GEOSCIENCES AND ENGINEERING

A Publication of the University of Miskolc

Volume 8, Number 12

Special Issue of the EFOP-3.6.2-16-2017-00010 *Sustainable Raw Material Management Thematic Network – RING 2017* Project

TABLE OF CONTENTS

FOREWORD

When someone has a look at the map of Hungary, a ring formed by the cities of Miskolc, Pécs, Sopron, and Szeged is clearly visible. This idea, namely "the alliance of the ring" was the initial spark behind the project, which now is approaching its completion. The EFOP-3.6.2-16-2017-00010 *Sustainable Raw Material Management Thematic Network – RING 2017* Project – in numbers – in brief: 4 cities, 4 partner universities, 5 research cells, more than 160 university lecturers–researchers, 200 students and young researchers and 140 other contributors did research and built this network together. In the 38 months so far more than 500 publications have been issued, of which more than 340 were in a language other than Hungarian (mainly in English), more than 330 people took part in research management and research skills improvement trainings, almost 100 potential Horizon 2020 partners contacted, almost 60 guest researchers–lecturers invited from EU/EGT or Carpathian Basin countries and more than 100 conference presentations held by our students during the 4 Sustainable Raw Materials International Project Weeks (IPWs) organized within the project.

The four networking universities – the University of Miskolc, the University of Sopron, the University of Pécs and the University of Szeged – joined their human and physical resources and carried out common scientific work in the following research cells:
- Innovative utilization of large-scale industrial and mining waste and by-products (SILICATE)
- Recovery of valuable materials from waste electronic and electrical equipment (WEEE)
- Municipal solid waste as a secondary source of raw materials (MSW)
- Utilization of lignocelluloses (LIGNOCELLULOSE)
- Utilization of wastewater and sewage sludge, low CO^2 emission technologies (CO2)

SILICATE Research Cell. The population of our earth is growing significantly, which means a continuous, drastic increase in both the demand for raw materials and the demand for energy for the future. This results in the formation of large amounts of solid by-products, the utilization of which is one of the most important tasks today. This amounts to nearly 800 million tonnes per year. Also, a significant amount of by-products are metallurgical slags, which represent around 500 million tonnes per year worldwide. Furthermore, approximately 120 million tonnes of red mud are generated annually during alumina production. These by-products and wastes, predominantly containing silicates, are joined by other mineral-derived materials, such as natural pozzolanic materials (pumicite, trass) or glass waste, the recovery of which has not been resolved. Recognizing the need for raw materials, the European Union's

raw materials strategy was developed, the importance of which is reflected in the Horizon 2020 calls for 'industrial leadership' and 'societal challenges' pillars.

Based on the above problems, the following thematic research directions were created in the project related to the Innovative Silicate Bearing Waste Recycling Research Group: nano grinding and the development of fine grinding for mechanical activation; geopolymer raw materials; geopolymer foam; mineralogical investigation of silicate bearing wastes and recycled products; utilization of construction and demolition waste and industrial by-products; and legal issues of the recycling of silicate bearing waste and of selective mining.

The basic goal of the research cell is to develop the preparation processes of primary and secondary raw materials of mineral origin in order for them to appear on the market as higher value-added products. One of the utilization possibilities is the production of geopolymers suitable for various applications (thermal insulation systems, micro-cement, concrete, heat-resistant materials). The subject of the present research is the development of technologies and products whose properties can be controlled by mechanical process engineering operations (mainly by grinding or classification); thus, the characteristics suitable for the purpose can be planned in advance.

As a result of our research we found that grinding had a key role in order to prepare a more reactive raw material for geopolymers by mechanical activation, as well as for nano-grinding of ilmenite, vivianite, hematite and cuprite. Geopolymer composites with appropriate mechanical stability could be obtained with various raw materials such as fly ash, red mud, and biomass. It was found that the cell structure of geopolymer foam, and thereby its compressive strength and density, can be controlled by grinding of the raw material. Utilization of construction and demolition waste and industrial by-products (fly ash and alumina dross) is possible in building materials and as potential raw material for road construction, while concrete and brick waste may hold potential for preparing geopolymers. Regarding the legal issues of recycling silicate bearing waste, researchers examined the rules on utilization of fly ash in Hungarian and EU law and introduced the dilemmas that lawmakers have to face when it comes to its utilization. Furthermore, selective mining sites were investigated in the Borsod coal basin in north-eastern Hungary, with the Dubicsány deposit found to be the most promising.

WEEE Research Cell. The European Commission has adopted a new Circular Economy Action Plan – one of the main blocks of the European Green Deal, Europe's new agenda for sustainable growth. The new Action Plan announces initiatives along the entire life cycle of products, targeting for example their design, promoting circular economy processes, fostering sustainable consumption, and aiming to ensure that the resources used are kept in the EU economy for as long as possible. Waste electrical and electronic equipment (WEEE) or e-waste is electrical and electronic equipment (EEE) that becomes waste. High added value products usually require special materials, and without them production is not possible (e.g.: indium in LCDs). Nowadays some important raw materials mainly come from non-European

countries, for example Rare Earth Elements (REE) from China. The E-waste generation was 44.7 million metric tons globally (in 2016), and only 20% of this amount is collected and recycled. The amount of WEEE is increasing because of the intensification of technological developments, increasing population, rapid societal and economic development (developing countries' access to modern technologies), changes in consumer habits (mobile phones, decreasing product lifetimes). On the one hand, untreated WEEE is hazardous to the environment and human health; on the other hand WEEE is a resource which should be used. WEEE processing faces many challenges, e.g. extreme small concentrations of valuable elements, composite materials, thin layers, covering materials, rapid changes in EEE technologies, substitution of elements, and market price variation of elements.

Various types of lithium-ion batteries were investigated, such as mobile phone batteries, notebook batteries and hybrid vehicle batteries. Structural and material compositions were determined (mobile, laptop, and car) and processing possibilities were investigated to avoid explosion during recycling. Mechanical and chemical treatment processes were developed in the case of the first two battery types. The most valuable materials recycled from the anode and cathode were cobalt and lithium.

In the case of LCD and LED, mechanical treatment processes were investigated. In addition to that, chemical and biological solubilisation experiments were carried out in order to solubilize the indium from waste LCD panels, and in a preliminary experiment, the potential of bioleaching of LEDs (light emitting diode) was examined as well. The newest types of displays (OLED) were also procured and analysed. These are used nowadays in mobile phones as well as in TVs, and shipment of them is increasing.

The solid-state drive (SSD) was introduced in the late 2000s as a new technology for storing data. Fundamental data for searching for appropriate treatment options of SSDs were analysed, such as the mass balance of the components of SSDs, material composition of the parts in SSDs, and size reduction of SSDs. The increasing demand for SSDs worldwide also fosters the research regarding SSDs recycling to ensure high effectivity and efficiency in handling "end of life" SSDs in the future.

To understand the structure of WEEEs and WEEE parts, CT measurements were performed in the 3D Lab of the University of Miskolc with a XYLON FF35 dual tube computer tomography equipment. For the measurements additional sample preparation was not necessary, because whole sample pieces could be placed inside the instrument. The sorting of WEEE parts was investigated by a camera with shape recognition software with one- and two dimensional code on the examined image. Market price tendencies were also examined from the economist's point of view, especially for EU critical raw materials.

MSW Research Cell. On the one hand quality and quantity enhancement of residue derived fuel (RDF) was one of the main topics of this research cell. The factors that affect fuel quality during the mechanical treatment process and the enhancement options after treatment were identified. Fuel particle size distribution, as well as heat value, moisture, ash, heavy metal and chlorine content of each size fraction were

measured for an entire year. The results showed close correlation between particle size and both physical and chemical characteristics of the fuel. Components that make the combustion challenging, e.g. chlorine, heavy metal, ash and moisture, are concentrated in the <10 and 10–20 mm size fractions of the RDF, while their low heat values were only half of those measured in case of the >30 mm fractions. Another working group of the MSW research cell carried out intensive research work on the development of mechanical processing technologies for residual municipal solid wastes (RMSW). The KLME (combined air flow, electric and magnetic) separator was patented and built into the new RMSW processing plant in Zalaegerszeg-Búslakpuszta. Industrial scale processing tests were performed.

Our research ambitions also covered the enhancement of secondary raw material production during manual sorting processes (in material recovery facilities), by means of near infrared (NIR) optical separators that required preliminary data collection and assessment. Time series analyses were performed within one year to show the variation of the composition of the waste issuing from separate collection, the changes in particle size distribution of those fractions that promise optimum operation for near infrared (NIR) optical separators, as well as the correlation between the sorting position, the waste type and the picking number. Based on these analyses, only 61 wt% of the incoming material can go through the optical separators, after diversion of the oversize (>350 mm; 18 wt%) and the small (<70 mm; 21 wt%) fractions. The measurements showed that the >350 mm fraction contains 60 wt% cardboard and 9.4 wt% LDPE film, while the 70–350 mm fraction contains 34.5 wt% paper, 18.5 wt% PET bottle and 9.5% cardboard.

The third main axis addresses non-destructive measurement methods, aiming at characterizing heterogeneous waste deposits, potentially suitable for secondary raw material extraction. Our research cell developed models with a completely new approach to electrical impedance spectroscopy and tomography measurement evaluations. In the case of spectroscopy, besides producing high-quality data, it is important to use appropriate models, since the models used in today's practice grant primarily mathematical interpretations of the measurement data. In our case (mainly by modifying existing models), we have produced models that, in addition to being mathematically aligned with the data, produce information (material characteristics) that can be used physically, taking into account the dielectric properties of the investigated material. With regard to tomography, we have developed a new image reconstruction process based on a completely new numerical process, also developed by the University of Pécs. During modelling, the test substance, as a continuum, is converted into a concentrated parameter linear network. The matrix of the resulting linear equation system contains the concentrated parameter equivalents of the material characteristics. With this method, we were able to achieve a higher resolution and sensitivity than that documented in the literature at simulation level. As a consequence of the proprietary numerical process, a universal analytical solution scheme was found for second-order ordinary differentials in the one-dimensional case. We are currently working on its two-dimensional extension.

LIGNOCELLULOSE Research Cell. There are three research groups established within the research cell: BIOMASS, BARK, and MUSHROOM. The aim of the work of the BIOMASS research group was to investigate the new directions of dendromass production, harvesting mechanisation and utilization. The task was very complex, because the increased demand for woody raw material puts a lot of pressure on forests, and in order to achieve a sustainable raw material supply other additional options need to be considered. Thus, the potential of base materials with high lignocellulose content was analysed going beyond forested areas, also on agricultural land, such as in agroforestry or short rotation woody energy plantation systems. In the future, these may play an increasingly important role in the local raw material supply.

The important part of the project was to examine the right choice of forest management method, which plays an important role in the efficient development of the useable amount of dendromass. Forestry research begins with the mechanization of planting the seeds or seedlings. The group also examined highly mechanized logging technologies, because the use of the modern mechanization systems is expected to occur more frequently in the future.

It was also essential to analyse the factors that are influencing wood quality. To achieve a circular economy and carbon sequestration, efforts must be made to utilize wood first in the wood industry, while energy utilization should be the last option. Tree dimensions and wood quality (the presence or absence of wood defects, which can be related to origin or age) determine the composition of the forest assortment that can be produced during harvesting; these factors were also measured. The usability of woody materials is also affected by biotic and abiotic forest damage, which has been increasing worldwide in recent years.

In the third part of the research, attention was particularly focused on finding new ways of utilizing woody materials and industrial by-products, e.g. the production of lignocellulose biofuels and wood mixture pellets. Both have strict requirements for the raw material, which was examined from ecological, economical and sustainability points of view.

Cultivation of wood produces large quantities of renewable raw materials each year. 10% of produced round wood is bark, which in most cases has been dumped in landfills. However, tree bark can be a perfect raw material for production of thermal insulation panels. Some trees have high resin and wax content, which is beneficial because no glue is required when gluing boards together. Boards are heat treated mainly to reduce water uptake and thickness swelling. There are several factors influencing the thermal conductivity values of wood-based materials, of which temperature, moisture, and density are the most crucial parameters. The results show that 0.06W/mK insulation value can be achieved, which is very close to the values of consumable materials. Thermal insulation panels were produced with different density and different treatments, and the results show the potential of a successful bio-product from bark, which could be competitive on the market. The use of bark as a formaldehyde absorber is another possibility.

To characterize the properties and condition of the biomass, we chose FT-IR spectrometry as an analytical technique providing chemical information. A chemometric data analysis strategy (Spectrum Preparation + PCA-LDA) was used to evaluate FT-IR spectra. The spectra of plant foliage and wood, as well as that of fungi decomposing woods, are characteristic. The effect of genetic origin (species type) and environmental condition is reflected in the spectra. Different plant foliage, wood samples, and fungal cultures can also be distinguished by group analysis of their spectra. Degradation of wood by fungi can be monitored by PCA-LDA evaluation of indicative spectra.

As part of the project in interinstitutional cooperation, we applied our developed spectrometry-based evaluation strategy to both plastic and wastewater samples. FT-IR spectrometry also proved to be suitable for the identification and separation of plastics and for the monitoring of wastewater purity. Using various pre-treatments can promote the hydrolysis and increase the total biogas yield in case of the lignocelluloses. Application of mechanical, thermal and chemical pre-treatment have many advantageous effects but these are expensive and their toxic by-products can cause many problems. In contrast, biological pre-treatments have benefits such as cost-effectiveness and environmental friendliness. Two different fungi species; oyster mushroom (*Pleurotus sp.*) and chicken of the woods (L*aetiporus sulphureus*) were applied for the pre-treatment of poplar and willow samples. The moisturised and chopped wood samples were inoculated with fungi strains and incubated in room temperature for 28–180 days. The alteration of cellulose and lignin content of samples were measured during the treatment. The biogas yields of pre-treated lignocelluloses in anaerobe digestion were tested under thermophilic (55 ºC) conditions in semi-continuous feeding lab fermentors. Correlations between the rate of fungal decomposition of wood sample and specific methane yield in anaerobe trials were revealed.

CO2 Research Cell. Water is a strategically essential material, and therefore the significance of water recycling and wastewater treatment technologies is of primary importance. Membrane separation, biotechnological approaches, advanced oxidation processes and agricultural fertilization alone or in combination are currently proven technologies in many areas, including wastewater treatments and utilization. The main limitation of the various filtration processes is the accumulation of matter at the membrane surface or in the pores, leading to two phenomena: concentration polarization and membrane fouling. Several combined approaches, including sonication, Fenton-oxidation and ozonation-coupled ultrafiltration have been successfully applied to increase the efficacy and decrease the costs of ultra- and nanofiltration techniques. Membrane fouling was substantially reduced by Vibratory Shear Enhance Processing. Novel self-cleaning nanocomposite membranes were also developed for better reusability of the filters. Oily wastewaters were also successfully treated with a combined microbiological/filtration method. A novel dielectric measurement technique was introduced for monitoring the sludge utilization process filtration.

Oily wastewater can be treated by biotechnological methods using "oil-eating" microbes. Moreover, natural waters are frequently contaminated by toxic hydro-

phobic materials. Annually, a huge amount of hazardous compounds is released into the environment, including xenobiotics, oils, oil derivatives, drugs. etc.; majority of them reaches and contaminates the groundwater zones and gets involved in water recycling. Various biotechnological approaches were successfully applied for treatment of contaminated groundwater and of wastewater containing fat/drugs both at aerobic and anaerobic zones. A unique strain capable of degrading drug intermediates was isolated, characterized and applied for treatment of industrial wastewater. Lubricant oils are widespread pollutants, therefore their degradation is extremely important. Culture dependent and culture independent, biostimulation, bioaugmentation strategies were designed and applied for intensified/accelerated removal of such contaminants for industrial interest. Together with industrial partners, the elimination of diesel oil contaminations in the groundwater of an abandoned military base was studied and an anaerobic microbial-enhanced energy recovery process was suggested to convert pollutants into biomethane. Methane/biogas, an important alternative energy carrier, can be produced from various sources, including wastewater, organic materials and energy plants. A variety of biomass sources, such as tomato and wood wastes, willow, microalgal biomass, algae-treated wastewater, could be efficiently converted into biogas and thus CO_2 emissions can be reduced. The processes were followed by numerous standard analytical and high-throughput biological methods. Various treatments including enzymatic or microwave pretreatments, and bioaugmentation were applied for intensification of biogas production and to increase the final yields. Microalgae can capture CO_2 and produce clean gaseous energy carriers, such as hydrogen. In collaboration, a carbon-free sustainable process was developed for continuous but cyclic production of photobiohydrogen from water.

Heterogeneous photocatalysis is one of the most investigated advanced oxidation processes which can be applied in wastewater purification technologies. This technology is quite advantageous: it is highly flexible, needs low energy input, and has low or no toxicity impact. Usually, nanostructured materials are used as photocatalysts, which are obtained after complicated synthesis procedures; however, natural minerals can also be applied. In the project, the applicability of natural minerals as photocatalysts was demonstrated in wastewater treatment technologies. Natural rutile nanoparticles in the size range of 20–100 nm could be successfully used for degradation of drug pollutants and xenobiotics, including ibuprofen and phenol in wastewater. Natural ilmenite showed significant photocatalytic activity towards the degradation methylene blue dye, suggesting its applicability in the decolorization process in dye, textile and paper industrial wastes/wastewaters. Natural cuprite nanomaterial obtained by nanogrinding was demonstrated to be an efficient degrader of a model drug pollutant, salicylic acid.

Sewage sludge utilization has three main directions: a) energetic utilizations, such as biogas/biohydrogen production, incineration, thermochemical conversions into solid, liquid and gaseous fuels; b) direct usage as fertilizer; c) composting as an indirect fertilizer. In the project, the agricultural applicability of wastewater sludge was tested. Our study focused on examining the changes in the extractable components of a Chernozem soil and the soil's biological activity as a consequence of low-dose

municipal sewage sludge compost applications. The results clearly showed significantly increased soil-bound K2O, P2O5 and NO2− + NO3− contents linked to the sewage sludge treatments, but the toxic element content did not increase significantly. Microbiological analysis revealed that the sewage sludge treatments increased the number of the aerobic microbes and the biochemical activities in the samples. Consequently, low doses of municipal sewage sludge compost can be a sustainable fertilizing practice, taking advantage of their high N, P and K contents that are slowly converted to their soluble/bioavailable forms, thus preventing their excessive leaching into the groundwater. The measurements of CO_2 emissions on arable lands treated with sewage sludge confirm that the daily rhythm of soil moisture and temperature changes have much stronger effects on the CO_2 respiration than the low-dose sewage sludge treatments.

Dear Reader, accept this publication as a little taste of the work and results of the project!

Miskolc, 25 November 2020

Best regards,

J. Faitli, scientific leader of the project
G. Mucsi, leader of the SILICATE research cell
S. Nagy, leader of the WEEE research cell
T. Kiss, leader of the MSW research cell
I. Czupy, leader of the LIGNOCELLULOSE research cell
G. Rákhely, leader of the CO2 research cell

SUMMARIZING RECENT ACHIEVEMENTS OF THE SILICATE WASTE RESEARCH GROUP, UNIVERSITY OF MISKOLC, WITHIN THE RING 2017 PROJECT

GÁBOR MUCSI[1] – ROLAND SZABÓ[1] – NÓRA HALYAG[1] –
MÁRIA AMBRUS[1] – ISTVÁN KOCSERHA[2] – RÓBERT GÉBER[2] –
FERENC MÁDAI[3] – FERENC KRISTÁLY[3] – FERENC MÓRICZ[3] –
ÁDÁM RÁCZ[1] – KATALIN BOHÁCS[1] – ÉVA GREGUS[1] –
CSILLA CSÁK[4] – GYÖRGY MARINKÁS[5] – ÁKOS DEBRECZENI[6] –
JÓZSEF MOLNÁR[6]

[1]*Institute of Raw Materials Preparation and Environmental Processing,
University of Miskolc*
[2]*Institute of Ceramic and Polymer Engineering, University of Miskolc*
[3]*Institute of Mining and Geology, University of Miskolc*
[4]*Department of Labour and Agricultural Law, University of Miskolc*
[5]*Department of European Law and International Private Law, University of Miskolc*
[6]*Institute of Mining and Geotechnical Engineering, University of Miskolc*

Abstract: In the present paper the main research results are summarized that were carried out under the umbrella of the project entitled *Sustainable Raw Material Management Thematic Network – RING 2017* and that are related to the Innovative Silicate Bearing Waste Recycling Research Group. The following thematic research directions were created: nano grinding and the development of fine grinding for mechanical activation; geopolymer raw materials; geopolymer foam; mineralogical investigation of silicate bearing wastes and recycled products; utilization of construction and demolition waste and industrial by-products; and legal issues of silicate bearing waste recycling and selective mining. As a result of the research work it was found that geopolymer composites can be produced from various waste streams. Shortcomings of the current regulation and the soft-law regulating tools are addressed, which are meant to shape the future development of the field.

Keywords: waste utilization, grinding, geopolymer, hydraulic binder, selective mining

1. INTRODUCTION

The population of our earth is growing significantly, which means a continuous, drastic increase in both the demand for raw materials and the demand for energy for the future. In terms of energy, the BP Statistical Review of World Energy (2013) stated that coal-based energy production is one of the most prominent in the world in terms of energy production, due to its economical extraction and favourable price. This results in the formation of large amounts of solid by-products (fly ash and slag),

the utilization of which is one of the most important tasks today. This amounts to nearly 800 million tonnes per year. Also, a significant amount of by-products are metallurgical slags, which represent around 500 million tonnes per year worldwide. Furthermore, approximately 120 million tonnes of red mud are generated annually during alumina production. These by-products and wastes, predominantly containing silicates, are well complemented by other mineral-derived materials, such as natural pozzolanic materials (pumicite, trass) or glass waste, the recovery of which has not been resolved. The steady decline in the volume of primary raw materials and the rise in their prices worldwide encourages professionals to research the large-scale availability of secondary raw materials. Examples include industrial and mining by-products and wastes such as fly ash and slag from coal-fired power stations, glass waste of various origins, red mud from alumina production, waste from the production and preparation of mining, or metallurgical slag. Due to their good physical and chemical properties, these materials are excellent for use in the construction or building materials industries, among others.

Most industrial by-products and waste are currently deposited in landfills, which is disadvantageous in several respects. First, the landfills reduce valuable agricultural and industrial land and pose an environmental risk (water and air pollution) in the event of improper disposal. Furthermore, the utilization of the by-product in question as a raw material would mean the rational and sustainable management of the primary mineral resources and raw materials. Last but not least, it also contributes to the reduction of CO_2 emissions, as a significant amount of CO_2 is produced during the production of the cement to be replaced. The right quantity and quality of raw materials are essential for the European economy as well as for the Hungarian economy. Recognizing these needs, the European Union's raw materials strategy was developed, the importance of which is reflected in the Horizon 2020 calls for 'industrial leadership' and 'societal challenges' pillars.

Therefore, the basic goal of our research group is to develop the preparation processes of primary and secondary raw materials of mineral origin in order for it to appear on the market as a higher value-added product. One of the utilization possibilities is the production of geopolymers suitable for various applications (thermal insulation systems, microcement, concrete, heat-resistant materials). These are inorganic polymers which can be prepared by reacting aluminosilicate oxides and aluminosilicates in an alkaline medium. The thermal insulation properties of the fly ash-based geopolymer can be enhanced by creating a foam structure. These materials are characterized by excellent fire and chemical resistance, which makes it possible to use them as a refractory or – with low thermal conductivity – thermal insulation material. The subject of the present research is the development of technologies and products whose properties can be controlled by mechanical process engineering operations (mainly by grinding, classification); thus, the characteristics suitable for the purpose can be planned in advance. Our primary goal is to develop a thermal insulation material that is air permeable, non-combustible and priced lower than other mineral-derived thermal insulation materials. This is made possible by a thermal insulation material with a foam structure obtained from the utilization of a secondary raw

material. Another utilization solution for secondary raw material-based foam products is the development of special functional materials whose high specific surface area is provided by the open-pore foam structure: for example, the production of ion exchange materials that can be used for either remediation, environmental or energy purposes.

Last but not least, supplementary cementitious materials (SCMs) are of great importance. They can be obtained at significantly lower prices than products currently on the market (e.g. microsilica, metakaolin), while also producing high-strength, acid-resistant, heat-resistant products. These materials can be manufactured from waste materials, therefore one of our focus is SCM development from secondary materials sources.

Based on the above-mentioned research areas, an additional goal of the project is to investigate the legal circumstances of waste processing and utilization in the European Union as well as on the Hungarian level.

2. THEMATIC RESEARCH RESULTS

2.1. Application of nano-grinding and the development of fine grinding for mechanical activation

Within the framework of the project developments in various fine grinding areas were carried out. In the first topic the differences and similarities of the wet and dry grinding in a stirred media mill were investigated from energetic and mechanochemical point of view. Grinding experiments in batch stirred media mill were carried out with zeolite and kaolin. The grinding experiments were carried out at different stress energy and stress number values and the grinding was measured during milling. After grinding, X-ray diffraction (XRD), Fourier Transform Infrared Spectroscopy (FTIR), and particle size analysis by laser scattering were carried out on the ground materials. It was found that wet stirred media milling was much more effective than dry stirred media milling from the size reduction point of view. However, more significant changes were observed in the structure during dry grinding, based on FTIR measurements. Dry grinding is more effective in amorphisation than wet grinding, as observed from the evolution of amorphous fraction based on XRD. More progressive crystallite size decrease and amorphous fraction increase is observed with the higher energy dry grinding. Based on the above, it can be stated that dry stirred media milling is much more effective for the mechanochemical activation, while the wet process is more suitable for particle size reduction [1]. The same milling experiments were carried out in with limestone and with quartz. The aim of the measurements was to understand the main differences in the method of wet and dry stirred media milling. Based on the results, in the case of the non-cohesive quartz dry grinding was more effective than wet in the comparison of the product median at a certain specific grinding energy. For limestone, which is a cohesive material, the wet process was much more efficient. Connecting to the development of the mechanical activation in a stirred media mill, a continuous dry grinding stirred media milling system was developed within in the project, where mainly the effect of the

operational parameters on the product particle size was investigated [2] and also the system itself was modified and developed in numerous steps [3]. As a final step the system received a self-developed airflow control that ensures an even amount of air inside the mill during operation.

The second main topic was carried out in cooperation with the University of Szeged, where wet stirred media milling and nano-grinding of different Ti, Fe and Cu-oxide and phosphate minerals were performed. During the experimental work nano-grinding of ilmenite, vivianite, hematite and cuprite was carried out in a continuous operation wet stirred media mill. During the experiments the particle size distribution and specific surface area of the ground materials were determined after certain grinding times and the specific grinding energy was measured, thus determining the grinding kinetics of the different minerals. After the milling, scanning electron microscopy (SEM) and FTIR measurements were carried out on the samples to characterize the nanoparticles. The nano rutile, ilmenite, vivianite and cuprite particles produced were later applied as photocatalysts for the development of novel wastewater treatment technologies by the colleagues from Szeged.

2.2. Investigations concerning possible geopolymer raw materials

Nowadays several studies are being conducted on the use of waste materials in order to eliminate the increasing toxic threat to the environment. The solution is an economically viable utilization of waste materials in new products for other applications rather than disposal in landfills. The new product can be formed by alkali activation of alumina-silicate materials containing highly reactive phases. The possible raw materials can be power plant fly ash, ground granulated blast furnace slag, red mud, silica fume, or rice husk ash, but other mine tailing waste can also be successfully utilized in geopolymer production. In most studies fly ash is used as a source material [4, 5, 6, 7], as millions of tonnes of fly ash are generated each year by coal-fired power stations.

Fly ash *(Figure 1)* is the fine solid particulate residue separated from the flue gas of a power station burning pulverized coal, where the particle size, amorphous content, loss on ignition, morphology and origin influence the stability of fly ash used in a geopolymer. Fly ash also possess pozzolanic properties, which allows it to serve as a reagent for the synthesis of geopolymers, which is an inorganic amorphous polymeric Si-O-Al framework formed by alkali activation with alkali hydroxide and alkali silicate solution [8]. The result is a cement-like product with better mechanical properties (compressive strength, flexural, splitting tensile strength), better physical properties and higher durability (resistance to chloride, sulfuric acid, thermal, freeze-thaw cycles). Besides these advantages, geopolymerization can trap and fix toxic metal elements from fly ash. The process and the final properties depend on the Si/Al ratios, the type and the amount of the alkali solution and the curing conditions.
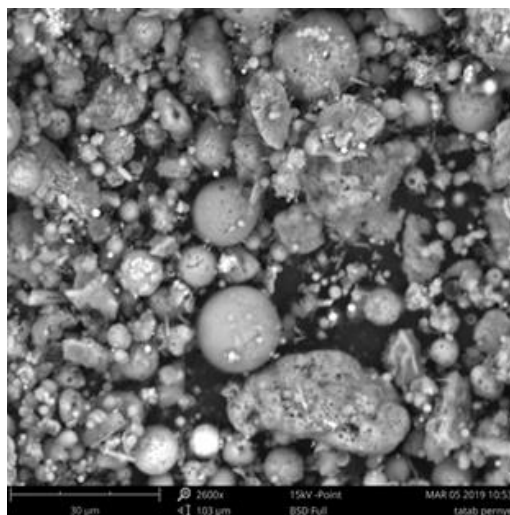
Figure 1
SEM image of brown coal fly ash from Tatabánya

The mechanical properties and durability can be improved by the mechanical activation of fly ash, by slightly changing the Si/Al ratios, alkali solutions, curing conditions, or by adding other types of wastes, such as slag or red mud [9] and/or fibers to reach the optimal chemical composition for geopolymerization with better mechanical properties. Experiments with mechanical activation of brown coal fly ash from Tatabánya revealed that with an optimized liquid/solid ratio (0.82) and appropriate activator solution composition (25 wt.% 8 M NaOH solution and 75 wt.% water glass), the uniaxial compressive strength of the specimens can be increased. As seen in *Figure 2*, the highest average compressive strength values could be achieved with 5–10 minutes grinding; however, further grinding time resulted in decreasing strength values [10].

The addition of fly ash can also improve the mechanical properties of raw materials with high crystallinity and low reactivity, by bounding the undissolved inert particles together to achieve enhanced compressive strength. The best results can be obtained by mixing in half proportions the binding reactive fly ash and the highly crystalline rhyolite tuff with alkaline solution consist of 75 wt.% waterglass and 25 wt.% 6 M NaOH, which reaches 22.5 MPa compressive strength. This result is better than the compressive strength of a geopolymer made of only fly ash (9.44 MPa).

Along with fly ash, the application of red mud as a possible supplementary geopolymer raw material has also been an area of investigation during the past decade. Due to its availability and high alkalinity, it has proven to be an appropriate material for geopolymerisation [11, 12]. With the use of red mud sample from Almásfüzitő, the preparation of fly ash–red mud-based geopolymers exhibited 5.5 MPa maximum compressive strength with the addition of 15% red mud. Furthermore, a linear correlation was observed between the compressive strength and the specimen density

of the specimens. Overall, the experiments proved that the red mud could substitute some of the alkali activators for geopolymer production [9].
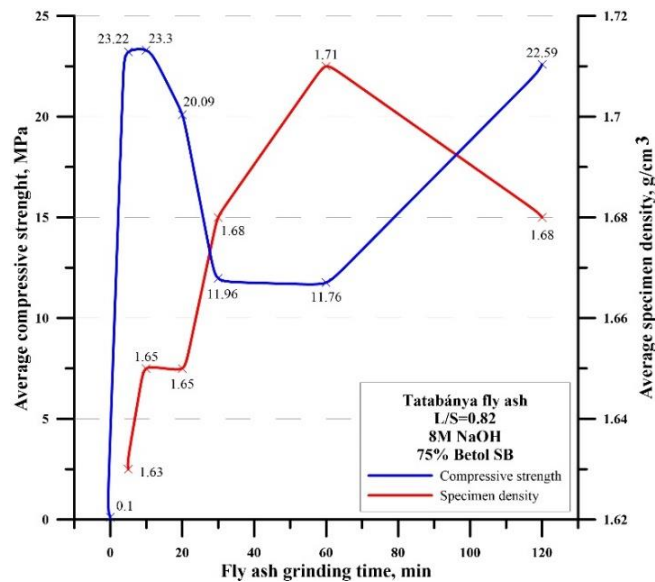
Figure 2
Average compressive strength and specimen density of
ground fly ash geopolymers [10]

As geopolymer exhibits brittle behavior due to its low tensile strength, several composites have been developed to increase flexural strength or heat resistance. The addition of natural or artificial fibers [13] can change brittle behavior to ductile or quasi- ductile with significant improvement in mechanical properties, depending on the type and length of the fiber, which can improve the strength, reinforce-matrix interaction by fiber-bridging behavior, heat resistance and resistance against chemical and physical corrosion [14].
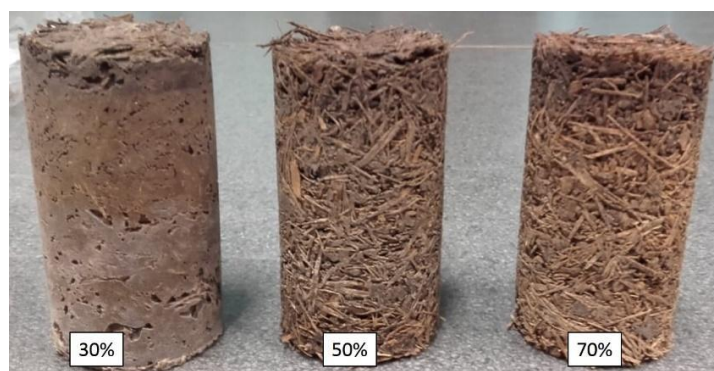
Figure 3
Biomass-geopolymer composites [15]

A joint research project with the University of Sopron included the investigation of biomass-geopolymer composites. Using woody biomass from the Botanical Garden of the University of Sopron, fly ash based geopolymer specimens were prepared using 30 wt.%, 50 wt.% and 70 wt.% biomass fibers *(Figure 3)*. With increased biomass fiber content, decreased specimen density was experienced. Based on the microstructural analysis, the fibers were compatible with the geopolymer matrix, with the prepared composites applicable for sound or heat insulation or as a lightweight composite.

2.3. Effect of the amount of foaming agent and fly ash fineness on the properties of geopolymer foam

The rate of foaming of the geopolymer (and thus its properties) can be influenced by several parameters such as the foaming method, the amount of foaming agent and surfactant, or the rheological properties of the initial mixture (geopolymer paste) [16, 17, 18, 19, 20, 21].

The generation of gas into the geopolymer paste can be realized by adding foaming agents. Chemical foaming agents form gaseous products (such as O_2 and H_2) and other byproducts by thermal decomposition or chemical reactions. Metal powders (such as aluminum or silicon) and hydrogen peroxide are used most frequently for the fabrication of geopolymer foams [22]. Based on the experimental results it was found that the higher content of foaming agent (aluminum powder) resulted in lower compressive strength, specimen density and higher porosity of fly ash-based geopolymer foam. However, for a given foaming agent content, no change in the strength and density values of geopolymer foam is detected [23].

The rheology of the mixture can be easily changed by the amount of added liquid activator, i.e. by the liquid/solid ratio (L/S ratio) or by using a superplasticizer [20, 21, 24]. However, the rheology of geopolymer paste can also be controlled at a given L/S ratio by the size reduction of the solid component, by grinding. At the start of grinding, the particle size of the material becomes finer relatively quickly, and the work required for grinding (optionally grinding time) is approximately proportional to the new surface formed, i.e. the degree of dispersion of the resulting product. It was found that the geopolymer paste with a given fly ash content (55 w/w%), with originally non-Newtonian (Bingham-plastic) behavior, became a Newtonian fluid – regardless of the fly ash type (lignite or brown coal) – over a given specific surface area of fly ash (about 3,000 cm^2/g) due to increasing the fly ash fineness. Based on the experimental results it was found that the flow behavior of the geopolymer paste significantly influenced the porosity, the size and the amount of the pores, and thus the compressive strength of the brown coal fly ash-based geopolymer foam made using hydrogen peroxide foaming agent. Due to the high viscosity of the geopolymer paste the formation of pores was inhibited, so the pore size of geopolymer foam was too small. In case of very low viscosity the oxygen gas can easily escape from the geopolymer paste and as a result of this the geopolymer foam had a compact structure with few bigger pores [6, 25].

Overall, it can be stated that not only by changing of the amount of foaming agent but also by modifying the rheology of geopolymer paste, the pore structure of geopolymer foam can be changed, thereby altering its compressive strength and density.

2.4. Mineralogical investigation of silicate bearing wastes and recycled products

X-ray powder diffraction investigations were carried out on the Bruker D8 Discover instrument of the 3DLab (Institute of Mineralogy and Geology, University of Miskolc). The measurements were run in Bragg-Brentano geometry (θ- θ goniometer, reflection mode, top-loaded sample holders) with Cu K-alpha radiation (40 kV, 40 mA), using a LynxEye XE-T energy-dispersive position-sensitive detector with 2° detector window opening, in high resolution mode to cut fluorescence from Fe. Patterns were recorded in the 2–70 °(2θ) range with 0.007 °(2θ)/24 sec counting time. Crystalline phases were identified from ICDD PDF4 (2018) database with the Search/Match module of the Bruker Diffrac*Plus* EVA.11 software. Quantitative composition was calculated by Rietveld refinement using fundamental parameters approach (FPA) from instrumental convolutions and crystal structure data from the Crystallography Open Database [26] and American Mineralogist Crystal Structure Database [27]. Amorphous content was calculated by the amorphous hump method. The chemical analysis was completed by a Rigaku Supermini 200 type WD-XRF, which has an air-cooled 200W X-ray tube with Pd target (50kV, 4.00mA). The measuring was done at 1.2–1.6 Pa pressure with ZSX driver and evaluation programme. The peak and the background(s) angle positions were measured by LiF crystal in the range of $_{22}$Ti – $_{92}$U, PET crystal in the range of $_{13}$Al – $_{21}$Sc and RX25 crystal in the range of $_{8}$O – $_{12}$Mg. For detection scintillation counter (SC) for heavy elements and P10 gas flow proportional counter (F-PC) for light elements was used. The grain size of the sample was crushed under 65 μm, then it was dried at 120 °C for 2 h. For powder pellet preparation 4,000 g of the dried powder was mixed and homogenized with 1,000 g of Cereox binder (ultra-pure and fine polyethylene powder), and the mixture was pelletized with Ø32 mm at 25 tonnes. As additional data, the L.O.I. (Loss on Ignition) was measured at 1050 °C.

Statistical methods were applied in order to characterize the correlation between change of rare-earth element (REE) content along vertical profiles, cross-correlated as well with the change in mineral and major element composition.

The red mud samples investigated by XRD have the same major phases – hematite and cancrinite – while minor and accessory phases vary both in type and amount. Based on the Rietveld refinement data, cancrinite is present both as carbonate and an OH⁻ enriched species of the cancrinite group, although a reliable distinction requires vibrational spectroscopy analysis [28]. Hydrogarnets, the byproduct of the Bayer process, were identified as hibschite [29] and katoite [30]. Although in some samples grossular was observed, our results have now indicated the presence of almandine. Carbonates appear as calcite and dolomite, but in some of the samples aragonite is also detected. Kaolinite, illite, gibbsite, böhmite and diaspore are residual ore minerals,

while nordstrandite in traces, observed by Bolanz et al. [31], could be a residual phase or crystallized after red mud deposition. Quartz, zircon and anatase are also possible residual phases. Amorphous material content is in the range of 10–20 wt.%, different for each sample.

Goethite found in important amounts could be also a residual bauxite phase, but if it forms as a precipitated product of red mud, it could have an important role in fixing REEs existing in solution. Hematite is a potential carrier phase for Ce^{4+}, as shown by detailed investigations of Bolanz et al. [31]. None the less, REE bearing phases cannot be evidenced by XRD. An approximated limit of detection for REE minerals could be around 1-2 wt.% due to the severe peak overlapping of the >10 crystalline phases. However, chemical analysis suggests quantities < 1 wt.% for such phases.

The main chemical components are Fe_2O_3 (hematite and goethite, mainly), Al_2O_3 and SiO_2. The Na_2O is contained in the cancrinite structure, while most of CaO is carbonate (calcite) form, also contributing to cancrinite, hydrogarnets (hibschite and katoite) and dolomite. The toxic heavy metal content is low, especially Pb, Cu and As < 100 ppm. The somewhat elevated Cr content (400–600 ppm) may be fixed in the crystal structure of hematite, thus immobilized with regard to leaching. These properties make the investigated red mud materials suitable for incorporation into silicate-based products, like geopolymers. The composition of amorphous phase observed by XRD is a mixed aluminum-silicate with Na, as a residue of silicate crystallization from the Bayer process. The anion exchange property of cancrinite – to remove $(OH)^-$ and replace it by $(CO_3)^{2-}$ – makes the material suitable for CO_2 sequestration also.

Cross-correlation matrixes built up on component changes along the vertical profiles of red mud residue storage facilities show that there are only tiny differences between REE profiles. The cross-correlation calculations show that profiles of La-Pr-Nd-(Sm) are very similar and these comprise one group. There is another group of heavy REEs (Dy-Ho-Er-Tb-Gd) where the profiles show close similarities. Cross-correlation values show similarities for TiO_2-Al_2O_3-Fe_2O_3, which practically do not change along the profile. Among the more changeable components, stronger similarity is found among SiO_2 and Na_2O and Al_2O_3. This is explained by the fact that after hematite the second most common mineral phase in the samples is the cancrinite. Mineral composition changes along the profile indicate that rare earth elements and Yttrium (REY) show good correlation with cancrinite. The best correlation values are with hematite concentration of which shows very little changes along the profile. Incorporated in mineral phases, REE are primarily associated with phosphates. This observation is supported by microprobe analysis of aggregated samples from cells VIII and IX, detecting primarily xenotime and monazite grains.

2.5. Utilization of construction and demolition waste and industrial by-products as potential raw materials for the building industry and road construction

Several by-products are issued during different production technologies. One serious issue is how to handle and utilize construction and demolition (C&D) waste in an

appropriate way. These materials are generated in significant quantities year by year, while storage of them as waste can be harmful to the environment in the long term. Therefore, our team focused on two main research directions: utilization of C&D waste and industrial by-products (fly ash and alumina dross) in building materials and as potential raw material for road construction. Reviews on these fields are made in [32, 33].

In an experimental series, the effects of different curing conditions on geopolymer foam were analyzed [34]. Foams were prepared using Class F type fly ash and sodium-hydroxide activator and were cured in a furnace or in autoclave for six hours. The temperature range was varied between 60–90 °C and the pressure of autoclave was changed between 2–7 bar. Results showed that autoclaving has less effect on the compressive strength than being cured in a furnace. Within the pressure and temperature ranges investigated, autoclaving produced no change in the properties of the samples.

C&B (concrete and brick waste) and industrial by-product (alumina dross) powders were used to prepare geopolymers [35]. As the performance of geopolymers is highly dependent on the properties of the initial powders, different methods (particle size distribution, density, elemental and chemical composition, microstructural analysis) were used to reveal the features of these powders. For preparing samples, an alkali activator (NaOH solution in different concentrations) and waterglass (Na_2SiO_3) were applied. After curing, compression strength was determined at the age of 7 and 28 days. The test results confirmed that not only the type and amount of waste materials affect the forming of a geopolymer structure, but the concentration of alkali activator is important as well. We found that samples with concrete powder had the highest compressive strength (>17 MPa) after 28 days. According to this result, concrete may be a potential raw material for preparing geopolymers. The brick powder may also be suitable as a raw material; however, in this case the use of a proper concentration of alkali activator is required. During the reaction of metallic Al of aluminum dross and liquid activator solution content a low density foamed geopolymer was prepared, which may be useful for thermal insulating applications.

Asphalt is a special composite material, which consists of bitumen as a binder and a high volume of mineral aggregates in a specific particle size distribution. Mining of these minerals will cause the depletion of natural sources and thus it is necessary to search for potential materials to substitute these minerals in part or in full. Aluminum dross, brick powder and concrete powder were investigated as potential asphalt filler (d < 0.063 mm) for road construction [36, 37]. Different tests (particle size distribution, elemental composition, electron microscopy) suitable to characterize the powder samples were made. Limestone filler, which is one of the best fillers in asphalt, was used as a reference material. The cohesion between the binder and fillers were also revealed. According to the hydrophilic coefficient, we found that aluminum dross has an advantageous property, because it is similar to limestone powder. Brick powder also shows good results. To sum up, aluminum dross and brick may be used in asphalt pavements as fillers.

2.6. Legal issues of silicate bearing waste recycling

In their article 'The legal categorization of Fly ASH in EU and the Hungarian law' [38] the authors examined the rules on utilization of fly ash in Hungarian and EU law and introduced the dilemmas that lawmakers have to face when it comes to its utilization[1]. They also examined the sustainability of the coal combustion power plants – which are major sources of fly ash – from an economic and environmental aspect. Regarding the relevant EU law they came to the conclusion that it is rather divergent[2]. The authors devoted a section to the case law of the European Court of Justice (CJEU), which has a paramount role in shaping EU law by elaborating definitions and clarifying the law.

In their article, called 'A KKE országok hulladékgazdálkodási szabályozása és azok konformitása az uniós joggal – Az EuB vonatkozó joggyakorlatának elemzése / Waste management regulations in East-Central European countries and their conformity with EU law – Analysis of related CJEU case-law' [39] the authors – building on Csilla Csák's earlier writings [40, 41] – examined the rules on waste management in the EU law and in the legal systems of Central and Eastern European countries with special regard to industrial wastes like fly-ash and construction and demolition waste. In this article too, they examine the related case law of the CJEU.

In their forthcoming article 'A hőszigetelő anyagokra vonatkozó uniós szabályozás, különös tekintettel a geopolimer alapú hőszigetelő anyagokra / The law of the European Union of heat insulating materials, with special regard to the geopolymer based insulating materials' the authors provided an overview of the energy policy of the EU and its environmental protection objectives and examine how the law on the heat insulation of the buildings fits into this policy, which aims at reaching the highest possible energy efficiency by decreasing the demand of the consumer side. Considering the fact that in the EU the major part of the energy consumption is contributable to the energy demands of buildings, modern and efficient heat insulation of the buildings is a major step in reaching the energy-efficiency goal. In connection with this, the authors introduced the shortcomings of the current regulation and the soft-law regulating tools, which are meant to shape the future development of the area.

2.7. Opportunity for selective mining in the Borsod coal basin in northeastern Hungary

Numerous underground coal mines were in operation in the Borsod coal basin in the northeastern part of Hungary until the beginning of this century. The main areas of

---

[1] As an example: while the EU law prefers utilization of waste materials in order to create a circular economy, the principle of proximity – which shall be taken into consideration – does not facilitate the utilization of fly ash, since this principle – alongside economic considerations – excludes the transportation of material for greater distances.

[2] While the Waste Directive – which classifies fly ash as waste and thus determines its legal standing – provides the regulatory framework, other directives, regulations and decisions of the Commission provide for the detailed rules of utilizing fly ash.

utilization of the mined-out coal were power and heat generation and supplying households with fuel, mostly for heating. So almost the whole output of the mines was burned. Only a part of the by-products of this mining activity is available. Coal combustion products of household heating became scattered throughout the region over the past centuries; just the part – probably smaller – from industrial consumers is available on the sites of power stations and other plants. Mine waste that was disposed on the mine sites consists of mostly country rocks of the coal seams containing variable amounts of coal. The coal content of the waste was certainly burnt or slowly oxidized during this long time. The mine waste disposal sites were reclaimed during the past two decades. Consequently, new mine waste and coal processing by-products can be obtained only from the operation of new mining operations.

Several cases were examined to select the proper mine site throughout the northern part of Hungary. Finally, the Dubicsány deposit was found to be the best of them. Its mineable reserves are estimated at 50 million tonnes with a little bit more than 12 MJ/kg calorific value, enabling operation of more than three decades. The main difference between the classic and the future ways of utilization is that this time only coal chemistry can be taken into account to extract its carbon content, but burning it as fuel in power plants is practically excluded. The subjects of research were sustainability as well as technical, safety and economic aspects. The following main results of the research can be summarized as follows [42, 43]:

- Research confirmed the well-known facts of coal quality properties that calorific value can be estimated accurately as a function of ash and moisture content furthermore sulfur, volatile and carbon contents. A very fine analysis was made for all properties using data of over 5600 samples demonstrating linearity. Estimations proved to be accurate as coefficients of determination were fairly high ($0.7670 < R^2 < 0.9948$) and estimated errors of calorific value were low (0.335 MJ·kg^{-1} < D(ΔF) < 2.248 MJ·kg^{-1}). A huge number of samples (5648) were analyzed and extremely good correlation (a 0.9845 coefficient of determination and 0.814 MJ·kg^{-1} mean residual square of estimation) was found for calorific value and carbon content. This proves that calorific value can be considered a basic parameter for coal chemistry, even instead of carbon content, for the given deposits.
- Water hazard and quantity of mine water was examined to assure safe mine operation and the least possible environmental impact. The mine dewatering method considered it a part of potable water supply for the inhabitants and industrial water for the mine.
- All of the coal properties were found to vary throughout the deposits, both horizontally and vertically. Therefore, a 3D numerical analysis is being developed to enable selective cutting and accurate quantity and quality design of the mine output. As coal quality changes (deteriorates) from the covering layer of Seam V downwards, determining the proper height of the coal face of the longwalls *(Figure 4)* is an extremely important question. This is also important for the correct selection of the longwall equipment, thus enabling selective

cutting. The aim of the numerical analysis was to find the distribution functions of the mass and the heat content, and furthermore the mean calorific value of the coal as a function of coal face height for the four parts of the mine. Future owners will be able to use these results for proper decisions in mine valuation and mining engineering design.
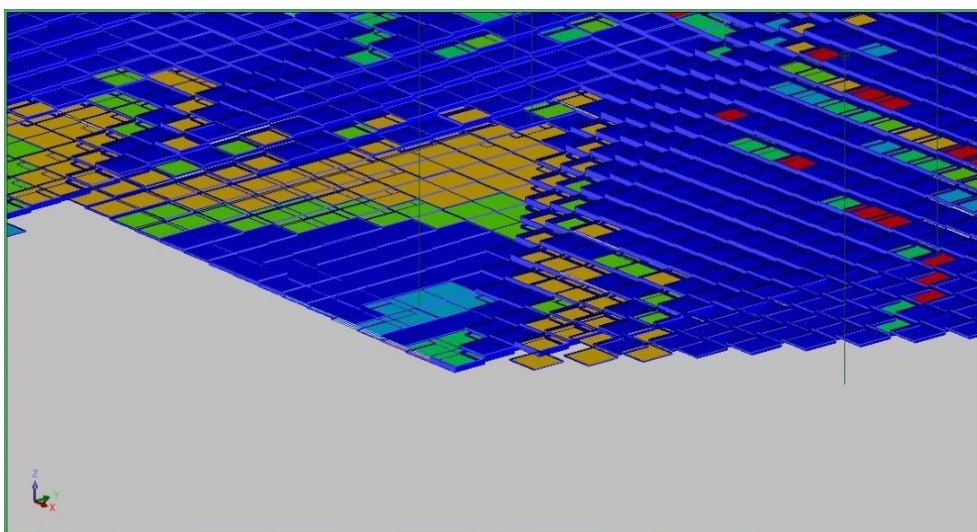
Figure 4
Ortographic view of a zoomed smaller part of the 3D block model of Seam V of the Dubicsány deposit highlighting its fine resolution
Drawn by Tompa R., 2018

3. SUMMARY

The following research results were achieved by the Silicate Bearing Waste Recycling Research Group in the RING 2017 project:
- grinding had a key role in the project in order to prepare a more reactive raw material for geopolymers by mechanical activation, as well as for nano-grinding of ilmenite, vivianite, hematite and cuprite;
- a geopolymer composite with appropriate mechanical stability could be obtained with various raw materials like fly ash, red mud and biomass;
- it was found that the cell structure of geopolymer foam, and thereby its compressive strength and density, can be controlled by grinding of the raw material;
- a mineralogical investigation of red mud was carried out in order to monitor the metal components, revealing that REE are primarily associated with phosphates;
- utilization of construction and demolition waste and industrial by-products (fly ash and alumina dross) is possible in building materials and as potential raw material for road construction, while concrete and brick waste may hold potential for preparing geopolymers;

- regarding the legal issues of recycling silicate bearing waste, researchers examined the rules on utilization of fly ash in Hungarian and EU law and introduced the dilemmas that lawmakers have to face when it comes to its utilization;
- selective mining sites were investigated in the Borsod coal basin in northeastern Hungary and the Dubicsány deposit was found to be the most promising.

REFERENCES

[1]   Rácz, Á., Bohács, K., Kristály, F., Gregus, É., Mucsi, G. (2018). Comparison of wet and dry stirred media milling from energetic and mechanochemical point of view. *IMPC 2018 – 29th International Mineral Processing Congress,* pp. 454–463.

[2]   Rácz, Á., Tamás, L., Gombkötő, I., Csőke, B., Faitli. J. (2017). Effect of the milling parameters on the product dispersity and energy consumption in a continuous dry air-transported stirred media mill. *Proceedings of the 15th European Symposium on Comminution and classification.*

[3]   Rácz, Á., Tamás, L. (2018).: Optimization of the air flow rate in a laboratory scale horizontal continuous dry stirred media mill. *Proceedings of the 9th International Symposium on Fine Grinding and Dispersing*, pp. 26–27.

[4]   Mucsi, G., Kumar, S., Csőke, B., Kumar, R., Molnár, Z., Rácz, Á., Mádai, F., Debreczeni, Á. =(2015). Control of geopolymer properties by grinding of land filled fly ash. *International Journal of Mineral Processing,* 143, pp. 50–58.

[5]   Kumar, S., Mucsi, G., Kristály, F., Pekker, P. (2017). Mechanical activation of fly ash and its influence on micro and nano-structural behavior of resulting geopolymers. *Advanced Powder Technology,* 28 (3), pp. 805–813.

[6]   Szabó, R., Gombkötő, I., Svéda, M., Mucsi, G. (2017). Effect of grinding fineness of fly ash on the properties of geopolymer foam. *Archives of Metallurgy and Materials,* 62 (2B), pp. 1257–1261.

[7]   Mucsi, G., Csöke. B. (2012). Power plant fly ash as valuable raw material. *Geosciences and Engineering,* 1, pp. 223–236.

[8]   Davidovits, J. (1989). Geopolymers and Geopolymeric Materials. *Journal of Thermal Analysis and Calorimetry,* 35 (2), pp. 429–441.

[9]   Mucsi, G., Szabó, R., Rácz, Á., Kristály, F., Kumar, S. (2019). Combined utilization of red mud and mechanically activated fly ash in geopolymers. *Rudarsko-Geolosko-Naftni Zbornik,* 34 (1), pp. 27–36.

[10]   Ambrus, M., Szabó, R., Csőke, B., Mucsi G. (2019). Tailoring the Mechanical Properties of Landfilled Fly Ash Geopolymers by Grinding. In: McCarthy, M. J. et al. (eds.). *Proceedings of the EuroCoalAsh 2019*, 10–12 June 2019, Dundee, Scotland, pp. 346–355.

[11]   Ascensão, G., Seabra, M. P., Aguiar, J. B., Labrincha, J. A. (2017). Red mud-based geopolymers with tailored alkali diffusion properties and pH buffering ability. *Journal of Cleaner Production,* 148, pp. 23–30.

[12]   Nie, Q., Hu, W., Huang, B., Shu, X., He, Q. (2019). Synergistic utilization of red mud for flue-gas desulfurization and fly ash-based geopolymer preparation. *Journal of Hazardous Materials,* 369, pp. 503–511.

[13]   Zhang, Z., Yao X., Zhu H., Hua S., Chen Y. (2009). Preparation and mechanical properties of polypropylene fiber reinforced calcined kaolin-fly ash based geopolymer. *Journal of Central South University,* 16, pp. 49–52.

[14]   Sakulich, A. R. (2011). Reinforced Geopolymer Composites for Enhanced Material Greenness and Durability. *Sustainable Cities and Society,* 1 (4), pp. 195–210.

[15]   Ambrus, M. Papné Halyag, N., Czupy, I., Szalay, D., Mucsi, G. (2019). Macro- and Microstructural Analysis of Biomass-fibre Reinforced fly ash Geopolymer. *II. Sustainable Raw Materials. International Project Week and Scientific Conference*, Szeged, Hungary, May 6–9, 2019.

[16]   Abdollahnejad, Z., Pacheco-Torgal, F., Félix, T., W. Tahri, W., Aguiar, J. B. (2015). Mix design, properties and cost analysis of fly ash-based geopolymer foam. *Construction and Building Materials,* 80, pp. 18–30.

[17]   Hlaváček, P., Šmilauer, V., Škvára, F., Kopecký, L., Šulc, R. (2015). Inorganic foams made from alkali-activated fly ash: Mechanical, chemical and physical properties. *Journal of the European Ceramic Society,* 35 (2), pp. 703–709.

[18]   Sanjayan, J. G., Nazari, A., Chen, L., Nguyen, G. H. (2015). Physical and mechanical properties of lightweight aerated geopolymer. *Construction and Building Materials,* 79, pp. 236–244.

[19]   Favier, A., Habert, G., d'Espinose de Lacaillerie, J. B., Roussel, N. (2013). Mechanical properties and compositional heterogeneities of fresh geopolymer pastes. *Cement and Concrete Research,* 48, pp. 9–16.

[20] Papa, E., Medri, V., Benito, P., et al. (2016). Insights into the macroporosity of freeze-cast hierarchical geopolymers. *Royal Society of Chemistry Advances,* 6 (29), pp. 24635–24644.

[21] Franchin, G., Scanferla, P., Zeffiro, L., et al. (2017). Direct ink writing of geopolymeric inks. *Journal of the European Ceramic Society,* 37 (6), pp. 2481–2489.

[22] Bai, C., Colombo, P. (2018). Processing, properties and applications of highly porous geopolymers: A review. *Ceramics International,* 44, pp. 16103–16118.

[23] Szabó R., Mucsi G. (2017). Lignittípusú, pernyealapú geopolimer habok előállítása és tulajdonságai. *Műszaki Földtudományi Közlemények,* 86 (1),pp. 30–39.

[24] Nematollahi, B. Sanjayan, J. (2014). Effect of different superplasticizers and activator combinations on workability and strength of fly ash based geopolymer. *Materials and Design,* 57, pp. 667–672.

[25] Szabó, R., Mucsi, G. (2019). Effect of fineness of lignite fly ash on the properties of geopolymer foam. In: Czupy Imre (ed.). *III. RING – Fenntartható Nyersanyag Gazdálkodás – III. Sustainable Raw Materials Konferenciakötet – Proceedings.* Sopron, Magyarország, Soproni Egyetem Kiadó, pp. 92–100.

[26] Grazulis, S., Chateigner, D., Downs, R. T., Yokochi, A. T., Quiros, M., Lutterotti, L., Manakova, E., Butkus, J., Moeck, P., Le Bail, A. (2019). Crystallography Open Database – an open-access collection of crystal structures. *Journal of Applied Crystallography,* 42, pp. 726–729.

[27] Downs, R. T., Hall-Wallace, M. (2003). The American Mineralogist Crystal Structure Database. *American Mineralogist,* 88, pp. 247–250.

[28] Chukanov, N. V., Pekov, I. V., Olysych, L. V., Zubkova, N. V., Vigasina, M. F. (2011). Crystal chemistry of cancrinite-group minerals with an AB-type framework: a review and new data. II. IR spectroscopy and its crystal-chemical implications. *The Canadian Mineralogist,* 49 (5), pp. 1151–1164.

[29] Sun, C., Chen, J., Tian, K., Peng, D., Liao, X., Wu, X. (2019). Geochemical Characteristics and Toxic Elements in Alumina Refining Wastes and Leachates from Management Facilities. *International Journal of Environmental Research and Public Health,* 16, p. 1297.

[30] Ye, N., Yang, J., Ke, X., Zhu, J., Li, Y., Xiang, C., Wang, H., Li, L., Xiao, B. (2014). Synthesis and Characterization of Geopolymer from Bayer Red Mud with Thermal Pretreatment. *Journal of the American Ceramic Society,* 97, pp. 1652–1660.

[31] Bolanz, R. M., Kiefer, S., Göttlicher, J.; Steininger, R. (2018). Hematite (-Fe$_2$O$_3$) — A potential Ce^{4+} carrier in red mud. *Science of the Total Environment,* 622–623, pp. 849–860.

[32] Géber, R., Kocserha. I. (2018). Current research trends in foamed construction and building materials: A review. *Materials Science and Engineering,* 43 (1), pp. 42–53.

[33] Udvardi B., Géber R. (2019). Aktualitások az útépítésben hasznosítható másodlagos nyersanyagok területén. *Útügyi Lapok,* 7 (12), pp. 33–41.

[34] Géber, R., Szabó, R., Kocserha, I. (2019). Preparation of geopolymer foams using autoclave curing. *Materials Science and Engineering,* 44 (2), pp. 13–22.

[35] Udvardi, B. Román, K., Kurovics, E., Géber, R., Kocserha, I. (2019). Preparation and investigation of geopolymers generated from construction, demolition and industrial wastes. *WIT Transactions on Engineering Sciences,* 124, pp. 49–59.

[36] Udvardi, B., Géber, R. Kocserha, I. (2019). Examination of different waste materials for road construction. *Preparation of ceramic materials, Proceedings of the XIIIth International Conference,* pp. 17–24.

[37] Udvardi, B., Géber, R., Kocserha, I. (2019). Examination of the utilization of aluminum dross in road construction. *IOP Conf. Series: Materials Science and Engineering,* 613, p. 012053.

[38] Csák Cs., Marinkás, Gy. (2019). The legal categorization of Fly ASH in EU and the Hungarian law – analysis of related CJEU case-law. *Journal of Geoscience and Engineering,* (forthcoming); the same in Hungarian: Csák, Cs. and Marinkás, Gy. A pernye jogi besorolása az Európai Uniós és a magyar jog alapján. – A kapcsolódó EuB joggyakorlat elemzése. Jog, Állam, Politika IX/4, pp. 125–138.

[39] Csák Cs., Marinkás Gy. (2019). A KKE országok hulladékgazdálkodási szabályozása és azok konformitása az uniós joggal – Az EuB vonatkozó joggyakorlatának elemzése. *Miskolci Jogi Szemle,* XIV/1, (2), pp. 5–18.

[40] Csák Cs. (2014). Hulladék vagy melléktermék? – avagy a mezőgazdasági maradványanyagok jogi megítélése. *Őstermelő: Gazdálkodók Lapja Plusz,* 2, pp. 14–16.

[41] Csák Cs. (20111). A hulladék fogalmának értelmezése az uniós ítélkezési gyakorlat alapján. *Sectio Juridica et Politica,* Miskolc, Tomus XXIX/2, pp. 423–434.

[42]   Molnár, J., Debreczeni, Á., Tompa, R. (2018). Challenges and Opportunities of Underground Coal Mining in Northeastern Hungary. In: Proc. Universitaria SIMPRO 2018, *8th International Multidisciplinary Scientific Symposium,* 11–13 October 2018, Petrosani (Romania), pp. 347–352. ISSN L 1842-4449. URL: https://www.upet.ro/simpro/2018/downloads/Proceedings%20SIMPRO%202018.pdf. Downloaded: 10. 12. 2018.

[43]   Debreczeni, Á., Molnár J., Tompa R. (2019). Opportunities of Re-Establishing Underground Mining in the Borsod Coal Basin in North-Eastern Hungary. In: Kotwica, Krzysztof (ed.). *New trends in production engineering*. Monograph, Part 2, Sciendo, Warszawa, pp. 179–187.

EVALUATION OF CRM POTENTIAL IN FLY ASH OF HUNGARIAN COAL POWER PLANTS

FERENC MÓRICZ[1] – FERENC MÁDAI[2] – JÁNOS FÖLDESSY[3] –
GÁBOR MUCSI[4] – IMRE GOMBKÖTŐ[5]

[1, 2, 3] *Institute of Mineralogy and Geology, University of Miskolc*
[4] *Institute of Raw Material Preparation and Environmental Processing,
University of Miskolc*
[5] *EIT RawMaterial – CLC East*

1. INTRODUCTION

In 2010, the Raw Materials Supply Group defined 14 types of raw material qualified as critical to the resource supply for the European economy by 2030. This list of critical raw materials (CRM) was revised first in 2014 and then 2017 again and the number of raw materials designated to be critical to the EU economy were elevated to 20, then 27. Hungary – like most EU Member States – is a net importer of most of the critical raw materials, it has a significant dependence on distant sources. Despite this fact the country is significantly behind in the research of energy and other mineral sources and with the development of exploitation and technologies of production (National energy strategy 2011; Mineral resource utilization and reserve management action plan 2013, amended for energy minerals in 2018).

As the most important secondary resource, samples of coal fly ash (CFA) from storage facilities were evaluated for their potential for providing rare elements as well as for their utilization as added-value construction materials (Blengini et al. 2019).

2. BACKGROUND

The objective of the overall study was to identify the potential for critical raw materials (CRM) in Hungary both from primary and secondary sources using archive data mining and exploration methods, investigating not only the occurrence and amount but in parallel determining applicable processing and recovery methods for the identified sources, promoting its business availability as well.

Most of the archive research reports were written before the digital age, thus archivation and digitalization of the materials was also necessary. Approximately 150 different geological reports were identified to contain meaningful assay data of the CRMs. These were widely different in the time of sampling, the assay methods, the sensitivity of assays, etc. None of this information was detailed and reliable enough to make quantitative estimates (Less 2012, 2013).

The diverse origin and the usually undocumented material properties (of mine wastes, among others) did not make this systematic approach fully applicable in the case of potential secondary raw materials. Instead, some important, high volume types were selected (coal-based fly ash, fluorite flotation tailing, e-waste, quartz-sand processing waste), and the survey focused on these materials (Blengini et al. 2019).

The waste materials of fly ash of thermal power plants were fully mapped. Apart from discussing the material properties, several possible applications and uses – like concrete additive, asphalt component, geopolymers, and minor element source – have been discussed and tested. A monograph contains the results of the investigations (Mucsi 2014), introducing a complex approach to utilization of this landfill waste. It gives an overview of Hungarian coal fuel materials from different coal basins, the results of geochemical research on selected CFA storage materials, and a literature review of recovery technologies of rare elements from CFA, as well as giving the theoretical background and experimental results on the utilization of the bulk material as geopolymers or other value-added construction materials.

The laboratories used were the geochemical laboratory of the MFGI (Hungarian Geological and Geophysical Institute), and the ALS Global. The data evaluation was published in a REE monograph (Szakáll 2014) and a summary volume (Földessy 2014).

The Hungarian Mining and Geological Survey in 2018 completed a detailed assessment of the CRM potential of different Hungarian coal basins and formations. (Püspöki 2018)

3. LOCATIONS OF HUNGARIAN COAL BASINS AND COAL POWER PLANTS

Coal combustion power plants (CCPPs) were the predominant facilities of electric power generation for Hungary until 1982, when the Paks nuclear plant came into operation. Most of the thermal plants were run on sub-bituminous coal of Eocene-Miocene age, one (Visonta) on Late-Miocene lignite and one (Pécs) on the Jurassic bituminous coal of the East Mecsek Mts. From the 1980s, most of the coal-based PPs were refit to run on combined fuel sources – coal plus oil and/or gas, or biomass – and later some of them were totally converted to oil, gas or biomass fuel. *Table 1* summarizes the relevant CCPPs, the accompanying fly ash storage, fly ash waste volumes, their current status as extractive waste facilities (Blengini et al. 2019).

The only active fly ash tailings facility is located at the Mátra power plant (near Visonta); others are under closure and many of them has been completely restored. Active and still not restored tailings facilities have little environmental impact, while containing enriched concentration of some rare elements, among them many CRMs as well. Elevated concentration of radioactive elements is known only from the Pécs fly ash storage facility, where from the bulk samples Th concentration reached 40–48 ppm and U concentration 16–20 ppm (Blengini et al. 2019).
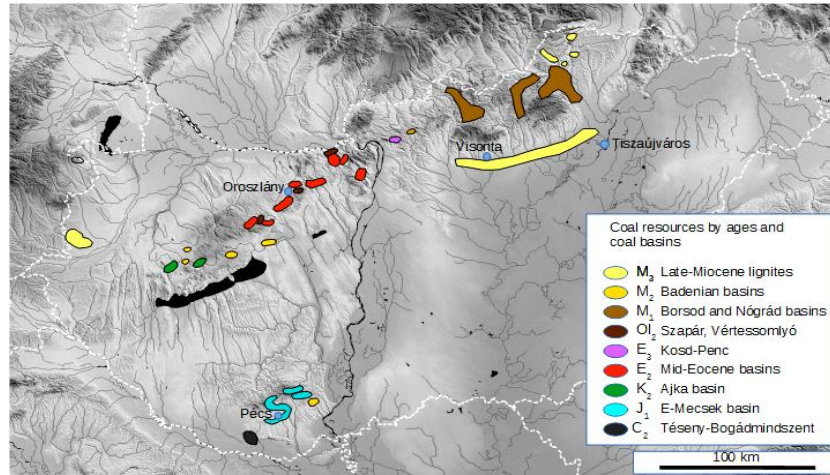
Figure 1
Coal basins of Hungary and the location of the four power plants and
CFA storage facilities referred to in this study (Püspöki 2018)

Table 1
Technical data on Hungarian CCPPs operating in the last 50 years and
associated fly ash storage (Gáspár 2005)

CCPP	current status	area of the tailings facility [ha]*	volume of the tailings facility [Mm³]*	fuel material used	current tailings facility status
Ajka	active	88	20.7	bituminous coal, biomass	partly closed/ active
Berente	closed	15	19.1	sub-bituminous coal, biomass	restored
Várpalota (Inota)	closed	180	27	sub-bituminous coal	restored
Visonta	active	51	7.6	lignite (until 2008), later lignite + biomass	active
Oroszlány (Vértes PP)	closed	105	21	sub-bituminous coal, biomass	under closure
Pécs	active	233.3	39.2	bituminous coal (until 2004), later gas, later biomass	closed, under restoration
Komló	active	4	1.1	sub-bituminous coal, later gas + biomass	restored
Tatabánya (Bánhida)	closed	25	4.6	sub-bituminous coal	under restoration
Dorog	active	25	1.2	sub-bituminous coal. later gas + biomass/coal	restored
Tatabánya	active	27	28	sub-bituminous coal, gas, biomass	restored
Tiszapalkonya	closed	255	14.1	sub-bituminous coal, later oil and gas	restored
In total*		**1,009.5**	**184.2**		

(*after Gáspár, 2005)

As a consequence of the Ajka red mud accident in 2010, all tailings management facilities in Hungary are under strict and regular inspection. An extraordinary inspection completed in October 2010 just after the Ajka accident by the Environmental, Nature Conservation and Water Inspectorate concluded that there is no geotechnical risk connected to active or not restored TMFs. Fly ash storage facilities were also assessed during this inspection. As can be seen from Table 1, total area of the CFA comprises more than 1000 ha which is not utilized. However, the most important environmental driver and social benefit of the CFA utilization is the substitution of primary resources in different construction material producing technologies. (Blengini et al. 2019)

4. ECONOMIC POTENTIAL

Complex utilization of CFA is an actual issue globally. Despite the well-known fact that CFA is enriched in several rare elements, its recovery can be economic and/or socially acceptable only if the bulk material also finds some way of utilization. Rare element content can be recovered only as by-products if the cost of the rather complex treatment is covered (Blengini et al. 2019).

The bulk of the CFA is used as pozzolanic material for the cement industry, while another emerging mode is the utilization of its main volume as geopolymer composites that can directly be used for construction industry as heat or sound insulating panels, pavement panels etc. (Csőke et al. 2007; Mucsi et al. 2015; Mucsi et al. 2017). There is still high potential in coal combustion by-product utilization: 80% of the global utilization comes from three countries: China (335 Mt/year), USA (118 Mt/year), India (105 Mt/year) (Mucsi & Csőke 2014). The highest rate of utilization is reached in Japan (96.4%), while the lowest rates are in Africa and in the Middle-East (10.5%). Just over 50% of US coal fly ash is beneficially reused (Kolker et al. 2017; Blengini et al. 2019).

Utilization of CFA as the bulk component for geopolymers is based on its high aluminum-silicate content. Compared to utilization of the CFA as a pozzolanic material in the cement industry, an important benefit is that the geopolymerization process takes place at much lower temperatures and CO_2 release is only 10–20% that of cement production (Davidovits 2011). Due to the flexible production technology, geopolymer-based final products are found as bricks and insulation panels (fire, heat and sound), pavement blocks, water insulation layers, and roofing composites (Xia & Sanjayan 2016).

Recovery of rare elements from CFA is also a hot topic today. While technologies for recovery of some rare elements as Ge and/or Ga are known even on the commercial scale (e.g. Jandova et al. 2002), in-depth research on recovery of REE from CFA began in last years. Articles on REE recovery tend to be published mainly by researchers in the USA and Japan (Blengini et al. 2019).

Articles on REE recovery typically discuss laboratory-scale dissolution experiments. The reason why recovery technologies for REE are far behind compared to other elements is the diversity of solubility of different rare elements: Ga and Ge

are easily soluble, while REE are much less soluble and occur mostly in the amorphous phase. REEs are dissolved primarily in the amorphous alumina-silicate glass phase which forms during high-temperature combustion. Ca- and Fe-bearing Al-silicates are comparatively enriched in REE, presumably due to the similarity in ionic radii between Ca^{2+} and LREE, and between Fe^{2+} and HREE ions (Kolker et al. 2017).

According to Kashiwakura et al. (2013), REEs are fixed in the CFA by two processes: by vaporization surface-deposition and by dissolution/accompaniment in silicate-rich CFA particles (SiO_2, mullite, amorphous) when they melt. REEs in the coal occur primarily as minor elements in mineral phases such as monazite, allanite, zircon, xenotime, etc. and subsidiary – especially HREEs – as absorbed on organic matter.

During combustion, transition of REEs from the original mineral phases can go to newly-formed CFA phases in two ways (Kolker et al. 2017):
  – melting/breakdown of original phases with partitioning the REE into the melt,
  – size reduction by thermal shock shuttering of the REE-bearing phases to nano-particles and diffusion into the glass phase.

Partitioning and speciation of REEs depend on combustion technologies. In high-temperature combustion (1,500–1,700 °C), waste material melts and REEs dissolve in the silicate glass. In dry combustion (1,100–1,400 °C) similar melting may take place, while in fluidized bed combustion (900 °C) melting does not takes place, thus REEs remain in the original mineral phases.

Detailed textural investigation of CFA with the SHRIMP-RG ion microprobe method revealed that REE partitioning into the glass phase shows uniformity, therefore the main distribution mechanism is not the persistence of trace element-bearing phases with thermal shock shuttering, but the high-temperature vaporization and dissolution of REEs (Kolker et al. 2017). These fine textural investigations are important in order to find out the effective recovery method of REEs from CFAs. Nitric acidic extraction experiments did not result in high fraction REE recovery, which shows that more aggressive methods are needed to introduce commercial-scale REE recovery from CFA (Kolker et al. 2017). Possible ways may be HF or Na-peroxide treatment to destroy the Al-silicate glass before acidic digestion; however, neither of them is likely to be viable on a commercial scale.

5. CHARACTERIZATION OF THE MATERIAL FROM CCPP

Bulk samples were collected from 4 CCPP sites: from the Vértes (Oroszlány), Tiszapalkonya and Pécs PP fly ash storage facilities and two fresh fly ash samples from the Visonta PP. These samples were analyzed for physical-technical and chemical characteristics. Data of both major and rare elements are available from the bulk samples.

5.1. Physical and technical characterization

For further utilization the most important parameters of the fly ash materials from the 4 sites are summarized in *Table 2*. As the main parameters, the table presents the ash content of the coal, the average grain and bulk density of the ash, the BET and Blaine specific surface, and the HCl insoluble residual rate.

Averaged particle size distribution analysis was also done on all of the four investigated fly ash samples. The graph *(Figure 2)* clearly shows that the CFA from the Pécs storage facility has the highest share of fine particles, resulting also in the highest specific surface values *(Table 2)*.

Table 2

Physical and technical properties of the investigated CFA samples
(Kovács 2001; Mucsi & Csőke 2014; Gáspár 2005)

	Vértes PP Oroszlány (CFA storage)	**Pécs (CFA storage)**	**Visonta (fresh CFA)**	**Tiszapalkonya CFA storage**
Average ash content of the coal fuel used (%)	40	55–60	15–25	40–43
Average grain density of CFA (cm^3/g)	2.22	2.08	1.93	1.59
Compacted bulk density (cm^3/g)	0.95	1.08	0.72	0.86
BET specific surface (cm^2/g)	19,000–29,000	35,000–60,000	30,000–40,000	25,000–30,000
Blaine specific surface (cm^2/g)	2,800–4,410	4,050–4,100	3,600–7,800	3,000–3,400
Residue not dissolvable in cold HCl (%)	70.2–73.5	80.0–85.4	64.0–67.6	NA
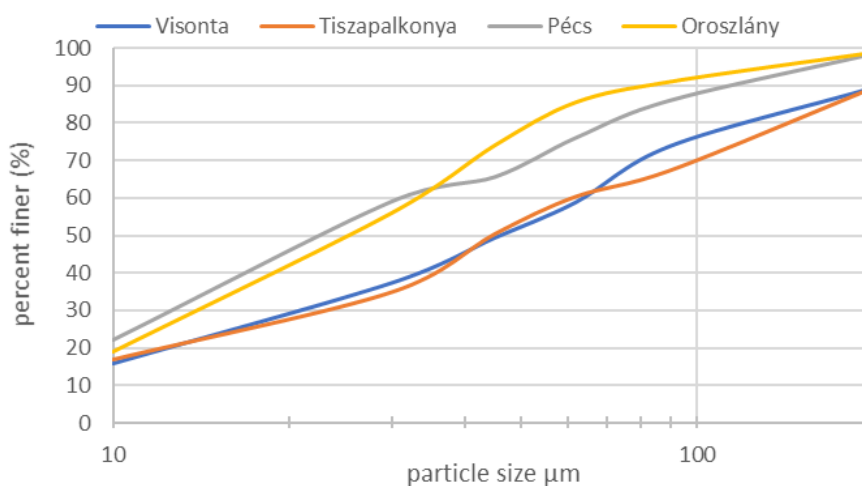
Figure 2
Averaged particle size distribution of the four analyzed CFA samples
(Lachner et al. 2002)

5.2. Chemical characterization

Data on major and rare elements are available for types of CCPP fly . The main element chemistry of the samples *(Table 3)* shows a pozzolanic type of fly ash material. Fresh CFA from Visonta (lignite) shows a relative abundance of CaO, while the Pécs and Tiszapalkonya fly ashes are depleted in CaO (Mucsi et al. 2015).

Table 3

Major element composition of the investigated Hungarian CFAs (Mucsi 2014)

Sample / element	SiO_2	Al_2O_3	TiO_2	Fe_2O_3	MnO	MgO	CaO	Na_2O	K_2O	LOI	SO_3
Vértes (CFA storage)	42.8	23.1	0.83	7.57	0.03	1.30	6.37	0.57	1.05	8.43	2.92
Pécs (CFA storage)	53.6	20.3	0.98	8.67	0.18	1.35	2.17	<0.03	3.09	3.91	<0.15
Visonta-1 (fresh CFA)	43.1	15.2	0.50	12.7	0.17	3.02	13.4	0.45	1.21	2.26	4.39
Visonta-2 (fresh CFA)	44.4	15.2	0.52	12.2	0.18	3.13	12.8	0.54	1.31	2.17	3.50
Tiszapalkonya (CFA, d<63 μm)	57.0	23.9	0.47	4.26	0.02	0.85	1.40	1.05	1.22	1.84	<0.15
Tiszapalkonya (CFA, d = 63 – 106 μm)	62.7	25.2	0.54	4.94	0.02	0.96	1.68	1.06	1.54	0.96	<0.15
Tiszapalkonya (CFA, bulk sample)	61.9	26.3	0.48	4.26	0.02	0.90	1.53	0.99	1.42	1.80	<0.15

From the aspect of chemical properties one of the most important parameters of the fly ash samples is the SiO_2-Al_2O_3-CaO concentration. *Figure 3* shows the place of the 4 investigated samples on the triangular diagram of the three most important main elements.
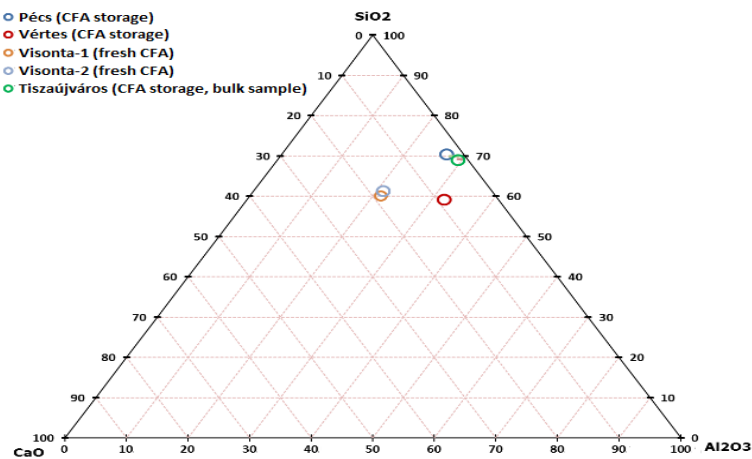
Figure 3

Triangular diagram of the fly ash samples as a function of SiO_2-Al_2O_3-CaO concentration

In addition to the main element concentration – which is important from point of for geopolymerization – the trace element concentration is an essential data, especially the rare elements and the CRMs. Rare element contents of the CFA samples are summarized in Table 4, obtained from the CriticEl database.

Abundancy of some rare elements relative to the CFA global average values (Ketris & Yudovich 2009) was found only for the samples from the Pécs CFA storage. Results show here the increased abundance of REE (especially La and Ce), Zr (3.5X), Nb (7.3X), Ta (5.5X) and Co (6.1X). Total REE content form the Pécs samples is found as 891 ppm, which is 2.5 times higher compared to the global CFA average. Rare element concentrations of the sample from the Vértes CFA storage reaches or very slightly overrides the global average values in case of Sc, V, Co, Y, La, Ce, Er and U. Rare element values from the Visonta CFA samples in general represent 0.4-0.6 times the global CFA average, while the Tiszapalkonya sample for lighter rare elements (Sc, V, Co) reaches the half of the global average, but for other rare elements it is far below (10–20 times) of that. In Tiszapalkonya the fuel used was a mixture of different brown coals from NE-Hungary and biomass since 2002 what may be the reason of the very low rare element concentrations. (Blengini et al. 2019)

Table 4

*Rare and rare-earth element composition
of the investigated Hungarian CFAs* (Mucsi 2014)

rare elements (ppm)	Vértes (CFA, bulk sample)	Pécs (CFA, bulk sample)	Visonta–1	Visonta–2	Tiszapalkonya (CFA storage)		
			(fresh CFA, bulk sample)		(d<63 μm)	(d = 63–106 μm)	(bulk sample)
Be	5.53	12.90	4.16	3.80	4.40	0.42	0.43
Sc	29.40	9.17	9.50	16.60	12.90	11.60	11.60
V	242.0	124.0	118.0	123.0	66.70	79.00	58.50
Co	34.00	195.00	21.00	8.67	79.20	27.50	20.20
Ga	22.30	30.40	18.10	17.10	16.30	1.85	1.23
Ge	1.00	1.74	0.68	0.66	0.79	<0,25	<0,25
Y	55.40	69.60	26.80	25.50	27.90	2.91	2.61
Zr	137.0	743.0	102.0	105.0	150.0	17.60	13.80
Nb	14.10	146.00	10.80	11.00	21.80	2.41	1.87
Σ REE	357.76	891.04	148.59	144.81	323.31	19.36	18.56
Ta	1.22	9.58	0.95	1.00	2.01	<0,25	<0,25
Th	19.90	41.50	14.40	13.30	28.40	2.95	2.93
U	17.90	16.80	7.46	6.77	7.74	0.83	0.76

It should be noted that an increased germanium concentration of the Mecsek bituminous coal (fuel for the Pécs PP) was detected in the 1960s (Csalagovits & Víghné 1969). According to this source, the average Ge-content in coal ash samples from different mines of the Mecsek coal basin varied from 11 ppm (Pécsbányatelep, southern limb) to 72 ppm (Komló) and 82 ppm (Szászvár, northern

limb). Conversely, only 1.74 ppm germanium was measured from the Pécs PP's CFA storage samples, which is at least an order of magnitude less than the previously mentioned results. According to Ketris & Yudovich (2009), the coal ash global average concentration of Ge is 15 ppm, which is in the same order of magnitude as that reported by Csalagovits & Víghné (1969) from the Mecsek coal ashes.

It has been concluded that the results obtained by Li-metaborate digestion and ICP-MS method, but in case of germanium were systematically undermeasured, beacause its volatile behaviour on high temperature. This was proved on four coal samples from the Mecsek Mts. by repeated analysis carried out by the IDAEA laboratory (Spain) using a low temperature sequential extraction method of digestion. Applying the low temperature digestion, the obtained Ge-concentrations were 4–10 times over that of the results obtained by the Li-metaborate digestion. The same range of Ge-content was also proved from samples from the Pécs-Vasas quarry, completed within the frame of the recent reambulation project (Püspöki, 2018). The Germanium data in *Table 4* should be considered as strongly undermeasured due to inappropriate digestion. Measurements on CFA samples should also be repeated using the low-temperature digestion.

Rare earth element concentrations are slightly promising only for Pécs PP's CFA and only for Low REEs (La, Ce, Pr, Nd, Sm), overriding the global CFA average at least two times *(Figure 4)*. Reliability of the REE data is proved by the distribution of these elements, as it follows the Oddo-Harkins rule *(Figure 5)*.
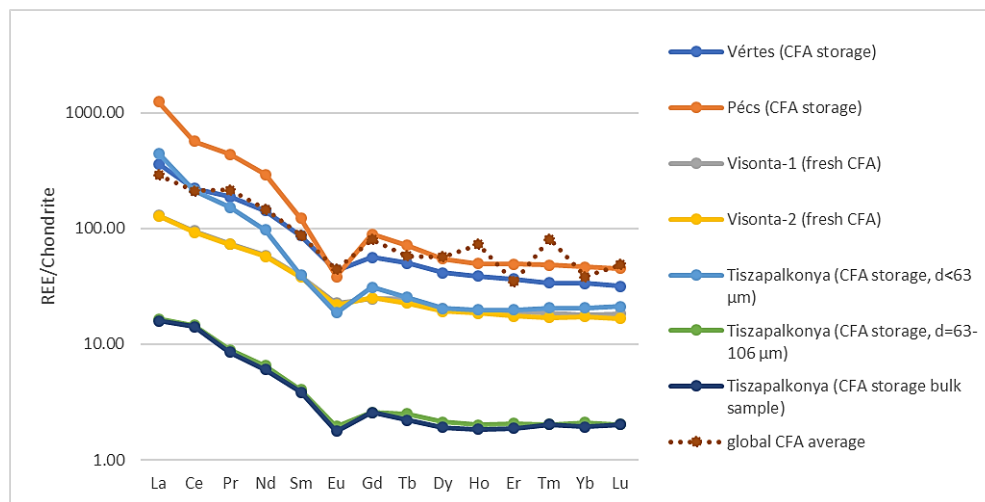
Figure 4
REE concentrations normalized to the C1 chondrite
from the analyzed CFA samples
(Source: CriticEl database)
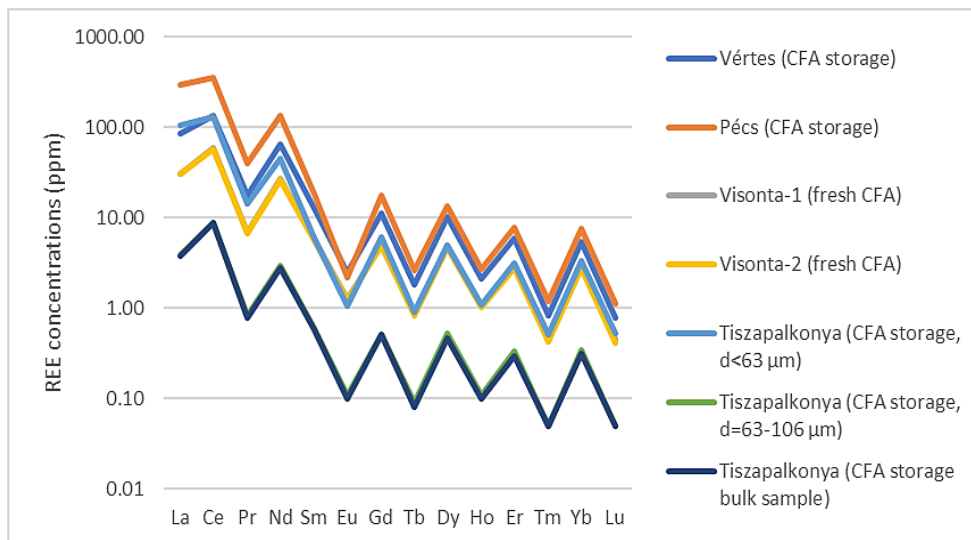
Figure 5
*Distribution of REE concentrations in order of their atomic number
from the analysed sample* (Source: CriticEl database)

Data from three fractions of the Tiszapalkonya CFA shows a strong increase in rare elements in the fine fractions compared to the coarse fractions and the bulk sample *(Table 4)*. REE concentrations of the fine fraction (d<63 μm) are 10–30 times higher than those of the coarser (63–106 μm) fraction. This remarkable difference is connected to different formation temperatures: the fine fraction forms at high temperatures (over 1100 °C) where the melt silicate material adsorbs the rare element by surface deposition of vaporized elements or dissolves tiny rare element-rich particles. This phenomena has been observed for several fly ash materials (Kolker et al. 2017; Blengini et al. 2019)

New data from the Mecsek coals obtained by the coal reassessment project (Püspöki 2018) have confirmed the old data (Csalagovits & Víghné 1969) on elevated concentrations of germanium and also the results obtained by the CriticEl project on Nb, Ta, Zr, Co and REEs. These new data also support the importance of further detailed assessment of the Pécs PP CFA storage facility.

Research on physical and chemical properties of the Pécs PP' CFA has shown that it can be used as a geopolymer raw material (Mucsi & Csőke 2014). According to Davidovits (2011), geopolymerization of CFA can be reached also by acidic dissolution, therefore complex utilization of the fly ash – extraction of rare elements and subsequent utilization of the bulk material – can be achieved. On the other hand, as was shown by a recent project supported by the US Department of Energy (Carlson 2017), 0.1 kg Na-P1 type zeolite can be produced per kg of CFA from the residual material left after efficient REE extraction.

6. LIMITATIONS FOR THE RECOVERY OF CRITICAL AND OTHER RAW MATERIALS

Although resources are available at Hungary, the recovery possibilities of them are limited. These difficulties are mostly legislative and economic in corresponding the structure and diversity of the industry exist in Hungary.

Currently there is no metal production from primary mineral resources at all in Hungary – not counting the limited steel production in Dunaújváros – which means that the upstream part of the primary raw material value chain is technically missing in Hungary. There are no active, large scale exploration projects and potential investors are even discouraged by the overly bureaucratic legislation and tender policy, in combination with conflicting land use priorities. That means new exploration projects are hard to initiate even if the funds were available and there are no existing incentives in place to support these actions. This is despite the fact that data supporting such investment decisions for large scale exploration projects are available. The missing non-ferrous metal smelters resulting in high metal content waste are processed to some extent but utilized in other EU countries, where copper, aluminum lead or zinc smelters are operating. The amount of these waste streams collected in Hungary alone is not able to financially sustain the investment and operation of a non-ferrous smelter plant. Unfortunately, even if there would be a sufficient amount of metallic wastes, the recovery of most of the existing metals in these waste streams would require an expensive and complex combined, mechanical and metallurgical process that would bring the financial feasibility into question anyway. Further complicating the waste scene is the fact that the ownership of different waste streams and stocks (tailings and waste rock) is sometimes complex and also doubtful in some cases. (Blengini et al. 2019):
- coal mining was shut down 18–20 years ago;
- old fly ash dumps, closed, partly restored;
- combined combustion of different fuels: coal, biomass: heterogeneity of the waste material, varying composition in different layers.

7. RECOMMENDATIONS FOR FURTHER DEPLOYMENT

Based on the available geochemical data, storage volume and bulk density, the potential resources for rare elements in the Pécs and Vértes CFA storage facilities comprise a few dozen metric tons to thousands of metric tons *(Figure 6)*. CFA of the Pécs PP storage exceeds the world CFA average values for Co (6X), Zr (3.5X), Nb (7.3X), Ta (5.6X) and LREE (2 – 4.6 X).

These data and results contributed to fill in some gaps in the data and improved the knowledge base that is necessary to find out a comprehensive utilization scheme for CFA storage materials, such as those generated at the Pécs and Vértes PPs. This experience can be improved and replicated on a larger scale (Blengini et al. 2019).
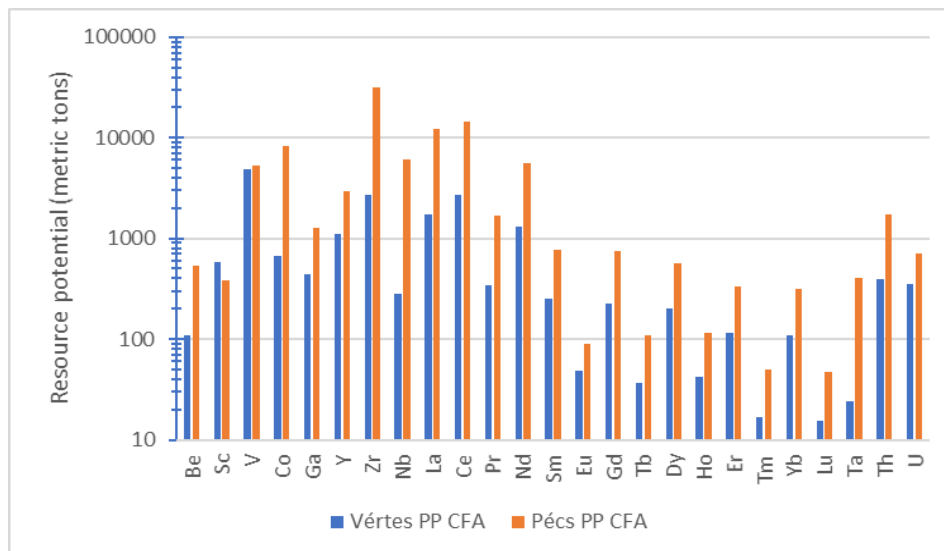
Figure 6
Estimated resource potential of rare elements
from Vértes and Pécs PP's CFA storage

Further research is recommended in order to find out a complex utilization scheme for the Pécs PP's CFA storage material, focusing on the following issues:

I. Systematic sampling in full profile to check whether vertical migration of rare elements has taken place within the facility after the deposition.

II. Systematic sampling in order to characterize the lateral and vertical heterogeneity of the CFA material. As in many other Hungarian landfill or mine waste facilities, it may be the case that materials from other waste streams had been also deposited at this site.

III. Detailed research is recommended for speciation of CRMs of fly ashes, using state- of-the-art analytical methods (e.g. FIB-SEM, computer tomography) in order to support the appropriate recovery technologies.

IV. Development of the appropriate recovery technology based on the latest research results (mechanical activation, selective leaching, combined grind-leaching process, etc.).

V. Investigation of synergetic utilization of FA with other silicate or alumino-silicate waste streams in order to improve geopolymer properties by developing composite materials (i.e. fiber-reinforced geopolymer).

VI. Economic feasibility of the CRM recovery may only be realistic if the bulk material is also utilized. Therefore R&D is necessary to obtain value-added products from the residue: synthetic zeolites and/or utilization of this as geopolymer construction blocks. The latter one was an important topic within the frame of the CriticEl project.

REFERENCES

[1]   Blengini, G. A., Mathieux, F., Mancini, L., Nyberg, M., Viegas, H. M. (eds.) (2019). *JRC Science of Policy Report – Recovery of critical and other raw materials from mining waste and landfills*. https://publications.jrc.ec.europa. eu/repository/bitstream/JRC116131/aaa_20190506-d3-jrc-science-for-policy -recovery_of_rm_from_mining_waste_and_landfills_4_07_19_online_final.pdf.

[2]   Carlson, G. (2017). *Economical and Environmentally Benign Extraction of Rare Earth Elements from Coal & Coal Byproducts*. https://www.netl.doe. gov/File%20Library/Events/2017/crosscutting/20170322-Track-C/20170322 _1330C_Presentation_FE0027155_Tusaar.pdf.

[3]   Csalagovits, I., Víghné, F. M. (1969). Trace elements of the waste rocks and coal. (in Hungarian) *Ann. Inst. Geol. Publ. Hung.,* 51, pp. 518–574.

[4]   Csőke, B., Mucsi, G., Opoczky, L., Gável, V. (2007). Modifying the hydraulic activity of power station fly ash by grinding. *Cement International,* 5 (6), pp. 86–93.

[5]   Davidovits, J. (2011). *Geopolymer chemistry and application*. Institut Geopolimére, Saint-Quentin France, pp. 283–286.

[6]   Földessy, J. (ed.) (2014). *Basic research of the strategic raw materials in Hungary*. CriticEl monograph series No. 10, Miskolc, Milagrossa Kft.

[7]   Gáspár, L. (ed.) (2005). Secondary raw materials for road construction. (in Hungarian) Budapest, IHU Kht.

[8]   Jandova, J., Vu, H. (2001). Processing of germanium-bearing fly ash. *Metallurgy, Refractories and Environment*, Technical University of Košice: Košice, Slovakia, pp. 107–112.

[9]   Kashiwakura, S., Kumagai, Y., Kubo, H., Wagatsuma, K. (2013). Dissolution of Rare Earth Elements from Coal Fly Ash Particles in a Dilute H_2SO_4 Solvent. *Open J. Phys. Chem.,* 03, pp. 69–75.

[10]   Ketris, M. P., Yudovich, Y. E. (2009). Estimations of Clarkes for Carbonaceous biolithes: World averages for trace element contents in black shales and coals. *International Journal of Coal Geology,* 78 (2), pp. 135–148.

[11] Kolker, A., Scott, C., Hower, J. C., Vazquez, J. A., Lopano, C. L., Dai, S. (2017). Distribution of rare earth elements in coal combustion fly ash, determined by SHRIMP-RG ion microprobe. *Int. J. Coal Geol.,* 184, pp. 1–10.

[12] Kovács, F. (2001). Fly ash and slag materials of brown coal power plants, their properties and utilization. (in Hungarian) *Publications of the University of Miskolc, series A, Mining,* Vol. 55, pp. 67–76.

[13] Lachner, L. (2002). *Application of soot as binder in the road building* (in Hungarian). http://internet.kozut.hu/ume/ume/e-UT_05_02_41.pdf.

[14] Less, Gy. (ed.) (2012). *Mineral resources of strategic importance II* (in Hungarian). CriticEl monograph series No. 2, Miskolc, Milagrossa Kft.

[15] Less, Gy. (ed.) (2013). *Mineral resources of strategic importance I* (in Hungarian). CriticEl monograph series No. 1, Miskolc, Milagrossa Kft.

[16] Ministry of National Development [Hungary] (2011). National Energy Strategy 2030. http://2010-2014.kormany.hu/download/7/d7/70000/Hungarian%20Energy%20Strate gy%202030.pdf.

[17] Mucsi, G. (ed.) (2014). *Complex utilization of power plant fly ashes* (in Hungarian). CriticEl monograph series No. 6, Miskolc, Milagrossa Kft.

[18] Mucsi, G. Csőke B. (2014*). Physical and chemical properties of power plant fly ashes* (in Hungarian). CriticEl monograph series No. 6, Miskolc, Milagrossa Kft., pp. 67–79.

[19] Mucsi, G., Kumar, S., Csőke, B., Kumar, R., Molnár, Z., Rácz, Á., Mádai, F., Debreczeni, Á. (2015). Control of geopolymer properties by grinding of land filled fly ash. *International Journal of Mineral Processing,* Vol. 143, pp. 50–58.

[20] Mucsi, G., Szabó, R., Nagy, S., Bohács, K., Gombkötő, I, Debreczeni, Á. (2017). Development of polystyrene -geopolymer composite for thermal insulating material and its properties with special regards to flame resistance. *IOP Conference Series: Materials Science and Engineering,* Vol. 251, pp. 1–8.

[21] Püspöki, Z. (ed.) (2018). *The Hungarian coal resource and its utilization opportunities* (in Hungarian). Webpge of Magyar Bányászati és Földtani Szolgálat, https://mbfsz.gov.hu/sites/default/files/file/2018/06/07/a_hazai_szenvagyon_ es_ hasznositasi_lehetosegei.pdf.

[22] Szakáll, S. (ed.) (2014). *Rare earth elements in Hungarian geological formations* (in Hungarian). CriticEl monograph series No. 5, Miskolc, Milagrossa Kft.

[23] Xia, M., Sanjayan, J. (2016). Method of formulating geopolymer for 3D printing for construction applications. *Mater. Des.,* Vol. 110, pp. 382–390.

MECHANICAL AND STRUCTURAL PROPERTIES OF BIOMASS-GEOPOLYMER COMPOSITES

MÁRIA AMBRUS[1] – NÓRA PAPNÉ HALYAG[1] – IMRE CZUPY[2] – DÓRA SZALAY[2] – GÁBOR MUCSI[1]

*[1]Institute of Raw Materials Preparation and Environmental Processing,
University of Miskolc*
[2]Faculty of Forestry, University of Sopron

Abstract: With the ever-increasing demand in the construction and building industry, not only the need for sustainable and environmentally friendly building materials but the application of locally available additive materials has been the focus of much research. Geopolymers are a novel material type, produced by the polycondensation and polymerisation of solid aluminosilicates by an alkali solution. Various geopolymer composites can be prepared with the addition of different artificial and natural materials, preparing for example fiber-reinforced or lightweight materials with increased heat, fire and acid resistance. Geopolymers are considered more environmentally friendly due to the lower CO_2 emissions during their production (compared to ordinary Portland cement), and the use of locally available natural materials to improve their properties can provide further benefits.

The examined geopolymer composites from woody biomass and fly ash based geopolymer were prepared with 25 wt.%, 50 wt.% and 75 wt.% biomass addition. The base materials exhibited good compatibility, especially between the fibrous phloem and the geopolymer matrix. The increased biomass content resulted in lowered flexural and compressive strength, but due to the decreased specimen densities, the application of the composites as lightweight construction material could be a feasible option.

Keywords: biomass, fiber addition, fly ash, geopolymer composite, mechanical pro-perties

1. INTRODUCTION

Geopolymers are inorganic materials synthetized at room or elevated temperatures from solid silica and alumina containing primary or secondary raw materials in mainly alkaline and possibly acidic aqueous medium. During the geopolymerisation process, a 3D aluminosilicate framework is produced, creating the geopolymer matrix. The resulting material has numerous application fields, such as fire-resistant materials, thermal insulation, high-tech resins, toxic and radioactive waste containment, composites for the aircraft and automobile industries, etc. [1, 2].

Fly ash is a coal combustion product collected from flue gas by gas filtration equipment, which is mostly deposited into ponds for storage. Some possible utilisations include concrete production, mine reclamation, soil amendment, filler material

in road construction, etc. Furthermore, because of its high availability and possible reactivity, it has proven to be a suitable geopolymer base material, as well [3].

The addition of small quantities of natural fibers to reinforce both traditional cementitious materials and geopolymers has proven to be suitable to improve the mechanical properties of the brittle cementitious matrices. Some of the examined geopolymer composites have included the addition of cotton [4, 5], wool [6, 7], sawdust [8], sisal [9, 10], coconut [11], and bamboo fibers [12].

In this article, the results of the examination of woody biomass–flyash based geopolymer composites are summarized. The flexural and compressive strength, specimen density, structural changes, and microstructural properties were analyzed.

2. MATERIALS AND METHODS

2.1. Base materials

The woody biomass was from an approximately 45-to-60-year-old linden (Tilia) tree, originating from the Botanical Garden of the University of Sopron, collected in 2018. The diameter of the logs was 30–40 cm. After separating the cork and phloem from the wood, the fiber production was carried out with hammer mill with a screen size of 10 mm.

The lignite fly ash was collected from Mátra Power Station. Before use, the sample was dried at 105 °C then sieved to remove >1 mm particles, such as unburned coal, slag and other contaminants. The moisture content of the fly ash was 25.0% and the loss on ignition was 0.37 wt.%. The particle and bulk densities were 1.84 g/cm^3 and 0.63 g/cm^3, respectively.

The cumulative and frequency distributions of the fly ash particles were analyzed with a Horiba LA-950 V2 laser particle size analyzer *(Figure 1a)*. The characteristic particle sizes were $x_{10} = 13.36$ μm, $x_{50} = 65.78$ μm and $x_{90} = 187.18$ μm. In the frequency curves, two local maximum points can be observed, at ~11 μm and ~100 μm. The geometric specific surface was calculated by the particle size analyzer to be 956.02 cm^2/g. The BET specific surface was measured using a Gemini VII 2390 Series Surface Area Analyzer, the value was 14.68 m^2/g.

In case of the woody biomass, the cumulative and frequency distributions *(Figure 1b)* were measured with sieve analysis. According to the frequency distribution, the 0.5–1 mm size fraction contained the highest amount of sample, with considerable amounts from both the friable cork and the fibrous phloem.
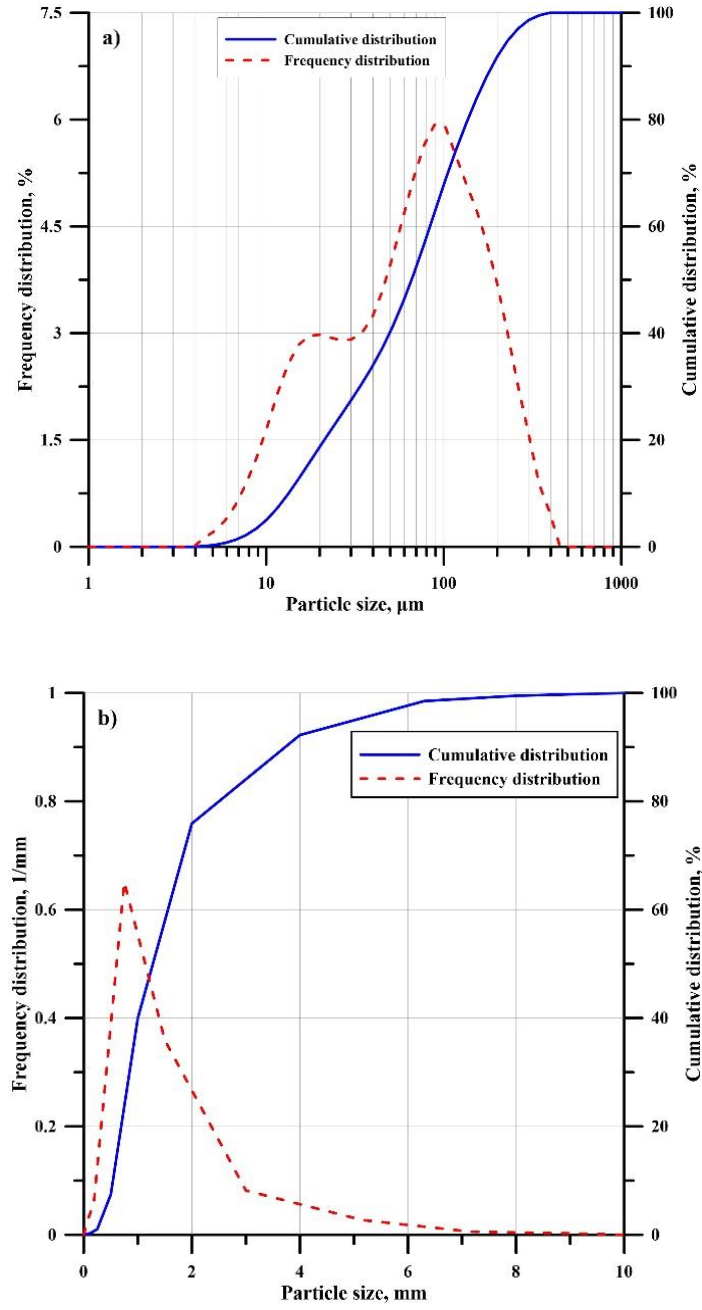
Figure 1
Cumulative and frequency distribution curves: a) fly ash; b) biomass

2.2. Geopolymer mixtures

The biomass and fly ash were mixed in three ratios: 25 wt.% biomass – 75 wt.% fly ash, 50 wt.% biomass – 50 wt.% fly ash and 75 wt.% biomass – 25 wt.% fly ash.

The activator solution consisted of 27 wt.% 8 M NaOH solution and 75 wt.% water glass with the following composition: 25.3% SiO_2, 13.7% Na_2O, 2.7% K_2O and 48.3% H_2O.

The liquid-to-solid ratio was 1 : 1.

During geopolymer production, the fly ash was mixed with the activator solution before the woody biomass addition. The mixtures were poured into molds and homogenized for 1 minute using a vibrating table. After a 1-day aging under sealed conditions, the specimens were heat treated at 60 °C for 6 hours. The cooled down geopolymer composites were held under sealed conditions for an additional 5 days before the strength measurements of the 7-day-old specimens could be carried out.

2.3. Test methods and apparatus

For flexural strength tests, the dimensions of the specimens were $40 \times 40 \times 160$ mm, while the compression strength test bars were of 60 mm height and 40×40 mm cross-section. The flexural and compression strength tests were carried out using three and six specimens, respectively, based on the standard MSZ EN 196-1:2016 at the age of 7 days.

Microstructural analyses on fly ash-biomass composites were performed by Fourier transform infrared spectroscopy (FT-IR), where stretching and bending vibrations of chemical bonds of functional groups in samples were detected by JASCO FT-IR 4200 type Fourier Transformed Infrared Spectrometer in reflection mode, with diamond ATR. The infrared transmission spectra of samples were recorded for $400–4000$ cm^{-1} at spectral resolution of 4 cm^{-1} using a Perkin-Elmer spectrum to measure the absorption spectra of the bonds. The spectrum is baseline corrected.

The morphology of the fly-ash based geopolymer replaced by biomass was observed by Phenom ProX electron microscopy equipped with EDS detector. The fly ash–biomass composite samples after compressive strength measurement were stacked onto the carbon adhesive. The measurement conditions include accelerating voltage 10 and 15 kV, in point analysis mode with spectrum collection time of 60 s. The images were taken at varying magnification.

3. RESULTS

3.1. Strength and specimen density values

The results of the flexural and uniaxial compressive strength, and the specimen density measurements are summarized in *Figure 2*, with the fit curves to each test result.
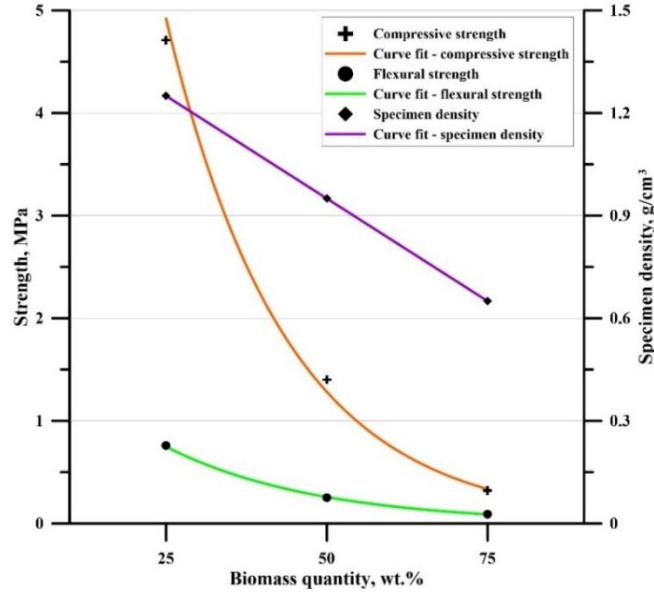
Figure 2
Results of strength and specimen density measurements

With 25 wt.% biomass addition, the flexural strength was 0.75 MPa, which decreased to 0.25 MPa and 0.09 MPa as the biomass quantity was increased. The decrease in the flexural strength can be described with $R^2 = 0.997$ using *Equation (1)*. During the flexural strength tests, the specimens failed to break after reaching the breaking point, exhibiting the flexible behavior characteristic to fiber-reinforced geopolymers. However, the decreasing flexural strength hinders the applicability of the composites as fiber-reinforced building material.

$$y = -0.043x + 0.777 \tag{1}$$

For the compressive strength the same tendency could be observed, as the highest uniaxial compressive strength was 4.71 MPa, achieved with 25 wt.% biomass. With higher biomass content, the strength values exponentially decreased to 1.40 MPa with 50 wt.%, and 0.32 MPa with 75 wt.% biomass. The strength decrease can be characterized by *Equation (2)*, the $R^2 = 0.999$. The decrease in the uniaxial compressive strength values can be explained by the higher amount of geopolymer matrix in the composites with lower biomass quantity, which provides the dense structure and strength to the samples.

$$y = -0.054x + 2.938 \tag{2}$$

Increasing the amount of biomass in the composites led to linear decrease in the specimen density values [*Equation (3)*, $R^2 = 1$]. The initial 1.25 g/cm^3 was decreased to 0.95 g/cm^3, then 0.65 g/cm^3 with the addition of biomass. This can be due to the density difference between the fly ash and the woody biomass: the higher the amount of lower density biomass in the composites (as a replacement of the higher density fly ash), the lower the density becomes.

$$y = -0.012x + 1.55 \tag{3}$$

Based on the strength and specimen density results, it can be concluded that even though the addition of high quantity of woody biomass decreased the flexural and uniaxial compressive strength of the specimens, due to the decreased specimen density, the production of a lightweight building material from the biomass-geopolymer composite could be a potential area of utilization. However, further experiments should be conducted to confirm the applicability of the prepared materials.

3.2. Microstructural analysis

FT-IR

First, we measured the spectra of the raw materials to compare the structural changes caused by alkali activation. Wood fiber consists of mainly cellulose, hemicellulose and lignin. Cellulose is a linear polymer which is insoluble in water and is the main component of wood fiber, forming the frame of the cell wall. Hemicellulose and lignin form the surrounding intercellular substance. Hemicellulose is chemically polysaccharide of low molecular weight, so it can be dissolved in water. Lignins are polymeric aromatic constituents in plant cell walls, which bond fibers and give stiffness to wood. Hemicellulose and cellulose are mainly composed of oxygen functional groups which are present in the lignocellulose material such as hydroxyl, ether, carbonyl, while lignin is a complex, systematically polymerized, highly aromatic substance and acts as cementing matrix that holds between and within both cellulose and hemicellulose units. Wood fibers can be used in various forms as reinforcement. The FT-IR spectra of the raw materials can be seen in *Figure 3*. The biomass shows strong broad overlapping bands between 3654–2721 cm^{-1}. The main band of the wood spectra centered at 3329 cm^{-1} indicates the OH stretching vibration in hydroxyl groups, which all main wood components contain. The smaller band at 2915 cm^{-1} and 2849 cm^{-1} can be derived from asymmetric C-H and symmetric C-H bonds, present in cellulose and hemicellulose. The strong band at 1604 cm^{-1} indicates the bonding of $C = C$ or $C = N$. The band at 1413 cm^{-1} can be ascribed as O-H vibrations and $C = O$ vibrations in cellulose. The C-O carbonyl band in lignin and xylan units was observed at 1229 cm^{-1}. The main absorption band centered at 1034 cm^{-1} is a superposition of broad overlapping bands coming from the C-O stretching vibration of cellulose, hemicellulose and lignin. The absorption bands from 900 to 400 cm^{-1} region are strongly reduced in intensity. The band at 837 cm^{-1} is assigned to C-O-C stretching as an amorphous absorption band.

In the case of fly ash, small bands at 1614 cm^{-1} correspond to the H-O-H bending vibrations. The peak identified at 1465 cm^{-1} can be related to the O-C-O stretching vibration of a carbonate phase. The main absorption band is located between 1270 and 833 cm^{-1} and is attributed to the Si-O-Al and Si-O-Si asymmetric stretching vibrations. The band at 812 cm^{-1} is attributed to the bands present in the fly ash source as quartz or mullite. The peak at 559 cm^{-1} is assigned to the Si-O-Al bending vibration. Bands with low intensity at the low wavenumber side belong to Si-O Si-O-Si bending vibrations [13].
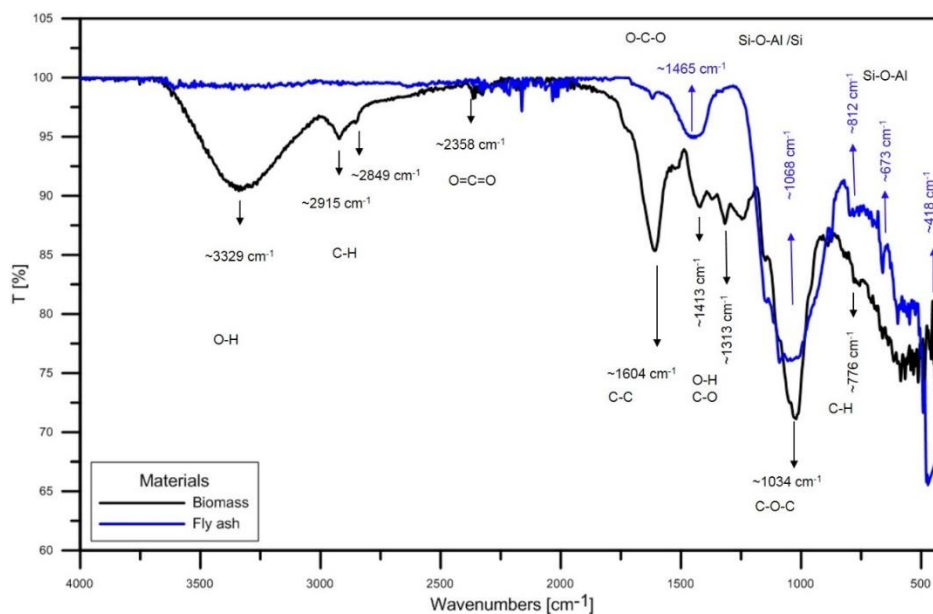
Figure 3
FT-IR spectra of the raw materials (wood fibers and fly ash)

As is illustrated in *Figure 4*, after alkali activation of the fly ash based geopolymer replaced by 25 wt.% biomass, the spectrum shows a new band at 1700 cm^{-1} derived from the C = O vibrations of biomass. The band of fly ash shifts from 1465 cm^{-1} to 1401 cm^{-1}, which might be formed from remaining unreacted activator and CO_2. The main absorption band located at 1068 cm^{-1} shifts to 979 cm^{-1} with the replacement of biomass. The bands of fly ash between 800 cm^{-1} and 500 cm^{-1} coming from Si-O-Al decreases significantly, which may indicate reaction. The most obvious changes of the absorption band of the composite are the disappearing of the O-H stretching band at 3329 cm^{-1} and the small C-H bands at 2915 cm^{-1} and 2849 cm^{-1} coming from the biomass. The increasing portion of biomass shows absorption bands at 3310 cm^{-1}, 2922 cm^{-1}, and 2360 cm^{-1} that can be derived from the biomass. In the case of 50 wt.% replacement the band of C-O centered at 1401 cm^{-1} shows the most intense absorption band of all of the composites, indicating the highest amount of carbonate formation due to the alkali activation. The intensity of the main Si-O-Al band decreases as the

fly ash content decreases. At the low wavenumber side of the spectra the biomass derived amorphous absorption band become more intense. The replacement of fly ash with 75 wt.% biomass shows a band at 979 cm^{-1} with the lowest intensity due to the low proportions of fly ash.
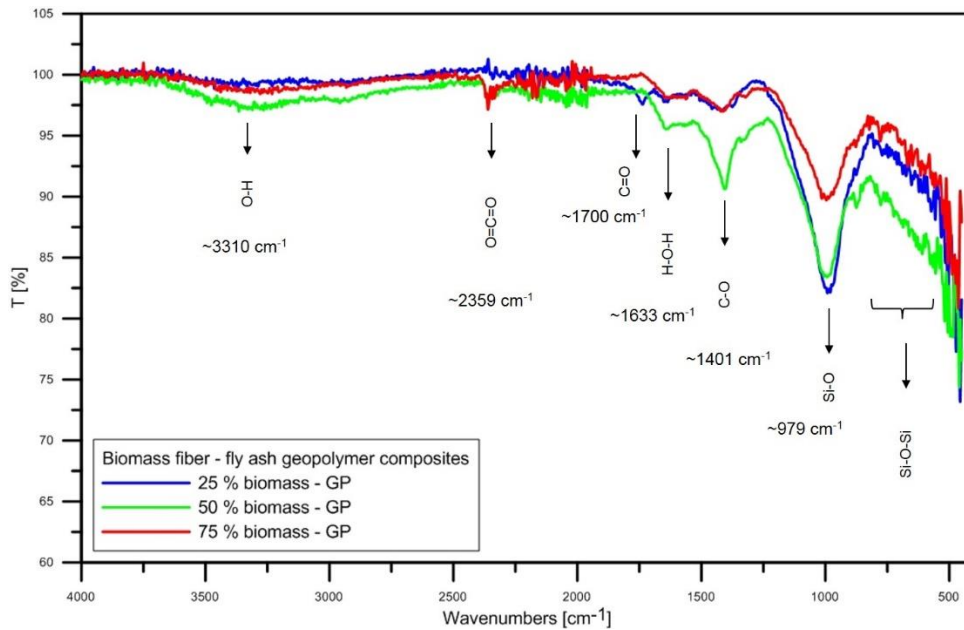
Figure 4
FT-IR spectra of the fly ash based geopolymer
with different portions of wood fibers

Scanning electron microscopy

The analysis was performed first on raw fly ash then on fly-ash based geopolymer replaced by 25, 50 and 75 wt.% crushed wood fibers. *Figure 5* shows raw fly ash particles with spherical shapes and smooth surfaces of different sizes. Most particles are hollow and filled with fragments.

The fly ash biomass composites were compact, with micro-porosity and holes formed during polycondensation. Both fly ash and wood particles underwent significant changes of morphology and chemical composition in the geopolymer due to the alkali reaction. The spherical fly ash particles are built into the amorphous geopolymer framework of aluminosilicate. The composite contains undissolved solid particles of fly ash with higher amounts of Si, Al, and Fe, or partially dissolved fly ash particles. In *Figure 5*, partially reacted fly ash particles can be seen. The area of the unreacted particles is the most sensitive to mechanical loading. All of the samples with different replacement of biomass show micro cracks, which resulted in lower compressive strength, and increased porosity. The micro cracks could have formed

as a result of drying of geopolymer concrete specimens. The strong chemical bond between the geopolymer gel and wood fiber can be the main reason for higher flexural and compressive strength.
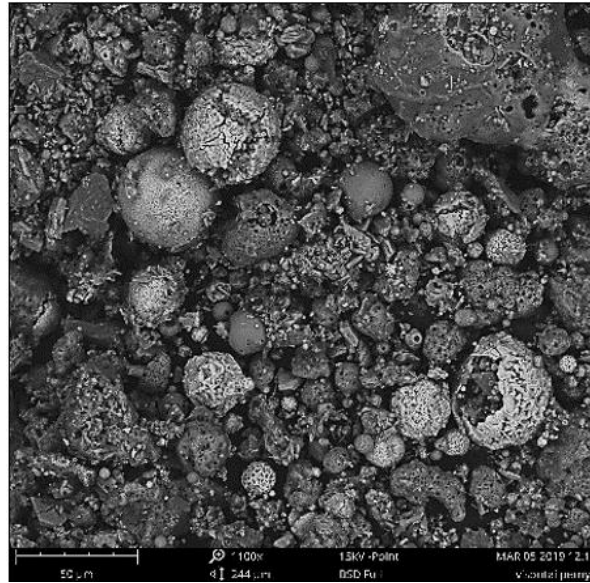
Figure 5
Fly ash with its spherical particles (Sample from Visonta, Mátra Power Plant)
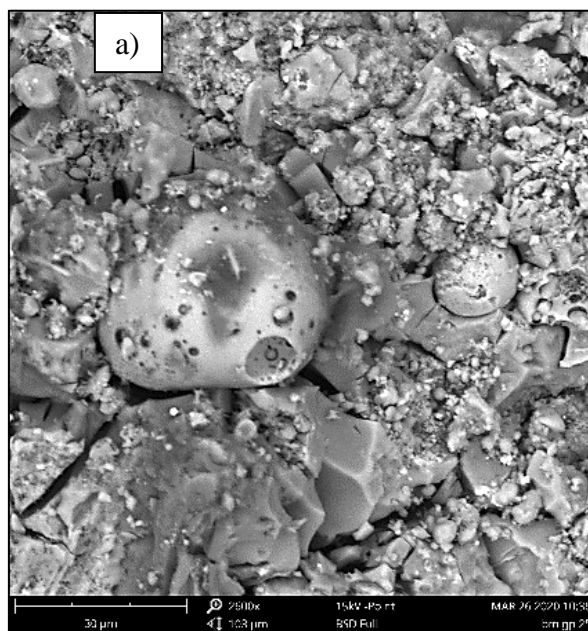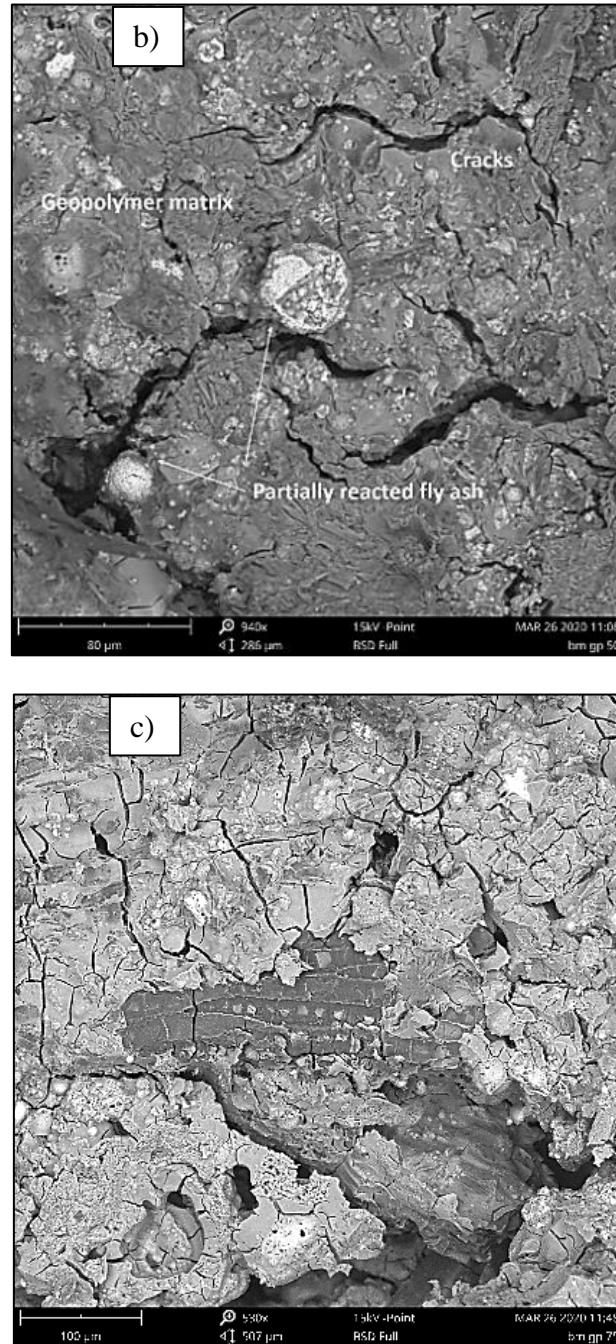
Figure 6

Microstructure of the fly ash based geopolymer replaced by 25 wt.% wood (a),
50 wt.% wood (b) and 75 wt.% wood fibers (c)

The SEM images in *Figure 6* indicate that there was good adhesion between the fibrous wood particles and the geopolymer matrix at the interface zone. The wood particles may bridge the micro and macro cracks of the brittle matrix. In the case of 25% by weight replacement there were unreacted fly ash particles among the wood fibers, but with an increasing amount of wood, the number of fly ash particles decreased as they built into the geopolymer gel (50 wt.% replacement). The fibers are covered with this newly formed geopolymer gel binding the fibers together. In the case of 75 wt.% replacement the wood fibers are covered with dense, fractured geopolymer gel, but the fibers were not bound together due to the low amount of fly ash meaning low compressive strength.

Table 1

The results of EDS analysis in the case of geopolymer and wood fiber

Element	Weight concentration (%)	
	Geopolymer	**Wood fiber**
Oxygen	30.18	43.98
Silicon	29.83	2.3
Calcium	12.89	0.55
Carbon	7.4	46.72
Sodium	6.72	5.16
Potassium	5.06	0.39
Aluminum	4.14	0.44
Sulfur	1.83	0.09
Iron	1.68	0.3
Magnesium	0.26	0.06

The data from the elemental analysis of the geopolymer gel and the uncoated wood surface are summarized in *Figure 7* and *Table 1*. The composition of the geopolymer gel contains high amount oxygen, silicon and calcium, which is a part of the C-S-H (calcium-silicate-hydrate) gel responsible for mechanical properties in the fly ash biomass composite. The potassium and sodium content of the geopolymer originates from the alkali solution of NaOH and water glass mixture, while the rest of the trace elements, i.e. sulfur, iron, etc., correspond to the composition of the fly ash used. The chemical composition of the biomass fiber consists of mainly C and O with a low amount of Na. The lack of H in the EDS analysis data is due to the inability of the instrument to identify hydrogen during the analysis. The polygonal structured part of the wood (cork) is not appropriate for geopolymer gel formation, as proved by the lack of geopolymer on its surface with a trace amount of Si, Al and Ca, which are more dominant in the geopolymer gel.

a)

b)
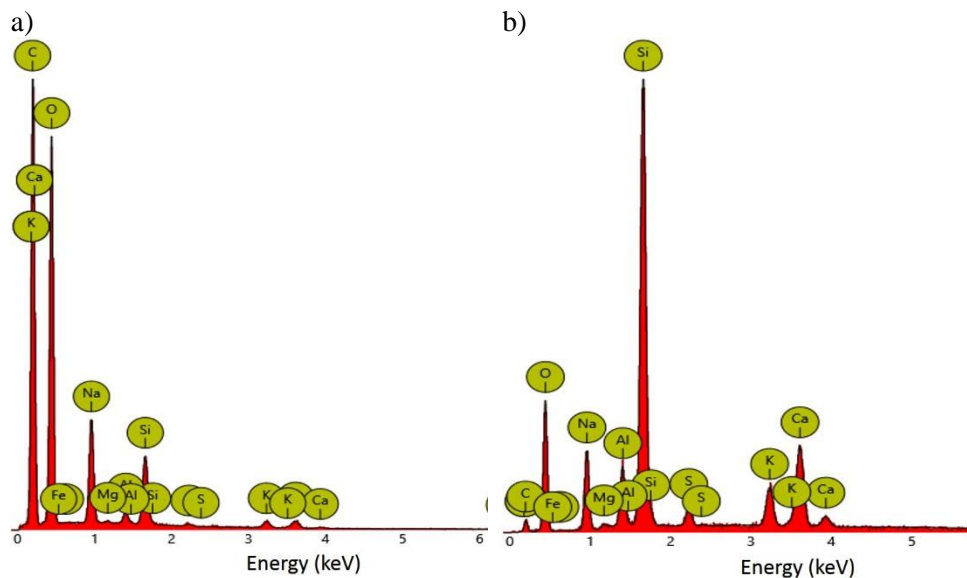
Figure 7

The spectrum of a) the geopolymer gel and b) the wood fiber after alkali activation

4. CONCLUSIONS

In the article, experimental results of biomass-geopolymer composites were presented, with 25 wt.%, 50 wt.% and 75 wt.% woody biomass addition to fly ash based geopolymer. The flexural and uniaxial compressive strength test values of the specimens could be described with exponential decrease as the biomass quantity was increased in the geopolymer matrix. The specimen density of the specimens linearly decreased as the higher density fly ash was replaced with lower density biomass. The main components of the base materials could be identified by the FT-IR analysis and the shifts of bands in the spectra of the composites indicated the geopolymerization reaction. As the biomass quantity was increased in the composites, the bands corresponding to the biomass became more dominant in the spectra. The SEM images showed unreacted fly ash particles in all three composite samples, along with micro cracks on the geopolymer structure. The fibrous phloem of the woody biomass was coated with the geopolymer gel, while the friable cork part was not compatible with the geopolymer matrix. Based on the results of the microstructural analysis and the strength tests of the biomass-geopolymer composites, it can be concluded that cork of the sample mainly acts as filler in the composite.

ACKNOWLEDGEMENTS

REFERENCES

[1] Davidovits, J. (1991). Geopolymers: Inorganic polymeric new materials. *Journal of Thermal Analysis*, 37, pp. 1633–1656, DOI: 10.1007/BF01912193.

[2] Zhuang, X. Y., Chen, L., Komarneni, S., Zhou, C. H., Tong, D. S., Yang, H. M., Yu, Hao Wang, W. H. (2016). Fly ash-based geopolymer: clean production, properties and applications. *Journal of Cleaner Production*, 125, pp. 253–267, DOI: 10.1016/j.jclepro.2016.03.019.

[3] Nath, S. K., Kumar, S. (2019). Reaction kinetics of fly ash geopolymerization: Role of particle size controlled by using ball mill. *Advanced Powder Technology*, 30 (5), pp. 1079–1088, DOI:10.1016/j.apt.2019.02.003.

[4] Alomayri, T., Shaikh, F. U. A., Low, I. M. (2014). Synthesis and mechanical properties of cotton fabric reinforced geopolymer composites. *Composites Part B: Engineering*, 60, pp. 36–42, DOI: 10.1016/j.compositesb.2013.12.036.

[5] Alomayri, T., Shaikh, F.U.A., Low, I. M. (2013). Thermal and mechanical properties of cotton fabric-reinforced geopolymer composites. *Journal of Materials Science*, 48, pp. 6746–6752, DOI: 10.1007/s10853-013-7479-2.

[6] Alzeer, M., MacKenzie, K. J. D. (2012). Synthesis and mechanical properties of new fibre-reinforced composites of inorganic polymers with natural wool fibres. *Journal of Materials Science*, 47, pp. 6958–6965, DOI: 10.1007/s10853-012-6644-3.

[7] Ranjbar, N., Zhang, M. (2020). Fiber-reinforced geopolymer composites: A review. *Cement and Concrete Composites*, 107, p. 103498, DOI: 10.1016/j.cemconcomp.2019.103498.

[8] Duan, P., Yan, C., Zhou, W., Luo, W. (2016). Fresh properties, mechanical strength and microstructure of fly ash geopolymer paste reinforced with sawdust. *Construction and Building Materials*, 111, pp. 600–610, DOI: 10.1016/j.conbuildmat.2016.02.091.

[9] Da Silva Alves, L. C., dos Reis Ferreira, R. A., Bellini Machado, L., de Castro Motta, L. A. (2019). Optimization of metakaolin-based geopolymer reinforced with sisal fibers using response surface methology. *Industrial Crops and Products*, 139, p. 111551. DOI: 10.1016/j.indcrop.2019.111551.

[10] Silva, G., Kim, S., Aguilar, R., Nakamatsu, J. (2020). Natural fibers as reinforcement additives for geopolymers – A review of potential eco-friendly

applications to the construction industry. *Sustainable Materials and Technologies*, 23, e00132, DOI: 10.1016/j.susmat.2019.e00132.

[11] Korniejenko, K., Frączek, E., Pytlak, E., Adamski, M. (2016). Mechanical properties of geopolymer composites reinforced with natural fibers. *Procedia Engineering*, 151, pp. 388–393, DOI: 10.1016/j.proeng.2016.07.395.

[12] Sá Ribeiro, R. A., Sá Ribeiro, M. G., Sankar, K., Kriven, W. M. (2016). Geopolymer-bamboo composite – A novel sustainable construction material. *Construction and Building Materials*, 123, pp. 501–507, DOI: 10.1016/j.conbuild mat.2016.07.037.

[13] Pandey, K. K., and Pitman, A. J. (2004). Examination of lignin content in a softwood and a hardwood decayed by a brown-rot fungus with acetyl bromide method and Fourier transform infrared spectroscopy. *Journal of Polymer Science Part A – Polymer Chemistry*, 42, pp. 2340–2346. DOI: 10.1002/pola. 20071.

CONSTRUCTION AND DEMOLITION WASTES AS POTENTIAL ASPHALT FILLERS

R. GÉBER[1] – I. KOCSERHA[2] – T. FERENCZI[3] – F. KRISTÁLY[4] – F. MÓRICZ[5] – Á. RÁCZ[6]

[1,2] *Institute of Ceramics and Polymer Engineering, University of Miskolc,*
H-3515 Miskolc-Egyetemváros
[3] *Institute of Metallurgy, University of Miskolc, H-3515 Miskolc-Egyetemváros*
[4,5] *Institute of Mineralogy and Geology, University of Miskolc,*
H-3515 Miskolc-Egyetemváros
[6] *Institute of Raw Material Preparation and Environmental Processing,*
University of Miskolc, H-3515 Miskolc-Egyetemváros

Abstract: The purpose of this research work was to investigate the usability of powdered construction and demolition (C&D) wastes as potential asphalt fillers. During the research, mineral and chemical composition, particle size distribution, BET-specific surface area and pore volume of recycled concrete powder (RCP) and roof-tile powders (RTP) were determined and compared to limestone filler as the reference material. Results show that mineral composition, particle size distribution, specific surface area and pore volume are good indicators to reveal the most important features of these potential asphalt fillers. Particle size distribution fundamentally affects all of the properties of these powders. The results show that RTP has some positive properties, especially its specific surface area, that may influence the adsorption of bitumen; therefore, this material may be a good asphalt filler. With the proper comminution of C&D waste a suitable particle size distribution can be achieved in order to use these fillers in asphalt pavements.

Keywords: asphalt filler, construction & demolition waste, porosity, specific surface area

1. INTRODUCTION

Asphalt is a composite constructional building material consisting of a mineral skeleton in a specific particle size distribution and binder material. According to ÚT 2-3.301-1:2010 Hungarian Road Paving Technical Specification [1], the mineral part of asphalt mixtures basically consists of natural rocks in specified particle sizes: aggregate (d > 2.0 mm), sand (2.0 mm > d > 0.063 mm) and filler (d < 0.063 mm). In Hungary, mainly andesite and basalt are used as aggregate, while limestone is used as filler for pavements. However, there is a growing demand worldwide for the use of waste materials and secondary raw materials. Substitution of mineral materials of asphalt mixtures generally depends on geographical and economic features.

Several by-products are issued during production technologies which could be used in road construction as secondary raw material. Such materials include oil-drill

cuttings [2], fly ash [3,4], boron waste [5], waste lime [6,7], and steel slag [8,9]. In Asia – mainly in developed Far-Eastern countries – it is a serious problem how to handle and utilize construction and demolition waste (C&D) – mostly brick and concrete – originating from demolition in acorrect appropriate way [9]. These materials are generated in significant quantities year by year, while storage of them as waste can be harmful for the environment in the long term. Utilization of construction and demolition waste as road construction material is beneficent in several ways. Not only can the exploitation of natural raw material (rocks) be decreased but also the storage of waste in landfills. Recognizing its potential, research is carried out for the utilization of such waste.

Chen et al. [10] examined the application of brick powder as recycled asphalt filler. They made comparative measurements in which they examined the generally used limestone powder and brick powder to be used as alternative filler. Beside material structure examinations of fillers, they also made a general examination of asphalt mixtures, such as indirect tensile modulus test, water sensitivity, static and dynamic creep tests and fatigue test. Their results showed that asphalt mixtures made with brick powder have a higher modulus compared to the control mixture made with limestone powder. This presumes better rutting resistance, improves water sensitivity and fatigue life. Furthermore, brick powder also decreases the degree of permanent deformation.

Wu et al. [11] made asphalt mastics utilizing recycled red brick powder (RBP) on which they made rheological examinations, besides testing the most significant physical features (penetration, softening point, high temperature viscosity). Based on their results, application of RBP may have some positive effect on high-temperature properties of asphalt mastic, but at the same time may have some negative effect on its low-temperature properties.

Chen et al. [12] examined the applicability of recycled fine aggregates powder (RFAP) in asphalt mixture. Besides compositional and morphological examinations of powders, they have made conventional asphalt technological tests on the asphalt mixtures made with these fine powders, such as indirect tensile modulus test, three-point bending test, water sensitivity, dynamic creep test and fatigue test. Then results were compared with mixtures made with generally used limestone powder, showing that concrete powders improve water sensitivity, high temperature performance and fatigue resistance of asphalt mixture, but at the same time decrease low temperature performance to some extent.

Besides fine sand and stone dust mix, Sutradhar et al. [13] have examined waste concrete dust and brick dust as possible asphalt fillers. Marshall Stability (MS) values of asphalt mixtures made with concrete dust and brick dust increased, which indicates the usability of optimal quantity of waste as filler.

Fillers play a significant role in mineral mixtures. Several features of asphalt concrete depend on quantity and features of fillers. It is subservient to use mainly carbonate rocks as fillers, such as limestone powder, which is basic and adsorbs well to bitumen. The binder material of asphalt pavements, bitumen sticks together the

larger aggregates that carry the load of traffic. Therefore, mineralogical, physical and surficial properties of mineral aggregates need to be favorable. The contact between fillers and bitumen depends on the adsorption processes taking place on their interface. Physical adsorption is affected by the porosity and the specific surface area of the fillers. According to numerous research articles [14, 15], the bond between bitumen and siliceous fillers is mechanical (generated by the Van der Walls forces) while the bond between bitumen and another filler (for example limestone) is chemical.

The amount of pores, cracks and small crystals stuck on the surface of a filler grain increases the specific surface area and therefore affects the adsorbable amount of bitumen. Compared to other grains, the specific surface area of fillers in the mineral skeleton of an asphalt mixture is considerably higher, therefore they are able to adsorb a great part of bitumen in compound. When choosing fillers, mineral composition has great importance, that is, the material has to be pure. The presence of clay minerals is unfavorable, for instance, as it decreases mechanical strength, resistance to mechanical weathering, and finally leads to failure of pavement sooner than planned.

In Hungary, up to 30% of construction and demolition waste is from concrete, brick, tile and ceramics. Being a member of the European Union, Hungary is also subject to targets set in the Waste Framework Directive introduced in 2008 [16]. The Directive sets target values to reach for 2020: 70% preparation for re-use, recycling and other recovery of construction and demolition waste.

These experimental results may promote the applicability of such waste in road construction.

2. MATERIALS AND METHODS

2.1. Sample preparation

During the research we examined construction and demolition waste materials (recycled concrete powder – RCP, recycled roof-tile powder – RTP). As reference material, limestone powder was chosen that was previously grinded by the producer. The required particle size of powders was produced from waste concrete and roof tiles by a hammer, then grinded by a planetary ball mill. After grinding, fine powders were fractioned by a standard sieve of 0.063 mm nominal particle size. Samples were then dried to weight constancy and placed in air-proof storage for further examinations.

2.2. Testing methods

Mineralogical composition of samples was determined by X-ray powder diffraction (XRD) on a Bruker D8 Advance diffractometer (Cu-Kα source, 40 kV and 40 mA generator settings) in parallel beam geometry obtained with a Göbel mirror and Vantec1 (1° window opening) position sensitive detector. Measurements were carried out in the 2–70°(2θ) range with 0.007°(2θ)/120 sec goniometer speed. Crystalline components were identified by Search/Match algorithm in DiffracPlus EVA, using

the ICDD PDF2 2005 database. Quantitative composition was calculated by Rietveld refinement in TOPAS4, using empirical instrumental profile modelling (on ASTM SMR 640d Si standard) and crystal structure data from ICSD and AMCSD [17].

Chemical composition was determined by X-ray fluorescence spectrometry (XRF) on a Rigaku SuperMini 200 tabletop wavelength dispersive spectrometer (Pd –source, 50 kV and 4 mA) using in-house and USGS standards. Peak intensity determinations were done with 10 second background measurement on the left and right flank and 40 secondss on the peak maximum. Limits of detection in silicate matrix are from 0.01 wt% (light elements) to 0.001% (heavy elements).

Particle size distribution (PSD) of the ground material was measured by a HORIBA LA-950V2 laser diffraction particle size analyzer in wet mode using distilled water as dispersing media and sodium-pyrophosphate as dispersing agent, applying the Fraunhofer theory as evaluation method. Before the measurements 1-minute ultrasonic treatment was applied on the samples for better dispersion.

For morphological tests a Carl Zeiss EVO MA10 scanning electron microscope (SEM) was used. High resolution electron micrographs were taken in different magnifications for further observation. The aim of this technique was to observe the morphology and geometrical features of powders, as well as to reveal traces of porosity. Morphological analysis was made on the fractioned portions of powders during microstructural examination.

Specific surface area (SSA) of the powders (by BET method) was determined by a TriStar 3000 instrument (manufactured by Micromeritics). The method of this instrument is based on physical absorption and capillary condensation, and it works in volumetric mode. The fine powder samples were prepared with the use of a SMARTPREP instrument. Adsorption-desorption isotherms, BET-specific surface area and pore volume of samples according to the BJH method [18] were determined.

3. RESULTS AND DISCUSSION

Table 1 contains the mineral composition of the tested powders determined by XRD.

The calcite containing Mg in limestone is probably a component formed in veinlets, without major importance. Limestone is a compact, low porosity material, resulting in angular grains by crushing, determined by the rhombohedral cleavage of calcite (quartz and illite do not influence its properties). RCP (recycled concrete powder) and RTP (recycled roof-tile powder) could be compared to the previously mentioned materials as high temperature contact metamorphic rock (RTP) and high temperature rock altered by hydration (RCP). Based on their chemical compositions (SiO_2 content), the rocks range from acidic to basic: RCP > RTP > limestone. However, the interaction with bitumen is at the level of single grains, so quartz grains with carbonate coating could form good bonding, while bytownite grains with a smectite coating could give bad results.

Mineral	Group	Sample, w%		
		Limestone	RCP	RTP
Calcite	carbonates	97.6	76.0	–
Calcite, magnesian		1.4	–	–
Bytownite An85	feldspars	–	–	26.3
Albite		–	3.4	–
Microcline		–	1.2	8.7
Grossularia	garnet	–	0.7	–
Diopside	inos	–	–	19.4
Illite 2M1	micas	0.6	–	–
Biotite 1M		–	0.7	–
Larnite	olivines	–	1.3	–
Hatrurite		–	1.7	–
Akermanite	other	–	0.7	–
Quartz	oxides	0.4	–	22.4
Cristobalite low		–	–	2.1
Periclase		–	0.4	–
Hematite		–	–	5.1
Amorphous (alumino-silicate material)	–	–	14.0	16.0

Table 2 shows the chemical composition of tested powders determined by XRF. The sum of measurements is the total amount of material that could be measured and quantified according to calibration standards. The loss on ignition (LOI) was determined by 2 hours heating at 1,200 °C. The LOI is given by CO_2 content for limestone and adsorbed H_2O for RCP and RTP. The LOI values of RCP and RTP are linked to the amorphous materials, since all the crystalline components are anhydrous. This indicates a state of alteration by hydration, which may result in the formation of hydrated layers in cracks and on grain surfaces, leading to an increase in surface reactivity and bonding capacity.

Component, w%	Sample		
	Limestone	RCP	RTP
SiO_2	1.5	67.4	54.2
Al_2O_3	0.8	4.2	17.1
MgO	0.28	1.73	4.15
CaO	55.0	14.6	10.2
Na_2O	<0.01	0.46	0.68
K_2O	0.15	0.84	2.95
Fe_2O_3	0.07	1.14	6.04
MnO	0.005	0.147	0.113
TiO_2	0.010	0.155	0.753
P_2O_5	0.072	0.062	0.154
S	<0.005	0.4	0.005
LOI	42	9	4

The particle size distributions of the tested fillers can be seen in *Figure 1*.
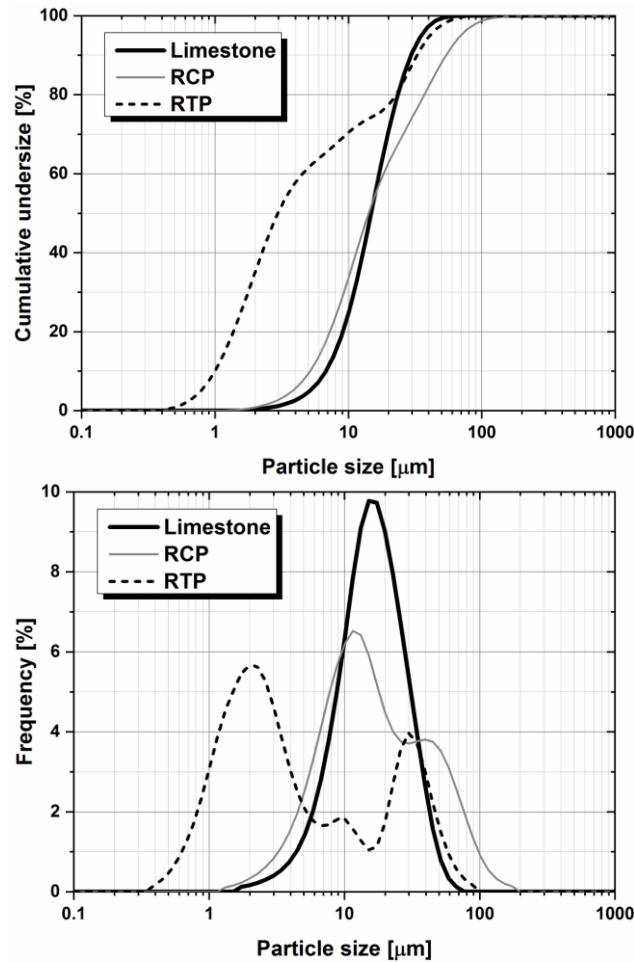
Figure 1
Particle size distribution of powders

According to *Figure 1* and *Table 3*, RTP proved to be the finest among the prepared fillers. The maximum particle size of limestone is the smallest with 67 µm. RCP has the highest median value with 14.23 µm. From the point of view of d_{80}, RTP is the finest, while RCP is the coarsest. RTP has the highest calculated surface area, which is 26,079 cm²/cm³. The fineness modulus (FM) is a practical mathematical method to describe the fineness of a material, based on which RTP proved to be the finest. RCP has the highest FM value, so from this point of view this material proved to be the coarsest. Coefficient of uniformity (U_c) shows width of particle size distribution, that is, how wide the size range is in which the grains are present in the material.

From this point of view, limestone has the lowest U_c, the narrowest distribution, while RTP has the widest.

Common values and parameters derived from particle size distribution

Parameter	Unit	Limestone	RCP	RTP
D_{50}	μm	14.82	14.23	2.92
D_{80}	μm	23.56	37.09	22.82
D_{95}	μm	35.23	69.69	41.11
Fineness Modulus, *FM*	–	3.13	3.41	2.06
Coefficient of Uniformity, U_c	–	2.52	3.58	4.54
Surface area, *S (calculated)*	cm^2/cm^3	5,058.6	5,672	26,079

Morphology and surface characteristics of the examined powders are shown by SEM micrographs in *Figure 2*.
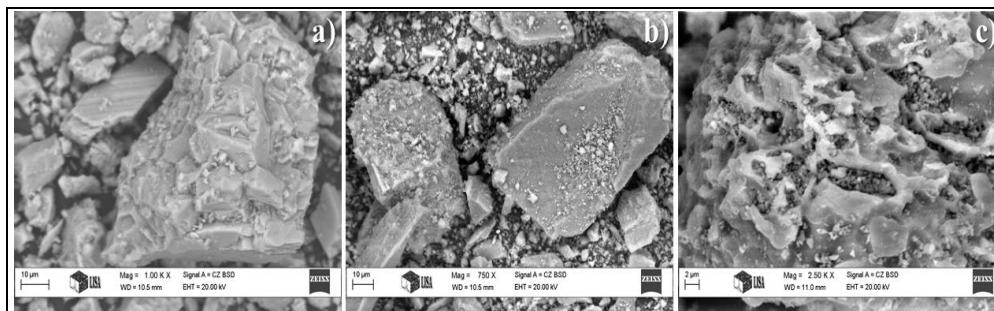
Figure 2
SEM micrographs of powders: a) Limestone, b) RCP, c) RTP

In the SEM micrograph of the limestone *(Figure 2a)* used as reference material, relatively big, solid calcite grains can be seen. It is visible that small grains have adhered on their surface. It is well recognizable that bigger planar faces and planar fractures formed on other grains during grinding. Based on this, we can conclude a relatively small surface area, which is favorable in view of bitumen quantity to be used.

Figure 2b shows the morphology of RCP, which reflects particle size distribution. In the view field, several 10 μm grains can be seen, besides some large grains. Just like on the other samples, adherence of the finest grains to the bigger ones can be observed in case of RCP. Also occurring in the sample are polygonal shaped and plated grains whose surface and planar fracture is relatively smooth.

Figure 2c, the high resolutional SEM micrograph of RTP powder, shows a diversified picture. A continuous glassy phase can be observed, as well as the characteristically submicronic crystalline grains in between. Formation of the glassy phase is due to the process of firing of tile at high temperature (normally ~1100 °C). The surface

of the glassy phase is coherent and there are no signs of higher porosity on it. Contrary to the surface property of the other samples, in case of RTP no extensive fracture planes can be observed.

The test results of nitrogen adsorption tests are summarized in *Table 4*. The lowest specific surface area belongs to the reference limestone powder (0.92 m^2/g), while RCP has the highest SSA value (2.27 m^2/g). The SSA value of limestone powder is favorable referring to the quantity of bitumen to be used in asphalt mixture production. In case of using limestone powder as filler we do not need to calculate with excess bitumen. Application of RCP may result in an increased bitumen requirement, which affects –mainly worsens – other features of the asphalt mixture (bleeding, rutting).

Table 4.

Results of Nitrogen adsorption test

Property	Unit	Limestone	RCP	RTP
BET specific surface area, SSA	m^2/g	0.92	2.27	1.65
BJH desorption average pore diameter	nm	45.27	26.82	21.27
BJH desorption cumulative surface area of pores (values were determined between 1.7 nm and 300.0 nm diameter region)	m^2/g	0.98	2.51	1.38
BJH desorption cumulative pore volume of pores (values were determined between 1.7 nm and 300.0 nm diameter region)	cm^3/g	0.0111	0.0168	0.0073

The BET specific surface area value of RTP is rather interesting. Based on particle size distribution it is already known that this powder is the finest. This statement is supported also by the FM value, furthermore this material has the highest surface calculated from PSD. Nevertheless, based on BET value (1.65 m^2/g), RTP has the second lowest SSA value after limestone. The surface of glassy phase present in great quantity is adequately smooth and free of bigger pores and this phenomenon causes a BET value decrease of the powder.

Nitrogen adsorption method was used to define porosity of the powders. Average pore diameter of the materials, cumulative surface area of pores and cumulative volume of pores were defined by the Barret–Joyner–Halenda (BJH) method according to desorption isotherms. This method assumes pores are cylindrical. It is suitable to determine pores with diameter of 1.7 nm–300 nm, therefore mesopores (d: 2–50 nm) and macropores (d > 50 nm) can also be revealed.

In view of porosity value defined from desorption isotherm, limestone has the highest average pore diameter (45.27 nm), while the smallest pores (12.99 nm) can be found in RTP. From the point of view of cumulative pore area RCP has the highest (2.51 m^2/g) and limestone has the lowest (0.98 m^2/g) pore surface.

4. CONCLUSION

This research focused on the examination of two powdered waste materials which may be potential paving material. One conventional asphalt filler (limestone) and two waste materials (recycled concrete and roof tiles) were investigated in their powder form. Mineral composition, particle size distribution, specific surface area and pore volume are useful features to characterize the powders. If the specific surface area and pore volume is high the grains can adsorb much more bitumen on their surface, which may cause fast ageing of this binder. If an optimal particle size distribution is achieved during the comminution process of waste materials, roof tile powder may be a potential good asphalt filler.

ACKNOWLEDGEMENT

REFERENCES

[1] ÚT 2-3.301-1:2010. *Hungarian Road Paving Technical Specification* (in Hungarian).

[2] Dhir, R. K., Csetenyi, L. J., Dyer, T. D., Smith, G. W. (2010). Cleaned oil-drill cuttings for use as filler in bituminous mixtures. *Construction and Building Materials*, 24, pp. 322–325.

[3] Xie, J., Wu, S., Pang, L., Lin, J., Zhu, Z. (2012). Influence of surface treated fly ash with coupling agent on asphalt mixture moisture damage. *Construction and Building Materials*, 30, pp. 340–346.

[4] Sharma, V., Chandra, S., Choudhary, R. (2010). Characterization of fly ash bituminous concrete mixes. *Journal of Materials in Civil Engineering*, 22 (1), pp. 1209–1216.

[5] Gürer, C., Selman, G. S. (2016). Investigation of properties of asphalt concrete containing boron waste as mineral filler. Materials Science (Medziagotyra), 22 (1), pp. 118–125.

[6] Do, H. S., Mun, P. H., Keun, R. S. (2008). A study on engineering characteristics of asphalt concrete using filler with recycled waste lime. *Waste Management*, 28, pp. 191–199.

[7] Pasandín, A. R., Pérez, I., Gómez-Meijide, B., Pérez-Barge, N. (2015). The effect of hydrated lime on the bond between asphalt and recycled concrete aggregates. *Petroleum Science and Technology*, 33 (10), pp. 1141–1148.

[8] Chen, J.-S., Wei, S.-H. (2016). Engineering properties and performance of asphalt mixtures incorporating steel slag. *Construction and Building Materials*, 128, pp. 148–153.

[9] Fang, F. T., Chong, Y. C., Nyunt, T. T., Loi, S. S. (2013). Development of environmentally sustainable pavement mix. *International Journal of Pavement Research and Technology*, 6 (4), pp. 440–446.

[10] Chen, M., Lin, J., Wu, S., Liu, C. (2011). Utilization of recycled brick powder as alternative filler in asphalt mixture. *Construction and Building Materials*, 25, pp. 1532–1536.

[11] Wu, S., Zhu, J., Zhong, J., Wang, D. (2011). Experimental investigation on related properties of asphalt mastic containing recycled red brick powder. *Construction and Building Materials*, 25, pp. 2883–2887.

[12] Chen, M., Lin, J., Wu, S. (2011). Potential of recycled fine aggregates powder as filler in asphalt mixture. *Construction and Building Materials*, 25, pp. 3909–3914.

[13] Sutradhar, D., Miah, M., Chowdhury, G. J., Sobhan, M. A. (2015). Effect of using waste material as filler in bituminous mix design. *American Journal of Civil Engineering*, 3 (3), pp. 88–94.

[14] Gezentsvey, L. B. (1960). *Road asphalt concrete*. Moscow, Stroynadat.

[15] Anderson, D. A. (1996). Influence of fines on performance on asphalt concrete mixtures. *International Center for Aggregates Research (ICAR), 4th Annual Symposium.*

[16] European Union. *Directive 2008/98/EC on waste* (Waste Framework Directive). https://ec.europa.eu/environment/waste/framework/.

[17] Downs, R. T., Hall-Wallace, M. (2003). The American Mineralogist Crystal Structure Database. American Mineralogist. 88, pp. 247–250.

[18] Barrett, E. P., Joyner, L. G., Halenda, P. P. (1951). The Determination of Pore Volume and Area Distributions in Porous Substances. I. Computations from Nitrogen Isotherms. *Journal of the American Chemical Society*, 73 (1), pp. 373–380.

VALUABLE ELEMENTS IN WASTE ELECTRICAL & ELECTRONIC EQUIPMENT (WEEE) AND THEIR POSSIBLE RECOVERY METHODS INTRODUCTION

VALÉRIA MÁDAI-ÜVEGES[1] – LJUDMILLA BOKÁNYI[1] –
RICHÁRD ZOLTÁN PAPP[2] – ZOLTÁN SZAMOSI[3] –
ROLAND ROBERT ROMENDA[1] – SÁNDOR NAGY[1]

[1]*Institute of Raw Material Preparation and Environmental Processing*
[2]*Institute of Mineralogy and Geology*
[3]*Institute of Energy Engineering and Chemical Machinery*
University of Miskolc, H-3515 Miskolc-Egyetemváros

Nowadays the amount of waste of electrical and electronic equipment (WEEE) is increasing due to the increasing variety of equipment types, increasing number of users and decreasing lifetime of such equipment. According to the Global E-waste Monitor 2017, by 2016 the world had generated 44.7 million metric tons (Mt) of e-waste and only 20% has been recycled through appropriate channels [1].

The composition and structure of e-equipment is changing fast due to new models and technologies. High-tech equipment contains very valuable materials, such as critical elements. Processing such end-of-life equipment is an inevitable environmental and economic target of the society. According to the new Circular Economy Action of the European Union (EU), the new Action Plan announces initiatives along the entire life cycle of products, targeting for example their design, promoting circular economy processes, fostering sustainable consumption, and aiming to ensure that the resources used are kept in the EU economy for as long as possible.

This paper gives a short introduction to research work in the field of WEEE processing, in the case of Li-ion batteries, LCDs (Liquid Crystal Display), LEDs (Light Emitting Diodes) and SSDs (Solid-State Drive), in the framework of RING 2017 Project. The combination of applied processes is also shown, such as mechanical and chemical-biological treatment methods.

1. LITHIUM-ION BATTERIES

1.1. About lithium-ion batteries

Since the advent of Li-ion batteries in the 1990s, they have been gaining ground as an energy storage cell for electrical devices, especially mobile devices, notebooks, electric and hybrid cars. From their early, rapid spread, it could be expected that after becoming waste, they would occur in large quantities within this type of waste. Pro-

cedures must be developed for their disposal and processing that allow as much as possible of the valuable secondary raw materials contained in them to be recovered.

The batteries are quite simple in structure (batteries of notebooks, mobile phones). Between the two metal electrodes, which are usually copper and aluminum, there is a lithium-based electrolyte and, for charge storage, a separator film between the anode and the cathode [2]. Although these batteries may vary depending on their capacity, size, and manufacturer, the average chemical composition of a typical lithium-ion battery can be given as below [3].

Table 1
Chemical composition of Li-ion batteries [3]

Chemical elements	Weight percentage [%]
Cobalt	7
Lithium	7
Nickel	4
Manganese	5
Copper	10
Aluminium	15
Graphite	16
Others	36

1.2. Safety aspects of the recycling of Li-ion batteries

A battery cell has an anode and cathode for energy storage and for energy load. A battery can be a unique cell or a connection of cells for higher energy load, for example the batteries of laptops. The lithium is oxidized inside the anode to Li^+ and gives an electron. During energy transmission the Li^+ diffuses to the cathode across the electrolyte. During charging the process is the reverse. In case of damage, physical impact, overheat, or short circuit of the Li-batteries the thermal runaway can be started, which results in explosion-like energy release, accompanied by heat and flame.

Possibilities to avoid explosion during recycling

Prior to recycling safety should be considered [5]. The first option to avoid explosion is to discharge the battery fully, which can be done by immersing it in at least 5 m/m% NaCl solution for 48 hours. After the discharging step the device should be dismounted into metal cover, cathode, anode and organic separators. The anode and cathode are crushed in a mill, and then the particles should be sieved at 75 micrometers. The ≤ 75 μm particles are the mixed electrode parts ($LiCoO_2$ and graphite). With that method an explosion can be avoided and 66.75% of the fine powder is $LiCoO_2$ which can be recovered from a Li-battery [4].

The second possibility is that the carefully dismounted batteries are cooled with liquid nitrogen for 5 minutes. This cryogen step makes the battery ineffective in terms of explosion. After the freezing, the end of the top metal cover can be dismounted also and other part of the metal cover of the battery can be cut with a saw with longitudinal slash. Then the inner part of the battery is accessible [6].

There is a research group [7] where the wet crushing of Li-ion batteries was examined. The crusher was a wet cutting mill. Using water every kind of explosion or fire can be avoided.

Some of the researchers do not perform any discharging step to avoid explosion. Dry crushing [7] requires a crusher which is relatively stronger than the common ones, so that in case of explosion it should not be destroyed. The housing of the crusher must be strengthened, which makes the investment cost higher.

1.3. Disassembling

In our research in the mechanical preparation tests the batteries of several mobile phones were disassembled manually. For safety reasons, the batteries were placed in 10 m/m% NaCl solution to reduce the residual voltage below 0.5V. During the manual disassembling, the composition and structure of the examined batteries was determined, so that during the subsequent comminution, it was easier to identify the components in each size fraction. After considering several shredders, hammer mills have proven to be suitable for sufficient liberation without the production of the overground particles. It can be clearly seen from *Figure 1* and *Table 2* that after the separation into particle size fractions, the various components were clearly concentrated in different particle fractions.

It can be seen that the individual foils are enriched in the coarser particle fractions, so an air flow separator and after that an electrodynamic separator can be used to separate them. Using a scanning electron microscope and chemical analysis, the composition of the finest fraction was determined. The most valuable cobalt and lithium materials from the anode and cathode were concentrated in the finest size fraction of <0.5 mm (mass yield of <0.5mm fraction was as high as 42.30%).

Table 2

Component content in the size fractions after shredding

Size fractions x, [mm]	Separator foils, c_{SF} [%]	Aluminium foils, c_{AlF} [%]	Copper foils, c_{CuF} [%]	Plastic and others, c_{PO} [%]	SUM [%]
8…20	34.53	17.82	5.25	42.40	100.00
4…8	14.48	55.24	14.10	16.18	100.00
2…4	10.20	48.80	29.20	11.80	100.00
1…2	14.66	47.41	26.72	11.21	100.00
0.5…1	9.68	64.51	13.98	11.83	100.00
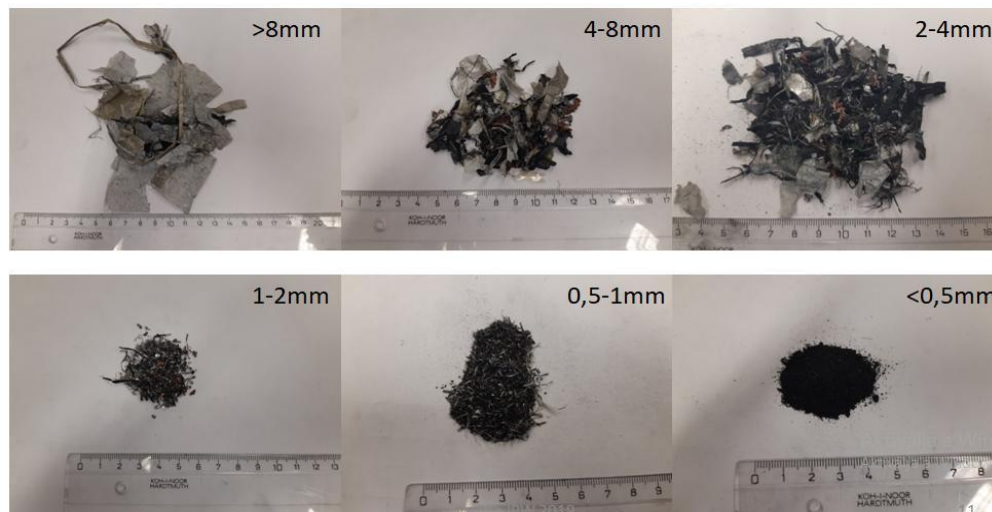
Figure 1.
Size fractions of the lithium-ion battery, shredding by hammer mill [22]

2. SOLID STATE DRIVES (SSD) AND LIGHT EMITTING DIODES (LED)

2.1. SSD processing

The solid state drive (SSD) is a storage device which contains non-volatile memory [8, 9], such as the NAND flash memory introduced in the late 2000s [10]. Due to its benefits like processing speed, durability, and energy consumption, SSD has become the prima donna in the data storage market. Based on data from Statista [11], the shipment of SSD keeps increasing in each quarter of the year, with the last recorded in the second quarter of 2018 being 47.8 million units shipped.

An SSD does not have a moving or rotating part, which makes its components relatively simple, and is only composed of a case containing a Printed Circuit Board (PCB), where several of the main parts are attached. The main components of an SSD are [9, 12]:

- Input/Output Interface or I/O interface: The I/O interface is a connector that connects the power and data to the SSD. Types of I/O in the SSD are SATA, PCIe, and SAS.
- Controller: Manages all functions in the SSD, such as data transmission and allocating data load to flash memory.
- Flash Memory: is where the data is stored. Commonly used flash memory is NAND type.
- Printed Circuit Board (PCB): is a printed board where the three parts above are attached.
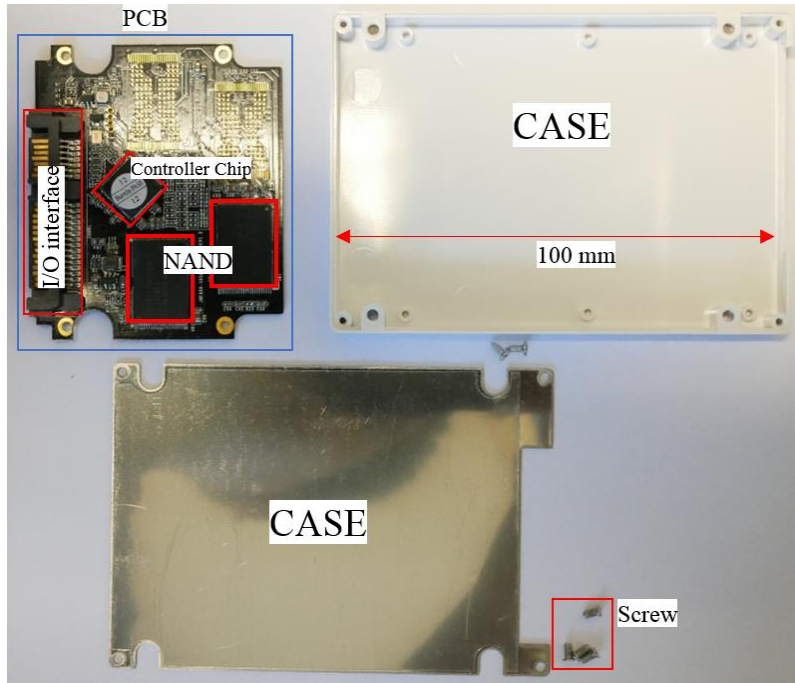
Figure 2
Components of SSD [13]

The average composition of two SSDs (Kingston A400 and Goodram CX400) is shown in *Table 3*.

Table 3
Parts of SSD [13]

Name of part	Mass, m_i [g]	Mass yield [%]
Case	26.0648	70.60
Controller Chip	0.1933	0.52
NAND Chip	1.1052	2.99
Gold Pin	0.2519	0.68
I/O interface	1.2634	3.42
PCB (Base board)	7.4474	20.25
Other	0.5654	1.53
SUM	36.8914	100.00

The weight of SSD mainly depends on the case material, which covers up to 70 m/m% of the total mass of the SSD. The other parts which also can affect the total weight of SSD are the NAND chips. The precious metal found on the surface of the SSD's components is gold (Au), which is found in the gold pins and the vias in the PCB. The material used to attach the component to the PCB is mainly tin (Sn) [13].

The results from the comminution test show the possibility of SSD disassembling by using mechanical means. The PCB is still intact with a little damage on its edge, while some of the components are liberated from the PCB due to the crushing in hammer shredder (type UK 60/40). Moreover, the distribution of the components in the size fractions can be grouped based on the majority of the materials found in them: (1) case materials are concentrated in the ≥ 45 mm size fraction, (2) the PCBs in the 20….45 mm size fraction, (3) the NAND chips in 10–16 mm size fractions, and (4) the gold pins can be found below 4 mm. Based on the distribution of materials in the size fractions, it should be possible to separate the components above from the flow of the comminuted SSD [13].

2.2. CT measurement of LED and SSD

To understand the structure of WEEE parts, computer tomograph (CT) measurements were performed in the 3D Lab of the University of Miskolc using XYLON FF35 Dual tube computer tomography. For imaging of a LED and SSD NAND a FeinFocus 190 kV nano-focus X-ray tube was used. *Table 4* contains the parameters of the measurements.

Table 4
Measurement parameters of the micro-CT imaging

Number of projections	1080
Rotation angle	360°
FOD (focus-object distance)	90 mm
FDD (focus-detector distance)	700 mm
Magnification	8.52x
Voxel size	16.9 μm
High voltage	190 kV
Tube current	260 μA
Scan time	9 min 2 sec
Type on anode	W
Type of filter	Sn; 0.5 mm
Detector framerate	2 Hz

Additional sample preparation for the measurements was not necessary, because the whole samples could be placed in the instrument.

With the help of the CT measurements exact 3D models of the LEDs *(Figure 3)* and SSD NAND *(Figure 4)* can be determined. The macroscopically not observable metal parts can be easily identified and their volume can be estimated.

In the CT images the LED electrodes and the connection between them can be observed. These electrodes contain several different metal layers (indium-titan-oxide

(ITO), gallium nitride GaN), but due to their tiny thickness, the different parts cannot be separated mechanically from each other. The uneven soldering of the electrodes, the plastic cover and the copper film beneath the electrodes also can be recognized.

In the case of the SSD NAND, macroscopically only the black plastic casing and the soldering can be observed. The CT images show the complex, internal metal structure of it with two separated parts and the connections.
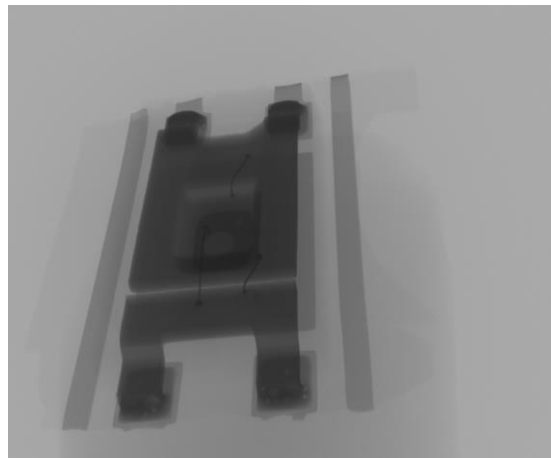
Figure 3
SAMSUNG LED projection
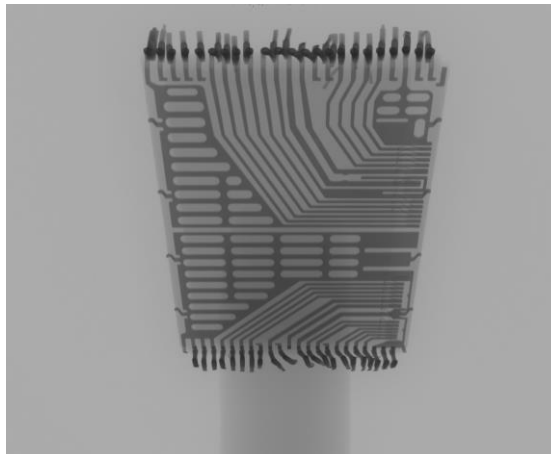
Figure 4
SSD NAND projection

3. RECYCLING OF METALS FROM DISPLAY PANELS AND LEDS BY CHEMICAL AND BIO SOLUBILIZATION

Research in the field of critical raw materials recovery has come into prominence in the last decade. One potential secondary source of these materials is electronic waste. Electronic waste has in most cases a very complex structure and the elements of interest are frequently presented in a thin layer. Many records can be found in literature related to the bioleaching of precious metals from PCBs, but there are only a few recently released publications reporting the bioleaching possibilities on LCD (Liquid Crystal Display) or LED (Light Emitting Diode) substrate [14, 15, 16].Chemical and biological solubilization experiments were carried out in Bioprocessing Laboratory of Institute of Raw Materials Preparation and Environmental Processing in order to solubilize the indium from waste LCD panels, and in a preliminary experiment the potential of bioleaching of LEDs (light emitting diodes) was examined as well.

The main methodological difference between our work and the mentioned in above literature is that the mechanical pre-treatment of the waste LCD panels was carried out before leaching experiments, which was reported by Nagy et al. [17], and later it was proven that the method is highly beneficial regarding mass transfer as well [17, 18]. In the case of LED, SMD 3528 white 2700K type was ground in a planetary ball mill (Fritsch Pulverisette 5) followed by hand sieving at 1 mm gap size to separate the magnetic flocs from the powdered material. The fraction below 1 mm was ground further for an additional 20 minutes, and then separated at 0.315 mm by hand sieving *(Figure 5)*.
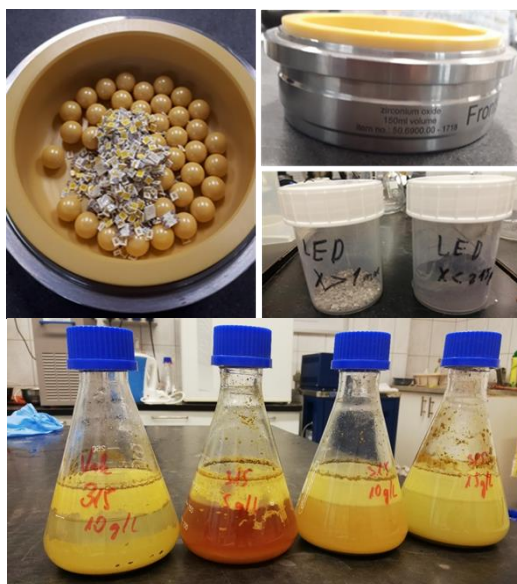
Figure 5 (left)
Fritsch Pulverisette type planetary ball mill and the LED samples before and after grinding, and right: tenth day of the bioleaching experiment (<0,315 mm) [20]

In the case of chemical leaching experiments on an LCD panel, 1M HCl and 1M H_2SO_4 solutions were applied for the single stage leaching and the effect of the temperature and residence time was investigated using a Wise Cube heatable shaker. Furthermore, multistage leaching was also studied using a weak (0.5M) acetic acid in the first stage for selective Fe removal and 1M HCl solution in the second stage in order to recover indium. Comparing the results of chemical leaching test of LCD panels, it was revealed that the 1M HCl solvent was more effective for In solubilisation from the LCD glass as compared with 1M H_2SO_4, since the recovery values were higher under several conditions and the In recovery was almost complete. Considering the alien metal presence in the solution, like Fe, the best leaching parameters were chosen as follows: 1 hour retention time, 55 °C and 1M HCl as solvent at 1 : 1 S/L ratio. Another attempt was when the selective solubilization of iron in weak acetic acid was targeted at first, and In should have been dissolved in the second stage in HCl. This attempt ended with a modest success. Iron was only slightly dissolved in the acetic acid, moreover In was detected as well in the solution of the first leaching stage with 16–19% recovery. The optimal circumstances for the selective dissolution of iron should be further investigated [19].

In case of bioleaching experiments, *Acidithiobacillus ferridurans* (Karitas) and *A. ferrooxidans* (Pech) autotrophic bacteria were used without adaptation to the material source. The bacteria were cultivated for 5 days before the experiments in a Silverman-Lundgren (9K) nutrient solution with Fe_2SO_4 as the main nutrient. The leaching experiments were carried out in a Wise Cube shaker, as in case of chemical leaching experiments, but residence time was varied from 7 up to 17 days, and a constant temperature of 28 °C was kept. The leaching ability of the 9K solution without bacteria was also investigated, the changes in pH were measured, and the metal content of the pregnant solution was analyzed by ICP-OES in case of LCD, and by AAS spectrometry in case of LED solutions.

Based on the results, it was revealed that the formation of jarosite precipitate during bioleaching test is unavoidable, and the co-precipitation or adsorption of the dissolved metals occurs on this precipitate;, therefore, total separation from the residual solid material and further treatment are both necessary. Based on the pH curves *(Figure 6)* it can be stated that when the electronic waste came into contact with the bacterium solution, the pH increased, but after 3 days, it started to decrease. The metal recovery in the solution showed differences between the Karitas and Pech bacteria, and in every experiment, the solution containing the bacterium was more effective than the quasi- sterile 9K solution. *Table 5* shows the experimental data of LCD dissolution experiments.

Indium recovery values from LCD panels obtained in bioleaching experiments were far weaker compared to the chemical leaching, as the best result obtained was 75.53% In recovery in the solution [21], but the reproducibility of this experiment with a different LCD panel sample was not adequate, so further experiments should be performed.

Table 5

Parameters and best results of chemical and biological experiments
on LCD panels

	1M HCl; 1:1 solid to liquid ratio, 55ºC, 1h retention time	9K sterile solution, 1:10 solid to liquid ratio, 7 days retention time	Karitas bacteria containing 9K solution, 1:10 solid to liquid ratio, 7 days retention time
In recovery from LCD (%)	99	68.46	75.53

Our preliminary bioleaching experiments with Karitas bacterium on the LED substrate showed that there is a difference between the bio-leachability of the fraction above 1 mm (magnetic flocs), and the powder fraction. For the bioleaching experiment, the applied 5-10-15 g/L solid:liquid ratio of <0.315 mm LED sample has no inhibitor effect, copper was leached successfully, but the 15 g/L solid concentration of >1 mm LED sample had an inhibiting effect for bacterial metal extraction; this concentration can be toxic, or the powder fraction contains more easily recoverable copper species than the >1 mm LED sample. The inhibitor effect could be seen in case of Sn and Ni for the >1 mm fraction as well, although the recoveries were below 2.25%. In the case of powder fraction, the best Ni recovery was as high as 9%, and it was reached applying the lowest solid concentration. Based on these results, the adaptation of the bacteria to the particular substrate is very desirable.
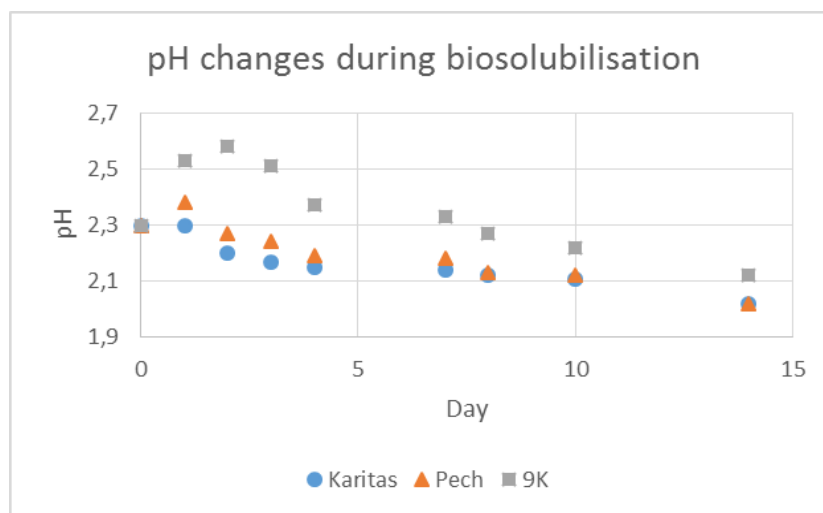
Figure 6

pH changes in course of pre-treated LCD panel bioleaching experiment

4. SUMMARY

Electrical and electronic equipment (EEE) and consequently its waste (WEEE) contains a large number of valuable elements; however, their structural forms (e.g. powder, layer) and composition can differ significantly. The collection method of WEEEs also affects the further processing. From the introduced examples it can be seen that the proper selection of treatment methods and the combination of methods is essential. Usually mechanical preparation should be followed by thermal, chemical or biological techniques. Treatment methods can be designed for each WEEE flow, but the low concentrations and technological changes in EEE production along with incomplete waste collection can significantly encumber recycling and recovery of materials.

REFERENCES

[1] Baldé, C. P., Forti V., Gray, V., Kuehr, R., Stegmann, P. (2017). *The Global E-waste Monitor – 2017*. United Nations University (UNU), International Telecommunication Union (ITU) & International Solid Waste Association (ISWA), Bonn/Geneva/Vienna.

[2] Zhang, Zhengming, Fang, Weifeng, Ma, Ruijun (2019). Brief Review of Batteries for XEV Applications. *eTransportation*, Volume 2, November.

[3] Pagliaro, Mario, Meneguzzo, Francesco (2019). Lithium battery reusing and recycling: A circular economy insight. *Heliyon*, Volume 5, Issue 6, June, e01866.

[4] Yu, J., He, Y., Ge, Z., Li, H., Xie, W., Wang, S.(2018). A promising physical method for recovery of $LiCoO_2$ and graphite from spent lithium-ion batteries: Grinding flotation. *Sep. Purif. Technol.*, Vol. 190, pp. 45–52.

[5] Xu, J., Thomas, H. R., Francis, R. W., Lum, K. R., Wang, J., Liang, B. (2008). A review of processes and technologies for the recycling of lithium-ion secondary batteries. *J. Power Sources*, Vol. 177, pp. 512–527.

[6]   Wang, M., Zhang, C., Zhang, F. (2016). An environmental benign process for cobalt and lithium recovery from spent lithium-ion batteries by mechanochemical approach. *Waste Manag.*, Vol. 51, pp. 239–244.

[7]   Zhang, T., He, Y., Ge, L., Fu, R., Zhang, X., Huang, Y. (2013). Characteristics of wet and dry crushing methods in the recycling process of spent lithium-ion batteries. *J. Power Sources*, Vol. 240, pp. 766–771.

[8]   Baxter, A.: *SSD vs HDD*. [Online]. Available: https://www.storagereview.com/ssd_vs_hdd. [Accessed May 2019].

[9]   Ommi, A. K. Y. (2016). *Solid State Drive (SSD) Overview*. June 2016. [Online]. Available: http://www.tsmtutorials.com/2016/06/ssd-overview.html. [Accessed May 2019].

[10]   Brant, T. (2019). *SSD vs. HDD: What's the Difference?* January 2019. [Online]. Available: https://www.pcmag.com/article/297758/ssd-vs-hdd-whats-the-difference. [Accessed May 2019].

[11]   Statista (2019). *Solid State Drive (SSD) Shipments Worldwide from 2013-2018, by quarter (in million units)*.

[12]   Thierolf, T., Uriarte, J. (2010). *Solid State Drive Architecture*. [Online]. Available: http://meseec.ce.rit.edu/551-projects/fall2010/. [Accessed March 2019].

[13]   Fadhil, Muhammad Faisal, Romenda, Roland Róbert, Papné Halyag, Nóra, Nagy, Sándor (2019). A basic analysis for designing the treatment of solid-state drive (ssd) waste. In.: *III. Sustainable Raw Materials* (Imre Czupy), Soproni Egyetem Kiadó, Sopron, pp. 166–177.

[14]   Jowkar, M. J., Bahaloo-Horeh, N., Mousavi, S. M., Pourhossein, F. (2018). Bioleaching of indium from discarded liquid crystal displays. *Journal of Cleaner Production*, 180, pp. 417–429.

[15]   Willner, J., Fornalczyk, A., Gajda, B., Saternus, M. (2018). Bioleaching of indium and tin from used LCD panels. *Physicochemical Problems of Mineral Processing*, 54 (3), pp. 639–645.

[16]   Pourhossein, F., Mousavi, S. M. (2018). Enhancement of copper, nickel, and gallium recovery from LED waste by adaptation of Acidithiobacillus ferrooxidans. *Waste Management*, 79, pp. 98–108.

[17]   Nagy, S., Csőke, B., Gombkötő, I., Faitli, J., Magyar, T., Oláh, B. (2014). Mechanical preparation of LCD TVs and monitors. In: Yianatos, Juan, Doll, Alex, Gomez, Cesar (ed.). *IMPC 2014, XXVII International Mineral Processing Congress.*, Santiago de Chile, pp. 200–209.

[18]   Nagy, S., Bokányi, L., Üveges, V., Ambrus, M., Gaydardzhiev, S., Mucsi, G. (2018). Influence on various mechanical preparation methods on LCD on the leac-hability of critical elements. *Proceedings of the International V4 Waste Recycling 21 Conference*, Miskolc, pp. 77–87.

[19]   Bokányi, L., Varga, T., Mádai-Üveges, V., Bruncszlik, A., Garai, K. (2014). Recovery of In as a critical element from waste LCD panels. *Proceedings of the 14 th International Mineral Processing Symposium*, pp. 645–651.

[20]   Simon, K. (2019). *Bioleaching processes for waste recycling with Acidithiobacillus ferrooxidans*. TDK work, Univ. of Miskolc.

[21]   Mádai-Üveges, V., Varga, T., Bokányi, L. (2018). Experimental comparison: acidic and bio solubilisation of indium from liquid crystal displays. *Proc. of the International V4 Waste Recycling 21 Conference*, Miskolc, pp. 28–34.

[22]   Orosz Kinga Andrea, Romenda Roland, Mádainé Üveges Valéria, Nagy Sándor (2019). Mobiltelefonokból származó lítium-ion akkumulátorok felépítésének és apríthatóságának vizsgálata. *III. RING – Fenntartható nyersanyag-gazdálkodás konferencia*, 2019. október 10–11., Soproni Egyetem Kiadó, Sopron, ISBN 978-963-334-353-1.

LCD SCREENS AS POTENTIAL SOURCES OF ELEMENTS

V. MÁDAI[1] – V. MÁDAINÉ ÜVEGES[2] – T. KURUSTA[3]

[1]*askcesar@uni-miskolc.hu*
[2]*ejtmuva@uni-miskolc.hu*
[3]*ejttamas@uni-miskolc.hu*
[1]*Institute of Mineralogy and Geology, Faculty of Earth Science and Engineering,
University of Miskolc Hungary*
[2, 3]*Institute of Raw Material Preparation and Environmental Processing,
Faculty of Earth Science and Engineering, University of Miskolc, Hungary*

Abstract: Because of the dramatic growth of liquid crystal display (LCD) production in the last decade, large numbers of used LCD screens are being produced. From the used whole LCD panel, Indium-Tin-Oxide (ITO) nanoparticles can be generated, or indium can be extracted by hydrometallurgy. The recycled glass material is used as a source material for heat and sound insulating fiberglass, or as cement additives it is a valuable Si source. Recycling of this boron silicate glass material is challenging because of contaminating metals like antimony, arsenic, lead, and strontium. In our study ground LCD waste glass was investigated as a potential source of metals. The waste LCD monitors were disassembled by hand and the LCD screen covering plastic layers were dismantled using a thermal shock. After intensive grinding in cutting, planet, and ball mills, a powder finer than 100 microns was investigated by X-ray diffractometry (XRD), scanning electron microscope with energy dispersive detector (SEM EDS), differential thermal analyzer (DTA), and wavelength dispersive X-ray fluorescent spectrometry (WDXRF). Beside the content of almost 6 percent strontium, transition metals like Sn, W, Cr, Ni and Ba were detected in the 1,000 to 5,000 ppm range. Considering the literature, Sr atoms are situated in cyclosilicates, mainly combeite, in the place of Ca. Transition metals are generally found in the islands produced by structure modifiers in the amorphic glass structure or from remnants of the grinding bodies.

Keywords: LCD, X-ray diffraction, scanning electron microscopy, differential thermal analyzer, LCD glass scrap materials

1. INTRODUCTION

Increasing use of equipment containing liquid crystal is part of our modern lifestyle [1]. The life expectancy of these devices amounts to 3–8 years [2], therefore the amount of waste from these devices is constantly increasing [3]. The display panel constitutes over 40% of these types of equipment [4], [5]. LCD glass is a pure, alkali-free material, composed of SiO_2, Al_2O_3, B_2O_3, and alkaline earth oxides [6]. LCD glass is produced by stirrer melting above 1,600 °C, using high-purity raw materials to guarantee the display quality. These glasses have excellent homogeneity. Unlike LCD glasses produced before 2010, current LCD glass materials do not contain toxic

components, which indicates that the resulting waste glass is environmentally friendly. The waste glass can be divided into three categories: 1) LCD cullet from LCD glass manufacturers, 2) LCD process waste glass (LCDPWG) from LCD panel manufacturers, and 3) waste glasses from end-of-life LCD devices (EOLLCDWG). LCD cullet is recycled as a secondary raw material for alkali-free borosilicate fiber glass (so-called E-glass). This material is used for producing alkali borosilicate glass wool or soda lime silicate container glass [7], [8]. LCD cullet is the main raw material to supply B_2O_3 to E-glass and glass wool and can also be used to supply Al_2O_3 to soda lime silicate container glass. The reuse of LCDPWG as a raw material for LCD glass is impossible due to contaminates such as coatings on its surfaces. Introduction of LCDPWG to raw material for the original LCD glass or other colorless glass production produces a slightly grayish color. Many studies have introduced LCDPWG as a raw material in the production of glass-ceramics [9], [10], sintered ceramics [11], insulating foamed glass [12] and cement [13]. In the case of end-of-life LCD waste glass produced before 2010, toxic components such as arsenic and antimony oxide cause serious difficulties in their recycling [6]. Because of it, they are disposed of as unusable waste material [14].

In the present work, EOLLCDWG was examined as a commercial metal source. The results are discussed from the viewpoint of possible sources of the metals and their structural positions in the bearing glass structure. As the EOLLCDWG composition fluctuates considerably depending on the glass supplier, the recycling of it is difficult in a process that is sensitive to composition change. However, as metal sources, these fluctuations are not remarkable.

2. EXPERIMENTAL MATERIALS

In the research project three samples were investigated with L-C, S-C and V-C signs. The L-C and S-C materials are ground glass materials of two market leader LCD manufacturers. In both cases the date of manufacturing is 2017. The third sample (V-C) is a mixture of the first two samples, because in everyday practice the recycling process of used LCD panels is generally manufacturer independent, but in small amounts (less than 10%) it contains LCD material released in 2012. The used LCD screen panels were thermally shocked by heating in furnace up to 200 °C, then they were suddenly cooled down in air and the coating plastic and metal bearing films were taken out by hand. The stripped glass material was crushed and milled in cutting, planet and ball mills. After 40 minutes of milling, the grain size distributions of the samples were measured by Retsch Technology Camsizer X2 laser equipment. The average grain size was under 100 μm. The powders, as bulk samples, were measured by X-ray diffraction (XRD), scanning electron microscopy with energy dispersive detector (SEM EDS), differential thermal analyzer (DTA) and wavelength dispersive X-ray fluorescent spectroscopy (WDXRF).

3. RESEARCH METHODS

3.1. X-ray Diffraction (XRD)

The phase compositions of ground LCD panels were analyzed by X-ray powder diffraction (XRD) method, using a Bruker D8 Discover X-ray spectrometer equipped with Cu anode X-ray source and energy dispersive Lynxeye detector. The grains of the samples were crushed under the size of 5 μm in a ceramic mortar. Mineral phases were identified on the basis of PDF-2 database (release 2010), formalized by the ICDD.

3.2. Scanning Electron Microscopy with Energy Dispersive Detector (SEM EDS)

The morphology and approximate elemental content of milled LCD material was determined using scanning electron microscopy (SEM). The observation was made by means of a Jeol 8600 Superprobe electron microscope, equipped with an energy dispersive spectrometer (EDS)-based system for elemental composition analysis. The powder samples for SEM investigations were coated with an approximately 50 nm layer of carbon to achieve conductivity on the sample surfaces.

3.3. Differential Thermal Analyzer (DTA)

The thermal dependent properties, like endothermic or exothermic reactions, together with mass increases or reductions were investigated by computer-controlled MOM Derivatograph-C equipment. Heating rate was 10 °C/min, heating range was from 20 °C up to 1,000 °C. The original powder sample masses were under 0.5 g, generally 0.1 or 0.2 g. Results were analyzed by the MOM developed WinderC software.

3.4. X-ray Fluorescent Spectroscopy (XRF)

The elemental compositions of ground samples were measured by a wavelength dispersive Rigaku Supermini 200 type benchtop sequential spectrometer. The X-ray source was an air cooled Pd-anode with 50 kV voltage, 4.00 mA heating current and 200 W power. Primary beam filter was Zr. Reflecting crystals for the wavelength dispersive technology were: LiF(200), PET, and XR25 crystals. The grains of the samples were crushed under the size of 65 μm in a ceramic mortar, than they were dried out at 120 °C for 2 h. From the already dried powders, 0.2 g were measured out and mixed by Cereox binder (ultra-pure and fine polyethylene powder) and homogenized in an agate mortar. These mixtures were pressed into pellets of 32 mm diameter by pressure of 25 tonnes. Both the calibration and measuring of each element was done at 1.2–1.6 Pa pressure with the Rigaku ZSX driver and evaluation program.

4. RESULTS AND DISCUSSIONS

The X-ray diffraction *(Figure 1)* showed mainly amorphous, rather non-crystalline phases in every sample.
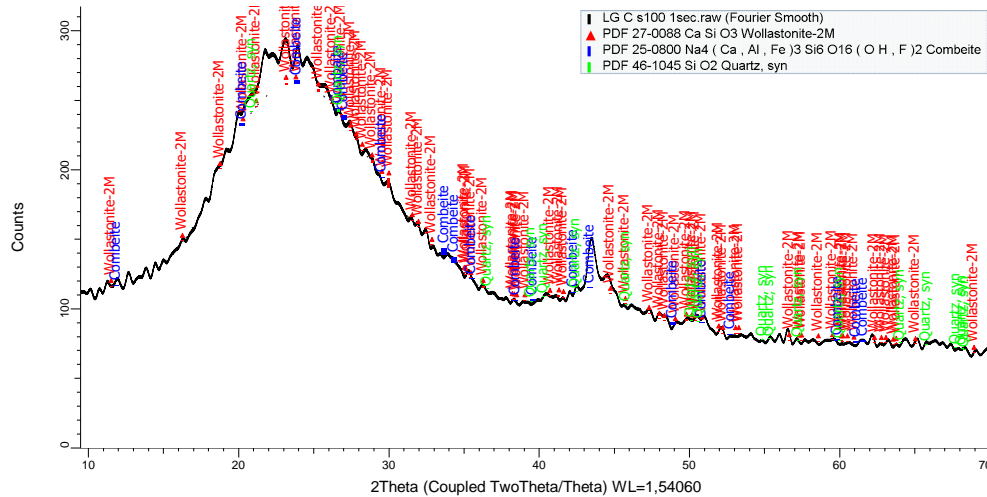
Figure 1

Fourier smoothed X-ray diffraction pattern of L-C sample. Identifiable main crystalline phases are wollastonite, combeite and quartz. The glassy phase, with high amorphous content, can be seen in the form of extended area under the wavy baseline.

Instead of well reflecting oxide remnants, Al-Si-Ca dominated glass (short range ordered) phases was identified. Similar results were generated by electron microscopic (SEM EDS) investigations: mainly Si-Al dominated grains, and some Ni, Fe and Cr dominated patches appeared *(Figure 2)*.
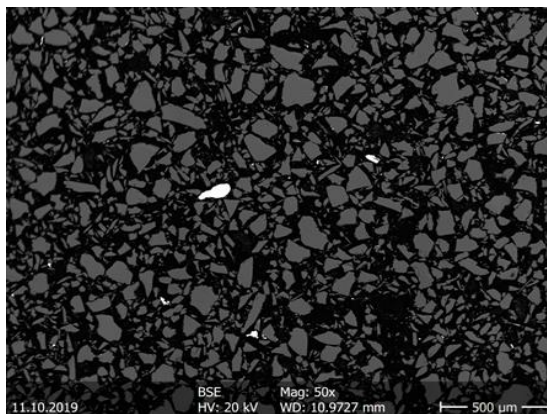
Figure 2
Scanning electron microscopic picture of L-C sample. Grains dominated by high atomic numbers are bright patches in the middle section of the picture. The surrounding dark gray materi-al is composed of glass grains, mainly with Si-Al elemental composition.

From the literature, the X-ray diffraction pattern can be explained as reflections of wollastonite, combeite and quartz structures, in a glassy (Q1-Q2) type matrix. In the combeite structure the Ca is substituted by Sr (Fujikura et al. 2012).

In every sample, on the elemental maps of the electron microprobe *(Figure 2)*, among the glass dominated powder grains (dark green glass grains), the high atomic numbered metal bodies (white patches) are remnants of the grinding bodies of the mills of high energy cutting and crushing, or broken parts of the not completely removed foils of the LCD screen structure.

The thermal behavior was very similar in the case of the three samples. On the thermogravimetric curve (smoother green line) of the thermal analytical pattern *(Figure 3)* after a significant mass reduction some very poor but identical mass increases appear, while later mass decreases can be seen.
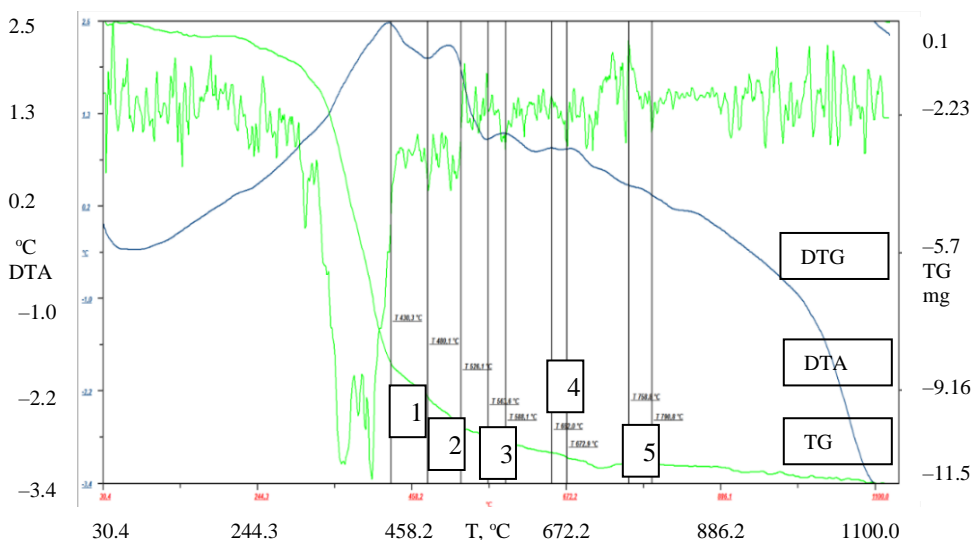
Figure 3
Differential thermal analytical pattern of L-C sample. Contiguous smoother green line is thermogravimetric (TG) curve. The extensively alternating green curve is differential TG (DTG) pattern. Blue shows the differential thermal analytical (DTA) curve. Vertical straight lines are on the borders of slight mass increases: tiny hills on the TG curve. Some of the possibly metal oxide productive phases are 1, 2, 3, 4, and 5. The left vertical axis shows the changes of temperature of the sample (DTA) (°C). Horizontal axis is scaled in temperature (°C), and on the right side, vertical axis is scaled for TG in mass (mg).

From left to right between the black vertical lines, five small heaps can be identified (marked with numbers). The first two (1, 2) are right beside each other. The others (3, 4, and 5) are more distinct. Considering the literature, the first serious mass decrease is caused by the remnants of coating film evaporation or oxidation. When

repeating the heating in a traditional furnace, a strong smell was sensed. The cause was organic material (plastic film remnant) oxidation [15]. As the temperature increases, fine mass increases are detected, showing the results of oxidation of metals. Following this, slight mass reductions can be seen on the TG-curve, which are the deteriorations of the formerly generated metal oxides [16].

The three samples showed similar element content. From the WDXRF measurements *(Table 1)* Si-Al-Ca dominated materials can be identified, but Sr (6%) and Cr, Ni, Sn and W (about 0.1%) and In (about 0.03%) were also measured. The main elements were measured as oxides in mass percent (m/m%). Every other constituent was measured in ppm.

Table 1

Element and metal-oxide constituents of the three samples measured by WDXRF method

Elements (oxides)	SiO_2	Al_2O_3	MgO	CaO	Na_2O	K_2O	Fe_2O_3
Sample/Unit	m/m%	m/m%	m/m%	m/m%	m/m%	m/m%	m/m%
L-C	56.7	12.5	0.32	9.08	0.08	0.18	1.60
S-C	60.4	13.5	0.38	9.46	0.10	0.18	2.28
V-C	63.1	14.3	0.98	9.38	0.10	0.16	2.32
Elements	Cl	Ga	Br	Mo	In	Sn	W
Sample/Unit	ppm	ppm	ppm	ppm	ppm	ppm	ppm
L-C	505	51	20	187	379	2,198	899
S-C	479	40	27	348	361	2,174	1,087
V-C	249	N.A.	20	301	280	1,533	1,089
Elements	Hg	Cu	Sr	Ba	Cr	Co	Ni
Sample/Unit	ppm	ppm	ppm	ppm	ppm	ppm	ppm
L-C	305	1138	59,200	5,600	2,110	276	1,528
S-C	258	50	57,200	5,700	2,944	358	2,166
V-C	216	42	31,600	2,500	2,760	438	2,096

From *Table 1* and *Figure 4* it can be clearly seen that each material was rich in metals. The light element (C, H, O) cannot be seen in *Table 1*, because the WDXRF spectrometer is unable to detect this elemental group. Cl as a detected light element comes from the plastic parts of the screens, or together with Br can be chemical components of pigment green 36. The highly transparent type of this substance is used in color filters in the LCD and TFT displays [17]. At the same time chlorine and bromine as additives decrease the glass melt viscosity. The source of Ga in the LCD–TFT panels may be the amorphous oxide semiconductor indium-gallium-zinc-oxide (IGZO). IGZO was introduced as a new TFT channel material from 2004 [18]. Gallium in glass technology plays a crucial role. In ternary As containing colorless glasses, Ga, In and other transition elements are main glass components [19]. Molybdenum is used in limited amounts as a single layer for a gate or S/D electrode and as a metal electrode for smaller panel sizes of less than 20″. This metal also has good

direct contact resistance properties with ITO or IGZO pixel electrodes, and is used as an amorphic Si diffusion barrier or capping layer for Al or Cu electrodes [18] The sources of In and Sn are the ITO layer remnants.
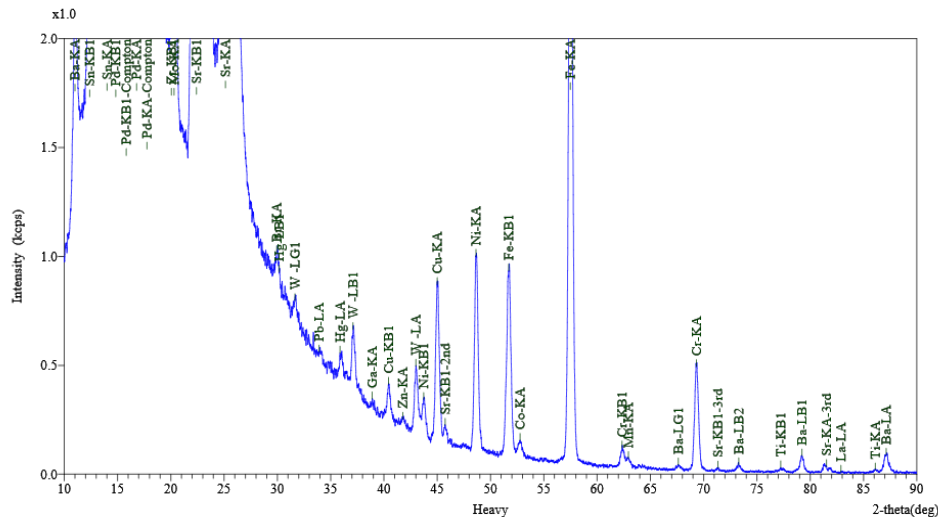
Figure 4

Results of WDXRF measurement of L-C sample. Peak intensities in kilo counts per second. The material is rich in Fe, Sn, W, Cu, Sr, Ba, Cr and Ni

Tungsten is generally applied in low-temperature poly-silicon technology type TFT screens. In these high resolution LCDs, molybdenum or molybdenum–tungsten alloys are used mainly as gate metal because of their low resistance, good etchability, high temperature stability and controllability of layer stress [18]. Mercury can be present as pollution on the surfaces of glass grains from the possible contact with broken cold cathode fluorescent lamps containing high amount of mercury vapor. From the viewpoint of glass technology Hg is a reducing agent through the color controlling processes in glass production [19]. For larger monitors and TVs, Cu and Al alloys are used to produce low-resistance bus lines. These alloys of source-drain electrodes require under- and capping layers for ohmic contacts and contacts with pixel electrodes [18]. Moreover, Cu can be used in glass technology as a color modifier. For similar purposes iron, chromium, and nickel are applied individually or in a mixture of iron to undergo redox reactions with copper during the processing of alkali borosilicate glasses [20]. Sr as a glass additive may favor the formation of Q2 ring structures at the expense of chain structures in the glasses. Ring silicate structures may result in a more expanded glass network generation [21].

The addition of barium to the glass-structure increases the refractive index and at the same time Ba is a basic glass forming element [19]. Cr with low thin film resistivity was used as data line metal for TFT-LCD in the early days of notebook PC production,

but nowadays, because of environmental considerations, it has been replaced by Mo [18]. During laser chemical vapor deposition process of the thin film transistor's open-circuit repair method, because of the high resistivity of tungsten and molybdenum, cobalt is used [18]. At the same time Mo, W, Cr, Co, Ni, are steel additives. Their presence in the investigated material might be the results of mechanical or mechano-chemical reactions between the grinding bodies and crystallized-semicrystallized glass material that took place during the high energy grinding process.

5. CONCLUSIONS

In our research, three samples were examined showing similar material properties. In two cases, the investigated panels were grouped by the type of producer. Two WEEE samples came from two used LCD panels produced in 2017 by two market leader companies. The third one was a mixture of the former two and in a small amount (less than 10%) it also contained LCD material released in 2012, because in recycling technology different types of LCD equipment are handled. X-ray diffraction showed a glassy but partly crystallized material. The main phases were wollastonite, combeite and quartz. Electron probe analyses showed mainly glassy particles with some high atomic numbered patches, which are individual metallic grains. Thermal measurement showed a mainly glassy material with some plastic remnants and a low amount of metal components. In WDXRF measurements, the metal contents of these LCD glass scrap materials were surprisingly high: the examined WEEE materials were Si-Al-Ca dominated waste, but were a promising source of elements such as Sr, (6%) Sn and In (about 0.1%, respectively), and the amounts of W, Cr and Ni were interestingly high as well (about 0.03%).

Three main elemental sources can be identified explaining the metal content. One part of the detected metals comes from the remnants of the not perfectly removed thin film transistor layer. The TFT layer was removed by hand before the crushing and milling processes, applying fast heating up in a furnace and cooling down on free air. The other source is the glass material itself. The third elemental bearing source is the pigment material in the LCD structure.

REFERENCES

[1]   Hermans, J. M.; Peelen, J. G.; Bei, J. R.: Recycling of the TV glass: profit ordoom? Am. Ceram. Soc. Bull. 2001, 80, pp. 51–56. In: Góra, J., Franus, M., Barnat-Hunek, D., Franus, W. (2019). Utilization of Recycled Liquid Crystal

Display (LCD) Panel Waste in Concrete. *Materials,* 12, p. 2941; DOI:10.3390/ma12182941.

[2] Guo, Y. J.; Liu, Q.; Qiao, Q.; Liang, J.; Yang, D.; Ren, Q.: The processing and management of the thin film transistor of the waste liquid crystal display. J. Environ. Eng. Technol. 2011, 1, 168–172. In: Góra, J., Franus, M., Barnat-Hunek, D., Franus, W. (2019). Utilization of Recycled Liquid Crystal Display (LCD) Panel Waste in Concrete. *Materials*, 12, p. 2941, DOI:10.3390/ma 12182941.

[3] Miklósi P. (2005). Elhasznált LCD-eszközök hasznosításának lehetőségei. *X. Fiatal Műszakiak Tudományos Ülésszaka*, Kolozsvár, 2005. March 18–19. DOI: 10.36243/fmtu-2005. 34.

[4] Cramer, S. C.; Schmidt, F.; Clasen, R.; Jasen, S. (1995). Recycling of TV-glass: Problems and perspectives. *Glastech. Ber. Glass Sci. Technol.*, 68, pp. 191–196.

[5] Menad, N. (1999). Cathode Ray Tube Recycling. *Resour. Conserv. Recycl.*, 26, pp. 143–154. [CrossRef]

[6] Ellison, A., Cornejo, I. A. (2010). Glass substrates for liquid crystal displays. *Int. J. Appl. Glass Sci.*, 1, 87e103. https://doi.org/10.1111/j.2041-1294.2010. 00009.x.

[7] Kim, K., Hwang, J. (2011). Recycling of TFT-LCD cullet as a raw material for fibreglasses. *Glass Technol. Eur. J. Glass Sci. Technol.*, Part A, 52, 181 e184.

[8] Kim, K., Kim, K., Hwang, J. (2014). Thin film transistor-liquid crystal display cullet: a raw material for production of commercial soda lime silicate glasses. *J. Clean.Prod.*, 79, 276e282. https://doi.org/10.1016/j.jclepro.2014.05.036.

[9] Lin, K. L. (2007). Use of thin film transistor liquid crystal display (TFT-LCD) waste glass in the production of ceramic tiles. *J. Hazard. Mater.*, 48, (1e2), 91e97. https://doi.org/10.1016/j.jhazmat.2007.02.004.

[10] Fan, C. S.; Li, K. C. (2013). Production of insulating glass ceramics from thin film transistor-liquid crystal display (TFT-LCD) waste glass and calcium fluoride sludge. *J. Clean. Prod.*, 57, 335e341. https://doi.org/10.1016/j.jclepro. 2013.06.002.

[11] Kim, K., Kim, K., Hwang, J. (2015). LCD waste glass as a substitute for feldspar in the porcelain sanitary ware production. *Ceram. Int.*, 41, 7097e7102. https://doi.org/10.1016/j.ceramint.2015.02.018

[12] Lee, C. T. (2013). Production of alumino-borosilicate foamed glass body from wasteLCD glass. *J. Ind. Eng. Chem.*, 19, 1916e1925. https://doi.org/10.1016/ j.jiec.2013.02.038.

[13] Lin, K. L., Chang, W. K., Chang, T. C., Lee, C. H., Lin, C. H. (2009). Recycling thin film transistor liquid crystal display (TFT-LCD) waste glass produced as glass ceramics. *J. Clean. Prod*., 17, 1499e1503. https://doi.org/10.1016/ j.jclepro.2009.05.012.

[14] Bihlmaier, A., Volker, M. (2013). WEEE scrap optical glass for the production of foam glass-foaming properties and heavy metal release. *Glass Technol. Eur. J. Glass Sci. Technol*., Part A, 54, 42e44.

[15] Cui, Q. B., Aimin, L., Ningbo, G. (2013). Combustion and Pyrolysis of Electronic Waste: Thermogravimetric Analysis and Kinetic Model 2013. *International Symposium on Environmental Science and Technology* (2013 ISEST) Procedia Environmental Sciences 18, pp. 776–782. DOI: 10.1016/j.proenv.2013.04.104.

[16] Ortuño, N., Conesa, J. A., Moltó, J., Font, R. (2012). Thermogravimetric Study of the Decomposition of Printed Circuit Boards from Mobile Phones. *19th International Symposium on Analytical and Applied Pyrolysis* At: Linz (Austria).

[17] Kadish, K., Guilard, R., Smith, K. M. (2003). *The Porphyrin Handbook. Applications of Phthalocyanines*. Elsevier Science, Vol. 19, Academic Press.

[18] Souk, J., Morozumi, S., Luo, F-C., Bita, I. (eds.) (2018). *Flat Panel Display Manufacturing*. John Wiley and Sons Ltd., https://www.wiley.com/en-hu/Flat+Panel+Display+Manufacturing-p-9781119161349

[19] Vogel, W. (1994). *Glass Chemistry*. Springer-Verlag, Berlin, Heidelberg, 2nd edition, DOl: 10.1007/978-3-642-78723-2.

[20] Henry, N., Deniard, P., Jobic, S., Brec, R., Fillet, C., Bart, F., Grandjean, A., Pinet, O. (2004). Heat Treatments Versus Microstructure in a Molybdenum-rich Borosilicate. *Journal of Non-Cryst. Solids*, 333, pp. 199–205.

[21] Fujikura, K., Karpukhina, N., Kasuga, T., Brauer, D. S., Hill, R. G., Law, R. V. (2012). Influence of Strontium-Substitution on Structure and Crystallisation of Bioglass® 45S5. *Journal of Materials Chemistry*, 22, p. 7395. DOI: 10.1039/C2JM14674F.

ANALYSIS OF CRITICAL RAW MATERIALS THROUGH THE EYES OF ECONOMISTS

BEATRIX VARGA – KITTI FODOR

Intstitute of Economic Theory and Methodology, Faculty of Economics,
University of Miskolc, Hungary
stbea@uni-miskolc.hu

Abstract: In recent times there have been many changes in the world. New technologies are constantly evolving and the pace of change is accelerating. If this trend does not change, it will become increasingly difficult to say what new changes the future holds. The impact of these developments can be felt in many areas of life. One such area is critical raw materials (CRM). Due to the actuality of the topic and the fact that CRM are related to all areas of life, we had the opportunity to examine the raw materials from several perspectives, including a historical overview and statistical analysis. In this paper, our aim is to summarize the results of the last research period.

Keywords: critical raw materials (CRM), cluster analysis,

1. CRITICAL RAW MATERIALS IN HISTORY

The history of mankind and the use of mineral resources are closely linked. We can associate each historical period with raw materials that are necessary for the development of that period. Ages go, raw materials come. Throughout the history of mankind, we have witnessed the rise and disappearance of raw materials. So we examined which raw materials were of strategic importance in each historical period, in other words, which were the critical raw materials for the economic development of those periods.

Obsidian and flint were strategically the most important raw materials during prehistoric times, because they were easily cracked and made into arrowheads, which were essential for getting food. The use of different metals became possible only when fire could be harnessed for forging. Copper was the first raw material for the production of metal tools. With the development of alloying technology, around 4000 B.C., we reach the Bronze Age. Bronze is an alloy of copper and tin and is harder than copper. The appearance of iron marks the end of prehistoric times.

Let us start the list of minerals from ancient times with halite. Salt was an essential raw material in ancient times for the preservation of food, and accordingly it was very expensive. At the end of the 8th century in the Chinese Empire, more than half of the government revenue came from the salt tax. In ancient times, seven metals enjoyed a key role: lead, gold, silver, iron, mercury, tin, and copper. In ancient states, precious metals were primarily used as money or made into jewelry. Lead was often used for making jewelry or sarcophagi. From ancient times to the late Middle Ages, lead acetate was used as a sweetener and as an ingredient in cosmetics. In other

words, half of the empire was poisoned with lead, and the poisoning of the rich was more intensive. Symptoms of lead poisoning can be observed in several Roman emperors, including Claudius, Caligula and Nero. Already in ancient times the strategic raw materials of later days – coal and oil – were being used. Coal mining began industrially in England in the 13th century. Coal was used for heating and for the production of high-quality steel, and oil was used as a medicine or insecticide. From the mixture of petroleum and burnt lime came the "Greek fire", one of the most formidable weapons until the invention of gunpowder in 1350.

The next important stage is the Industrial Revolution. In heavy industry, the appearance and spread of steam engines multiplied the required amount of iron and coal. Demand for coal and iron further increased due to the rapid construction of railways and thus iron and coal mining gained in importance. Brick was increasingly used in the field of architecture. The mass production of the automotive industry required many new materials, such as gasoline, rubber, plastics, batteries and glass. Even at this time, coal was the main source of energy, but at that time the use of crude oil had also begun.

The period between the two world wars is extremely important in the history of flight, as it is when regular air travel began. After World War II, space exploration began developing more dynamically and soon tourists will be moving into space. However, during this period, further changes were made in the field of science and technology. Microelectronics was developing at an ever faster rate, which was necessary for the development and spread of mass communication and telecommunications. All of these technical solutions required the use of newer raw materials.

In the 1970s, world models of earth threats emerged, in which separate chapters were devoted to extremely diminishing raw materials. Meadows et al. in their book *The Limits to Growth* (1972) [1] considered the depletion of eight stocks of metal as critical in view of the known world reserves [2]-[4]. Fortunately, their dire predictions have not materialized up to this point, which may be due to changes in technology and the search for newer reserves *(Figure 1)*.
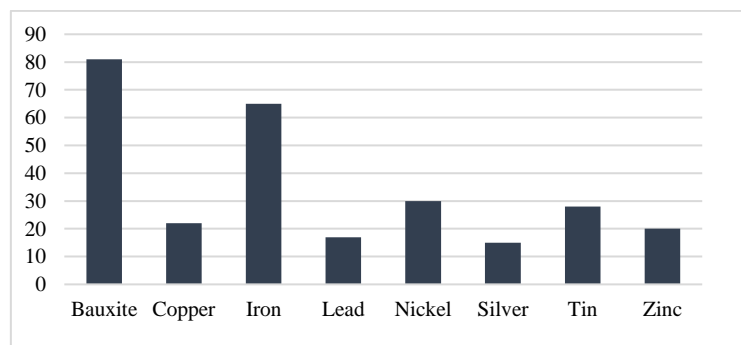
Figure 1
Expected lifetime of known stocks with 2% annual increase in production (years)
Source: Meadows, 1992

2. CRITICAL RAW MATERIALS IN THE 21ST CENTURY

Today, there is another industrial revolution that we are part of. The "steam engines" of this new revolution are cyber-physical systems and digitalization. Many new information and communication technologies have emerged and are spreading. We have smartphones in our pockets, flat-screen smart TVs in our homes, laptops and computers in our offices. In addition, the use of electric cars and drones is spreading. New innovations not only change our daily lives, but rewrite again and again the list of elements to which we attach strategic importance. Countries and organizations have responded to these changes and are monitoring the changes.

The European Commission has also recognized this change and since 2011 has been paying close attention to the evolution of critical raw materials. The European Commission categorizes those raw materials as critical that are of high economic importance and have a high supply risk [5]–[13].

There is no generally accepted, "worldwide" method for identifying critical raw materials, which means that the same raw materials are not necessarily strategically important raw materials for each country. A comparison of the critical raw material lists of the United States of America and of the European Commission shows that arsenic, cesium, rubidium, strontium and uranium were not included in the European Commission's survey at all, and that aluminum, chromium, lithium, manganese, potash, rhenium, tellurium, tin, titanium and zirconium are not considered critical by the European Commission, but have been identified by the Americans as critical raw materials [6]–[15].

These raw materials play a key role in today's technology, which is especially true for high-tech electronics and mechanical engineering, since it is difficult to find an element in the periodic table that would not be used in these production areas. For production they are required only in small quantities, but they have unique properties and special application areas. These factors make their substitution difficult.

In many cases, these rare raw materials are mined in politically unstable countries, and often these countries have a monopoly or oligopoly in terms of production. For example, the Democratic Republic of the Congo is an important country for cobalt mining. This country was ranked by the Fund for Peace in 2020 as the 5th most fragile country in the world [16]. However there is a country which has a key role in the mining of not only one critical raw material: China controls 90% of the rare earths market, and thanks to that power, it can dictate not only prices but also access to certain raw materials [17]–[18].

3. CRITICAL RAW MATERIALS FROM STATISTIC VIEW

In addition to reviewing each historical age, we examined raw materials using statistical tools. We created a database based on the research of the European Commission that contains 73 raw materials; 54.8% of these elements were categorized as critical in 2017. The database includes 15 variables, for example the name of the raw material, supply risk, economic importance, EU import reliance, end-of-life re-cycling input rate, major world producers and critical classification in 2011, 2014, and

2017. We had two goals for the statistical analysis, for which we chose two methodologies: cluster analysis and logistic regression.

3.1. Logistic regression

Logistic regression is a method for classifying observation units, in which these individuals are classified into predefined groups of the dependent variable. Using logistic regression, we created a complex model consisting of two regression models. Raw materials were classified as critical by the complex model which were considered critical by both regression models; however, if only one or neither of the models rated a material as critical, then the given raw material was not considered critical according to our analysis.

The explanatory variables in the first regression model were economic significance (EI) and supply risk (SR), while the explanatory variables in the second regression model were end-of-life recycling rate, EU import dependence, and the ratio of primary producer volume. In both cases, the dependent variable was an alternative variable that shows whether or not the raw material was classified as critical in 2017 by the European Commission.

Both regression models have high classification accuracies of 88.7% and 93.2%. In total, only three raw materials – hafnium, silicon, and tantalum – were misclassified. Of these, tantalum and hafnium are located on the border of critical and noncritical raw materials, which is also supported by the diagrams in *Figure 2*.
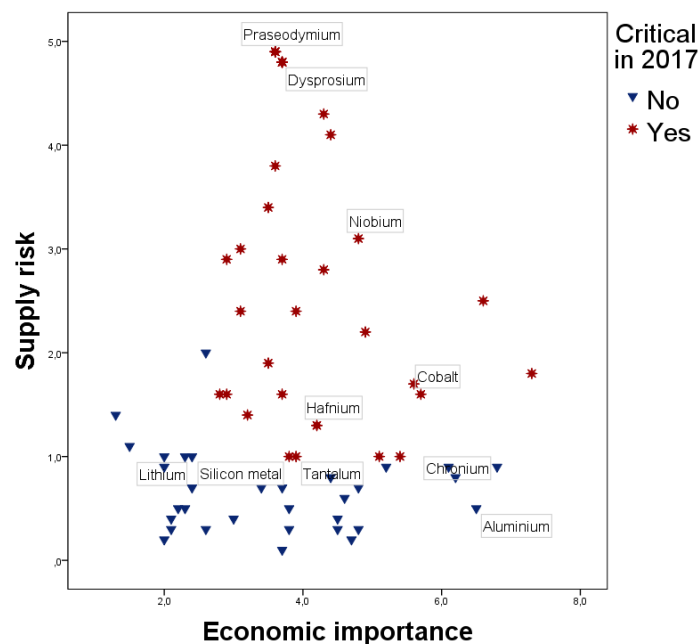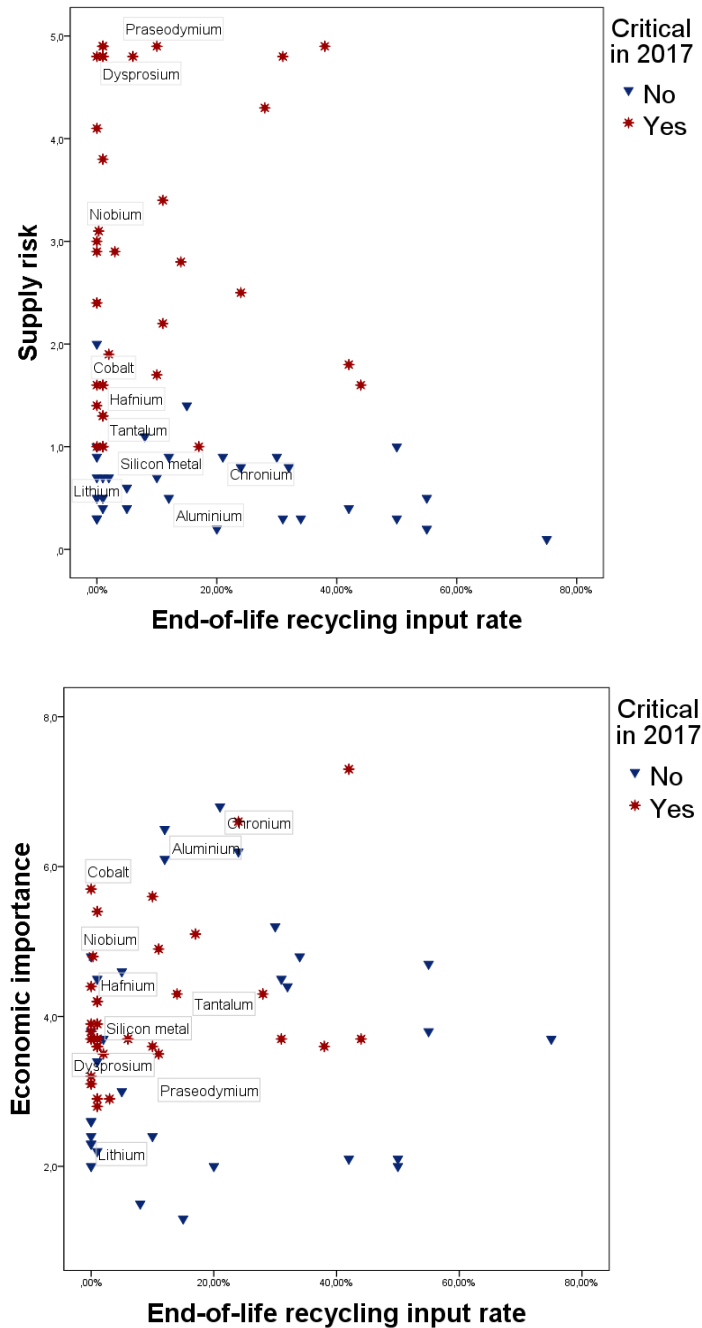
Figure 2
Representation of raw materials based on economic importance, supply risk,
end-of-life recycling input rate
Source: Own editing based on the data of European Commission

The upper left-hand chart in *Figure 2* shows the representation of the examined raw materials according to their economic importance (x axis) and supply risk (y axis). It can be observed that non-critical raw materials (in blue) are basically located at the bottom of the figure, i.e. the supply risk of these raw materials is low. The upper right-hand chart shows the raw materials by supply risk (y axis) and recycling rate (x axis). The dimensions of the third, lower figure are economic importance (y axis) and recycling rate (x axis). All three figures suggest that the boundary between the two groups is not sharp if we categorize materials along only two dimensions.

Therefore, in the next section, we discuss the conclusions that can be drawn if the variables used in *Figure 2* are considered simultaneously. The result of this is reflected in *Figure 3*.

3.2. Cluster analysis
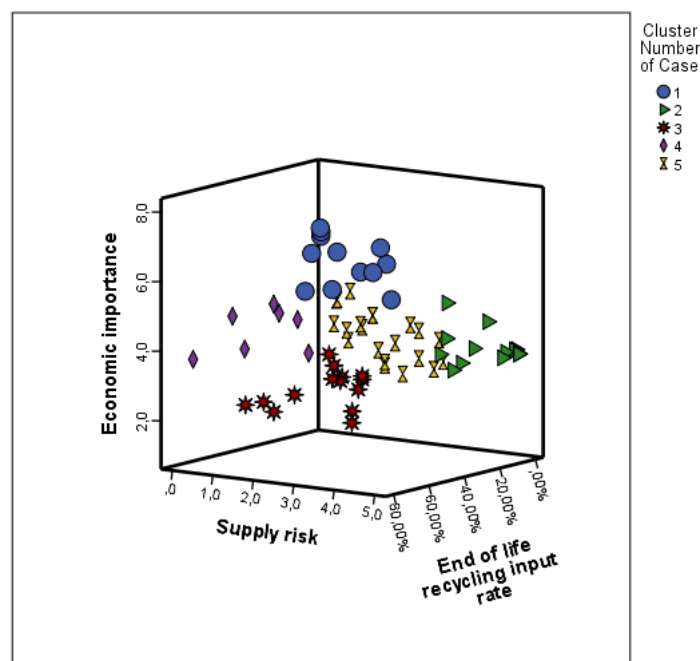
Figure 3
Raw material clusters in 3D scatter
Source: Own editing, SPSS output

Another goal is the identification of groups with the help of hierarchical cluster analysis and the identification of clusters that are important from the perspective of innovation. Cluster analysis means the grouping of items that are similar to each other, and its goal is to categorize the observed units into homogeneous groups. There are several methods of cluster analysis to choose from, for example hierarchical and

partitioning methods, model-based methods, etc. Each method has its own advantages and disadvantages, and we strove to perform our analysis keeping this in mind. We chose hierarchical cluster analysis because there was no a priori information about the number of the clusters, and the hierarchical method can help in defining the number of clusters. Further information regarding our analysis will be addressed in the following parts of the study [19]–[22].

So our goal was to assign the raw materials into homogeneous groups. Presumably, this can help with the identification of important raw materials in regards to innovation. The clusters were based on EI (economic importance), SR (supply risk) and EoL (End of life recycling input rate). Since the scaling of these three variables is different, standardization was used. The SPSS software package offers several options when it comes to standardization, and we chose "z-score" from these. We paid extra attention to the management of outliers. The identification of outliers was done with the "nearest neighbor" method. We identified two outliers, which were magnesium and titanium.

Based on a dendrogram, we reached the conclusion that the creation of 5 clusters would be ideal. We used Ward's Method and Squared Euclidean distance. As the three-dimensional scatter plot *(Figure 3)* shows, the groups are nicely separated from each other.

For validation we used the Rand Index. The Rand Index is a measure of the similarity between two clusterings. Based on Table 1, the value of the Rand Index is 0.961. This means that similar groups were created using the two methods.

Table 1

Rand Index results

			Cluster method 1		Total
			Pair assigned to		
			the same cluster	different cluster	
Cluster method 2	Pair assigned to	the same cluster	490	56	546
		different cluster	42	1897	1939
Total			532	1953	2485

Source: Own editing

For testing the internal validity we used the Average Silhouette Width (ASW). The mean of the values was 0.5 and the maximum was 0.772. We did not get a negative value. In the case of silhouette calculations, a value close to 1 indicates that the clustering can be considered good for the given cluster number, so we can conclude that the clustering can be considered moderately good.

The highest values were in the first and second groups, which are extremely important for innovation. The lowest value was in the third group. This may be because the classification of materials in this group is constantly changing. More information about this will be included in the characterization of the clusters.

The main characteristics of the resulting clusters can be summarized as follows:

The first cluster was named 'Innovation dependent' because this group has the highest economic importance. Only 1% of the world's production takes place in Europe, so import dependence can also be considered high. From the exceptionally high economic importance, we concluded that the members of this cluster are key players in today's technological innovations. This is also indicated by the presence in the group of cobalt, which is required for the lithium-ion battery of electric cars.

The next cluster contains "Treasures of Asia". The raw materials in the second cluster are of medium economic importance, but their supply risk is extremely high. The reason is that their production in Europe is minimal. The main producer, with the exception of ruthenium, is located in Asia.

The members of the third cluster are the "Emerging Criticals". Europe yields 10% of the world's total production, so the dependence on import is also moderate. However, the analysis of the EU confirms that these raw materials are becoming increasingly important, since a growing number of them are classified as critical.

The name of the fourth cluster is "Harmless". The raw materials in this group have neither a significant supply risk nor high economic importance. One third of global production comes from Europe and most of the major producers are located outside of Asia. In 2017, none of the raw materials in the cluster received a critical classification.

The last, fifth cluster is characterized by moderate-high economic importance and the lowest supply risk. The recycling rates of these materials are high. The group was named "Recyclables".

3.3. Comparison of the results

As mentioned above, the classification of three raw materials using our complex model also proved to be incorrect. Based on the European Commission's analysis in 2011 and 2014, these elements were not classified as critical, or only in one year, but in 2017, all three had become critical. This changed position is also supported by our cluster analysis, in which all three elements were located in the same cluster, which we call "Emerging Criticals".

4. CONCLUSION

The topic of critical raw materials through the ages is a good illustration of the changing world we live in, and it is changing even faster now than before. As the years have passed, technology has evolved, demands have grown, and different raw materials have become strategically important.

To answer the question of what will come in the future is not easy. Not only newly discovered deposits can provide a solution, but also, as we mentioned, new or partially new technologies. For example the newest model of Lamborghini, the Lamborghini Sian, debuted in autumn 2019. This is a hybrid car whose special feature is that energy is stored with capacitors. The capacitors are recharged during braking, and the car is able to drive the electric motor immediately after applying the

accelerator pedal. But the Sian is not an affordable car for the general market; only 63 of them have been made, as shown by the numbers on the back wing, and its price is more than HUF 1 billion [23]. We do not know whether tomorrow's strategic raw material was used in the production of this car, but we can imagine it may be so.

But what can we say about clusters? Can we say that from the five clusters there is one which is significantly more important from the perspective of innovation than the others? There is indeed a cluster that includes only critical raw materials, but it cannot be stated that it is more important than the other clusters. Consider the batteries of electric cars, for example, which require manganese, lithium, cobalt, nickel, graphite, aluminum and copper. This is only a single product, but it affects 4 out of the 5 groups. However, the analysis can be of help with the adjustment of attitude toward each group and raw materials.

It is important that we not lose sight of the fact that our world is constantly changing and new technologies are emerging; these factors make it difficult to predict in advance what raw materials will be needed. At any time, technologies that are still new today may become history tomorrow, and rewrite the list of strategically important raw materials.

REFERENCES

[1]   Meadows, D. H. et al. (1972). *The limits to growth: A report for the Club of Rome's project on the predicament of mankind*. New American Library, New York.

[2]   Laszlo, E. e. a. (1978). *Goals for Mankind.* Scarborough: The New American Library of Canada Limited.

[3]   Imre, K. (1980). *Világmodellek - A Római Klub jelentéseitől az ENSZ kezdeményezéséig.* Budapest, Közgazdasági és Jogi Könyvkiadó.

[4]   Meadows, D. H., Meadows, D. L. Randers, J. (1992). *Beyond the Limits.* London, Earthscan publications Limited.

[5]   Gombkötő I., Magyar T.: *Mik azok a kritikus nyersanyagok, mi lenne velünk nélkülük?* https://matarka.hu/koz/ISSN_2062-204X/4_evf_2_sz_2013/ISSN_2062-204X_4_evf_2_sz_2013_058-078.pdf.

[6]   CriticEl – Kritikus Elemek project website. http://kritikuselemek.uni-miskolc.hu/.

[7]   CRM Alliance website. http://criticalrawmaterials.org/.

[8] European Commission (a) (2017). Methodology for establishing the EU list of critical raw materials (Publications Office of the EU, Luxembourg), https://publications.europa.eu/en/publication-detail/-/publication/2d43b7e2-66ac-11e7-b2f2-01aa75ed71a1.

[9] European Commission (b) (2017). Study on the review of the list of Critical Raw Materials – Criticality Assessment (Publications Office of the EU, Luxembourg), https://publications.europa.eu/en/publication-detail/-/publication/08fdab5f-9766-11e7-b92d-01aa75ed71a1/language-en.

[10] European Commission (c) (2017). Study on the review of the list of Critical Raw Materials – Critical Raw Materials Factsheets (Publications Office of the EU, Luxembourg), https://publications.europa.eu/en/publication-detail/-/publication/7345e3e8-98fc-11e7-b92d-01aa75ed71a1/language-en.

[11] European Commission (d) (2017). Study on the review of the list of Critical Raw Materials – Non-critical Raw Materials Factsheets (Publications Office of the EU, Luxembourg), https://publications.europa.eu/en/publication-detail/-/publication/6f1e28a7-98fb-11e7-b92d-01aa75ed71a1/language-en.

[12] European Commission: *Critical Raw Materials*. https://ec.europa.eu/growth/sectors/raw-materials/specific-interest/critical_en.

[13] European Commission (2016): EU takes legal action against export restrictions on Chinese raw materials, https://ec.europa.eu/commission/presscorner/detail/en/IP_16_2581.

[14] *Interior Releases 2018's Final List of 35 Minerals Deemed Critical to U.S. National Security and the Economy* (18 May 2018). https://www.usgs.gov/news/interior-releases-2018-s-final-list-35-minerals-deemed-critical-us-national-security-and [30

[15] Gere, L.: *A Föld stratégiai fontosságú nyersanyagai*. (19. April 2018) http://www.geopolitika.hu/hu/2018/04/19/a-fold-strategiai-fontossagu-nyersanyagai/#_edn8.

[16] The Fund for Peace: *Fragile states index*. https://fragilestatesindex.org/country-data/.

[17] Hobot P. (2017). *Lassan vége az olajkorszaknak, mostantól a kobaltért, a volfrámért és a héliumért folyik a verseny*. https://qubit.hu/2017/11/20/lassan-vege-az-olajkorszaknak-mostantol-a-kobaltert-a-volframert-es-a-heliumert-folyik-a-verseny [25 Nov 2019].

[18] Horváth Á. (2017). Kongón múlhat az eletromos autógyártás jövője. https://index.hu/gazdasag/penzbeszel/2017/08/14/femes_jovo/ [26 Nov 2019].

[19] Hajdu O. (2003). *Többváltozós statisztikai számítások*. Központi Statisztikai Hivatal, Budapest.

[20]   Malhotra N. K. (2008). *Marketingkutatás*. Akadémiai Kiadó, Budapest.

[21]   Sajtos L., Mitev A. (2007). SPSS kutatási és adatelemzési kézikönyv. Alinea Kiadó, Budapest.

[22]   Varga B., Szilágyi R. (2011). *Kvantitatív információképzési technikák*. https://www.tankonyvtar.hu/hu/tartalom/tamop425/0049_08_kvantitativ_in-formaciokepzesi_technikak/3268/index.html.

[23]   Lövei, G. (2019). Lágy-hibrid rendszerrel jut el a csúcsra a Lamborghini Sián. http://www.automotor.hu/hirek/lagy-hibrid-rendszerrel-jut-el-a-csucsa-a-lamborghini-sian/ [04 Jan. 2020].

[24]   Hegedűs, Zs. (2014). „Natural security" az Amerikai Egyesült Államokban. *Nemzet és Biztonság*, 2014/4. szám, pp. 22–29.

[25]   Major, A.: *Ezek lesznek a jövő legértékesebb nyersanyagai, de van velük egy kis gond.* (12 July 2019), https://www.portfolio.hu/uzlet/20190712/ezek-lesznek-a-jovo-legertekesebb-nyersanyagai-de-van-veluk-egy-kis-gond-330833

[26]   The International Raw Materials Observatory, https://intraw.eu/reports-factsheets/ [23 Oct 2019].

[27]   U.S. Government Accountability Office (GAO) (2010). *Rare Earth Materials in Defense Supply Chain.* https://www.gao.gov/new.items/d10617r.pdf [14. May 2020].

LITHIUM AND LITHIUM BATTERIES
FROM AN ECONOMIST'S POINT OF VIEW

ZSOLT PÉTER – DÁNIEL OROSZ

Institute of World and Regional Economics, University of Miskolc

Abstract: Batteries operate an ever-growing number of electrical and electronic devices. When these devices break down or become obsolete, they are disposed of. As our resources are limited, it makes sense to recycle or re-use the materials of the devices and the batteries that run them, as it saves material, energy, and money.

There are basically two barriers to recycling that are closely related. When designing most products, the aspects of saleability and the profit are dominant, the aspects of recycling (disassembly, easy separation of the used materials) rarely appear. While in the case of acid (lead-based) batteries the recycling is already close to 100% due to the value of the materials used, the technology developed, the recycling is economical. In the case of lithium-based power sources the solution is much more complicated. These types show much greater variety in their format and chemical composition. Technology is still developing rapidly, the capacity of batteries and the range of materials used are constantly changing.

In this study, we review the international literature focusing on the latest economic issues in the recycling process, with special reference to lithium-based models. We survey the cost structure of the most recent battery producing technologies, gathering data about the expenses of recycling and the expected advantages.

Keywords: batteries, materials of the batteries, recycling, lithium-based models

1. INTRODUCTION

The use of batteries and cells is indispensable in our daily lives. While a few decades ago we could easily name and count the number the tools or devices that operated in our homes with a power supply that is independent of the electrical network, nowadays it would be difficult to count the devices used in a household. The almost exponential increase in the use of batteries has occurred not only in the case of households. Similar growth has happened for batteries not directly affecting final consumers. Batteries and cells have a high degree of variation in their characteristics (basic materials, auxiliary materials, coatings, sizes, purposes of use, lifetime, etc.).

The significant number of such factors can be considered as major challenges for those trying to recycle worn-out batteries. In our paper we briefly review the major steps of the development of batteries and we examine the significant changes made in the past decades, mainly in terms of production, sales, and types and materials used, with special regard to the recent popular lithium-based models.

2. RESULTS AND DISCUSSION

The first object thought to be like a battery dates from the time of the Parthian Empire (between 250 BC and 250 BC). There are only speculations about its use, but it was probably used in the galvanization of metals. The first chemical power source capable of producing electricity in the modern sense was made by Alessandro Volta, which was. Recharging was not yet possible with this structure until 1859, when the French physicist Gaston Planté invented the battery. The principle of operation, despite the more than a century and a half that have passed since then, has not changed, while the production technology, the structure, the range of materials used have changed significantly [1].

The literature classifies chemical power sources into two main groups. Primary batteries are those that cannot be recharged simply or efficiently, so they are typically discarded after use. Their structure is characterized by the electrolyte in the primary cell being contained in an absorbent or separating material. Their general characteristics are cheapness and small size. They are used to provide memory capacity in portable electrical appliances, lighting, photographic equipment, games, computers, etc. They are suitable for long-term energy storage where continuous use is common, their capacity is typically small, the vast majority of them are in single-cell cylindrical, flat or button cell format, some of which are multi-channel, i.e. elementary cells. [2]

Secondary batteries are rechargeable and their main purpose is energy storage. Their use is often occasional or intermittent, they are discarded when the device in which they are used is permanently destroyed, or when their capacity is significantly reduced due to a large number of recharges, and this is already a problem during use. There are also so-called spare batteries in which the key components (usually the electrolyte) are separated before activation, so that no chemical damage or self-discharge can occur before use. These batteries are capable of extremely long-term energy. [2]

Recycling a lithium-based battery is complicated due to the variety of unique materials used in the design of the cells. Recycling can be done by pyrometallurgical means (furnace melting), which is economically viable if the cathode contains cobalt or nickel. During hydrometallurgical recycling, the materials are dissolved in an alkaline medium. At current market prices, this method can only be worthwhile if the cathode contains cobalt or nickel. In direct recycling, the discharged cells are placed in a container to which CO_2 is added and the supercritical carbon dioxide extracts the electrolyte from the cells, which can thus be recycled after further processing. [3]

3. ECONOMIC ISSUES OF RECYCLING WITH SPECIAL REGARD TO LITHIUM-BASED TYPES

Different sources approach the benefits of recycling in different ways. Basically, three approaches, or combinations thereof, characterize the literature. The savings are typically related to the amount of recycled materials, the energy saved, and, in rare cases, the cost of recycling, and characterized by expected benefits.

There are technological problems with recycling that have a significant impact on economy. Mixing lithium-ion batteries with lead-acid batteries can be a serious problem, which can cause fires and explosions: Cross-contamination must be avoided, meaning that segregation systems are required for large-format batteries, which increases recycling costs. [4]

Qinyu Q. et al. [5] characterize the recycling of electric cars with specific data. The cost-benefit analysis of battery-free vehicles and batteries is based on the recycling and revenues of salable materials. The recycling of car batteries faces relatively few problems, as a large amount of materials produced with similar technology is available at the same time, and the price of the extracted materials can be said to be high. The shortcoming of the analysis is that it unfortunately does not cover the proportion of metals in batteries *(Table 1)*.

Table 1

Costs and revenues for the recycling of electric vehicles

COSTS	USD/kg (2017)
Vehicle (without battery)	
Acquisition	0.01
R & D	0.01
Manpower	0.01
Management	0.01
Maintenance	0.01
Amortization	0.02
Other	0.03
Battery	
Acquisition	2.87
Recycling	3.73
REVENUE	**USD/kg (2017)**
Steel	0.27
Aluminum	1.90
Iron	0.16
Copper	5.61
Lithium-nickel-manganese-cobalt oxide	27.01

Source: [5]

Future recycling will ideally be able to handle batteries with the same characteristics in a uniform way. Clear, user-friendly markings on the packaging indicate the right technology. The delivery of used power sources to recycling companies should be unhindered and the quality of products made from recycled materials should be the same as those made from completely new raw materials.

4. HISTORICAL OVERVIEW OF LITHIUM USE

A significant amount of lithium was first used during World War II. Its most important field of application at that time was the aircraft industry. There was a slight

decline in the post-war years, but the Cold War period put demand back on an increasing trajectory (more was needed for hydrogen bomb fusion fuel and for the production of nuclear fusion weapons [6].

The use of lithium has also become popular in other fields. With lithium the melting temperature of glass can be reduced and the melting parameters of alumina can also be favorably influenced. [7] However, the areas of use mentioned above dwarfed the demands of the military industry. Then, due to the end of the arms race, demand for lithium dropped significantly in the early 1990s. As a result, prices started to fall. The decline in market prices accelerated further when the U.S. Department of Energy sold much of its inventory. [8]

Since the middle of the 1990s, the typical technology of production has changed a lot, further reducing prices. The extraction of lithium from salt water began, and this process could be done at a lower cost than mining. Most of the mines were closed or concentrated on other economically extractable materials in the ores. [8]

In the 2000s, there was a technological shift in the field of mobile devices and they became more widespread, especially in the markets of developed countries. Within a few years, NiCd and NiMh batteries were replaced by lithium-based batteries due to the fact that they were far superior to their competitors in terms of capacity, number of recharges, and slower wear. In 2004, the Lithium-ion types became dominant in the market of non-acidic (lead-based) batteries: their total capacity approached 80,000 MWh by 2016, while the share of other types was around 3–5,000 MWh *(Figure 1)*. [9]

Figure 1
Global Battery Sales (Excluding Lead/Acid Batteries)
Source: [10]
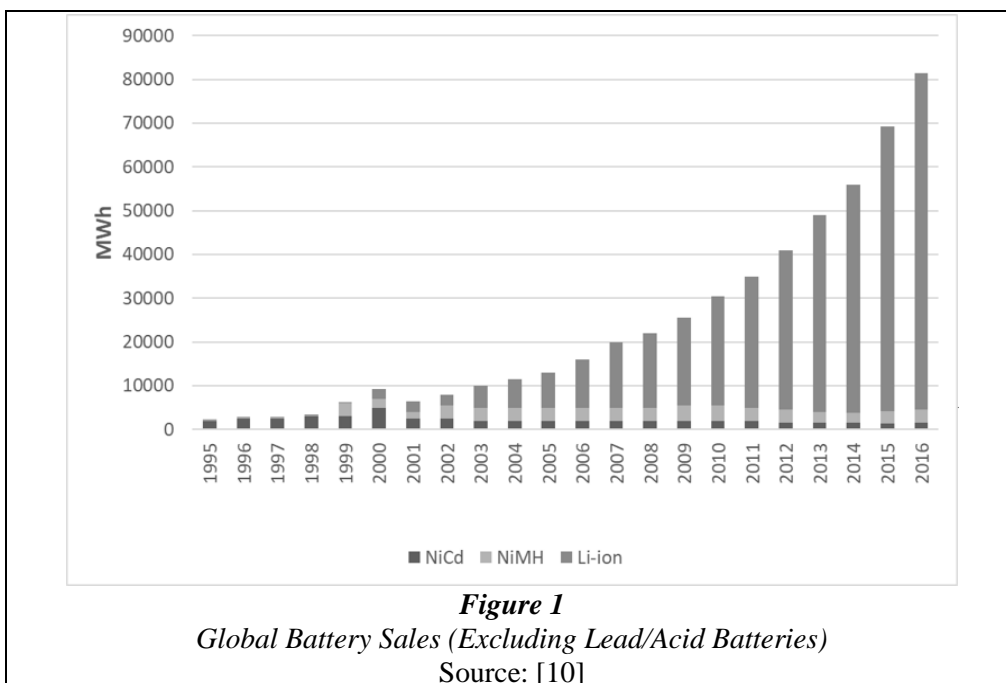
Although acid (lead-based) batteries may appear obsolete due to the hazardous nature of the materials used and their heavy weight, they still account for the vast majority (>80%) of the total capacity of batteries produced to date. Sales of lead batteries no longer have the potential for growth, and stagnation and then decline can be predicted in the future, as their typical area of use is passenger cars with internal combustion engines, which may even disappear completely within a few decades.
Figure 2 shows the changes in the market for "other" technologies by area of use without the values of lead batteries (still dominant). It is clear that the market for mobile devices will continue to grow, with the emergence of dynamically growing areas (electric cars and buses) leading to highly exponential growth. The figure also highlights that while China is not necessarily the market leader in technology, the world's most populous country in terms of in-vehicle batteries is already ahead of its rivals in volume.

There is also dynamically increasing industrial use, and in other areas; for instance, we are also seeing extremely dynamic growth for power tools. This increase, of course, could not have occurred without the decrease in the price of the finished product (e.g., 1 Wh of the standard 18650 lithium battery decreased from \$2.60 in 2000 to \$0.15 in 2015). [10]
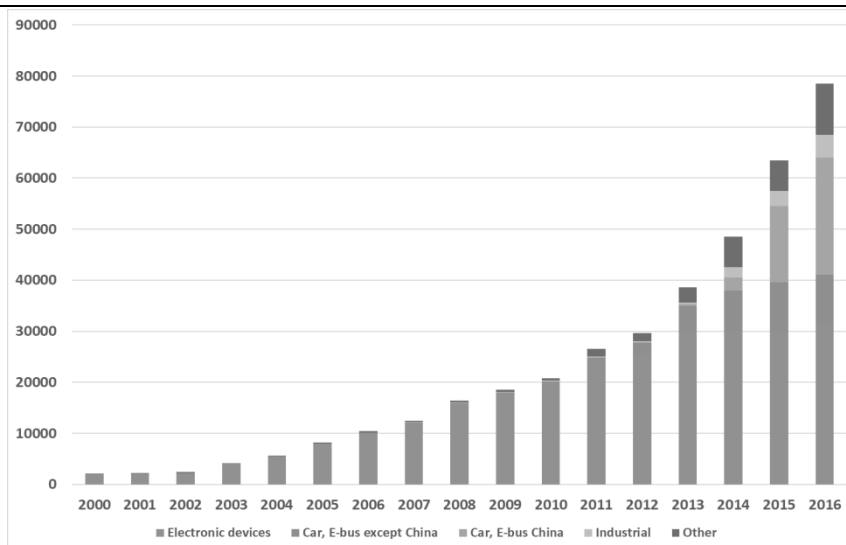
Figure 2
Dynamics of lithium battery use
Source:[10]

There have also been significant market reorganizations in the field of battery production according to the market share of the producing countries. The technology was first developed and transferred to mass production by Japan, and as an early

follower, South Korea caught up within a few years, surpassing the Japanese share by 2012 [10].
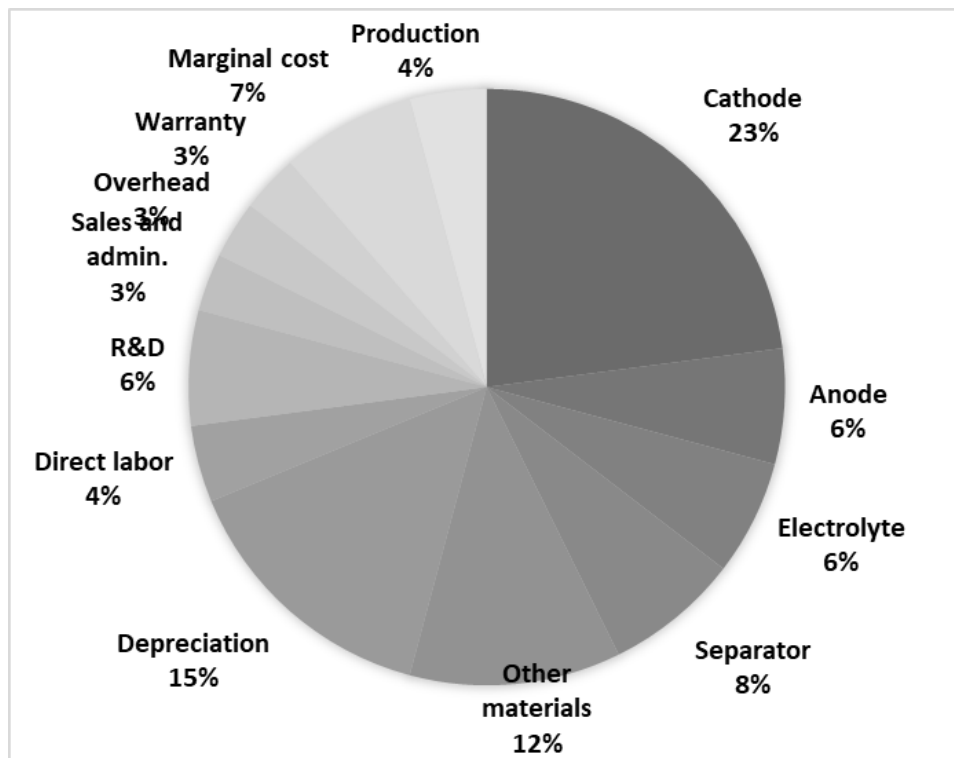
Figure 3
Average cost of manufacturing lithium-ion batteries in 2016 (%)
Source:[10]

China produced slow growth from 2005 until 2011, when the explosion of the "smart" mobile devices market in particular set it on a much higher growth trajectory than before, making it a clear market leader by 2015.

The current cost distribution for the production of lithium batteries is 55% material cost (cathode 23%, anode 6%, electrolyte 6%, separator 8%, other materials 12%, etc.) 45% non-material (depreciation 15%, direct labor 4%, R&D 6%, sales and administration 3%, overhead 3%, production 4%, other 7%) *(Figure 3)*. [10]

From the early 1990s, lithium production increased almost unbroken, while the price of lithium experienced extremely significant fluctuations. Demand and supply did not meet in several periods: the sale of US reserves and Chile's entry into the market from 1994 to 2004 reduced prices to a previous fraction, which only returned to previous levels due to the growing demand of the 2000s. [11]

Figure 4
Change in the price of lithium and the amount mined (1990–2015)
Source:[12]
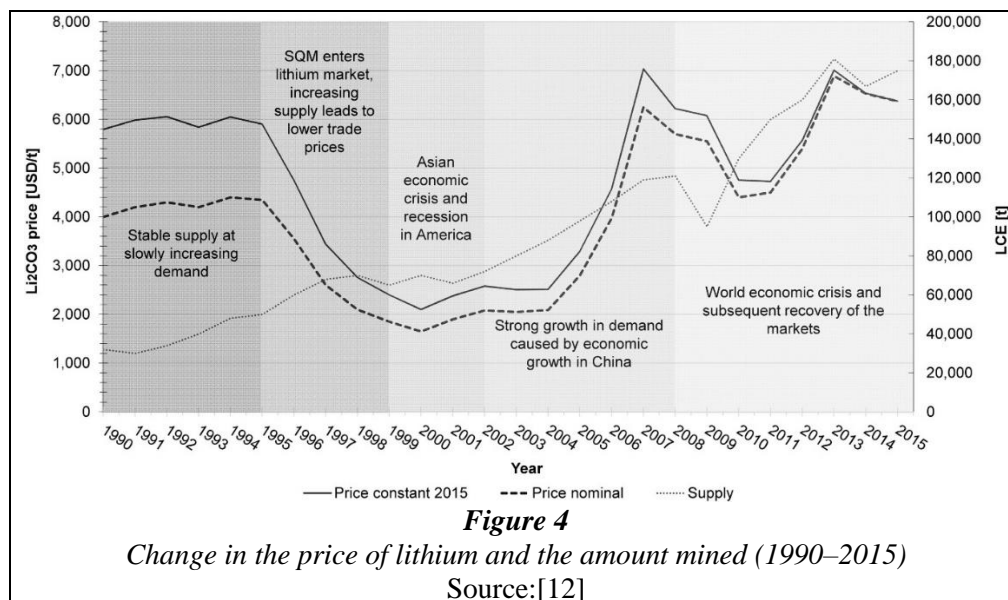
The crisis broke this trend and then the saturation of the mobile device market led to a correction again. [13] With the construction of Gigafactory, one of the world's largest lithium-ion battery factories, Tesla greatly increased supply, leading to lower prices *(Figure 4)*. [14]

5. CONCLUSION

Demand for lithium-based batteries has grown exponentially in recent years, somewhat contradicted by the fact that demand for lithium has different characteristics. The reasons are mainly due to the significant development of the materials used per unit mass and the saturation of the mobile device market. Prices have been dominated over the last few decades mainly by (sudden) changes in supply. China has become an unavoidable factor in recent years (the writings of Chinese authors have also become dominant in the literature). The current predictable trends are most at risk from possible technological leaps in the development of batteries (new cathode/anode coatings or technological changes).

REFERENCES

[1]   Bernard F. S. (2002). *Origin of Electrical Power*. National Museum of American History. http://americanhistory.si.edu/powering/past/prehist.htm.

[2]   Linden, D.. Reddy, T. B. (2001). *Handbook of Batteries*. Third Edition, McGraw-Hill Handbooks, http://dl.booktolearn.com/ebooks2/engineering/electrical/9780071624213_lindens_handbook_of_batteries_cd2a.pdf

[3]   Gaines, L. (2018). Lithium-ion battery recycling processes: Research towards a sustainable course. *Sustainable Materials and Technologies*, Volume 17, September 2018, e00068. https://doi.org/10.1016/j.susmat.2018.e00068

[4]   Gaines L. (2014). The future of automotive lithium-ion battery recycling: Charting a sustainable course. *Sustainable Materials and Technologies*, Volumes 1–2, December 2014, Pages 2–7. https://doi.org/10.1016/j.susmat.2014.10.001

[5]   Qinyu Q. et al. (2018). *Electric vehicle recycling in China: Economic and environmental benefits.* Resources, Conservation and Recycling. Volume 140, January 2019, pp. 45–53. https://doi.org/10.1016/j.resconrec.2018.09.003

[6]   http://www.pioneerresources.com.au/lithium.php.

[7]   Ebensperger, A., Maxwell, P., Moscoso, C. (2018). The lithium industry: its recent evolution and future prospects. *Resources Policy*, 30 (4), pp. 218–231.

[8]   Joyce, O. A. (1994). *Commodity Report 1994: Lithium*. United States Geological Survey, Reston, Virginia.

[9]   Elzea, K. J. (2001). *Lithium, Industrial minerals & rocks: commodities, markets, and uses.* Littleton, Colo.: Society for Mining, Metallurgy, and Exploration.

[10] Pillot C.: *The Rechargeable Battery Market and Main Trends 2016–2025*. Avicenne Energy. Lisbon, Portugal, September 20th, 2017, conference presentation.

[11] Maxwell P. (2015). Transparent and opaque pricing: The interesting case of lithium. *Resources Policy*, 45, pp. 92–97.

[12] Martin G et al. (2017). Lithium market research – global supply, future demand and price development. *Energy Storage Materials* Vol. 6, pp. 171–179.

[13] Robert B. (2013). Evaluating and forecasting the lithium market from a value perspective. *Roskill Presentation, 5th Lithium Supply and Markets Conference*, Las Vegas, pp. 29–31.

[14] Chatsko, M. (2015). *The Tesla gigafactories are coming. can global lithium supply keep up?* https://www.fool.com/investing/general/2015/04/26/the-tesla-gigafactories-are-coming-can-global-lith.aspx.

EFFECT OF INDUSTRIAL BY-PRODUCTS USED AS ADDITIVES ON THE PROPERTIES OF CONCRETE

ALI M. SALEM[1] – ÁDÁM HÉJJAS[1] – PÉTER KOLLÁR[1] –
ANITA K. DOLGOSNÉ[2] – ZOLTÁN ORBÁN[1]

Faculty of Engineering and Information Technology, University of Pécs
[1]Structural Diagnostics and Analysis Research Group
[2]Department of Environmental Engineering

Abstract: Concrete is a widely used material for the construction industry, as it is characterized by compressive strength, durability, availability, and fire resistance as compared to other construction materials. Cement – a significant ingredient used for preparation of concrete mix – entails environmental pollution due to the enormous production and usage of clinkers in cement products and contributes to the greenhouse effect and global warming. Therefore, it is essential to reduce the amount of cement in the concrete industry as much as possible by using alternative solutions to produce eco-friendly concrete. The sustainability of concrete can be improved by using a large volume of fly ash, ground granulated blast furnace slag (GGBS), silica fume, etc. as cement replacing materials and in this way utilizing wastes that contribute to the decrease of CO_2 emissions into the atmosphere. This paper investigates the effects of partial substitution of cement using GGBS and fly-ash at varying percentages on the properties and quality of concrete in comparison with conventional concrete.

Keywords: *construction industry, sustainability, fly-ash, ground granulated blast furnace slag, recycled concrete aggregate*

1. INTRODUCTION

The construction industry is considered as one of the most essential sectors of a country's social and economic development [1], with one the highest environmental effects, as it consumes large amounts of energy and natural resources and produces enormous amounts of waste [2]. Concrete is the most widely used material in the construction industry, with a global production of ca. 1 m^3 per capita per year. Concrete is a composite material made up of cement, course aggregate, fine aggregate, water, and admixtures. Portland cement (PC) which is the main constituent of concrete, had a global production of 4.3 billion tonnes in 2014 [2, 3] and contributes to 6–8% of the global CO_2 emissions [4, 5] that have led to a climate crisis and to depleting the environment [6]. Therefore, it is essential to reduce the amount of cement used by the concrete industry as much as possible. Currently, processes of construction industry have been investigated in order to reduce carbon dioxide emissions and enhance the performance of concrete with reducing the construction costs [7]. To maintain sustainability and protect the environment, eco-friendly ap-

proaches must be considered, including utilizing industrial wastes that can substitute for natural materials [8].

Rapid industrialization and urbanization have contributed to increasing the industrial wastes that represent a critical issue [9]. Thus, it is required to manage such wastes efficiently and effectively. One possible way is the use of industrial wastes as a supplementary binding material by partially replacing cement with suitable materials. This replacement will lead to decreased cement consumption, thereby helping to reduce greenhouse emissions [9]. Waste and supplementary binding materials such as silica fumes, rice husk, fly-ash, lime, and ground granulated blast-furnace slag (GGBS) have pozzolanic properties, meaning they can be used as partial replacements for cement [10]. Therefore, recycling the waste materials used in concrete is essential to conserve natural resources. Fly ash and GGBS are commonly used in concrete as supplementary cementitious materials, as they can reduce the porosity and improve the durability of concrete and improve the interface with the aggregate [11].

GGBS is a by-product from production of iron and steel-making. The slag is a mixture of silica, lime, alumina and the same oxides that are used for the production of Portland cement, but in different proportions [12, 13]. Fly ash is generated in power plants constituting about 60–88% of total combustion residues [14].

The reuse of industrial wastes is justified in cement production as well as construction because of reducing the consumption of natural resources [15]. The main aim of this paper is to assess the effects of partial replacement of cement by fly ash and GGBS on the compressive strength and fresh concrete properties. The cement replacement was carried out by waste materials using varied percentages of fly ash and GGBS.

2. PREVIOUS STUDIES

Nicula et al. [16] studied some design mixes with minimum partial replacement of cement with granulated ground blast furnace slag and silica fume. In this experiment it was found that water absorption decreases with the partial replacement of GGBS and silica fume. Also, it was concluded that tensile strength and freeze-thaw resistance increase compared to the reference mix. Moreover, the results of the tests showed a possible way to reduce carbon dioxide emission by partial replacement of cement with granulated ground blast furnace slag and silica fume [16]. Salem et al. [17] reported that recycled aggregate concrete (RAC) had lower resistance to thawing and freezing compared to conventional concrete. Singh et al. [18] evaluated the effect of RAC with fly ash and GGBS at various percentages. They designed M25 grade with RAC percentages of 50, 60, 70, 80, 90 and 100. He found that the fly ash and GGBS improved the workability of concrete. Modulus of rupture and the compressive strength of RAC increased with replacement of GGBS (20%) and fly ash (30%). Abou-Zeid et al. [19] concluded that RAC exhibited lower resistance and higher water permeability to chloride ion penetration compared to natural concrete.

Ayoub et al. [20] investigated the use of RAC as replacement of coarse aggregate on short-term concrete properties. She concluded that the RAC replacement level decreased the compressive strength of the concrete. However, RAC replacement up to 50% still provided medium-high target strength. Nath and Sarker [21] found that incorporation of fly ash in concrete enhanced its workability while it decreased the water permeability of concrete significantly at 28 days and further reduction was found at 6 months. Kisku et al. [22] reviewed hundreds of research papers about RAC and concluded that using mineral admixtures could improve the properties of RAC. They recommended further research into the long-term behavior of RAC with respect to mechanical and durability properties and the addition of unconventional materials waste as cement replacement materials. Berndt [23] studied the combined effects of the use of RAC and partial cement replacement on enhancing the sustainability of concrete. He reported that concrete mixes with 50% blast furnace slag as a cement replacement produce the best results in terms of durability and mechanical properties when either recycled or natural aggregate was used. Kim et al. [24] investigated the impacts of using GGBS as cement replacement on concrete strength. They concluded that the optimum quantitative ratio of GGBS is 30%. Moreover, they found that using slag in concrete significantly decreased CO_2 emissions (up to 68%), based on the level of cement replacement. Kou et al. [25] examined the effect of replacements of natural aggregate by RAC and replacement of cement by fly ash (Class F) at 0, 25, and 35 percent. They concluded that the compressive strength, static modulus of elasticity and tensile strength values of the concrete at all ages decreased as the fly ash content and the RAC increased. However, the use of fly ash (Class F) up to 35% with a w/b ratio between 0.45–0.55 and the substitution of natural aggregate with RAC could result in improved properties. They found that due to the pozzolanic effects of fly ash at later age, mainly between 28 to 90 days, increased compressive strength was achieved despite a relatively high w/b ratio.

3. EXPERIMENTAL PROGRAM

The laboratory program included the design and test of five concrete mixes. For all mixes, fresh concrete properties (workability, air content, fresh concrete density) and hardened properties (compressive strength) were tested, and the results have been evaluated.

3.1. Materials

3.1.1. *Cement, fly ash and GGBS*

CEM I 42.5 N Portland cement according to EN 197-1 with normal initial strength, Class F low-calcium fly ash and GGBS were used in the concrete mixes. The CEM I 42.5 N Portland cement was obtained from the Duna Drava Cement Factory while fly ash and GGBS were from ISD Dunaferr Dunai Vasmű Zrt., Hungary. The chemical composition of cement, fly ash and GGBS is shown in *Table 1*. *Table 2*

presents the physical properties of the cement, fly ash and GGBS used in the tests. The surface area was measured by air permeability test according to the European standard EN 196-6 [26].

Table 1

Chemical Composition of cement, fly ash and GGBS

Chemical Composition (%)	SiO_2	Al_2O_3	Fe_2O_3	MgO	SO_3	CaO	K_2O
Cement	20.52	4.61	2.59	4.17	2.7	63.25	0.5
Fly ash	52	25	12	0.9	1.08	5	1.9
GGBS	39.18	10.18	2.02	8.52	–	32.82	0,3

Table 2

Physical properties of cement, fly ash and GGBS

Properties	Materials		
	Cement	Fly ash	GGBS
Density (kg/m^3)	3150	2300	2870
Specific surface area (m^2/kg)	352	396	425

3.1.2. Aggregates

Recycled concrete aggregate and natural aggregates were used in the concrete mixtures. In this study, RAC sourced from a recycling facility in Pecs, Hungary was used. Recycled aggregate was produced by crushing concrete specimens sourced from a recycling facility in Pecs, Hungary with a hammer. The RAC was washed and sieved in a standard way. Aggregates with a density of 2,400 kg/m^3, a fineness modulus of 6.89 and a maximum particle size of 16 mm were used as natural aggregate.

3.1.3. Superplasticizer

For all concrete mixtures, superplasticizer admixture was used to control the consistence class F3 through the slump of 100–150 mm. This superplasticizer is available as a dark-brown 40–42% solid aqueous solution with a density of 1,210 kg/m^3.

3.2. Specimen preparation and curing

The fine aggregate, coarse aggregate and cement were dry mixed for about a minute. Cement was then added and dry blended for a further minute. This was then followed by the addition of two thirds of the total mixing water *(Figure 1)*. After two minutes of mixing, the remaining mixing water was added with the superplasticizer. Mixing was ceased after four minutes for all mixes.

a)   b)
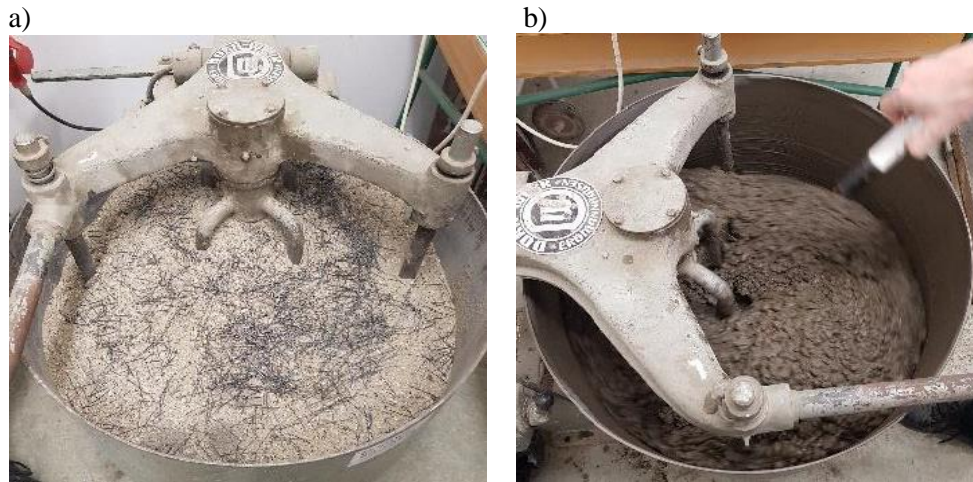
Figure 1
Mixing process: a) dry mixing; b) wet mixing

From each concrete mixture, three 150 mm cubic samples were cast for the determination of the compressive strength. Casting of cubes was conducted in two layers. Each layer was compacted by internal vibration and the top surface was leveled and smoothed using a trowel. After casting, all of the molded specimens were placed on a vibration table. The vibrating procedure was executed in order to obtain a more homogeneous mix. After 24 h, the concrete specimens were demolded and cured under laboratory condition of $95 \pm 5\%$ RH and 22 ± 2 °C until the time of the compressive strength tests.

Table 3
Percentage of binder content: Cement, fly ash and GGBS
in mix design proportion

Mix Scenario	Binder content (%)		
	Portland Cement	**Fly ash**	**GGBS**
S0	100	0	0
S1	85	10	5
S2	85	5	10
S3	70	20	10
S4	70	10	20

3.3. Mix proportions

After many trials the final mix proportions were selected to have a slump between 90 and 120 mm at a constant water–cement ratio (w/c) of 0.45. The mix proportions of the conventional mix were cement content of 430 kg/m^3, fine aggregate of 655 kg/m^3, coarse aggregate of 1,175 kg/m^3 and water content of 190 kg/m^3. The slump was adjusted by adding different dosages of the superplasticizer. In this study, fly ash and GGBS were used as 0, 5, 10 and 20% by weight replacements of

cement. The percentage of cement replacement by fly ash and GGBS in the designed mixes is presented in *Table 3*.

3.4. Testing

3.4.1. Fresh concrete tests (Workability, air content and density)

The workability of concrete was determined in terms of slump, noted immediately after mixing the concrete. The slump test was carried out in accordance with EN 12350-2, and the air content was tested according to EN 12350-7, as shown in *Figure 2*. The density of fresh concrete was tested according to EN 12350-6 for each mix in a fresh state.

a)

b)
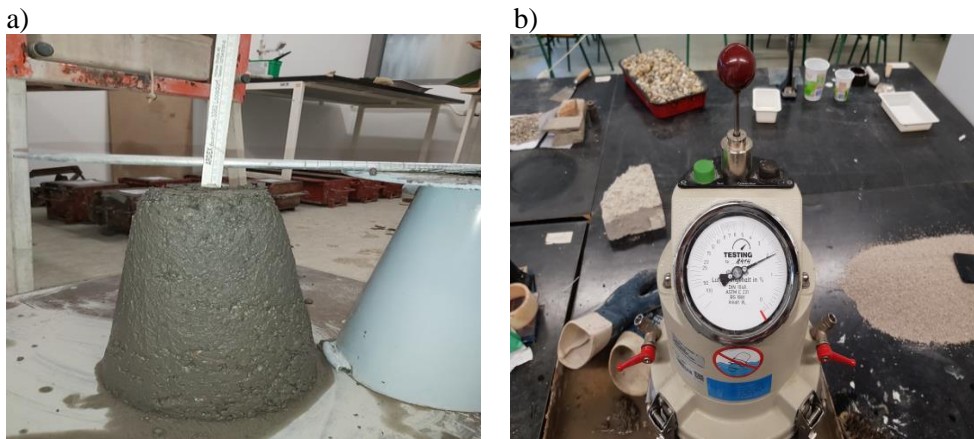
Figure 2
a) Slump test
b) Air content test of fresh concrete

3.4.2. Hardened test (Compressive strength)

The compressive strength of the concrete was determined for three cubes of 150 mm size at the age of 28 days for each mix. The test was carried out according to EN 12390-3:2001.

4. RESULTS AND DISCUSSION

4.1. Workability

The measured slump of the conventional mix was 75 mm, while the slump of the mix proportion with cement replacement with 10% fly ash and 5% GGBS was 102 mm, and 92 mm for the mix with cement replacement of 5% fly ash and 10% GGBS, respectively. The better workability for the mix proportion with more fly ash is attributed to the spherical shape of the fly ash particles. Similar reports of the effect of cement replacement on the workability are available in the literature, e.g.,

Reddy et al. [27] reported that the slump value was increased by replacing cement with various percentages of fly ash and GGBS.

4.2. Compressive strength

The compressive strength of all mixing scenarios was determined at 28 days age. *Figure 3* shows the compressive strength results for the conventional mix and for mixes obtained by adding varying percentages of fly ash and GGBS additives as 5%, 10% and 20% partial Portland cement replacements.
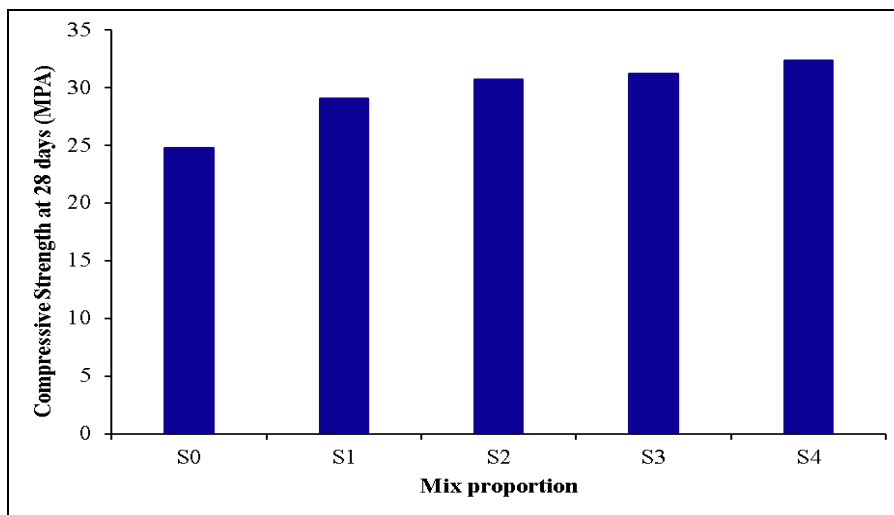
Figure 3
Compressive strength values for different mix proportions

The results show that the compressive strength was slightly increased by adding some percentage of fly ash and GGBS to the concrete mix. Furthermore, the mix proportion with cement replacement by 10% fly ash and 20% GGBS achieved 30.5% higher compressive strength than that of the conventional mix. Consistent with the present result, Prince et al. [28] also reported that by cement replacement with 20% fly ash and 30% copper slag 39 MPa compressive strength was achieved. Therefore, it can be concluded that with 30% of cement replacement by fly ash and GGBS the desired compressive strength of the concrete could be reached. Partial replacement of cement with industrial waste additives proved to be an effective and sustainable technique for reducing carbon dioxide emissions.

Further studies on strength and other characteristics of concrete with different ratios of fly ash and slag used as cement replacing materials should be made in order to gain information to help with common acceptance and practical application.

5. CONCLUSIONS

The studied approach aims to make material substitutions to decrease CO_2 emissions, save energy and reduce the environmental impact of concrete. This objective was achieved by partial replacement of cement with large volumes of fly ash and ground granulated blast furnace slag (GGBS). This paper focused on the impacts of the use of partial cement replacement to improve the sustainability of concrete. Therefore, as an experimental point of view, this research focused on finding the optimum percentage of these materials to achieve beneficial effects regarding the strength and workability of concrete. The results showed that adding fly ash and GGBS to the concrete mix can increase workability. It was also concluded that 30% replacement of cement with fly ash and GGBS resulted in the highest compressive strength among the mixes analyzed. Partial cement replacement with fly ash and GGBS in concrete gradually raised the compressive strength as the replacement percentage increased. The results should encourage the use of fly ash and GGBS in concrete technology and help change the perception of people towards the recycling of materials and the partial replacement of cement with industrial by-products as additives.

REFERENCES

[1]   Ashfaque, A. J., Samiullah, S. (2018). Effect of steel fibers on the compressive and flexural strength of concrete. *Int. J. Adv. Appl. Sci*., 5, pp. 16–21.

[2]   Kisku, N., Joshi, H., Ansari, M., Panda, S., Nayak, S., Dutta, S. C. (2017). A critical review and assessment for usage of recycled aggregate as sustainable construction material. *Constr. Build. Mater*, 131, pp. 721–740.

[3]   Agenda 21, the Rio Declaration on Environment and Development, the Statement of Forest Principles, the United Nations Framework Convention on Climate Change and the United Nations Convention on Biological Diversity. *United Nations Conference on Environment and Development (UNCED)*, Rio de Janeiro, 3–14 June 1992.

[4]   Philip, A., Mathew, A. (2016). Experimental Study on Mechanical Properties of Geopolymer Concrete Using GGBS. *IJSR*, 5 (5), pp. 2465–2468.

[5]   McLaren, R. J., DiGioia, A. M. (1987). *The typical engineering properties of fly ash*. In Geotechnical Practice for Waste Disposal '87, pp. 683–697. ASCE.

[6]   Lehne, J., Preston, F. (2018). *Energy, Environment and Resources Department, Innovation in Low-Carbon Cement and Concrete*. Projects: Energy, Environment and Resources Programme, Innovation in Low-Carbon Cement and Concrete. Available: https://reader.chathamhouse.org/making-concrete-change-innovation-low-carbon-cement-and-concrete#.

[7]   Raili, K., Hurme, M. (2016). Cement Industry Greenhouse Gas Emissions – Management Options and Abatement Cost. *Journal of Cleaner Production*, 112, pp. 4041–4052., DOI:10.1016/j.jclepro.2015.07.055.

[8]   Davidovits, Joseph. (1994). Properties of geopolymer cements. In Proceedings, *First international conference on alkaline cements and concretes*, Vol. 1, pp. 131–149. Scientific Research Institute on Binders and Materials Kiev, Ukraine.

[9]   Kim, Y., Hanif, A., Usman, M., Munir, M. J., Kazmi, S. M. S., Kim, S. (2018). Slag waste incorporation in high early strength concrete as cement replacement: Environmental impact and influence on hydration; durability attributes. *J. Clean. Prod*, 172, pp. 3056–3065.

[10]   Phul, A. A., Memon, M. G., Shah, S. N. R., Sandhu, A. R. (2019). GGBS and Fly Ash Effects on Compressive Strength by Partial Replacement of Cement Concrete. *Civil Engineering Journal*, Vol. 5 (4), pp. 913–921.

[11]   Oner A., Akyuz, S. (2007). An experimental study on optimum usage of GGBS for the compressive strength of concrete. *Cement & Concrete Composites*, 29, pp. 505–514.

[12]   Sha, W., Pereira, G. B. (2001). Differential scanning calorimetry study of hydrated ground granulated blast-furnace slag. *Cement Concrete Res*, 31, pp. 327–329.

[13]   Domone, P. L., Soutsos, M. N. (1995). Properties of high-strength concrete mixes containing PFA and GGBS. *Mag Concr Res*, 47, pp. 355–67.

[14]   Panda, R., Sahoo, T. K. Effect of Replacement of GGBS and Fly Ash with Cement in Concrete. In: Das B., Barbhuiya S., Gupta R., Saha P. (eds). *Recent Developments in Sustainable Infrastructure*. Lecture Notes in Civil Engineering, Vol 75, 2021, Springer, Singapore. https://doi.org/10.1007/978-981-15-4577-1_68.

[15]   Han, F. H., He, X. J., Zhang, Z. Q., Liu, J. H. (2017). Hydration heat of slag or fly ash in the composite binder at different temperatures. *Thermochim. Acta*, 655, pp. 202–210.

[16]   Berndt, M. L. (2009). Properties of sustainable concrete containing fly ash, slag, and recycled concrete aggregate. *Construction and Building Materials*, 23 (7), pp. 2606–2613.

[17]   Nicula, L. M., Corbu, O., M. Iliescu, M. (2018), Studies based on cement mortar composites with blast furnace slag powder and ultrafine silica. In *Proceeding of 18th International Multidisciplinary Scientific GeoConference SGEM* 2018, 3–6 December 2018, Vienna, Austria. DOI: 10.5593/sgem2018 V/6.4/S09.063

[18]   Salem, R. M., Burdette, E. G., Jackson, N. M. (2003), Resistance to freezing and thawing of recycled aggregate concrete. *ACI Mater. J*., 100 (3), pp. 216–221.

[19]   Singh, S. B., Mahalakshmi, N., Thammishetti, N. (2014). Mechanical Properties of Recycled Coarse Aggregate (RCA) Concrete. *International Journal of Applied Engineering Research*, 9 (3), pp. 363–372.

[20]   Abou-Zeid, M. N., Shenouda, M. N., McCabe, S., El-Tawil, F. A. (2005). Reincarnation of concrete. *Concr. Int*., 27 (2), pp. 53–59.

[21]   Ayob, A., Razali, M. E, Alias, S., Ahmad, A. G., Ali, D. S. H. (2017). Engineering Behavior of Concrete with Recycled Aggregate. In *MATEC Web of Conferences*, 87, p. 01002. DOI: 10.1051/matecconf/20178701002.

[22]   Nath, P., Sarker, P. M. (2013). Effect of Mixture Proportions on the Drying Shrinkage and Permeation Properties of High Strength Concrete Containing Class F Fly Ash. *KSCE Journal of Civil Engineering*, 17 (6), pp. 1437–1445. DOI 10.1007/s12205-013-0487-6.

[23]   Kisku, N., Joshi, H., Ansari, M., Panda, S. K., Nayak, S. Dutta, S. C. (2017). A critical review, and assessment for use of recycled aggregate as sustainable construction material. *Constr. Build. Mater*., 131, pp. 721–740. https://doi.org/10.1016/j.conbuildmat.2016.11.029.

[24]   Berndt, M. L. (2009). Properties of sustainable concrete containing fly ash, slag, and recycled concrete aggregate. *Construction and Building Materials*, 23 (7), pp. 2606–2613.

[25]   Kim, Y., Hanif, A., Usman, M., Munir, M. J., Kazmi, S. M. S., Kim, S. (2018). Slag waste incorporation in high early strength concrete as cement replacement: Environmental impact and influence on hydration & durability attributes. *Journal of Cleaner Production*, 172, pp. 3056–3065. https://doi.org/10.1016/j.jclepro.2017.11.105.

[26]   Kou, S. C., Poon, C. S., Chan, D. (2009). Influence of Fly Ash as Cement Replacement on the Properties of Recycled aggregate concrete. *Journal of Materials in Civil. Engineering*, 19 (9), pp. 709–717. DOI:10.1061/(ASCE) 0899-1561(2007)19:9(709).

[27]   EN 196-6 (2010) Methods of testing cement — part 6: determination of fineness.

[28] Reddy, A. N., Anitha, D., Tilak, U. V. (2014). Performance of alkali activated slag and alkali activated slag+ fly ash with various alkali activators. *International Journal of Engineering and Technical Research*, 2 (1), pp. 73–78.

[29] Prince, M. J. R., Singh, B. (2013). Bond Behaviour of Deformed Steel Bars Embedded in Recycled Aggregate Concrete. *Construction and Building Materials*, 49, pp. 852–862. DOI:10.1016/j.conbuildmat.2013.08.031.

SUSTAINABLE CONCRETE
FROM RECYCLED CRUSHED AGGREGATES

LEVENTE BALOGH[1] – KINGA KÁRPÁTI[1] – ZOLTÁN HAVASI[1] – CSABA VÉR[2] – ZOLTÁN ORBÁN[1]

[1]*Structural Diagnostics and Analysis Research Group,*
Faculty of Engineering and Information Technology, University of Pécs
[2]*Department of Environmental Engineering,*
Faculty of Engineering and Information Technology, University of Pécs

Abstract: Concrete is the most widely used construction material, and therefore its application has a high environmental impact concerning the raw materials used in its manufacturing. The number of concrete buildings reaching the end of their designed life has gradually increased in recent years. The aging of existing buildings creates large problem in landfills due to the huge amount of waste materials that result from the construction and demolishing operations. Producing recycled aggregates from these concrete wastes, instead of dumping it in landfills, is a promising way to make the concrete industry more sustainable and waste-free. This paper demonstrates some of the results of an experiment where properties of recycled concrete, incorporating different percentages of reclaimed crushed aggregates, were compared with those of a reference conventional concrete. It was found that the performance of concrete mixes with reclaimed crushed aggregates satisfied the target design properties. However, the results point out some necessary changes in the optimal composition of recycled concrete mixes and define targets for further research.

Keywords: recycled concrete, reclaimed crushed aggregates, concrete properties

1. INTRODUCTION

Concrete consists of a uniform composite of different materials that are bonded together to form a solid and durable mixture. Cement, fine aggregates, coarse aggregates and water are constituents needed to produce a conventional concrete. Portland cement is one of concrete's main component and cement production needs an enormous amount of energy; this makes the cement industry one of the significant sources of carbon-dioxide emissions. It is estimated that about 5% of the global anthropogenic CO_2 emissions are produced by the cement industry [1]. The global interest in achieving sustainable development in the construction industry and protecting the environment has significantly increased over the last two decades; thus, governments around the world are adopting sustainable policies to achieve environmental and economic gains. These policies discourage landfills by applying taxes or even banning landfilling, requiring that construction and demolition waste be reused in the economic cycle. Furthermore, the idea of producing

useful products from these demolished wastes is not new, since preliminary work was carried out by Gluzhge as long ago as 1946, after the Second World War [2]. However, real progress and noteworthy advancements have been made only over the last two decades.

Generally, construction and demolished rubble contains components other than concrete, like tiles, soil, bricks, and wood, especially when the rubble is produced as a result of disasters such as wars, earthquakes, and floods. The existence of different contaminants reduces the quality of recycled aggregate, and these contaminants are difficult to remove. Although it is possible to produce high quality recycled aggregates that have properties similar or close to that of natural aggregates, the treatments (removing contaminants, classifying, washing, screening, multiple crushing stages, etc.) needed to obtain this quality cost of money, time, power and also produce CO_2 emissions. According to CSI report from 2009 [3], recycled aggregates are commonly used for one of the following applications: raw material for the cement industry, soil stabilizing or improving, pavement bricks, road construction subbase material, and embankment fill.

The potential use of recycled coarse aggregate from the concrete of demolished buildings, as replacement of natural aggregate, is also considered for the production of structural concrete. As a recent example from Hungary, the demolition of the 25-story Magasház in Pécs resulted in 22,549 tonnes of concrete debris [4]. The utilization of this material is underway.

Reclaimed concrete material (RCM), a by-product of the manufacturing process of precast concrete products in concrete plants, has different features: it often contains well-graded aggregates (usually mineral aggregates), bonded by a hardened cementitious paste. The management and sensible re-use of these waste materials will also be a great challenge for civil engineers in the future [5] [6].

This paper focuses on the analysis of the basic properties of concrete mixes prepared with recycled aggregates that were reclaimed from hardened concrete specimens. Consistency, water absorption and compressive strength results were compared to those of conventional concrete mixes. The aim of the research is to analyze how the properties of a specific conventional concrete change when using recycled aggregates gained from crushed concrete samples.

2. MATERIALS USED AND TESTS CARRIED OUT

A considerable amount of concrete waste as by-product of a normal manufacturing activity is produced every day in a local concrete lab in Pécs. To simulate the situation of construction and demolishing, waste from test cubes were collected after tests from various concrete classes. These cubes were crushed to produce reclaimed aggregates and then the aggregates were washed and sieved.

A standard concrete composition of grade C30/37-XC4-XV3(H)-16-F3 was designed using the natural and reclaimed aggregate fractions described in *Table 1*.

Name	Source	Type	Aggregate size range
OH 0/4	natural	fine	0–4 mm
OK 4/8	natural	course	4–8 mm
OK 8/16	natural	course	8–16 mm
Z 0/11	reclaimed	mixed	0–11 mm
Z 0/16	reclaimed	mixed	0–16 mm

Figure 1

Crushed concrete pieces obtained from cube specimens

The aggregates of graded course aggregate and sand were obtained from a quarry site near Pécs. The material for Z 0/11 was produced by cracking, chopping and grading concrete blocks, curbstones, paving slabs, and other paving elements, while the material for aggregate Z0/16 was made by crushing the pieces of 81 test cubes *(Figure 1)*.

The cement type used was CEM II/A-M (V-LL) 42.5 N composite, which contains supplementary materials of fly ash and limestone. The Z0/11 aggregate from crushed concrete samples was rich in fine particles and was not sufficient for larger particle ranges. Therefore the Z0/16 reclaimed aggregate was further decomposed into fractions 0/4 and 4/16.

For fresh concrete primarily the consistency was tested, while for the hardened concrete the compressive strength, the density and the water absorption. The testing of fresh concrete was carried out in accordance with MSZ EN 12350:2009 while MSZ EN 12390:2009 standard was used for testing the hardened concrete.

Determination of the water absorption of the aggregates was carried out in accordance with MSZ EN 1097-6:2013. In doing so, the water absorption of 10 larger pieces of concrete scrap was tested after one and two hours and until a constant weight in saturated condition was reached. The measured water absorption values showed large discrepancy between the concrete pieces, within the range of 4.9% and 10.4%. The analysis of water absorption clarifies that the recycled aggregate

contains more than one kind of material. It is evident that due to this significant amount of water absorption, pre-wetting of the aggregates is particularly important before mixing.

The particle size distribution curves of the recycled aggregates are shown in *Figure 2*.

Z 0/4

Z 4/16
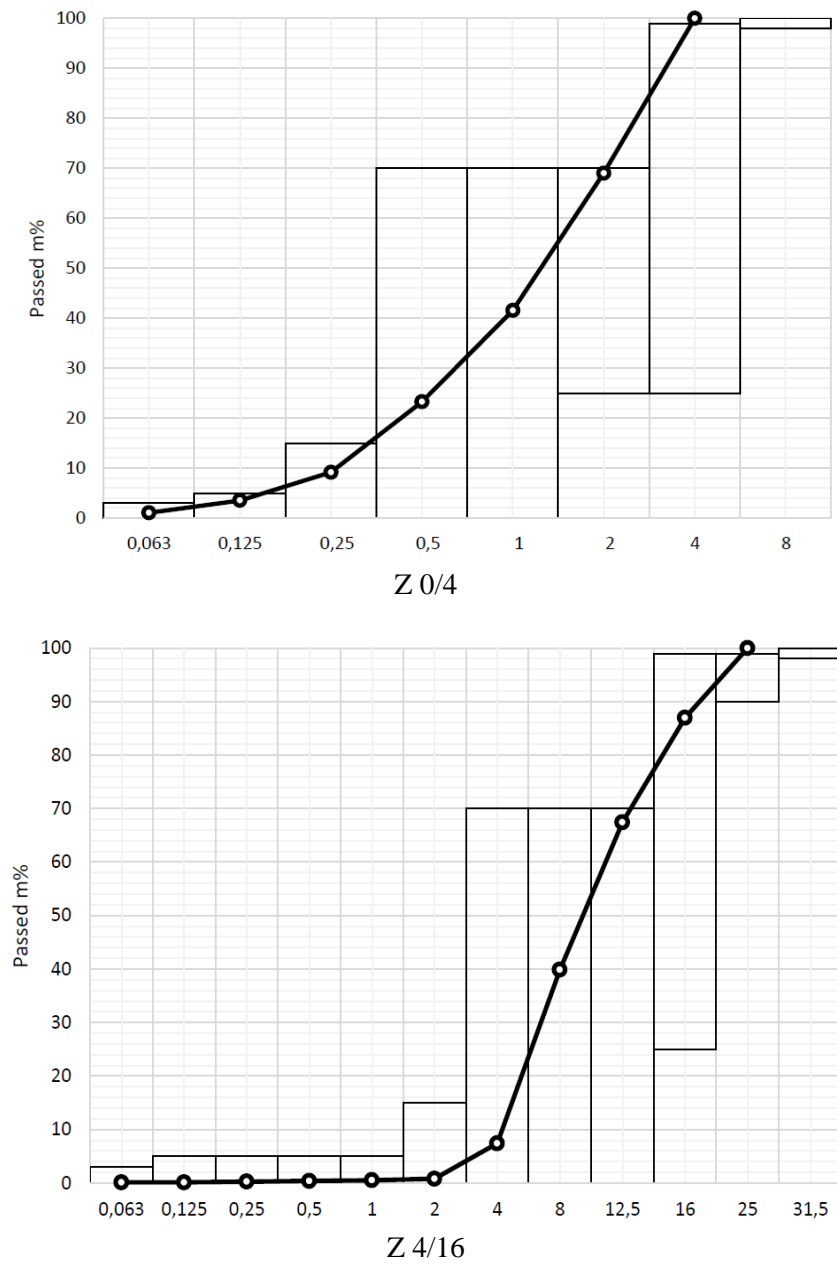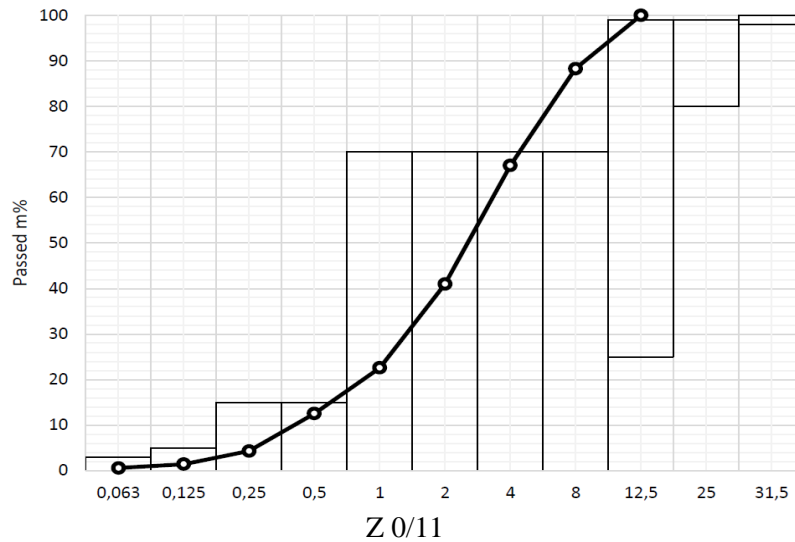
separated fractions

Figure 2
Particle size distribution curves of recycled aggregates

Surprisingly, the particle size distribution of the recycled material Z0/4 was better than that of the classified sand (OH 0/4). The particle size distribution of the material describes a gradually increasing logarithmic curve. However, there is a minor derogation from particle size distribution of 2 mm. In the case of Z4/16, the initial part of the curve is constant, followed by a gradually increasing log curve, since the

fine content is negligible, unlike the case of Z0/11, whereas the material has broader fractions of sand and gravel. This is the reason why the curve leaves the range between the sieve sizes of 4 mm and 12.5 mm. Regardless of this, there is no peak or fracture in the curve; a gradually increasing log curve can be seen here as well.

The measured average density of the particles was 2.62 g/cm^3 for the natural aggregates and 2.31 g/cm^3 for the reclaimed aggregates. There were no measurable differences between the pieces.

The aim to design the composition of the aggregates is to create a mixture of aggregates with a standardized fineness modulus, passing between the designated limiting curves from materials of a given fineness modulus and of a sieve curve. The analysis was performed by using five different kinds of aggregate mixtures. *Table 2* shows the designed compositions of aggregate mixes used.

Table 2

Designed composition of aggregates for concrete mixes

Mix number	OH 0/4 (natural)	OK 4/8 (natural)	OK 8/16 (natural)	Z0/11 (recycled)	Z0/16 (recycled)
Mix 01 (reference))	45%	25%	30%		
Mix 02	25%	5%	30%	40%	
Mix 03	10%		30%	60%	
Mix 04	25%	15%	20%		20% Z 0/4 20% Z 4/16
Mix 05	15%	10%	15%		30% Z 0/4 30% Z 4/16

The water content and density of the fresh concrete were affected by the type and composition of aggregates used for the mixes (see *Figures 3* and *4*).
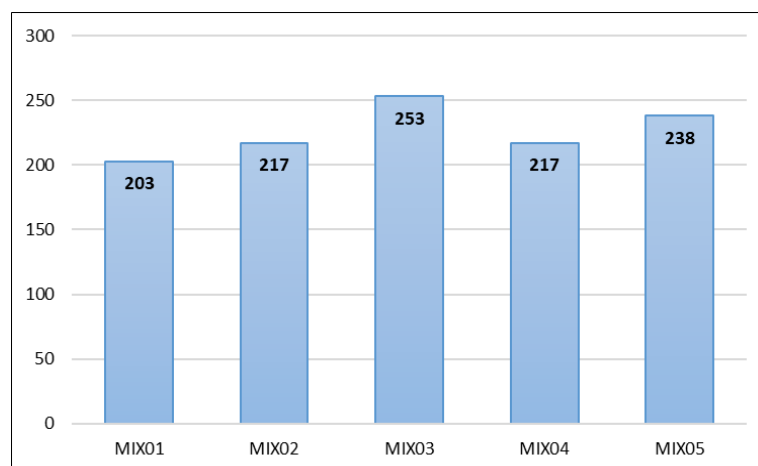
Figure 3

Water content of fresh concrete mixes (l/m^3)
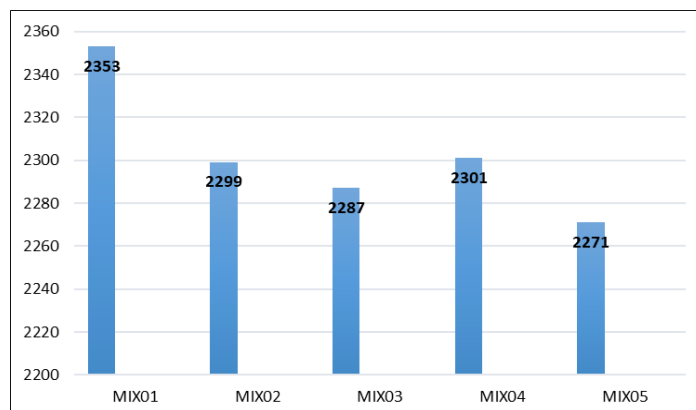
Figure 4
Density of fresh concrete mixes (kg/m^3)

The hardened concrete cube specimens were tested at 28 days of age for compressive strength (according to MSZ EN 12390-3:2009), density and water penetration (MSZ EN 12390-8:2009). *Table 3* and *Figures 5* and *6* summarize some of the test results obtained for the hardened specimens.

Table 3
Measured properties of hardened concrete at 28 days

Mix number	Compressive strength (MPa)	Density (kg/m^3)	Water penetration (mm)
Mix 01 (reference)	48,4	2327	N/A
Mix 02	56,2	2263	19
Mix 03	50,7	2252	25
Mix 04	51,2	2257	20
Mix 05	49,7	2205	29
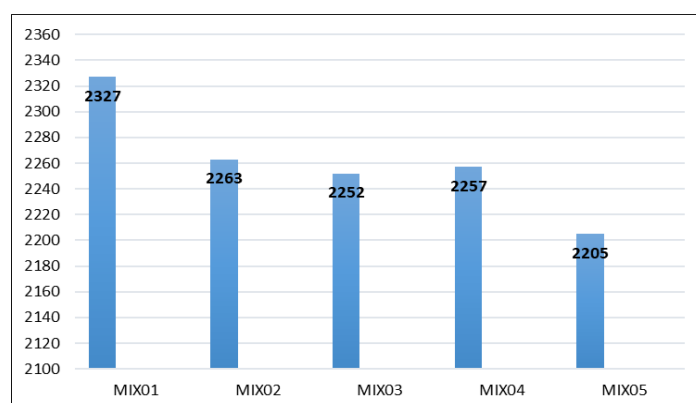
Figure 5
Density of hardened concrete specimens (kg/m^3)
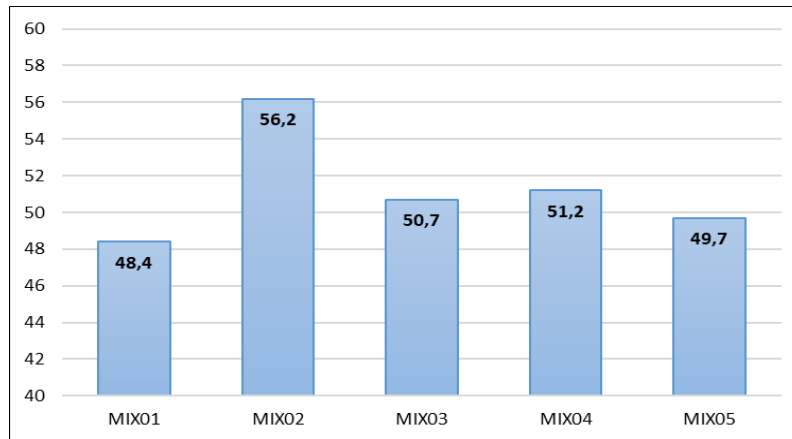
Figure 6
Compressive strength of hardened concrete specimens (MPa)

3. CONCLUSIONS

Some of the properties of concretes containing recycled aggregates reclaimed from hardened test cubes were investigated and compared to conventional concrete mix was investigated. Properties of five concrete mixes containing various amounts of reclaimed aggregates were tested in both fresh and hardened states. It should be noted that the maximum allowable replacement percentage of natural aggregates by the EN-206 standard is 30%, but some of the mixes deliberately contained higher amounts.

As was expected, the water content and density of the fresh concrete mixes were strongly affected by the type and composition of aggregates used for the mixes. It was concluded from the tests that it becomes more and more difficult to keep the planned consistency of the fresh concrete as the amount of recycled aggregates in the mixes increases.

Based on the tests carried out on fresh concrete mixes, it seemed likely that the samples containing recycled materials in increasing quantity would not reach or even approach the requirements of C30/37 concrete class. In spite of that, unexpectedly good results were obtained on the hardened concrete samples. The compressive strength result of each mixture reached the lowest bound defined for the planned concrete grade. What is more interesting, all mix compositions but one gave better results for strength than those achieved by the standard recipe.

Originally, the mixes were designed for the XV3(H) exposure class. The maximum allowed water penetration value of concrete with XV3(H) exposure class is 22 mm. Half of the samples reached a lower level water penetration value, but the rest of the samples yielded worse results.

As for compressive strength, it was found that the recycled aggregates did not downgrade the quality of concrete; the strength of the samples 60% recycled by

weight complied with the requirements of the targeted concrete class, as did the samples from the reference mixes. On the other hand, the way that the higher porosity of the recycled material affects the behavior can be seen when testing the water penetration. In some of the specimens where recycled aggregates were used, the measured water penetration values exceeded the acceptable limit (22 mm) given for the defined exposure class. This can be explained by the fact that these materials are more porous than natural aggregates; consequently, water can penetrate into these concrete specimens more easily under pressure.

The results of the tests encourage the use of recycled concrete aggregates to achieve more sustainable concrete technology by saving natural aggregate raw materials from being exhausted.

REFERENCES

[1]   Worrell, E., Price, L., Martin, N., Hendriks, C., Meida, L. O. (2001). Carbon dioxide emissions from the global cement industry. *Annual Review of Energy and the Environment*, 26, pp. 303–329.

[2]   Gluzhge, P. J. (1946). The work of scientific research institute. *Gidrotekhnicheskoye Stroitelstvo*, No. 4, pp. 8–27. (In Russian)

[3]   CSI Cement Sustainability Initiative Report (2009). World Business Council for Sustainable Development, www.wbcsd.org.

[4]   Jakab R. (2018). A pécsi magasház bontásából származó hulladékok kezelése, utóhasznosítása. *Beton*, XXVI. évf. III. szám, p.13. (In Hungarian)

[5]   Anastasiou, E. (2018). Investigation of the Use of Recycled Concrete Aggregates Originating from a Single Ready-Mix Concrete Plant. *Applied Sciences*, 8 (11), p. 2149, https://doi.org/10.3390/app8112149.

[6]   Malešev, M., Radonjanin, V., Marinković, S. (2010). Recycled concrete as aggregate for structural concrete production. *Sustainability*, 2 (5), pp. 1204–1225., https://doi.org/10.3390/su2051204.

INDUSTRIAL TESTS WITH A RESIDUAL MUNICIPAL SOLID WASTES PROCESSING PLANT WITH THE NEWLY DEVELOPED KLME COMBINED SEPARATOR

JÓZSEF FAITLI[1] – BARNABÁS CSŐKE[1] – ROLAND ROMENDA[1] – ZOLTÁN NAGY[2] – ÁDÁM RÁCZ[1]

[1]*University of Miskolc, Institute of Raw Material Preparation and Environmental Processing*
[2]*3B Hungária Kft., Hungary, Zalaegerszeg*

Abstract: Municipal waste management is slowly moving from landfilling to waste processing. This paper focuses on a separation device in a new waste processing plant in western Hungary. The plant, put into operation in July 2018, has mechanical-physical technology including a pre-shredder, a drum screen to separate the bio-fraction, a newly developed combined air flow, magnetic and eddy-current separator (KLME), two NIR sorters and a final shredder. The main products of the technology are the bio-fractions and inert fractions (still landfilled at the first stage), material streams for recycling, Fe, Al, PET and PVC and secondary fuel material (RDF) for energetic utilization. This paper reports on the process engineering tests and characteristics of three different designs of the KLME separator. Three industrial-size mechanical processing tests have also been carried out with samples of more than 10 t each. Research work of the second development stage has also begun. A pilot-scale pyrolysis reactor has been made and fundamental research is ongoing to produce bio-fraction and RDF pellets as fuel for this machine.

***Keywords:** KLME separator, residual municipal solid wastes (RMSW), combined energetic utilization of bio-fraction and RDF, rotary shear*

1. INTRODUCTION

Modern lifestyles result in significant municipal waste generation, and if we would like to maintain or even improve the living standards we have achieved, sustainable waste management is necessary. Even developed countries have to take the long-term generation of residual municipal solid wastes (RMSW) into account, because even with the application of a sophisticated selective collection system there are still large amounts of residual materials that have to be non-selectively collected and handled [1, 3, 25, 26]. There are many different country-specific solutions for processing technologies for RMSW. In Europe, a widely used concept is mechanical or biological pre-treatment. This method reduces the environmental impact when some portion of the RMSW is still finally disposed in landfills [29]. The main problem with this technology is the very heterogeneous nature of RMSW, which does not allow the use of universal processing technologies. However, tech-

nologies usually contain a pre-shredding or bag-opening step, classification with drum or cascaded sieve and upgrading steps with different separator and sorting machines [8, 13, 23, 27]. Finally, the degradable fine bio-fraction can be biologically treated by aerobic or anaerobic processes to reduce the mass, volume and biological hazard potential of the waste [2, 22].

There are three main types of these technologies: Mechanical–Biological Stabilization (MBS), Mechanical-Physical Stabilization (MPS) and Mechanical–Biological Treatment (MBT) [2, 5, 12, 21]. Both the MBS or MPS technologies use the same steps to treat the solid waste, namely shredding, screening, metal and plastic sorting and separation. The only difference between these two technologies is the method of biological treatment. In physical treatment methods, physical drying technologies are utilized after metal sorting, while MBS uses aerobic or anaerobic digestion to stabilize the organic components in the residual municipal solid waste [4, 14, 28]. Mechanical–Biological Treatment is more complex than other two approaches, because after pre-shredding the waste is divided into two size fractions by a drum screen (50-80 mm). The fine fraction goes to biological treatment while the coarse fraction is treated with mechanical methods to make recyclable products and Refuse-Derived Fuel (RDF) [6, 16, 17, 18, 19, 20, 24, 30].

As of 2017, there were 26 RMSW processing plants in Hungary, mainly mechanical–physical plants [15]. Typically the key machinery for comminution, separation and sorting is imported from abroad (with the exception of the recently commissioned plant). The main products of these plants is bio-fraction, some small material streams for waste-to-material recycling (such as Fe, Al and PET), and refuse derived fuel (RDF). At this point in Hungary the bio-fraction is mainly landfilled. A small proportion of the bio-fraction is stabilized by aerobic decomposition before landfilling. There is ongoing intensive research about better handling and utilization for the bio-fraction in the country. The bio-fraction generally contains organic, biodegradable materials but it also contains a lot of metals, plastics, and inert wastes, and therefore its treatment is difficult. The current Hungarian situation is that the rate of separation of the valuable materials from RMSW for recycling is rather low because of the existing low aftermarket and processing industry capacities; recycling of this material stream is still not very developed. The municipality of Zalaegerszeg decided on the improvement of the MSW management of the region according to European Directives. In the near past, 100% of the RMSW was landfilled in the up-to-date landfill of the community. A consortium formed from a machine and technology producer (3B Hungary Ltd.), a scientific partner (the Institute of Raw Materials Preparation and Environmental Processing, University of Miskolc), and a public waste managing service company (Zala-Müllex Ltd.) is working on the development and construction of an RMSW processing technology targeting no-landfilling for this waste stream [10]. The development and construction of the mechanical-physical processing plant – the first stage – was supported by an EU-funded grant. A new waste processing plant was built in Zalaegerszeg (Búslakpuszta) to treat residual municipal solid wastes of the region (60,000 tons/year). The new plant, which is almost entirely developed in Hungary and con-

structed and equipped by Hungarian firms, was inaugurated on 13 July 2018. Since the inauguration, the technology has been slightly modified based on the experience gained from industrial size operational tests. The originally developed bag opener machine was replaced by a two-rotor rotary pre-shredder and feeder machine. Three different designs of the KLME separator were built and tested. On 25-26 September 2019 three industrial-size tests were carried out with samples of more than 10 t each. The tests were run with a previously optimized parameter setup and the outputs and the necessary intermediate belt conveyors were sampled. A new fluid dynamics study is starting to further optimize the operation of the KLME separator and data was necessary to map the recent situation. This paper reports on the process engineering evaluation of these tests.

2. MATERIALS AND METHODS

Before the design of the processing technology a sampling campaign was carried out in the collection area [10] to gain fundamental data for technological design. Before the classification of waste types the waste bags must be opened. Thus, the first unit of mechanical–physical RMSW plants is either a pre-crusher or a bag opener placed before the classification (drum screen or cascade sieve) unit. Generally a rotary pre-shredder is applied for opening bags; however, it has a serious disadvantage, since this machine mixes up the Fe and plastic particles and the resultant intergrown particles cause problems for the downstream separation. The energy need of a rotary pre-shredder is also significant. Therefore, a bag opener machine *(Figure 1)* was developed and made in Zalaegerszeg [10, 11].

Figure 1	**Figure 2**
The moving floor conveyor and the bag opener machine	*The rotaries of the Metso M&J PreShred 1000 machine*

A big rotor with teeth for the bag opener rotates opposite to the moving floor conveyor; therefore the bags are lifted and torn into the hydraulically supported standing teeth. Unfortunately, during the operational tests, two problems with this bag opener machine were revealed: insufficient bag opening and uneven feed for the technology. Even feed is crucial for the smooth operation of RMSW processing

technology and clean products. Therefore, the bag opener machine was exchanged for a Metso M&J PreShred 1000 two-rotor rotary shredder *(Figure 2)*.

The technological flowsheet of the plant as it was inaugurated was published in [10, 11]. The technology has since been modified, and the current version (as of October 2019) is shown in *Figure 3*. The industry standard drum screen is equipped with a drum screen with 60 mm circular openings. The separated bio-fraction (–60 mm) will be temporarily landfilled after this first stage of development. The pre-shredded coarse fraction (+60 mm) goes into the newly developed KLME separator.
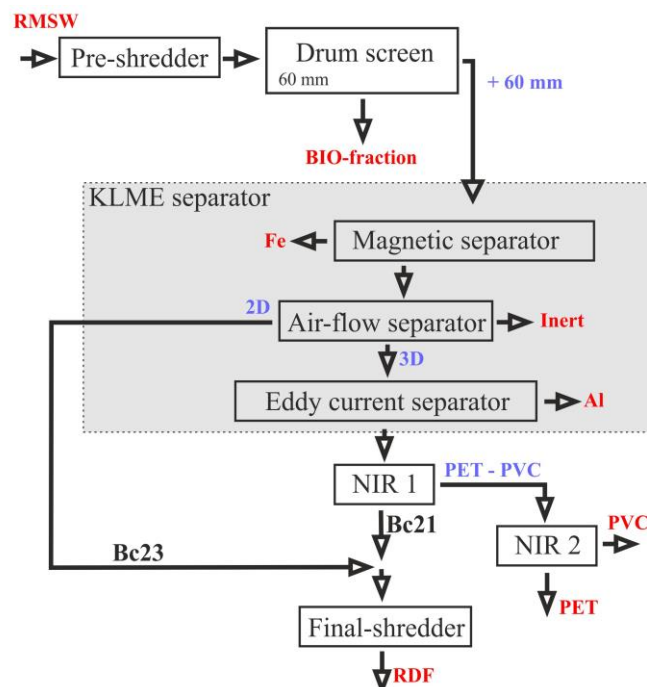
Figure 3
RMSW processing technology

As was reported earlier [9, 10, 11], many model machines were made before building the industrial size prototype KLME machine. The schematics of the KLME separator with exhaust cage were published earlier [10, 11]. To the best of our knowledge, the KLME separator is the only machine in the world that combines four separators in one unit without intermediate conveyors and bins. Therefore, space and energy requirements are smaller. The exhaust cage design was made first and afterward two other designs followed it. It is instructive to follow the development steps and key points to understand why modification was necessary. In the first technological version the 60–200 mm intermediate size fraction was fed into the KLME separator by a vibrated feeder. The air nozzle was located in the bottom

of the first part of the vibrated plateau. Heavy particles fell through the air beam onto the magnetic drum. Magnetic particles were dragged into the Fe product output, while heavy inert particles (rocks, bricks and so on, as well as wet and therefore heavy books, shoes, etc.) fell into the inert product output. Light particles were blown and transported by the air beam. When a particle falls into the air beam, the initial acceleration part of particle settling is dominant, but afterwards, when the particle is being transported by the air beam, the particle settles in it and has sufficient time to settle; therefore the terminal settling velocity is dominant [9]. Another point is that the density of the particle (body) – and not the material density – determines both the initial and terminal particle settlings. The material density of aluminum cans and PET bottles is significantly different; however, their particle densities might be similar depending on how they had been compressed previously. Therefore the light particles in 2D shape (foils and papers) and in 3D shape (aluminum, plastics) light particles were also blown by the air beam. The 3D plastics and aluminum particles settle out from the beam and then an eddy-current separator separated them into two products. The 2D-like foils and paper sheets were sucked into the surface of the exhaust cage, because there is a strong suction from the inside of this cage supplied by two auxiliary fans. The rotating cage transported the 2D particles into the 2D output. Unfortunately, clogging often occurred on the surface of the exhaust cage when the earlier applied hammer pre-crusher [10, 11] was operated for the comminution of the +200 mm particle size materials. When the crushed small particles reached the KLME separator, these small particles clogged the 10×10 mm square openings of the exhaust cage. Therefore, the KLME separator and especially its 2D separator were redesigned and a new industrial prototype was made. This 2nd design is labelled the KLME separator with nailed roller. The fans of the exhaust cage were removed and the 2D channel was redesigned. The schematic drawing of the KLME separator with nailed roller is shown in *Figure 4*. Industrial process engineering tests with the KLME separator with the nailed roller were carried out in the plant at different parameters. These tests showed that this construction is more suitable but there were still operational issues, such as clogging of the nails on the roller and separation issues of the foils (2D) from the 2D air channel. Thus the KLME separator was redesigned for the third time and a new industrial prototype was made. It has to be mentioned here that this design idea originates from János Vad. Some mock-up units made from wood sheets were made to study two phenomena: the Coanda effect and air beam dragging. The Coanda effect is well known in the literature. In 1910, the Romanian engineer Henri Coanda observed that air flows near surfaces would bend because of the fluid dynamics influence of the surfaces [7]. The second issue, air beam dragging (distraction) by a neighboring wall, was experienced with the earlier designs of the KLME separator. On the basis of the preliminary tests with mock-up devices a new industrial KLME separator was built *(Figure 5)*.
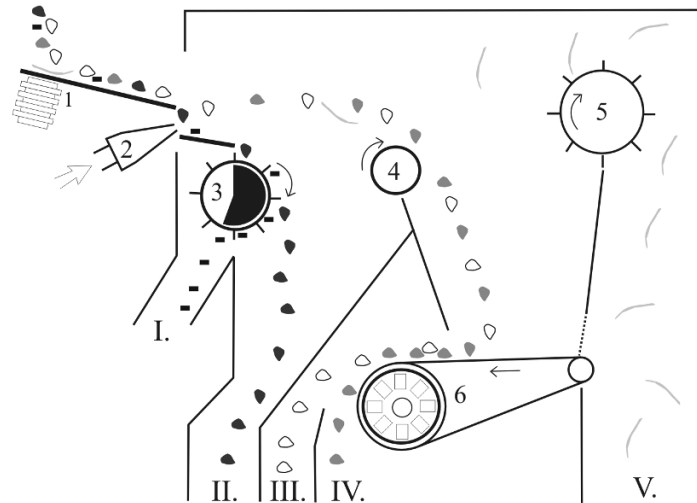
Figure 4
The KLME separator with nailed roller schematics
Main technological units are: *Vibrated feeder, 2. Air nozzle, 3. Magnetic drum, 4.*
Rotated auxiliary cylinder, 5. Nailed roller, 6. Eddy current separator.
Numbers and short names of products are: *I. Magnetic, II. Inert, III. Al, IV. 3D, V. 2D.*
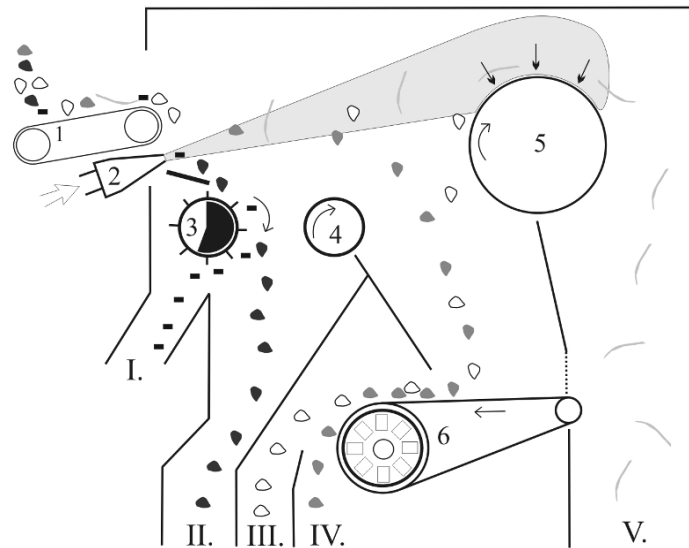
Figure 5
The KLME separator with Coanda roller schematics
Main technological units are: *1. Vibrated feeder, 2. Air nozzle, 3. Magnetic drum,*
4. Rotated auxiliary cylinder, 5. Coanda roller, 6. Eddy current separator.
Numbers and short names of products are: *I. Magnetic, II. Inert, III. Al, IV. 3D, V. 2D.*

The air beam released by the nozzle and induced by the centrifugal impeller fan should reach the upper ¾ part of the Coanda roller. If the operation is sufficient the air coming out from the nozzle with the retrained air together will flow above the Coanda roller into output V. If this flow pattern is fulfilled the evolved Coanda effect helps effective 2D separation, because 2D shaped particles are "sucked" onto the drum surface by the Coanda effect and the rotating drum transports them to output V. However, experimental difficulties were experienced with the mock-up units with targeting the air beam into the proper section of the Coanda roller. The angle of the air nozzle was changed systematically; however, the design of the KLME housing and its inner structure strongly influence the propagation direction of the air beam. Improper design can propagate the air beam upward, way above the Coanda drum, or downward into the eddy-current separator. In such a case, it was not the angle of the nozzle that determined the direction of the blown-in air beam. In the case of the upward beam distraction, additional air was sucked in from above the beam, an eddy formed between the air beam and the upper wall, and its result was upper beam distraction. After redesigning the separator these problems were eliminated and now the direction of the air beam propagation can be set precisely by setting the angle of the air nozzle. Another significant modification was the change of the vibrated feeder into a short feeder belt conveyor. The particles before the air nozzle must be evenly distributed. If evenly distributed particles fall into the air beam good separation is the consequence. The feed with the vibrated feeder was not sufficiently even, so particle bulks were formed and that caused bad separation. *Figure 6* shows the most recent version of the KLME separator.

Figure 6
The KLME separator

On the left upper side an air chamber for the exhaust air output can be seen above the 2D belt conveyor *(Figure 6)*. Before the end of the technology there are two near infrared (NIR) sorters *(Figure 7)*. The first one is set to remove the PET and PVC particles and the second one cleans the PET product from this stream by removing the PVC. By this way the technology separates the Al, PET and Fe materials for waste-to-material recycling and the PVC is also removed from the produced RDF, which is necessary for the thermal utilization. The final machine of the technological flowsheet *(Figure 3)* is a one-rotor shredder produced by Metso (Fine Shred) with radial cutting gap.

Figure 7
The NIR sorters

Three industrial size processing experiments were carried out on 25th and 26th September 2019. *Table 1* shows the mass and origin of the processed samples. The gross and net masses of a waste collecting vehicle transporting a sample were measured by a weighbridge with a resolution of 10 kg. Before each test all the machine parameters were set and checked and the equipment was emptied out.

Table 1
The mass and origin of samples

Mark of the test	Test A	Test B	Test C
Collection area (municipality) of RMSW	Zalaegerszeg city center	Andráshida, Babosdöbréte	Teskánd, Csatár, Bokföld (4,280 kg), Zalaegerszeg Hegyföld (1,600 kg), Zalaegerszeg Kertváros (6,700 kg)
Mass of raw sample [kg]	10,600	10,440	12,580

Feed was started by a bucket loader into the hopper of the pre-shredder. Time measurement was started when the material appeared at the bottom of the pre-shredder. At a given point in time the equipment was stopped and samples of a given length of three conveyor belt sections were taken. Time measurement was stopped finally when the material flow terminated at the bottom of the pre-shredder. The mass of each product was measured by appropriate nominal range and resolution balances (40 t, 150 kg, 20 kg, 5 kg, 1 kg nominal ranges). Samples were taken from all products during the industrial size tests, except from RDF, because that had earlier been analyzed semi-continuously. However, the composition of the RDF product was examined by taking samples from belt conveyor Bc21 and Bc23 *(Figure 3)*. These two belts convey the materials into the final shredder. All samples were sieved by a 50 mm quadratic opening 1.2 × 1.2 m size sieve frame. The +50 mm size fractions were hand sorted into many material categories. The –50 mm size fractions were hand sorted only into two categories: particles in the correct and in the incorrect place, namely, a significant amount of –50 mm aluminum particles were in the Al product.

Mechanical pre-treatment experiments with the bio-fraction and RDF were carried out from September 2018 to August 2019. Samples were taken many times during the experimental runs of the mechanical-physical RMSW processing plant. Moisture content was measured in a drying oven at 105 °C until mass equilibrium. Empirical particle size distribution was measured by hand sieving with different laboratory sieve series. Material composition was determined by hand sorting with the help of some auxiliary equipment (magnets, Raman spectrometer, FTIR spectrometer, XRF spectrometer). For the separation of the non-ferrous metal, rock and glass particles a counter-current air flow separator was used, and a pilot-scale flat-die pelletizing machine was used for the pelletizing experiments with RMSW bio-fraction and RDF. These machines were made by the Institute of Raw Material Preparation and Environmental Processing, University of Miskolc. The nominal capacity of this pelletizer machine is 100–200 kg/h, depending on the physical features of the fed material. The outer diameter of the flat die is 200 mm, the length of the holes is 28 mm and their inner diameter is 8 mm. For the laboratory comminution of the prepared samples a cutting mill was used (diameter and length of the rotor: 300 × 600 mm, inside sieve opening: 10 and 20 mm, nominal capacity: 200 kg/h, tangential speed of tip point: 26.3 m/s). Ash content and calorific value were measured by the accredited laboratory of the Department of Combustion Sciences, University of Miskolc.

3. RESULTS AND DISCUSSION

Experiments had been carried out previously to determine an optimized setup of all the technical parameters of the RMSW processing plant. Two tests were planned with identical parameters with a moderate capacity and the third one with slightly increased capacity. *Table 2* shows the unchanged main technical parameters for all three tests. The pre-shredder machine acts as a controllable feeder as well. The

revolution number of its rotors determines the mass flow rate of feed. During Test C this revolution number was increased from 35 1/min to 40 1/min. Because of the increased feed, the speed of the moving floor conveyor and the revolution number of the drum screen were also increased. The changed parameters are shown in *Table 3*.

Table 2

Unchanged main technical parameters of Tests A, B and C

Parameter	Value
KLME accelerating feed belt conveyor speed	0.537 m/s
KLME air nozzle air flow rate (blown in)	8,100 m^3/h
Air flow rate in the 2D separation chamber (exhausted)	13,000 m^3/h
Revolution number of the eddy-current separator pole motor	2,820 1/min
NIR1 and NIR2 feed belt conveyor speed	3 m/s
Belt conveyor speed before the Metso rotary final-shredder (Bc21)	0.689 m/s

Table 3

Varied main technical parameters

Parameter	Test A	Test B	Test C
Revolution number of pre-shredder rotors	35 1/min	35 1/min	40 1/min
Moving floor conveyor speed	0.057 m/s	0.057 m/s	0.059 m/s
Tangential speed of the drum screen perimeter	1.11 m/s	1.11 m/s	1.17 m/s

Figure 8
Photo of sample of Test C to be fed

As an example, *Figures 8, 9* and *10* show photos of the fed sample and the products of Test C. *Figure 8* shows the feed and *Figure 9* shows photos of the separated four material streams intended for waste-to-material recycling. These are Fe, Al,

PET and PVC *(Figure 9)*. *Figure 10* shows photos of the separated two material streams intended for waste-to-energy local thermal utilization after the second development stage. By just looking at the products many conclusions can be drawn. At first glance it is seen that there are many 2D plastic particles (foils) in the Fe product (6.81 m/m% for Test B, *Table 5*). This is a consequence of the change of the first comminution machine from a bag opener into the rotary pre-shredder. The bag opener machine did not crumple the foil and Fe particles together; therefore the Fe product was cleaner than that shown here (though not other products). The rotary pre-shredder does crush them together; therefore, there are many intergrown Fe–foil particles in the Fe product. Though the visible volume percentage is high, the mass percentage of the foil compared to Fe is low. When the total amount of a sample had been processed and all the materials were in the product containers the net weight of each product was measured.

Figure 9
Products of Test-C for waste-to-material recycling: a) Fe; b) Al; c) PET; d) PVC

a)   b)
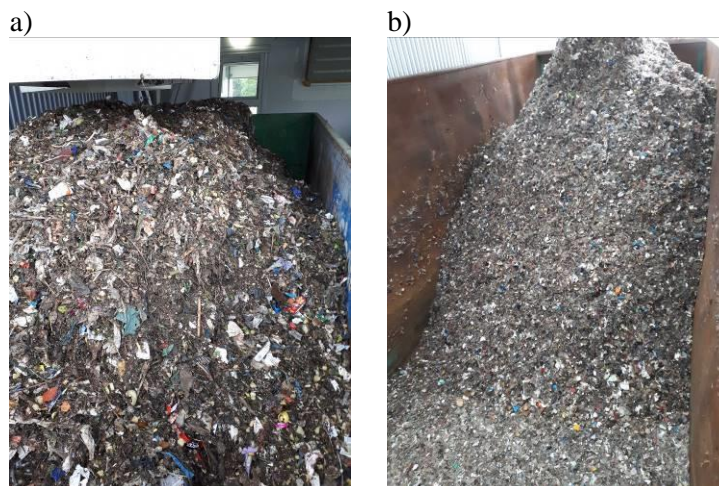
Figure 10

Products of Test C for waste-to-energy local thermal utilization: a) Bio-fraction; b) RDF

Table 4

Products mass yield data of the industrial tests

Product of technology	Test A		Test B		Test C	
	Mass [kg]	**Mass yield of product [%]**	**Mass [kg]**	**Mass yield of product [%]**	**Mass [kg]**	**Mass yield of product [%]**
Bio-fraction (-60 mm)	5,860	55.6	6,100	59.5	6,840	56.7
Fe (all magnetic)	268.7	2.6	328	3.2	129.56	1.1
Inert (Si)	552.9	5.3	502	4.9	658.6	5.5
Al	13.5	0.1	12.5	0.1	13.84	0.1
PET	345.2	3.3	225	2.2	123.47	1
PVC	9.15	0.1	7.8	0.1	19.8	0.2
RDF	3,465	33	3,065	30.0	4,270	35.4
Total	**10,514.45**	**100**	**10,240.3**	**100**	**12,055.27**	**100**
Measured capacity	15 t/h		17 t/h		17 t/h	

Table 4 shows the mass data of each product as well as the calculated mass yields of products in mass percentage units. The composition of the bio-fraction was not examined during the described industrial tests, as it had been investigated earlier. In the case of the RDF the two material streams (the 3D particles on the Bc21 belt

conveyor and the 2D particles on the Bc21 conveyors) were sampled by taking all the materials on a 4 m belt length on the stopped conveyor. In this way the mass flow rates of these belts were also determined and the composition of the RDF product could be calculated. The RDF of this plant had been extensively tested before, too. *Table 5* shows the component content of the Fe, Inert, Al, PET and PVC products (see *Figure 3*) and indirectly shows the component content of the RDF product of Test B as an example. The sorted material components are shown in the left-hand column of *Table 5*.

Table 5

The component contents (m/m%) of the products of Test B

Material components	Product					Belt conveyor	
	Fe	Inert (Si)	Al	PET	PVC	3D-Bc21 (RDF)	2D-Bc23 (RDF)
3D – HDPE, PS, PP	–	4.74	0.40	4.43	10.27	7.51	4.52
3D – PET	0.37	0.43	–	**49.89**	13.48	7.51	2.26
2D – foil	6.81	2.16	1.60	3.33	3.85	9.25	**56.56**
2D – paper	0.12	8.19	1.20	4.43	4.49	18.50	10.18
Composite	0.37	1.29	2.81	0.22	0.13	2.89	–
Al	–	3.02	**90.62**	–	0.39	1.16	–
Fe	**81.16**	3.45		–	0.64	1.16	–
Textile	1.86	1.72	0.24	**16.63**	10.91	22.54	6.79
Stone (glass)	–	19.40	–	–	–	–	–
Bio	1.24	9.914	0.08	–	–	0.58	0.45
Other combustible	3.10	25.43	0.24	16.63	44.93	15.03	3.39
Other (fine: -50 mm, non-identifiable)	4.96	20.26	2.81	4.43	10.91	13.87	15.84
Total	100	100	100	100	100	100	100

All product samples were first sieved on a 50 × 50 mm opening screen. From the undersize fractions only particles in the correct product were sorted out. For example in the Fe product the – 50 mm Fe (magnetic) particles were sorted out and their mass was added to the Fe component, because the technology separated these particles into the right product. Therefore, they have to be taken into account in the final material balance, even though they would have been included in the bio-fraction with this equipment because they are smaller than the drum screen openings.

During Test A the feed mass flow rate was 15 t/h at 35 1/min pre-shredder rotor revolution number. 55.8% of the feed was yielded into the bio-fraction product. The mass flow rate of the KLME separator feed was 6.4 t/h. The mass yield of the RDF product was 33.2%, therefore, the capacity of the final-shedder was 4.9 t/h. The aluminum content of the Al product was very high (87.2 m/m%). The magnetic content of the Fe product was moderate, only 59.8 m/m%. The PET product contained 49.9 m/m% PET from which about 8 m/m% was PET textile.

During Test B the throughput of the plant was 17 t/h, despite the fact that the pre-shredder rotor revolution number was the same (35 1/min). This is a considerably higher capacity. The only explanation is that the material – especially its moisture content – was higher. 59.5 m/m% of the fed material was yielded into the biofraction. The mass flow rate of the KLME separator was 6.9 t/h. The RDF yield was 30 m/m%; therefore, the final shredder operated with 5.1 t/h. The products were considerably cleaner, the aluminum content of the Al product was 90.6 %, the magnetic material content of the Fe product was 81.2 m/m% and the PET product contained 49.89 m/m% PET bottles and sheets and additionally about 14 m/m% PET textile.

Although in Test C the revolution of the rotors of the pre-shredder was increased by 14 % up to 40 1/min, the measured throughput was also 17 t/h. This is also because of the material, with a little lower moisture content in this case. 56.7 m/m% was the bio-fraction yield, and 7.3 t/h was the KLME feed. The capacity of the final shredder was 6 t/h and 35.4 m/m% of the feed was distributed into the RDF product. The Al product contained 84.9 % aluminum; the Fe product contained 71.65 % magnetic particles. The PET content of the PET product was the highest, 73.5 m/m%, which contained 46.1 m/m% PET bottles and sheet and 27.4 m/m% textile PET as well.

Table 6

The mass flow rate of the individual machines during the industrial tests

Mass flow rate of machines	Test A [t/h]	Test B [t/h]	Test C [t/h]
Pre-shredder	15	17	17
Drum screen	15	17	17
KLME separator	6.4	6.6	7.3
NIR I sorter	5.5	5.7	6.2
NIR II sorter	0.5	0.4	0.2
RDF final shredder	5	5.1	6

Table 6 contains the measured and calculated mass flow rates of the individual machines during the industrial tests. This table contains a clue as to why the measured capacity of Test B is so high. In this case the mass flow rate of the KLME separator is lower (6.6 t/h) than in Test C (7.3 t/h); therefore, a higher percentage of

material went into the bio-fraction. This is logical, since the soil-like state bio-fraction adsorbs more internal moisture, and this explains the measured data.

4. CONCLUSIONS

The municipality of Zalaegerszeg (Hungary) decided to improve its MSW management in order to decrease landfilling in the area to near to 0 %. The first stage of this conceptual plan has been carried out because a mechanical–physical RMSW processing plant has been constructed. Since then the plant has been operating in test mode and some modifications have been made. Three different industrial size prototypes of the KLME separator have been made. The best construction so far is the KLME separator with a Coanda roller. The earlier installed bag opener machine was exchanged for a two-rotor rotary pre-shredder and feeder machine. Three industrial size mechanical processing tests with samples of more than 10 t each were carried out to analyze the current operation and yield and quality of products. Smooth and stable plant operation was experienced with quite stable yields of products with satisfactory purity, despite the very heterogeneous nature of raw RMSW.

REFERENCES

[1] Aich A., Ghosh, S. K. (2016). Application of SWOT analysis for the selection of technology for processing and disposal of MSW. *Procedia Environmental Sciences*, 35 pp. 209–228.

[2] Alexa, L., Bokányi, Lj., Csőke, B., Varga, T. (2017). A Novel Complex MSW Biomass Processing System with the Economic and Environmental Target to Maximize Waste-to-Energy Output. *19th European Conference and Exhibition*, 6–10 June 2011, Berlin, pp. 1851–1857.

[3] Csőke B. (2003). A hulladék, mint nyersanyag. (Waste as Raw Material). *BKL Bányászat*, 136, Vol. 6. pp. 415–430.

[4] Csőke B., Faitli J., Györfi A., Alexa L., Ferencz, K. (2006). Production of Secondary Raw Materials and Fuels through the Preparation of Municipal Wastes. IMPC 2006, Sept. 3-6. 2006. Istanbul. *Proceedings of the XXIII In-*

ternational Mineral Processing Congress (Ed. Önal et al.), Promed. Ad. Agency, Istanbul, pp. 230–235.

[5] Csőke B., Alexa L., Olessák D., Ferencz K., Bokányi Lj. (2009). Mechanikai-biológiai hulladékkezelés kézikönyve. (Handbook of Mechanical – Biological Waste Treatment), Profikomp könyvek, Global Kiadó, Gödöllő.

[6] Csőke B., Faitli J., Mucsi G., Antal G., Bartók F. (2012). Comminution of Forest Biomass by Modified Beater Wheel Mill in a Power Plant. *International Journal of Mineral Processing*, Volumes 112–113, pp. 13–18.

[7] Crivio O., Doroftei I. (2016). Some experimental results on Coanda effect with application to a flying vehicle. 7th International Conference on Advanced Concepts in Mechanical Engineering, *IOP Conf. Series: Materials Science and Engineering*, 147 (1), pp. 338–344.

[8] Everett, J. W., Peirce J. J.: The development of pulsed flow air classification theory and design for municipal solid waste processing. *Resources, Conservation and Recycling*, 4, pp. 185–202.

[9] Faitli J., Romenda R. Szűcs M. (2017). Egyedi TSZH szemcsék mozgásának vizsgálata modell légáramkészülékben (The examination of the motion of single MSW particles in a model air flow separator). In: Szigyártó I. L. Szikszai A. (eds.). *XIII. Kárpát-Medencei Környezettudományi Konferencia*, Cluj Napoca, Romania, 5–8 April 2017. Ábel Kiadó, pp. 228–237.

[10] Faitli, J., Csőke, B., Romenda, R., Nagy, Z. Németh, S. (2018). Developing the combined magnetic, electric and air flow (KLME) separator for RMSW processing. *Waste Management & Research*, 36 (9), pp. 779–787.

[11] Faitli, J., Csőke, B., Romenda, R., Nagy, Z., Németh, S. (2019). Industrial Tests with a New Mechanical – physical RMSW Processing Plant in Búslakpuszta, Hungary. In: Moustakas K., Loizidou, M. (ed.). *Proceedings of the 7th International Conference on Sustainable Solid Waste Management*. Herakleion, Grece, pp. 1–8. Paper: Session XIV paper 14.

[12] Fei, F., Wen, Z., Huang, S., Clercq, D. D. (2018). Mechanical biological treatment of municipal solid waste: Energy efficiency, environmental impact and economic feasibility analysis. *Journal of Cleaner Production*, Volume 178, pp. 731–739.

[13] Gombkötő, I., Nagy, S., Csőke, B., Juhász, G.: Effect of particle shape and orientation on separation efficiency of eddy current separator. In: *Indian Institute of Metals* (ed.) *XXVI International Mineral Processing Congress*, *Proceedings*. New Delhi, India, 24–28. September 2012. Paper No. 538.

[14] Hanc, A., Novak, P., Dvorak, M., Habart, J., Svehla, P. (2011). Composition and parameters of household bio-waste in four seasons. *Waste Management*, 31, pp. 1450–1460.

[15] Leitol Cs. (2018). Visszacsatoláson alapuló több szempontú műszaki, környezeti és közgazdasági elemzés alkalmazása a mechanikai-biológiai hulladékkezelő művek technológiai tervezésében. (The application of multi standpoint technical, environmental and economic analysis in the feedback technique design of mechanical – biological MSW processing plants). PhD Thesis, University of Pécs, Hungary.

[16] Lungu, M. (2005). Separation of small nonferrous particles using an angular rotary drum eddy-current separator with permanent magnets. *International Journal of Mineral Processing*, 78 pp. 22–30.

[17] Maraspin, F., Bevilacqua, P., Rem, P.: Modelling the throw of metals and non-metals in eddy current separations. *International Journal of Mineral. Processing*, 73, pp. 1–11.

[18] Miller, S., Miller, R. (2009). Air separation of recyclable materials, United States Patent, Patent No. US7584856 B2.

[19] Miller, S., Miller, R. (2013). Separation system for recyclable material, United States Patent, Patent No. US8618432 B2.

[20] Montejo, C., Costa, C., Ramos, P., del Carmen Marquez, M. (2011). Analysis and comparison of municipal solid waste and reject fraction as fuels for incineration plants. *Applied Thermal Engineering*, Volume 31, Issue 13, September 2011, pp. 2135–2140

[21] Nelles, M., Morscheck, G., Grünes, J. (2012). MBT in Germany and Europe, development, status and outlook. International 9th ASA Recycling Days MBT as a Supplier of Secondary Raw Materials, Hanover, Germany 29 February–2 March pp. 1–16.

[22] Pace, S. A., Yazdani, R., Kendall, A., Simmons, C. W., VanderGheynst, J. S. (2018). Impact of organic waste composition on life cycle energy production, global warming and Water use for treatment by anaerobic digestion followed by composting. *Resources, Conservation and Recycling*, Volume 137, pp. 126–135.

[23] Pap, Z., Gombkötő, I., Nagy, S. Debreczeni, Á. (2014). Determination of separability of different particles by eddy current separator: A statistical approach, In: Yianatos, J., Doll, A., Gomez, C., (ed.). *XXVII International Mineral Processing Congress, Proceedings,* Santiago de Chile, Chile, 20–24 October 2014, pp. 141–149.

[24] Połomkam, J., Jędrczak, A.: Efficiency of waste processing in the MBT system. *Waste Management*, Volume 96, pp. 9–14.

[25] Pomberger, R., Sarc, R., Lorber, K. E. (2017). Dynamic visualisation of municipal waste management performance in the EU using Ternary Diagram method. *Waste Management*, 61. pp. 558–571.

[26] Rada, E., Istrate, I. Ragazzi, M. (2009). Trends in the management of residual municipal solid waste. *Enviromental Technology*, (7), pp. 651–661.

[27] Siddiqui, A. A., Richards, D. J., Powrie, W. (2013). Biodegradation and flushing of MBT wastes. *Waste Management*, Volume 33, Issue 11, pp. 2257–2266.

[28] Thiel, S., Thomé-Kozmiensky, J. K. (2010). Mechanical-biological pre-treatment of waste, Hope and reality. In: *Papers and Proceedings of the ISWA World Congress 2010 – Urban Development and Sustainability – a Major Challenge for Waste Management in the 21th Century*, Hamburg, Germany, 15–18. November, pp. 1–16.

[29] Trulli, E., Ferronato, N., Torretta V., Piscitelli, M., Masi, S. Mancini, I. (2018). Sustainable mechanical biological treatment of solid waste in urbanized areas with low recycling rates. *Waste Management*, Volume 71, pp. 556–564.

[30] Zhang, S., Forssberg, E., Arvidson, B. Moss, W. (1999). Separation mechanisms and criteria of a rotating eddy-current separator operation. *Conservation and Recycling*, 25 pp. 215–232.

SUSTAINABLE DENDROMASS MANAGEMENT RESEARCH TO MEET THE GROWING ENERGY DEMAND IN HUNGARY

V. PAPP[1] – D. SZALAY[1] – A. VÁGVÖLGYI[1] – A. HORVÁTH[1] –
T. MAJOR[1] – K. SZAKÁLOSNÉ MÁTYÁS[1] – A. VITYI[1] –
N. SZIGETI[1] – K. KOVÁCS[1] – I. CZUPY[1*]

[1]*Institute of Forest and Environmental Techniques, Faculty of Forestry*
University of Sopron
*czupy.imre@uni-sopron.hu

Abstract: Woody biomass plays a significant role in Hungarian energy production. However, growing raw material needs can only be sustainably met in long term through conscious forest management and by exploiting additional dendromass production opportunities. This article summarizes research results of the Innovative Biomass Utilization Group relevant to the project entitled *Sustainable Raw Material Management Thematic Network – RING 2017*. The work of the research group examines several factors affect yield and influencing economic aspects, such as forest regeneration, damage and harvesting solutions in a time when timber quality is declining and forest damage is increasing. Also carrying out analyses of the opportunities for further woody biomass cultivation outside the forest area (agroforestry, short rotation woody energy plantations). The study pays attention particularly to new ways of utilizing woody materials, e.g. the production of lignocellulosic biofuels and wood mixture pellets.

Keywords: woody biomass, dendromass production, dendromass utilization, energy tree

1. INTRODUCTION

Using biomass for energy and other industrial purposes is becoming an important option for reducing greenhouse gas emissions worldwide. This article presents the new directions of dendromass production and harvesting mechanisation, damage events, and novel utilization opportunities in the framework of the RING 2017 project. These research areas are all linked in terms of a secure raw material supply for wood industry, planned heating and electricity power plants or other energy producing plants. The woody biomass, also known as dendromass, is the most widely used biomass based raw material at present. The research is also justified because production and consumption of wood products are currently forecast to increase over the next 20–30 years [1, 2, 3, 4]. According to the WWF Living Forest Model, annual wood removals will be three times higher in 2050 compared to the volume reported in 2010. The main driver of growing demand is the projected massive escalation in wood use for bioenergy purposes in addition to the rising demand for solid wood and paper products. This is partly due to the increasing supply and demand of developing

Asian countries (mainly China and India). The FAO's (Food and Agriculture Organization of the United Nations) analysis, on the other hand, finds that the biggest change is caused by the rapid increase in energy demand. This is especially true in Europe as a result of the EU's renewable energy policy [1].

Biomass already plays a significant role in Hungary's energy supply. Primary energy demand is more than 1,100 PJ, of which 12.5% was covered by renewable energy sources in 2017 [5]. Biomass and other municipal biowaste amounted to three-quarters of renewable energy, with most of this being dendromass [6]. According to the National Energy Strategy 2030 with an outlook to 2040 (2020), the goal in Hungary is to increase the share of renewable energy sources to a minimum of 21% of gross final energy consumption by 2030. The strategy envisages a further increase in the use of biomass, and its role will be primarily in the increased use of heating based on renewable resources, in the Green District Heat Program and in renewable energy production for own use.

The increased demand for wood puts a lot of pressure on forests, which is further enhanced by the extraction of damaged timber in some countries. These factors jointly may cause significant reduction in forest cover, which can severely deplete the region's forest carbon sinks as major factors in reducing emissions. The right choice of forest management method plays an important role in the development of a usable amount of wood. Logging must be in constant balance with forest regeneration. In order to achieve a circular economy and carbon sequestration, efforts must be made to utilize wood first in the wood industry, and energy utilization should be the last option. Therefore, it is essential to analyze not only the factors influencing quantity but also those affecting quality. Wood quality and tree dimensions (the presence or absence of wood defects, quantity of wood defects or measurements) determine the composition of the forest assortment that can be produced during harvesting. The appearance of certain wood defects is age-related; therefore, the proper choice of cutting age plays an important role in the variations of assortment composition.

In addition, the state of a forest's health (specifically, insects and diseases or abiotic damages) has an effect on the qualitative parameters as well as the quantitative parameters of living stock. Furthermore, origin (seed or root sprout) also influences assortment composition.

The usability of woody material is also affected by the increasing biotic and abiotic forest damage observed worldwide in recent years. The extraction of damaged timber changes the possibilities of utilization, since less wood is expected to be used in the furniture industry and a higher amount of low quality materials will be used for energy purposes. The rising frequency and intensity of extreme weather, such as droughts, long periods of high temperature, heavy rains, and floods, makes trees more susceptible to physical damage, disease, and pests [7]. Furthermore, a wide range of other climate-related variables, ranging from wind speed and atmospheric moisture content to snow pack and atmospheric CO_2 concentration [8] are associated with disturbance change.

Such various abiotic damage events have changed logging procedures. For example, Slovenia was hit by a major ice storm in late January 2014. Six million cubic

meters of wood, more than the typical annual nation-wide wood harvest, had to be felled as a direct consequence of the glaze ice, while almost three million cubic meters more was left to rot in forests [9]. In terms of emergency felling, beech, oak, and pine trees suffered the most damage in Hungary in recent years. In the area which belonging to Egererdő Plc. harvesting forced by ice, storm, or wind damage requires innovative harvesting solutions; therefore, these kinds of harvests present a challenge to foresters [10]. This is one reason why highly mechanized logging technologies are being utilized more frequently in Hungary. One example is the CTL (Cut To Length) work system where felling, skidding, delimbing, assorting, chopping, bunching, and reviewing are completed with a harvester, while skidding and forwarding are done with a forwarder.

As a result of new technological developments, harvesters may no longer be confined to softwood forests only. Several studies conducted on black locust, Turkey oak, beech, and oak stands have justified the use of these machines in hardwood stands. Evaluating the results of the cost and time analyses, we concluded that in several cases harvesters are more efficient than traditional tree felling with chainsaws [11].

Figure 1
Harvesters in Hungary

Current Hungarian biomass utilization occurs mainly in thermal and electric power plants and to a lesser extent in biogas plants or in pellet, briquette, and chipboard production. The most frequently utilized raw material is dendromass from forests or by-products from the wood industry. However, the new EU directives strongly support the use of forestry and agricultural residues or other industrial lignocellulose containing by-products. The collection of residues requires a more advanced technology and its current application is low. But forest areas are not the only way to think about the supply of woody raw materials. In the future, the role of energy plantations in low-quality agricultural areas may increase significantly. The research area of agroforestry is also related to the topic of energy plantations. The dendromass from such areas can supplement residues well and a good tool for increasing carbon

sequestration in the agricultural field. Both agroforestry and woody energy plantations require a well-organized system [13].

Currently, three classes of woody energy plantations exist in Hungary, e.g. rolling energy plantations (>20 years, intended for energy recovery); short rotation energy plantations (mostly 3–5 years of rotation, intended for energy recovery); and woody industrial plantations. The total area of plantations established in Hungary was 4,489 ha in 2019 [14]. Woody energy plantations have different yields, ranging from 5 to 25 atro t/ha/year depending on the cultivation area, technology, climate, and tree species/clones [15, 16]. With a calculation of an average dry matter of 10 t/ha/yr, this results in approximately 40–45,000 tons of woody material. Utilization of this material has been achieved, and free potential can be reached only with establishment of new plantations. The establishment, cultivation and harvesting of plantations requires a high degree of mechanization, which determines their economic feasibility.

One of the other alternatives is the widespread implementation of agroforestry in agricultural areas. This could make a significant contribution to meeting future needs of woody biomass and mitigate the loss of wooded areas. Applying agroforestry practice can also increase forest management efficiency, for example, by supporting reforestation. According to the FAO definition the agroforestry system is a dynamic, ecologically based natural resource management system that integrates trees into farms and the agricultural landscape, thereby diversifying farms and maintaining production for land users. It incorporates a variety of farming practices by combining crops, livestock, and trees with the aim of optimizing these components to achieve a community's economic, social, environmental, and cultural needs. The combination and structure of associated species or varieties can be very diverse in agroforestry systems. As agriculture has changed, intensive crop and livestock production has taken hold, reducing the occupation of small diverse production systems such as agroforestry farms. Recently, agroforestry has begun spreading again and plays an increasingly important role in climate adaptation and safe production [17, 18]. In a study conducted in the context of the AGFORWARD project, experts estimated the extent of agroforestry in the EU to be 15.4 million hectares in 2016. This represents 3.6% of the total area and 8.8% of the utilized agricultural area. In the same study, the area covered by agroforestry systems in Hungary is estimated at 38,100 ha, which is 0.4% of the country's territory and 0.8% of the areas under agricultural cultivation [19].

The increasing demand for renewable energy ensures the importance of new energy production methods using various woody biomass and by-products. Material compacting such as pelleting is a rapidly growing biomass utilization sector. Though pellets are primarily made from wood or herbaceous plants, various waste materials and their mixtures can also be utilized for energy purposes. Waste pellets can be used in larger industrial plants or in combustion plants with appropriate flue gas cleaning and filtering equipment. The varying proportions of paper sludge (waste from paper industry) and pine wood shaving pellets are an excellent opportunity to harness lignocellulose by-products [20].

Lignocellulose biofuel production is another new woody biomass utilization opportunity. Meeting the RED II (Renewable Energy Directive II) legislation is a

challenge that encourages biofuel production, without intensification of food conflict. Although conversion rates and production capacity of lignocellulose biofuels production are lower than those of conventional biofuels, the investment cost can be up to ten times higher [12]. Thus, their market presence usually requires some form of support and high amount of utilizable dendromass. For these reasons there are currently only five commercial scale lignocellulose biofuel plants in Europe [12]. Dendromass with high free potential, e.g. forest residues and SRC (short rotation coppices) characterized by high bark content [21], is also responsible for high ash and alkaline content [22, 23, 24]. These properties make it much more difficult to complete the whole biofuel production process because the pyrolysis bio-oil yield decreases laterally with the increasing ash content [24, 25].

2. METHODS

SRC (short rotation coppices)

Figure 2
Cultivation and utilization of dendromass
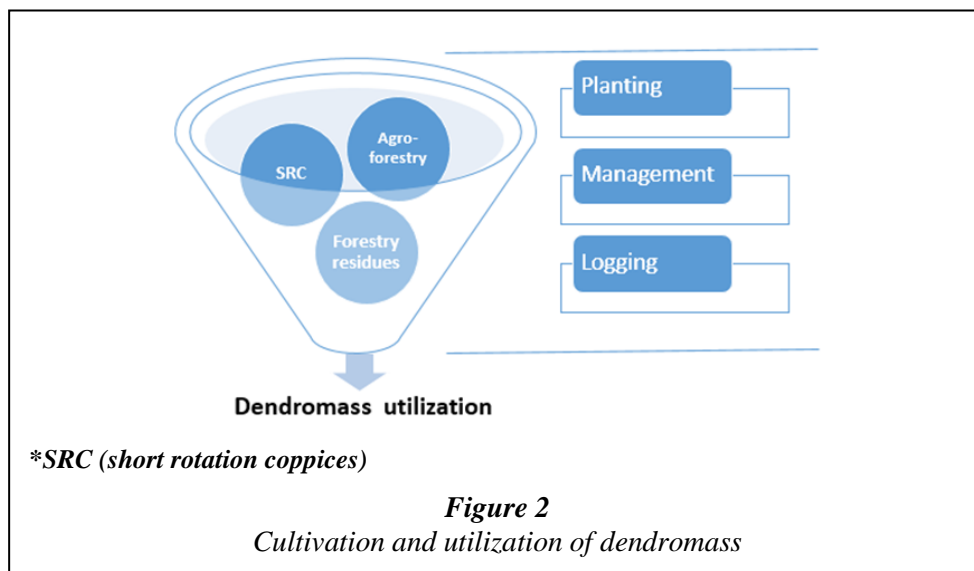
This article covers many areas of dendromass cultivation and utilization. The field of research is diverse, with a common focus on new opportunities in the production, harvesting, and utilization of woody materials.

2.1. Forests

2.1.1. Assortment composition

The objective of the research was the examination of the effect of seed or root sprout origin for yield and quality. We completed our research in the two most prominent black locust *(Robinia pseudoacacia)* areas: Nyírerdő PLC (located in Szabolcs-Szatmár-Bereg and Hajdú-Bihar county) and SEFAG Ltd (located in Somogy

county). The primary consideration during the selection of the forest sites was that they be located on soils providing equal production potential. We applied final cutting data from the period 2010 to 2017 in our research.

Different filtering was performed on the data before the examinations began. The database contained 5–100% mixed forest parts. Of these, only forest sites containing at least 90% black locust were considered for the evaluation. In the case of forest areas where not only black locust can be found, we reduced to match the proportion of black locust according to the proportion of the mixed forest in the produced timber volumes.

The data is projected to1 ha filtered area, and the resulting m³/ha data serve as a basis for comparative analyses.

2.1.2. Examination of abiotic and biotic damage

As an indirect consequence of climate change, logging due to forest damage is playing an increasing role in the future. Different damage events, such as storm damage or insect damage, all require different harvesting technologies. Harvesters and forwarders can be suitable solutions for harvesting operations after damage events. Data on forest damage events were collected in the area of Egererdő PLC for 15 years through the annual claim report and information on the evolution of yields by area and species was also collected. The data comes from field surveys and accurate logging of harvested timber. The main abiotic and biotic damages by tree species were summarized and the annual and regional summary of emergency felling was compiled. Major damage events in 2009 and 2014 causing the biggest problems in beech forests were analyzed; these included ice, wind, tornado, and storm damage. Among the types of biotic damage, bark beetle damage in spruce stands caused the most destruction.

In addition, the 15-year average gross and net yields for the main tree species were determined, which could then be compared to the evolution of yields.

2.1.3. Harvesting technology

In the past few years, multi-operational logging machines have been used for logging domestic forests. These are special forestry machines that can perform two or more operations at the same time (e.g. felling, preassembly, debranching, etc.). Clearcutting, thinning, preparatory cutting, and sanitary cutting as well as selective cutting were all completed with these machines.

We conducted a national survey on this topic. The number of machines working in Hungary has increased consistently since 2005. It is very difficult to determine the actual number of machines, especially retrospectively. Specific data from forestry, logging entrepreneurs, and machine dealers exists, while data can also be inferred and estimated from specialist articles, news and social media. In the future, forest damage can be an interesting area of research.

Field surveys with continuous time measurement were conducted to analyze and evaluate harvester work-day structure and performance. In addition to recording the

duration of individual actions, the total volume of the timber processed in each cycle and the distances of changeovers were also recorded.

The following types of actions were distinguished during the survey [11, 26]:

- <u>Grabbing the tree (GT):</u> equals the time required for the machine operator to place the harvester head onto the base of the tree, using the manipulator arm.
- <u>Felling and processing the log (F):</u> involves the time for felling, preassembly, debranching of the log as well as the conversion into assortments and piling by assortments.
- <u>Changeover (C):</u> is the duration of machine displacement.
- <u>Felling only (FO):</u> time spent on logging very thin or poor quality (e.g. completely rotten) logs, which do not yield valuable assortments.
- <u>Arranging branch material (B):</u> transfer and rearrangement of branches obstructing the path of logging.
- <u>Arranging timber (T):</u> transfer and arrangement of timber stacks obstructing the path of logging.
- <u>Rest period (R):</u> time for meeting personal needs.
- <u>Service (S):</u> duration of machine needs (e.g. chain change, refueling).
- <u>Troubleshooting (TH):</u> time for fixing technical defects in the machinery.
- <u>Waiting (W):</u> other time losses (e.g. phone calls).

Examinations of logging damages are a very important task in Hungarian forests as well. Field work was aided by the influencing factors identified in a questionnaire survey. A protocol form was created. This contained possible answers to the relevant aspects so that the conditions of the exploration under investigation can be circled during field trips and interviews. This form, which only takes a few minutes to fill out, allows for the categorization of all the extractions according to the same criteria. The field data captures took place in 1–5 ha private forests. The allocation of ground plots was in the Borostyánkő and Kőszeg mountains. It is important to note that accessibility in the area of the examined forests was 45.5 lm/ha (linear meter pro hectare), which is very high. In comparison, this value usually ranges from 4 to 22 lm/ha in domestic forests, with an average of 7.2 lm/ha. The aim of the study is not to generalize the measurement results, but to investigate the usability of the invented and applied test in the practice.

Reforestation occurs naturally, and regrowth in different age distribution and density is prevalent. In order to protect natural regeneration, it is important to keep the wild game at a tolerable level, which is achieved through intensive hunting. A short-tree working system was used with harvesters and forwarders.

Data measured in the plots:
- Skidding trail distances,
- Plot areas,
- Tree species, number of pieces, breast height diameters, tree heights,
- Stem damage, damage size, depth of skidding trails.

2.2. Dendromass cultivation outside forest area

However, the role of forests must be primarily in carbon sequestration and meeting the needs of the wood industry. By reorganizsation of agricultural land use, with a greater involvement of agroforestry systems and woody energy plantations, the growing demand for dendromass can be sustainablye met in an ecologically and economically advantageous way.

2.2.1. Energy plantations

Energy plantations are suitable for the utilization of low-quality agricultural land, so a large amount of dendromass can be produced in the future without losing valuable agricultural land cover. This may reduce logging of forests and lead to longer-term carbon sequestration. Here we present a summary of energy plantation research. The topic is multifaceted, covering several areas.

In the recent period, the area of energy plantations has not increased as expected. A SWOT analysis was used to explore the causes. In the course of the SWOT analysis, we examined and summarized the practical experiences regarding the strengths, weaknesses, opportunities, and threats of energy tree plantations in Hungary on the basis of the literature.

The study reviews the background of the present legislation (Government Decree 135/2017 [VI.9.]) as well as the direct and indirect support possibilities of woody energy plantations with the help of the available plans, action programs, legislation, and websites. We contacted the Forestry Directorate of the National Food Chain Safety Authority (NÉBIH) of Hungary to acquire current data, and we analyzed the cultivation technology currently employed. We paid special attention to the harvesting technology.

2.2.2. Agroforestry

Complex yield and site studies were performed in a one-year- old experimental afforested area of 0.66 ha. Half of the area was intercropped while the other half was left in between the rows of trees without cover for control. Intercrop– typically corn in Hungary – if well chosen (e.g. crop variety with below average growth), creates a competitive and partial shade, thus potentially stimulating the growth of young trees. Tree planting was completed with 8,000 seedlings/ha, in a 2.5 m ×30 cm installation network, mixed species *(Quercus robur, Pyrus pyraster, Tilia tomentosa, Betula pendula)*. Alleys were oriented to NS (prevailing wind direction: NE) and cultivated with ploughing and chemical weed control. Crop line spacing was 70 cm wide double-lines, resulting in a 90-70-90 cm spacing of tree and corn lines. The crop (Dekalb 4592) was planted using an MTZ-82 tractor and two-line drill. The experimental area was not irrigated and the same management practices were applied for the saplings in both intercropped and the control plot. In order to compare the effect of intercropping on the microclimate of the afforested area, soil moisture (soil conductivity) and soil temperature were measured. Tests were made in the driest period (July and

August) when sandy soil with humus heats up rapidly and strong radiation from the top and the bottom at the same time affects the young plants negatively, increasing significantly the risk of dehydration.

2.3. New methods of energy utilization

2.3.1. Industrial pellets

One important area of utilization of woody by-products is pelleting. The utilization of various forestry and industrial by-products may play an increasingly important role in the future. In the current study, we produced pellets using paper industrial by-products and sawdust. During pelletization studies, paper sludge composition is variable. The utilization of paper sludge as pellets is a new research area. Because of the high inorganic content of paper sludge, energy recovery is difficult and large amounts of ash and slag are often produced. The examination of ash content is particularly important, due to the high ash content can damaged the pellet burning equipment.

The approximately 60 kg of paper sludge prior to the tests had a 30% moisture content. Therefore, the material was spread for natural drying, and pelleting started two days later; moisture content was measured to reach the optimum 11-12%. The material was compacted into small pieces of 0.5 to 2 cm thick that were easy to crumble. The size of the fraction required for pelleting was produced with a hammer grinder.

After grinding, 50 to 55% of the material was in the range 2.5 mm to 1 mm. The paper sludge was then mixed in different proportions to the pine-based wood shavings. The pelletization was carried out with a Kahl type pellet press at 800 bar pressure, with a flat sticker and feeding system.

We investigated the changes in ash content and calorific value of pure paper sludge and mixtures of different proportions. The heating value was determined by calorimetric tests. The ash content was measured by a glow furnace system. The moisture content was continuously measured by an automatic wet content analyzer.

2.3.2. Utilization of woody material as biofuel base material

The measurements were completed at the Bajti Experimental Plantation of the Forest Research Institute (NAIK ERTI) in Hungary. The plantation was completed in three repetitions and cultivated with a coppicing technology. The test area has a clayey loam forest soil in hornbeam-oak climate in medium deep topsoil, which was not irrigated. Nutrient replenishment and watering is not used. We selected 4 species/clones with the highest yield in the area. The sampling was executed from each of the four tree species/clones in December 2013; average-sized stems were cut at the age of three. Every 50 cm an approx. 1 cm wide section from the shoot was sampled.

Afterwards, the bark was removed from the wood with a peeler knife and the absolute dry matter was weighed separately. The bark percentage for the different diameters can be obtained using the equation below.

The data were classified according to diameter. The resulting values based on the thickness of the shoots were also applied to the shoots harvested in the summer of 2013 at three different vegetation years. This method resulted in a high number of elements. In all cases, we summed the weight of the bark and debarked wood, from the cutting height to the tip. It was followed by the calculation of the bark percentage for the whole shoots, then for the whole plant and for one hectare.

The ash content was also examined. We conducted our examination with a Hőker LS-12 laboratory muffle furnace. During the measurements, we separately determined the ash content of tree in bark and only bark in triple repetition. During the measurements, we determined the moisture content of the shredded samples using a BOECO SMO 01 moisture meter.

3. RESULTS

3.1. Results of forests

3.1.1. Assortment composition

The right choice of forest regeneration type has a major impact on carbon sequestration capabilities. It influences the quality and quantity of assortment compositions and through that, it has an effect on useable wood production, which is an important issue today due to climate change. The quality and quantity of assortment compositions are defined by standards, but depending on the market demand can differ.

In Nyírség, black locust is found mainly on two genetic soil types, namely banded brown forest soils ('kovárvány') and humic sand soil. We found a greater number of black locust stocks of seed origin although most regeneration today occurs from sprouts. Root sprout origin stands were not found in this area. During our examinations, we compared the seed and rootstock origin tree stocks on the same production areas; we also examined the impact of different production areas for assortment composition.

Our investigation results reveal no significant economic difference between different origin tree stocks on humic sand soil, however, significant differences are observed in the assortment composition. The economic parameters are calculated based on the price of harvested timber in 2016.

On banded brown forest soils ('kovárvány') brown forest soil significant differences exist both in the assortment composition and in the price income of tree utilization.

Our analysis indicates a significant difference in the assortment composition of black locust on banded brown forest soils ('kovárvány') and humic sand soil, with benefits to the tree stand cultivated on banded brown forest soils ('kovárvány').

In the area of SEFAG PLC, the black locust stocks are found on nine genetic soil types. Of these, all three origins (seed, root sprout, stump sprout) stocks can be found only on brown soil and rusty brown forest soil. Therefore, we compared the assortment composition of the three origin stocks on these two genetic soil types as well as of root sprout and stump sprout origin stocks on humic sand soil and root sprout

and seed origin stands on 'kovárvány' brown forest soil. The brown soil result was interesting: the volume of timber harvested per hectare was lower in the seed origin stands than in the sprout origin stands.

There is no significant difference between the two sprout origin (root sprout and stump sprout) stands here. Sprouting does not rule out quality wood production, although the effect of multiple sprouting would certainly be visible. No notable difference between sprout and seed origin stands on rusty brown forest soil was found, but the quality of stump sprout origin stands was much lower. A higher yield of wood can be found here in the cases of seed and root sprout than in the case of the similar origin stands of brown soil.

Finally, we compared the assortment composition and sales returns of tree utilization of the two black locust producing areas in the Nyírség and Somogy regions. However, comparisons could only be made for two genetic soil types, since only these occur in both forest regions. In 'kovárvány' brown forest soil, we could compare seed and root sprout origin stands with the humic sand soil and root sprout origin stands.

Table 1 summarizes the volume of wood harvested per ha and the wood utilization income per ha in the areas of the two forestry companies (forest regions). The primary consideration in the selection of forest plots was to have the selected stands on soil with the same site potential. The different climatic factors were not studied.

Table 1
Summary of the difference between the two forestry companies

	Origin	Genetic soil type	SEFAG PLC.	Nyírerdő PLC.
Produced timber volume [m³/ha]	Seed	'kovárvány' brown forest soil	152.7	170.0
	Root sprout	'kovárvány' brown forest soil	143.7	110.0
		Humic sand soil	97.7	130.0
Income [million HUF/ha]	Seed	'kovárvány' brown forest soil	2.60	3.86
	Root sprout	'kovárvány' brown forest soil	2.42	2.20
		Humic sand soil	1.56	2.77

Marked differences between the assortment compositions of the two areas of SEFAG Plc exist in case of root sprout; these differences extend to wood utilization income as well because the location of the forestry site influences the produced assortments significantly. In case of the Nyírerdő PLC sites, the volume of the harvested wood is more evenly distributed among the various assortments

Marked differences between the assortment compositions of the two areas of SEFAG Plc exist in case of root sprout; these differences extend to wood utilization income as well because the location of the forestry site influences the produced assortments significantly. In case of the Nyírerdő PLC sites, the volume of the harvested wood is more evenly distributed among the various assortments.

3.1.2. Results of the harvesting research

3.1.2.1. Working day structure

Based on measurements, the average working time structure of the harvests in Hungary can be determined *(Figure 3)*. Almost 50% of the working time is spent by the machine and its operator for felling, preassembly, and debranching of the log as well as the conversion into assortments and piling by assortments. The second most important action is 'changeover'. The proportion of other operations is below 10% on average.

Figure 3
Working day structure of harvesters
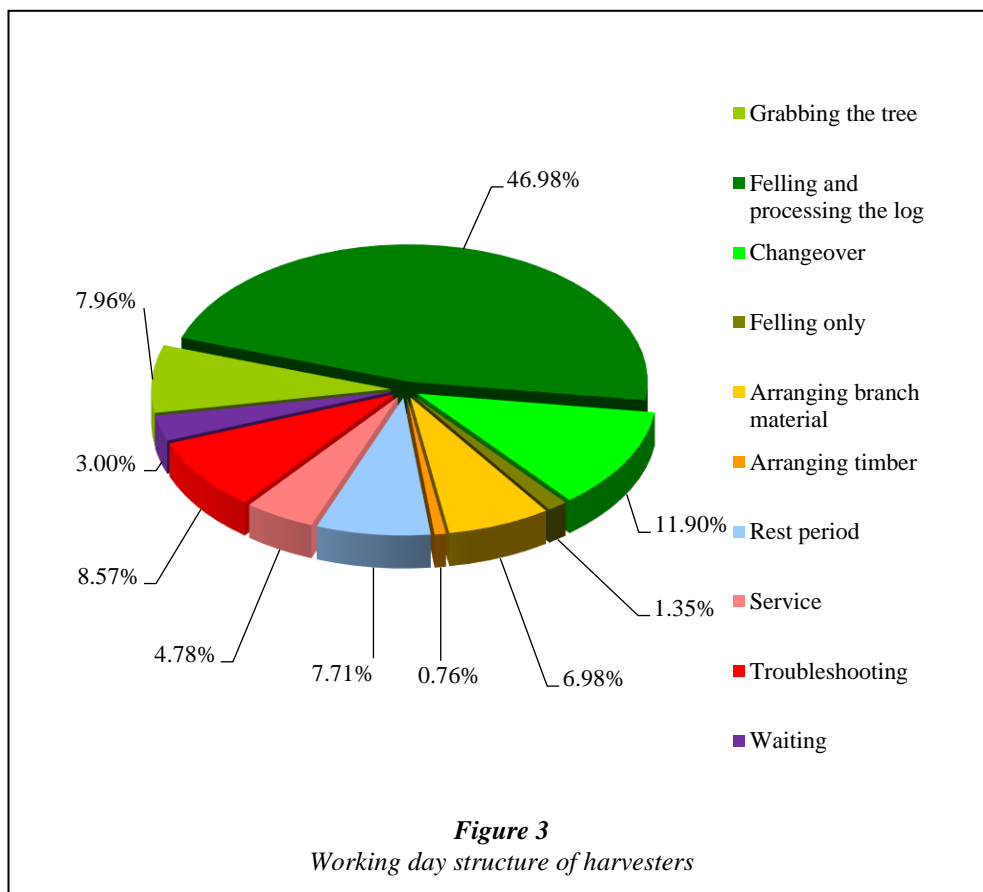
When examined separately, the proportion of actions *(Figure 4)* for the harvesting of deciduous and pine stands shows no substantial difference.

Figure 4
Averages of work completed by harvesters
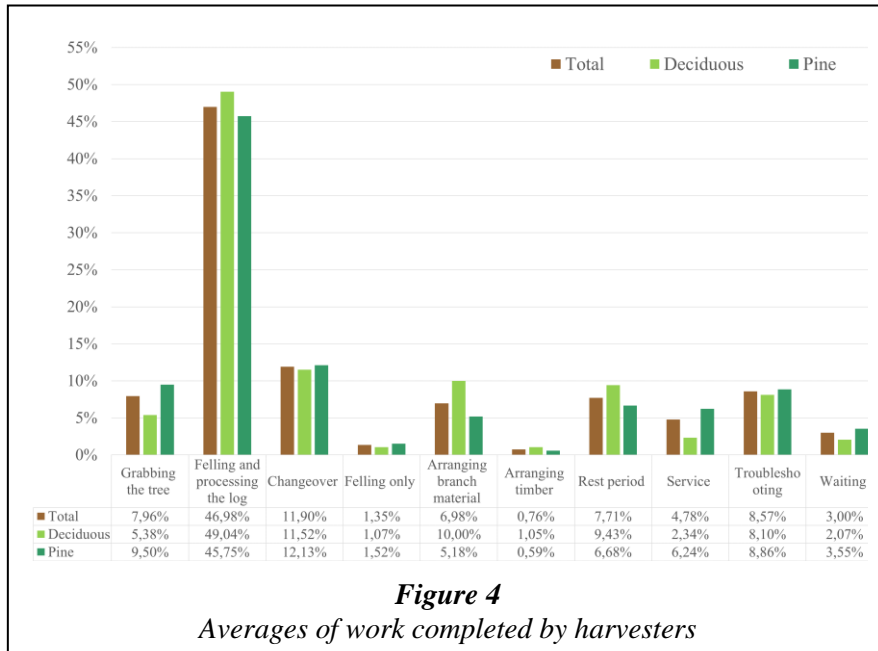
The hourly performance of the machines during the examination is shown in *Figures 5* and *6*.

Figure 5
Harvester performance in deciduous and pine stands

Figure 6
Working day structure of harvesters
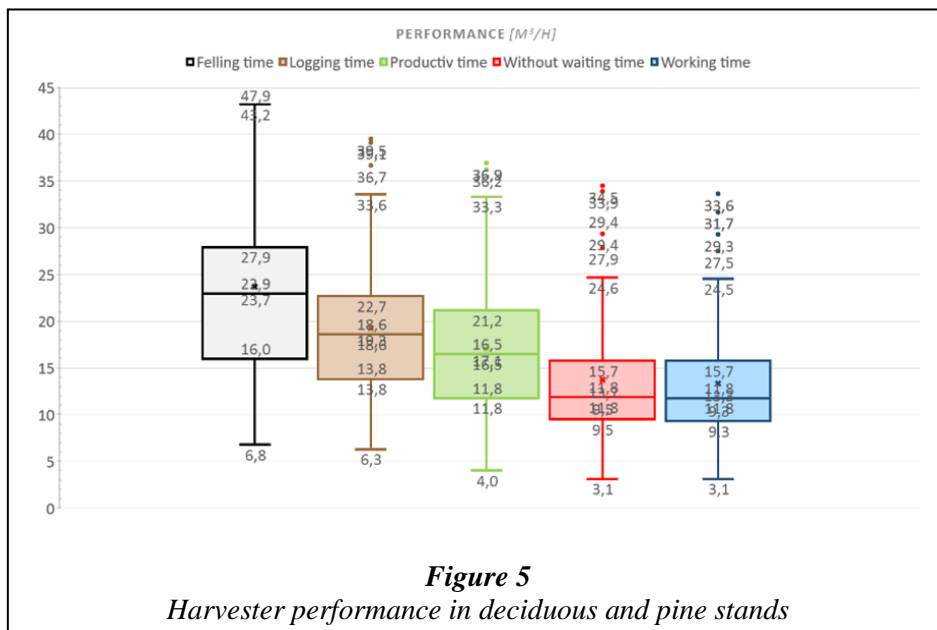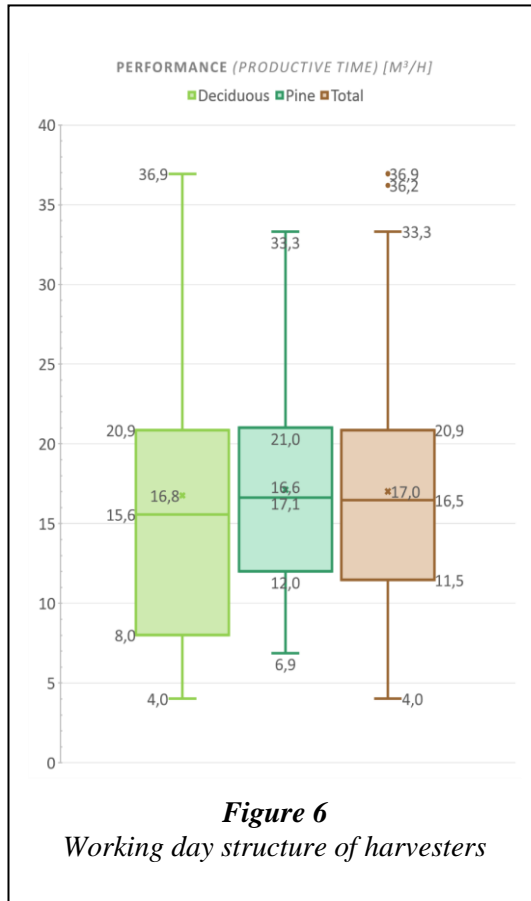
Machine performance is highly variable (working time: 3.1–33.6 m³/h, productive time: 4.0–36.9 m³/h) mainly due to the differences in the characteristics of the tree stand and tree use. The average performance range during working: 8.9–15.7 m³/h, in productive time: 11.8–21.2 m³/h.

Examining the achievements of the deciduous and pine stands in productive time, we find that the standard deviation of the results is higher for the deciduous stands; and in the case of pine, the average performance range is narrow-wer. In deciduous stands, the productivity of the machines varied between 8.0 and 20.9 m³/h, while in the pine forest it ranged from 12.0 to 21.0 m³/h.

3.1.2.2. Logging damage

The basis of the research was the examination of 10 kinds of logging, which types are presented in *Figures 3* and *4*. Great emphasis has been placed on recording the conditions so that the values obtained can serve as a basis for comparison.

An evaluation table *(Figure 7)* was prepared to process the data, which contains all the measured data. The evaluation was completed with Microsoft Office Excel to facilitate usability. Each page has data for a plot and its evaluation, so it is easy to review and evaluate each plot in its own right. At the bottom of the page, sample data for each harvesting is summarized.

Examination results for the injuries (damage during logging, that affects trees and soil) of the remaining wood pieces were in accordance with the literature and our expectations, see *Figure 7*. Beech (7.8%), spruce (7.2%), and fir (7.5%) were damaged at a higher rate, while oak (2.7%), larch (3.3%), and Scotch pine (6.0%) were damaged at a lower rate.

The average skidding trail distance was 16.2 m; the minimum was 14.4 m; the maximum was 18.4 m. The average skidding trail width was 3–3.5 m. On average, 16.7% of the forest area is covered by a skidding trail system.
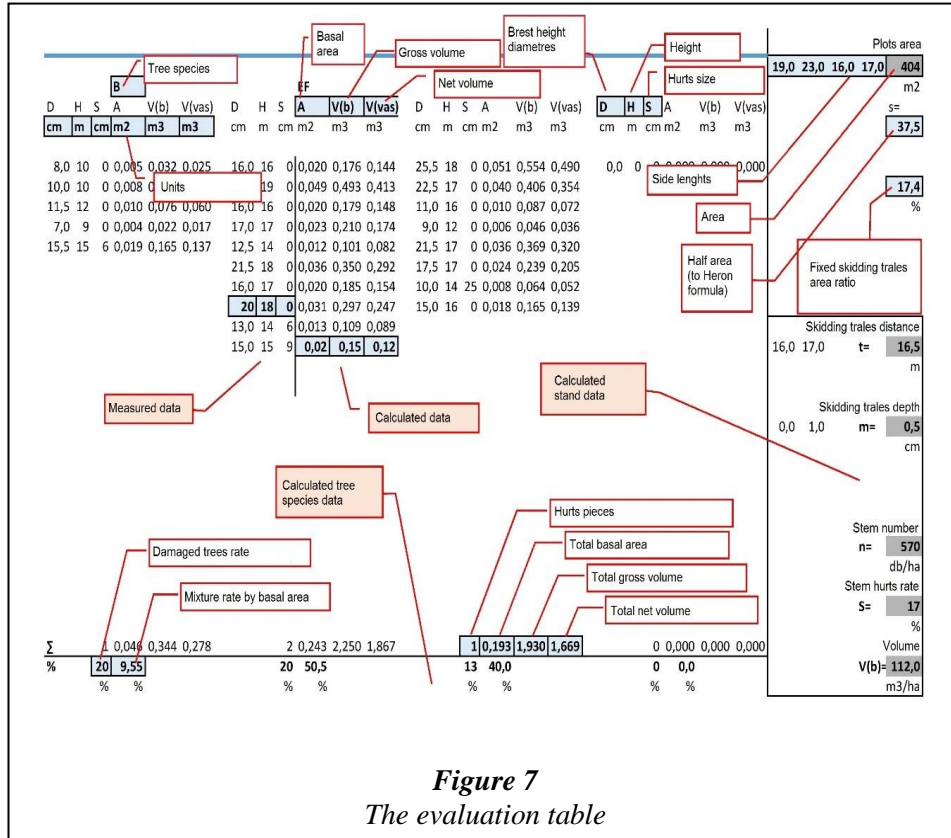
Figure 7
The evaluation table

Skidding trail depth was also measured. This revealed that a depth of more than 1-2 cm was formed where the slope increases (above 20°), and the soil carrying capacity or the branch carpet thickness is not sufficient. Only two test areas had a critical proximity skidding trail (soil damage) of more than 10 cm. Thanks to the soil integrity, the root system did not suffer from any major numerical damages.

The skidding trail system allowed enough space for the movement of the machines; consequently, no stump damage occurred. After 30–40% thinning intensity, depending on the conditions, stem injury was 0–19%. The average rate of damaged trees was 8–9%.

3.1.3. Results of biotic and abiotic damage research

Of the damage occurring in forestry, this article deals only with damage to a larger territory of major tree species, which affects an area of more than five hectares.

Significant amounts of damaged wood were harvested in the beech forest due to storm and the ice damage in 2014 *(Figure 8)*.
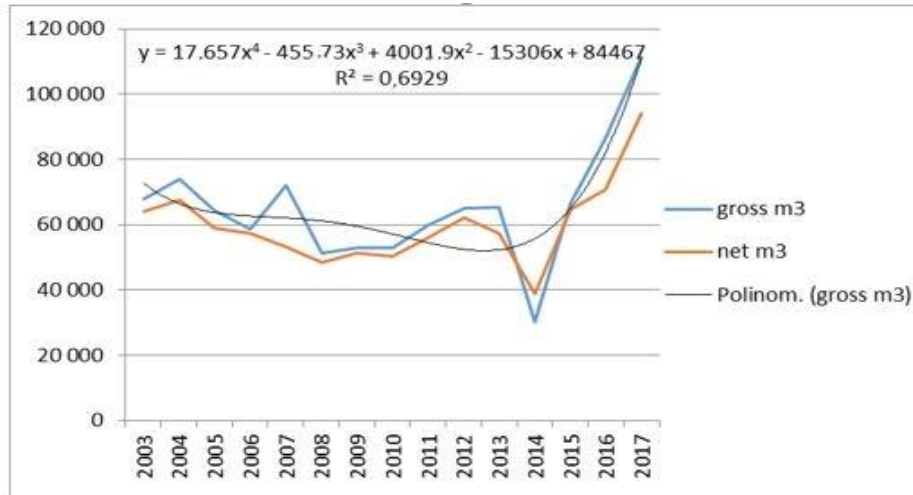
Figure 8
Beech (Fagus sylvatica) annual total harvest (2003–2017)

Logging as a result of that storm continued in the following years, as shown in *Figure 9* Then in 2017, a snowfall in the spring caused problems reaching the already leaf-covered forest.

Forest management activities and emergency felling from 2014 onwards have shown outstanding values. The average annual output of beech has nearly doubled due to storm, ice, and snow damage.
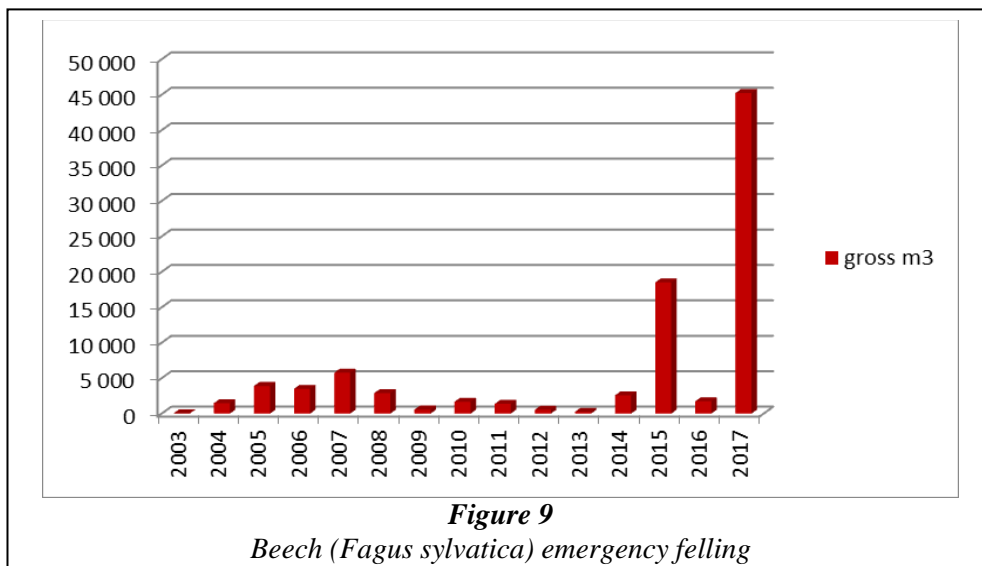
Figure 9
Beech (Fagus sylvatica) emergency felling

Bark beetles weaken spruce and fir. Average winter temperatures have also increased in recent years, making it easier for pests to overwinter. As a result, storms, wind, and ice damage are more prominent on weakened stocks. The situation is exacerbated by the increase in summer and winter temperatures in recent years as well as the extreme heat that often occurs in summer. The health logging and forced logging of pine trees was due to storm, wind, and ice damage, and their combined effects. *Figure 10* highlights the increase in forced and annual logging of spruce and fir due to damage over the last 7–8 years.

$$y = -3.3874x^4 + 132.37x^3 - 1423.7x^2 + 5053.1x + 8814.1$$
$$R^2 = 0.8394$$

Figure 10
Total annual logging data of spruce and fir
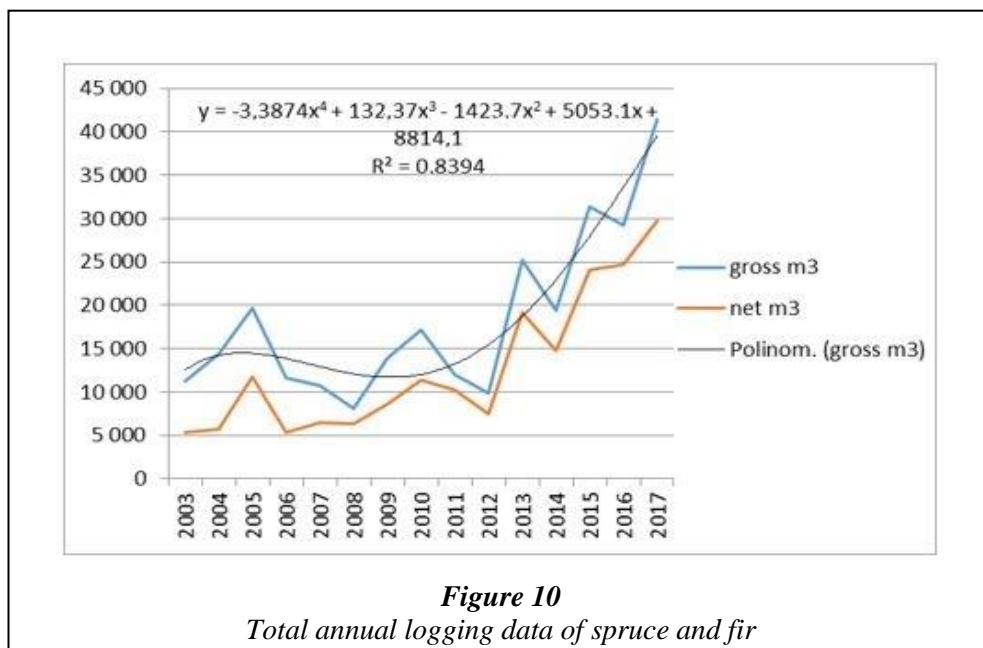
3.2. The role of dendromass production outside forest areas

3.2.1. Energy plantation results

The dendromass supply can be supplemented from outside forest areas. In tree plantations a large amount of raw material can be produced in a short time. Cultivation is possible in low quality agricultural areas, provided the appropriate tree species are planted. If ecological concerns are taken into consideration during implementation,excellents results and effort to conserve biodiversity can be achieved with little loss of space. Furthermore, adaptation to the changing climate is properly executed. Legislative developments in recent years support the establishment of energy plantations. New legislation (Decree 135/2017 [VI. 9.]) addresses woody energy plantations in a more transparent manner and establishes a new plantation category. In some cases, the cutting cycle has been lengthened. Site exploration and the related

expert consulting have been made obligatory before planting, and the list of usable wood species has been expanded.

Despite legislative changes and many ecological benefits and reliable mechanization technology, the area of tree plantation has not increased. By means of SWOT analysis, our research sought to understand what helps or hinders the expansion of energy tree plantations in Hungary. An abbreviated summary of the SWOT analysis is provided in *Table 2*.

Table 2

Summary of SWOT analysis

INTERNAL FACTORS		
	Strengths	**Weaknesses**
Energetic viewpoint	Quickly reproducible, renewable energy source; Favorable energy balance	Lower energy density than fossil fuels
Technological viewpoint	Favorable yields and firing parameters; Less weather and climate sensitivity; Less need for fertilizer	Different cultivaton technology from agricultural food crops; Varying moisture content; More complicated and costly utilization technology; Soil preparation, plant protection, as well as game control is important in the first years; Plantation should be planted years before power plants are installed
Environmental viewpoint	Soil melioration; Biodiversity enlargement; Carbon sequestration	Potential negative impact on groundwater table
Economic viewpoint	Income and workplace creation, rational land use; Improvement machine utilization, harvest can be postponed	Increased administrative tasks; Absence of support background, high investment, shipping, storage costs, late returns (3–5 years)
EXTERNAL FACTORS		
	Opportunities	**Threats**
Energetic viewpoint	Achieving energy targets; Decentralized energy production; Stable raw material production; Sustainable energy management; Reducing import dependence; Energy storage in wood	
Technological viewpoint	Versatile usability; Integration into agroforetry system; Promotion of the conversion to the circular economy	Lack of market expansion; Inappropriate species selection
Environmental viewpoint	The country's environmental perception is improving; Carbon sequestration, melioration, improving of ecological environment; Less climate sensitivity, utilization of less-favored areas; Outplacing of wood ash, biofertilizer, sewage, sewage sludge, sewage sludge compost, liquid manure	Negative counter-arguments among farmers; Food conflict; Loss biodiversity; Appearance of new pathogens, pests; Decrease in resistance

Economic viewpoint	EU financial support; Development of rural region; Attitude shaping of the population; Workplace creation; Enhancement of revenue; Growing demand	The economy and politics favor gas imports; Buyer prices do not cover cost of production; Declining planting motivation due to sales and species selection failure and lack of support

From the research, it turned out that energy tree plantations have many more opportunities and strengths than weaknesses and threats. Weaknesses and threats are mainly due to technological and economic difficulties, so they were analyzed separately.

The results show that the recent changes eliminating the direct and indirect support of short rotation coppices (SRC), leaving only area-based and greening-related support, have significantly reduced the willingness of farmers to establish SRC in Hungary. According NÉBIH data, support for roundwood plantations for industrial purposes, which has been available since 2016, did not increase farmer willingness to plant. At the same time, plantations were established close to secure markets with buyers like Pannon Power Plant and Bakonyi Power Plant because the wood chips from plantations play a significant role in the supply of raw materials to power plants. The economics of plantations are greatly influenced by the mechanization used.

Analysis of technological aspects shows that cultivation technology differs from the technology used in forest management and is highly dependent on the size of the cultivated area *(Figure 11)*.

We have concluded that one part of the cultivation technology of energy tree plantations (site-preparation, preparation of soil, sowing, planting of saplings, cultivation, transport of wood chips, transport of bunches and winding up) can be carried out with agricultural and forestry machinery. The difference we can find is in cutting and harvesting technology. For example, the working systems for short rotation wood energy plantations essentially determine the producing technology (rotation, initial spacing), the type of harvesting (chopping, rolling or whole tree), and the size of the area.

Harvesting costs account for 50–80% of the gross production costs; thus, the choice of the optimal harvesting method is a key factor [27]. Depending on the rate of harvesting mechanization, the following working systems can be isolated:
- manual harvesting;
- mechanical multiple harvesting (periodic, multiphase, multipass);
- mechanical single harvesting (singlepass).

The type of the stand – coppicing or roller wood energy plantation – needs to be considered when choosing a working system.

Making the surface suitable for the preparation of the soil; Elimination of ground irregularities; Cutting out bushes and shrubs; Clearing away non-woody	**SITE-PREPARATION**	landscaping→push blade; bushwhacking→stem crusher; chemical weed control→ sprayer
Implementing optimal physical state for the soil; Rotation of the soil; Pounding of clods, grading the surface of the soil	**PREPARATION OF THE SOIL**	deep ploughing (25-50cm)→deep plough, subsoiler; deep turning (50-70cm)→trench plough; ground surface finishing→tiller, land plane, harrow
Sowing black locust seeds; Planting saplings of black locust and domestic poplar species; Propagation of hybrid poplar clones and willow by cuttings, besides the plantation of hybrid poplar clones and willow by canes	**PLANTING**	sowing→sower; planting of saplings →tree-planting machine; propagation by cuttings→ cutting machine, sapling-planting machine, hole-digger
Ensuring optimal conditions for the species of the energy tree-plant; Loosening of the soil, weed control; Weed control	**CULTIVATION**	mechanical soil tending →tiller, cultivator, forestry soil loosener; mechanical weed control→stem crusher; chemical weed control →sprayer, grounting machine
Production of chips suitable for combustion. Production of wood chips by mobile chipping; Chipping by one of the following series of actions: - felling-chipping, - felling-harvesting-chipping, - felling-bunching-transport of bunches-chipping	**HARVESTING**	one-step harveting→mobile chipper; multi-step harveting→ brushcutter, chainsaw, feller, harvester, buncher, chipper, hydraulic crane trailer
Transport of the chips or bunches between the production site and the power plant.	**TRANSPORT OF WOOD**	chips trasport →lorry, trailer; bunches transport→hydraulic crane trailer, forestry truck, trailer
Making the site suitable for the field growing of plants; Rooting up of tree trunks; Cutting out of the roots; Ploughing up the soil; Pounding of clods, grading the surface of the soil	**WINDING UP THE PLANTATION**	grubbing →chock grapple, stem chipper; root cutting→root cutter; trench ploughing (50-70cm)→trench plough; finishing of the ground surface→tiller, land plane, harrow

Figure 11
The activities and the corresponding machinery required in the cultivation technology of energy tree-planting

Manual harvesting

This method can be applied in smaller ground plantations. Clearing saws, U-bolt chainsaws, and chainsaws are the tools used for base and controlled felling in coppiced stands. U-bolt chainsaw can be used to cut trees with a diameter of 10 cm at most. Chainsaws are the tools used in roller wood energy plantations.

Timber chopping can be carried out in the following ways:
- timber is chopped with mobile choppers and then transported to the place of use;
- timber is forwarded to the edge of the ground or to a formed landing, where chopping occurs later with a mobile or installed chopper. The chips are transported by vehicles to the users.

Mechanical multiple harvesting

In the case of mechanical multiple harvesting, the harvest and chopping of timber at different times – in some cases in different places – can occur. A variety of machines complete harvesting, hauling, and processing work. Chopping can be completed at the felling site, at the landing, or at the place of use.

Mechanical single harvesting

With mechanical single harvesting, the base cutting and chopping happens simultaneously. The machines do the felling and chopping and deliver the timber to a storage unit (container, trailer).

Harvesting and transporting tasks are influenced by several factors. It takes complex planning to choose an appropriate harvesting method, which is encumbered by defining different transporting opportunities. Continuously changing and suddenly arising factors such as weather can present obstacles and induce rapid redesign tasks. In summary, it can be stated that harvesting operations in the cultivation technology of energy tree plantations are of the utmost importance both technically and economically. Access to a well-established logistics system is required to supply the right quantity of timber for the power producing unit in a timely manner.

3.2.2. Supporting afforestation through agroforestry

The application of agroforestry practices can play an important role in improving the quantitative and qualitative parameters of dendromass production from wooded areas in the future. The history of the Carpathian Basin demonstrates a tradition of intercropping in forest restocking. Recent observations and studies in Hungarian systems have shown that this has positive effect on the soil microclimate and the growth of saplings, thereby increasing the survival rate of trees.

A common feature of agroforestry systems is that its elements interact and can therefore lead to more ecologically and economically sustainable farming [28]. A number of domestic and international practical examples confirm that the positive effect of trees present in the agricultural system is reflected in the improvement of both the quantity and quality of production [29, 30, 31, 32, 33, 34]. The profitability of the production system can be increased through the introduction of trees in agricultural areas, such as a combination of coppicing or timber tree plantations with agricultural crops, which can be supplemented with livestock and beekeeping if honey crops are included.

Various types of agroforestry practices are becoming increasingly well-known and widespread among farmers today. This is partly due to the fact that agroforestry areas are more diversified than unilateral forms of agricultural production (e.g. plantation farming, large-scale livestock farming, monoculture), thus increasing income security through diversification of income. For production, a special ratio called the Land Equivalent Ratio (LER) is used to calculate the relative performance of agricultural systems [35]. This ratio compares the relative yield of a component of a crop combination compared to sole stands of the same species *(Figure 12)*.

A well-established and efficiently operated agroforestry system can produce a total biomass yield of up to 30–40% higher than systems with plant cultures grown separately. This is due to the use of woody vegetation, which provides protection to crops and livestock, a more favorable microclimate, and diversity, while simultaneously producing wood that complements the yield of the agricultural crop [29, 30].

Figure 12
The Land Equivalent Ratio (based on [36] and [37])
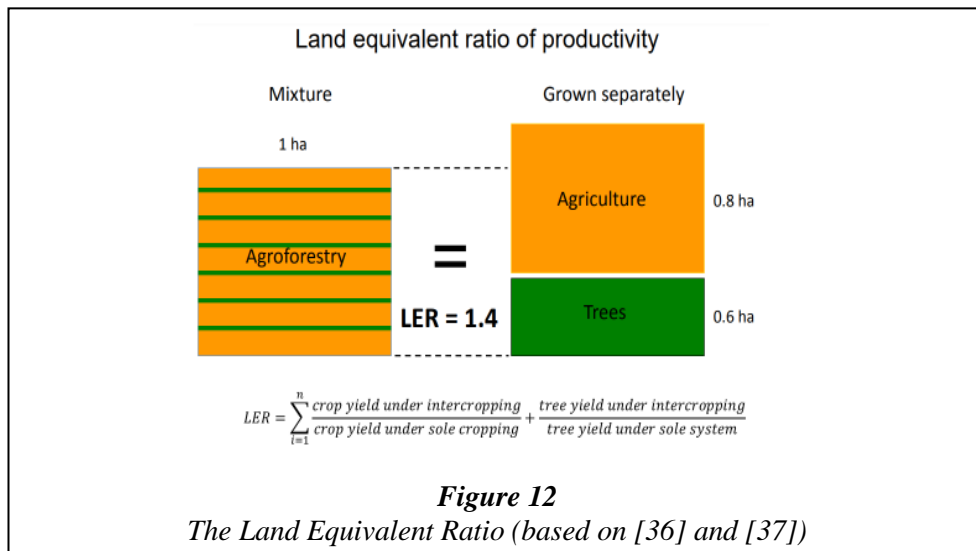
A comparison of the growth parameter revealed that saplings in an intercropped area showed stronger growth than those grown separately, with the two areas having the same characteristics [17].

In the agroforestry area, soil temperature and water management were much more balanced than in the control. The positive effect was particularly strong in drought periods; the drought damage loss was significant in the control area, while no loss was observed in the intercropped forest plantation. The daily average temperatures of the intermediate area during the arid period were significantly lower than the values of the control area [41] (*Figures 13* and *14*).
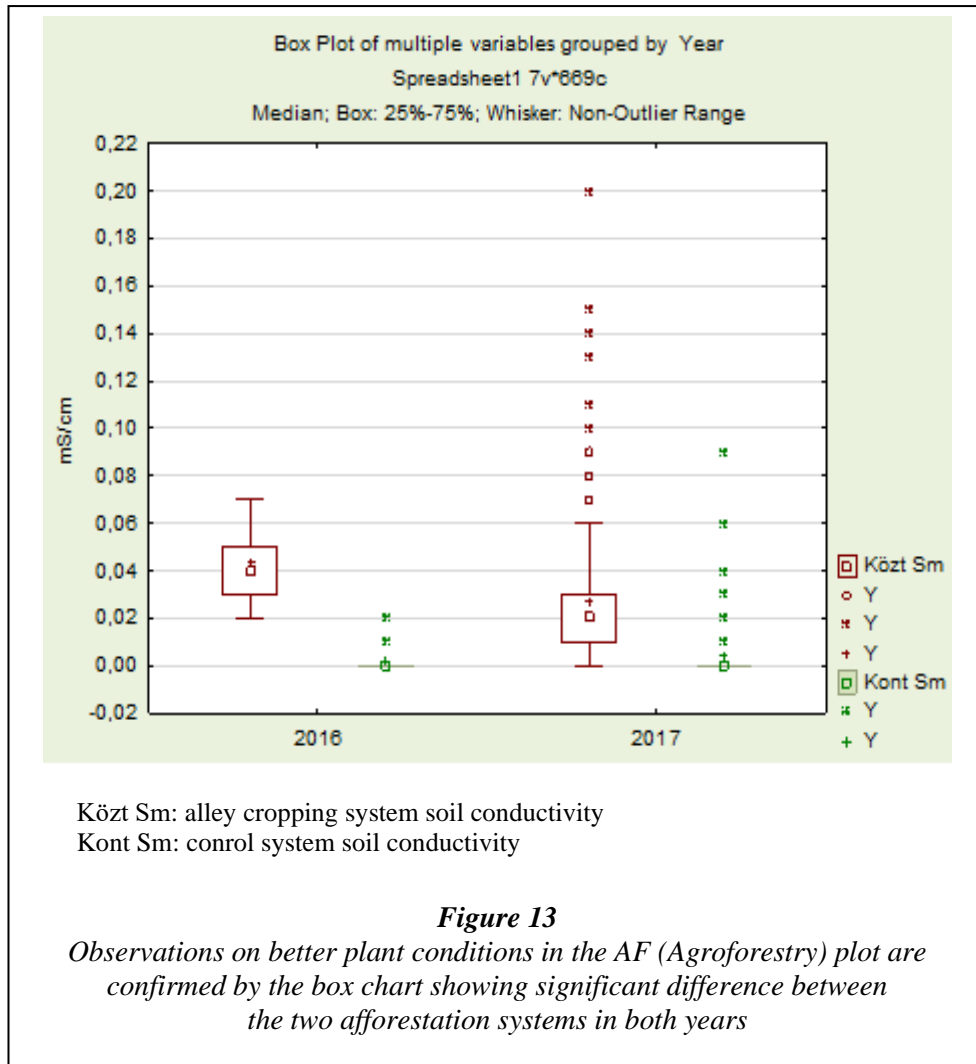
Alley cropping is the cultivation of food, forage or specialty crops between rows of trees. It is a larger version of intercropping or companion planting conducted over a longer time scale. Alley cropping can provide profitable opportunities for row crop farmers, hardwood timber growers, nut growers.
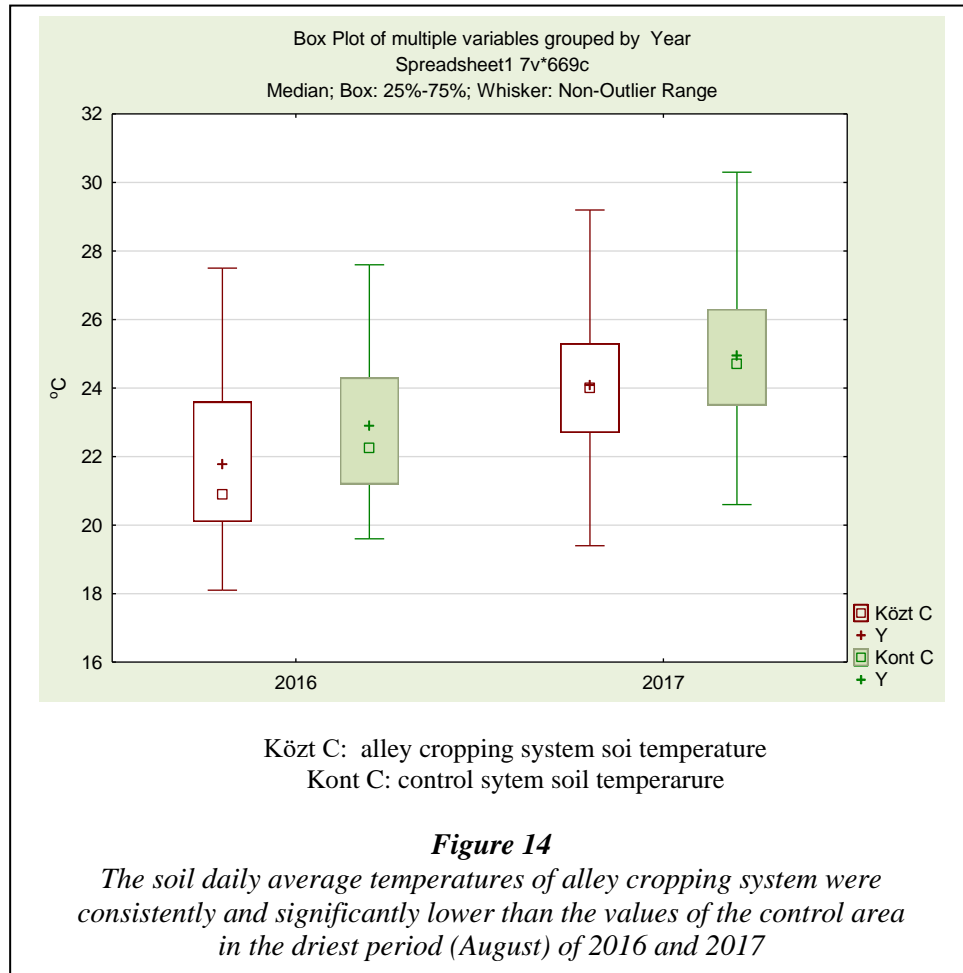
Experimental areas are affected by wildlife damage. Experience shows that wildlife tended to damage the intermediate culture while leaving trees intact [17, 18].

However, a significant contribution to meeting future needs for woody biomass and mitigating the loss of wooded areas can be achieved not only by the re-introduction of intercropping in young forest plantations, but also through the introduction of agroforestry in agricultural areas. In practice, agroforestry has always spread or diminished depending on whether farmers obtained additional income from the cultivated timber or advantages for their own use. While enjoying the added benefits, farmers rarely saw it as having major value. However, in response to new market opportunities, industrial tree planting on farms is spreading across Europe. Parallel to this, new research areas exploring competition between tree and food crops and ways of making the most of land have emerged. Given that agricultural land accounts for almost half of the EU area and the high adaptability of agroforestry systems, there

would be enormous potential in terms of wood production if woody vegetation is integrated into existing agricultural systems, even if only less productive areas with lower soil quality index are considered.

Közt Sm: alley cropping system soil conductivity
Kont Sm: conrol system soil conductivity

Figure 13

*Observations on better plant conditions in the AF (Agroforestry) plot are
confirmed by the box chart showing significant difference between
the two afforestation systems in both years*

Közt C: alley cropping system soi temperature
Kont C: control sytem soil temperarure

Figure 14
The soil daily average temperatures of alley cropping system were
consistently and significantly lower than the values of the control area
*in the driest period (August) of 2016 and 2017*

3.3. New methods of energy utilization

3.3.1. Industrial pellets results

Paper sludge has a high ash content as it contains large amounts of inorganic SiO_2 and AlO_3. The ash content was determined by a glow furnace test; the average of five samples was 39.8%. The calorific value was 11.8 MJ/kg for dry matter and 10.7 MJ / kg at 11% moisture before pelletization. By increasing the mixing ratio, a linear rise in ash content was expected, as demonstrated by the following equation. The ash content is particularly important in the utilization of pellets. If the ash content is too high, problems may occur during firing. The results of ash content measurement are shown in Table 3.

Ash content change in paper sludge and wood blend pellets

Paper sludge mixing ratio (%)	5	10	20	30		40	50
Ash content (%)	3.1	6.5	9.8	12.7		16.2	19.6

The "a" and "b" values of "a * x + b = y" equation are the parameters of the regression equation, where denotes the mixing ratio, y the ash content of the samples. From a practical point of view, the intersection points are also important, as can be concluded by the ash content of the base material. The ash content results and the regression line are visible in *Figure 15*.

Figure 15
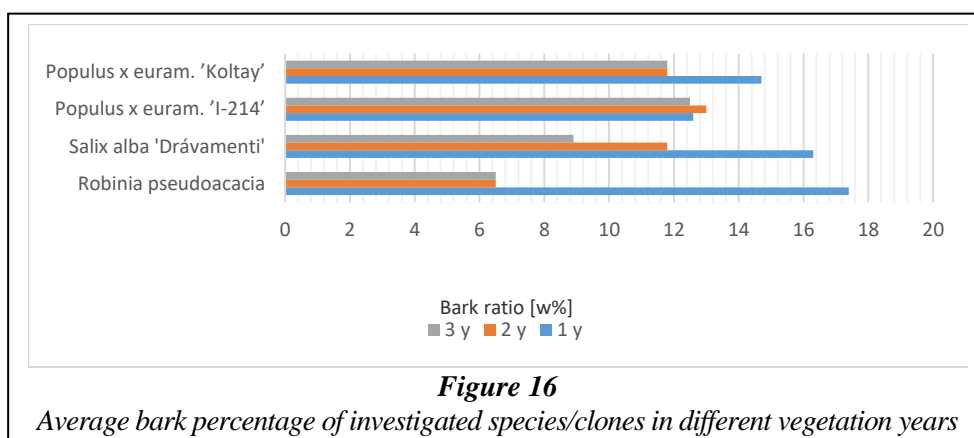**Ash content change and regression line in blend pellets**
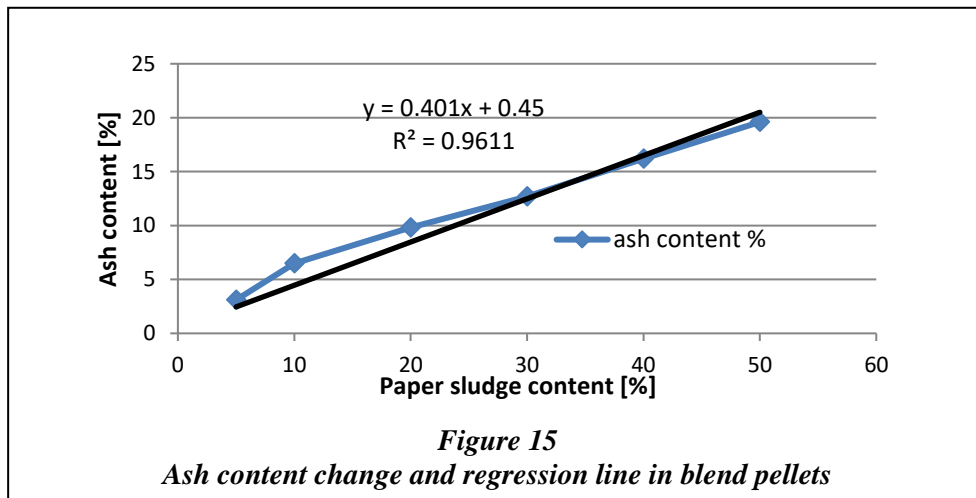
As expected, the calorific value decreased with the increase in paper sludge. Measurements were repeated three times; the mean of the results is shown in *Table 4*.

Table 4
Heating value of paper sludge and wood blend pellets

Mixing ratio of paper sludge %	Heating value MJ/kg
5	17.5
10	16.9
20	16.1
30	15.3
40	14.6
50	13.8

In the course of our previous research studies, we have dealt with wood pellet and agripellet energy balance and EROEI (Energy Returned on Energy Invested), by the amount of invested and recoverable energy [38]. When using paper sludge for pellets, EROEI values are considerably smaller due to the relatively low calorific value as compared to wood pellets or agripellets. The other problem is high humidity; achieving optimum levels of 11–12% under operating conditions requires a significant energy input need for drying. Although there is no industrial data on pelletizing energy for paper sludge, an approximate value can be provided. An average value was taken into account from the technological energy demands presented in the previous research of wood pellet production [39] (120 MJ/t for delivery, 1,700 MJ/t for primary electric energy of pelletizing pellet, 1,500 MJ / t for drying, 200 MJ/t for pellet delivery, etc.) so an estimated value for energy input can be entered. Assuming 80% efficiency in recovery, the calorific value of the samples tested can be estimated by the amount of recoverable energy [39]. By increasing the mixing ratio of paper sludge due to the decreasing heat values, the EROEI values are, of course, also lower. Since the amount of recoverable energy is much lower than it is in pure wood pellets, the EROEI estimates are also lower, at 50% mixing only around 2-3.

3.3.2. Biofuels results

Figure 16
Average bark percentage of investigated species/clones in different vegetation years

During our research we determined the bark percentage for the four species/clones in different vegetation years. The highest bark percentage was typically obtained in the first vegetation year when stem diameter is still small; the average value ranged from 12 to 18%. In later years, the bark percentage depended on the specific growth rate of species/clones. The difference of the bark percentage in the 2nd and 3rd vegetation year is only significant in the case of willow thanks to intensive shoot growth in the third vegetation year. *Figure 16* demonstrates the values for the different vegetation years, which refer to the absolute dry weight.

A relationship between diameter and bark content was established and the values were classified. Bark content changed the most in the case of poplar clones, from

nearly 5% to 33% from the cutting height to the tip. In the case of willow and black locust, the value was lower, ranging between 3–20%. Generally, the bark percentage decreased rapidly in the small diametric classes up to 25 mm, and then we observed a slight increase *(Figure 17)*.

Figure 17
Average bark percentage in the different diameter classes
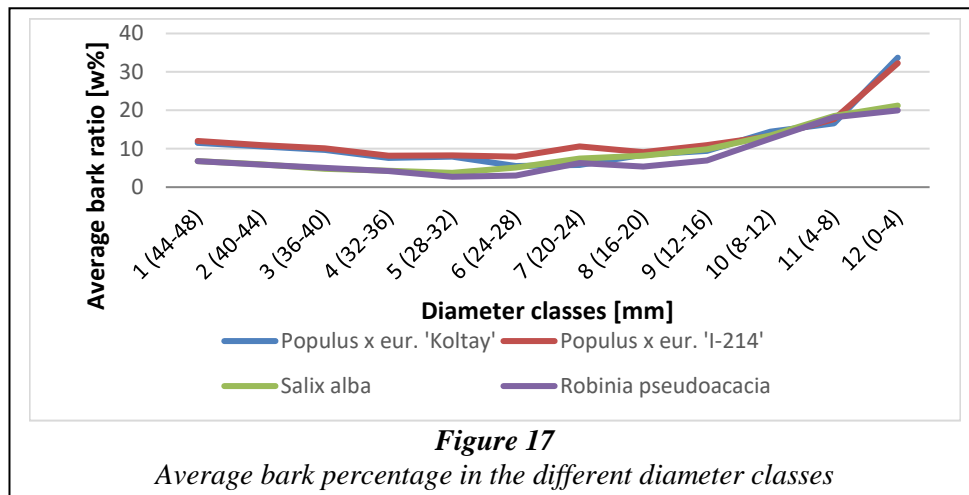
Base material ash content is an important feature from the perspective of thermal processes. Therefore, we also examined this property for the investigation of the bio-fuel production applicability. The high ash content was mainly caused by the high bark rate. Thus, as a first step, we determined bark ash content. The result shows that the ash content varied between 5.8 and 7.2% depending on tree species. Compared to that, the barked wood shows 3 to 4 times lower ash content *(Figure 18)*.

Figure 18
The mean ash content of bark for the different wood species/clones
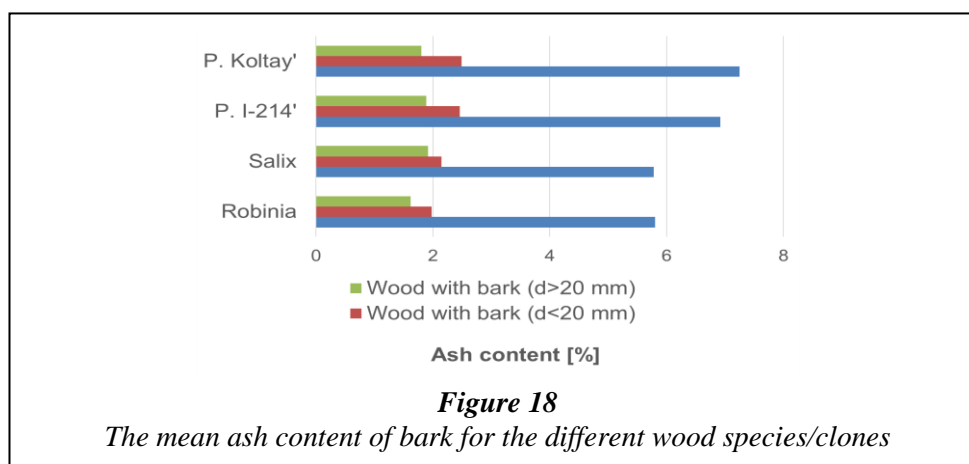
Choosing the right cultivation technology is a significant factor in ash content reduction. A shorter cutting cycle would ensure a continuous supply for the power plant and easier harvesting. However, in the first vegetation year especially, the weight ratio of the small shoots is more than 80% in the cases of willow and black locust, which results in a high ash content.

4. CONCLUSION

Concerning a wide range of issues in the production, harvesting, and utilization of dendromass, the following conclusions can be made.

The final conclusion is that highly mechanized logging work systems in the studied forest areas in the Borostyánkő and Kőszeg mountains, do not cause much damage and there is no significant difference in the work time structure, due to well-chosen machines, well-established networks, and well-organized work schedules. The developed measuring systems are well-suited for gathering data needed to analyze the logging.

Of the biomass sources that may be used for energy production, woody energy plantations show the greatest potential from both the productive and the environmental point of view. In the woody plantations, we can produce large amounts of biomass in a relatively short time and this can be used for energy or industrial purposes. This can also be particularly important for the supply of raw materials to a larger heating or power plant.

However, the area of tree plantations in Hungary has not increased significantly in recent years, mainly due to a lack of adequate support background. Therefore, it cannot be considered a relevant factor in the security of energy supply.

Overall, similar to European trends, biotic and abiotic damage and yields have increased significantly in the studied area over the last decade. Logging has also increased significantly over the past seven years due to meteorological damage when compared to the average of previous years. If these events continue as an indirect consequence of climate change, they will affect future yield trends. It can also be observed that the damaged wood is of lower quality, so the utilization of wood and the assortment structure are also transformed. Consideration should be given to changing the species structure and promoting the plantation of climate-resistant tree species, which poses a major challenge for forestry.

The pressure on the forestry sector can be significantly reduced by the widespread introduction of agroforestry in agricultural areas as well as the re-introduction of intercropping in young forest plantations, which could make a significant contribution to meeting future needs of woody biomass and mitigate the loss of wooded areas. According to agroforestry research, soil temperature and water management were much more balanced when intercropping was used than in the control area. The positive effect was particularly strong in drought periods, which is of high importance in mitigating the effects of climate change.

The use of paper sludge and pine wood mixtures for pellets raises a number of questions. The high ash content creates problems for residential equipment; hence,

only industrial scale utilization can be optimal. The high moisture content of sludge is also problematic during pelletization. In the case of energy, it would be optimal to produce pellets if some kind of waste heat was used in the drying process of paper sludge. The utilization of wood materials as liquid biofuel is greatly influenced by the bark content. SRC plantations show a correlation between bark content, vegetation time, and tree species.

Overall, from afforestation to timber harvesting, agroforestry and energy plantations, all contribute to a sustainable supply of raw materials. In the future, it must be borne in mind that the utilization of the various by-products and the material of the energy plantations will take on a more central role. If so, the wood of forests will be maintained for a longer time, and carbon sequestration will also be more optimal.

REFERENCES

[1]   UNECE-FAO (2011). The European Forest Sector Outlook Study II. 2010-2030. Publishing Service, United Nations, Geneva.

[2]   WWF Living Forests Report (2012). Forests and Wood Products. Chapter 4 Published in December 2012 by WWF – World Wide Fund for Nature, Gland, Switzerland.

[3]   Jonsson, K., Blujdea, V., Fiorese, G., Pilli, R., Rinaldi, F., Baranzelli, C., Camia, A. (2018). *Outlook Of The European Forest-Based Sector: Forest Growth, Harvest Demand, Wood-Product Markets And Carbon Dynamics Implications*. Sisef-Soc Italiana Selvicoltura Ecol Forestale 2018. From: https://ec.europa.eu/jrc/en/publication/outlook-european-forest-based-sector-forest-growth-harvest-demand-wood-product-markets-and-carbon.

[4]   EUROSTAT (2018). *Wood products - production and trade*. Agriculture, forestry and fishery statistics. Printed by Imprimeries Bietlot Frères in Belgium, ISBN 978-92-79-75764-8.

[5]   EUROSTAT (2020). Share of energy from renewable sources. https://appsso.eurostat.ec.europa.eu/nui/show.do?dataset=nrg_ind_ren&lang=en.

[6]   KSH Hungarian Central Statistical Office (2018). Elsődleges megújuló energiaforrások termelése energiaforrások szerint (2000–). https://www.ksh.hu/docs/hun/xstadat/xstadat_eves/i_ui012b.html

[7] Sierota, Z.; Grodzki, W.; Szczepkowski, A. (2019). Abiotic and Biotic Disturbances Affecting Forest Health in Poland over the past 30 Years: Impacts of Climate and Forest Management. *Forests*, 10 (1), p. 75.

[8] Seidl, R., Thom, D., Kautz, M., Martin-Benito, D., Peltoniemi, M., Vacchiano, G., Wild, J., Ascoli, D., Petr, M., Honkaniemi, J., Lexer, J. M., Trotsiuk, V., Mairota, P., Svoboda, M., Fabrika, M., Nagel, T. A., Reyer, Ch. P. O. (2017). Forest disturbances under climate change. *Nature Climate Change*, Vol. 7, Slovenian Forest Survive, pp. 395–402.

[9] Slovenian Forest Survive (2019). *Annual Forest Report, Five Years After Ice Storm, Damage to Slovenian Forests Remains*. Total Slovenia News. https://www.total-slovenia-news.com/lifestyle/3019-five-years-after-ice-storm-damage-to-slovenian-forests-remains-video

[10] Papp, V., Babiczki, L., Grédics, Sz., Szalay, D. (2019). Timber Harvest Due to Biotic and Abiotic Damage by the Example of Egererdő Plc. In: Czupy, I.: Exceeding the Vision: Forest Mechanisation of the Future. *Proceedings of the 52nd International Symposium on Forestry Mechanization*, Sopron, Hungary. e-book. pp. 495–502.

[11] Horváth A. (2015). *Többműveletes fakitermelő gépek a hazai lombos állományok fahasználatában*. Doctoral dissertation, Nyugat-Magyarországi Egyetem, Sopron.

[12] Szalay D. (2018). *Energetikai célú dendromassza termesztés és hasznosítás lehetséges szerepe a lignocellulóz biohajtóanyag üzemem alapanyag ellátásában.* Doctoral dissertation, Soproni Egyetem, Sopron.

[13] Szalay, D.; Jákói, Z.; Papp, V. (2019). Possible Role of Agricultural Woody By-products in Lignocellulose Biofuel Production In Hungary. *Journal of International Scientific Publications: Agriculture & Food Journal*, Vol. 7, pp. 211–220.

[14] Nemzeti Élelmiszerlánc-biztonsági Hivatal (NÉBIH) (2020). Erdészeti Igazgatósága személyes kapcsolatfelvétel útján adatgyűjtés.

[15] Marosvölgyi B. (1995). *Energetikai célú és a racionális földhasznosítást is szolgáló faültetvények komplex vizsgálata*. Research report. University of Forestry and Wood Industry, Sopron, pp. 28–31.

[16] Marosvölgyi B., Kürtösi A., Tamás R., Tóth G., Petznik P., Körmendi P. (1999). *Az ERTI által létesített energetikai faültetvényeken végzett utóméréseiről, és egyéb vizsgálatokról*. University of Sopron, Sopron.

[17] Vityi, A., Kovács, K. (2018). Improve the efficiency of afforestation by the use of alley cropping system. In: *Proceedings of the 4th European Agroforestry Conference: Agroforestry as Sustainable Land Use* (eds.: Nuria, Ferreiro-

Domínguez, María, Rosa Mosquera-Losada). Nijmegen, Hollandia, European Agroforestry Federation, pp. 457–461.

[18] Kovács K., Vityi A. (2017). Erdőtelepítés támogatása agroerdészeti rend-szerekkel." In: Bidló A., Facskó F. (eds.). *Soproni Egyetem Erdőmérnöki Kar VI. Kari Tudományos Konferencia: a konferencia előadásainak és posztereinek kivonatai*, Sopron, Hungary, Soproni Egyetem Kiadó, pp. 81–84.

[19] Den Herder, M., Gerardo, M., Mosquera-Losada, R., Palma, J., Sidiropoulou, A., Santiago Freijanes, J. J., Crous–Duran, J., Paulo, J., Tomé, T., Pantera, A., Papanastasis, V., Mantzanas, K., Pachana, P., Papadopoulos, A., Plieninger, T., Burgess, P. J. (2016). *Current Extent And Trends Of Agroforestry In The EU27*. Deliverable 1.2: AGFORWARD (613520).

[20] Papp, V., Szalay, D., Hodúr, C., Czupy, I. (2019). Production and laboratory testing of paper sludge and wood chips blend pellets. *IOP Conference Series: Earth and Environmental Science*, 307 Paper: 012010.

[21] Szalay, D., Papp, V., Hodúr, C., Czupy, I. (2019). Examination of bark content for different species of short rotation coppice. *IOP Conference Series: Earth and Environmental Science*, 307 Paper: 012001.

[22] Szalay, D., Kertész, Sz., Papp, V. (2019). Examination of Ash Content for Different Species of Short Rotation Coppice. *Journal of International Scientific Publications: Agriculture & Food Journal*, Vol. 7, pp. 221–231.

[23] Frankó, B., Galbe, M., Wallberg, O. (2015). Influence of bark on fuel ethanol production from steampretreated spruce. *Biotechnology for Biofuels*, 8 (1), DOI: 10.1186/s13068-015-0199-x2015.

[24] Tröger, N., Richter, D., Stahl, R. (2013). Effect of feedstock composition on product yields and energy recovery rates of fast pyrolysis products from different straw types. *J Anal Appl Pyrol.*, 100, pp. 158–165.

[25] Dou, C., Chandler, D. S., Resende, F., Bura, R. (2017). Fast Pyrolysis of Short Rotation Coppice Poplar: An Investigation in Thermochemical Conversion of a Realistic Feedstock for the Biorefinery. *ACS Sustainable Chemistry & Engineering*, 5 (8). DOI: 10.1021/acssuschemeng.7b01000 2017.

[26] Horváth, A. L., Szné. Mátyás, K., Horváth, B. (2012). Investigation of the Applicability of Multi-Operational Logging Machines in Hardwood Stands. *Acta Silvatica et Lignaria Hungarica*, Vol. 8, Magyar Tudományos Akadémia Erdészeti Bizottsága, Sopron, pp. 9–20.

[27] Liebhard P. (2009). *Energetikai faültetvények*. Cser Kiadó, Budapest.

[28] Leakey, R. R. B. (2012). Multifunctional agriculture and opportunities for agroforestry: implications of IAASTD. In: Nair P. K. R., Garrity D. (eds.).

Agroforestry-the future of global land use. *Advances in agroforestry*, Vol. 9, Springer, Dordrecht, pp. 203–216.

[29] Gál J. (1963). A mezőgazdasági terméshozamok növekedése az erdősávok védelmében. The increase of agricultural yields in protection zone of forest belts. *Scientific Publications of the University of Forestry and Timber Industry*, 1963/1–2., pp. 43–81.

[30] Dupraz, C., Burgess, P. J., Gavaland, A., Graves, A. R., Herzog, F., Incoll L. D., Jackson, N., Keesman, K., Lawson, G., Lecomte, I., Mantzanas, K., Mayus, M., Palma, J., Papanastasis, V., Paris, P., Pilbeam, D. J., Reisner, Y., van Noordwijk, M., Vincent, G., van der Werf, W. (2005). *SAFE, Silvoarable Agroforestry for Europe: Synthesis Report.* http://www1.montpellier.inra.fr/safe/english/index.htm

[31] Suliman, A., Ahmed, M. (2013). Assessing the Land Equivalent Ratio (LER) of Two Leguminous Pastures (Clitoria and Siratro) Intercropping at Various Cultural Practices and Fencing at Zalingei, Western Darfur State –Sudan. *ARPN Journal of Science and Technology*, 2 (11), pp. 1074–1080.

[32] Abdul, K. (2013). Comparative study of different densities of poplar in wheat based agroforestry system in central punjab. *Geography*, https://www.researchgate.net/publication/28346983_comparative_study_of_different_densities_of_poplar_in_wheat_based_agroforestry_system_in_central_punjab

[33] Nyoki, D., Ndakidemi, P. (2017). Assessing the land equivalent ratio (LER) of maize (Zea mays L.) intercropped with Rhizobium inoculated soybean (Glycine max [L.] Merr.) at various P and K levels. *International Journal of Biosciences*, 10 (3), pp. 275–282.

[34] Vityi, A., Kiss Szigeti, N., Schettrer, P., Marosvölgyi, B. (2017). *Lessons learnt: Alley cropping in Hungary*. Contribution to Deliverable 4.11 Lessons learnt from innovations within agroforestry for arable farmers, Agforward project.

[35] Abdullahi, I. N., Anyaegbu, P. O. (2017), The performance of Soybean using Moringa as alley to improve soil productivity in North-Central Nigeria. *African Journal of Agricultural Research*, 12 (14), pp. 1182–1189.

[36] Nair, P. K. R. (1993). *An Introduction to Agroforestry*. Springer Science & Business Media, Springer Netherlands, Amsterdam.

[37] Briggs, S. (2015). *A farmer's perspective on Agroforestry*. Seminar Presentation. Can agro-ecological approaches contribute to sustainable intensification 10th June 2015, Edinburgh. https://www.nature.scot/sites/defa ult/files/2017-12/Seminar%20Presentation%20-%20Edinburgh%20-%20June%2020015%20-%20Agroforestry%20and%20sustainable%20intensification%20-%20Stephen%20Briggs.pdf

[38] Papp V., Marosvölgyi B. (2012). A pellet mint megújuló energiaforrás előállítása, hasznosítása és energetikai értékelése. *Energiagazdálkodás*, 53 (2), pp. 18–21.

[39] Papp V. (2018). *Energetikai pelletek előállításásnak és hasznosítsának ökoenergetikai vonatkozásai*. PhD dissertation, Univerity of Sopron.

[40] Barkóczy Zs. (2009). *A dendromassza alapú decentralizált energiatermelés alapanyagbázisának tervezése*. PhD dissertation, Sopron.

[41] Vityi, A., Kovács, K., Dufla, F., Bácsmegi, L., Nagy, I. (2016). Improve the efficiency of afforestation by the use of agroforestry practices. In: Marie, Gosme, Paulo, J. A., Borek, R., Burgess, P. J., Dupraz, C., Domínguez, N. F., Freese, D., González-Fernández, P., Hartel, T., Lamersdorf, N., Lawson, G., Lojka, B., Méziére, D., Moreno, G., Mosquera-Losada, M., Palma, J., Pantera, A., Paris, P., Pisanelli, A., Plieninger, T., Reubens, B., Rois, M., Rosati, A., Smith, J., Vityi, A. (eds.). *Proceedings of 3rd European Agroforestry Conference*, Montpellier, France, European Agroforestry Federation, pp 144–145.

SUSTAINABLE RAW MATERIALS SUPPLY OF LIGNOCELLULOSIC BIOFUELS IN HUNGARY

D. SZALAY[1*] – A. VÁGVÖLGYI[1] – I. CZUPY[1] –
SZ. KERTÉSZ[2] – S. BESZÉDES – C. HODÚR[2] – V. PAPP[1]

[1]*Institute of Forest and Environmental Techniques*
Faculty of Forestry, University of Sopron
[2]*Department of Process Engineering, Faculty of Engineering, University of Szeged*
*szalay.dora@uni-sopron.hu

Abstract: The current publication summarizes the main results of the lignocellulosic biofuel research carried out within the project *Sustainable Raw Material Management Thematic Network – RING 2017*. In the first part of the paper, we explore the different type of currently available biomass residues potential and summarized for each Hungarian county. In the next part, we identify the main factors that significantly influence the sustainable raw material supply of a lignocellulosic biofuel production plant and investigate the additional feedstocks, which may be useable in the future. The results show a large amount of available biomass residues with more than 330 PJ energy potential. Particularly, the amount of generated agroresidues is outstanding, almost half of which can be used for energy production. However, the collection, storage and utilization for biofuel production of agroresidues is less developed than for woody material.

Keywords: lignocellulosic biofuel research, biomass, dendromass,

1. INTRODUCTION

Biofuels have a key role to play in combating climate change in the future through lowering greenhouse gas emissions. The prescribed biofuel ratio target values for member states of the EU is also encouraging the application of biofuel blends. According to the RED II (Renewable Energy Directive II) regulation, member states will have to meet targets of 14% renewable energy use in road and rail transport by 2030. At the same time, decision-makers have recognized that crop-based biofuels encroach upon land used for food crop production through indirect land use. According to estimates, the land area used for growing biofuel feedstock in 2018 covered about 5% of the total crop area [1]. The growing areas for corn, sugar cane, or palm were enlarged through the conversion of rainforests and grasslands. This has reduced the net carbon dioxide absorption capacity and increased emissions. Droughts, forest fires, biotic and abiotic damage are becoming more frequent as a result of the changing climate. Carbon stored in forest biomass is released and contributes to climate change.

The occasional yield loss of conventional biofuel raw materials is already a problem today. A doubling of cereal consumption for food and animal feed due to population growth and changes in consumption structure in the 21st century only adds to this problem [2]. The intensified application of mechanical soil cultivation technology with irrigation and the vast use of fertilizers has made the satisfaction of cumulative demands possible. However, fertilizer production is an energy-intensive industry [3]. For these reasons, the EU legislation restricts the use of food crops for energy purposes. The maximum contribution of conventional biofuels will be frozen at 2020 consumption levels, plus an additional 1% with a maximum cap of 7% of road transport fuel in each member state. The proportion of advanced fuels to be achieved must grow gradually and its proportion was set at least 3.5% by 2030. With the help of lignocellulosic biofuels there is an opportunity to meet the target.

Commercial-scale production of lignocellulosic biofuels from forestry and agricultural by-products is under development, and its increased use in transport sector will be viable in the near future [8]. The use of wood industry by-products is already largely realized today.

The conversion of lignocellulosic feedstock to liquid biofuels requires much more complex technology than first generation biofuels. Overall, conversion rates and production capacity are lower, but the investment cost can be up to ten times higher compared to advanced biofuels [4]. To achieve a sustainable raw materials supply for the planned expansion, an extensive raw material analysis is absolutely necessary.

2. METHODS

The following methodology was used to calculate the available raw material potential reserves. As a starting point for calculations of forest residue amounts, we used Hungary's wood use data from the compilation of Statistical Mirror in 2013, "Features of Forest Management", by the Hungarian Central Statistical Office (KSH) [5]. Subsequently, this logging data was updated from the 2016 Forest Balance Sheet and created the gross volume of timber harvested per county per tree species. The by-product volume is worth an average of 17% relative to the gross volume of timber produced. The data were retrieved in a humid state while 50% moisture content was assumed. When cubic meters were converted to metric tons, the wood weight ratio of the species harvested by clear cutting in the country based on the 2016 forest balance sheet data was considered and multiplied by the density values specific to the tree species.

National wood use data as described for forest residues were calculated to estimate the stump and root amount. Larger quantities of stumps can only be technically harvested in areas where clear-cutting has been executed within the end use. However, stumping and subsequent rotational soil preparation are limited to flat or slightly undulating surfaces and can only be performed on some genetic soil types, e.g. sandy soil [6]. Therefore, it mostly takes place with black locust, poplar, and pine as characteristic tree species. After that, the black locust, poplar, and for-

est pine areas were determined according to the table of the NÉBIH Forest Inventory by Tree Species Group and the Current Forest Association Group, followed by the gross volume count of these trees. Root stump logs account for 15–25% of the aboveground tree mass for black locust and up to 10–20% for poplar and pine [6].

The potential estimation of grape and fruit tree areas was derived from the Hungarian Central Statistical Office (KSH) 2017 Land by Field Cultivation Table [7]. According to the methodology of the Statistical Office, grape-growing areas producing propagating material are also included. Vineyards produce about 1–2.5 tons of pruning residues per hectare per year, with an average of annual 1.5 t/ha. Fruit tree thinning produces a smaller amount of prunings annually, with larger amounts every 4-5 years; on average, we can count on 2.5 t/ha per year. Since the by-products can only be cost-effectively collected in vineyards with larger contiguous areas, only vineyards above 3 ha were taken into account during the calculation. The breakdown by size categories made in 2005 and 2007 Census of Vine and Fruit Plantations was used for the calculations.

Since woody energy plantations are also a potential lignocellulosic biofuel feedstock, we conducted a survey of these as well. The survey was based on the area data collected by the Forestry Directorate of the NÉBIH in 2018. Furthermore, we used the average yearly yields for the calculations.

Table 1 summarizes the characteristics of dendromass feedstock.

Table 1

Features of dendromass base materials [8, 9]

Type of by-product	Generated by-product [t/ha or %]	Heating value (at w% 15−20) [MJ/kg]
Forest residues	12%	14−15
Grape pruning	1.5 t/ha	14.5−15
Orchard residues	2.5 t/ha	14.5−15.5
Woody energy plantations	10 t_{dry}/ha	18

For comparison, the by-products of arable herbaceous plant production have also been surveyed. Hungary has a great deal of arable land due to favorable weather conditions; the volume of agricultural residues in the country is remarkable. Calculations were completed by determining the harvested area of different agricultural crops based on KSH 2018 data tables. Area size changes every year due to crop rotation. As a result, five-year averages (2013–2017) were considered. By-product mass determination was possible using KSH 2018 main product yield data. We also considered 5-year averages here due to crop yield fluctuations. Data in the literature on the main product ratio (seed:stem ratio) to the by-product were collected and used to determine the residue amounts. *Table 2* summarizes these data.

Using formulas (1) and (2) the determination of the theoretical and energetical biomass potential is possible.

Features of by-products of herbaceous plants [10, 11, 12, 13, 14, 15, 16]

Type of stem, stalk	Seed:stem ratio	Heating value at harvest [GJ/t]	Moisture content at harvest [%]
Corn stem	1 : 1.5	12	30–40
Wheat straw	1 : 1.2	13	10–15
Barley straw	1 : 1.2–1 : 1.5	13	15–20
Rye straw	1 : 1.8	13	15–20
Oat straw	1 : 1.3	13	15–20
Triticale straw	1 : 1.2	13	15–20
Sunflower stem	1 : 2	14	25–35
Rape seed straw	1 : 1.4	14	15–20

Theoretical biomass potential:

The energy potential of the amount of studied annually generated biomass.

Forest residues per county:

$$E_{ei\,for} = \frac{V_{br} * a * k * F}{10^6}$$

(1)

where:

$E_{ei\,for}$ – theoretical annual energy potential of forest residues in a county (PJ/yr)
i – county (i=1 to i=20)[1]
V_{br} – gross volume of wood use in the county (m³/yr)
a – crop yield relative to main product (~17%)
k – average multiplication factor at m³ to metric ton conversion (national ave. approx. 0.6 for dry wood)
F– calorific value of the residues (MJ/kg).

Agricultural residues per county:

$$E_{ei\,agr} = \frac{\sum_n T_n f_n m_n F_n}{10^6}$$

(2)

where:

$E_{ei\,agr}$ – theoretical annual energy potential of agricultural residues in a county (PJ/yr)
i – county (i=1 to i=20)
T_n – 5-year average of the growing area of the plant type "n" (ha)
f_n – 5-year average yield of the main product of the plant type "n" (t/ha*yr)

---

[1]   Hungary has 19 counties plus the capital city of Budapest, which is counted here as a county.

m_n – ratio of the yield of the by-product to the main product of the plant type "n"
F_n – calorific value of the by-product of the plant type "n" (MJ/kg).

Gross energy potential of biomass residues in Hungary per county (PJ/yr):

$$E_i = \Sigma\, E_{ei\,for.} + \Sigma\, E_{ei\,agr} \qquad (3)$$

Energetical biomass potential

This is the amount of biomass that can be used for energy purposes. To determine this value, we considered the various sustainability, environmental and technical interests, as well as the biomass amounts potential users requires.

In the case of forestry residues, larger quantities of raw material can only be cost-effectively collected in areas practicing clear-cutting within end use. According to the KSH OSAP 1254 data collection, the use of clear cutting occurred in 47% of the total national harvested gross timber volume in 2016 [19]. Only the 3–7 cm thin wood parts from end uses felling can be harvested technically and ecologically, which represents 12% of the total wood weight [6].

In the case of agricultural residues, it would be optimal to return 20–30% of the stem mass to the soil for soil fertilizing [17, 18]. We also determined the average amount of straw used for animal litter per year based on the data from the literature and from the number of Hungarian livestock recorded by KSH *(Table 3)*.

We summarized the biomass demand of currently operating users and potential users (those planning to become users) through the collection of data in the literature and electronically-available data from the website of the companies.

Table 3
Specific straw needs for bedding [20]

Farm animals	Straw needs for bedding	
	[kg/head/day]	[kg/head/year]
Cattle	3.8	1,400
Sow	1.4	511
Sheep	1.1	220
Poultry	–	3.3

3. RESULTS

3.1. Residues potential

Based on the calculation methods given in the methodology, the nationally generated theoretical annual potential of biomass by-products is shown in *Table 4*.

Table 4

Theoretical annual biomass potential in Hungary [8, 21]

Type of biomass	Amount (dry) [1000 t]	Energy [PJ]
Forest residue	1,000	11.0
Stump	160	1.8
Fruit tree pruning	165	2.6
Vineyard pruning	57	1.0
Agricultural herbaceous residue (stalk, stem)	22,700	314.0
Short rotation coppice (SRC)	4.4	0.08

3.1.1. Forest residues and stumps

Almost 1 million metric tons of forest residues, calculated in the wet state at the harvest, are generated annually, in theory. Within this figure, about 700,000 tons can be collected, once technical, ecological and economical aspects are taken into account. Roughly 7.7 PJ of energy can be gained through forest residue utilization. Stump amounts are only an additional available potential from forestry. This technology can be mainly used in Somogy, Szabolcs-Szatmár-Bereg, Bács-Kiskun, Pest and Hajdú-Bihar Counties. It is worth mentioning that the annual yield of black locust, poplar, and pine has shown a slight increase over the last five years, but the biomass of root and stump is technically unusable so far.

3.1.2. Orchards, vineyards

According to our survey, the amount of collectable fruit tree prunings is about 165,000 tons annually, which would provide 2.6 PJ of usable energy. In vineyards, 57,000 thousand tons of prunings can be realistically collected, which equals nearly 1 PJ of energy.

3.1.3. Agricultural residues

Corn is the most cultivated crop in Hungary, with a cultivation area of about 1.1 million hectares. This is followed by wheat with 1 million hectares, and sunflower with a cultivation area of 625,000 hectares. According to our calculations, corn production generates more than 11 million tons of by-products in Hungary annually. The amount of wheat straw is also large; on average more than 6 million tons every year. Sunflower stalks amount to 3.3 million tons, while the amount of rapeseed stalks is just over 1 million tons per year. The quantity of barley straw is also significant, around 1.4 million tons per year.

3.1.4 Short rotation coppice

In Hungary, energy plantations are worth mentioning, primarily with regard to woody plantations. However, energy plantation size is not significant when com-

pared to Western European countries. According to 2019 NÉBIH Forestry Directory data, energy plantations in Hungary occupy a total of 4351 ha, of which about 80% is cultivated with poplar due to the suitability of the species in the available areas. Miscanthus plantations only comprise about 360 ha in the country [22].

3.2. Impact of climate change on collectable raw material

Future indirect effects of climate change will increase biotic and abiotic damage. The number of forest pests is forecast to grow due to average annual temperature increases and warmer winters [26]. Most intense forms of damage have occurred in the last 20 years. Moreover, this damage has generally accumulated over the past 10 years [26]. Therefore, in our previous research study we began focusing on forest damage-induced logging, which will affect the useable amount of raw materials for energy recovery in the future [23]. In agriculture harmful effects can be eliminated in a relatively short time period with the help of appropriate agrotechnical methods, while in forestry this is only possible over a longer time frame and only through appropriate tree species choices.

Drought and favorable periods for crop production have a strong impact also on the amount of agricultural by-products generated. Based on KSH data, 2012 was one of the worst drought years of the last decade, and we took this year into account in our research. According to yields, the most favorable weather occurred in 2016. The generated amount of by-products that could be harvested annually nationwide in these two years is compared to the average of 2013–2017 and shown in *Table 5*.

Table 5

Change in the theoretical amount of by-products annually [8]

	National data	2012 "worst year"	2016 "favorable year"	2013–2017 "average"
Corn	growing area [ha]	1,191,291	1,011,563	1,115,955
	average crop yield [t/ha]	4.0	8.6	6.9
	harvestable stalk [t]	**7,147,746**	**13,049,162**	**11,550,134**
Sunflower	growing area [ha]	615,097	629,675	625,488
	average crop yield [t/ha]	2.1	3.0	2.7
	harvestable stalk [t]	**2,583,407**	**3,778,050**	**3,377,635**
Rapeseed	growing area [ha]	164,916	256,679	238,346
	average crop yield [t/ha]	2.5	3.6	3.0
	harvestable stalk	**577,206**	**1,293,662**	**1,001,053**

The amount of rapeseed stalk showed the biggest difference, but this was mainly due to the changing size of harvested area. Crop yield loss per hectare was 30% in 2012 compared to the most favorable year, while in the case of rapeseed stalk, less than half could be collected. Of the examined cereals, corn had the largest yield fluctuation. Less than half of the corn crop and corn stalk could be collected in the worst year compared to the favorable year. The fluctuation is the smallest in the case of sunflower, and there is no significant difference in the harvested area or yields. However, it should be mentioned that only a weak-medium correlation can be detected between the yield of main products and by-products n recent years, which can impair the accuracy of the survey [24].

In addition to the quantitative change caused by climate change, agroresidues are also affected by plant breeding methods *(Figure 1)*. The plant breeding methods have an important role influencing the long-term energy strategies through of the amount of generated biomass.

Figure 1
Changes in straw and stem specific quantities due to plant breeding activities [26]
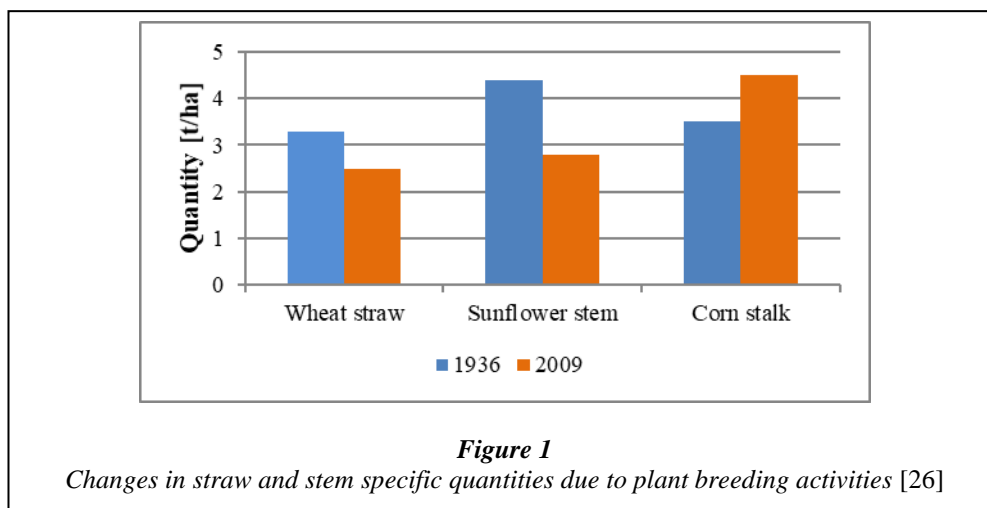
In terms of raw material supply, woody energy plantations can be an additional solution for lignocellulosic biofuel plants, which can be successfully grown even in low-quality agricultural areas. Energy plantations can be much better protected against biotic and abiotic damage. Unfortunately, dry summers represent a high risk, especially in planting years. Up to 50% of shoots planted during dry summers do not sprout and need to be replaced. The expected yield is also far from optimal, since drought inhibits photosynthesis; leaves become smaller; shoots become elongated; leaves untimely wilt and fall; and peak dehydration may occur [27].

The frequency of persistently cold winters is decreasing. Nevertheless, their episodic occurrence in Hungary should be taken into account even with a slightly warmer global climate. In principle, frosts in April–May and September–October will become less frequent, but as the growing season lengthens, the risky periods

will also shift towards the cold season. Early frosts shorten the vegetation period, thereby inhibiting the "ripening" of wood [27]. Late spring frost can cause severe damage to some poplar clones; their shoots often die completely. This poses a particular risk to clones originating from less frigid regions [27] *(Figure 2)*. The photos of two different poplar clones were taken in the same area, at the same time. The variety on the left with mostly dead shoots is highly sensitive to spring frost. The plant emerges much later, produces a lower number of shoots, and results in a lower yield at harvest. The poplar variety shown in the picture on the right is not sensitive to late spring frost. Breeding and tree species selection as well as choosing varieties according to the given climatic and soil conditions are of great importance during planting.

Figure 2
Effect of spring frost on different poplar clones [8]
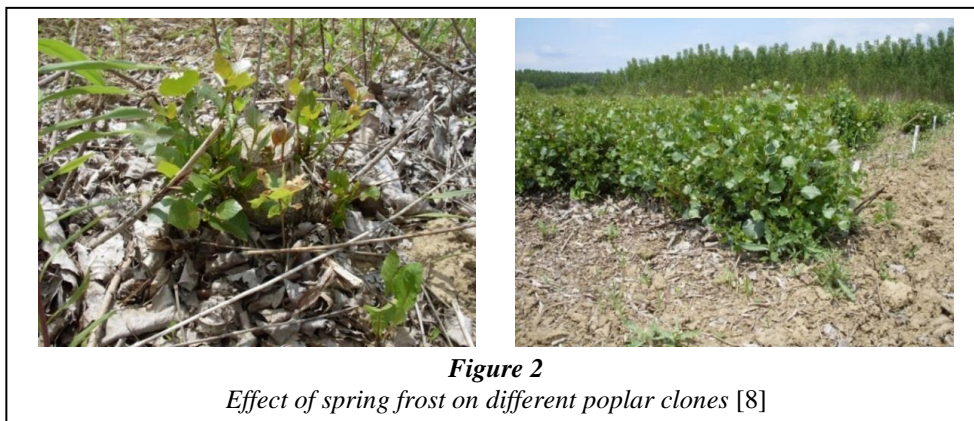
Figure 3 illustrates the yield differences of the different poplar clones under the same climatic and soil conditions.

The annual change in precipitation based on climate scenarios is expected to be characterized by a slightly negative trend in Hungary by 2100. About 90% of the country's territory is at risk of drought. Drought can change the mechanical properties, the chemical composition of soil, organisms within soils and the wildlife of a plantation over time. In addition to the decrease in soil moisture, a drier climate may also lead to a drop in the groundwater level. This causes a greater decline in yields, especially in summer energy plantations. In addition to direct climatic effects, indirect effects such as plant diseases and pests may also occur. For this reason, it is important to choose the right tree species.

Increasing CO_2 emissions from burning fossil fuels has a fertilizing effect on most plants because CO_2 is a component of photosynthesis. Experiments on the effects of enriched atmospheric CO_2 on plants have been completed in several cases around the world. Based on their results, the mass of aboveground woody biomass may rise by up to 25–38% due to increasing photosynthesis. This may change the mass ratio of plant components, e.g. the mass of leaf, stem, and root system. On the other hand, plant stock characteristics also change due to altered conditions. For

example, plant biomass increases, plant stocking density increases, water utilization improves, and the C:N ratio changes, all of which also affects the infectious characteristics of pathogens and the nutritional characteristics of animal pests. However, the beneficial effect can only be achieved if the necessary water supply is available.

Figure 3
Height difference of two different poplar clones with the same environmental and soil conditions [8]

3.3. Utilized residues by main potential users

An important part of the base material survey is the examination of the current operating and planned potential users. Forest and agricultural by-products are only partially collected, and are most often sold to power plants, perhaps to a smaller extent to heating plants, boilers, and pellet and briquette factories.

3.3.1. Dendromass utilization

Different information is available on the currently used quantities because the largest collectors and purchasers obtain some of their by-products from forests in other countries. According to the literature, about 4.5% of the thin wood part of the collectable forest residues is utilized [6].

Pécs Power Plant is the largest forestry residue utilizer in Hungary. Smaller amounts are utilized in the cities of Pornóapáti, Hangony, Csitár-Nógrádgárdony, Mátészalka, Szakoly, Miskolc, Pannonhalma, Homrogd, and Szombathely. In Tiszaújváros, forestry residues are used for wood pellet production. In addition, a

common form of forest residue utilization today is collection by local people for their personal use. In the Kiskunság Forestry and Wood Processing Co. (KEFAG) area, for example, the local population harvests 3,000–4,000 m^3 of tree branches to obtain cheap fuel for own energy needs. An additional 10,000 m^3 of logging waste collection is done mechanically.

Tree stumps offer further potential from forest management. There have been attempts to utilize stumps in the country (Pécs, Szakoly), but this is not typical due to challenges with harvesting and burning. Furthermore, the presence of a significant amount of bark and contamination causes problems during biofuel production; hence, we did not include it as a potentially useable base material.

The main users of forestry and woody by-products are pellet and briquette manufacturers. Their number has been rising steadily due to significant export demand. Exports make up about 70% of the total Hungarian production. At the same time, pellet production is largely restrained by the cheap inflow of pellets from Ukraine. The utilization of raw materials is usually done with bark-free by-products in a mixture. Of the larger manufacturers, forest residues are utilized by the Eko Fire Pellet Ltd. in Tiszaújváros, for example.

There are several paper mills in Hungary. Most of their raw material is derived from forests that have been deliberately planted for industrial use. The mills also manufacture products from waste paper. As in Hungary, the global wood-based panel industry primarily uses low quality wood resources and turns them into value-added products. One of the forms of using by-products from forestry and the wood industry is chipboard manufacturing. Falco Zrt. in Szombathely is the best-known chipboard manufacturing plant in Hungary. Furthermore, the Swiss Crono OSB factory in Vásárosnamény started operations in 2016. Veneer sheet production (e.g. Derula Kft. in Szolnok) mainly uses poplar logs, which are produced on industrial plantations. In this process the by-products are not used [29].

Upcoming projects may also modify the available raw material. Mátra Power Plant (Visonta) recently received a permit for the construction of a mixed-fueled (Refuse-derived fuel RDF 75.2% and biomass 24.8%) power plant in Halmajug. This is expected to amount to 84,836 t of BIOMIX per year. About 30% of this is stem and straw, 15% is forest and wood by-product, and the remainder is biomass from food processing. The 49.9 MW wood chip-fired block at Pécs utilizes 400,000 tons of woody biomass each year – mostly residues from forestry and sawmills including wood chips and sawdust, but also sunflower shells. However, by the end of November, about a quarter of the fuel used in the woodchip block may be replaced by the so-called "Mecsek mix". This product contains commercially available quality-assured fuel biomass and pre-sorted PVC-free plastics, paper, and textiles from Pécs and its surroundings [28].

Despite the cost-effective 50 km transport distance of wood chips, raw material can also arrive at the larger power plants from even longer distances. This implies neighboring counties, and they can, in fact, become potential raw material suppliers.

3.3.2. Agricultural residues (stalk, stem) utilization

Corn stalks represent the largest quantity of agricultural residues. Currently, the most common way of utilizing corn stalks is to simply plow them into the soil, which is done to approx. 93-94% of the stalks [30]. However, large amounts of lignocellulose should not be returned the soil because it launches a pentosane effect (cellulose effect). Optimal values for straw and stem quantities used for soil improvement vary in the literature, but according to most analyses, 20–40% of stem weight is the best [17, 18, 31]. Large amounts of nitrogen fertilizer are needed to avoid cellulose effects; this would significantly increase costs and environmental hazards. From an ecological perspective, we calculated with a max. 50% useable amount together with technical losses.

The utilization of wheat straw in livestock farming is significant. Straw is fed primarily to ruminants, but only in small quantities. Due to its low usable energy concentration, straw cannot replace hay as feed; thus, straw can only be used effectively in small daily doses as supplementary feed. The utilization of by-products as fodder may be higher in drought years if the amount of harvested crop does not meet national needs. However, the amounts used for bedding are significant. According to the calculations described in the methodology, the required amount of litter has increased by 7% in the last two years and by 13% in the last decade. Straw is also utilized in some power plants. The district heating system of Pécs can supply approximately 60% of the region's heat demand, which means 200,000 tons of straw purchased from the local farmers. The Oroszlány Power Plant is capable of burning 100,000 tons of straw annually [32, 33]. The available potential is lower than 1.5 million tons [8].

Rapeseed stem also represents significant quantities of by-products. It can be easily balled; the technology of harvesting is well-known. Its utilization began to be examined during the biodiesel production boom. When mixed with different materials, rapeseed stem could be a valuable raw material for agripellet production [34]. The usable potential of sunflower stems is also significant, but their harvesting is still problematic; therefore, utilization for energy purposes cannot be achieved by current methods.

For the time being, the corn stalk utilization is relatively low. Pécs utilizes about 10,000 tons and the Mátra Power Plant consumes about 100,000 tons of corn stalks. Mátra also uses straw in smaller quantities. Other agricultural by-products are utilized in Szakoly, Szerencs, and Homrogd. The plant in Dorog uses sunflower stems.

As far as potential users are concerned, the biogas plants are mainly based on animal by-products such as manure, animal carcasses, and meat processing industry by-products. A major agricultural products such as silage corn or sugar sorghum silage usually complements these products. It should be emphasized that the whole plant is chopped during the preparation of silage maize, so we did not consider it as a potential raw material in the previous section (3.1.3.). There are only

three or four biogas plants utilizing some types of plant stalk or straw, but not to a significant extent.

The annual raw material consumption of agripellet plants in Hungary is not yet significant. In Polgárdi, Vertikál Plc. processes a few hundred tons. In Szentes the amount of annually produced pellets is 3,600 tons/year, which includes wheat, corn and rapeseed stalk. In Agárd-Pálmajor, Agripellet Ltd. produces 4,200 tons of pellets per year, of which rapeseed straw and sunflower husk represent a smaller portion. In addition, straw pellets are produced in smaller quantities in some plants (Jászladány, Vép). In the future, it will be possible to produce torrefication pellets from agricultural by-products, but the technology is not yet widespread [34].

In the neighboring countries, larger biomass recovery plants located near the Hungarian border could be a further source of demand. There is a plan to develop an advanced bioethanol production plant based on agricultural by-products with a capacity of 50,000 tons (63 million L/year) in Leopoldov, Slovakia [35]. It will be located at a distance of 110 km from the border, which can only show an uptake market in drought years, because of the larger collection area due to smaller yield. In October, 2014, Beta Renewables and BioChemtex signed an agreement with Energochemica SE to produce commercial lignocellulose based ethanol from 55,000 tons of wheat straw, rapeseed, and maize stalks in Strazske, also in Slovakia [36]. A demand for raw materials could be manifested, since Strazske is less than 50 km from the border.

A biofuel plant with fermentation technology, which is expected to use wheat and other cereal straw to produce 63 million liters of biofuel per year, is planned for construction in southwestern Romania. However, the realization of this plant is not yet certain.

3.4. Gross energy potential of biomass residues per county
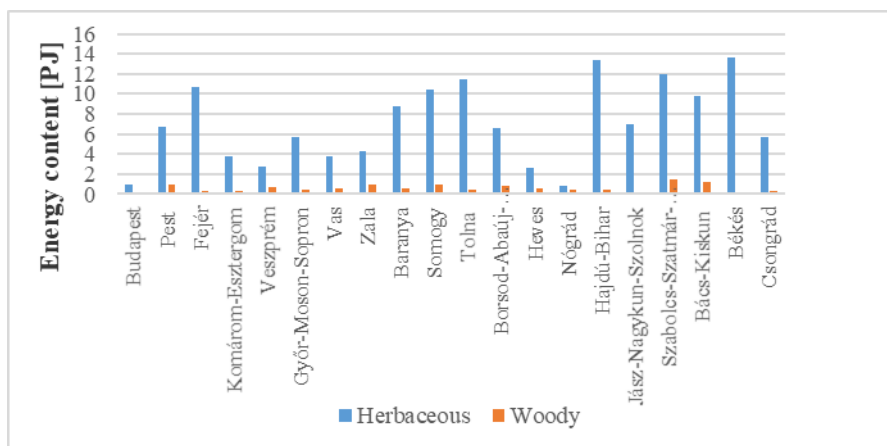
Figure 4
Distribution of energy originated from herbaceous and woody collectable by-products by county [8]

The amount of generated woody and herbaceous by-products were aggregated for each county. *Figure 4* shows the amount of agricultural by-products is dominant and adds up to 92% of the total energy content of potential that can be obtained with its utilization. However, the collection, storage, and utilization of soft-stemmed by-products all are less developed compared to those of woody by-products.

The total energy amount of collectable by-products in Hungary is about 152 PJ.

3.5. Evaluation of raw materials so far not used for energy purposes

Meeting the needs of potential users can be facilitated by planting new woody energy plantations. The 250,000–300,000 hectares of uncultivated land area in Hungary could be well utilized for this purpose. Based on data from the Forestry Directorate of NÉBIH, the creation of energy plantations for energy recovery has been completely absent over the past year. Lack of support and the start of a rival grant F 5 billion tender for the planting of new woody plantations for industrial purposes are the reasons for this. The main priority of support is to promote carbon sequestration in agriculture and forestry. Furthermore, optional additional activities include the establishment of electric fences (4.8 EUR/m) and fences (5.8 EUR/m) if appropriate conditions are met. The smallest eligible area is 0.5 hectares. The requirement for disbursement of support is the sale of more than 50% of the generated dendromass for wood industrial purposes within 20 years; the establishment of woody and short rotation plantations for energy production purposes are ineligible activities.

However, woody industrial plantations also generate large amounts of residues (10%) and bark (15–17%) that can be used for energy purposes. The production of industrial wood is about 70%. According to [39], the average increment of the total wood yield is 27 m^3/ha/year at age 12. Calculating the data reveals that up to 5 t/ha of usable biomass per year can be generated. Approximately 1.0–1.5 t/ha/year of biomass can be used for energy recovery if bark residues are excluded from the calculations. However, if we use 49% of biomass for energy purposes, an additional 5 tons of absolute dry matter becomes available. Besides, we can calculate in the material from pruning, which is generated during the formation of the 6–8 m high branch-clear trunk in the first three years of the plantation.

Agroforestry is an intermediate solution. This can be a highly advanced production method today and is becoming a viable option for land use as it offers many ecological and environmental benefits [40]. Agroforestry is a type of climate-smart agriculture practice of deliberately integrating woody vegetation (trees or shrubs) with crop and/or animal systems. Through intercropping, the carbon sequestration in trees compared to herbaceous plants occurs in the deeper layers of the soil, due to their deeper root system. Therefore, these cultivation systems are a good tool for increasing carbon sequestration in the agricultural field. In addition, intercropping technology helps to prevent the growing fire risk of dendromass production, especially in southern European countries [41].

Several EU projects are working on extending the amount of raw materials via the agroforestry method. The aim of the AgroCop project is to maximize the production of both high quality timber and wood for energy use by combining the available advantages of agroforestry systems (AFS) and short rotation coppice (SRC) [45]. The AGFORWARD project (2014–2017) aimed to promote agroforestry practices in Europe that will advance sustainable rural development with the active participation of Hungarian partners [46]. The AFINET project is an ongoing project with Hungarian participants (University of Sopron Cooperative Research Centre Non-profit Ltd.) [47].

Another possible raw material is waste wood, which has not been utilized yet due to the problem of surface treatment (except of untreated waste wood for pellet and briquett production). At the same time, research studies from abroad claim the chemicals used for surface treatment can be degraded, thereby enabling use of the material for energy purposes to have low environmental risk [42, 43, 44]. We calculate 0.5–0.7 million m^3/year of wood material from this area in the longer term [38].

4. DISCUSSION

The choice of biofuel feedstock has undergone a strong transformation in the last decade. The range of raw materials that are less dangerous to the food supply but at the same time sustainable has expanded. The advantage is that several types of raw materials can be introduced into the system at the same time with proper construction.

However, based on the described results, it will become increasingly difficult to plan the raw material supply for both food crop-based and lignocellulosic biofuel plants in the future. The increased frequency of extreme weather events, especially droughts during the growing season, will increase the uncertainty of a sustainable raw material supply. The consequence of the crop loss for biofuel production was also manifested in the drought period of the year of 2007. Many of the planned bioethanol plants at that time did not materialize. Although the climate in Hungary is more favorable for corn production than it is in most countries in Western Europe, Hungary's yield is still below the average of many other EU countries. This is accompanied by the above-mentioned yield fluctuations. For example, in 2003 and 2007 less than 35–40% of corn was produced in Hungary compared to the national average of in that decade. The same value was at most 18% in Austria and Germany [26]. The yield loss could be decreased in Hungary by using appropriate agricultural technology. Furthermore, as a result of climate change, we can expect a rise in temperature in Hungary, which may lead to a narrowing of the growing area of rapeseed, which is a raw material for biodiesel production that prefers cooler, wetter areas.

Increased use of forest and agricultural residues is necessary on the one hand to avoid food conflicts and on the other hand to comply with legal requirements. Forestry labor shortages make it increasingly difficult to harvest the forest residues. Mechanization development would help alleviate this, but it would entail higher

costs. Beyond forestry residues timber harvested by forced cutting is likely to be used for energy purposes. The pyrolytic utilization of this material is aided by the fact that the damaged wood can be harvested with relatively low moisture contents; thus, instead of drying the wood, the energy can be used to produce heat and electricity, which improves the economy of the industry.

Agricultural by-products demonstrate high potential, but their low bulk density makes transportation costly over long distances. In addition, the conversion rate of agricultural by-products is also low. Extreme weather effects must be taken into account when planning biofuel plants; these effects can increase the collection area of agroresidues by up to 70% [37]. Meeting ecological needs (soil improvement) doubles the base material footprint. Furthermore, agricultural by-products are also used in animal husbandry. Harvesting and storing corn stalks with high moisture content is still cumbersome. Nevertheless, according to the raw material footprint – which is suitable for given the collection area – forest residues require higher raw material collection for biofuel production with the same energy content. Moreover, the risk of Indirect Land Use Change (ILUC) can be reduced with the use of agricultural residues. Short rotation coppices (SRC) requires the smallest collection area [37].

Overall, a large amount of useable residues is available for the supply of raw material to potential lignocellulosic biofuel plants in Hungary. However, it must be considered that for all forestry and agricultural lignocellulosic feedstocks, more frequent plant protection activities should be conducted to mitigate effects of climate change threats. These activities will increase CO_2 emissions as well as costs through the use of machinery and the production of pesticides.

5. SUMMARY

The course of the survey in 2018 revealed that many agricultural by-products, especially corn stalk, are available for energy production purposes. However, the harvesting and utilization of these by-products for biofuel production have not been fully developed.

Climate change, together with the current operating and potential users, significantly influences the locally usable amount of biomass. Hereby, the raw material supply of a scheduled plant can be accomplished with longer transport distances. Commercially operated decentralized technology primarily enables the utilization of dendromass. Although harvesting of forest residues is still problematic, forestry development in this direction is underway. Occasional biotic and abiotic damage events in forests increase the amount of dendromass that can be used for energy purposes.

the framework of the Széchenyi 2020 Program. The realization of this project is supported by the European Union, co-financed by the European Social Fund.

REFERENCES

[1]   Biodiesel Magazine (2020). *Biofuels require little arable land but provide many benefits*. http://biodieselmagazine.com/articles/2516887/biofuels-require -little-arable-land-but-provide-many-benefits

[2]   Spiertz, J. H. J., Ewert, F. (2009). Crop production and resource use to meet the growing demand for food, feed and fuel: opportunities and constraints. *NJAS – Wageningen Journal of Life Sciences*, 56 (4), pp. 281–300.

[3]   Neményi M. (2009). *Megújuló energiaforrások kutatási-fejlesztési tevékenysége a karon*. (Research and development activities on the field of renewable energy sources in the faculty.) http://www.mtk.nyme.hu/fileadmin/user _upload/szti/biomotion/biofuels_in_hungary.pdf

[4]   Szalay D., Papp V., Marosvölgyi B. (2018). Lignocellulóz biohajtóanyag üzemek alapanyag-felhasználásának jelenlegi helyzete. In: Kiss T., Dolgosné Kovács A., Vér Cs., Máthé P.: Sustainable Resource Management. *I. RING – Conference*. Pécs, Magyarország, pp. 168–175. (Current situation of raw material use in lignocellulosic biofuel plants.)

[5]   Hungarian Central Statistical Office (KSH): *013-as erdőgazdálkodás jellemzői statisztikai tükör (Statistical Mirror in 2013 Features of Forest Management)*. https://www.ksh.hu/docs/hun/xftp/stattukor/regiok/orsz/erdogazd12.pdf

[6]   Szakálosné M. K., Horváth B., Major T., Horváth A. (2013). *Magyarországi erdők energetikai célokra hasznosítható faanyaga*. Alföldi Erdőkért Egyesület Kutatói Nap: Tudományos eredmények a gyakorlatban. Lakitelek (Woody biomass sources of hungarien forestries for energy purposes. Researchers' Day of the Association for the Great Plain Forests: Scientific results in practice).

[7]   Hungarian Central Statistical Office (KSH): *2017 Land by Field Cultivation Table* (2017-es évre vonatkozó Földterület művelési ágak szerint megnevezésű tábla). https://www.ksh.hu/docs/hun/xstadat/xstadat_eves/i_omf003.html

[8]   Szalay D. (2018). *Energetikai célú dendromassza termesztés és hasznosítás lehetséges szerepe a lignocellulóz biohajtóanyag üzemem alapanyag ellátásában*. Doktori értekezés. Soproni Egyetem. Sopron. (Production and Utilization of Dendromass for Energy Purposes and Possible Role in the Base Material Supply of Lignocellulose Biofuel Plant. PHD Thesis. University of Sopron.)

[9]   Boris, C., Zoran, S., Novic, D. (2011). Geographic distribution of economic potential of agricultural and forest biomass residual for energy use: Case

study Croatia. Energy 2011 https://www.researchgate.net/publication/22300 6293_Geographic_distribution_of_economic_potential_of_agricultural_and_ forest_biomass_residual_for_energy_use_Case_study_Croatia 2015. 10. 11.

[10] Sembery P., Tóth, L. (2004). *Hagyományos és megújuló energiák*. Szaktudás Kiadó Ház, Budapest (Conventional and renewable energies. Szaktudás Publishing House).

[11] Fogarassy Cs. (2001). *Energianövények a szántóföldön*. SZIE GTK Európai Tanulmányok Központja, Gödöllő. ISBN 963 9256 47 1 (Energy crops on the arable land. Center for European studies of SZIE GTK).

[12] Radics L. (ed.) (1994). *Szántóföldi növénytermesztéstan*. Egyetemi jegyzet, Budapest (Crop production on plow land. University note).

[13] Barótfi I. (ed.) (2003). *Környezettechnika*. Mezőgazda Kiadó, Budapest, ISBN: 978 963 9239500 (Environmental technology. Mezőgazda Publiusher).

[14] Papp V., Marosvölgyi B. (2010). A pelletálás energiamérlegének vizsgálata. Tudományos eredmények a gyakorlatban. Szolnok, pp. 101–105. (Investigation of the energy balance of pelletization." Scientific results in practice.)

[15] Papp, V., Beszédes, S., Szalay, D. (2019). Opportunities and challenges of agripellet production in Hungary. *Agriculture and Food*, Vol. 7, pp. 197–204.

[16] Papp V., Szalay D., Gaál L. (2016). Agripellet előállítás alapanyagbázis vizsgálata Magyarországon. *Journal of Central European Green Innovation*, 4, 2, pp. 89–102.

[17] EBTP (2013). European Biomass Technology Platform-Agricultural residues as feedstocks for biofuels production. http://biofuelstp.eu/agri-residues.html.

[18] Kline, R. (2014). *Estimating crop residue cover for soil erosion control*. Soil factsheet. Ministry of Agriculture. British Columbia, pp. 1–4.

[19] Hungarian Central Statistical Office (KSH). KSH OSAP 1254 sz. adatgyűjtése. *Beszámoló az erdősítésekről és a fakitermelésekről a 2016. évben.* (KSH OSAP 1254 data collection report on national reforestation and harvested gross timber volume in 2016), https://portal.nebih.gov.hu/documents/10182/206281/M%C3%A9rleg-2016.pdf/a723b1fd-c5b2-497c-8049-4 f149fb99bd0.

[20] Maga J. (2012). *A szalma energetikai hasznosításának lehetőségei Szlovákiában. Innovációval a zöld jövőért*. Konferenciakiadvány (Opportunities for energy utilization of straw in Slovakia. Innovation for a green future. Conference proceedings).

[21] Szalay, D., Jákói, Z., Papp, V. (2019). Possible Role of Agricultural Woody By-products in Lignocellulose Biofuel Production In Hungary. *Journal of*

International Scientific Publications: Agriculture & Food Journal, Vol. 7, pp. 211–220.

[22]   Miszkuly S. (2019). Szóbeli tájékoztatás (personal communication).

[23]   Papp, V., Babiczki, L., Grédics, Sz., Szalay, D. (2019). Timber Harvest Due to Biotic and Abiotic Damage by the Example of Egererdő Plc. In: Czupy, I. Exceeding the Vision: Forest Mechanisation of the Future. *Proceedings of the 52nd International Symposium on Forestry Mechanization*. Sopron, Hungary e-book. pp. 495–502.

[24]   Bai A., Tarsoly P. (2011). *A hazai melléktermék-hasznosítás. Agrárium*. Debreceni Egyetem (Utilisation of by-product in Hungary. University of Debrecen).

[25]   Szalay D. (2009). *Biomassza alapú cseppfolyós üzemanyag előállításának lehetőségei, különös tekintettel a második generációs bioüzemanyagokra.* MSC-diplomadolgozat, Nyugat-magyarországi Egyetem, Sopron (Possibilities for the production of biomass-based liquid fuels, especially second-generation biofuels. MSc Thesis, University of West Hungary).

[26]   Szalay D., Palocz-Andresen M. (2013). A biomassza termesztés és feldolgozás függősége a klímaváltozástól. Alföldi Erdőkért Egyesület, Kutatói nap kiadványa, Lakitelek, pp. 89–93. (Dependence of biomass cultivation and processing on climate change. Association for the Great Plain Forests, Researcher's Day Publication).

[27]   Liebhard P. (2008). *Energetikai faültetvények. Rövid vágásfordulójú faanyagtermelés. A jövő nyersanyaga*. Cser Kiadó, Budapest (Energy tree plantations. Short - cut timber production. The raw material of the future. Cser Publisher).

[28]   Veolia (2019). *Újabb lépés a körforgásos gazdaságért: speciális tüzelőanyag-mix a pécsi erőműben* (Another step for the circular economy: a special fuel mix at the Pécs power plant). https://www.veolia.hu/hu/hirek/ujabb-lepes-korforgasos-gazdasagert-specialis-tuzeloanyag-mix-pecsi-eromuben

[29]   DERULA (2019). *Cégünkről* (About our Company). http://www.derula.hu/hu/s/3195/cegunkrol

[30]   Haszon Agrár (2010). Mit kezdjünk a kukoricaszárral? (What to do with the corn stalk?) http://www.haszon.hu/agrar/noevenytermesztes/533-mit-kezdjuenk-a-kukoricaszaral.html

[31]   Mann, L., Tolbert, V., Cushman, J. (2002). *Potential environmental effects of corn (Zea mays L) stover removal with emphasis on soil organic matter and erosion*. Agriculture, Ecosystems & Environment.

[32] Energiainfo: *3,5 milliárdért venne szalmát a pécsi biomassza erőmű* (The Pécs biomass power plant would buy straw for 3.5 billion). http://www.en ergiainfo.hu/35-milliardert-venne-szalmat-pecsi-biomassza-eromu/.

[33] Vértesi Erőmű Zrt.: *Általános információk* (General Information). http://www.vert.hu/altinf.aspx.

[34] Papp V. (2018). Energetikai pelletek előállításának és hasznosításának öko-energetikai vonatkozásai. PhD-disszertáció, Soproni Egyetem, Sopron. (Eco-Energy Aspects of Production and Utilization of Energetic Pellets.) PhD thesis, University of Sopron.

[35] Biofuel News: Advanced biofuels plant to be built in Slovakia https://biofu els-news.com/display_news/12889/advanced_biofuels_plant_to_be_built_in _slovakia/

[36] Chemicalparks (2014). Green chemistry investment by Energochemica SE group for Ethanol at Strážske Chemko in Slovakia. https://chemicalparks. eu/investment-projects/500

[37] Szalay, D., Papp, V., Czupy, I. (2018). Analysis of the Base Material Footprint of Conventional and Lignocellulosic Biofuel Production. *IOP Conference Series: Earth and Environmental Science*, 159 (1), p. 8.

[38] Molnár S., Pásztory Z., Komán Sz. (2013). A faenergetika minőségi fejlesztésének szakmai megalapozása (mire elég a magyar dendromassza?!) FATÁJ online. (Professional foundation for the quality development of wood energy (what is the Hungarian dendromass enough for?!) www.fa taj.hu.

[39] Nagy I. (2016). Csodavárás helyett egy lehetséges megoldás – jövőnk az iparifa-ültetvény! (Part 1). *Erdő-mező online*. (Instead of waiting for a miracle, one possible solution – our future is the industrial tree plantation!) http://erdo-mezo.hu/2016/02/07/csodavaras-helyett-egy-lehetseges-megoldas -jovonk-az-iparifa-ultetveny-1-resz/.

[40] Jose, S. (ed.) (2010). *Agroforestry for Ecosystem Services and Environmental Benefits*. Springer Kiadó, http://www.tankonyvtar.hu/hu/tartalom/tamop 425/0027_BTRI13/ch01s02.html.

[41] Kumar, B. M., Nair, P. K. R. (eds.): *Carbon Sequestration Potential of Agroforestry System*. Springer Netherlands, Amsterdam.

[42] Clausen, C. A., Smith, R. L. (1998). CCA removal from treated wood by chemical, mechanical, and microbial processing. *Proceedings of the 4th International Wood Preservation Symposium*, The Challenge-Safety and Environment. https://www.fpl.fs.fed.us/documnts/pdf1998/claus98b.pdf.

[43]   Clausen, C. (2004). Improving the two-step remediation process for CCA-treated wood. Part I. Evaluating oxalic acid extraction. *Waste Management*, 24 (4), pp. 401–40.

[44]   Sierra-Alvarez, R. (2009). Removal of copper, chromium and arsenic from preservative-treated wood by chemical extraction-fungal bioleaching. Waste *Manag.*, 29 (6), pp. 1885–1891.

[45]   AGROCROP. Project proposal webpage, https://sites.google.com/site/agro benkcrop/services.

[46]   AGFORWARD. Project webpage, https://www.agforward.eu/index.php/en/ home-redirect.html.

[47]   AFINET. Project webpage, https://euraf.isa.utl.pt/afinet

THE UTILIZATION OF TREE BARK AS THERMAL INSULATION PANELS AND FORMALDEHYDE ABSORBER

Z. PÁSZTORY – A. NOVOTNI

Innovation Center, Simonyi Karoly Faculty of Engineering
Wood Sciences and Applied Arts
University of Sopron

Abstract: Recently the mitigation of global warming and the circular economy have been emphasized for providing sustainable development in the developed world. The reduction of global warming first requires the use of all the renewable materials produced by nature and secondly the recycling of all the materials after production and use. Tree bark is a byproduct of forestry and its utilization has been only marginal. However, bark has many advantageous properties. In a project to utilize waste, bark was investigated and viable utilization methods were worked out. Tree bark can be a perfect raw material for production of thermal insulation panels. The results show that 0.06 W/mK insulation value can be achieved, which is very close to commercial available materials, but the economic balance is much better. The improvement of its properties can be done by different treatments which make it more resistant to water uptake and thickness swelling. Bark has high porosity and the dry material has a quite large inner surface with active molecules which can absorb significant amounts of volatile organic molecules such as formaldehyde. The investigation shows that poplar bark can absorb about 0.9 mg formaldehyde (HCHO)/g bark. This property provides another utilization area for bark products. This article summarizes some of the possibilities and research results related to tree bark.

Keywords: *tree bark, thermal insulation, thermal treatment, formaldehyde absorption*

1. INTRODUCTION

One of the main purposes of forestry is the cultivation of wood, which produces large quantities of renewable raw materials each year. The worldwide annual production of round wood is estimated at 3,591 million m^3 [1]. On average, 10% of produced round wood is bark. Even in the middle of the twentieth century, the disposal of huge amounts of bark, which in most cases had been dumped in landfills, was a major problem [2]. The amount of bark removed from the timber harvested in Hungarian forests is 500–600,000 cubic meters annually [3].

Bark can take many forms, depending on the species, its age and other ecological factors, and may be different in different parts of a tree [4–6]. The proportion of bark to the tree body can be 5–28% [3, 7].

There has been a growing focus on the industrial use of bark in recent decades, for better utilization of renewable materials and to avoid the waste of biological

products such as cellulose and lignin besides other organic substances. Bark could be an outstandingly important raw material because of its special chemical components and unique structure.

Recently, the most frequently used insulation materials are artificial materials made of non-renewable materials such as polystyrene, fiberglass, or glass wool. A low but increasing ratio of renewables-based materials can be found on the market, most of which use cellulose and other plant fibers for manufacturing insulation materials that are environment friendly and renewable. This article summarizes the research results on the production of bark-based insulating panels.

2. USE OF BARK AS THERMAL INSULATION BOARD

The use of bark as thermal insulation board is still in its early stages. However, laboratory results are outstanding in terms of thermal conductivity values and also for embodied energy and recyclability. It is uncertain how the difficulties in lumbering quality differences can be handled.

Some trees have a quite high resin and wax content, which is beneficial because no glue is required when gluing boards together; it is enough to press them at high temperatures. Thermal insulation boards are made with wood chips and bark, where the bark content is usually 25% [8]. Kain et al. [9] made insulation boards out of *Pinus sylvestris* cortex, creating comparatively light bark boards for thermal insulation. The heat storage capacity was better than commonly known insulation materials.

Kain et al. [10] used spruce bark pieces as pressed panel from thermal insulation while making insulation for a log wall on which winter temperatures were modeled, and the temperature profile was simulated. Bark conducted heat more slowly than other materials used for blowing, so it can be used as insulation material. Kain et al. [11] made insulating boards using separated bark from *Pinus sylvestris*, *Picea abies*, and *Abies alba*. They found that the heat and sound insulating properties were very good, and the mechanical properties met the requirements of the standards. Furthermore, its formaldehyde emission was minimal. The bark of *Larix decidua* is suitable for thermal insulation boards, which have relatively small coefficients of thermal conductivity (0.065–0.09 W/mK) [12]. Moreover, the boards could be glued with tannin resin, free from formaldehyde and artificial resins, so they are more environmentally friendly.

Cryptomeria japonica is widely used in the construction industry in Japan, where its bark (which is rich in fiber and long lasting) is separated. Experiments were made on its thermal insulation properties in which it was coarsely and finely chopped, and boards were made with expanded polystyrene foam. The coarse and fine chopping did not make a difference, as the coefficients of thermal conductivity were 0.073 and 0.076 W/mK, respectively, in contrast with the 0.045 W/mK of the Styrofoam board [13].

In the following chapters, we will present three type of insulating panels made of bark.

2.1. Insulation panels and thermally modified bark

The thermal modification of wood is a well-known method of treatment. With heat treatment, dimensional stability and resistance against wood degrading organisms improves, while some strength properties decline [14]. Several variables affect the results achieved during heat treatment, including tree species, chamber design, treatment duration and temperature, an oxidative or neutral atmosphere or a mix, etc. [15], [16], [17], [18].

Boards are heat treated mainly to reduce water uptake and thickness swelling. Lehmann [19] treated chips at 204 °C for 15, 30, and 45 minutes and found that particleboard dimensional stability increased slightly, but strength properties decreased. Tomek [20] studied the heat treatment (1–8 minutes; 230°–300 °C) of oak chips. The water absorption (WA) and thickness swelling (TS) of the particleboard made from the treated material was reduced; the modulus of rupture (MOR) increased. Lee et al. [21] investigated the physical-mechanical properties of particleboard made from heat-treated rubber wood (*Hevea brasiliensis* (Willd. ex A. Juss.) Müll.Arg.). Four different temperatures (50, 100, 150 or 200 °C) and three different durations (one, two, or three hours) were investigated in dry and wet conditions. The heat treatment of the particles improved the dimensional stability, but mechanical properties decreased with the duration of the heat treatment. Ohlmeyer & Lukowsky [22] investigated single-layer pine particleboard. The particles were treated at 240 °C. The modification decreased the equilibrium moisture content (EMC), the WA, and the TS. The internal bond (IB), the modulus of elasticity (MOE), and the MOR of the particleboard decreased as well. Mendes et al. [23] compared the effect of thermal pre-treatment of strand-type particles on the physical-mechanical properties of Oriented Strand Board (OSB) panels produced from *Pinus taeda* L. The particles were treated at 200 °C and 240 °C. Thermal treatment of particles at 200 °C negatively affected the physical and mechanical properties of the control panels, while thermal treatment at 240 °C significantly improved the physical properties and weakened the mechanical properties. Paul et al. [24] examined the physical and mechanical properties of OSBs made from Scots pine (*Pinus sylvestris* L.) chips treated at 220 °C and 240 °C for 30 minutes, which resulted in decreased thickness swelling and increased dimensional stability. The pre-treatment left the internal bond strength unaffected and greatly reduced its bending properties (MOE, MOR). Boonstra et al. [25] investigated a two-stage steam pre-treatment (with temperatures below 200 °C) of particleboard made of Norway spruce (*Picea abies* (L.) H. Karst.) and Scots pine (*Pinus sylvestris* L.) chips. The WA and TS decreased, as did the IB. Kwon & Ayrilmis [26] investigated the physical and mechanical properties of flakeboard made of heat-treated flakes (at 150, 170 and 190 °C; 2 hours). The TS, WA, MOR, MOE decreased as temperature increased, while IB strength increased.

Sometimes thermal post-treatment was used, but steam injection and post-treatment only work with isocyanate, phenol-melamine-urea-formaldehyde (PMUF), melamine-urea-formaldehyde (MUF), and phenol-formaldehyde adhesives [25]. The

swelling of the heat-treated particleboard decreased in tests by Ernst [27]. Suchsland & Enlow [28] reduced the swelling with one to two hours of heat treatment at 218 °C, and the mechanical properties of phenolic bonded particleboard were not adversely affected. Menezzi & Tomaselli [29] examined the effect of thermal post-treatment on OSB dimensional stability. The thermal treatment was effective and reduced the TS, EMC, but did not affect WA. The longer the treatment, the better the dimensional stability became. Oliveira et al. [30] evaluated the effect of post-heat treatment on the physical and mechanical properties of MDF panels. The dimensional stability of the MDF increased, but all the thermally treated panels revealed a significant decrease in their MOR and MOE. Ayrilmis et al. [31] also examined the thermal post-treatment of MDF. The heat treatment improved the TS, but WA and linear expansion properties were adversely affected. The MOR and MOE values decreased with increasing temperature. Another study by H'ng et al. [32] investigated post-heat treated particleboard made of rubber wood (*Hevea brasiliensis* (Willd. ex A.Juss.) Müll.Arg.) in a laboratory press at 100, 150, and 180 °C for 90, 180, and 270 seconds. The thermal treatment reduced the TS, but the WA was not affected.

Thermal conductivity also decreases with thermal treatment [33, 34, 35]. Sekino & Yamaguchi [36] reduced the thermal conductivity of their insulation panels made of wood shavings by carbonizing the wood material. Similar processes can occur during heat treatment, as the structure and the composition of the wood and bark are similar, but not the same.

According to Pásztory et al. [37], the thermal conductivity (0.067 W/mK) of poplar bark panels lies in the middle of the heat conducting range of other wood-based panels (0.05–0.08 W/mK). The thermal conductivity of these insulation panels made of bark can be reduced by heat treatment. By treating the particles with one hour of heat before the panels are manufactured, the thermal conductivity of a panel – at the same density – decreased to 0.064 W/mK. In fact, after three hours of treatment, the thermal conductivity of a panel with a density of about 5% is the same as that of the control panel (0.067 W/mK). That is, by heat treating the particles prior to panel production, the thermal insulation properties of the panels can be improved. A big problem with natural thermal insulation materials is that their moisture content changes in parallel with atmospheric humidity, which strongly influences heat conduction. Pre-manufacturing heat treatment of the raw material bark changes its chemical structure, thus decreasing the water absorption and swelling of the manufactured panels [34].

2.2. Density optimization

There are several factors influencing the thermal conductivity values of wood-based materials, of which temperature, moisture, and density are the most crucial parameters. Researchers generally agree that thermal conductivity increases proportionally as a function of temperature, moisture content and density [38]. It is reported in [39] that the thermal conductivity values of wood and wood-based materials increases linearly with rising density in the range of 200 to 800 kg/m^3. Thus, in the building

supply market, low density fiberboards or softboards are usually commercially available as thermal insulation materials. According to the EN 316 standard, low-density fiberboards are porous panels having a density between 230 and 400 kg/m^3 [40].

In addition, it is known that density has a significant positive influence on the mechanical performance of wood-based panels, since it is acknowledged that the higher the density the stronger the mechanical properties are [12]. Even though mechanical behavior is not a priority for insulation, and panels with lower mechanical properties can be used as insulating materials in buildings [41], wood panels should withstand a minimum performance during their handling, installation and maintenance as thermal insulation panels.

In an experiment of Pásztory et al. [42], bark particleboards were formatted according to a defined initial weight and target densities, at 20 mm thickness. However, possibly due to inhomogeneities of bark particles during the manual process or their compression during the hot press, the boards with a target density of 350 kg/m^3 had a mean density value of 387.57 kg/m^3, 10.73% higher than expected. As expected, the thermal conductivity values as well as the static bending properties and internal bonding of the experimental panels were significantly increased by raising the density of bark from 250 kg/m^3 to 350 kg/m^3. The panels with mean thermal conductivity values of 250, 300 and 350 kg/m^3 were calculated to be 0.059 W/mK, 0.063 W/mK and 0.079 W/mK, respectively. In the literature the thermal conductivity values were within the range of 0.06 W/mK up to 0.10W/mK, when comparing them to the thermal conductivity of other insulation panels made from wood or agricultural residues (bio-resources).

2.3. Formaldehyde adsorption

An indoor air-pollution problem of volatile organic compounds (VOC) like formaldehyde (HCHO) has arisen, with over 500 VOC having been detected [43, 44]. Carbon nitride nanotubes have been studied to adsorb formaldehyde with activated carbon and various inorganic porous materials, [45], [46], [47]. Extracts of bark are examined in the literature [48, 49, 50, 51], although there are only a few research studies focusing on the HCHO adsorption of bark itself [52], [53]. However, it was shown that using bark even as a bio-indicator can be advantageous, since it can adsorb gases from the air [54, 55, 56]. Numerous tree species such as oaks (*Quercus* sp.), elm (*Ulmus* sp.), willow (*Salix* sp.), poplar (*Populus* sp.), ash (*Fraxinus* sp.), maple (*Acer* sp.), lime (*Tilia* sp.), pine (*Pinus* sp.), yew (*Taxus baccata* L.), black locust (*Robinia pseudoacacia* L.), olive tree (*Olea europea* L.), cedar (*Cedrus atlantica* Endl.), cypress (*Cupressus sempervirens* L.), and eucalyptus (*Eucalyptus* sp.), among others, have been used to detect contaminants adsorbed from the air [57]. Among them, poplar bark is also useful for detecting pollutants through adsorption [58]. Due to its unique structure, its porous nature and the high extract content, bark can be a promising adsorbent material. Suberin and condensed tannins are important constituents of tree bark, but there are several other types of substrate materials in bark (in different proportions), such as waxes, terpenes, flavonoids, and alkaloids

[59, 60, 61, 62, 63]. Tannin in bark, having different types of flavan-3-ol units [64][65], can react with formaldehyde vapor [66, 67].

According to our measurements Pannónia (*Populus Euramenricana*) poplar bark can adsorb 0.9 mg/g of formaldehyde. Formaldehyde emissions of an uncontaminated bark sample were also investigated by Pásztory et al. [68], and 0.0036 mg/g was measured, which is significantly lower than that of the adsorbed amount of formaldehyde. Consequently, poplar bark can be used as a formaldehyde absorber when built into materials such as boards glued together by formaldehyde adhesives.

3. CONCLUSIONS

Tree bark is produced in high amounts worldwide by forestry and this by-product has not been widely used. This literature review investigated some tree bark species for different uses and showed a good potential for using them. Some of the possible treatments and applications are listed below.

- Thermal insulation panels were produced with different density and different treatments, and the results show the potential for a successful bio-product that can be competitive on the market.
- By means of different treatment the properties of bark particles and panels can be improved, according the optimized parameters of the product. By thermal treatment at 200 °C or higher the thermal conductivity of the panel will decrease and also other physical parameters will become more advantageous.
- A special utilization possibility for tree bark is usage as an absorbent. The investigated poplar bark was able to absorb significant amount of formaldehyde from the atmosphere and thus cleaned the air.

These utilizations are only possible examples and further investigation is needed for exploring wider utilizations of this versatile material produced by nature.

REFERENCES

[1] FAO (2017). *FAO Yearbook: Forest Products 2009–2013*. Rome.

[2] Weißmann, G. (1976). Reinigung Ölhaltiger Abwässer mit Rinde. *Holz Zentralblatt*, 50, pp. 661–662.

[3] Molnár S. (2004). *Faanyagismeret.* Budapest, Mezőgazdasági Szaktudás Kiadó.

[4]   Fekete Z. (1951). *Erdőbecsléstan: a faállományszerkezettan és a faterméstan vázlatával*. Budapest, Akadémiai Kiadó.

[5]   Gencsi, L. (1980). *Erdészeti növénytan*. Budapest, Mezőgazdasági Kiadó.

[6]   Butterfield, B. G., Meylan, B. A., Ilona, P. (1997). *A fatest háromdimenziós szerkezete = Three-dimensional structure of wood*. Budapest, Faipari Tudományos Alapítvány.

[7]   Guidi, W., Piccioni, E., Ginanni, M., Bonari, E. (2008). Bark content estimation in poplar (Populus deltoides L.) short-rotation coppice in Central Italy. *Biomass and Bioenergy*, 32 (6), pp. 518–524. DOI: 10.1016/j.biombioe. 2007.11.012

[8]   Harkin, J. M., Rowe, J. W. (1971). *Bark and its Possible Uses*. Madison, Forest Products Laboratory, U.S. Forest Service.

[9]   Kain, G., Barbu, M.-C., Teischinger, A., Musso, M., Petutschnigg, A. (2012). Substantial Bark Use as Insulation Material. *Forest Products Journal*, 62 (6), pp. 480–487. DOI: 10.13073/fpj-d-12-00052.1

[10] Kain, G., Barbu, M. C., Hinterreiter, S., Richter, K., Petutschnigg, A. (2013a). Using Bark as a Heat Insulation Material. *BioResources*, 8 (3). DOI: 10.15376 /biores.8.3.3718-3731

[11] Kain, G., Heinzmann, B., Barbu, M-C. (2013b). Softwood bark for modern composites. *Pro Ligno*, 9, pp. 460–468.

[12] Kain, G., Güttler, V., Barbu, M.-C., Petutschnigg, A., Richter, K., Tondi, G. (2014). Density related properties of bark insulation boards bonded with tannin hexamine resin. *European Journal of Wood and Wood Products*, 72 (4), pp. 417–424. DOI: 10.1007/s00107-014-0798-4

[13] Sato, Y., Konishi, T., Takahashi, A. (2004). Development of Insulation Material Using Natural Tree Bark. *Transactions of the Materials Research Society of* Japan, No. 5, 29 (5), pp. 1937–1940.

[14] Rowell, R. M., Youngs, R. L. (1981). *Dimensional Stabilization of Wood In Use*. DOI: 10.2737/fpl-rn-243, https://www.fs.usda.gov/treesearch/pubs/5888.

[15] Rapp, A. O. (2001). Review on heat treatments of wood COST Action E22; proceedings of the special seminar held in Antibes, France, on 9 February 2001. In *Review on heat treatments of wood COST Action E22; proceedings of the special seminar held in Antibes, France, on 9 February 2001*. Luxembourg: Off. for Off. Publ. of the Europ. Communities.

[16] Tjeerdsma, B. F., Militz, H. (2005). Chemical changes in hydrothermal treated wood: FTIR analysis of combined hydrothermal and dry heat-treated wood. *Holz Als Roh- Und Werkstoff*, 63 (2), pp. 102–111. DOI: 10.1007/ s00107-004-0532-8.

[17] Esteves, B. M., Pereira, H. M. (2009). Wood modification by heat treatment: A review. *BioResources*, 4 (1), pp. 370–404.

[18] Navi, P., Sandberg, D. (2012). *Thermo-hydro-mechanical Processing of Wood*. Lausanne, Switzerland, EPFL Press.

[19] Lehmann, W. F. (1964). *Retarding dimensional changes of particle boards*. Corvallis: Oregon State University, Forest Research Laboratory.

[20] Tomek, A. (1966). Die Heißvergütung von Holzspänen, ein neues Verfahren zum Hydrophobieren von Spanplatten. *Holztechnologie*, 7, pp. 157–160.

[21] Lee, S. H., Ashaari, Z., Jamaludin, F. R., Yee, C. N., Ahamad, W. N. (2016). Physico-mechanical properties of particleboard made from heat-treated rubberwood particles. *European Journal of Wood and Wood Products*, 75 (4), pp. 655–658. DOI: 10.1007/s00107-016-1145-8

[22] Ohlmeyer, M., Lukowsky, D. (2004). Wood-Based Panels Produced from Thermal-Treated Material: Properties and Perspectives. In: *Wood-Frame Housing Durability and Disaster Issues Conference*, pp. 127–132.

[23] Mendes, R. F., Júnior, G. B., Almeida, N. F. D., Surdi, P. G., Barbeiro, I. N. (2013). Effects of thermal pre-treatment and variables of production on properties of OSB panels of Pinus taeda. *Maderas. Ciencia y Tecnología*, pp. 141–152. DOI: 10.4067/s0718-221x2013005000012

[24] Paul, W., Ohlmeyer, M., Leithoff, H., Boonstra, M., Pizzi, A. (2005). Optimising the properties of OSB by a one-step heat pre-treatment process. *Holz Als Roh- Und Werkstoff*, 64 (3), pp. 227–234. DOI: 10.1007/s00107-005-0073-9.

[25] Boonstra, M. J., Pizzi, A., Ohlmeyer, M., Paul, W. (2006). The effects of a two stage heat treatment process on the properties of particleboard. *Holz Als Roh- Und Werkstoff*, 64 (2), pp. 157–164. DOI: 10.1007/s00107-005-0055-y.

[26] Kwon, J. H., Ayrilmis, N. (2015). Effect of heat-treatment of flakes on physical and mechanical properties of flakeboard. *European Journal of Wood and Wood Products*, 74 (1), pp. 135–136. DOI: 10.1007/s00107-015-0961-6.

[27] Ernst, K. (1967). Möglichkeit zur Verminderung der Quellung bei Spanplatten. *Holztechnologie*, 8, pp. 41–47.

[28] Suchsland, O., Enlow, R. C. (1968): Heat treatment of exterior particleboard. *Forest Products Journal*, 18 (8), pp. 24–28.

[29] Menezzi, C. H. S. D., Tomaselli, I. (2005). Contact thermal post-treatment of oriented strandboard to improve dimensional stability: A preliminary study. *Holz Als Roh- Und Werkstoff*, 64 (3), pp. 212–217. DOI: 10.1007/s00107-005-0052-1.

[30]   Oliveira, S. L., Freire, T. P., Mendes, L. M., Mendes, R. F. (2017). The Effect of Post-Heat Treatment in MDF Panels. *Materials Research*, 20 (1), pp. 183–190. DOI: 10.1590/1980-5373-mr-2016-0259.

[31]   Ayrilmis, N., Laufenberg, T. L., Winandy, J. E. (2009). Dimensional stability and creep behavior of heat-treated exterior medium density fiberboard. *European Journal of Wood and Wood Products*, 67 (3), pp. 287–295. DOI: 10. 1007/s00107-009-0311-7.

[32]   H`ng, P., Lee, S., Lum, W. (2012). Effect of Post Heat Treatment on Dimensional Stability of UF Bonded Particleboard. *Asian Journal of Applied Sciences*, 5 (5), pp. 299–306. DOI: 10.3923/ajaps.2012.299.306.

[33]   Kol, H. Ş., Sefil, Y. (2011). The thermal conductivity of fir and beech wood heat treated at 170, 180, 190, 200, and 212°C. *Journal of Applied Polymer Science*, 121 (4), pp. 2473–2480. DOI: 10.1002/app.33885.

[34]   Korkut, S., Aytin, A. (2015). Evaluation of physical and mechanical properties of wild cherry wood heat-treated using the thermowood process. *Maderas. Ciencia y Tecnología*, pp. 71–178. DOI: 10.4067/s0718-221x2015005000017

[35]   Pásztory, Z., Horváth, N., Börcsök, Z. (2017). Effect of heat treatment duration on the thermal conductivity of spruce and poplar wood. *European Journal of Wood and Wood Products*, 75 (5), pp. 843–845. DOI: 10.1007/s00107-017-1170-2.

[36]   Sekino, N., Yamaguchi, K. (2010). Carbonizing binderless wood shaving insulation panels for better insulation and durability Part 1: Relationship between thermal conductivity and carbonizing temperature. *Proceedings of the International Convention of Society of Wood Science and Technology and United Nations Economic Commission for Europe – Timber Committee October 11–14, 2010*, Geneva: Switzerland, Paper, 8.

[37]   Pásztory, Z., Tsalagkas, D., Horvath, N., Börcsök, Z. (2019). Insulation Panels Made from Thermally Modified Bark. *Acta Silvatica et Lignaria Hungarica*, 15, pp. 23–34. DOI:10.2478/aslh-2019-0002.

[38]   Sonderegger, W., Niemz, P. (2009). Thermal conductivity and water vapour transmission properties of wood-based materials. *European Journal of Wood and Wood Products*, 67 (3), pp. 313–321. DOI: 10.1007/s00107-008-0304-y.

[39]   Sonderegger, W., Martienssen, A., Nitsche, C., Ozyhar, T., Kaliske, M., Niemz, P. (2012). Investigations on the physical and mechanical behaviour of sycamore maple (Acer pseudoplatanus L.). *European Journal of Wood and Wood Products*, 71 (1), pp. 91–99. DOI: 10.1007/s00107-012-0641-8.

[40]   Troppová, E., Švehlík, M., Tippner, J., Wimmer, R. (2014). Influence of temperature and moisture content on the thermal conductivity of wood-based

fibreboards. *Materials and Structures*, 48 (12), pp. 4077–4083. DOI: 10.1617/s11527-014-0467-4.

[41] Güler, C., Büyüksarı, Ü. (2011). Effect of production parameters on the physical and mechanical properties of particleboards made from peanut (Arachis hypogaea l.) Hull. *BioResources*, 6, pp. 5027–5036.

[42] Pásztory, Z., Börcsök, Z., Tsalagkas, D. (2019). Density optimization for the manufacturing of bark-based thermal insulation panels. *IOP Conference Series: Earth and Environmental Science*, 307, p. 012007. DOI: 10.1088/1755-1315/307/1/012007.

[43] Chi, C., Chen, W., Guo, M., Weng, M., Yan, G., Shen, X. (2016). Law and features of TVOC and Formaldehyde pollution in urban indoor air. *Atmospheric Environment*, 132, pp. 85–90. DOI: 10.1016/j.atmosenv.2016.02.043.

[44] Plaisance, H., Blondel, A., Desauziers, V., Mocho, P. (2013). Field investigation on the removal of formaldehyde in indoor air. *Building and Environment*, 70, pp. 277–283. DOI: 10.1016/j.buildenv.2013.08.032.

[45] Beheshtian, J., Peyghan, A. A., Bagheri, Z. (2012). Formaldehyde adsorption on the interior and exterior surfaces of CN nanotubes. *Structural Chemistry*, 24 (4), pp. 1331–1337. DOI: 10.1007/s11224-012-0172-2.

[46] Boonamnuayvitaya, V., Sae-Ung, S., & Tanthapanichakoon, W. (2005). Preparation of activated carbons from coffee residue for the adsorption of formaldehyde. *Separation and Purification Technology*, *42*(2), 159–168. doi: 10.1016/j.seppur.2004.07.007

[47] Li, J., Li, Z., Liu, B., Xia, Q., Xi, H. (2008). Effect of Relative Humidity on Adsorption of Formaldehyde on Modified Activated Carbons. *Chinese Journal of Chemical Engineering*, 16 (6), pp. 871–875. DOI: 10.1016/s1004-9541(09)60008-2.

[48] Chen, C. M. (1982). Effects of Extraction on the Quantity of Formaldehyde Requirement in Reaction of Extractives of Bark and Agricultural Residues with Formaldehyde. *Holzforschung*, 36 (2), pp. 65–70. DOI: 10.1515/hfsg.1982.36.2.65.

[49] Chen, C. M., Hatano, Y. (1990). Study of the molecular weight of bark extracts and products of their reaction with formaldehyde. *Biomass*, 21 (1), pp. 65–74. DOI: 10.1016/0144-4565(90)90048-o.

[50] Chen, C. M. (1991). Effects of Extraction on Reaction of Bark Extracts with Formaldehyde. *Holzforschung*, 45 (1), pp. 7–12. DOI: 10.1515/hfsg.1991.45.1.7

[51] Takano, T., Murakami, T., Kamitakahara, H., Nakatsubo, F. (2008). Mechanism of formaldehyde adsorption of ( )-catechin. *Journal of Wood Science*, 54 (4), pp. 329–331. DOI: 10.1007/s10086-008-0946-8.

[52] Funaki, M., Fukuta, H., Nishizawa, M., Yamagishi, T. (2004). Adsorption of formaldehyde on the bark of Larix kaempferi. *Natural Medicines,* 58, pp. 104–108.

[53] Takano, T., Murakami, T., Kamitakahara, H., Nakatsubo, F. (2008). Formaldehyde adsorption by karamatsu (Larix leptolepis) bark. *Journal of Wood Science*, 54 (4), pp. 332–336. DOI: 10.1007/s10086-007-0940-6.

[54] Böhm, P., Wolterbeek, H., Verburg, T., Musílek L. (1998). The use of tree bark for environmental pollution monitoring in the Czech Republic. *Environmental Pollution*, 102 (2–3), pp. 243–250. DOI: 10.1016/s0269-7491(98)00082-7.

[55] Saarela, K.-E., Harju, L., Rajander, J., Lill, J.-O., Heselius, S.-J., Lindroos, A., Mattsson, K. (2005). Elemental analyses of pine bark and wood in an environmental study. *Science of The Total Environment*, 343 (1–3), pp. 231–241. DOI: 10.1016/j.scitotenv.2004.09.043.

[56] Mandiwana, K. L., Resane, T., Panichev, N., Ngobeni, P. (2006). The application of tree bark as bio-indicator for the assessment of Cr(VI) in air pollution. *Journal of Hazardous Materials*, 137 (2), pp. 1241–1245. DOI: 10.1016/j.jhazmat.2006.04.015.

[57] Pásztory, Z., Mohácsiné, I. R., Gorbacheva, G., Börcsök, Z. (2016). The Utilization of Tree Bark. *BioResources*, 11 (3), pp. 7859–7888., DOI: 10.15376/biores.11.3.

[58] Berlizov, A., Blum, O., Filby, R., Malyuk, I., Tryshyn, V. (2007). Testing applicability of black poplar (Populus nigra L.) bark to heavy metal air pollution monitoring in urban and industrial regions. *Science of The Total Environment*, 372 (2–3), pp. 693–706. DOI: 10.1016/j.scitotenv.2006.10.029

[59] Bianchi, S. (2017). *Extraction and characterization of bark tannins from domestic softwood species*. PhD Thesis, University of Hamburg.

[60] Hathway, D. E. (1958). Oak-bark tannins. *Biochemical Journal*, 70 (1), pp. 34–42. DOI: 10.1042/bj0700034.

[61] Kurth, E. F. (1947). The Chemical Composition of Barks. *Chemical Reviews*, 40 (1), pp. 33–49. DOI: 10.1021/cr60125a003.

[62] Narasimhachari, N., Rudloff, E. V. (1961). The Chemical Composition Of The Wood And Bark Extractives Of Juniperus Horizontalis Moench. *Canadian Journal of Chemistry*, 39 (12), pp. 2572–2581. DOI: 10.1139/v61-339.

[63] Navarrete, P., Pizzi, A., Bertaud, F., Rigolet, S. (2011). Condensed tannin re-activity inhibition by internal rearrangements: Detection by CP-MAS 13C NMR. *Maderas. Ciencia y Tecnología*, 13 (1), pp. 59–68. DOI: 10.4067/s0718-221x2011000100006.

[64] Porter, L. J. (1992). Structure and Chemical Properties of the Condensed Tannins. *Plant Polyphenols*, Basic Life Sciences, vol 59. Springer, Boston, MA, pp. 245–258. DOI: 10.1007/978-1-4615-3476-1_14.

[65] Schofield, P., Mbugua, D., Pell, A. (2001). Analysis of condensed tannins: a review. *Animal Feed Science and Technology*, 91 (1–2), pp. 21–40. DOI: 10.1016/s0377-8401(01)00228-0.

[66] Pizzi, A. (1980). Tannin-based adhesives: new theoretical aspects. *International Journal of Adhesion and Adhesives*, 1 (1), pp. 13–16. DOI: 10.1016/0143-7496(80)90028-7

[67] Pizzi, A. (2003). Natural Phenolic Adhesives I. *Handbook of Adhesive Technology, Revised and Expanded*. Marcel Dekker Inc. DOI: 10.1201/9780203912225.ch27.

[68] Pásztory, Z., Halász, K., Börcsök, Z. (2019). Formaldehyde Adsorption–Desorption of Poplar Bark. *Bulletin of Environmental Contamination and Toxicology*, 103 (5), pp. 745–749. DOI: 10.1007/s00128-019-02718-7.

MORPHO-STRUCTURAL PROPERTIES OF NANOGRINDED RUTILE AS POTENTIAL PHOTOCATALYST FOR WATER TREATMENT

ENIKŐ ESZTER ALMÁSI[1, 2] – ZSOLT PAP[1, 3, 4] – ÁDÁM RÁCZ[5]– KATALIN BOHÁCS[5] – GÁBOR MUCSI[5]– GÁBOR RÁKHELY[1, 6]

[1]*Institute of Environmental Science and Technology, University of Szeged, Szeged, Hungary*
[2]*Vulcano Research Group, Department of Mineralogy, Geochemistry and Petrology, University of Szeged, Szeged, Hungary*
[3]*Nanostructured Materials and Bio-Nano-Interfaces Center, Interdisciplinary Research Institute on Bio-Nano-Sciences, Babeş–Bolyai University, Cluj-Napoca, Romania*
[4]*Institute of Research-Development-Innovation in Applied Natural Sciences, Babes-Bolyai University, Cluj-Napoca, Romania*
[5]*Institute of Raw Material Preparation and Environmental Processing, University of Miskolc, Miskolc, Hungary*
[6]*Department of Biotechnology, University of Szeged, Szeged, Hungary*

Abstract: Titanium dioxide (TiO_2) is a widespread photocatalytic material for water treatment and can be found in three different crystalline structures: rutile, anatase and brookite. Rutile is thermodynamically stable, and its mineral version can be used as a promising photocatalyst for the decomposition of organic pollutants. These materials are relatively cheap and are easy to obtain. Nanoground natural rutile samples were used for photocatalytic degradation of ibuprofen and phenol under visible light and UV irradiation. The natural rutile samples were characterized using X-ray diffraction (XRD), Raman spectroscopy, and X-ray fluorescence spectroscopy (XRF). The results showed that 33% ibuprofen and phenol was photodegraded after 22 h visible-light irradiation. It was found that sample Rutile_180 (180 minutes grinding time) was the most efficient catalyst under visible-light irradiation. Interestingly, this sample contained particles in the size groups of >1 μm, 0.5–1 μm and <0.5 μm, in order of frequency.

Keywords: rutile, photocatalysis, grinding, water treatment

1. STATE OF ART

Rutile is a naturally occurring titanium dioxide (TiO_2) polymorph and can be found in three different crystalline structures: stable rutile (tetragonal), metastable anatase (tetragonal) and brookite (orthorhombic). Anatase transforms irreversibly to rutile at elevated temperatures. This transformation does not have an exact crystallisation temperature; usually the process occurs at 600 C [1], although the temperature value can vary from 400 to 1,200 °C [2–4]. Rutile can contain several elements that can substitute Ti, for example: Al, V, Fe, Cr, Hf, W, V, Ta, Sn, Sb [5–7]. TiO_2 has attracted attention for various application such as photocatalysis, sensor devices, pigments, dye-sensitized solar cells, cosmetics and protective coatings [8] and has some applications in the earth sciences [6].

Numerous publications are available in which the applied TiO_2 degraded organic contaminants such as pesticides [9, 10], herbicides (Ioannis K. Konstantinou et al. 2000; Mehrabadi & Faghihian 2019), phenol [13, 14], or pharmaceuticals (e.g. paracetamol, diclofenac, ibuprofen) [15, 16]. Phenol is a crystalline substance that is colorless at room temperature, has hygroscopic properties, and is soluble in water and slightly in organic solvents. This compound can be found in surface waters or in ground waters [17]. Many industries rely on phenol and phenolic compounds; therefore, these organic materials are often found in different wastewaters.

Pharmaceutical compounds have been found in many types of environmental matrices, including groundwater, surface water, wastewaters, and even drinking water [19]. Pharmaceuticals, including ibuprofen, are persistent in the environment, where they are observed in part due to the limited efficiency of current wastewater treatment [20]. Ibuprofen, a non-steroidal anti-inflammatory drug, is one of the most frequently used active pharmaceutical ingredients worldwide, especially prescribed for the treatment of arthritis and for toothaches, muscle aches, migraine, fever, and painful menstrual periods [21].
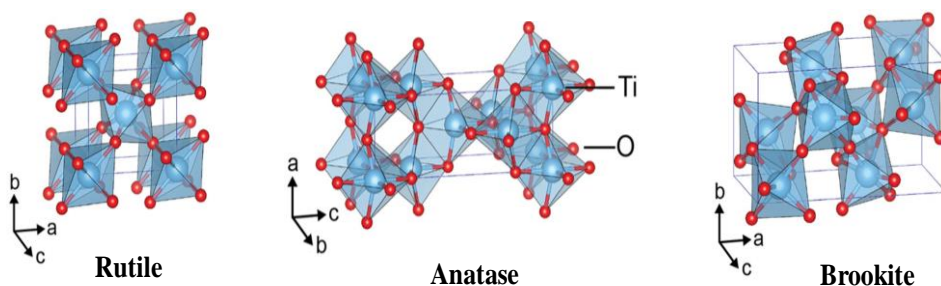
Figure 1
Crystal structure of TiO_2 polymorphs (Haggerty et al. 2017)

In the aquatic environment pharmaceutical residue presents at low levels and its continuous input into the environment has been found to impact a wide range of aquatic species in terms of abnormal development, lack of metamorphosis, and irregular behavior and reproduction [22, 23].

In the present work, natural rutile samples with different grinding times were investigated by different methods [Raman spectroscopy, X-ray diffraction (XRD), X-ray fluorescence (XRF)] and their photocatalytic properties were examined under visible and UV light.

2. CHARACTERIZATION

In rutile and anatase structures, the basic building block consists of a titanium atom surrounded by 6 oxygen atoms in a distorted octahedral configuration. Oxygen atoms at the apices of the octahedron and the two bonds between titanium are slightly longer.

2.1. Rutile

Rutile has a tetragonal unit cell (a = b = 4.584 Å and c = 2.953 Å [24]). The coordination number of titanium is 6, surrounded by an octahedron containing 6 oxygen atoms. The usual color of this mineral is brown, reddish brown, red, blood red, brownish yellow, pale blue and sometimes violet. The crystal habitat is prismatic or acicular, elongated and striated parallel to [001]. The cleavage alongside [110] is good, for [100] is moderate, while the clevage is is possible also at [092] and [011]. Hardness shown on the Mohs scale is 6.0–6.5. Rutile is a heavy mineral, with a density of 4.23 g·cm^{-3}, but density can range up to 5.50 g·cm^{-3} [25]. Associated minerals in nature are hematite (Fe_2O_3), muscovite $KAl_2(AlSi_3O_{10})(OH)_2$ (quartz (SiO_2), anatase (TiO_2), barite ($BaSO_4$), orthoclase ($KAlSi_3O_8$), calcite ($CaCO_3$), ilmenite ($FeTiO_3$), siderite ($FeCO_3$), and brookite (TiO_2). Rutile and anatase have the same symmetry despite having different structures. The TiO_6 octahedrons are organized into a four-fold symmetry in rutile, while in anatase, the octahedrons are connected at the four edges.

3. Occurence

Rutile is an accessory mineral in igneous rocks (it appears in mantle xenoliths and meteorites) and metamorphic rocks and – being a stable heavy mineral – it occurs also in sedimentary rocks [6]. Rutile is a common accessory mineral in plutonic igneous rocks, and it was detected in deep mantle sources such as kimberlites [26], pegmatites [27] and laproites [28]. It also appears in xenoliths of metasomatized peridotites [29], granitic rocks [30] and metallic ore deposits [31]. Rutile is mainly formed during high medium-grade metamorphic processes [32], but it can also appear in low-grade metamorphic rocks [33]. Large specimens of rutile crystals were found in pegmatites [34] such as granite greisen [35] and skarns [36]. Rutile has also been found in some altered igneous rocks (gneisen, schists) as accessory minerals.

In the Carpathian region, rutile is omnipresent, such as in the chloritic schists of the Tulgheş epimetamorphic series in the Corbu and Borsec region. The rutile crystals found in these regions were oriented intergrowths and organized in acicular aggregates [37]. In the Ditrău Alkaline Massif, the Jolotca deposits, rutile is present in the ore-forming phase mainly bound to ilmenite. The typical forms in this case are grey prismatic crystals of 1-2 cm or in disseminated state [38, 39]. In the Căliman Caldera of the silicified rocks rutile was observed in the miscroscopic form as bipyramidal and acicular crystals together with cassiterite [40]. In the miarolitic cavities of basalt at Racoş, rutile was observed as 0.5 mm size acicular crystals [41].

In Hungary, rutile is an accessory mineral of migmatites, sedimentary (placers, bauxite, sand) and metamorphic rocks. Rutile appears as black prismatic crystals in siliceous rocks at Fony in Tokaj Mountains. In the Mecsek Mountains at Ófalu, rutile appears in quartz veins of metamorphic rocks as black to reddish brown columnar crystals.[42].

4. APPLICATIONS OF TiO₂

Titanium dioxide has several applications, one of which is photocatalysis. This includes sterilization [43], water splitting [44], air purification [45] and pollutant degradation as well [2,46]. Titania itself is relatively cheap with high oxidation capacity; it is considered photostable, non-toxic and widely available. TiO₂ has been widely used in paper and cosmetic products (Lu et al. 2015), pigment in paints [48], as well as high-tech applications such as solar cells [49], biomedical devices [50] and semiconductors [51]. Rutile has some application in the earth sciences: rutile contains Nb, Ta and other HFSE (high-field-strength elements) , which elements are widely used as geochemical fingerprints of geological processes: subduction-zone metamorphic and magma evolution [52]; rutile's Fe content has a metamorphic origin indicator, because metamorphic rutile contains mostly >1000 ppm Fe (Gomathi Thanga Keerthana et al. 2018; Zack et al. 2004a). The partitioning of zirconium (Zr) into zircon or other Zr-rich phases with rutile has a strong dependence on temperature (Zack, et al. 2004b).

Interestingly, natural rutile has already proven to work as a photocatalyst, and has been used for the degradation of different pollutants under visible light: methylene blue [56, 57], methyl orange [58], indigo carmine [59], halohydrocarbons (Lu et al. 2004), phenol [61], etc.

5. TiO₂ SYNTHESIS

To obtain titania nanoparticles several different methods have been reported in the literature, such as hydrothermal crystallization [53, 62] or solvothermal crystallization [63, 64], sol-gel [65–67], direct oxidation [68, 69], precipitation [70, 71], thermal decomposition [72, 73], chemical vapor deposition [74, 75], hydrolysis [76, 77], a sonochemical method [78, 79], micelle and inverse micelle based methods [80, 81], ball milling [82, 83], spray pyrolysis [84,85], and microwave induced crystallization [86–88]. The production of TiO₂ nanoparticles from natural rutile mineral has also been attempted using spray pyrolysis and sonication [89], sol-gel methods and ball milling [90].

6. STRATEGY OF TiO₂ MODIFICATIONS

Large number of publications have focused on TiO₂ modification in order to enhance its photocatalytic properties [91]. Three essential TiO₂ modification strategies have been applied:
1. doping with non-metal and metal elements, to enhance light absorption and to prevent recombination of electrons and holes;
2. creating composites with other conductors and semiconductors to form a heterostructure that provides suitable energy levels for synergic light absorption for enhanced utilization of solar energy;
3. loading metal nanoparticles (Au, Ag, Pt, Pd, etc) to act as a surface plasmon resonance photosensitizer for driving visible light [92].

7. MATERIALS

Natural rutile (TiO_2) from Brazil was used as the raw starting material *(Figure 1A)*. The rutile is deep grey in color with submetallic luster and its grain size values were between 3 and 5 cm. The crystals were short prismatic ones. Cracks were observed on the rutile crystals' surface and also brownish iron (III) oxide, which was removed using oxalic acid aqueous solution. The photocatalytic efficiencies were determined using the aqueous solution of phenol (Spectrum 3D, analytical grade) and ibuprofen (Fluka, >99.0% purity) as water contaminant.

8. METHODS AND INSTRUMENTATION

8.1. Grinding methods

In the first step the rutile samples were ground under 106 μm in a Retsch planetary ball mill and designated as sample Rutile-000. This was used as a feed for the nanogrinding. For the natural rutile grinding a stirred media mill (Netzsch MiniCer, Netzsch GmbH, Germany) was used in continuous closed-circuit mode. The liners of the grinding chamber and the stirrer rotors were made of ZrO (zirconia). The circumferential tip speed of the rotor was set at a constant 9.3 ms^{-1} consequently during the experiments. Yttrium-stabilized zirconium oxide (ZY Premium, Sigmund, and Lindner, Germany) grinding media was applied during grinding. The filling ratio of grinding ball in the milling chamber was 70 v/v%. Mass concentration of the suspension was 0.2 m/m%. Samples were taken after 30, 60, 150, 180, 240- and 300-min grinding time (the samples were coded based on the grinding times, e.g. Rutile-030 denotes the sample milled for 30 minutes). Up to 180 min grinding time 0.8–1.0 mm grinding media was used, then it was changed to a smaller one (0.6–0.8 mm) for more effective grinding. Suspension samples were taken from the outflow of the pipe in which the suspension re-enters the stirrer vessel. The volumetric flow rate of the pump was $2.5e^{-05}$ m^3s^{-1}. The power draw of the mill was measured by the Netzsch measuring system, and data were registered in the computer. In this way, the specific grinding energy could be calculated.

The rutile particle size, microstructure and the morphology were analyzed by cold field-emission scanning electron microscope (SEM), Hitachi S-4700 Type II (accelerating voltage: 10 kV). The samples for SEM measurements were attached to a carbon adhesive pad, which was fixed to an aluminum sample holder.

The rutile mean primary crystallite size values and crystal phase identification were determined by a Rigaku MiniFlex II diffractometer equipped with a graphite monochromator and functioning with Cu-K_α radiation (λ = 0.15406 nm, 30 kV, 15 mA). The scanning speed was 1(2θ°) min^{-1}. The XRD measurements were recorded in the 2θ° range from 20°–40°. The mean primary crystal size values were calculated using the Scherrer equation.

The rutile crystalline structure was determined by Thermo Scientific DXR confocal Raman microscope, equipped with a diode-pumped frequency-doubled Nd:YAG laser (532 nm laser, 8 mW laser power, 10X objective lens, spot size of

approximately 1 µm). The acquired spectra were recorded at 2 cm^{-1}, while a 25 µm pinhole confocal aperture was used for each measurement.
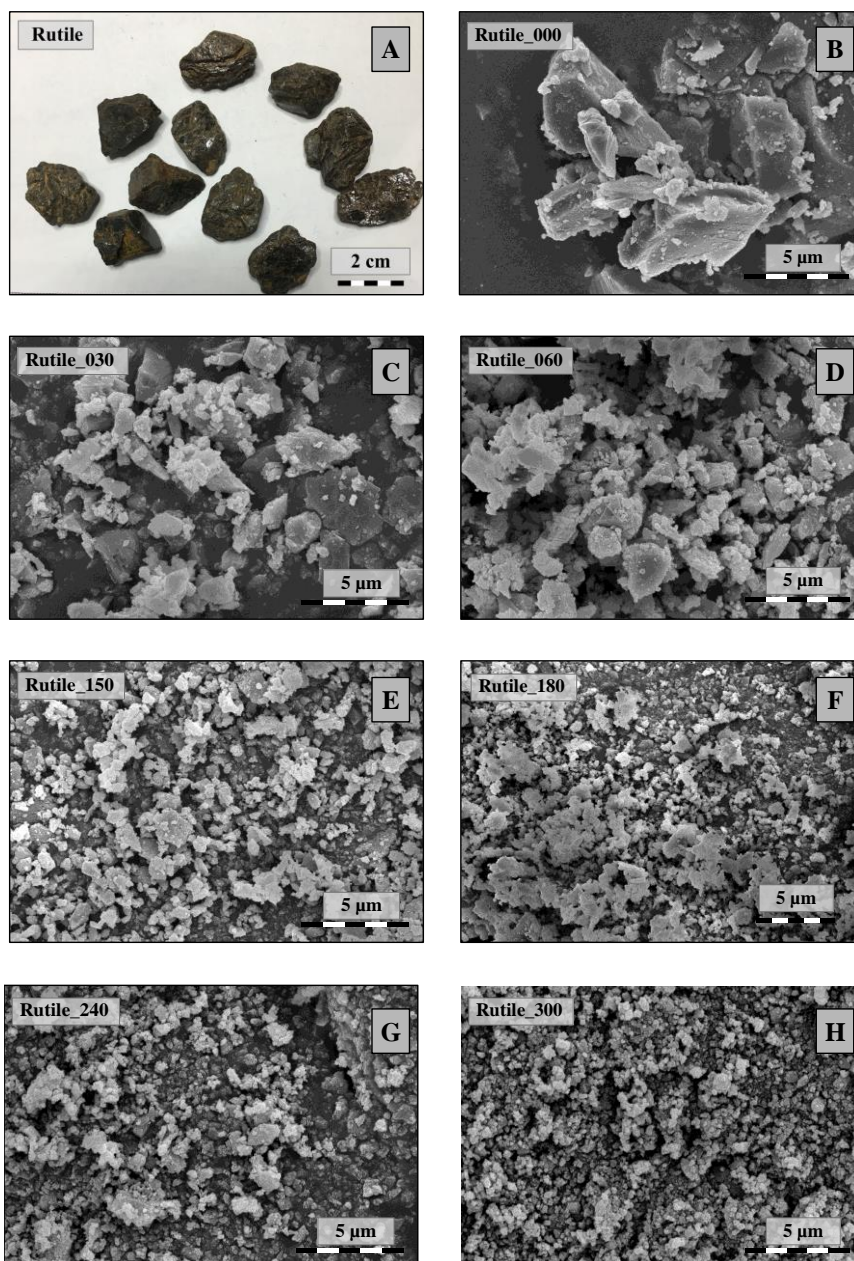
Figure 2
Photographs of the short prismatic rutile crystal and scanning electron micrographs of the samples obtained at different milling times

The trace element content of the samples was measured with a Horiba Jobin Yvon XGT-5000 X-ray fluorescent spectrometer, equipped with Rh X-ray source. The records were made at 30 kV excitation voltage, 0.5 mA anode current and 1000 s measuring time.

The specific surface areas of the grinding rutile were determined by nitrogen adsorption at 77K, using a BELCAT-A device. The specific surface area was calculated via the BET method.

The photocatalytic activity of the natural rutile was determined by the photodegradation of the ibuprofen and phenol under visible light and UV irradiation. 100 mL of the photocatalyst dispersion ($C_{rutile} = 1.0$ g/L) containing ibuprofen ($C_{ibuprofen} = 0.1$mM) or phenol ($C_{phenol} = 0.1$mM) was used in the experiments. The photoreactor used for the visible light experiments is an open glass tube with double walls, surrounded by thermostating jacket maintained at 25.0 °C (Power Star HCl-TC 75W/WDL type) with a $NaNO_2$ solution (1 M, in a thermostating jacket absorbing UV photons ($\lambda < 400$ nm). The UV photoreactor was irradiated by six fluorescent lamps (Vilber-Lourmat T-6L UV-A, 6 W power, radiation maximum at 365 nm). Prior to the photocatalytic experiments the suspensions were sonicated in the dark for 15 min, and then vigorously stirred by a magnetic stirrer during the measurements. Dissolved oxygen concentration was maintained constant by bubbling air through the reactor. 1.5 mL samples were taken out a specific time (0, 10, 20, 30, 40, 50, 60, 80, 100, 120, 180, 240, 300, 360, 420 and 1320 min), and was centrifuged for 3 min (at 13,400 rpm) and filtered with a 0.2 μm Whatman Anotop Syringe Filter.

The ibuprofen concentration was determined by an Agilent 8453 UV-Vis spectrophotometer and the detection wavelength was $\lambda = 222$ nm using a 0.2 cm cuvette.

The phenol concentration change was determined with High Performance Liquid Chromatography (Merck-Hitachi L-7100 low-pressure gradient pump equipped with a Merck-Hitachi L-4250 UV–Vis detector and a Lichrospher RP 18 column) applied as eluent methanol/water mixture (50:50). Detection wavelength for phenol was at λ=210 nm.

9. MORPHO-STRUCTURAL PROPERTIES

The first step in the characterization of the rutile was to determine the crystal phases and particle size. The XRD patterns of the rutile samples *(Figure 3)* suggested a clear presence of rutile (TiO_2, JCPDS card No. 00-900-1681 and 900-4141): diffraction peaks located at 27.44°, 36.08°, 39.20°, corresponded to the (110), (101) and (200) crystallographic planes.

The morphology and the crystal size of ground rutile is shown in *Figure 1B-H*. The surface of rutile particles was smooth. The particle size of the ground rutile samples was heterogeneous in each case. After 300 min grinding the rutile sample showed homogenous polyhedral particles. The SEM micrographs showed the decreasing rutile crystal size with the increase in grinding energy.

In the starting sample (Rutile_000) the following fractions were identified: ≥ 3 μm, 2.5–3 μm, 2–2.5 μm, 1.5–2 μm, 1–1.5 μm, 0.5–1 μm and ≤ 0.5 μm sized particles. The prolongment of the grinding time was simultaneous with the decrease of the rutile crystal size as well. The duration of milling processes the number of ≤ 0.5 μm sized particles increased. The particle size values of ground rutile (Table 1) are in good agreement with the crystallite sizes determined by the Scherrer equation [93]. Raman spectra of the rutile samples *(Figure 4)* shows typical peaks of rutile at 247, 447 and 612 cm^{-1}, reinforcing the XRD results.

After the simple ball milling, the average crystal size was 136.06 μm, while after the application of stirred media mill, the primary crystallite size significantly decreased with the grinding time. After 30 minutes the primary crystallite size of natural rutile was 53.76 nm, while after 300 minutes the primary crystallite size was decrease to 20.10 nm.

Figure 3
The XRD patterns of the rutile samples obtained
after specific grinding times
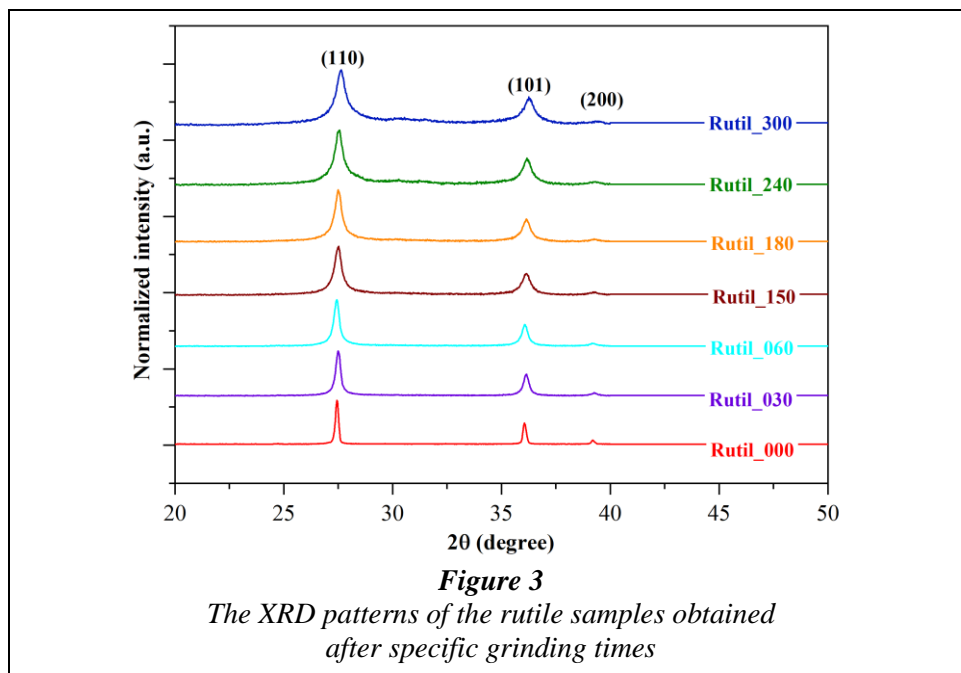
Elemental doping is an effective strategy to tune the band gap of TiO_2 [94]. The doping elements used for TiO_2 were non-metal elements as well, such as N, S, C, B, P, I, F, and metal-ions (dominantly transition metals): Cu, Co, Ni, Cr, Mn, Mo, Nb, V, Fe etc. [95–97]. These elements can enhance the photocatalytic activity [98, 99], although not in every case [100]. Among the positive results Fe^{3+} and V and in the natural rutile under visible light irradiation induced good photocatalytic activities [56, 58, 60].

The investigated natural ground rutile samples (Rutile-180) showed larger quantities of the elements Hf (4165 ppm), Nb (2475 ppm), Nd (1092 ppm), Zr (57630 ppm) and W (230 ppm). The other rutile sample, which received the highest amount of grinding energy, Rutile_300, showed lower quantities of trace elements, which were previously mentioned Hf (1487 ppm), Nb (506 ppm), Nd (506 ppm), Zr (19210 ppm). These changes may have several reasons, including slow dissolution in water during the grinding process. The elements listed here are usually concomitantly present with Ti, therefore their appearance is not surprising. The list of other elements is given in *Table 2*.

Table 1

The primary crystallite size, band gaps and specific surface areas of the investigated rutile samples

Sample	Grinding time (min)	Median crystal size (μm) from SEM micrograph	Primary crystallite size (nm)	Specific surface area ($m^2 \cdot g^{-1}$)	Ibuprofen degradation (%)	Surface normalized degradation rate of ibuprofen (mM/m^2) $\cdot 10^{-5}$	Phenol degradation (%)	Surface normalized degradation rate of phenol (mM/m^2) $\cdot 10^{-5}$
Rutile_000	0	1.9	132.0	1	–		9.8	983.6
Rutile_030	30	0.9	53.8	11	16.2	7.61	13.0	118.3
Rutile_060	60	0.8	44.1	20	–		16.2	81.2
Rutile_150	150	0.7	31.3	41	–		14.0	34.1
Rutile_180	180	0.7	31.4	49	31.2	1.40	33.1	67.6
Rutile_240	240	0.6	25.3	59	–		11.4	19.4
Rutile_300	300	0.5	20.1	80	32.6	0.84	12.1	15.1

The specific surface area of ground rutile is 1, 11, 20, 41, 49, 59, 80 $m^2 \cdot g^{-1}$ *(Table 1)*. It can be observed that the specific surface area of the ground rutile increases with a decrease in particle size; during the milling processes the external surface area increased.

Table 2

Trace elements concentrations of ground natural rutile samples, XRF analysis

Trace elements concentrations (ppm)	Sample name	
	Rutil_180	**Rutil_300**
Ti (%)	87.45	90.19
Zr (%)*	5.76	1.92
Cu	71	64
Hf	4,165	1,487
Nb	2,475	506
Nd	1,092	506
Ta	164	106
U	74	54
W	230	174
Zn	48	0
LOI (%)	6.71	6.93

LOI - Loss on ignition

*the high amount originates from the milling processes

Figure 4
Raman spectra of the ground natural rutile samples
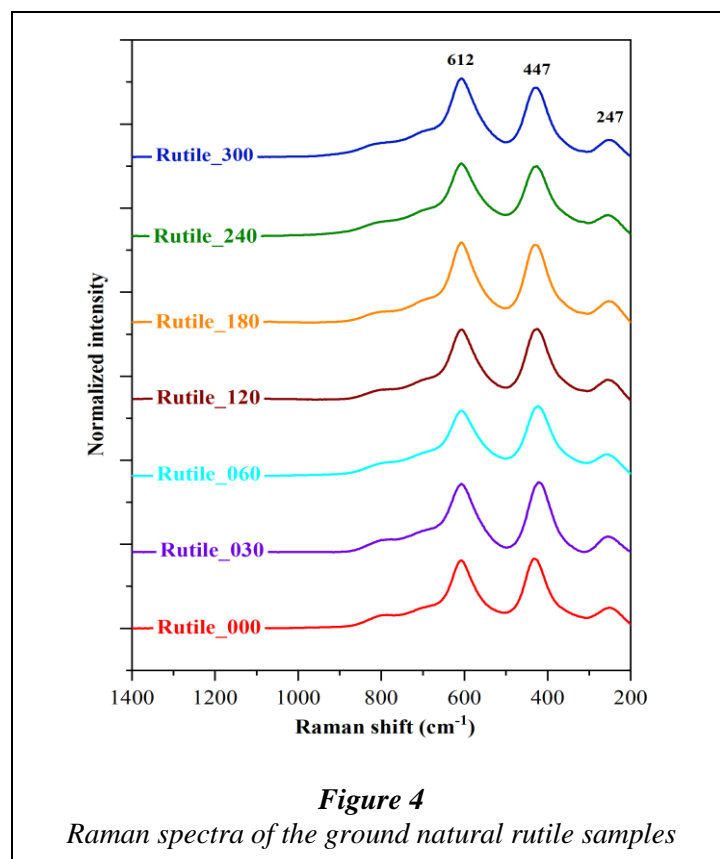
10. THE PHOTOCATALYTIC ACTIVITY OF GROUND RUTILE

The degradation efficiency of phenol with ground natural rutile was less than 35%. Additionally, with the HPLC method, two main oxidation byproducts of phenol (hydroquinone and pyrocatechol) were detected. Interestingly, the sample which was pre-ground showed 10% phenol degradation. This suggested that the specific surface area also influences the photoactivity of the samples. Therefore, the specific surface area values were measured and the surface normalized photoactivity was also evaluated. The surface normalized photocatalytic activity of phenol decreased with increased nanomilling duration *(Figure 5)*.

The sample, that received planetary ball-milling, Rutile_000, shows higher ($983.6 \cdot 10^{-5}$ mM/m^2) activity than sample Rutile_300 ($19.4 \cdot 10^{-5}$ mM/m^2), which has the most grinding time. Surface normalized activity can be a good indicator of surface quality; however, in real applications the absolute activity is considered. The best samples for visible light phenol degradation were: Rutile_60, Rutile_180 and Rutile_300. Three samples were chosen from the grinding series (Rutile_30, Ru-

tile_180 and Rutile_300) to evaluate their photoactivity towards a real pollutant, ibuprofen. Every elected sample showed photocatalytic activity under visible light degradation. The highest ibuprofen degradation was shown by Rutile_300 (32.6%), while Rutile_30 achieved only 16.2%. The photocatalytic activity to ibuprofen increased with the grinding time, namely with the particle size. This trend towards higher activity and lower particle size was already described in the literature [101]. The natural rutile samples did not show detectable photocatalytic activity in UV for phenol and ibuprofen.
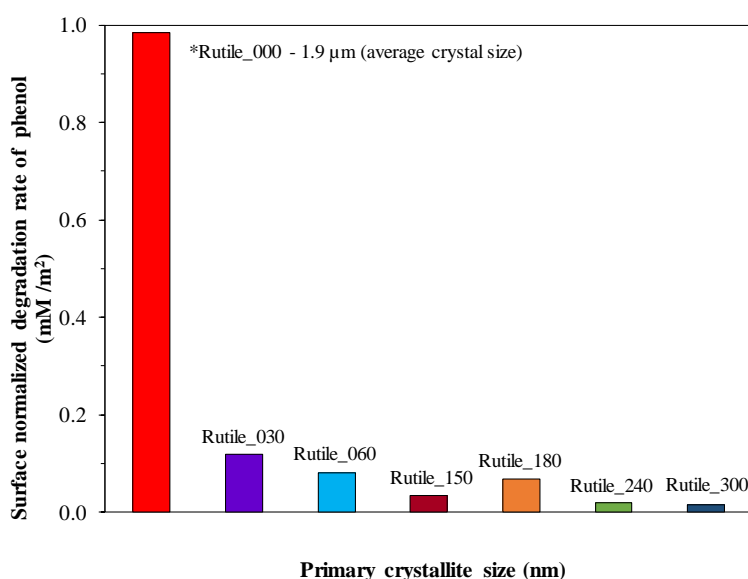
Figure 5
*The surface normalized degradation rate of phenol
from the ground natural rutile samples*

11. CONCLUSION

The photocatalytic efficiency of ground natural rutile was investigated by performing photocatalytic degradation of phenol and ibuprofen under visible light/UV light. The rutile mineral was ground for 30, 60, 150, 180, 240, or 300 minutes. The milling processes changed the morpho-structural properties and photocatalytic activity as well. The ground natural rutile samples did not show any activity under UV light. The most efficient sample under visible light irradiation was Rutile_180, which degraded 33.1% of the phenol and 31.2% of the ibuprofen. The results of the present study show that ground natural rutile samples exhibited good photocatalytic activity under visible light irradiation.

ACKNOWLEDGEMENT

REFERENCES

[1]   Li, G., Li, L., Boerio-Goates, J., Woodfield, B. F. (2005). High Purity Anatase TiO_2 Nanocrystals: Near Room-Temperature Synthesis, Grain Growth Kinetics, and Surface Hydration Chemistry. *Journal of the American Chemical Society*, 127 , pp. 8659–8666.

[2]   Mazza, T., Barborini, E., Piseri, P., Milani, P., Cattaneo, D., Li Bassi, A., Bottani, C. E., Ducati, C. (2007). Raman spectroscopy characterization of TiO_2 rutile nanocrystals. *Physical Review B*, 75, pp. 045416.

[3]   Hanaor, D. A. H., Sorrell, C. C. (2011). Review of the anatase to rutile phase transformation. *Journal of Materials Science*, 46, pp. 855–874.

[4]   Zhang, Jing, Xu, Q., Li, M., Feng, Z., Li, C. (2009). UV Raman Spectroscopic Study on TiO_2. II. Effect of Nanoparticle Size on the Outer/Inner Phase Transformations. *The Journal of Physical Chemistry C*, 113, pp. 1698–1704.

[5]   Carruzzo, S., Clarke, D. B., Pelrine, K. M. (2006). Texture, Composition, And Origin Of Rutile In The South Mountain Batholith, Nova Scotia. *The Canadian Mineralogist*, 44, pp. 715–7229.

[6]   Meinhold, G. (2010). Rutile and its applications in earth sciences" *Earth-Science Reviews*, 102, pp. 1–28.

[7]   Pe-Piper, G., Nagle, J., Piper, D. J. W., McFarlane, C. R. M. (2019). Geochronology and trace element mobility in rutile from a Carboniferous syenite pegmatite and the role of halogens. *American Mineralogist*, 104, pp. 501–513.

[8]   Di Paola, A., Bellardita, M. Palmisano, L. (2013). Brookite, the Least Known TiO_2 Photocatalyst. *Catalysts*, 3, pp. 36–73.

[9]   Zhu, X., Yuan, C., Bao, Y., Yang, J., Wu, Y. (2005). Photocatalytic degradation of pesticide pyridaben on TiO2 particles. *Journal of Molecular Catalysis A: Chemical*, 229, pp. 95–105.

[10] Wang, Y., Sun, C., Zhao, X., Cui, B., Zeng, Z., Wang, A., Liu, G., Cui, H. (2016). The Application of Nano-TiO_2 Photo Semiconductors in Agriculture. *Nanoscale Research Letters*, 11, pp. 529.

[11] Mehrabadi, Z. Faghihian, H. (2019). Clinoptilolite modified with TiO_2 for simultaneous elimination of two herbicides; 2,4-D and MCPA by UV and sunlight-assisted photocatalytic degradation. *Materials Research Bulletin*, 119, p. 110569.

[12] Ioannis, K., K., Theophanis, M. S., Vasilis, A. S., Albanis, T. A. (2000). Photocatalytic Degradation of Selected s-Triazine Herbicides and Organo-phosphorus Insecticides over Aqueous TiO_2 Suspensions. *Environmental Science and Technology*, 35 (2), pp 398–405.

[13] Guo, Z., Ma, R. Li, G. (2006). Degradation of phenol by nanomaterial TiO2 in wastewater. *Chemical Engineering Journal*, 119, pp. 55–59.

[14] Chowdhury, P., S. Nag, Ray, A. K. (2017). Degradation of Phenolic Compounds Through UV and Visible- Light-Driven Photocatalysis: Technical and Economic Aspects. *Phenolic Compounds – Natural Sources, Importance and Applications*. InTech, pp 395–417.

[15] Kanakaraju, D., Glass, B. D. Oelgemöller, M. (2014). Titanium dioxide photocatalysis for pharmaceutical wastewater treatment. *Environmental Chemistry Letters*, 12, pp. 27–47

[16] Lin, L., Wang, H., Jiang, W., Mkaouar, A. R., Xu, P. (2017). Comparison study on photocatalytic oxidation of pharmaceuticals by TiO_2-Fe and TiO_2-reduced graphene oxide nanocomposites immobilized on optical fibers. *Journal of Hazardous Materials*, 333, pp. 162–168.

[17] Agency for Toxic Substances and Disease Registry (ATSDR) (2008). *Toxicological profile for phenol* (D. of toxicology and environmental medicine/applied toxicology branch U. D. of health and human services Of [ed.]).

[18] Haggerty, James, E. S., Schelhas, Laura, T., Kitchaev, Daniil, A., Mangum, J. S., Garten, L. M., Sun, W., Stone, K. H., Perkins, J. D., Toney, M. F., Ceder, G., Ginley, D. S., Gorman, B. P., Tate, J. (2017). High-fraction brookite films from amorphous precursors. *Scientific Reports*, 7, p. 15232.

[19] Gracia-Lor, E., Sancho, J. V. Hernández, F. (2011). Multi-class determi-nation of around 50 pharmaceuticals, including 26 antibiotics, in environ-mental and wastewater samples by ultra-high performance liquid chroma-.tography–tandem mass spectrometry. *Journal of Chromatography A*, 1218, pp. 2264–2275.

[20] J Jallouli, N., Pastrana-Martínez, L. M., Ribeiro, A. R., Moreira, N. F. F., Faria, J. L., Hentati, O., Silva, A. M. T., Ksibi, M. (2018). Heterogeneous photocatalytic degradation of ibuprofen in ultrapure water, municipal and pharmaceutical industry wastewaters using a TiO_2/UV-LED system. *Chemical Engineering Journal*, 334, pp. 976–984.

[21]   Tanveer, M., Guyer, G. T. Abbas, G. (2019). Photocatalytic degradation of ibuprofen in water using TiO_2 and ZnO under artificial UV and solar irradiation. *Water Environment Research*, 91, pp. 822–829.

[22]   Achilleos, A., Hapeshi, E. Xekoukoulotakis, N.P. Mantzavinos, D. Fatta-Kassinos, D. (2010). UV-A and solar photodegradation of ibuprofen and carbamazepine catalyzed by TiO_2. *Separation Science and Technology*, 45, pp. 1564–1570.

[23]   Phasuphan, W., Praphairaksit, N. Imyim, A. (2019). Removal of ibuprofen, diclofenac, and naproxen from water using chitosan-modified waste tire crumb rubber. *Journal of Molecular Liquids*, 294, p. 111554.

[24]   Grant, F.A. (1959). Properties of rutile (titanium dioxide). *Review of Modern Physics*, 31, pp. 646–674.

[25]   Deer, W. A., Howie, R. A. Zussman, J. (2013). An introduction to the rock-forming minerals, The Mineralogical Society of Great Britain and Ireland, London.

[26]   Malkovets, V. G., Rezvukhin, D. I., Belousova, E. A., Griffin, W. L., Sharygin, I. S., Tretiakova, I. G., Gibsher, A. A., O'Reilly, S. Y., Kuzmin, D. V., Litasov, K. D., Logvinova, A. M., Pokhilenko, N. P. Sobolev, N. V. (2016). Cr-rich rutile: A powerful tool for diamond exploration V.G. *Lithos*, 265, pp. 304–311.

[27]   Okrusch, M., Hock, R., Schüssler, U., Brummer, A., Baier, M., Theisinger, H. (2003). Intergrown niobian rutile phases with Sc- and W-rich ferro-columbite: An electron-microprobe and Rietveld study. *American Mineralogist*, 88, pp. 986–995.

[28]   Kumar, A., Pankaj, P. Rao, K.K. (2016). A new find of lamproite dyke near Chintalapalle area, NW margin of the Cuddapah basin, eastern Dharwar craton, southern India. *Journal Geological Society of India*, 87, pp. 127–131.

[29]   Dawson, J. B. (2002). Metasomatism and partial melting in upper-mantle peridotite xenoliths from the Lashaine Volcano, Northern Tanzania. *Journal of Petrology*, 43, pp. 1749–1777.

[30]   René, M. (2019). Nb–Ta–Ti Oxides in Topaz Granites of the Geyersberg Granite Stock (Erzgebirge Mts., Germany). *Minerals*, 9, p. 155.

[31]   Carocci, E., Marignac, C., Cathelineau, M., Truche, L., Lecomte, A., Pinto, F. (2019). Rutile from Panasqueira (Central Portugal): An Excellent Pathfinder for Wolframite Deposition Eleonora. *Minerals*, 9, p. 9.

[32]   Force, E. R. (1991). Geology of titanium-mineral deposits, Geological Society of America, Boulder (Colo.).

[33] Luvizotto, G. L., Zack, T., Meyer, H. P., Ludwig, T., Triebold, S., Kronz, A., Münker, C., Stockli, D. F., Prowatke, S., Klemme, S., Jacob, D. E., von Eynatten, H. (2009) ,"Rutile crystals as potential trace element and isotope mineral standards for microanalysis. *Chemical Geology*, 261, pp. 346–369.

[34] Dill, H. G., Melcher, F., Füßl, M., Weber, B. (2007). The origin of rutile-ilmenite aggregates ('"nigrine"') in alluvial-fluvial placers of the Hagendorf pegmatite province, NE Bavaria, Germany. *Mineralogy and Petrology*, 89, pp. 133–158.

[35] Launay, G., Sizaret, S., Guillou-Frottier, L., Fauguerolles, C., Champallier, R., Gloaguen, E. (2019). Dynamic Permeability Related to Greisenization Reactions in Sn-W Ore Deposits: Quantitative Petrophysical and Experimental Evidence. *Geofluids*, 2019, pp. 5976545.

[36] Ordosch, A., Raith, Johann, G., Schmidt, S., Aupers, K. (2019). Polyphase scheelite and stanniferous silicates in a W-(Sn) skarn close to Felbertal tungsten mine, Eastern Alps. *Mineralogy and Petrology*, 113, pp. 703–725.

[37] Szakáll, S., Kristály, F. (2010) Mineralogy of Székelyland, Eastern Transylvania, Romania. Csík County Nature and Conservation Society, Sfântu Gheorghe.

[38] Ianovici, V. (1934). Étude sur le massif syénitique de Ditrau, région Jolotca distr. Ciuc (Transylvania). *Revista Muzeului Geologic-Mineralogic Al Universităţii Din Cluj Napoca*, 4 (2), pp. 1–53.

[39] Pál-Molnár, E. (2000). Hornblendites and diorites of the Ditró Syenite Massif, Department of Mineralogy, Geochemistry and Petrology, University of Szeged, Szeged.

[40] Teodoru, I., Teodoru, C. (1970). Faciesuri de metamorfism hidrotermal în Caldera Munţilor Călimani. [Hydrothermal metamorfism facieses in the Călimani Caldera]. *Dări de Seamă ale Şedintelor Institutului de Geologie şi Geofizică Romania*, 56, pp. 165–179.

[41] Almási, E. E. (2008). *Az alsórákosi bazaltben lévő karbonátos xenolitok ásványtani vizsgálata* [Investigation of the carbonate-derived xenoliths from basalts of Racoş]. Diploma Thesis, Cluj Napoca, *52 p.*.

[42] Szakáll, S., Udubasa, G., Ďuďa, R., Kvasnytsya, V., Koszonska., E. Novák, M. (2002). *Minerals of the Carpathians*. Granit publ., Prague, 479 p.

[43] Luo, L., Miao, L., Tanemura, S., Tanemura, M. (2008). Photocatalytic sterilization of TiO_2 films coated on Al fiber. *Materials Science and Engineering: B*, 148, pp. 183–186.

[44] Tang, J., Durrant, J. R., Klug, D. R. (2008). Mechanism of Photocatalytic Water Splitting in TiO2 . Reaction of Water with Photoholes, Importance of

Charge Carrier Dynamics, and Evidence for Four-Hole Chemistry. *Journal of the American Chemical Society*, 130, pp. 13885–13891.

[45] Zhong, L., Lee, C.-S., Haghighat, F. (2012) ,"Adsorption performance of titanium dioxide (TiO2) coated air filters for volatile organic compounds. *Journal of Hazardous Materials J*, 243, pp. 340–349.

[46] Singh, T., Srivastava, N., Mishra, P. K., Bhatiya, A. K., Singh, N. L. (2016). Application of TiO2 Nanoparticle in Photocatalytic Degradation of Organic Pollutants. *Materials Science Forum*, 855, pp. 20–32.

[47] Lu, P. J., Huang, S. C., Chen, Y.-P., Chiueh, L.-C., Shih, D. .-C. (2015). Analysis of titanium dioxide and zinc oxide nanoparticles in cosmetics. *Journal of Food and Drug Analysis*, 23, pp. 587–594.

[48] Middlemas, S., Fang, Z.Z., Fan, P. (2013). A new method for production of titanium dioxide pigment. *Hydrometallurgy Journal*, 131–132, pp. 107–113.

[49] Bai, Y., Mora-Seró, I., De Angelis, F., Bisquert, J., Wang, P. (2014). Titanium dioxide nanomaterials for photovoltaic applications. *Chemical Reviews*, 114, pp. 10095–10130.

[50] Visai, L., De Nardo, L., Punta, C., Melone, L., Cigada, A., Imbriani, M., Arciola, C. R. (2011). Titanium oxide antibacterial surfaces in biomedical devices. *Int J Artif Organs 2011*, 34, pp. 929–946.

[51] Humayun, M., Raziq, F., Khan, A., Luo, W. (2018). Modification strategies of TiO$_2$ for potential applications in photocatalysis: A critical review. *Green Chemistry Letters and Reviews*, 11, pp. 86–102.

[52] Rudnick, R. L., Barth, M., Horn, I., McDonough, Willian, F. (2000). Rutile-bearing refractory eclogites: missing link between continents and depleted mantle. ,*Science*, 287 (5451), pp. 278–281.

[53] Gomathi Thanga Keerthana, B., Solaiyammal, T., Muniyappan, S., Murugakoothan, P. (2018). Hydrothermal synthesis and characterization of TiO$_2$ nanostructures prepared using different solvents. *Materials Letters*, 220, pp. 20–23.

[54] Zack, T., von Eynatten, H., Kronz, A. (2004). Rutile geochemistry and its potential use in quantitative provenance studies. *Sedimentary Geology*, 171, pp. 37–58.

[55] Zack, T., Moraes, R., Kronz, A. (2004). Temperature dependence of Zr in rutile: empirical calibration of a rutile thermometer. *Contributions to Mineralogy and Petrology*, 148, pp. 471–488.

[56] Chuan, X. Y., Lu, A. H., Chen, J., Li, N., Guo, Y. J. (2008). Microstructure and photocatalytic activity of natural rutile from China for oxidation of methylene blue in water. *Mineralogy and Petrology*, 93, pp. 143–152.

[57] R Retamoso, C., Escalona, N., González, M., Barrientos, L., Allende-González, P., Stancovich, S., Serpell, R., Fierro, J. L. G., Lopez, M. (2019). Effect of particle size on the photocatalytic activity of modified rutile sand (TiO$_2$) for the discoloration of methylene blue in water. *Journal of Photochemistry and Photobiology A: Chemistry*, 378, pp. 136–141.

[58] Lu, A., Li, Y., Lv, M., Wang, C., Yang, L., Liu, J., Wang, Y., Wong, K. H., Wong, P. K. (2007). Photocatalytic oxidation of methyl orange by natural V-bearing rutile under visible light. *Solar Energy Materials and Solar Cells*, 91, pp. 1849–1855.

[59] Sajan, C. P., Basavalingu, B., Ananda, S., Byrappa, K. (2011). Comparative study on the photodegradation of Indigo Caramine dye using commercial TiO$_2$ and natural rutile. *Journal of the Geological Society of India*, 77, pp. 82–88.

[60] Lu, A., J. Liu, D. Zhao, Y. Guo, Q. Li, N. Li, (2004). Photocatalysis of V-bearing rutile on degradation of halohydrocarbons. *Catalysis Today*, 90, pp. 337–342.

[61] Yilleng, M. T., Gimba, E. C., Ndukwe, G. I. Bugaje, I. M. (2015). Assessing the Photo Catalytic Activity of Rutile Ore from the Middle Belt Region of Nigeria on the Degradation of Phenol in Water. *IOSR Journal of Applied Chemistry*, 8, pp. 36–43.

[62] Shivaraju, H. P., Byrappa, K., Kumar, T. M. S. V., Ranganathaiah, C. (2010). Hydrothermal Synthesis and Characterization of TiO$_2$ Nanosturctures on the Ceramic Support and their Photo-catalysis Performance. *Bulletin of the Catalysis Society of India*, 9, pp. 37–50.

[63] Mamaghani, A. H., Haghighat, F. Lee, C. S. (2019). Hydrothermal/ solvothermal synthesis and treatment of TiO$_2$ for photocatalytic degradation of air pollutants: Preparation, characterization, properties, and performance. *Chemosphere*, 219, pp. 804-825.

[64] Nam, C. T., Yang, W. D., Duc, L. M. (2013). Solvothermal synthesis of TiO$_2$ photocatalysts in ketone solvents with low boiling points. *Journal of Nanomaterials*, article 627385.

[65] Bessekhouad, Y., Robert, D., Weber, J. V. (2003). Synthesis of photocatalytic TiO$_2$ nanoparticles: optimization of the preparation conditions. *Journal of Photochemistry and Photobiology A: Chemistry*, *157*, pp. 47–53.

[66] Nachit, W., Touhtouh, S., Ramzi, Z., Zbair, M., Eddiai, A., Rguiti, M., Bouchikhi, A., Hajjaji, A., Benkhouja, K. (2016). Synthesis of nanosized TiO$_2$ powder by sol gel method at low temperature. *Molecular Crystals and Liquid Crystals*, 627, pp. 170–175.

[67] Su, C. Hong, B. Y., Tseng C. M. (2004). Sol-gel preparation and photo-catalysis of titanium dioxide. *Catalalysis Today*, 96(3), pp. 119–126.

[68] Malekshahi Byranvand, M., Nemati Kharat, A., Fatholahi, L., Malekshahi Beiranvand, Z. (2013). A Review on Synthesis of Nano-TiO_2 via Different Methods. *Journal of Nanostructures*, 3, pp. 1–9.

[69] Kumar, A., Pandey, G. (2018). Different methods used for the Synthesis of TiO_2 Based Nanomaterials : A Review. *American Journal of Nano Research and Applications*, 6, pp. 1–10.

[70] Buraso, W., Lachom, V., Siriya, P., Laokul, P. (2018). Synthesis of TiO_2 nanoparticles via a simple precipitation method and photocatalytic performance. *Materials Research Express*, 5, p. 115003.

[71] Li, Ye, Qin, Z., Guo, H., Yang, H., Zhang, G., Ji, S., Zeng, T. (2014). Low-temperature synthesis of anatase TiO_2 nanoparticles with tunable surface charges for enhancing photocatalytic activity. *PLoS ONE*, 9, pp. 1–19.

[72] Xiong, L., Xu, Y., Lei, P., Tao, T., Xiao, X. (2014). Synthesis and characterization of TiO_2/C by a simple thermal decomposition method. , *Solid State Ionics*, 268 (B), pp. 265–267.

[73] Mahajan, J., Jeevanandam, P. (2019). Novel thermal decomposition approach for the synthesis of TiO_2@Ag core-shell nanocomposites and their application for catalytic reduction of 4-nitrophenol. *Journal of Nanoparticle Research*, 21, p. 17., https://link.springer.com/article/10.1007/s11051-019-45 00-y#citeas

[74] Lee, H., Song, M. Y., Jurng, J. Park, Y. K. (2011). The synthesis and coating process of TiO_2 nanoparticles using CVD process. *Powder Technology*, 214 (1), pp. 64–68.

[75] Ding, Z., Hu, X., Yue, P. L., Lu, G. Q., Greenfield, P. F. (2001). Synthesis of anatase TiO 2 supported on porous solids by chemical vapor deposition. *Catalysis Today*, 68 (1–3), pp. 173–182.

[76] Mahshid, S., Askari, M., Ghamsari, M.S. (2007). Synthesis of TiO_2 nano-particles by hydrolysis and peptization of titanium isopropoxide solution. *Journal of Materials Processing Technology*, 189 (1–3), pp. 296–300.

[77] Zhang, J., Xiao, X., Nan, J. (2010). Hydrothermal-hydrolysis synthesis and photocatalytic properties of nano-TiO_2 with an adjustable crystalline structure. *Journal of Hazardous Materials*, 176 (1–3), pp. 617–622.

[78] Bahadur, N. M., Chowdhury, F., Obaidullah, M., Hossain, M. S., Rashid, R., Akter, Y., Furusawa, T., Sato, M., Suzuki, N. (2019). Ultrasonic-Assisted Synthesis, Characterization, and Photocatalytic Application of SiO_2@TiO_2

Core-Shell Nanocomposite Particles. *Journal of Nanomaterials*, 2019, article 6368789.

[79]   Arami, H., Mazloumi, M., Khalifehzadeh, R., Sadrnezhaad, S. K. (2007). Sonochemical preparation of TiO2 nanoparticles. *Materials Letters*, 61, pp. 4559–4561.

[80]   I Inaba, R., Fukahori, T., Hamamoto, M., Ohno, T. (2006). Synthesis of nanosized TiO_2 particles in reverse micelle systems and their photocatalytic activity for degradation of toluene in gas phase. *Journal of Molecular Catalysis A: Chemical*, 260 (1), pp.247–254.

[81]   Kluson, P., Luskova, H., Solcova, O., Matejova, L., Cajthaml, T. (2007). Lamellar micelles-mediated synthesis of nanoscale thick sheets of titania. *Materials Letters*, 61 (14–15), pp. 2931–2934.

[82]   Carneiro, J. O., Azevedo, S., Fernandes, F., Freitas, E., Pereira, M., Tavares, C. J., Lanceros-Méndez, S., Teixeira, V. (2014). Synthesis of iron-doped TiO_2 nanoparticles by ball-milling process: The influence of process parameters on the structural, optical, magnetic, and photocatalytic properties. *Journal of Materials Science*, 49, pp. 7476–7488.

[83]   Mishra, A., Roy, S. B. K. D. (2016). Development of Nano-TiO_2 by Mechanical Milling. *International Journal of Scientific Engineering and Research (IJSER)*, 4, pp. 67–69.

[84]   Choi, J., Yoo, K. S., Kim, J. (2018). Spray pyrolysis synthesis of mesoporous TiO_2 microspheres and their post modification for improved photocatalytic activity. *Korean Journal of Chemical Engineering*, 35, pp. 2480–2486.

[85]   Rozenberga-Voska, L., Grabis, J. (2017). Synthesis and photocatalytic activity of modified TiO_2 thin films prepared by spray pyrolysis. *Solid State Phenomena*, 267 SSP, pp. 3–6.

[86]   Scott, K. M., Radford, N. W. (2007). Rutile compositions at the Big Bell Au deposit as a guide for exploration. *Geochemistry: Exploration, Environment, Analysis* 7, pp. 353–361.

[87]   Calatayud, D. G., Jardiel, T., Peiteado, M., Caballero, A. C., Fernández-Hevia, D. (2014). Microwave-induced fast crystallization of amorphous hierarchical anatase microspheres. *Nanoscale Research Letters*, 9, pp. 1–5.

[88]   Suzuki, A., Yamaguchi, H., Kageyama, H., Oaki, Y., Imai, H. (2015). Microwave-assisted rapid synthesis of anatase TiO2 nanosized particles in an ionic liquid-water system. *Journal of the Ceramic Society of Japan*, 123, pp. 79–82.

[89] Arunmetha, S., Manivasakan, P., Karthik, A., Dhinesh Babu, N. R., Srither, S. R., Rajendran, V. (2013). Effect of processing methods on physicochemical properties of titania nanoparticles produced from natural rutile sand. *Advanced Powder Technology*, 24, pp. 972–979.

[90] Li, Yan, Xu, X., Li, Y., Ding, C., Wu, J., Lu, A., Ding, H., Qin, S., Wang, C. (2018). Absolute band structure determination on naturally occurring rutile with complex chemistry: Implications for mineral photocatalysis on both Earth and Mars. *Applied Surface Science*, 439, pp. 660–671.

[91] Moma, J., Baloyi, J. (2018). Modified Titanium Dioxide for Photocatalytic Applications. In tech Open. http://www.intechopen.com/articles/show/title/modified-titanium-dioxide-for-photocatalytic-applications.

[92] Ge, M.-Z., Cao, C.-Y., Li, S.-H., Tang, Y.-X., Wang, L.-N., Qi, N., Huang, J.-Y.,. Zhang, K.-Q., Al-Deyabe S., Lai, Y.-K. (2016). In situ plasmonic Ag nanoparticles anchored TiO2 nanotube arrays as visible-light-driven photocatalysts for enhanced water splitting. *Nanoscale*, 8, pp. 5226–5234.

[93] Holzwarth, U., Gibson, N. (2011). The Scherrer equation versus the 'Debye-Scherrer equation. *Nature Nanotechnology*, 6, pp. 534–534.

[94] Mathew, S., Ganguly, P., Rhatigan, S. , Kumaravel, V., Byrne, C., Hinder, S., Bartlett, J ., Nolan, M., Pillai, S. (2018). Cu Doped TiO$_2$: Visible Light Assisted Photocatalytic Antimicrobial Activity and High Temperature Anatase Stability. *Applied Sciences*, 8 (11), article 2067.

[95] Dvoranová, D., Brezová, V., Mazúr, M., Malati, M. A. (2002). Investigations of metal-doped titanium dioxide photocatalysts. *Applied Catalysis B: Environmental*, 37, pp. 91–105.

[96] Song, K., Han, X. Shao, G. (2013). Electronic properties of rutile TiO2 doped with 4d transition metals: First-principles study. *Journal of Alloys and Compounds*, 551, pp. 118–124.

[97] Zaleska, A. (2008). Doped-TiO$_2$: A Review. *Recent Patents on Engineering*, 2, pp. 157–164.

[98] Lv, C., Lan, X., Wang, L., Yu, Q., Zhang, M., Sun, H., Shi, J. (2019). Alkaline-earth-metal-doped TiO2 for enhanced photodegradation and H2 evolution: Insights into the mechanisms. *Catalysis Science and Technology*, 9, pp. 6124–6135.

[99] Huang, F., Yan, A., Zhao, H. (2016). *Influences of Doping on Photocatalytic Properties of TiO$_2$ Photocatalyst*. In: Semicond. Photocatal. – Mater. Mech. Appl., InTech.

[100] Pap, Z., Mogyorósi, K., Veréb, G., Dombi, A., Hernádi, K., Danciu, V., Baia, L. (2014). Commercial and home-made nitrogen modified titanias. A

short reflection about the advantageous/disadvantageous properties of nitrogen doping in the frame of their applicability. *Journal of Molecular Structure*, 1073, pp. 157–163.

[101] Murakami, N., Kawakami, S., Tsubota, T., Ohno, T. (2012). Dependence of photocatalytic activity on particle size of a shape-controlled anatase titanium(IV) oxide nanocrystal. *Journal of Molecular Catalysis A: Chemical*, 358, pp. 106–111.

STRUCTURE STABILITY AND PROPERTIES OF NANO MILLED CUPRITE AND ITS APPLICABILITY IN WASTEWATER TREATMENT

ENIKŐ ESZTER ALMÁSI[1, 2] – ZSOLT PAP[1, 3, 4] –
KATA SASZET[3, 5] – ÁDÁM RÁCZ[6] – GÁBOR MUCSI[6] –
NÓRA HALYAG[6] – GÁBOR RÁKHELY[1, 7]

[1]*Institute of Environmental Science and Technology, University of Szeged, Szeged, Hungary*
[2]*Vulcano Research Group, Department of Mineralogy, Geochemistry and Petrology,*
University of Szeged, Szeged, Hungary
[3]*Nanostructured Materials and Bio-Nano-Interfaces Center,*
Interdisciplinary Research Institute on Bio-Nano-Sciences,
Babeş–Bolyai University, Cluj-Napoca, Romania
[4]*Institute of Research-Development-Innovation in Applied Natural Sciences,*
Babes-Bolyai University, Cluj-Napoca, Romania;
[5]*Faculty of Physics, Babes-Bolyai University, Cluj-Napoca, Romania;*
[6]*Institute of Raw Material Preparation and Environmental Processing,*
University of Miskolc, Miskolc, Hungary
[7]*Department of Biotechnology, University of Szeged, Szeged, Hungary*

Abstract: Among the novel water treatment technologies, photocatalysis is one of the most prominent ones, where natural minerals have a high potential of applicability. In the present work nano ground, natural cuprite minerals properties were investigated, including morphological and structural peculiarities. Cuprite nanoparticles were obtained by wet stirring media milling. The samples were characterized using X-ray diffraction (XRD), Raman spectroscopy and scanning electron microscopy. During the grinding processes, the particle size and distribution were changed and the structure of the cuprite was also modified.

Keywords: wastewater, photocatalysis, wet milling, cuprite, nanomineral

1. INTRODUCTION

Nanotechnology generally refers to the fields of technology and sciences, and its general principle is to control properties of the material at the molecular and atomic scale. Nanoparticles become more reactive as the particles' size decreases; the ratio of its surface area to volume increases dramatically, thereby increasing the amount of available surface for chemical reactions (Plathe 2013). Nanominerals are a particular class of minerals, as they are rarely applied in nanotechnology (when they are, only in the form of composite systems with other materials). Mineral nanoparticles are minerals that exist in the nanorange. Although it is likely that many nano minerals are yet to be discovered, presumably the vast majority of them can exist as both mineral nanoparticles and the same mineral in the bulk state (Hochella et al. 2008).

The reactivity of these nanoparticles may be exploited in catalytic/ photocatalytic reactions in non-conventional water purification processes. The most commonly used method for nanoparticle production is wet stirring media milling, which could produce $d_{50} < 0.5$ µm ground materials [1].

Semiconducting minerals are unique, while this class of minerals is widely distributed in nature [2]. They affect and control redox-based biochemical and geochemical processes in nature, participate in near-surface geological processes (e.g. the formation of prebiotic organic molecules [3]). On Earth, hundreds of semiconductor minerals are available, which mainly belong to two mineral groups: sulfides (e.g. sphalerite (ZnS), pyrite (FeS_2), covellite (CuS)) and oxides (e.g. cuprite (CuS_2), rutile (TiO_2), hematite (Fe_2O_3)). These natural semiconducting minerals have the potential to be applied in environmental water treatment processes as efficient photocatalysts". In the present study we investigate the impact of different grinding times on natural cuprite samples by analyzing their morphology and structure changes (scanning electron microscopy, X-ray diffraction (XRD), Raman spectroscopy), and their photocatalytic activity using salicylic acid under UV light irradiation.

2. CHARACTERIZATION

Cuprite (Cu_2O) is an oxide mineral, named from the Latin word for "copper," *cuprum*, referring to the copper content of the mineral. Cuprite is a dark crystal with internal reflection. Its crystal system is cubic, hexoctahedral, while it appears in octahedral or cubic dodecahedral form or in a combination form. The unit cell parameters are a = b = c= 4.27 Å [4]. The hardness of the mineral on the Mohs scale: 3.5–4, and its density is 6.1 $g \cdot cm^{-3}$. Cuprite is a secondary mineral, appearing in the oxidized zone of copper sulfide deposits. Association minerals are usually azurite ($Cu_3(CO_3)_2(OH)_2$), malachite ($Cu_2CO_3(OH)_2$), native cooper (Cu), wüstite (FeO), magnetite (Fe_3O_4), hematite (Fe_2O_3) and limonite ($FeO \cdot nH_2O$). Its color varies from red to deep red and sometimes almost black, while showing cleavage in four directions of the forming octahedrons. Sometimes cuprite crystals transform entirely or partially to malachite and rarely to elemental copper. It should be mentioned that Cu_2O is unstable to oxidation, forming CuO.

3. OCCURRENCE

Cuprite occurs in the upper part of copper-bearing lodes and has a secondary origin, being produced by the alteration of copper sulfides. Cuprite can be found in the Altai Mountains, Ural Mountains and Sardinia, and in more isolated locations in Arizona, Bolivia, Chile, France and Namibia.

Cuprite occurs in the Carpathian region at Bălan (Romania), in the oxidation zone of the deposits, as massive aggregates, veinlets and fine-grained masses together with limonite [5]. In the marginal zones, it is frequently transformed into malachite [6]. In the Sărmanului Valley, Vârghiş cuprite was found in metabasites, and it is a secondary mineral accompanied by azurite and malachite [6]. In Hungary cuprite is a frequent mineral in a Cu-bearing ore deposit's oxidation zone, together with

copper, malachite and azurite, e.g. at Martonyi, Pátka, Pécs, Szabadbattyán, and Rudabánya. Various habits of cuprite crystals were found in the oxidation zone at Rudabánya:

    a. on the surface of copper aggregates, frequently found as small cuprite crystals

    b. attending large crystals (up to 4-5 cm) well developed rhombic dodecahedral and octahedral and sometimes altered to malachite [7].

4. APPLICABILITY OF CUPRITE

Cu_2O (cuprite) is a semiconductor with a direct bandgap and with promising applications in solar cells [8], lithium batteries [9], spintronics [10], supercapacitors [11], gas sensors [12], electrochemical sensors [13], photodetectors [14], superhydrophobic surfaces [15], field emission surfaces [16], and photocatalysts ([17,18].

5. SYNTHESIS

The literature has already described several methods for the synthesis of Cu_2O structures/nanoparticles/thin films *(Table 1)*. In these techniques, usually liquid-based chemistry is applied, because this technique is simple to execute, with low costs and not especially time consuming [19].

Table 1

Different methods for the synthesis of Cu_2O nanostructures

Methods	Nanostructure	References
Activated reactive evaporation	nanocrystalline thin films	[20]
Laser ablation	nanoparticles	[21]
Liquid phase synthesis	nanoparticles	[22]
Microemulsion	nanoparticles thin films	[23]
Microwave radiation	nanoparticles	[24]
Potentiostatistic deposition (reduction)	nanowires	[25]
Sono-chemical	nanoparticles	[26]
Spray pyrolysis	nanoparticles	[27]
Thermal oxidation	thin films	[28]

6. MATERIALS

Natural cuprite (CuO_2) from Rudabánya (Hungary) was used as the raw starting material. The cuprite sample was black, and the crystal size was 3 cm with octahedral geometry *(Figure 1A)*.

7. EXPERIMENTS

Grinding experiments were carried out in a stirred media mill (Netzsch MiniCer, Netzsch GmbH, Germany) in continuous closed-circuit mode. The liners of the grinding chamber and the stirrer rotors were made of ZrO_2 (zirconia). The circumferential tip speed of the rotor was 9.3 ms^{-1} during the experiments. Yttrium-stabilized zirconium oxide grinding media (0.6–0.8 mm) was applied during grinding. The filling ratio of grinding media in the milling chamber was 70 v/v%. Samples were taken after 60, 120, 180, and 240 min grinding time. Suspension samples were taken from the outflow of the pipe in which the suspension re-enters the stirrer vessel. The volumetric flow rate of the pump was $2.5e^{-05}$ m^3s^{-1}.

The microstructure, morphology and particle size of the cuprite was analyzed by cold field-emission scanning electron microscope (SEM), Hitachi S-4700 Type II (accelerating voltage: 10 kV). The samples for SEM measurements were attached to a carbon adhesive pad, which was fixed to an aluminum sample holder.

The X-ray diffraction (XRD) patterns were recorded on a Rigaku diffractometer. Specific parameters of the measurements were: $\lambda_{CuK\alpha}$ = 0.15406 nm, 40 kV, and 30 mA. The scanning speed was $1(2\theta°)$ min^{-1}. The XRD measurements were recorded in the $2\theta°$ range from 20°–60°. The mean primary crystal size values were calculated using the Scherrer equation [29].

The particle size distribution (PSD) of the raw and the ground materials were measured by HORIBA LA-950V2 laser diffraction particle size analyzer in wet mode using distilled water as dispersing media.

Raman measurements were recorded with a Thermo Scientific DXR Raman microscope, equipped with a diode-pumped frequency-doubled Nd:YAG laser with 10 mW maximum laser power. A laser irradiated the sample with a wavelength of 532.2 nm. A 5 × 5 µm area was used for gathering spectra of the catalysts.

The photocatalytic activity of the natural cuprite was determined by the photodegradation of salicylic acid under UV irradiation. 170 mL of the photocatalyst dispersion ($C_{cuprite}$ = 1.0 g/L) containing salicylic acid (C_{SA} = 0.5 mM) was used in the experiments. The UV photoreactor was irradiated by six fluorescent lamps (Vilber-Lourmat T-6L UV-A, 6 W power, radiation maximum at 365 nm). Preceding every experiment, the suspensions were sonicated in the dark for 10 min, and during the measurements, they were vigorously stirred by a magnetic stirrer. The concentration of the dissolved oxygen was kept constant by bubbling air through the reactor. Before the photocatalytic experiments, adsorption tests were conducted in the dark, under the same experimental conditions as the photocatalytic experiments, for 20 min, allowing the adsorption equilibrium to set. During the adsorption and photocatalytic tests 1.5 mL samples were taken out at specific times (adsorption sample: after 20

min, photocatalysis samples: 0, 10, 20, 30, 40, 50, 60, 80, 100, 120, 180, 240, 300, 360, 420, and 1,320 min), and were centrifuged for 3 min (at 15,000 rpm) and filtered with a Whatman Anotop Syringe Filter. The salicylic acid concentration was determined by a SPECORD 250 PLUS UV-Vis spectrophotometer, measuring in the spectral range of $\Delta\lambda = 200–450$ nm, using a cuvette with 10 mm path length.
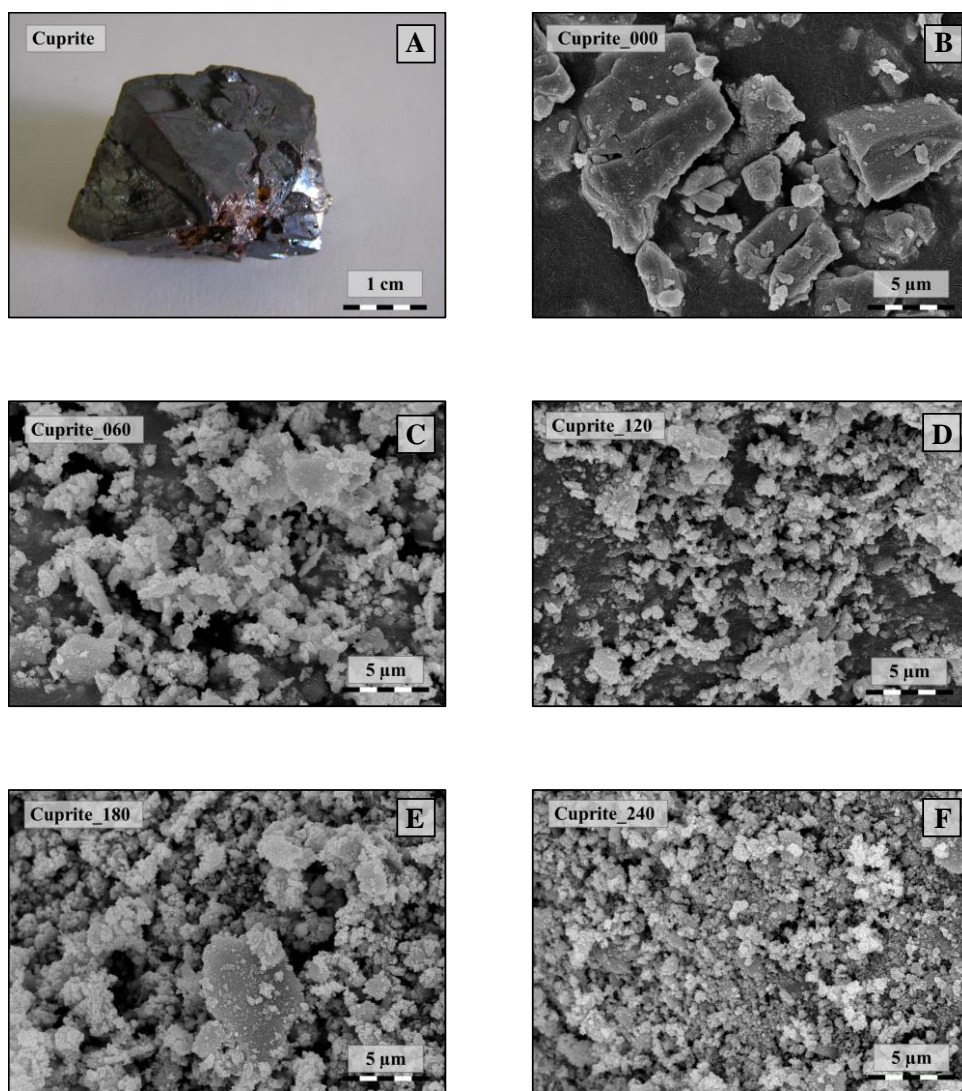
Figure 1
Photograph and scanning electron micrographs
of cuprite crystal obtained at different milling times

8. PROPERTIES OF NANO CUPRITE

The first step in the characterization of the cuprite was to determine its crystal phase composition and particle size. The XRD patterns of the ground cuprite *(Figure 2)* suggests a single mineral phase, cuprite (Cu_2O). The diffraction peaks were attributed to cuprite (Cu_2O) (JCPDS card No. 75-1531) and CuO (JCPDS card No. 48-1548); the four most intensive peaks located at 29.58°, 36.43°, 38.75°, 42.29° were attributed to the (110), (002), (111) and (200) crystallographic planes, respectively. The XRD patterns of the ground cuprite *(Figure 2)* suggested two mineral phases: Cu_2O and CuO, while in the starting sample (Cuprite_000), only Cu_2O was present. As the grinding time became longer new diffraction peaks appeared, such as the one at 38.75°, which is characteristic of CuO. This means that the structure of the cuprite changed during the grinding process. After 60 minutes, the new diffraction peak appeared.
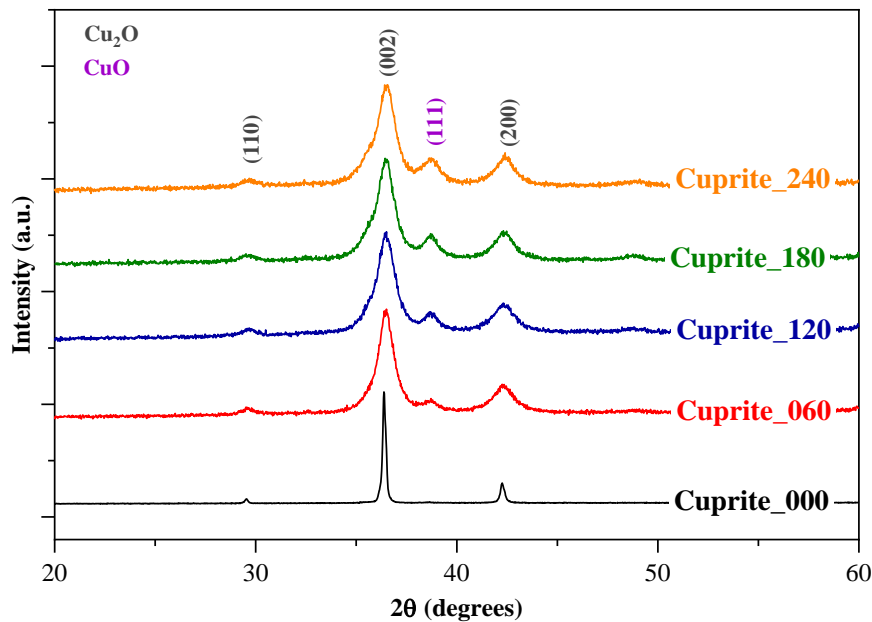
Figure 2

The XRD patterns of the cuprite samples obtained after specific grinding times

After the primary grinding process (chopping in a mortar), the average particle size determined from the SEM micrographs was ~0.91 μm, while after the application of stirred media milling size decreased significantly. After 120 minutes the average crystallite size was 9.4 nm, while after 180 minutes the crystallite size was 8.4 nm and at the end of the grinding procedure, the primary crystallite size value achieved 11.62 nm. This shows that the nano milling reached its original aim with a short grinding time and after a certain point, the particles lost their behavior as brittle

crystalline material. With the introduction of additional grinding energy, the grains suffered for the most part only plastic deformation, and the grinding energy was consumed after further milling for the transformation of Cu_2O to CuO. At the end of the experiment, the primary crystallite size increased, meaning that the milling energy is now invested in crystal size growth. This latter observation, however, needs further investigation.

The morphology and the crystal size of the ground cuprite samples are shown in *Figure 1B-F*. The surface of the cuprite particles was smooth. The particle size of the ground cuprite samples was heterogeneous in each case. After 240 min grinding the cuprite sample showed homogenous particles with non-specific geometry. The SEM micrographs showed a decrease in the size of the cuprite crystal. However, the situation with the primary crystallite size discussed earlier should be kept in mind. In the starting sample (Cuprite_000), the following fractions were identified: ≤0.5 µm, 0.5-1 µm, 1-2 µm, and 2-3 µm sized particles.

The advance of grinding time led to a decrease in the cuprite crystal size. The duration of milling processes favored the formation of particles with the size of ≤ 0.5 µm *(Figure 3)*.
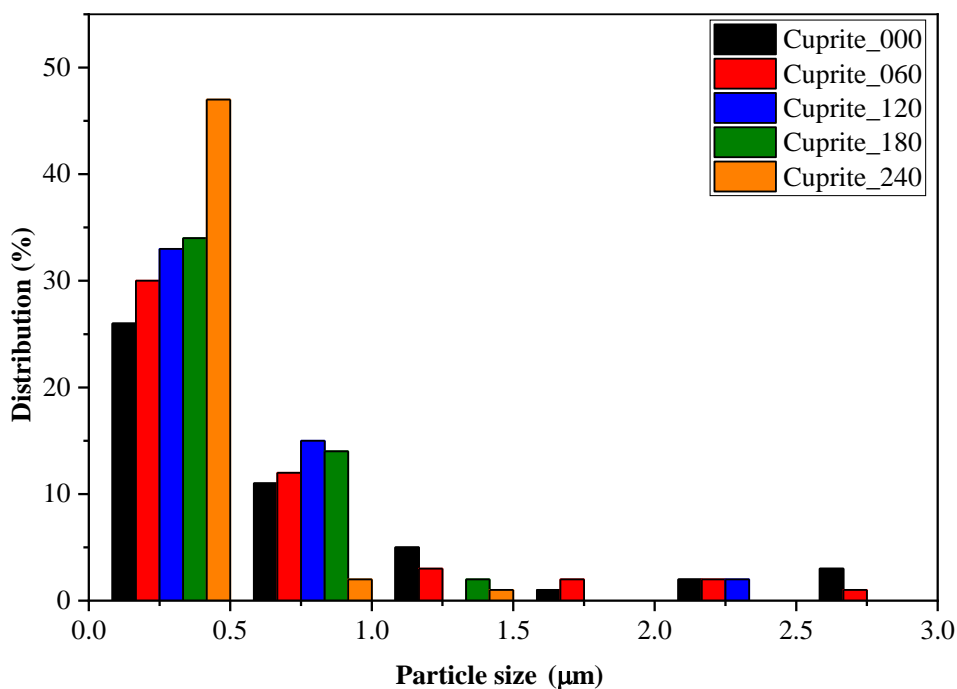
Figure 3
Particle size distribution of ground natural cuprite particles estimated from SEM micrographs

The particle size of ground cuprite determined from the SEM measurements showed a decrease in size of particles, but it was not valid for the primary crystallite size *(Table 2)* determined by Scherrer equation [29].

Table 2

Grinding times, crystal size and primary crystallite size of natural ground cuprite

Sample	Grinding time (min)	Median particle size (µm) from laser diffraction particle size analyzer	Median crystal size (µm) from SEM micrographs	Primary crystallite size (nm)	Grinding energy kJ/kg
Cuprite_000	0	n.a.	0.91	-	-
Cuprite_060	60	1.68	0.61	9.37	15,172
Cuprite_120	120	1.51	0.46	8.35	30,344
Cuprite_180	180	n.a	0.42	9.33	45,517
Cuprite_240	240	1.36	0.6	11.62	60,689

8.1. Particle size distribution by laser diffraction

Particle size distribution of the ground cuprite after 60, 120, or 240 min wet stirred media milling can be observed in *Figure 4*.
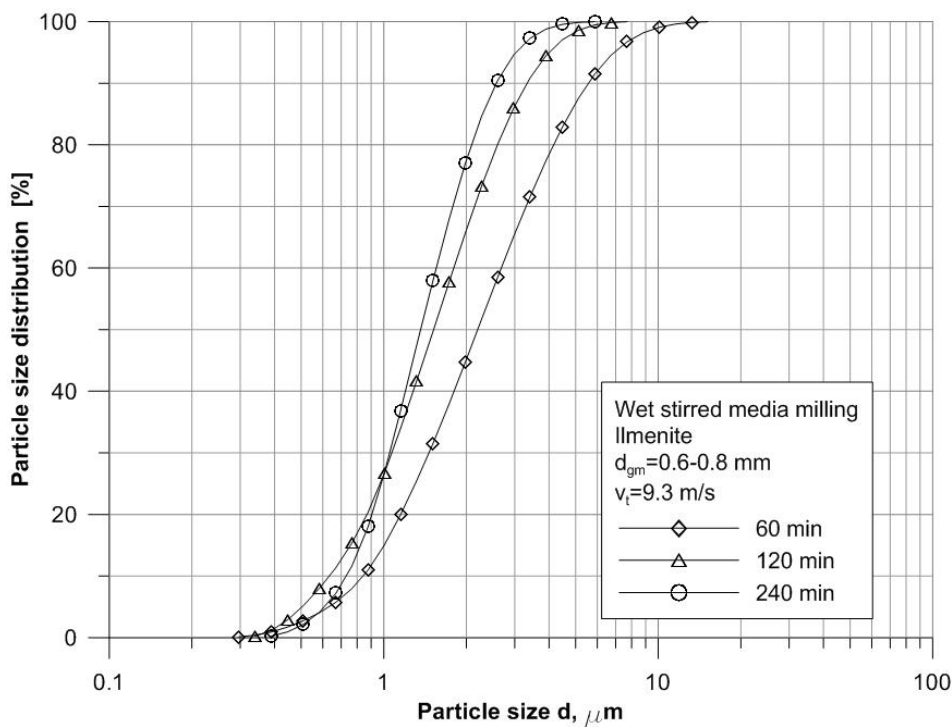
Figure 4

Particle size distribution of some selected ground cuprite samples, after 60, 120, 240 min wet stirred media milling

The median particle size of the cuprite decreased slightly during milling. The smallest median size was 1.36 μm at 60,689 kJ/kg specific grinding energy *(Table 2)*. In the case of cuprite, even after 60,000 kJ/kg the median particle size did not reach the nano size range. Only a small amount of the particles was under 0.5 μm – 2.7% after 60 min; 5.2% 120 min, 2.1% 240 min. Also, the maximal particle size of the ground cuprite remained quite coarse despite the extended stirred media milling.

Raman spectra of the cuprite samples *(Figure 5)* show two different phases by peak positions: Cu_2O and CuO. The specific peaks of Cu_2O was 109 (which is hardly identifiable) 125, 154, 219 and 635 cm^{-1} [30], while for CuO only one typical Raman band was found at 288 cm^{-1} [31]. The Raman results confirmed the transformation of Cu_2O to CuO and reinforced the data obtained from the XRD.
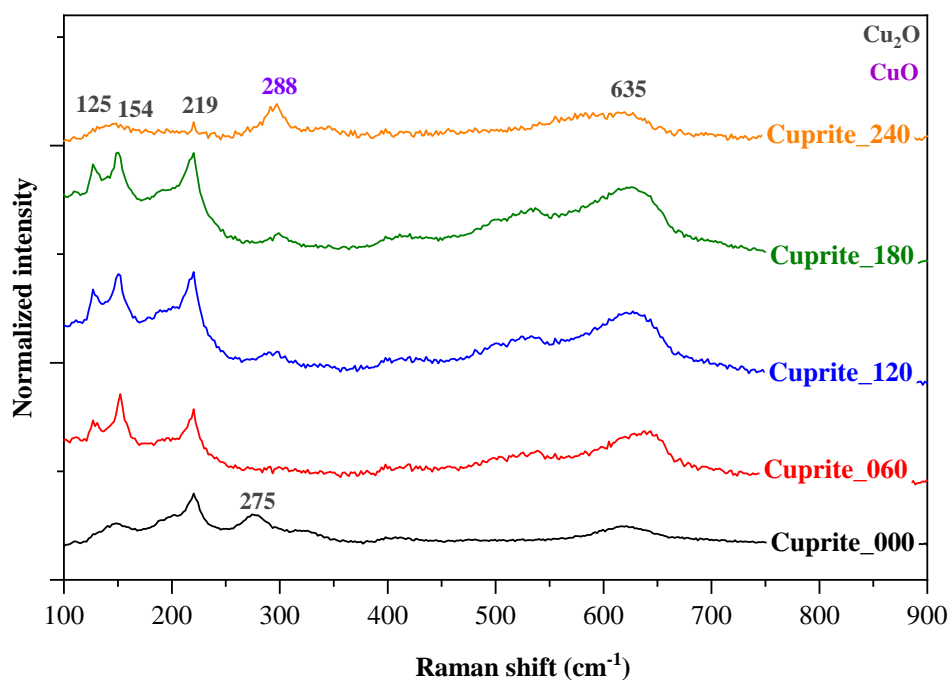
Figure 5
The Raman spectra of the ground natural cuprite samples

9. PHOTOCATALYTIC ACTIVITY

Although the photocatalytic activity was tested for these materials, achieving between 20-25% of degradation of salicylic acid (no significant differences were observed between the samples), the following issues should be considered:

- The mean primary crystallite size was quite low; therefore, after the filtering process, the small nanoparticles produced an intensive light scattering, conferring a high degree of uncertainty to the measurements.
- Salicylic acid is known to form surface complexes which cause light sensitization [32]; therefore, an additional enhancement mechanism should be also viable in the present case.
- The appearance of CuO, as discussed earlier in this work, could influence the overall activity either negatively or positively. Therefore, experiments elucidating this issue should be carried out.
- There was no difference between the photoactivity of any of the samples.

10. CONCLUSIONS

In the present paper nano cuprites based on a natural mineral source were investigated. The cuprite mineral was ground for 60, 120, 180, or 240 minutes using wet stirring media milling. The duration of milling processes changed the particle size, particle size distribution, and induced significant structural changes, which were demonstrated and explained by the presence of CuO. The samples showed photoactivity; however, specific issues need to be clarified in order to proceed with further investigations.

REFERENCES

[1] Knieke, C., Steinborn, C., Romeis, S., Peukert, W., Breitung-Faes, S. Kwade, A. (2010). Nanoparticle production with stirred-media mills: Opportunities and limits. *Chemical Engineering and Technology*, 33, pp. 1401–1411.

[2] Li, Y., Ding, C., Liu, Y., Li, Y., Lu, A., Wang, C., Ding, H. (2017). Visible Light Photocatalysis of Natural Semiconducting Minerals. In: An, T., Zhao, H., Wong, P. K. (eds.). Adv. *Photocatalytic Disinfect.* Springer,Heidelberg, Berlin, pp. 17–39.

[3] Schoonen, M., Smirnov, A., Cohn, C. (2004). A perspective on the role of minerals in prebiotic synthesis. *Ambio*, 33, pp. 539–551.

[4] Wells, A. F. (2012). *Structural inorganic chemistry*. Clarendon Press, Oxford.

[5] Ackner, M. I. (1855). *Mineralogie Siebenbürgens mit geognostischen Andeutungen*. Hermannstast, Steinhaussen.

[6]   Szakáll, S., Kristály, F. (2010). *Mineralogy of Székelyland*. Eastern Transyl-
      vania, Romania, Csík County Nature and Conservation Society, Sfântu
      Gheorghe.

[7]   Szakáll, S., Udubasa, G., Ďuďa, R., Kvasnytsya, V., Koszonska., E., Novák,
      M. (2002). *Minerals of the Carpathians*. Granit publ., Prague, 479 p.

[8]   Akimoto, K., Ishizuka, S., Yanagita, M., Nawa, Y., Paul, G. K., Sakurai, T.
      (2006) ,"Thin film deposition of Cu2O and application for solar cells. *Solar
      Energy*, 80, pp. 715–722.

[9]   Kim, E.-S., Kim, M.-C., Moon, S.-H., Shin, Y.-K., Lee, J.-E., Choi, S., Park,
      K.-W. (2019). Surface modified and size-controlled octahedral Cu2O
      nanostructured electrodes for lithium-ion batteries. *Journal of Alloys and
      Compounds*, 794, pp. 84–93.

[10] Li, H.-B., Wang, W., Xie, X., Cheng, Y., Zhang, Z., Dong, H., Zheng, R.,
      Wang, W.-H., Lu, F., Liu, H. (2015). Electronic Structure and Ferromag-
      netism Modulation in Cu/Cu_2O Interface: Impact of Interfacial Cu Vacancy
      and Its Diffusion. *Scientific Reports*, 5, pp. 15191.

[11] Kumar, R., Rai, P. Sharma, A. (2016). Facile synthesis of Cu_2O microstruc-
      tures and their morphology dependent electrochemical supercapacitor proper-
      ties. *RSC Advances*, 6, pp. 3815–3822.

[12] Wan, X., Wang, J., Zhu, L. Tang, J. (2014). Gas sensing properties of Cu_2O
      and its particle size and morphology-dependent gas-detection sensitivity.
      Journal of Materials Chemistry A, 2, pp. 13641–13647.

[13] Zhao, Z., Wang, Y., Li, P., Sang, S., Zhang, W., Hu, J., Lian, K. (2015). A
      highly sensitive electrochemical sensor based on Cu/Cu_2O@carbon nanocom-
      posite structures for hydrazine detection. *Analytical Methods*, 7, pp. 9040–
      9046.

[14] Liu, X., Du, H., Wang, P., Lim, T.-T., Sun, X. W. (2014). A high-performance
      UV/visible photodetector of Cu_2O/ZnO hybrid nanofilms on SWNT-based
      flexible conducting substrates. *Journal of Materials Chemistry C*, 2, pp. 9536–
      9542.

[15] Lei, S., Fang, X., Wang, F., Xue, M., Ou, J., Li, C., Li, W. (2019). A Facile
      Route to Fabricate Superhydrophobic Cu_2O Surface for Efficient Oil–Water
      Separation. *Coatings*, 9, pp. article 659.

[16] Hsu, C.L., Tsai, J.Y. Hsueh, T.J. (2015). Novel field emission structure of
      CuO/Cu_2O composite nanowires based on copper through silicon via technol-
      ogy. *RSC Advances*, 5, pp. 33762–33766.

[17] Singh, M., Jampaiah, D., Kandjani, A. E., Sabri, Y. M., Della Gaspera, E.,
      Reineck, P., Judd, M., Langley, J., Cox, N., Van Embden, J., Mayes, E. L. H.,

Gibson, B. C., Bhargava, S. K., Ramanathan, R., Bansal, V. (2018). Oxygen-deficient photostable Cu_2O for enhanced visible light photocatalytic activity. *Nanoscale*, 10 (13), pp. 6039–6050.

[18] Khiavi, N. D., Katal, R., Eshkalak, S. K., Masudy-Panah, S., Ramakrishna, S. & Jiangyong, H. (2019). Visible light driven heterojunction photocatalyst of CuO-Cu_2O thin films for photocatalytic degradation of organic pollutants. *Nanomaterials*, 9(7), article 1011.

[19] Sawant, S. S., Bhagwat, A. D., Mahajan, C. M., Bari, P., Rajasthan, J. (2016). Synthesis of Cuprous Oxide (Cu_2O) Nanoparticles – a Review The Cuprous Oxide (Cu_2O) is semiconductor metal which is nontoxic , low cost and has abundant source materials . Cu_2O has gained a renewed interest for various technological applications owi. *Journal of Nano- and Electronic PhysicS*, 8, pp. 1–5.

[20] Balamurugan, B., Mehta, B.R. (2001). Optical and structural properties of nanocrystalline copper oxide thin films prepared by activated reactive evaporation. *Thin Solid Films*, 396, pp. 90–96.

[21] Al-Antaki, A. H. M., Luo, X., Duan, X., Lamb, R. N., Hutchison, W. D., Lawrance, W., Raston, C. L. (2019). Continuous Flow Copper Laser Ablation Synthesis of Copper(I and II) Oxide Nanoparticles in Water. *ACS Omega*, 4, pp. 13577–13584.

[22] Gou, L., Murphy, C.J. (2003). Solution-Phase Synthesis of Cu_2O Nanocubes. *Nano Letters*, 3, pp. 231–234.

[23] Dodoo-Arhin, D., Leoni, M., Scardi, P., Garnier, E., Mittiga, A. (2010). Synthesis, characterisation and stability of Cu_2O nanoparticles produced via reverse micelles microemulsion. *Materials Chemistry and Physics*, 122, pp. 602–608.

[24] Nunes, D., Pimentel, A., Barquinha, P., Carvalho, P.A., Fortunato, E., Martins, R. (2014). Cu_2O polyhedral nanowires produced by microwave irradiation. *Journal of Materials Chemistry C*, 2, pp. 6097–6103.

[25] Wu, L., Tsui, L., Swami, N., Zangari, G. (2010). Photoelectrochemical Stability of Electrodeposited Cu_2O Films. *The Journal of Physical Chemistry C*, 114, pp. 11551–11556.

[26] Bhosale, M. A., Bhanage, B. M. (2016). A simple approach for sonochemical synthesis of Cu2O nanoparticles with high catalytic properties. *Advanced Powder Technology*, 27, pp. 238–244.

[27] Plankensteiner, N., Kautek, W., Dimopoulos, T. (2020). Aqueous Spray Pyrolysis of Cu_2O Films: Influence of Reducing Agent and Acetic Acid Addition. *Chemistry of Nanomaterials for Energy, Biology and More,* 6 (4), https://

onlinelibrary.wiley.com/action/showCitFormats?doi=10.1002%2Fcnma.2020 00006.

[28] Matsumura, H., Fujii, A., Kitatani, T. (1996). Properties of High-MobilityCu2OFilms Prepared by Thermal Oxidation of Cu at Low Temperatures. *Japanese Journal of Applied Physics*, 35, pp. 5631–5636.

[29] Holzwarth, U., Gibson, N. (2011). The Scherrer equation versus the 'Debye-Scherrer equation'" *Nature Nanotechnology*, 6, pp. 534–534.

[30] Solache-Carranco, H., Juárez-Díaz, G., Galván-Arellano, M., Martínez-Juárez, J., Romero-Paredes R., G., Peña-Sierra, R. (2008). Raman scattering and photoluminescence studies on Cu_2O. *5th International Conference on Electrical Engineering, Computing Science and Automatic Control, CCE 2008*, pp. 421–424.

[31] Vivas, L., Chi-Duran, I., Enriquez, J., Barraza, N., Singh, D.P. (2019). Ascorbic acid based controlled growth of various Cu and Cu_2O nanostructures. *Materials Research Express*, 6 (6), article 065033.

[32] Tang, W. R., Wu, T., Lin, Y. W. (2019). Salicylic acid-sensitised titanium dioxide for photocatalytic degradation of fast green FCF under visible light irradiation. *Micro and Nano Letters*, 14, pp. 359–362.

FINE STRUCTURAL FEATURES OF ILMENITE ACHIEVED BY WET MILLING AND ITS POTENTIAL IN THE DEGRADATION OF POLLUTANTS IN WASTEWATER

ENIKŐ ESZTER ALMÁSI[1, 2] – ZSOLT PAP[1, 3, 4] – KATA SASZET[3, 5] –
TAMÁS GYULAVÁRI[·6]– ÁDÁM RÁCZ[7] – GÁBOR MUCSI[7]–
NÓRA HALYAG[7] – GÁBOR RÁKHELY[1, 8]

[1]*Institute of Environmental Science and Technology, University of Szeged, Szeged, Hungary*
[2]*Vulcano Research Group, Department of Mineralogy, Geochemistry and Petrology,*
University of Szeged, Szeged, Hungary
[3]*Nanostructured Materials and Bio-Nano-Interfaces Center,*
Interdisciplinary Research Institute on Bio-Nano-Sciences,
Babeş–Bolyai University, Cluj-Napoca, Romania
[4]*Institute of Research-Development-Innovation in Applied Natural Sciences,*
Babes-Bolyai University, Cluj-Napoca, Romania;
[5]*Faculty of Physics, Babes-Bolyai University, Cluj-Napoca, Romania;*
[6]*Department of Applied and Environmental Chemistry,*
University of Szeged, Szeged, Hungary
[7]*Institute of Raw Material Preparation and Environmental Processing,*
University of Miskolc, Miskolc, Hungary
[8]*Department of Biotechnology, University of Szeged, Szeged, Hungary*

Abstract: Ilmenite nanoparticles were produced by wet stirred media milling. The grinding time influenced all the morpho-structural properties of the ilmenite, including the primary crystallite size, particle size distribution, and photocatalytic activities. However, the band-gap energy values were unchanged, even though changes in the samples' reflectance were observed. The applicability of ground ilmenite was explored by analyzing the degradation of methylene blue, achieving a maximum of 19 % conversion in 22 hours.

Keywords: photocatalysis, wet milling, ilmenite, wastewater, nanoparticle

1. INTRODUCTION

Photocatalytic degradation is clean, promising technology for the removal of dyes from different waters [1]. Dyes belong to environmental pollutants, which are released mostly by textile industries to the environment and are a major cause for some diseases [1]. Dyes are toxic, mutagenic, and teratogenic, carcinogenetic, so they are a serious health threat to humans and other organisms [2, 3]. In water, dyes block sunlight, decreasing or stopping water reoxygenation, and as a result the BOD (biochemical oxygen demand) value of those waters increases significantly, which is quite harmful for aquatic organisms [1]. Under environmental conditions many dyes

are stable and are resistant to biodegradation, so in order to remove them effective and environmentally friendly materials are needed [4].

Methylene blue is a very common dye that issued to color silk, hemp, bamboo, paper, and wood, as well as in the manufacture of inks in tissue staining and lake dyes [5]. Methylene blue released into water can cause serious pollution [6].The metal oxides (TiO_2, ZnO, CeO_2 and $FeTiO_3$), which are abundant in nature, have also been extensively used as photocatalysts. This is because of their biocompatibility, exceptional stability in a variety of conditions and capability to generate charge carriers when stimulated with required amount of light energy [7].

In the present study we investigated the effect of different grinding times on the natural ilmenite morpho-structural properties, using scanning electron microscope, X-ray diffraction (XRD), diffuse reflectance spectroscopy and a particle size analyzer, while the photocatalytic activity of methylene blue was also investigated under visible light irradiation.

1.1. Characterization of ilmenite

Ilmenite is a titanium-iron oxide mineral, idealized formula: $FeTiO_3$, otherwise called manaccanite. It is an opaque mineral whose color is black to brownish-red, with sub-metallic and metallic luster. It is the most important ore of titanium, a major source of titanium-dioxide (TiO_2) [8]. Titanium is usually found in igneous and metamorphic rocks as rutile (TiO_2), titanomagnetite (Fe_2TiO_4–Fe_3O_4) and ilmenite ($FeTiO_3$). 85% of titanium bearing minerals are used in making titanium dioxide for the pigment industry [9]. Titanium dioxide's applicability spectra includes manufacturing paper, printing inks, paints, paperboard, varnishes, rubber, lacquer, ceramics, floor covering, food and pharmaceuticals [10, 11]. The structure of ilmenite is derived from that of α-Fe_2O_3 by replacing every other layer of Fe atoms in the (001) planes by a layer of Ti atoms [12]. The main properties of ilmenite are the following:

- Crystal system: trigonal
- Crystal class: rhombohedral
- Unit cell: a = b = 5.0870 Å, c = 14.0420 Å [13].
- Color: iron-black, gray with a brownish tint in reflected light
- Crystal habit: lamellar exsolution in magnetite and hematite, granular to massive
- Cleavage: absent
- Density: 4.55 g/cm^3
- Hardness to Mohs scale: 5-6, weakly magnetic

Associations formed with hematite (Fe_2O_3), magnetite (Fe_3O_4), rutile (TiO_2), apatite ($Ca_{10}(PO_4)_6(OH,F,Cl)_2$), pyrrhotite ($Fe_{1-x}S$ (x = 0 to 0.2)), ulvospinel (Fe_2TiO_4 or $TiFe^{2+}_2O_4$). Also it should be mentioned that natural ilmenite can contain a large amount of hematite [14].

1.2. Occurrences

Ilmenite is the most abundant mineral on the Moon and is also available in large quantities on Earth [15] as a common accessory mineral in igneous and sedimentary rocks and in sands. Ilmenite is formed during magmatic cooling and concentrates via magmatic segregation [16]. Deposits are located on all five major continents: North and South America, Eurasia, Africa, and Australia [17].

In the Carpathian region, ilmenite occurs in teschenites from several localities in eastern Moravia, in rare tabular grains [18]. Ilmenite was observed as a frequent member of ore and gangue minerals, sometimes having undergone transformation to rutile at Bălan [19, 20]. Ilmenite is a frequent component around Jolotca of the mafic and ultramafic rocks [21–23]. Also, it is a common accessory mineral in Fe-Tibean peridotites at Szarvaskő. This ilmenite is in the form of microscopic grains or lamellar crystals and can be found in mianolitic cavities of basalt in the Balaton Highland at Nagygörbő, Uzsa, and Zalahaláp and also rarely in andesite cavities in the Mátra, Cserhát, and Tokaj Mountains. In the latter tabular crystals of ilmenite can be found growing to 2-3 mm in size.

1.3. Applications of ilmenite

Ilmenite is an antiferromagnetic semiconductor [24] and it has potential applications in high power electronic devices [15], high temperature integrated circuits [25], spintronics [26], or as a chemical catalyst and photocatalyst [27, 28]. Natural mineral ilmenite is the primary source for the production of bulk TiO_2 [17], because it is relatively cheap with a record of 140–165 USD/t [29] and the market price of pure TiO_2 has reached up to 2,000 USD/t [30]; therefore, it has been used for production of pigment through chemical routes [11]. Several researchers have successfully applied ilmenite or modified ilmenite to degrade organic compounds [31] via photocatalytic routes, such as phenol [32], acid orange 7 (Orange II) [33], methylene blue [12], malachite green, alkaline fuchsin, or Coomassie blue [1].

1.4. Ilmenite synthesis

$FeTiO_3$ can be synthesized under vacuum by a solid-state reaction at high temperatures above 1,200 °C. This synthesis results in large size particles and limited chemical homogeneity [34]. Among the popular techniques to synthesize $FeTiO_3$ are ball milling [35], chemical methods [36], co-precipitation [37], and the well-known sol-gel method [12, 38].

2. MATERIALS

Natural ilmenite from the Tellnes mine in Norway was used as the raw starting material *(Figure 1)*. The crystals were massive, black in color with submetallic luster and 2–4 cm in size. The preliminary photocatalytic efficiencies were determined using the aqueous solution of methylene blue (Sigma Aldrich, purity $\geq$ 95 %) as water contaminant.

Figure 1
Photomicrograph of natural ilmenite mineral

3. ANALYTICAL METHODS

3.1. Experiments

Grinding experiments were carried out in a stirred media mill (Netzsch MiniCer, Netzsch GmbH, Germany) in continuous closed-circuit mode. The liners of the grinding chamber and the stirrer rotors were made of ZrO_2 (zirconia). The circumferential tip speed of the rotor was 9.3 ms^{-1} during the experiments. Yttrium-stabilized zirconium oxide (0.6–0.8 mm) grinding media was applied. The filling ratio of the grinding media in the milling chamber was 70 v/v%. Samples were taken after 100, 180, and 240 min grinding times. Suspension samples were taken from the outflow of the pipe in which the suspension re-enters the stirrer vessel. The volumetric flow rate of the pump was $2.5e^{-05}$ m^{3}s^{-1}.

The microstructure, morphology and particle size of ilmenite were analyzed by cold field-emission scanning electron microscope (SEM), Hitachi S-4700 Type II (accelerating voltage: 10 kV). The samples for SEM measurements were attached to a carbon adhesive pad, which was fixed to an aluminum sample holder.

The crystal phase identification and primary mean crystallite size values were determined by a Rigaku MiniFlex II diffractometer equipped with a graphite monochromator and functioning with Cu-K$_\alpha$ radiation (λ = 0.15406 nm, 30 kV, 15 mA). The scanning speed was 1(2θ°) min^{-1}. The XRD measurements were recorded in the 2θ° range from 20°–50°. The mean primary crystal size values were calculated using the Scherrer equation.

A JASCO-V650 diode array computer controlled (SpectraManager Software) spectrophotometer with an integration sphere (ILV-724) was used to measure the DR spectra of the samples (λ–250–800 nm). To obtain the band-gap energy values, the well-known Kubelka-Munk approach was applied [39].

The particle size distribution of ilmenite samples was determined by a Horiba LA- 950V2 laser particle size analyzer (LPSA) in distilled water, using ultrasonic dispersing for minimum 1 min.

3.2. Photoreactor and photodegradation

The photocatalytic activity of the natural ilmenite was determined by the photodegradation of the methylene blue under UV irradiation. 170 mL of the photocatalyst dispersion ($C_{ilmenite} = 1.0$ g/L) containing methylene blue ($C_{MB} = 50$ µM) was used in the experiments. The UV photoreactor was irradiated by six fluorescent lamps (Vilber-Lourmat T-6L UV-A, 6 W power, radiation maximum at 365 nm). Preceding every experiment, the suspensions were sonicated in the dark for 10 min and during the measurements they were vigorously stirred by a magnetic stirrer. Dissolved oxygen concentration was kept constant by bubbling air through the reactor. Prior to the photocatalytic experiment's adsorption tests were conducted in the dark, under the same experimental conditions as the photocatalytic experiments, for 20 min, allowing the adsorption equilibrium to set. During the adsorption and photocatalytic tests 1.5 mL samples were taken out at specific times (adsorption sample: after 20 min, photocatalysis samples: 0, 10, 20, 30, 40, 50, 60, 80, 100, 120, 180, 240, 300, 360, 420 and 1320 min), and were centrifuged for 3 min (at 15000 rpm) and filtered with a Whatman Anotop Syringe Filter. The methylene blue concentration was determined by a SPECORD 250 PLUS UV-Vis spectrophotometer, measuring in the spectral range of $\Delta\lambda = 200–350$ nm, using a cuvette with 10 mm path length.

4. RESULTS AND DISCUSSION

4.1. Ilmenite characterization
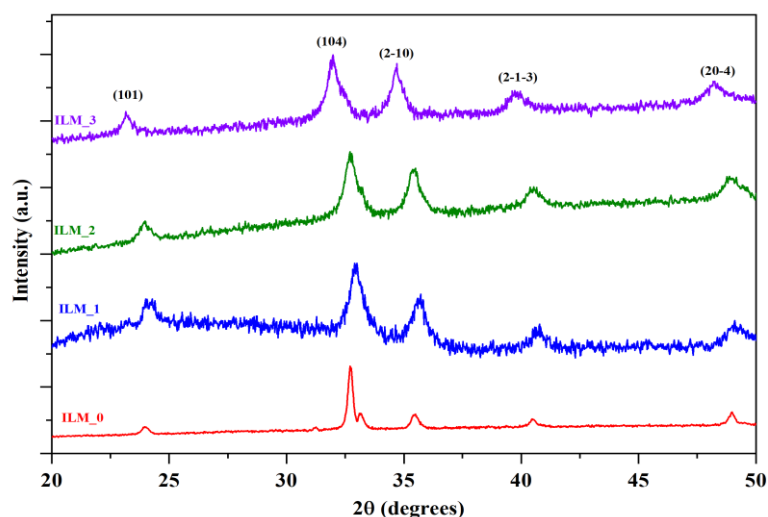
Figure 2
The XRD patterns of the natural ilmenite samples obtained after specific grinding times

The first step in the characterization of the ilmenite was to determine their crystal phase composition and particle size. The XRD patterns of the ground ilmenite *(Figure 2)* suggested a single mineral phase, namely ilmenite ($FeTiO_3$). All the diffraction peaks were attributed to ilmenite (JCPDS card No. 89-2811) and the five strongest diffraction peaks were directly identified at 23.10°, 31.90°, 34.66°, 39.70° and 48.23°, corresponding to the (101), (104), (2-10), (2-1-3) and (20-4) crystallographic planes, respectively.

The morphology and the crystal size of ground ilmenite are shown in *Figure 3*. The surface of the particles was smooth. The particle size of the ground ilmenite samples was heterogeneous in each case. After 240 min the ilmenite samples showed homogenous particles with non-specific geometry and decreased particle size, showing that the grinding time influenced the granulometric distribution of the particles. After the primary milling process, which was carried out with a classical ball mill, the average particle size determined using the SEM micrographs was ~150 μm, while after the application of stirred media milling, the primary crystallite size decreased. After 100 min the achieved crystallite size was 19.2 nm, while further significant changes were not observable with the prolongation of the grinding times *(Table 1)*.
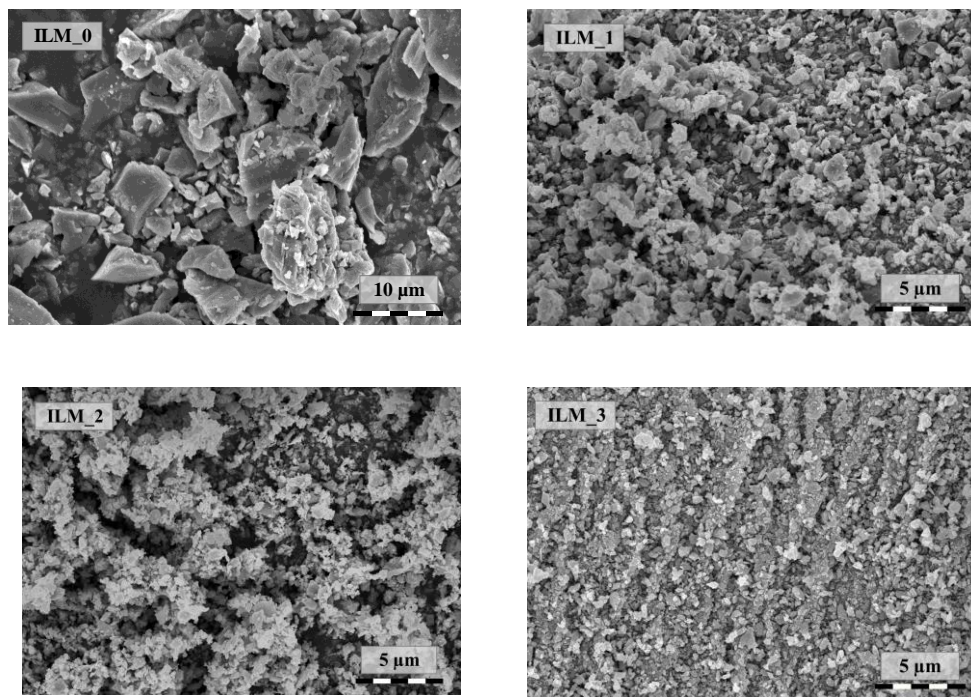
Figure 3
*Scanning electron micrographs of the natural ilmenite samples obtained
at different milling times*

Morphostructural properties of the ground ilmenite samples

Sample	Grinding time (min)	Primary crystallite size (nm)	Median crystal size (µm) from SEM micrograph	Bandgap Energy (eV)	Specific grinding energy kJ/kg	Methylene blue degradation (%)
ILM_0	0	–		–	0	0
ILM_1	100	19.20	0.56	1.36	9197.08	3.5
ILM_2	180	19.30	0.42	1.38	16554.74	19.25
ILM_3	240	18.90	0.33	1.41	22072.99	15.41

The particle size distribution of ilmenite ground materials after 0, 100, 180 and 240 min stirred media milling can be seen in *Figure 4*.
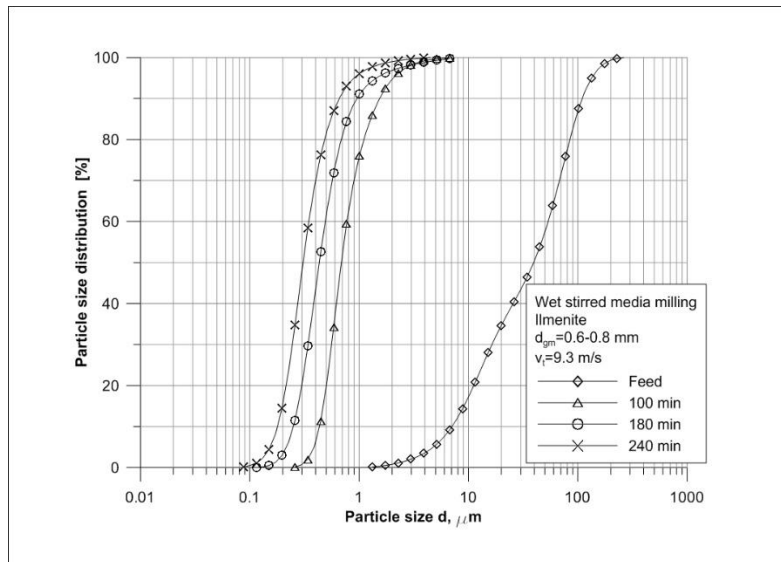
Figure 4
Particle size distribution of ilmenite ground material
after 0, 100, 180 and 240min grinding measured by LPSA

The feed material was prepared for the wet stirred media milling by pre-grinding in planetary ball mill and sieving under 106 microns. The median particle size of the feed was 39.48 µm, the particles were in the 1–100 µm size range, so the distribution was quite wide. The particle size was significantly reduced after 100 min grinding, the median particle size was 0.68 µm, and the distribution became much narrower, with the particles in the 0.2–6 µm size range. With longer milling times (180, 240) the particle size decreased continuously and the particle size distribution shifted continuously to the finer size range. The median particle size was 0.43 µm after 180 min, and 0.3 after 240 min grinding. Based on the LPSA measurement after 100 min

stirred media milling 21.3% of the ground ilmenite particles were under 0.5 μm. This value was increased to 63% after 180 min and to 82.3% after 240 min grinding. Compared to the particle size results gained by SEM measurement, these values are significantly lower.

In the starting sample (ILM_0) the following fractions were identified: ≤0.5 μm, 0.5-1 μm, 1-2 μm and ≥2 μm sized particles *(Figure 5)*. Only in the starting sample were particles identified as having ≥2 μm size (21%). The number of ≤0.5 μm sized particles increased as the duration of the milling process increased. In the starting sample the ≤ 0.5 μm sized particles were present (17%), while after 100 min of grinding this value increased even more to 72%, showing that the chosen grinding procedure is enough to increase the occurrence of nano-sized particles. After 240 the quantity of ≤ 0.5 μm sized crystals/aggregates was even higher, 98%.
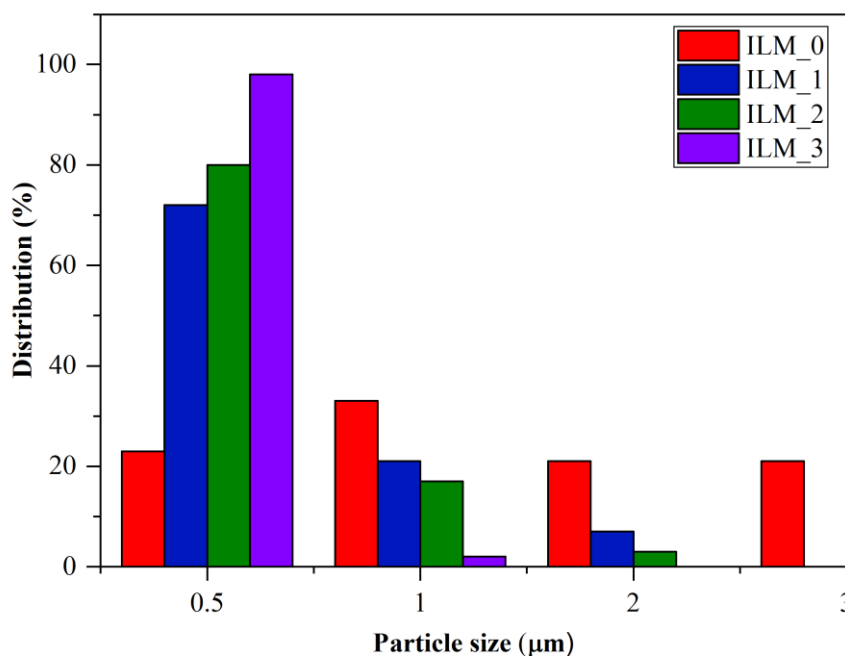
Figure 5
Particle size distribution of ground natural ilmenite particles estimated from SEM micrographs

Light absorption properties of the ground ilmenite samples were characterized by DRS measurements *(Figure 6)* and band-gap values *(Table 1)* were calculated using the Kubelka-Munk method. The band gap energies of ground ilmenite were 1.41–1.47 eV. These value were not close to the natural ilmenite band gap value, which is 2.5 eV [40]. The optical properties of ground natural ilmenite samples changed, showing a lighter color, but the evaluated band gap values did not change.
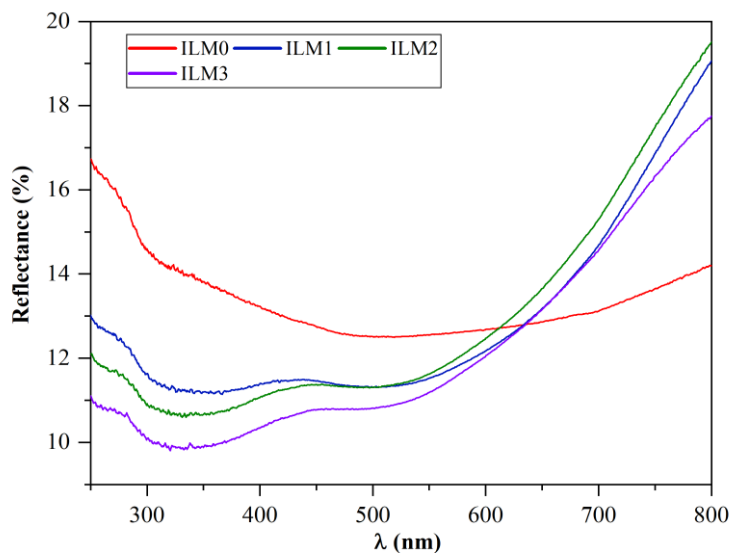
Figure 6
DRS spectra of the ilmenite samples

4.2. Degradation

Ground natural ilmenite showed photocatalytic activity in methylene blue degradation. Different ilmenite samples showed different photocatalytic activity in UV light irradiation. The highest achieved degradation yield was 19% (sample ILM_2), which is a remarkable result, considering that no chemicals were used to obtain these samples. The sample (ILM_0) that was pre-ground for nanomilling did not show any methylene blue degradation.

5. CONCLUSION

The photocatalytic performances for methylene blue degradation of ground natural ilmenite samples were examined. The minerals were ground for 100, 180, or 240 minutes. The photocatalytic efficiency of the ground natural ilmenite was investigated by performing the photocatalytic degradation of methylene blue under radiation of UV light. In the milling process, the particle size, particle size distribution and photocatalytic activity changed significantly. The 180-minute grinding time's natural ilmenite was the most efficient under UV light irradiation, degradeding 19.3% of the methylene blue in 22 h.

REFERENCES

[1] Kalantari, S., Emtiazi, G. (2016). Comparison of Ilmenite and Nano-Ilmenite for Dye Removal and Antibacterial Activities. *Journal of Nanosciences : Current Research,* 1 (1), article 1000101, 5 p.

[2] Tkaczyk, A., Mitrowska, K., Posyniak, A. (2020). Synthetic organic dyes as contaminants of the aquatic environment and their implications for ecosystems: A review. *Science of the Total Environment*, 717, pp. article 137222.

[3] Ismail, M., Akhtar, K., Khan, M. I., Kamal, T., Khan, M. A., M. Asiri, A., Seo, J., Khan, S. B. (2019). Pollution, Toxicity and Carcinogenicity of Organic Dyes and their Catalytic Bio-Remediation. *Current Pharmaceutical Design*, 25, pp. 3645–3663.

[4] Munusamy, S., Aparna, R. s.l., Prasad, R. g.s.v (2013). Photocatalytic effect of TiO_2 and the effect of dopants on degradation of brilliant green. *Sustainable Chemical Processes*, 1 (1), pp. 4.

[5] Li, G., Wang, B.-D., Sun, Q., Xu, W.-Q., Han, Y.-F. (2019). Visible-Light Photocatalytic Activity of Fe and/or Ni Doped Ilmenite Derived-Titanium Dioxide Nanoparticles. *Journal of Nanoscience and Nanotechnology*, 19, pp. 3343–3355.

[6] Shih, Y. J., Su, C. C., Chen, C. W., Dong, C. Di. (2015). Synthesis of magnetically recoverable ferrite (MFe_2O_4, M = Co, Ni and Fe)-supported TiO_2 photocatalysts for decolorization of methylene blue. *Catalysis Communications*, 72, pp. 127–132.

[7] Khan, M. M., Adil, S. F., Al-Mayouf, A. (2015). Metal oxides as photocatalysts. *Journal of Saudi Chemical Society*, 19, pp. 462–464.

[8] Nuilek, K., Memongkol, N., Niyomwas, S. (2008). Production of titanium carbide from ilmenite. *Songklanakarin Journal of Science and Technology*, 30, pp. 239–242.

[9] Samal, Sneha, Park, D. W. (2012). Nano-particle synthesis of titanium oxides from ilmenite in a thermal plasma reactor. *Chemical Engineering Research and Design*, 90, pp. 548–554.

[10] Samal, S., Rao, K. K., Mukherjee, P. S., Mukherjee, T. K. (2008). Statistical modelling studies on leachability of titania-rich slag obtained from plasma melt separation of metallized ilmenite. *Chemical Engineering Research and Design*, 86, pp. 187–191.

[11] Samal, S., Mohapatra, B. K., Mukherjee, P. S., Chatterjee, S. K. (2009). Integrated XRD, EPMA and XRF study of ilmenite and titania slag used in pigment production. *Journal of Alloys and Compounds*, 474, pp. 484–489.

[12] Chen, Y. H. (2011). Synthesis, characterization and dye adsorption of ilmenite nanoparticles. *Journal of Non-Crystalline Solids*, 357, pp. 136–139.

[13] Morosin, B., Baughman, R. J., Ginley, D. S., Butler, M. A. (1978). The influence of crystal structure on the photoresponse of iron–titanium oxide electrodes. *Journal of Applied Crystallography*, 11, pp. 121–124.

[14] Ye, F., Ohmori, A., Li, C. (2004). New approach to enhance the photocatalytic activity of plasma sprayed TiO_2 coatings using p-n junctions. *Surface and Coatings Technology*, 184, pp. 233–238.

[15] Pandey, R. K., Sunkara, S., Muthusami, J. (1996). Crystal growth and characterization of an oxide semiconductor (ilmenite) for novel electronic devices. *AIP Conference Proceedings*, 193, pp. 193–198.

[16] Edwards, R., Atkinson, K. (2013). *Ore deposit geology and its influence on mineral exploration*. Springer, [Place of publication not identified].

[17] Tao, T., Chen, Y., Zhou, D., Zhang, H., Liu, S., Amal, R., Sharma N., Glushenkov A. M. (2013). Expanding the Applications of the Ilmenite Mineral to the Preparation of Nanostructures : TiO_2 Nanorods and their Photocatalytic Properties in the Degradation of Oxalic Acid. *Chem. Eur. J.*, 19, pp. 1091–1096., doi:10.1002/chem.201202451.

[18] Szakáll, S., Udubasa, G., Ďuďa, R., Kvasnytsya, V., Koszonska., E., Novák, M. (2002). *Minerals of the Carpathians*. Granit publ., Prague, 479 p.

[19] Popescu, G. (1967). Asupra raporturilor structurale dintre mineralele metalice şi nemetalice din zăcământul Bălan. [On the structural relations of metallic and nonmetallic minerals from Bălan deposit]. *Revista Minelor*, 18, pp. 537–541.

[20] Petrulian, N., Steclaci, L., Oroveanu, F. (1971) ,"Studium mineralogic al minereului de la Bălan [Mineralogical investigation of the Bălan mineralization]. *Studii Cercetării Geologie, Geofizică şi Geographie, Serie. Geoogie*, 16, pp. 343–352.

[21] Ianovici, V. (1934). Étude sur le massif syénitique de Ditrau, région Jolotca distr. Ciuc (Transylvania). *Rev. Muz.., Univ. Cluj*, 4, pp. 1–53.

[22] Constantinescu, E., Anastasiu, N., Pop, N., Garbaşevski, N. (1983). Contributions á la connaissance des aspects paragénétiques de la minéralisation associée au massif alkalin de Ditrău. *Anuarul Institutul de Geologie si Geofizica*, 62, pp. 91–101.

[23] Pál-Molnár, E. (2000). Hornblendites and diorites of the Ditró Syenite Massif, Department of Mineralogy, Geochemistry and Petrology, University of Szeged, Szeged.

[24] Tang, X., Zhao, B. Y., Hu, K. A. (2006). Preparation of M-Ba-ferrite fine powders by sugar-nitrates process. *Journal of Materials Science*, 41, pp. 3867–3871.

[25] Krishen, K. (1994). *Dual-use space technology transfer conference and exhibition : proceedings of a conference and exhibition held at Lyndon* B. Johnson Space Center, Houston, Texas, February 1–3, 1994, in: National Aeronautics and Space Administration, [Place of publication not identified].

[26] Ribeiro, R. A. P., Camilo, A., de Lazaro, S. R. (2015). Electronic structure and magnetism of new ilmenite compounds for spintronic devices: $FeBO_3$ (B = Ti, Hf, Zr, Si, Ge, Sn). *Journal of Magnetism and Magnetic Materials*, 394, pp. 463–469.

[27] Lind, F., Berguerand, N., Seemann, M., Thunman, H. (2013). Ilmenite and nickel as catalysts for upgrading of raw gas derived from biomass gasification. *Energy and Fuels*, 27, pp. 997–1007.

[28] García-Muñoz, P., Pliego, G., Zazo, J. A., Bahamonde, A., Casas, J. A. (2016). Ilmenite ($FeTiO_3$) as low cost catalyst for advanced oxidation processes. *Journal of Environmental Chemical Engineering*, 4, pp. 542–548.

[29] Sheffield (2017). *Mineral sand market*. Available from: <http://www.554shef fieldresources.com.au/irm/content/mineral-sand-market.aspx?RID=385>.

[30] Tan, L. (2016). Asia buyers may switch to non-China TiO_2 after price surge. May 30. Website of ICIS. https://www.icis.com/explore/resources/news/ 2016/05/30/10002752/asia-buyers-may-switch-to-non-china-tio2-after-price-surge/.

[31] Lee, R. Bin, Lee, K. M., Lai, C. W., Pan, G., Yang, T. C. K., Juan, J. C. (2018). The relationship between iron and Ilmenite for photocatalyst degradation. *Advanced Powder Technology*, 29 (8), pp. 1779–1786.

[32] Moctezuma, E., Zermeño, B., Zarazua, E., Torres-Martínez, L. M., García, R. (2011). Photocatalytic Degradation of Phenol with Fe-Titania Catalysts. *Topics in Catalysis*, 54, pp. 496–503.

[33] Pataquiva-Mateus, A. Y., Zea, H. R., Ramirez, J. H. (2017). Degradation of Orange II by Fenton reaction using ilmenite as catalyst. *Environmental Science and Pollution Research*, 24, pp. 6187–6194.

[34] Ohara, S., Sato, K., Tan, Z., Shimoda, H., Ueda, M., Fukui, T. (2010). Novel mechanochemical synthesis of fine $FeTiO_3$ nanoparticles by a high-speed ball-milling process. *Journal of Alloys and Compounds*, 504, pp. 17–19.

[35] Tao, T., Glushenkov, A. M., Liu, H., Liu, Z., Dai, X. J., Chen, H., Ringer, S. P., Chen, Y. (2011). Ilmenite $FeTiO_3$ Nanoflowers and their Pseudo-capacitance. *The Journal of Physical Chemistry C*, 115, pp. 17297–17302.

[36] Mona, J., Kale, S. N., Gaikwad, A. B., Murugan, A. V. Ravi, V. (2006). Chemical methods to synthesize FeTiO3 powders. *Materials Letters*, 60, pp. 1425–1427.

[37] Yan, S., Ge, S., Qiao, W., Zuo, Y. (2010). Synthesis of ferromagnetic semiconductor $0.67FeTiO_3$–$0.33Fe_2O_3$ powder by chemical co-precipitation. *Journal of Magnetism and Magnetic Materials*, 322, pp. 824–826.

[38] Raghavender, A. T., Hoa Hong, N., Joon Lee, K., Jung, M.-H., Skoko, Z., Vasilevskiy, M., Cerqueira, M. F., Samantilleke, A. P. (2013). Nano-ilmenite $FeTiO_3$: Synthesis and characterization. *Journal of Magnetism and Magnetic Materials*, 331, pp. 129–132.

[39] Kubelka, P., Munk, F. (1931). Ein Beitrag Zur Optik Der Farbanstriche", *Zeitschrift Für Technische Physik*, 12, pp. 593–601.

[40] Wilson, N. C., Muscat, J., Mkhonto, D., Ngoepe, P. E., Harrison, N. M. (2005). Structure and properties of ilmenite from first principles. *Physical Review B – Condensed Matter and Materials Physics*, 71, pp. 1–9.

SOIL BIOREMEDIATION: A METHANOGENIC HYDROCARBON BIODEGRADER CONSORTIUM IN SOIL CONTAMINATED WITH DIESEL OIL AT GROUNDWATER LEVEL

K. LACZI[1] – J. M. SHUME[1] – A. BODOR[3] – N. BOUNEDJOUM[1] – T. KOVÁCS[4] – K. PEREI[1,2] – G. RÁKHELY[1,2,3]

[1]*Department of Biotechnology, Faculty of Science and Informatics; University of Szeged*
[2]*Institute of Environmental and Technological Sciences, University of Szeged;*
[3]*Institute of Biophysics, Biological Research Centre,*
Hungarian Academy of Sciences, Szeged;
[4]*Department of Biotechnology, Nanophagetherapy Center,*
Enviroinvest Corp., Pécs, Hungary

Abstract: Hydrocarbons are among the most frequent contaminants all over the globe. Because of their toxicity and recalcitrant properties, hydrocarbons have severe effects on the environment. In soil, hydrocarbon contaminations change the microbial compositions and hydrocarbon biodegraders usually emerge. Biodegradation of hydrocarbon pollutants is much more efficient under aerobic than microaerophilic or anaerobic conditions. Nevertheless, a substantial amount of contaminants occur in the anaerobic zone provoking a big challenge for environmental scientists. In this study, we investigated a weathered hydrocarbon contaminated site at the military base of Taszár, Hungary. We monitored 4 sampling sites (F1–F4) in 3 different depths (0.8–1 m, 5.5–5.8 m, 7.5–7.8 m). Total petrol hydrocarbon (TPH) measurements showed that the majority of the contaminations occurred at groundwater level (7.5 m). *Syntrophaceae* was the predominant microbial family in these contaminated zones, although microbes belonging to other hydrocarbon degrader families, *Commamonadaceae* and *Anaerolineaceae*, were also present. Acetoclastic methanogenic archaea such as the members of *Methanothrichaceae* could also be detected, which can convert acetic acid derived from hydrocarbon biodegradation into methane. Interestingly, at 5.5–5.8 m, the zones are inhabited by aerobic hydrocarbon biodegraders above the highly contaminated sections. We propose that this layer serves as a filter for volatile compounds.

Keywords: Hydrocarbons, soil bioremediation, methanogenesis, syntrophy

1. INTRODUCTION

Petrochemical products are the basis of modern society. From fossil fuels to plastics, crude oil-derived products are part of our daily life. The extensive usage of hydrocarbons makes them one of the most frequent contaminant groups. Hydrocarbon pollution poses a serious threat to the environment and human health. Hydrocarbons instantaneously interact with and change the properties of the environment. In soil, toxic hydrocarbon compounds impede the biogeochemical networks and decrease plant productivities. Biodiversity also decreases in hydro-

carbon-contaminated habitats [1]. Innate microorganisms can adapt to pollutions and eliminate them via a process called natural attenuation [2, 3]. A large number of bacterial groups have been identified as hydrocarbon degraders. Several metabolic pathways have also been described – for both aerobic and anaerobic - hydrocarbon mineralization [4–6]. In oxygen-limited deeper soil layers, the microbes have to utilize alternative electron acceptors, for example nitrate, ferric ion or sulfate. In the absence of electron acceptors, anaerobic hydrocarbon biodegradation can also be coupled to methanogenesis [7–10]. Methanogenic archaea utilize acetic acids derived from the hydrocarbon biodegradation for generating methane. This process can promote the energy recovery from organic pollutants. Under anaerobic conditions, hydrocarbon biodegradation is a slow process, since it is usually limited by the availability of electron acceptors and nutrients. Natural attenuation can be enhanced by various bioremediation methods such as biostimulation. In this case, nutrients and electron acceptors are introduced to the polluted area. Besides the physico-chemical parameters of soils, the composition of the microbial communities has a substantial impact on the efficacy of bioremediation processes. Metagenomic analysis of soils prior to remediation will provide insight into the composition and interactions of the local microbial community. In this study, our aims were to examine the microbial community of an area contaminated with diesel fuel and to identify the key components of the natural bioconversion processes.

2. MATERIALS AND METHODS

2.1. Sampling

Samples were taken from diesel oil contaminated soil of an abandoned military base in Taszár, Hungary. The military base was used by the Hungarian Army between 1936–1995 and then by US forces until 2004. Hydrocarbon contaminations have been there for many years. There were three sampling sites in the vicinity of two contamination sources. F1 was near a leaky underground fuel container, F2 was close to an above-ground fuel tank and F4 was at the edge of the contamination zone caused by the underground container. F3 was outside the base and served as a control sampling site. The GPS coordinates of the sampling sites were the following: F1: 46°22'37.1"N   17°53'52.1"E, F2: 46°22'36.6"N 17°53'48.4"E, F3: 46°22'35.5"N 17°53'49.3"E and F4: 46°22'36.5"N 17°53'51.4"E. Samples were taken at 3 depths: 0.8–1 m, 5.5–5.8 m, 7.5–7.8 m (groundwater level, which could be observed during sampling) with a petrol earth auger. Soil samples were collected from a 30 cm portion in the middle of a drill head spiral of approximately 100 cm length.

2.2. Total petrol hydrocarbon measurement

The TPH concentration of soil samples was measured by a Wilks InfraCal TPH/TOG analyzer as instructed by the manufacturer. TPH calibration was performed with diesel oil.

2.3. DNA extraction from the samples

DNA was extracted with the QIAGEN DNeasy PowerMax Soil Kit (QIAGEN N.V. Venlo, The Netherlands). All purifications were performed in triplicate except for F4 samples, which were done in duplicate.

2.4. DNA library preparation and sequencing

The libraries were prepared with Nextera XT DNA Library Preparation kit (Illumina Inc., USA). Paired-end sequencing of the libraries was carried out on the Illumina MiSeq next-generation sequencing platform (Illumina Inc.) using MiSeq reagent kit V3 with 2×300 cycles (Illumina Inc.).

2.5. Bioinformatical methods

All analyses were carried out on Debian GNU/Linux (version 4.19.67-2) platform. Sequencing reads were quality trimmed with Trimmomatic version 0.39 [11] with the following parameters: TRAILING:2, SLIDINGWINDOW:50:18, MINLEN:100. For taxonomic evaluation of the data, Kaiju 1.7.3 [12] and Diamond 0.9.29 were applied using the NCBI non-redundant protein database. The diamond alignment was meganized with MEGAN MetaGenome Analyzer Community Edition 6.18.5 [13]. MEGAN was used for cluster analysis of the samples with the Weighted Uniform UniFrac method [14].

2.6. Sample deposition

Raw sequencing reads were deposited into the EMBL-ENA MGnify database under the MGYS00001198 project ID.

3. RESULTS AND DISCUSSION

3.1. Total petrol hydrocarbon measurements

Analyzing the TPH concentrations of the samples revealed that a vast majority of the contamination was present at groundwater level (7.5–7.8 m). F2 samples from this depth had the highest TPH concentration: 4,414 ppm ± 443.7 ppm (Table 1). In addition, control samples at groundwater level also contained hydrocarbons, 213.6 ± 16.1 ppm, which was slightly above the threshold limit value. This can be explained by the relatively short distance between the F2 and F3 points (approx. 40 m). It is likely that some contaminants have reached the F3 point during the years. However, the measurement technique is based on infrared spectroscopy and measures C-H bonds in the molecule, therefore organic compounds other than hydrocarbons could give signals. This conception was also supported by GC/MS measurements (data not shown) of the samples. Hydrocarbon contamination could be measured only in F1, F2, F4 samples at 7.5 m depth by GC/MS. Hence, we considered the 7.5 m depth of these sampling points as the contaminated zones and measurements around 100 ppm as noise.

Depth	TPH concentration (ppm)			
	F1	**F2**	**F3**	**F4**
0.8–1 m	89.2 ± 22.9	106.3 ± 17.3	113.3 ± 28.6	76.4 ± 28.6
5.5–5.8 m	109.0 ± 16.6	89.1 ± 26.9	93.7 ± 28.0	91.9 ± 43.8
7.5–7.8 m	868.2 ± 53.8	4414.5 ± 443.7	213.6 ± 16.1	483.8 ± 125.3

3.2. Metagenomic analysis
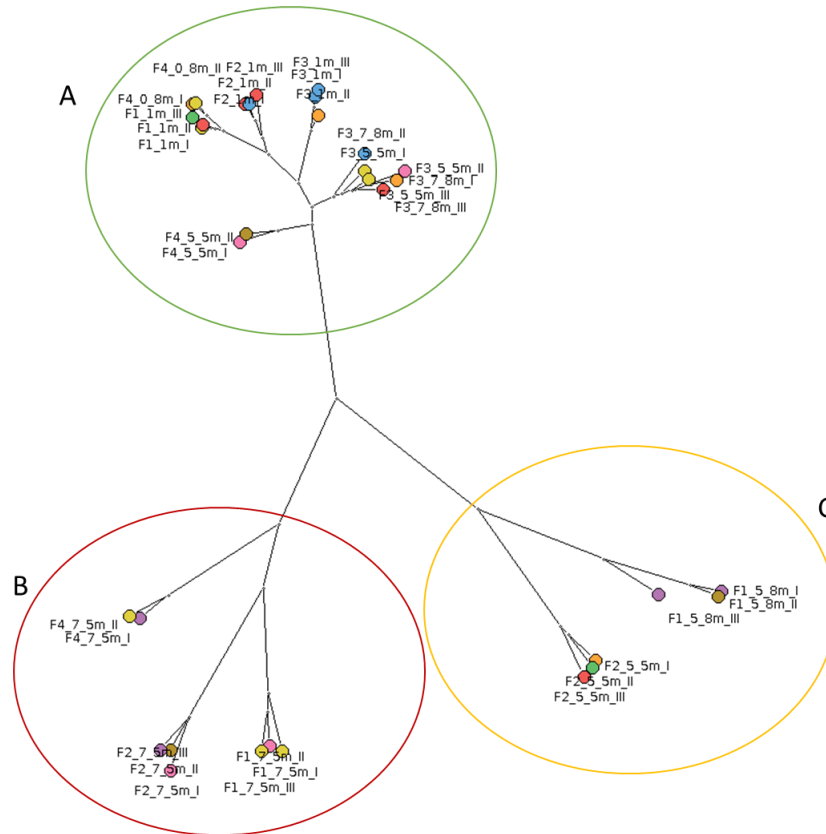
Figure 1
Neighbour-joining tree of the samples based on Weighted UniFraq distance matrix. Group A: samples from 0.8-1 m depth of all sampling points, 5.5 m and 7.8 m samples from the uncontaminated F3 point and 5.5 m samples from the F4 sampling point. Group B: All contaminated samples at 7.5 m depth; Group C: 5.5–5.8 m samples from the highly contaminated F1 and F2 sampling points

Preliminary metagenomic analyses were performed to disclose the composition of the microbial communities in the samples. Sequence read pairs were generated, and after quality trimming, 95.59% of the reads with an average length of 253.3 bp remained. Based on the cluster analysis, the samples are grouped into 3 different clusters *(Figure 1)*.

All samples are clustered together with their corresponding parallels. The grouping of the samples correlates with the concentrations of the contaminations. The 7.5 m samples, where hydrocarbons are present in high concentrations, form an individual group *(Figure 1B)*. The 5.5–5.8 m samples of F1 and F2 are clustered in a distinct group (*Figure 1*, C cluster). Even though the hydrocarbon concentration is around the threshold limit value in these samples, the contaminated zones have substantial effects on the compositions of their microbial communities at 2 m above the pollutions. On the other hand, the 5.5 m samples of F4 are not in the C cluster. In the 7.5–7.8 m samples of F4, the hydrocarbon concentration is much lower relative to those of F1 and F2. Therefore, in F4, the contaminated zone has no apparent effect on the microbial community composition in the soil layers above the contaminated zone (7.5–7.8 m).

Group A is more diverse than the other two groups *(Figure 1A)*. This group can be divided into two subgroups. The first subgroup contains all the samples taken from 0.8–1 m. The slight differences between these samples might be due to the distinct location of the sampling points on the field. The F1 and F4 samples are the closest neighbours (only 22 m distance), so they are clustered together while F2 (approx. 80 m away from F1) and F3 (approx. 77 m away from F1) samples diverge slightly from the group. The second subgroup contains the 5.5 m and 7.8 m samples from the uncontaminated control F3. In the absence of contamination, the variations in the microbial compositions at 5.5 m and 7.8 m are not significant. The F4 5.5 m samples are close to this cluster due to the lower contamination level at this zone.

Microbial composition varies among the contaminated and other samples. There are microbial groups that are completely missing from the hydrocarbon-contaminated samples, while other taxons emerge as a result of long-term exposure to hydrocarbons. The number of the otherwise predominant family, *Streptomycetaceae*, shows a strong decrease in the hydrocarbon-contaminated samples. *Nitrospiraceae* and *Mycobacteriaceae and Nocardiaceae* show similar tendencies. The most abundant family in the contaminated samples is *Syntrophaceae (Table 2)*. Few members of this family are known as hydrocarbon degraders [15]. These microorganisms are able to live in syntrophy with methanogenic archaea and thus such a consortium can convert hydrocarbons into methane [15–17]. Methanogenic archaea are also present in the contaminated samples at 7.5 m; *Methanothrichaceae* is the most abundant family *(Table 2)*. The members of this family are obligate acetoclastic methanogens and are often found in hydrocarbon-degrading consortia [18, 19]. Another acetoclastic methanogenic family is present in the contaminated samples, the *Methanoregulaceae (Table 2)*. This methanogenic family can also be found in association with hydrocarbon pollutants [10, 20]. The presence of *Syntro-*

phaceae and methanogenic archaea in the 7.5 m samples indicates a strict anaerobic environment and methanogenesis- coupled hydrocarbon degradation.

Table 2

Relative incidences of the most abundant microbes in the polluted zones

Family	Relative incidences in samples (%)					
	F1		F2		F4	
	5.5–5.8 m	7.5–7.8 m	5.5–5.8 m	7.5–7.8 m	5.5–5.8 m	7.5–7.8 m
Syntrophaceae		9.94		11.92		3.78
Anaerolineaceae		1.60		5.19		2.03
Commamonadaceae	10.19	2.66	13.50	9.42		
Methanothrichaceae		3.42		2.23		0.83
Methanoregulaceae		1.66		4.92		0.52

Another family that shows elevated abundance only in the contaminated zone is the obligate anaerobic *Anaerolineaceae (Table 2)*. This family is a member of the phylum *Chloroflexi*. Members of this family can be frequently found in hydrocarbon-contaminated environments in soil and sediments. However, their role in hydrocarbon biodegradation remains unclear [21–25].

The *Commamonadaceae* family was also detected in higher abundance in the contaminated zones, but only in the F1 and F2 samples (2.66% and 9.42%). Members of this family are associated with the biodegradation of aromatics [26]. Interestingly, this family is also present in the 5.5–5.8 m samples of these two sampling points. In the 5.8 m samples of F1 and F2, *Comamonadaceae* is predominant alongside with *Bradyrhzobiaceae* with 10.19% and 13.50% incidences, respectively. The latter also have members, inluding the genus *Afipia,* capable of degrading aromatics [27, 28]. The aromatic compounds of low molecular weight are volatile and might migrate to the upper layers of the soil. This phenomenon can also explain the substantial effect of the contaminated zones on the microbial composition of F1 and F2 5.5–5.8 m samples (*Figure 1*, cluster) even though the concentrations of the pollutions are around the detection limit.

Families including *Commamonadaceae*, *Erythrobacteraceae*, *Immundisolibacteraceae*, *Xanthomonas*, *Rhodocyclaceae*, *Sinobacteraceae*, and *Sphingomonadaceae* found in the 5.5-5.8 m samples of the F1 and F2 sites can also be associated with - mainly with aromatic - hydrocarbon biodegradation [29–37]. These data also imply the presence of aromatic compounds in the 5.5 m soil layer located above the contaminated zones. The microorganisms found in this layer use oxygenase enzymes to oxidize hydrocarbons foreshadowing the presence of oxygen in this layer. *Methylocystis* spp. are aerobic methanotroph microorganisms, which use methane monooxygenase to oxidate methane to methanol [38]. The presence of the *Methylocystaceae* in the 5.5–5.8 m layer in F1, F2 and F4 samples supports the active methanogenesis in the 7.5 m layer of the corresponding sampling points. Thus, the methane produced by the methanogenic archaea in the contaminated zone is utilized by *Methylocystis* in the 5.5–5.8 m layer.

4. CONCLUSION

The examination of the hydrocarbon-polluted site of the former military base of Taszár showed that the contamination had a radical effect on the microbial composition of the contaminated zone. At groundwater level (7.5–7.8 m) of the sites, anaerobic zones are formed where the anaerobic hydrocarbon biodegraders belonging to *Syntrophaceae* family are the dominant microbes alongside with the members of the *Commamonadaceae, Anaerolineaceae* and *Methanotrichaceae* families. Our results suggest that these microorganisms might live in syntrophy leading to active conversion of hydrocarbons to methane. This methanogenesis can be utilized in microbial enchanced energy recovery [39, 40]. Similarly to landfill gas management, the methane can be collected from the contaminated zone and used to reduce the costs of the intervention.

The high hydrocarbon concentrations in the contaminated zones strongly influenced the microbial composition of the zones above them at 5.5–5.8 m depth. In these zones, mainly aerobic hydrocarbon biodegraders are dominant, suggesting the seeping of volatile contaminants into this zone and the unexpected presence of oxygen. The 5.5–5.8 m zone might function as a filter preventing the volatile compounds from moving into the upper soil layers. Understanding the microbial interactions and metabolical pathways involved in the bioconversion could improve the efficiency of the bioremediation and lower intervention costs.

REFERENCES

[1]   Abbasian. F., Lockington, R., Megharaj, M., Naidu, R. (2016). The Biodiversity Changes in the Microbial Population of Soils Contaminated with Crude Oil. *Curr Microbiol*, 72, pp. 663–670.

[2]   Marić, N., Matić, I., Papić, P., Beškoski, V. P., Ilić, M., Gojgić-Cvijović, G., Miletić, S., Nikić, Z., Vrvić, M. M. (2018). *Natural attenuation of petroleum hydrocarbons — a study of biodegradation effects in groundwater (Vitanovac, Serbia)*. Environ Monit Assess, 190.

[3]   Truskewycz, A., Gundry, T. D., Khudur, L. S., Kolobaric, A., Taha, M., Aburto-Medina, A., Ball, A. S., Shahsavari, E. (2019). *Petroleum hydrocarbon contamination in terrestrial ecosystems — fate and microbial responses*. Molecules. MDPI AG.

[4] Fuchs, G., Boll, M., Heider, J. (2011). Microbial degradation of aromatic compounds — from one strategy to four. *Nat Rev Microbiol.*, 9, pp. 803–816.

[5] Wilkes, H., Buckel, W., Golding, B. T., Rabus, R. (2016). Metabolism of Hydrocarbons in n-Alkane-Utilizing Anaerobic Bacteria. *J Mol Microbiol Biotechnol*, 26, pp. 138–151.

[6] van Beilen, J. B., Funhoff, E. G. (2005). Expanding the alkane oxygenase toolbox: new enzymes and applications. *Curr Opin Biotechnol*, 16, pp. 308–314.

[7] Chang, W., Um, Y., Holoman, T. R. P. P. (2006). Polycyclic Aromatic Hydrocarbon (PAH) Degradation Coupled to Methanogenesis. *Biotechnol Lett*, 28, pp. 425–430.

[8] Jones, D. M., Head, I. M., Gray, N. D., Adams, J. J., Rowan, A. K., Aitken, C. M., Bennett, B., Huang, H., Brown, A., Bowler, B. F. J., Oldenburg, T., Erdmann, M., Larter, S. R. (2008). Crude-oil biodegradation via methanogenesis in subsurface petroleum reservoirs. *Nature*, 451, pp. 176–180.

[9] Zhu, X, Campanaro, S, Treu, L, Seshadri, R, Ivanova, N, Kougias, PG, Kyrpides, N, Angelidaki, I. (2020). Metabolic dependencies govern microbial syntrophies during methanogenesis in an anaerobic digestion ecosystem. *Microbiome*, 8, 22.

[10] Siddique, T., Semple, K., Li, C., Foght, J. M. (2020) Methanogenic biodegradation of iso-alkanes and cycloalkanes during long-term incubation with oil sands tailings. *Environ Pollut*, 258, p. 113768.

[11] Bolger, A. M., Lohse, M., Usadel, B. (2014). Trimmomatic: A flexible trimmer for Illumina sequence data. *Bioinformatics*, 30, pp. 2114–2120.

[12] Menzel, P., Ng, K. L., Krogh, A. (2016) Fast and sensitive taxonomic classification for metagenomics with Kaiju. *Nat Commun.*, 7, pp. 1–9.

[13] Huson, D. H., Beier, S., Flade, I., Górska, A., El-Hadidi, M., Mitra, S., Ruscheweyh, H. J., Tappu, R. (2016). MEGAN Community Edition – Interactive Exploration and Analysis of Large-Scale Microbiome Sequencing Data. PLoS Comput Biol, 12.

[14] Lozupone, C. A., Hamady, M., Kelley, S.T., Knight, R. (2007). Quantitative and qualitative β diversity measures lead to different insights into factors that structure microbial communities. *Appl Environ Microbiol.*, 73, pp. 1576–1585.

[15] Gray, N. D., Sherry, A., Grant, R. J., Rowan, A. K, Hubert, C. R. J-, Callbeck, C M., Aitken, C. M., Jones, D. M., Adams, J. J., Larter, S. R., Head, I. M. (2011). The quantitative significance of Syntrophaceae and

syntrophic partnerships in methanogenic degradation of crude oil alkanes. Environ Microbiol., 13, pp. 2957–2975.

[16] Berdugo-Clavijo, C., Gieg, L. M. (2014). Conversion of crude oil to methane by a microbial consortium enriched from oil reservoir production waters. *Front Microbiol*, 5.

[17] Wawrik, B., Marks, C. R., Davidova, I. A., McInerney, M. J., Pruitt, S., Duncan, K. E., Suflita, J. M., Callaghan, A. V. (2016). Methanogenic paraffin degradation proceeds via alkane addition to fumarate by *'Smithella'* spp. mediated by a syntrophic coupling with hydrogenotrophic methanogens. *Environ Microbiol*, 18, pp. 2604–2619.

[18] Cheng, L., Shi, S. bao, Yang, L., Zhang, Y., Dolfing, J., Sun, Y-g., Liu, L-y., Li, Q., Tu, B., Dai, L-rg., Shi, Q., Zhang, H. (2019). Preferential degradation of long-chain alkyl substituted hydrocarbons in heavy oil under methanogenic conditions. *Org Geochem*., 138, p. 103927.

[19] Sierra-Garcia, I. N., Belgini, D. R. B., Torres-Ballesteros, A., Paez-Espino, D., Capilla, R., Santos Neto, E. V., Gray, N., de Oliveira, V. M. (2020). In depth metagenomic analysis in contrasting oil wells reveals syntrophic bacterial and archaeal associations for oil biodegradation in petroleum reservoirs. *Sci Total Environ*, 715, p. 136646.

[20] Li, X., Li, Y., Zhang, X., Zhao, X., Sun, Y., Weng, L., Li, Y. (2019). Long-term effect of biochar amendment on the biodegradation of petroleum hydrocarbons in soil microbial fuel cells. *Sci Total Environ*., 651, pp. 796–806.

[21] Akbari, A., Ghoshal, S. (2015). Effects of diurnal temperature variation on microbial community and petroleum hydrocarbon biodegradation in contaminated soils from a sub-Arctic site. *Environ Microbiol*., 17, pp. 4916–4928.

[22] Peng, M., Zi, X., Wang, Q. (2015). Bacterial Community Diversity of Oil-Contaminated Soils Assessed by High Throughput Sequencing of 16S rRNA Genes. *Int J Environ Res Public Health*, 12, pp. 12002–12015.

[23] Sherry, A., Gray, N. D., Ditchfield, A. K., Aitken, C. M., Jones, D. M., Röling, W. F. M., Hallmann, C., Larter, S. R., Bowler, B. F. J., Head, I. M. (2013). Anaerobic biodegradation of crude oil under sulphate-reducing conditions leads to only modest enrichment of recognized sulphate-reducing taxa. *Int Biodeterior Biodegrad*, 81, pp. 105–113.

[24] Bruckberger, M. C,. Morgan, M. J., Bastow, T. P., Walsh, T., Prommer, H., Mukhopadhyay, A., Kaksonen, A. H., Davis, G. B., Puzon, G. J. (2020). Investigation into the microbial communities and associated crude oil-contamination along a Gulf War impacted groundwater system in Kuwait. *Water Res.*, 170, p. 115314.

[25] Júlio, A. D. L., de Cássia Mourão Silva, U., Medeiros, J. D., Morais, D. K., dos Santos, V. L. (2019). Metataxonomic analyses reveal differences in aquifer bacterial community as a function of creosote contamination and its potential for contaminant remediation. *Sci Rep.*, 9, pp. 1–14.

[26] Aburto, A., Peimbert, M. (2011). Degradation of a benzene-toluene mixture by hydrocarbon-adapted bacterial communities. *Ann Microbiol.*, 61, pp. 553–562.

[27] Al-Awadhi, H, Al-Mailem, D, Dashti, N, Hakam, L, Eliyas, M, Radwan, S. (2012). The abundant occurrence of hydrocarbon-utilizing bacteria in the phyllospheres of cultivated and wild plants in Kuwait. *Int Biodeterior Biodegrad*, 73, pp. 73–79.

[28] Lafortune, I., Juteau, P., Déziel, E., Lépine, F., Beaudet, R., Villemur, R. (2009). Bacterial diversity of a consortium degrading high-molecular-weight polycyclic aromatic hydrocarbons in a two-liquid phase biosystem. *Microb Ecol*, 57, pp. 455–468.

[29] Purohit, H. J., Dayananda, S., Prashant, P. (2019). Microbe-Assisted Biodegradation, Bioremediation and Metabolic Engineering. *Proc Indian Natn Sci Acad*, 85, pp. 963–983.

[30] Harwati, T. U., Kasai, Y., Kodama, Y., Susilaningsih, D., Watanabe, K. (2007). Characterization of Diverse Hydrocarbon-Degrading Bacteria Isolated from Indonesian Seawater. *Microbes Environ.*, 22, pp. 412–415.

[31] Corteselli, E. M., Aitken, M. D., Singleton, D. R. (2017). Description of Immundisolibacter cernigliae gen. Nov., sp. nov., a high-molecular-weight polycyclic aromatic hydrocarbondegrading bacterium within the class Gammaproteobacteria, and proposal of Immundisolibacterales ord. nov. and Immundisolibacteraceae fam. nov. *Int J Syst Evol Microbiol.*, Microbiology Society, Volume 67, Issue 4.

[32] Corteselli, E. M., Aitken, M. D., Singleton, D. R. (2017). Rugosibacter aromaticivorans gen. Nov., sp. nov., a bacterium within the family Rhodocyclaceae, isolated from contaminated soil, capable of degrading aromatic compounds. *Int J Syst Evol Microbiol.*, 67, pp. 311–318.

[33] Wang, L., Wang, W., Lai, Q., Shao, Z. (2010). Gene diversity of CYP153A and AlkB alkane hydroxylases in oil-degrading bacteria isolated from the Atlantic Ocean. *Environ Microbiol*, 12, pp. 1230–1242.

[34] Posman, K. M., DeRito, C. M., Madsen, E. L. (2017). Benzene degradation by a Variovorax species within a coal tar-contaminated groundwater microbial community. *Appl Environ Microbiol.*, 83.

[35] Patel, V., Cheturvedula, S., Madamwar, D. (2012). Phenanthrene degradation by Pseudoxanthomonas sp. DMVP2 isolated from hydrocarbon

contaminated sediment of Amlakhadi canal, Gujarat, India. *J Hazard Mater.*, 201–202, pp. 43–51.

[36] Jeon, C. O., Park, M., Ro, H. S., Park, W., Madsen, E. L. (2006). The naphthalene catabolic (nag) genes of Polaromonas naphthalenivorans CJ2: Evolutionary implications for two gene clusters and novel regulatory control. *Appl Environ Microbiol.*, 72, pp. 1086–1095.

[37] Mattes, T. E., Alexander, A. K., Richardson, P. M., Munk, A. C., Han, C. S., Stothard, P., Coleman, N. V. (2008). The genome of Polaromonas sp. strain JS666: Insights into the evolution of a hydrocarbon- and xenobiotic-degrading bacterium, and features of relevance to biotechnology. *Appl Environ Microbiol*, 74, pp. 6405–6416.

[38] Baani, M., Liesack, W. (2008). Two isozymes of particulate methane monooxygenase with different methane oxidation kinetics are found in Methylocystis sp. strain SC2. *Proc Natl Acad Sci U S A*, 105, pp 10203–10208.

[39] Gieg, L. M., Duncan, K. E., Suflita, J. M. (2008). Bioenergy production via microbial conversion of residual oil to natural gas. *Appl Environ Microbiol.*, 74, pp. 3022–3029.

[40] Gray, N. D., Sherry, A., Hubert, C., Dolfing, J., Head, I. M. (2010). *Methanogenic degradation of petroleum hydrocarbons in subsurface environments: Remediation, heavy oil formation, and energy recovery*. In Advances in Applied Microbiology (book series Edited by Allen I. Laskin, Sima Sariaslani, Geoffrey M. Gadd), 72, pp. 137–161. Academic Press Inc.

ISOLATION OF HYDROCARBONOCLASTIC BACTERIA FROM OILY WASTES AND THEIR PILOT APPLICATION FOR WATER AND SOIL DECONTAMINATION

ATTILA BODOR[1, 2, 3] – SÁNDOR MÉSZÁROS[1] – PÉTER PETROVSZKI[1] –
GYÖRGY ERIK VINCZE[1] – NAILA BOUNEDJOUM[1, 2] –
KRISZTIÁN LACZI[1] – GÁBOR RÁKHELY[1, 2, 3] – KATALIN PEREI[1, 2]

[1]*Department of Biotechnology, University of Szeged, Szeged, Hungary*
[2]*Institute of Environmental and Technological Sciences,*
University of Szeged, Szeged, Hungary
[3]*Institute of Biophysics, Biological Research Centre, Szeged, Hungary*

Abstract: Excessive consumption of petroleum products carries the risk that these toxic chemicals enter and accumulate in the environment via transportation, usage or improper storage, thus hazarding natural habitats or human health. Bioremediation is a cost-effective and environmentally friendly technique that involves the use of microorganisms or plants in order to neutralize environmental pollutants. Considering that bacteria occur not only in aqueous but even in oil phases, intermediates, by-products or wastes can pose hidden reservoirs of effective microbial degraders with potential application in oil bioremediation. Using mazut (a residual fuel oil from atmospheric distillation of crude oil) as an origin matrix, thirteen bacterial strains were isolated. The best performing strains, identified as *Rhodococcus* sp. PAE1 and *Rhodococcus* sp. PAE8, were able to degrade structurally variant hydrophobic compounds (including hexadecane, cooking oil, mazut or lubricant oil) in aqueous systems. Thus, they were used in further small-scale soil/groundwater experiments in order to model the bioremediation process of a local ares exposed to years lubricant oil pollution. Our study represents a targeted tool for the bioremediation of oil-polluted aquatic and terrestrial environments and revealed that oily wastes can be considered as valuable sources of new hydrocarbon-utilizing isolates.

Keywords: bioremediation, mazut, hexadecane, hydrocarbon-utilizing

1. INTRODUCTION

Since hydrophobic organic compounds pose serious risks to natural communities or human health, pollution of soils and waters by petroleum products or other oil-related compounds are still among the major environmental concerns that humankind must cope with. Petroleum products can enter into the environment through accidental oil spills or reckless human activity [1–5]. Areas close to vehicle traffic or where handling and maintenance operations of vehicles take place are considered to be particularly vulnerable, since the probability of contamination inevitably increases [6].

Mazut is a residual fuel oil from the atmospheric distillation process of crude oil [7]. It is a viscous mixture of hydrocarbons with high carbon number, PAHs, resins and cycloalkanes, often having complex structure with high heavy metal and sulfur content. These properties make mazut cumbersome for both biodegradation and further refining [7–8]. Nonetheless, mazut can be further processed by vacuum distillation in order to produce diesel oils, base oils, lubricants and heavy fuel oils [9]. Lubricant oils (LOs) are widely used for reducing friction in the engines of motorized vehicles such as cars, motorcycles or locomotives. Therefore, used lubricant oils (ULOs), containing long-chain hydrocarbons, additives and heavy metals, are considered widespread, hazardous pollutants and hence potential targets for environmental rehabilitation processes [10–12]. Several physicochemical and biological waste management techniques are available for neutralizing oil-related pollutants in the environment but most of these methods still need further developments [13–15]. Bioremediation utilizes the degradative capability of plants and/or microorganisms for the decontamination of polluted environments [16–19]. As an environmentally sound and cost-effective approach, it is considered to be one of the most promising rehabilitation technologies [16–18].

Bacterial communities occur in aqueous and even in oil phases [20]. Thus, isolation and examination of bacterial strains with the ability to degrade hydrocarbons from these oily environments can provide a promising tool for biological remediation and also a better understanding of the microbial community structure and in oil-polluted niches.

The aim of this study was to provide useful tools for the bioremediation of aqueous and terrestrial environments polluted by petrochemical products. To this end, isolation from mazut was carried out to gain new isolates with the ability to degrade petrochemicals and hydrophobic organic compounds, even if they have as high structural complexity as mazut and LOs do.

2. EXPERIMENTAL

2.1. Bacterial strains

Hydrocarbonoclastic bacteria were isolated from mazut using liquid minimal medium. Pure strains were selected, characterized [21] and tested for hydrocarbon biodegradation. The two most effective strains – PAE1 and PAE8 – were identified according to their 16S rDNA gene homology [22].

2.2. Biodegradation tests in aqueous systems

The best performing *Rhodococcus* sp. PAE1 strain was used in subsequent biodegradation tests performed in aqueous systems. Pollution of hydrophobic compounds was modelled by hexadecane, representing easily biodegradable *n*-alkanes; cooking oil, representing a wide-spread contaminant in municipal sewage; and mazut for a complex hydrocarbon mixture that is hard to biodegrade. All vials were capped and respiration activities were monitored by gas chromatography (GC). At the end of

the experiments, the remaining contaminants were extracted with diethyl ether or chloroform and then bioconversion (B%) values were calculated using gas chromatography coupled to mass spectrometry (GC-MS) and/or gravimetric data and applying the following equation [23]: $B\% = [(Contaminants_{cell-free\ samples}-Contaminants_{inoculated\ samples})/Contaminants_{cell-free\ samples}]x100$. Data are expressed as mean $\pm$ SE (standard error). Statistical significance was analyzed using one-way analysis of variance (ANOVA) followed by Duncan's test.

2.3. Small-scale *ex situ* soil bioremediation tests

The most effective hexadecane-degrader *Rhodococcus* sp. PAE1 and *Rhodococcus* sp. PE8 strains were tested for LO biodegradation and then used in small-scale soil experiments in order to model the bioremediation process of a long-time ULO-polluted area. Soil samples from a local ULO-polluted site were used to construct *ex situ* soil microcosms in order to model various bioremediation approaches. Rehabilitation treatments included biostimulation (BS, 30% soil moisture was set with the addition of minimal medium, which contained soluble, inorganic nutrients, such as nitrogen and phosporus) and bioaugmentation combined with biostimulation (BAS, in addition to biostimulation, oil-degrader *Rhodococcus* sp. PAE1 or *Rhodococcus* sp. PAE8 strains were introduced into the polluted soil at an inoculation level of 10^9 cells per gram soil). Non-treated control (NTC) samples represented a natural loss in the ULO-concentration. All samples were incubated for 40 days. All ULO-polluted soil microcosms were closed and respiration activities were monitored by gas chromatography (GC) for 30 days. The headspaces of the vials were refreshed every two days to maintain proper aeration. At the end of the experiments, the remaining ULOs were extracted with carbon disulfide as solvent. The extracts were analyzed with an infrared oil-measuring equipment to determine the concentration of total petrol hydrocarbons (TPHs). Bioconversion (B%) was calculated applying the following equation: $B\%=[(TPH_{non-treated\ soil}-TPH_{treated\ soil})/TPH_{non-treated\ soil}]x100$. Data are expressed as mean $\pm$ SE (standard error). Statistical significance was analyzed using one-way analysis of variance (ANOVA) followed by Duncan's test.

3. RESULTS AND DISCUSSION

3.1. Bacterial strains

Using mazut as an origin matrix, thirteen pure bacterial strains were isolated (one of them was pathogenic, thus, it was omitted from further experiments). The most important physiological and biochemical characteristics of all strains were determined. Data are summarized in *Table 1*.

Preliminary experiments revealed that eleven strains out of thirteen were able to utilize hexadecane as sole carbon and energy source (data not shown). After sequencing the 16S rDNA gene of the best hexadecane-utilizing strains PAE1 and PAE8, both of them were identified as members of the genus *Rhodococcus*, so in

further experimental works, the name *Rhodococcus* sp. PAE1 and *Rhodococcus* sp. PAE8 were used. *Rhodococci* play an important role in environmental and industrial biotechnology [23–27].

Table 1

Physiological and biochemical characteristics of the newly isolated bacterial strains

Characteristics	PAE1	PAE3	PAE4	PAE5	PAE6	PAE7	PAE8	PAE9	PAE10	PAE11	PAE12	PAE13
Gram staining	+	+	+	+	+	+	+	+	+	+	+	+
Cell length (µm)	2.48 ±0.3	2.09 ±0.33	1.94 ±0.26	1.95 ±0.27	0.77 ±0.12	1.91 ±0.13	1.87 ±0.24	2.09 ±0.19	2.08 ±0.22	1.96 ±0.20	1.97 ±0.24	1.90 ±0.16
Indole production	–	–	–	–	–	–	–	–	–	–	–	–
Hemolytic activity	–	–	–	–	–	–	–	–	–	–	–	–
Catalase activity	+	+	+	+	+	+	+	+	+	+	+	+
Casease activity	–	–	–	–	–	–	–	–	–	–	–	–
Lipase activity	+	+	+	+	+	+	+	+	+	+	+	+
Urease activity	–	–	–	–	–	–	–	–	–	–	–	–
Beta- galactosidase activity	–	–	–	–	–	–	–	–	–	–	–	–
Nitrate/nitrite reduction	w	w	w	w	–	w	w	w	w	w	w	w
Startch hydrolysis	–	–	–	–	–	–	–	–	–	–	–	–
Methyl red-test	–	–	–	–	–	–	–	–	–	–	–	–
Oxidation/ fermentation (OF) test	w	w	w	w	+	w	w	w	w	w	w	w
Tween 80 hydrolysis	+	+	+	+	–	+	+	–	–	–	+	+

3.2. Biodegradation tests in aqueous systems

Respiration activity of *Rhodococcus* sp. PAE1 was investigated in liquid mineral medium, artificially contaminated with 1% (m v^{-1}) of various hydrophobic pollutants. Three hydrophobic compounds were used as sole carbon and energy source: hexadecane represented the *n*-alkanes, cooking oil was used as a common contaminant in municipal sewages, and mazut represented the original isolation matrix of the new strain. According to the obtained results *(Figure 1)*, microbial activity decreased with the increasing structural complexity of the available substrates.

At the end of the incubation, the remaining amount of hydrophobic organic substrates was evaluated and bioconversion values were calculated for each carbon sources *(Figure 2)*. Coinciding with CO_2 measurements, bioconversion also decreased when a structurally more complex carbon source was available. Our results suggest that this newly isolated strain can be a targeted tool for the biodegradation of petroleum products in polluted waters.
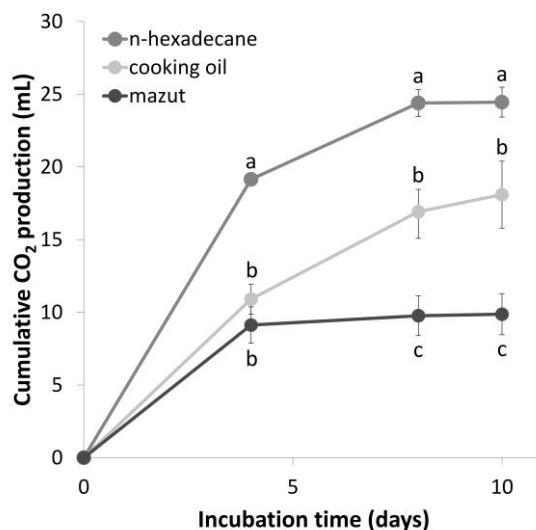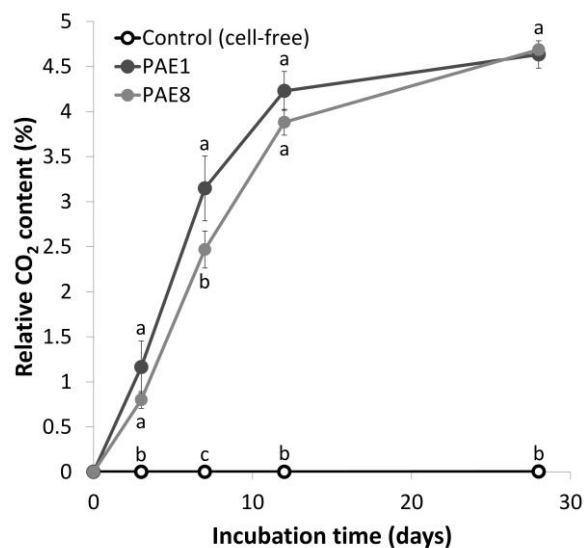
Figure 1

Cumulative CO_2 production of Rhodococcus sp. PAE1 in liquid mineral medium artificially contaminated with 1% (m v^{-1}) of various hydrophobic compounds. Different letters in the same incubation time represent a significant difference at P ≤ 5 (n = 3).
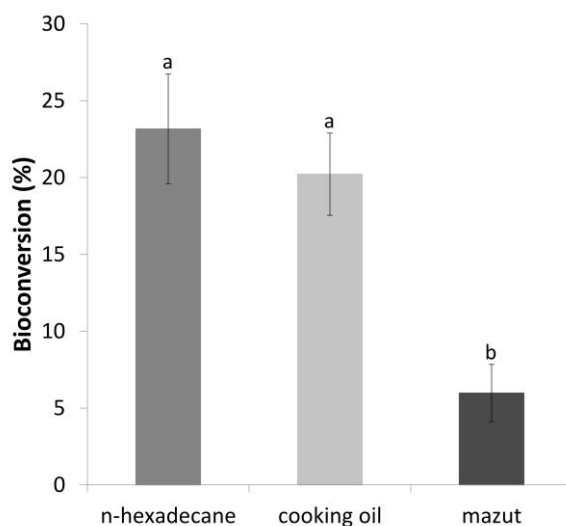
Figure 2

Bioconversion of 1% (m v^{-1}) n-hexadecane, cooking oil and mazut by Rhodococcus sp. PAE1 in liquid mineral medium. Different letters represent a significant difference at P ≤ 5 (n = 3).

Since *Rhodococcus* sp. PAE1 and *Rhodococcus* sp. PAE8 exhibited the highest respiration activities in preliminary experiments (data not shown) and *Rhodococcus* sp. PAE1 proved to be able to utilize structurally diverse hydrophobic compounds *(Figure 2)*, both strains were tested for lubricant oil biodegradation in liquid mineral medium. 1% (m v^{-1}) fresh LO was used as sole carbon and energy source. Aerobic biodegradation of hydrocarbons by hydrocarbonoclastic bacteria consumes oxygen alongside with the release of carbon-dioxide [28]. Thus, increasing relative CO_2 content was considered as an indirect measure of the microbial degradation of LO in the closed vials *(Figure 3)*.

Figure 3
Relative CO_2 content in the headspaces of the closed vials containing liquid mineral medium artificially contaminated with 1% (m v^{-1}) fresh lubricant oil. Different letters in the same incubation time represent a significant difference at $P \leq 5$ (n = 3).

Based on our results, *Rhodococcus* sp. PAE1 and *Rhodococcus* sp. PAE8 were able to utilize fresh LO as their sole carbon and energy source at a similar rate, thus, both strains can be potentially applied not only for water decontamination but even for modelling the bioremediation of a local ULO-polluted area.

3.3. Small-scale *ex situ* soil bioremediation tests

Respiration activity of ULO-polluted soil microcosms was followed with gas chromatography. According to the CO_2 production *(Figure 4)*, even NTC samples were active in respiration, indicating the presence of metabolically active microbiome in ULO-polluted soil. Respiration activity and thus microbial activity could be

increased by the supplementation of inorganic nutrients in BS samples. The most active respiration was observed in the soil samples inoculated with *Rhodococcus* sp. PAE1 (BAS_PAE1) and *Rhodococcus* sp. PAE8 (BAS_PAE8). Nevertheless, evolution of CO_2 in a hydrocarbon-polluted soil cannot be considered as sole evidence of hydrocarbon biodegradation due to the plentiful availability of organic matters and the compositional complexity of the soil matrix.
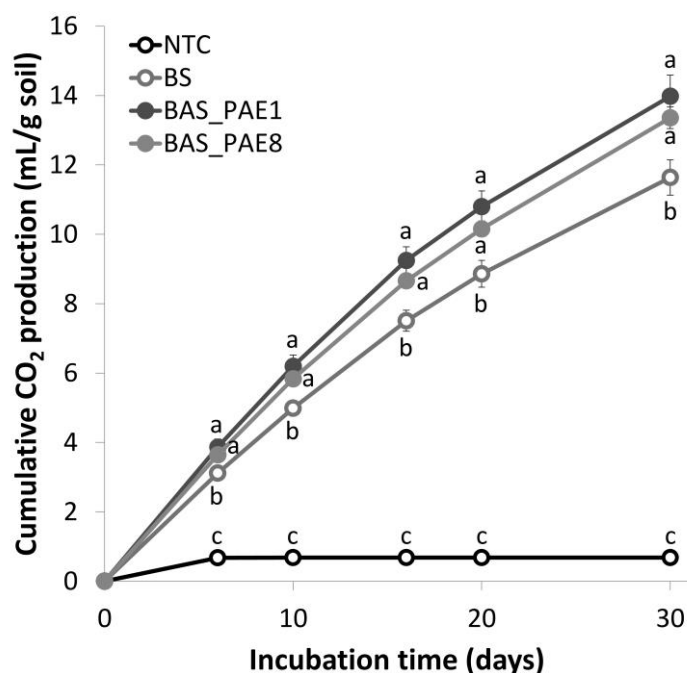
Figure 4

Cumulative CO₂ production in ULO-polluted soil microcosms
(NTC: non-treated control soil, BS: biostimulation, BAS_PAE1:
biostimulation+bioaugmentation using Rhodococcus sp. PAE1, BAS_PAE8:
biostimulation+bioaugmentation using Rhodococcus sp. PAE8).
Different letters in the same incubation time represent a significant difference
at P ≤ 5 (n = 3).

At the end of the experiment, remaining ULOs were extracted and TPH concentrations were evaluated in order to calculate TPH bioconversions in soil microcosms *(Figure 5)*. A considerable level of TPH bioconversion was observed in the biostimulated samples (BS), indicating the natural occurrence of ULO-degrading microorganisms even in heavily contaminated environments. Moreover, introduction of the newly isolated *Rhodococcus* sp. PAE1 and *Rhodococcus* sp. PEA8 significantly enhanced the TPH bioconversion to 38% and 40%, respectively.
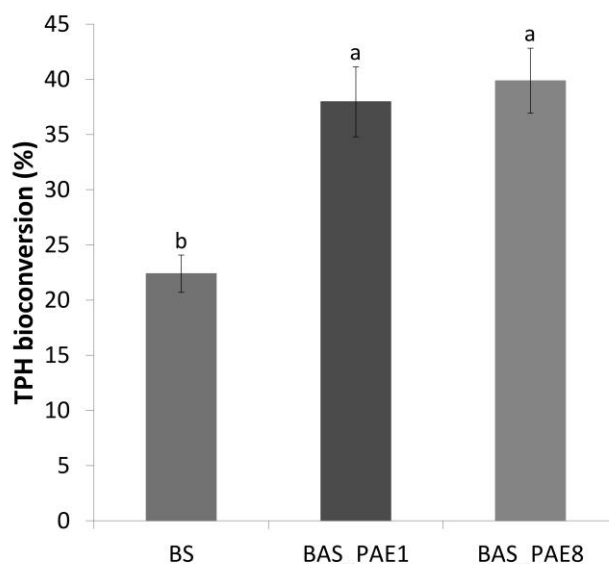
Figure 5
TPH bioconversion in ULO-polluted soil microcosms after 40 days of incubation
(BS: biostimulation, BAS_PAE1: biostimulation+bioaugmentation using
Rhodococcus sp. PAE1, BAS_PAE8: biostimulation+bioaugmentation using
Rhodococcus sp. PAE8). Different letters represent a significant difference
at $P \leq 5$ ($n \geq 15$).

4. CONCLUSION

Since bacterial communities occur in aqueous and even in oil phases, we hypothesized that oily wastes or by-products can provide undiscovered microbial degraders. Based on this assumption, 13 bacterial strains were isolated from mazut. The best performing hydrocarbon-utilizing isolates were identified as members of the genus *Rhodococcus* and assigned as *Rhodococcus* sp. PAE1 and *Rhodococcus* sp. PAE8. Despite the structural differences and complexities, *Rhodococcus* sp. PAE1 was able to utilize *n*-hexadecane, cooking oil and even mazut in liquid minimal medium. Further testing of *Rhodococcus* sp. PAE1 and *Rhodococcus* sp. PAE8 in aqueous systems showed that both strains were capable of LO biodegradation, and potentially applicable for ULO-polluted soil decontamination. Thus, ULO-polluted soil microcosms were constructed and then submitted to various biological treatments in order to model and evaluate options for the bioremediation of a long-term ULO-polluted site. Bioaugmentation with *Rhodococcus* sp. PAE1 or PAE8 significantly decreased the pollutant concentration compared to biostimulation. Although optimal conditions for the biodegradation are barely revealed and still need further

development, our results represent a targeted tool for the bioconversion of petroleum contaminants in aqueous and terrestrial environments. Additionally, this work highlights the fact that oily wastes and by-products can be potential sources of yet-to-be isolated hydrocarbonoclastic bacteria.

REFERENCES

[1]   Al Shami, A., Harik, G., Alameddine, I., Bruschi, D., Garcia, D.A., El-Fadel, M. (20179. Risk assessment of oil spills along the Mediterranean coast: A sensitivity analysis of the choice of hazard quantification. *Science of the Total Environment,* 574, pp. 234–245.

[2]   Alrumman, S. A., Standing, D. B., Paton, G. I. (2015), Effects of hydrocarbon contamination on soil microbial community and enzyme activity. *Journal of King Saud University-Science*, 27 (1), pp. 31–41.

[3]   Nikolopoulou, M., Pasadakis, N., Kalogerakis, N. (2013). Evaluation of autochthonous bioaugmentation and biostimulation during microcosm-simulated oil spills. *Marine Pollution Bulletin*, 72 (1), pp.165–173.

[4]   Nikolopoulou, M., Pasadakis, N., Norf, H., Kalogerakis, N. (2013). Enhanced ex situ bioremediation of crude oil contaminated beach sand by supplementation with nutrients and rhamnolipids. *Marine Pollution Bulletin*, 77 (1–2), pp. 37–44.

[5]   Fernández-Luqueño, F., Valenzuela-Encinas, C., Marsch, R., Martínez-Suárez, C., Vázquez-Núñez, E., Dendooven, L. (2011). Microbial communities to mitigate contamination of PAHs in soil—possibilities and challenges: a review. *Environmental Science and Pollution Research*, 18 (1), pp. 12–30.

[6]   Odjegba, V. J., Sadiq, A. O. (2002). Effects of spent engine oil on the growth parameters, chlorophyll and protein levels of *Amaranthus hybridus* L. *Environmentalist*, 22 (1), pp. 23–28.

[7]   Khorasani, A. C., Mashreghi, M., Yaghmaei, S. (2013). Study on biodegradation of Mazut by newly isolated strain *Enterobacter cloacae* BBRC10061: improving and kinetic investigation. *Iranian Journal of Environmental Health Science & Engineering*, 10 (1), p. 2.

[8]   Beškoski, V. P., Gojgić-Cvijović, G., Milić, J., Ilić, M., Miletić, S., Šolević, T., Vrvić, M. M. (2011). *Ex situ* bioremediation of a soil contaminated by

mazut (heavy residual fuel oil)–A field experiment. *Chemosphere*, 83 (1), pp. 34–40.

[9] Guo, B., Lyons, W. C., Ghalambor, A. (eds.) (2007). Petroleum Production Engineering: A Computer-assisted Approach. Elsevier, Gulf Professional Publishing, p. 312., https://doi.org/10.1016/B978-0-7506-8270-1.X5000-2.

[10] Lee, S. H., Lee, S., Kim, D. Y., Kim, J. G. (2007). Degradation characteristics of waste lubricants under different nutrient conditions. *Journal of Hazardous Materials*, 143 (1–2), pp. 65–72.

[11] Meeboon, N., Leewis, M. C., Kaewsuwan, S., Maneerat, S., Leigh, M. B. (2017). Changes in bacterial diversity associated with bioremediation of used lubricating oil in tropical soils. *Archives of Microbiology*, 199 (6), pp. 839–851.

[12] Lee, S. H., Ji, W., Kang, D. M., Kim, M. S. (2018). Effect of soil water content on heavy mineral oil biodegradation in soil. *Journal of Soils and Sediments*, 18 (3), pp. 983–991.

[13] Chmielewska, E., Nussbaum, M. T., Szytenchelm, R. (1997). An attempt to implement soil washing for central-europe cleanup activities. *Chemické listy*, 91 (6), pp. 438–443.

[14] Jones, D. A., Lelyveld, T. P., Mavrofidis, S. D., Kingman, S. W., Miles, N. J. (2002). Microwave heating applications in environmental engineering — a review. *Resources, Conservation and Recycling*, 34 (2), pp. 75–90.

[15] Paria, S. (2008). Surfactant-enhanced remediation of organic contaminated soil and water. *Advances in colloid and interface science*, 138 (1), pp. 24–58.

[16] Vidali, M. (2001). Bioremediation: an overview. *Pure and Applied Chemistry*, 73 (7), pp. 1163–1172.

[17] Fuentes, S., Méndez, V., Aguila, P., Seeger, M. (2014). Bioremediation of petroleum hydrocarbons: catabolic genes, microbial communities, and applications. *Applied Microbiology and Biotechnology*, 98 (11), pp. 4781–4794.

[18] Kang, J. W. (2014). Removing environmental organic pollutants with bioremediation and phytoremediation. *Biotechnology Letters*, 36 (6), pp. 1129-1139.

[19] Kis, Á. E., Laczi, K., Zsíros, S., Kós, P., Tengölics, R., Bounedjoum, N., Kovács, T., Rákhely, G., Perei, K. (2017). Characterization of the Rhodococcus sp. MK1 strain and its pilot application for bioremediation of diesel oil-contaminated soil. *Acta Microbiologica et Immunologica Hungarica*, 64 (4), pp. 463–482.

[20] Meckenstock, R. U., von Netzer, F., Stumpp, C., Lueders, T., Himmelberg, A. M., Hertkorn, N., Schmitt-Kopplin, P., Harir, M., Hosein, R., Haque, S.

Schulze-Makuch, D. (2014). Water droplets in oil are microhabitats for microbial life. *Science*, 345 (6197), pp. 673–676.

[21] Cowan, S.T. (2003). Cowan and Steel's Manual for the Identification of Medical Bacteria. Cambridge University Press.

[22] Dastager, S. G., Mawlankar, R., Tang, S. K., Krishnamurthi, S., Ramana, V. V., Joseph, N., Shouche, Y. S. (2014). *Rhodococcus enclensis* sp. nov., a novel member of the genus Rhodococcus. *International Journal of Systematic and Evolutionary Microbiology*, 64 (8), pp. 2693–2697

[23] Kis, Á., Laczi, K., Zsíros, S., Rákhely, G., Perei, K. (2015). Biodegradation of animal fats and vegetable oils by *Rhodococcus erythropolis* PR4. *International Biodeterioration & Biodegradation*, 105, pp. 114–119.

[24] Kis, Á. E., Laczi, K., Zsíros, S., Kós, P., Tengölics, R., Bounedjoum, N., Kovács, T., Rákhely, G., Perei, K. (2017). Characterization of the *Rhodococcus* sp. MK1 strain and its pilot application for bioremediation of diesel oil-contaminated soil. *Acta Microbiologica et Immunologica Hungarica*, 64 (4), pp. 463–482.

[25] Amoroso, M. J., Benimeli, C. S. and Cuozzo, S. A. (eds.) (20013). *Actinobacteria: application in bioremediation and production of industrial enzymes.* Boca Raton, USA, CRC Press.

[26] Alvarez, H. M. ed. (2010). *Biology of Rhodococcus*. Springer-Verlag, Berlin–Heidelberg.

[27] de Carvalho, C. C., Wick, L. Y. and Heipieper, H. J. (2009). Cell wall adaptations of planktonic and biofilm *Rhodococcus erythropolis* cells to growth on C5 to C16 n-alkane hydrocarbons. *Applied Microbiology and Biotechnology*, 82 (2), pp. 311–320.

[28] Rojo, F. (2009). Degradation of alkanes by bacteria. *Environmental Microbiology*, 11 (10), pp. 2477–2490.

THE EFFECTS OF SEWAGE SLUDGE DEPOSITION ON ECOSYSTEM CARBON EXCHANGE PROCESSES: POSSIBILITIES OF MODEL-BASED ASSESSMENTS

M. KISS[1] – K. BARTA[2] – Á. GULYÁS[1] – E. KRAJCSI[1] – A. FARSANG[2]

[1]*Department of Climatology and Landscape Ecology, University of Szeged, H-6722*
[2]*Department of Physical Geography and Geoinformatics, University of Szeged, H-6722*
Szeged, Egyetem u. 2. Hungary

Abstract: The growing interest in the concept of the circular economy calls for methodological development in several fields of environmental research and management. Life cycle analysis needs an integrated accounting of different production and waste treatment processes, which is the case also for carbon footprint calculations. If the aim is the assessment of sewage sludge utilization, model-based approaches are needed, because of the high number and the complex character of the related ecosystem processes. Our study gives a short overview of the actual background of this field, together with raising some methodological aspects of the relevant model development efforts. Owing to the detailed technical regulations, the industrial parts of the process can be relatively easily modeled, while the agricultural deposition of sewage sludge needs the use of the toolset of ecophysiological modeling. The main methodological aspects of integrated (technical-ecological) modeling are the following. As the agricultural management practices strongly affect the greenhouse gas exchange processes, models are preferred that represent these aspects in the parameterization. Spatially distributed models are suitable for a number of related decision-making processes. In general, the methodological elements of simplified performance assessments of other relevant fields have to be taken into consideration, together with the practical experiences of similar complex modeling systems (e.g. agricultural production and greenhouse gas).

Keywords: life cycle approach, sewage sludge deposition, ecosystem carbon exchange, ecophysiological model

1. INTRODUCTION

Contemporary environmental problems, especially global climate change, call for integrated efforts to mitigate the effects and to achieve sustainable solutions in every economic sector. One reasons for this is the complexity of the affected geoecological systems: the behavior of different ecosystems in situations such as rising temperatures or different agricultural management interventions is not always known. On the other side, almost every part of the agricultural or industrial processes has some effects on the greenhouse gas balance. These facts have led to the emergence of the concept of the circular economy, and the need for life cycle analyses as a type of

environmental assessment tool, and in a wider sense, as a new approach in environmental management. The circular economy describes an economic system that is based on business models which replace the "end-of-life" concept with reducing, reusing, recycling, and recovering materials in production/distribution and consumption processes, operating on different scales [1]. One method for its practical implementation is the life cycle assessment, which is an overall environmental analysis of products and services, through the life cycle from raw material extraction to waste treatment.

These developments have high relevance in the field of sewage sludge utilization. It can be considered a leading implementation of the concept, as due to the general availability of municipal wastewater treatment, millions of metric tons of dry matter are generated every year in the European Union [2]. Despite the strict regulations of the countries, the usage of sewage sludge in agriculture and for energy generation has an increasingly important role in the relevant sectors. Following this, there is a need for integrated experimental analyses of the different utilization possibilities, in a circular economy context and with the aim to be as applicable to other places and similar cases as possible [3].

A life cycle analysis of sewage sludge utilization focuses on the agricultural usage and the carbon footprint of the process, but the effects of the deposition on the carbon exchange processes of the agroecosystem also have to be investigated. For these types of assessments, model-based approaches can have a leading role. There are several reasons and cases in environmental sciences and applications where modeling provides a good solution, and sometimes the only solution. The complexity of the analyzed ecological systems (or their connections with industrial processes) might call for a simplified description, which is one of the main added values of models of complex systems [4]. Moreover, in the case of the development of such methods, which are intended to be widely usable in practice (in engineering, impact assessments, etc.), automated or mostly automated processes are advantageous, possibly with user-friendly software solutions. The multiscale character of environmental processes can also be handled in modeling approaches [5]. Therefore, we consider it important to develop model-based assessment methods to help carbon footprint estimations of sewage sludge disposal and related industrial and agricultural activities. Based on that, our aim is to provide a short review of the literature of modeling possibilities of this chain of activities, including the agricultural utilization. Then we raise and discuss some points on model choice and other methodological aspects, focusing on the sludge disposal's secondary effects on biogeochemical processes of agroecosystems. Our work is part of a wider project aiming at the holistic assessment of sustainability aspects of sewage sludge utilization. This paper serves as supporting material for a detailed, site-specific model-based assessment, based on the methodological background presented here.

2. MODELLING GREENHOUSE GAS FLUXES IN WASTEWATER AND SEWAGE SLUDGE TREATMENT PROCESSES AND AGROECOSYSTEMS

As the value chain of wastewater management consist mostly of carefully planned and regulated technical processes, calculations related to external effects (like greenhouse gas emissions) might be considered easier to make. It can be said that following the technical developments and the relevant policy initiatives, the modeling of the carbon footprint in this case has gone through the classical stages of model development. The first known quantitative connections make the development of empirical models and equation sets possible. One example for that is the set of IPCC Guidelines [6], which play an important role in the development of the scientific/technical background and the practical applications in this field. Later, based on the results of further research and experiences from practical applications, more complex process-based models have been developed [7], sometimes with user-friendly software implementations. The GestaBoues Tool (developed in France) takes into account direct, indirect and avoided emissions [8]. The BEAM calculator tool (Biosolids Emissions Assessment Model – (developed for Canadian circumstances) uses spreadsheets, which are suitable for general use by many municipalities [9]. And, following the widespread use and the popularity of life cycle assessments, a number of targeted software tools have been introduced for interested companies of different sectors, most of which are suitable for investigating the sewage sludge processing and end use (e.g. SimaPro, GaBi). The growing amount of modeling experience and results form a foundation for comparative assessments of relevant management alternatives [10]. However, large discrepancies could be found in the selection of the environmental emissions to be included in the life cycle assessments, or how they were estimated in the analysis [11]. This is especially true for the agricultural use of sewage sludge, as it is connected to complex agroecosystems. For them, the effects of different management options are not clarified totally, and the functioning of the system needs its own specific modeling framework.

Because of the above-mentioned aspects, there are several models of different subtargets and model complexities, which aim at assessing the greenhouse gas fluxes of different agricultural forms, under different management practices and different climatic circumstances. Agroecosystems are relatively well-studied because of the need for productivity estimations. But it has also been true for this field that the development of targeted models and software tools many times needed some new, primary (mostly field-based) results to add some missing parts. The challenges of modeling carbon exchange processes lie in the multi-domain character of the system. The results on the core process, the primary production of vegetation, are modified by several factors: the autotrophic and heterotrophic respiration serve as a source of carbon output. There is also the need for a clear distinction between the carbon input or output processes of the soil and the total ecosystem, and for the calculation of the effects of different agricultural management interventions. The subprocesses, which are ideally incorporated in the greenhouse gas balance models of ecosystems, can be seen in the architecture of the Biome-BGC model, which will be discussed later *(Figure 1)*.
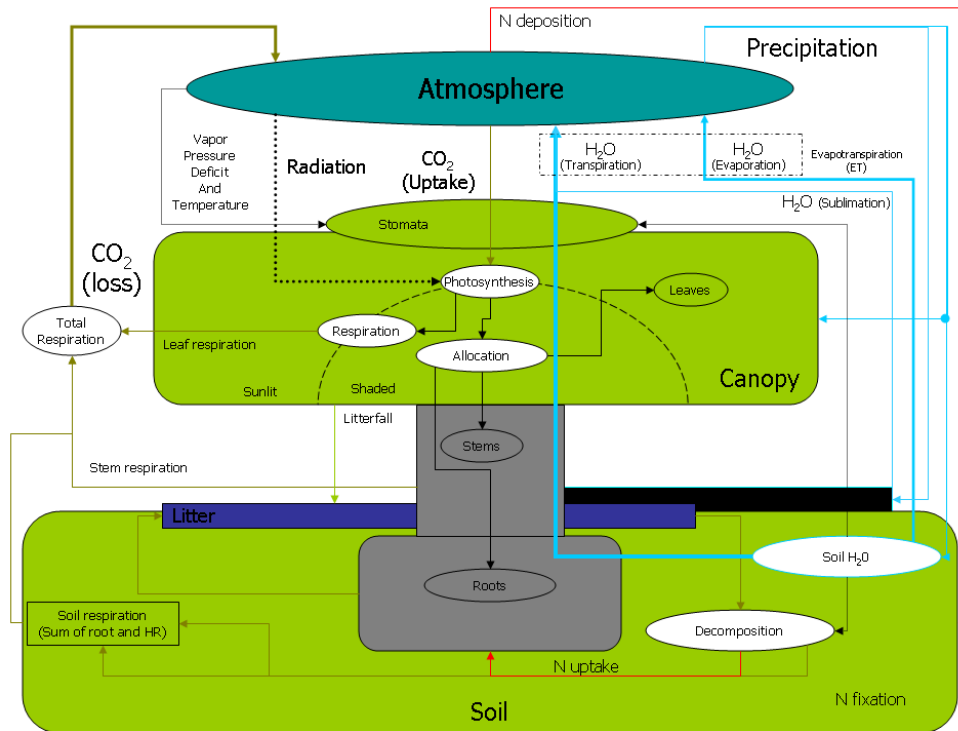
Figure 1
The structure of the Biome-BGC model [12]

Following the requirements above, there are a number of models that enable the detailed description of ecosystems and the assessments of different management (or even climate change) scenarios.

One of the first tools was the CENTURY model, which had been developed from the 1980s, and was implemented in FORTRAN language. It was able to simulate the dynamics of carbon, nitrogen, phosphorus and sulfur for different plant-soil systems (grassland systems, agricultural crop systems, forest systems, and savanna systems). The original version of the model runs in a monthly time step [13]. The improvement of the CENTURY model (e.g. for achieving better temporal resolution) resulted in the introduction of the DayCent model. This tool works based on daily meteorological data and provides daily outputs on fluxes of N gases and CO_2, together with net primary production and other ecosystem parameters [14].

The DNDC model was developed originally for quantifying carbon sequestration and emissions of nitrous oxide, nitrogen and carbon dioxide from agricultural soils in the USA, then was adapted to several other ecosystems and scenarios. Its main advantages are those related to usability: the user-friendly interface and the in-built library of default settings for several crops and soil types [15].

Another widely used, integrated ecosystem model is the Biome-BGC [12], which is point-based and works on a daily basis as well. It was introduced as an extension and generalization of the Forest-BGC model, dating back to the 1980s [16]. A huge advantage of the model is that it has been almost constantly developed and corrected until today, nowadays in the form of a modified model system: the Biome-BGC MuSo [17]. The latter abbreviation refers to the Multilayer Soil Module, which enables a more exact simulation of management interventions, which is especially important in the case of agricultural ecosystems. Similarly to most of the other similar tools, it works with the main model pools of leaf, fine root, fruit, soft stem, live wood, dead wood, coarse root, soil and litter [18].

Besides the above-mentioned tools, there are also some other modeling possibilities; for a comparison see e.g. Campbell and Paustian [19].

3. SOME ASPECTS OF MODEL SELECTION AND APPLICATION FOR IMPACT ASSESSMENT OF SEWAGE SLUDGE EFFECTS ON ECOSYS-TEM CARBON FLUXES

Although there are a number of easily available and potentially usable models to serve an integrated carbon footprint analysis of the land disposal of sewage sludge, there are some factors that should be taken into consideration in the modeling choice. As the intervention is characterized by a huge amount of additional organic matter input with a special chemical composition, the capability of detailed description of management actions (with a complex assessment of soil processes, especially fertilization) might be important. When croplands are in the focus of investigations, the multi-layer characterization of soils can highly improve model accuracy.

When models or results of models for distinct fields are to be somehow connected or integrated (like in this case with the industrial and ecosystem modeling part), the detailed and public documentation of the relevant elements is crucial. In the recent years, following the growing interest in sustainability assessments of different industrial or other economic activities, there is a need for generally usable targeted platforms. The development of such types of toolsets can be delivered through synthesizing relevant measurement and modeling results, or an expert-based development of simplified performance assessment tools [20], [21]. This systematic process may need to build on some elements of existing expert models. E.g. the AgroMo modelling framework is intended to integrate biogeochemcial and crop modelling to enable a holistic assessment of e.g. climate change effects [22]. In our opinion, some kind of similar integrated modeling system for wastewater treatment would highly improve the effectiveness of relevant decision-making processes. A related aspect is the open source availability of the referring software codes, which can help such modeling efforts very much.

The possibility of spatial extension of the model is definitely an advantage from this point of view, but it is also true that the current GIS capabilities and calculation capacities enable future improvement of models in this direction.

At last, the sequestration and storage of carbon by different types of vegetation is treated as an important ecosystem service, and has a central role in international

climate mitigation and biodiversity policies. As such, it can be valued also in monetary terms. This can also be the case for the industrial modeling part, which gives the possibility of an integrated economic assessment, e.g. with a cost-benefit analysis, which may improve the usability of modeling results in different practical applications.

In summary, the integrated modeling of the carbon footprint of the agricultural use of sewage sludge is feasible. The model development efforts needed for that could give usable methodological experience to other environmental management fields, because there is a constantly growing need for impact assessments with a life-cycle approach.

ACKNOWLEDGEMENT

REFERENCES

[1] Kirchherr, J., Reike, D., Hekkert, M. (2017). Conceptualizing the circular economy: An analysis of 114 definitions. *Resources, Conservation & Recycling*, 127, pp. 221–232.

[2] Bianchini, A., Bonfiglioli, L., Pellegrini, M., Saccani, C. (2016). Sewage sludge management in Europe: a critical analysis of data quality. *International Journal of Environment and Waste Management*, 18, pp. 226–238.

[3] Kiselev, A., Magaril, E., Magaril, R., Panepinto, D., Ravina, M., Zanetti, M. C. (2019). Towards Circular Economy: Evaluation of Sewage Sludge Biogas Solutions. *Resources*, 8, p. 91.

[4] Jørgensen, S. E., Fath, B. (2011). Concepts of Modelling. *Developments in Environmental Modelling*, 23, pp. 19–93.

[5] Wainwright, J., Mulligan, M. (2013). Environmental Modelling: Finding Simplicity in Complexity. 2nd edition, Wiley-Blackwell, 494 p.

[6] IPCC (2006). *IPCC Guidelines for National Greenhouse Gas Inventories. – Ch5: Wastewater treatment and discharge*. Intergovernmental Panel on Climate Change.

[7] Corominas, L., Flores-Alsina, X., Snip L., Vanrolleghem P. A. (2012). Comparison of Different Modeling Approaches to Better Evaluate Greenhouse Gas Emissions From Whole Wastewater Treatment Plants. *Biotechnology and Bioengineering*, 109, pp. 2854-2863.

[8] Pradel, M., Reverdy, A. L. (2012). *Assessing GHG emissions from sludge treatment and disposal routes: the method behind GESTABoues tool*. ORBIT2012, Global assessment for organic resources and waste management, Jun 2012, Rennes, France, 9 p.

[9] Brown, S., Beecher, N., Carpenter, A. (2010). Calculator tool for determining greenhouse gas emissions for biosolids processing and end use. *Environmental Science and Technology*, 44, pp. 9509–9515.

[10] Taseli, B. K.: Comparative Life Cycle Assessment of Sewage Sludge (Biosolid) Management Options. DOI: 10.5772/intechopen.91190.
Available from: https://www.intechopen.com/books/sustainable-sewage-sludge-management-and-resource-efficiency/comparative-life-cycle-assessment-of-sewage-sludge-biosolid-management-options

[11] Yoshida, H., Christensen, T. H., Scheutz, C. (2013). Life cycle assessment of sewage sludge management: A review. *Water Management & Research*, 31. pp. 1083–1101.

[12] Thornton, P. E., Running, S. W., Hunt, E. R. (2005). Biome-BGC: Terrestrial Ecosystem Process Model, Version 4.1.1. ORNL DAAC, Oak Ridge, Tennessee, USA. http://dx.doi.org/10.3334/ORNLDAAC/805

[13] Parton, W. J. (1996). The CENTURY model. In: David S. Powlson, D.S., Smith, P., Smith, J. U. (eds.): *Evaluation of Soil Organic Matter Models*. Springer-Verlag, Berlin–Heidelberg, pp. 283–291.

[14] Del Grosso, S. J., Parton, W. J., Mosier, A. R., Hartman, M. D., Brenner, J., Ojima, D. S., Schimel, D. S. (2001). Simulated interaction of carbon dynamics and nitrogen trace gas fluxes using the DAYCENT model. In: M. Schaffer, M., L. Ma, L. S. Hansen, S. (eds.): *Modeling Carbon and Nitrogen Dynamics for Soil Management*. CRC Press, Boca Raton, Florida, pp. 303–332.

[15] Gilhespy, S. L., Anthony, S., Cardenas, L., Chadwick, D., del Prado, A., Li, C., Misselbrook, T., Rees, R. M., Salas, W., Sanz-Cobena, A., Smith, P., Tilston, E. L., Topp, C. F. E., Vetter, S., Yeluripati, J. B. (2014). First 20 years of DNDC (DeNitrification DeComposition): Model evolution. *Ecological Modelling*, 292, pp. 51–62.

[16] Running, S. W., Coughlan, J. C. (1988). A general model of forest ecosystem processes for regional applications. I. Hydrologic balance, canopy gas exchange and primary production processes. *Ecological Modelling*, 42, pp. 125–154.

[17] Hidy, D., Barcza, Z., Marjanović, H., Sever, M. Z. O., Dobor, L., Gelybó, G., Fodor, N., Pintér, K., Churkina, G., Running, S., Thornton, P., Bellocchi, G., Haszpra, L., Horváth, F., Suyker, A., Nagy, Z. (2016). Terrestrial Ecosystem Process Model Biome-BGCMuSo v4.0: Summary of improvements and new modeling possibilities. *Geoscientific Model Development*, 9, pp. 4405–4437.

[18] Hidy, D., Barcza, Z., Hollós, R., Thornton, P. E., Running, S. W., Fodor, N. (2019). *User's Guide for Biome-BGCMuSo 6.0.* Excellence Center, Faculty of Science, Eötvös Loránd University, Martonvásár, p 71.

[19] Campbell, E. E., Paustian, K. (2015). Current developments in soil organic matter modeling and the expansion of model applications: a review. *Environmental Research Letters*, 10, p. 123004

[20] Peh, K. S.-H., Balmford, A., Bradbury, R. B., Brown, C., Butchart, S. H. M., Hughes, F. M. R., Stattersfield, A., Thomas, D. H. L., Walpole, M., Bayliss, J., Gowing, D., Jones, J. P. G., Lewis, S. L., Mulligan, M., Pandeya, B., Stratford, C., Thompson, J. R., Turner, K., Vira, B., Willcock, S., Birch, J. C. (20139. TESSA: A toolkit for rapid assessment of ecosystem services at sites of biodiversity conservation importance. *Ecosystem Services*, 5, pp. 51–57.

[21] Szkordilisz, F., Kiss, M., Égerházi, L. A., Kassai-Szoó, D., Gulyás, Á. (2016). Facilitating climate adaptive urban design - developing a system of planning criteria in Hungary. In: Habert, G., Schlueter, A. (eds.). *Expanding boundaries – Systems Thinking for the Built Environment : Sustainable Built Environment (SBE) Regional Conference*, Zürich, Svájc, VDF Hochschulverlag AG an der ETH Zürich, pp. 102–106.

[22] Barcza, Z., Fodor, N. (eds.) (2018). *The AgroMo approach: development of an integrated biogeochemical-crop model system in Hungary – synergy and cooperation of the model and the observations*. Detailed description about AgroMo, (available only in Hungarian).

OBSERVATION OF CONSEQUENCES OF SEWAGE SLUDGE DISPOSAL BY VEGETATION MONITORING OF CULTIVATED ARABLE LAND

F. KOVÁCS – ZS. LADÁNYI – M. HEGEDŰS

Department of Physical Geography and Geoinformatics, University of Szeged

Abstract: To observe the effects of sewage sludge disposal on fields used for crop production, we planned a multi-year, high-resolution data collection. Considering plant growth, more detailed weekly (high) time resolution and high spatial resolution were also necessary. Sentinel-2 multispectral imaging satellites provide finer resolution and optical data with a 3-to-5-day revisiting period. The vegetation indices applied can be used to evaluate the photosynthetic activity of the plants. There are some detectable differences between the areas affected by the placement of sewage sludge and those that are not affected. The advantage of sewage sludge placement is that nutrient replenishment eliminated biomass production differences between the monitored quadrates containing similar plants.

Keywords: sewage sludge, biomass production, Sentinel-2, spectral index

1. INTRODUCTION

Crop production and agricultural management have a strong impact on the rate of charging of the soil. The humus content in the A horizon of Chernozem soils in the Great Hungarian Plain may have been 1.5–2 times as higher at the time of the beginning of farming (cca. 10,000 years before) than as the current 2–4%. A significant proportion of soils on arable land are exposed to severe pressures, possibly showing signs of chemical and physical degradation, one of the main reasons for which is intensive agriculture [1]. The yield of cultivated crops will be affected in the near future by the increasingly extreme weather caused by climate change [2]. Thus, preserving and improving soil fertility is of common interest.

There is still a lack of a coherent strategy in the European Union regarding sewage sludge use in agriculture. There are several approaches to sewage sludge treatment, and many of them have targeted agricultural use [3, 4]. The agricultural use of sewage sludge is one means of nutrient supply. Valuable components can be recycled into the soils: organic matter, nitrogen, phosphorus and other plant nutrients [5]. The amount of sewage sludge is increasing with the progress of sewage disposal and treatment programs, and the safe use of this amount is also a problem, which is regulated in Hungary by Government Regulation 50/2001. (IV. 3.) and the Decree 36/2006. (V. 18.). Due to the extra nutrients in the sludge free of toxic substances, the development of the plants becomes more balanced, yield can increase and crop quality also improves. However, changes in the quality and quantity of organic matter in soils are slow, and soil improvement can be a long process [6].

To observe the effects of sewage sludge disposal on fields used for crop production, we planned a multi-year, high-resolution data collection. Considering plant growth, we aimed to achieve a more detailed weekly time resolution as well as high spatial resolution. The evaluation of the impact of the regular sewage sludge disposal on agricultural land based on biomass production was carried out for each land parcel based on the data and methods of multispectral remote sensing for the period of 2016, 2017, 2018 [7, 8].

Our further research aimed at more detailed, longer-term and higher time resolution impact assessment on different agricultural land parcels in a sample area of south-eastern Hungary. Using the SENTINEL-2 satellite images, the highest temporal and spatial resolution were applied for data collection. Our preliminary assumption suggests that crops under sewage sludge field application develop more dynamically. The process is, of course, complex, as land use changes and meteorological / climatological parameters influencing plant development also have to be considered.

2. DATA AND METHODS

The study area is located in the lowland interfluve area between the Körös River and Maros River, in the territory of Újkígyós settlement *(Figure 1)*.

Figure 1
The location of the soil quadrates (1t–10t) in the study area
and the land cover changes in the period 2016–2019

The area, formed by fluvial and eolian processes, belongs to the Körös River Catchment. The static groundwater level was measured at 2 m below the surface. It has an extent of 5.6 hectares where 2.5 m³/ha/year of treated municipal sewage has been applied regularly in autumn since 2013 on Chernozem and meadow Chernozem soils. Soil sampling was carried out in quadrats of 50 × 50 m² in the area, where 1t–4t were continuously treated areas. Quadrats 6t-7t are partly control areas, sewage sludge was deposited here only in 2018, while 9t-10t were control areas not treated with sewage sludge *(Table 1)*. The land coverage of the 1t–4t quadrats always differed from the 6t-7t and 9t-10t quadrats between 2017–2019. The biomass production of the 1t–4t quadrats can be distinguished from the others during the monitoring, and the values of 6t-7t and 9t-10t can be compared with each other depending on the time of sewage sludge placement.

Table 1

Crops produced in the quadrates and the sewage sludge placements

quadrats /year	2016	2017	2018	2019	sewage sludge placement
1t	maize	oil radish	winter wheat	colza	2017 autumn
2t	maize	oil radish	winter wheat	colza	2017 autumn
3t	maize	oil radish	winter wheat	colza	2017 autumn
4t	maize	oil radish	winter wheat	colza	2017 autumn
6t	colza	maize	maize	winter wheat	2018 autumn
7t	colza	maize	maize	winter wheat	2018 autumn
9t	sunflower	maize	maize	winter wheat	–
10t	sunflower	maize	maize	winter wheat	–

In addition to the scientific, agricultural applications of satellite remote sensing – eg. drought monitoring [9, 10] – new users are already increasing the number of drone applications based on business and agricultural economics. The high spatial resolution required by detailed land parcel-based surveys assumes the use of aerial imagery or very high-resolution satellite imagery, but their use is very expensive if we intend to comply with the very high time resolution required by the monitoring.

Free downloadable remote sensing data such as from LANDSAT is also applicable [11], but cannot alone supply good temporal resolution, which hardly allows plot scale evaluation of crop development in Hungary. The Sentinel-2 multispectral instrument (MSI) with refined spatial resolution allows for improved and accurate monitoring of the effect of sewage sludge with the presence of red-edge bands, which are not present in freely available multispectral sensors and whichwidens the spectral

windows, for instance the heavy metal stress discrimination at broader scales [12] Sentinel-2 multispectral imaging satellites provide finer resolution and optical data with a 3-to-5-day revisiting period *(Table 2)*. In the first period in 2016, only the Sentinel-2A satellite was in orbit and just the Level 1C (L1C) data product was available for download. In 2017, 2018, nd 2019 data from Sentinel-2A and -2B, at Level 2A (L2A, Bottom-of-Atmosphere (BoA) reflectance values) also became accessible. In the Sentinel-2 granule system, the study area is fully covered by one 100×100 km tile: 34TDS.

Only cloud-free images with atmospheric correction were evaluated (altogether 81 images). All available images in the vegetation period were used, which meant numerous images, mainly in 2018. Despite the high time resolution, we did not have data for July 2016 or May 2019 due to cloud coverage. We also used images from March to replace the fewer spring images.

Table 2

Sentinel-2 multispectral image parameters and database

Satellite / Sensor	Multispectral imagery	Applied spectral bands central wavelengths	Spatial resolution
Sentinel-2A / 2B	20 images / 2016 14 images / 2017 29 images / 2018 18 images / 2019	B2: 492.4 / 492.1 nm B4: 664.6 / 664.9 nm B8: 832.8 / 832.9 nm	10 m

The main application of multispectral remote sensing is the efficient observation of vegetation. Satellite images provide a cost-effective way of assessing the spatial and temporal patterns of biomass productivity by extracting vegetation indices. The NDVI and EVI vegetation indices applied can be used to evaluate the photosynthetic activity of the plants and the changes in biomass mass [13] (Equations 1, 2).

$$NDVI = \frac{NIR-Red}{NIR+Red} \tag{1}$$

$$EVI = G * \frac{NIR-Red}{NIR+C_1*Red+C_2*Blue+L} \tag{2}$$

where NIR indicates the near infrared band, Red indicates the visible red band, Blue indicates visible blue band, $L = 1$, $C_1 = 6$, $C_2 = 7.5$, and $G = 2.5$.

At a resolution of 10 m, there were few pixels in the area of sample quadrats (approximately 25 pixels/quadrat), which is why possible defective pixels may be more distorted. Insufficiently detailed time data density can make it difficult to compare results from different years.

The studied years had different weather conditions *(Figure 2)*. The investigated years show different distribution of precipitation. During the growing season, the average rainfall is approximately 340 mm and the average temperature is 17.3 °C. 2019 was very extreme, as in May there was twice the amount of precipitation

compared to the general average, however, in March, there was hardly any precipitation. Higher precipitation values were in June of 2016 and in March of 2018. 2017 was the driest year and 2018 was the warmest year.
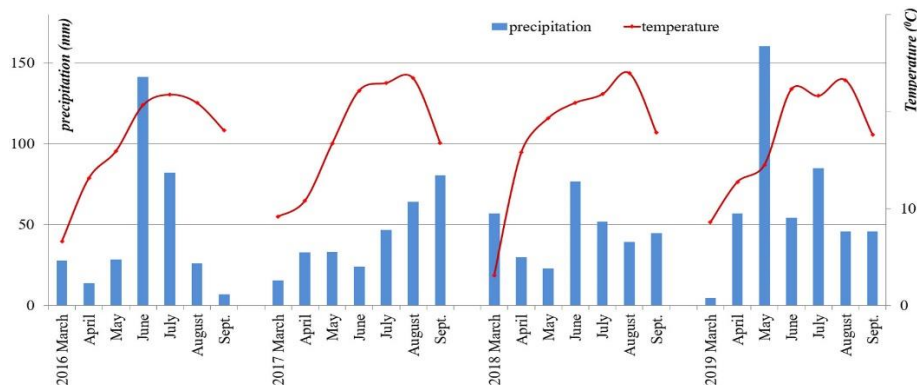
Figure 2
Temperature and precipitation for the study area (Békéscsaba station)
between 2016–2019

3. RESULTS AND DISCUSSION

The differences in the vegetation development of the plant types and in the land cover can be clearly seen in the vegetation index values derived from the images (*Figures 3* and *4*). Land use changes can also be detected (see *Figure. 1* and *Table 1*). The 1t–4t quadrats were always characterized by similar land use: they were covered by oil radish in 2017 and by winter wheat from 2018. Quadrats 6t-7t and 9t-10t also had similar land use, except for 2016; maize in 2017 and 2018 and winter wheat in 2019. According to the EVI/NDVI values, in 2016 the majority of the area was characterized by crop production showing a peak biomass production in May-June (e.g. winter wheat, oil radish). The cereals started to develop as early as spring and were harvested by July; this can be seen in green curve in 2018 in Fig. 3. In 2017-18, half of the sample area (1t–4t) remained similar, but the other half changed to other production, when the EVI/NDVI maximum production was in July-August (e.g. maize). The corn later started to develop and was harvested in August; it can be seen in the green curve in 2018 in Fig. 3. The biomass production on all areas peaked by June in 2019, but two types of crops were recognized in quadrats 1t–4t and 6t-7t, 9t-10t. NDVI values were higher and more easily saturated on the rich vegetation area, but the increase in biomass production was well assessed with them. In several years, plant types could be better distinguished in the NDVI data set (e.g. 2016), but the EVI as an enhanced index reduced the impact of soil and atmosphere. The study confirms that there is no single best index, rather it is worth using them together in the evaluation; for instance the difference between EVI and NDVI values of the 6t-7t areas in 2016 and 2017 were spectacular.
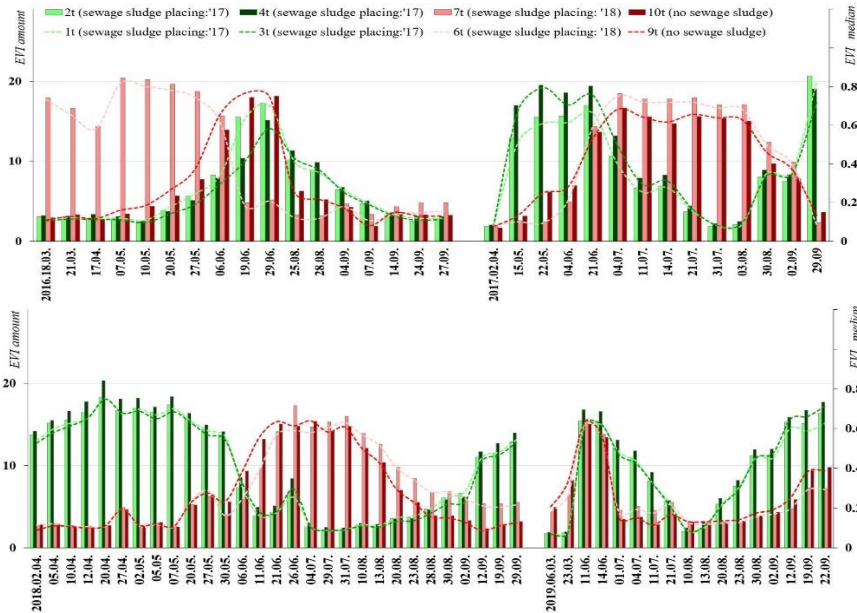
Figure 3
EVI values for all quadrat areas between 2016–2019
(dotted line is based on EVI median values, columns are EVI amount values)
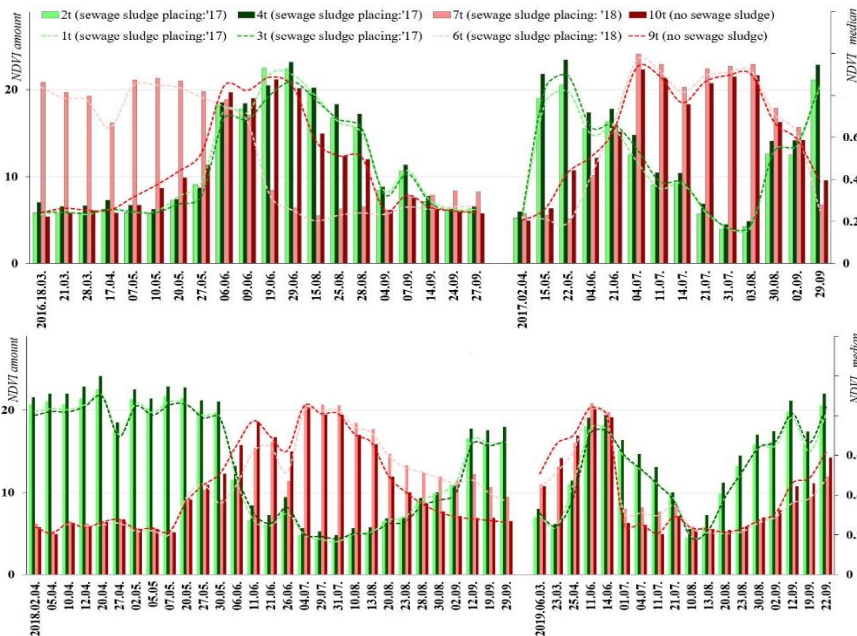
Figure 4
NDVI values for all quadrat areas between 2016–2019
(dotted line is based on NDVI median values, columns are NDVI amount values)

The effect of the 2017 placements is suggested by the NDVI values in 2018 in the 1t–4t quadrats, but this effect was contradicted by the high EVI values in 2016 in the 6t-7t quadrats. The profiles of the curves/columns after the placement of 2017 in the areas of 1t–4t became remarkably the same, which was not typical before. The advantage of sewage sludge placement was that it eliminated the differences in biomass production between quadrats containing similar crops by replenishing nutrients on monthly average images (*Figure 5* and *Figure 6*). The same can be observed in 2019 for quadrats 6t-7t, where there was sewage sludge placement in 2018.
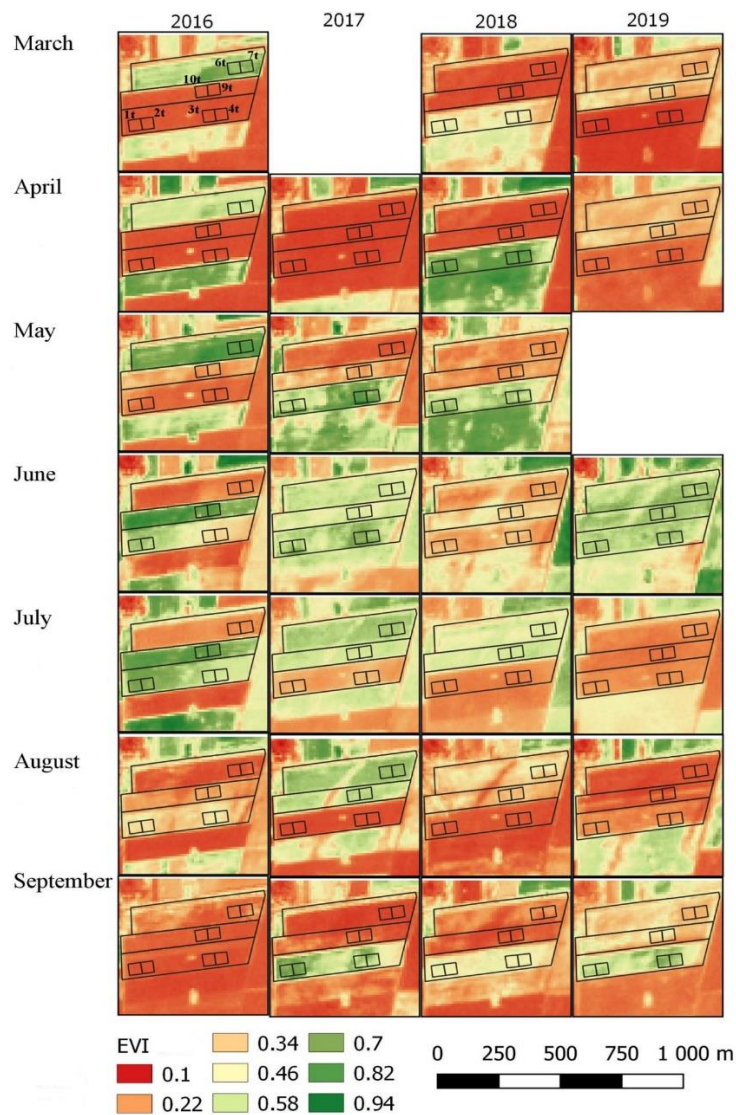
Figure 5
Vegetation production evaluated by EVI, 2016–2019
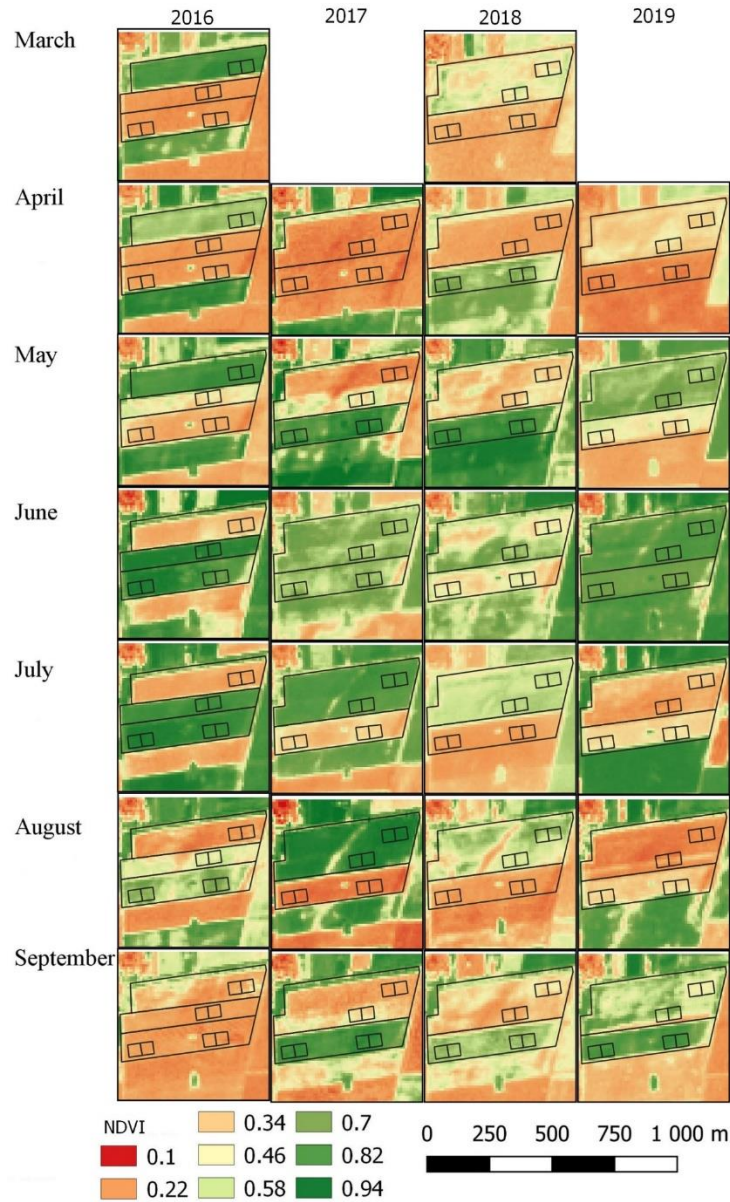
Figure 6
Vegetation production evaluated by NDVI, 2016–2019

When looking only in terms of peak values of biomass production on the 1t–4t quadrates, considering the placement in 2017 and changes in the crops produced, the data of the previous year were higher between 2016 and 2017. Assuming the same crop production between 2018–2019, the yield of 2019 showed values of 1.2–2.6 times, which also exceeded the production in 2017 recorded at the same time; here biomass

production increased after the field application of sewage sludge. This is reinforced by the fact that the index values for 2017 started with higher values than in the previous year, at higher temperatures and nearly equal precipitation values; excess nutrients from placement may also have played a role in the difference.

In the different biomass production periods of 6t-7t quadrats we experienced the richest vegetation in 2016–2017 years, up to 1.4 times more than in 2018. Between 2016 and 2019, the August-September period was comparable; here the actual values were somewhat higher, with a difference of up to 1.5 times. The impact of sewage sludge application is therefore noticeable, but we will need the data from 2020 to further verify this. Contrary to our expectations, the index values were higher in the 9t-10t control quadrats where there was no sludge placement than for the 6t-7t quadrats, where land use was similar.

In particular, the arid summers of 2017 and 2018 showed the location of the ancient alluvial geomorphological forms; the geographical factors influencing even the small area are indirectly outlined on the basis of the different soil conditions of the forms. They also cause a significant difference in yield within a land parcel (*Figures 5* and *6*).

4. CONCLUSION

Our goal was to monitor the impact of sewage sludge disposal on the vegetation development of arable land crops. Both the NDVI and EVI indices performed well for this purpose, as expected. There are some detectable differences between the areas with placement of sewage sludge and those that without it. If there is a rainfall event the plants affected by the placement of sewage sludge will benefit more from it next time period; in the case of an extreme situation due to a lack of rainfall plants suffer a smaller decrease in biomass production than the untreated areas. The advantage of sewage sludge placement is that nutrient replenishment eliminated biomass production differences between the monitored quadrates containing similar plants.

To detect significant differences, we continue data collection; 36 LANDSAT OLI images will be also included in the observation. Due to the differences in the crops produced, in addition to the four studied years, 2020 will also be monitored.

REFERENCES:

[1]   Rakonczai, J. (2018). *Global and geopolitical environmental challenges*. Corvinus University of Budapest.

[2]   Mezősi, G., Blanka, V., Ladányi, Zs., Bata, T., Urdea, P., Frank, A., Meyer, B. (2016). Expected mid- and long-term changes in drought hazard for the South-Eastern Carpathian Basin. *Carpathian Journal of Earth and Environmental Sciences*, 11 (2), pp. 355–366.

[3]   Kelessidis, A., Stasinakis, A. S.(2012). Comparative study of the methods used for treatment and final disposal of sewage sludge in European countries. *Waste Management*, 32 (6), pp. 1186–1195.

[4]   Thebo, A. L., Drechsel, P., Lambin, E. F., Nelson, K. L. (2017). A global, spatially-explicit assessment of irrigated croplands influenced by urban wastewater flows. *Environmental Research Letters*, 12 (7), p. 074008.

[5]   Tomócsik, A., Makádi, M., Orosz, V., Füleky, Gy. (2016). Effect of sewage sludge compost treatment on crop yield. *Agrofor International*, 1 (2), pp. 5–12.

[6]   Banerjee, M. R., Burton, D. L., Depoe, S. (1997). Impact of sewage sludge application on soil biological characteristics. *Agriculture. Ecosystems and Environment*, 66 (3), pp. 241–249.

[7]   Ladányi, Zs., Farsang, A., Gulácsi, A., Kovács, F. (2018). The impact of extreme weather conditions and municipal sewage disposal on vegetation using Sentinel images, SE Hungary. In.: Alapi, T., Ilisz, I. (eds.). *Proceedings of the 24th International Symposium on Analytical and Environmental Problems*, University of Szeged, pp. 325–329.

[8]   Babcsányi, I., Ladányi, Zs., Perei, K., Bodor, A., Barta, K., Kézér, A., Csányi, K., Pálffy, B., Farsang, A. (2019). Higher nutrient contents and biological activity in chernozem soils and enhanced biomass productivity linked to sewage sludge compost disposal. In: Gábor, Rákhely, G–Hodúr, C. (eds.). *II. Sustainable Raw Materials Conference Book – International Project Week and Scientific Conference*, Szeged, Hungary, University of Szeged, pp. 137–145.

[9]   van Leeuwen, B., Tobak, Z., Ladányi, Zs., Blanka, V. (2014). Satellite based soil moisture estimates for agricultural drought prediction. In: Cvetkovic, M., Zelenika, K. N., Geiger, J. (eds.). *6th Croatian–Hungarian and 17th Hungarian geomathematical congress*, Geomathematics - from theory to practice Zagreb, pp. 175–182.

[10]   Gulácsi A., Kovács, F. (2015). Drought monitoring with spectral indices calculated from MODIS satellite images in Hungary. *Journal of Environmental Geography*, 8 (3–4), pp. 11–19.

[11]   Sridhar, B. B. M., Vincent, R. K., Witter, J. D., Spongberg, A. L. (2009). Mapping the total phosphorus concentration of biosolid amended surface soils using LANDSAT TM data. *Science of the Total Environment*, 407, pp. 2894–2899.

[12] Zhang, Z., Liu, M., Liu, X., Zhou, G. (2018). A new vegetation index based on multitemporal Sentinel-2 images for discriminating heavy metal stress levels in rice. *Sensors*, 18, p. 2172.

[13] Bannari, A., Morin, D., Bonn, F., Huete, A. R. (1995). A review of vegetation indices. *Remote Sensing Reviews*, 13, p. 95–120.

MEASUREMENT OF SOIL CO₂ RESPIRATION ON ARABLE LAND TREATED BY SEWAGE SLUDGE COMPOST

M. TÓTH – I. FEKETE – K. BARTA – A. FARSANG

Department of Physical Geography and Geoinformatics,
University of Szeged, H-6722 Szeged, Egyetem u. 2., Hungary

1. INTRODUCTION

The key question of the global climate change is the change in the atmospheric concentration of carbon dioxide. It is obvious that the increase in CO_2 concentration in the last 100 years is caused by the accelerated utilization of fossil fuels, but we must not forget the effect of the intensive agriculture, with special attention to crop production on arable lands. This is responsible for the 30% of the global CO_2 emissions along with silviculture [1]. One part of this emitted carbon dioxide is lost forever from the soil; it is derived from the decreasing soil organic matter and unfortunately it can add to the atmospheric CO_2 concentration for a long time. Other part is in dynamic equilibrium with its environment and it has a daily and yearly cycle depending on soil biological activity. Photosynthesis plays the most important role on the input side of this cycle [2].

The problem of decreasing soil organic matter can be met favorably with problems of waste material emplacement derived from several different human activities. Examples are liquid manure from livestock ranches; fermented manure from biogas plants or sewage sludge from municipal wastewater treatment [3], [4]. There are two advantages of the deposition of these waste materials on arable lands: not only we have disposed of them, but they are useful fertilizer for soils and for plants. Their high organic matter content and nitrogen, phosphorus and potassium concentrations can improve soil quality and help increase crop yield. On the other hand, there are several risk factors in applying waste materials to arable lands, such as their high salt and nitrate content or toxic elements contained in them.

While these waste materials have positive effects on crop production and on the soil's biological activity, what is the effect on the global carbon cycle? Can this carbon surplus be built into the soil for long time? How can the intensified biological activity increase the soil respiration? Is it possible to show higher CO_2 emissions on arable lands treated with sewage sludge?

In this study we have investigated the changes in soil CO_2 flux on Chernozems treated with sewage sludge compost in the south-eastern part of Hungary. Besides the above questions we have tried to find answers to others: are there changes in soil CO_2 respiration after treatment; if so, how large are the changes; does what significantly exceed other influencing factors, e.g. effects of soil moisture and temperature?

2. MATERIAL AND METHODS

2.1. Study Area
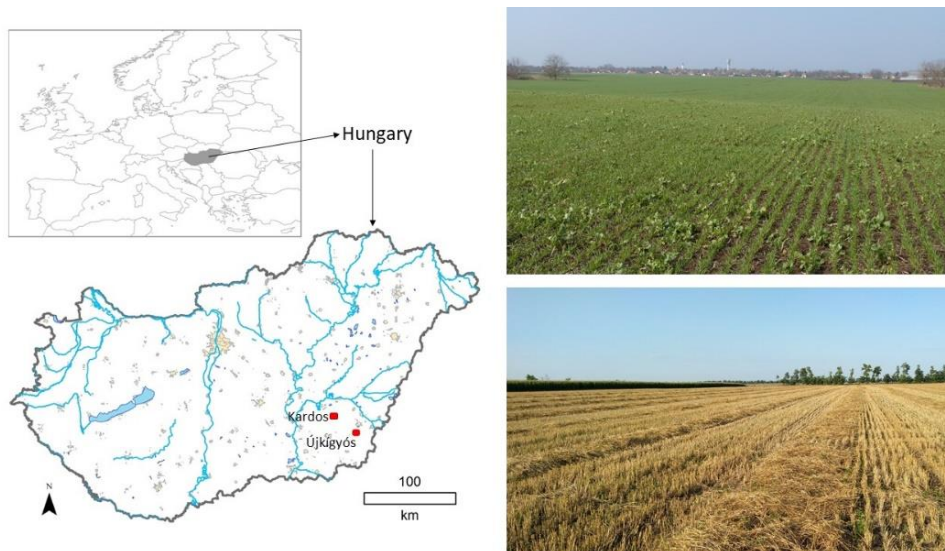
Figure 1
Location of the study areas and the arable lands
in springtime and after harvesting

One of the areas with the highest soil quality in Hungary is located in the south-eastern part of the country, in Békés County. Its soils are Chernozems formed on loess with loam and sandy loam texture. Their thickness is 100–120 cm and their humus content is still more than 2% in spite of long-term and very intensive cultivation. Two arable lands with 25.6 and 15.7 ha area were chosen near the settlements of Újkígyós and Kardos *(Figure 1)*. Both of them were covered with winter wheat in 2018 and 2019. Municipal sewage compost has been regularly applied to these fields since 2013 during October and November. The amount of sewage sludge compost was 2.5 m^3/ha/year at Újkígyós and 35 m^3/ha/year at Kardos, in a rotating manner. The compost was placed and plowed into the upper 30 cm of the soil.

2.2. Methods

Three treated study plots at each location (2.5 m^3/ha at Újkígyós in 2017 and 35 m^3/ha at Kardos in 2018) were assigned on both study areas in order to collect soil and plant samples for other parts of this project. The extent of these plots was 50×50 m and soil CO_2 flux was measured in the center of the parcels. A further three control plots at each site were chosen near them, which have never been affected by compost applications.

CO_2 respiration measurements were applied 5 times in 2019: twice in springtime (6 March 2019; 28 March 2019), twice in summer (19 June 2019 – before harvest;

16 July 2019 – after harvest) and once at the end of summer (28 August 2019) on both areas. The planned autumn measurements were cancelled due to the extremely low values of soil moisture, biological activity and CO_2 respiration [5].

We measured the CO_2 efflux with an EGM-5 portable gas analyzer. This system contains an SRC-2 closed dynamic chamber for collecting the air which flows from the soil to the atmosphere *(Figure 2)*.

Figure 2
Application of the EGM-5 under winter wheat near the village of Kardos

The system is closed; the air in this chamber is totally isolated from the ambient air. Also the system is dynamic because of the continuous circulating sample gas between the chamber and the infrared gas analyzer (IRGA). The core of the instrument is the IRGA, where measurement actually takes place, and the principle of the method is the infrared absorption of CO_2. As we know, infrared radiation can be absorbed by CO_2 and a nondispersive infrared (NDIR) sensor in EGM-5 can measure the absorbance in the CO_2 molecules' absorption band at 4.26 μm wavelength, where

the infrared radiation is completely absorbed by the carbon dioxide. As a result, it is a selective and sensitive method for measuring the concentration of CO_2 because of the minimal overlap with other ambient gas molecules. The built-in infrared source provides light in middle-infrared range and an optical filter corrects the light to the appropriate 4.26 μm wavelength. The absorption of carbon dioxide causes a decrease in the intensity of infrared radiation and the detector can measure the rate of decrease. Thus, the exact concentration of CO_2 is calculable from the ratio of the intensity of incident and transmitted light using the Lambert–Beer law. Furthermore, we can measure the soil moisture and soil temperature in the top 5 cm of soil using a Hydraprobe II sensor. The EGM-5 with this sensor provides data in every second on soil moisture between 0% and 100% and soil temperature between –10 °C and 55 °C. Thus, we can obtain a great deal of information about these two parameters in parallel with CO_2 efflux data [6].

Soil CO_2 respiration were measured each time in 10 repetitions in the middle of each assigned plot. That means that the value belonging to a given plot in a fixed time was created as the average of 10 measured data.

3. RESULTS AND DISCUSSION

The measured data and their main statistic parameters – after filtering false data – are summarized in *Table 1*.

The high values of standard deviations are caused by various conditions of measurements: soil moisture and soil temperature changed within a wide range and the vegetation was extremely different, from the bare soil surface via mature winter wheat until uncontrolled weeds. Although the measurements were taken on the same day on both treated and control plots, the measured data obviously show the role of the daily period of soil temperature and moisture. There are several scientific publications about the important role of soil moisture and temperature in CO_2 efflux (e.g. [7], [8], [9], [10], [11]) and our own measurements confirm that the daily rhythm of soil moisture and temperature changes have much stronger effects on CO_2 respiration than the treatments. This means that the differences measured inside a day are often caused from the few hours' differences between the measurement times.

Table 1

Averages of measured CO_2 respiration in 2019

| Plots	Average CO_2 respiration ($g \cdot m^{-2} \cdot h^{-1}$)	Number of cases	Min/Max	Standard deviation
Újkígyós – treated	0.930	47	0.566/1.586	0.244
Újkígyós – control	0.803	38	0.467/1.489	0.229
Kardos – treated	0.529	59	0.369/0.853	0.095
Kardos – control	0.532	59	0.351/0.808	0.107

Besides the summarized data, the last three measurement campaigns in Kardos can demonstrate the role of the soil temperature in the CO_2 flux very well *(Figure 3)*. The temperature dependent biological activity is the highest at about 30 °C and soil respiration decreases above it.
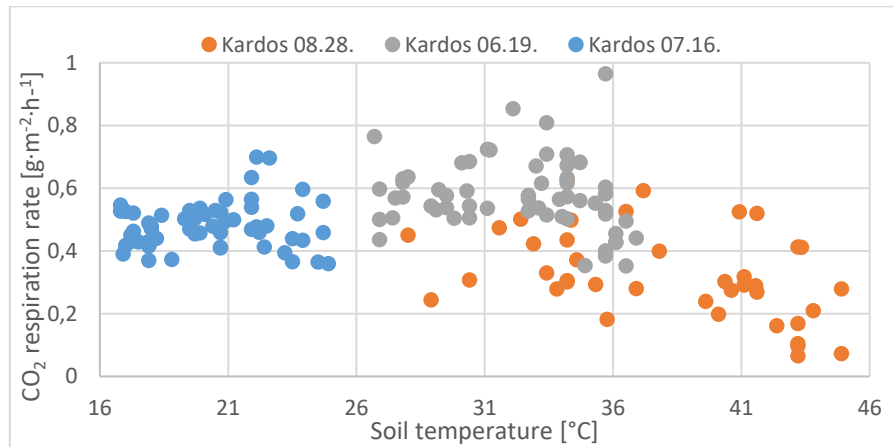
Figure 3
Respiration rates in function of soil temperatures
on three different days, near Kardos

An irrigation experiment provided further information on the role of soil moisture. Two small plots (plot A and B) were irrigated and CO_2 fluxes were measured in parallel on both plots *(Figure 4)*. The increasing soil moisture can cause the growth of respiration as far as field capacity. The main limiting factor for microbiological activity is the low amount of air in the soil pores above field capacity (25–30 v/v%). Results show that this harmful water surplus can obstruct the activity; the CO_2 respiration will decrease after this point [5].
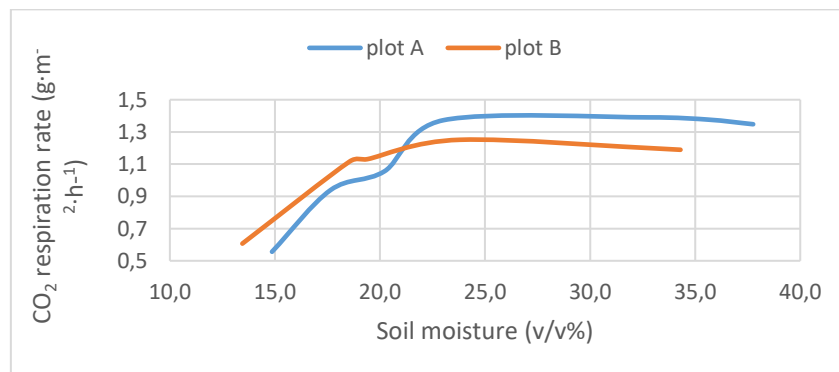
Figure 4
Respiration rates as a function of soil moisture during irrigating experiment

Our conclusion is that there was no obvious evidence to verify increasing CO_2 respiration after sewage sludge treatments on any study plot. The background of the undetectable changes could be the low doses and the fact that the effect of the soil moisture and temperature is higher by at least one order of magnitude than changes caused by the sewage sludge treatment. Measurements give evidence not only of this well-known correlation but they also highlighted the optimal values of soil moisture and temperature for biological activity via CO_2 respiration on the two study areas. The limiting factors of these two parameters are field capacity and a temperature around 30 °C.

The accurate establishment of the effects caused by sewage sludge treatment is possible if not only the measurement method is standardized but the surroundings conditions also, such as soil moisture and temperature. The best way to accomplish this is if the measurements are carried out at the same time of day in parallel on all plots with several sets of instruments.

REFERENCES

[1]   Anda A. (2016). Mezőgazdaság: fő tényező a globális felmelegedésben? (Agriculture: A major factor in global warming?) *Agrárium*, 6–7, pp. 79–81.

[2]   Powlson, D. S., Whitmore, A. P., Goulding, K. W. T. (2011). Soil carbon sequestration to mitigate climate change: a critical re-examination to identify the true and the false. *European Journal of Soil Science*, 62, February 2011, pp. 42–55.

[3]   Tuba G., Kovács Gy., Czellér K., Zsembeli J. (2019). A szennyvíziszap-komposzt hatása a kukorica termésére és a talaj néhány tulajdonságára. (The impact of sewage sludge on maize yield and certain soil characteristics) Növénytermelés 68/3. 2019, 73-89.

[4]   Uri Zs., Lukácsné Veres E., Kátai J., Simon L. (2005). Települési szennyvíziszapok hatása a talaj mikroorganizmusaira és enzimaktivitására (Effect of Variously Pre-treated Municipal Sewage Sludges on the Microbe Composition and Enzyme Activity of the Soil). *Agrokémia és Talajtan*, 54, pp. 439–450.

[5]   Tóth M. (2019). *A talajlégzés vizsgálata, valamint a kibocsátott CO_2 mérése EGM-5 gázanalizátorral*. (The examination of soil respiration and in situ CO_2

efflux measurement using EGM-5 gas analyzer). BSc Thesis Work, Szeged, p. 40.

[6]   PP Sytems (2018). *EGM-5 Portable CO₂ Gas Analyzer Operation Manual*. PP Systems, Amesbury.

[7]   Oh, N. H., Kim, H. S., Richter, D. D (2005). What Regulates Soil CO2 Concentrations? A Modeling Approach to CO2 Diffusion in Deep Soil Profiles. *Environmental Engineering Science*, 22/1.

[8]   Doetterl, S., Berhe, A. A., Nadeu, E., Wang, Z., Sommer, M., Fiener, P. (2016). Erosion, deposition and soil carbon: A review of process-level controls, experimental tools and models to address C cycling in dynamic landscapes. *Earth-Science Reviews*, 154, pp. 102–122.

[9]   Kovács Gy. (2014). *Mezőgazdasági hasznosítású talajok szén-dioxid-emissziójának vizsgálata Karcag térségében*. (Examination of carbon-dioxide emission of agricultural lands in Karcag region) Doctoral (PhD) Dissertation, University of Debrecen.

[10]   Tóth E., Koós S., Farkas Cs. (2008). A talaj szén-dioxid emissziója és nedvességtartalma közötti kapcsolat vizsgálata talajművelési tartamkísérletben. (Connection between soil carbon dioxide emission and soil moisture in long-term tillage experiment) In: *Talajvédelem különszám* (ed.: Simon L.), Talajtani Vándorgyűlés, Nyíregyháza. May 2008, pp. 175–184.

[11]   PP Systems: Measuring Soil CO₂ Efflux from Ant Nests in the Brazilian Rainforest. Application Note. p. 4. http://ppsystems.com/wp-content/uploads/ AN_ EGM-5_Measuring-Soil-CO2-Efflux-from-Ant-Nests-in-the-Brazilian-Rainfo rest.pdf

PALYNOFACIES AND ORGANIC THERMAL MATURITY OF THE UPPER MANCOS FORMATION IN THE SAN JUAN BASIN, NEW MEXICO, USA

A. H. MOGHAZI – M. K. ZOBAA – F. MÁDAI – M. HÁMOR-VIDÓ

Department of Geology, Aswan university, Aswan, Egypt
(aswanpalyno@gmail.com)
Department of Geosciences, University of Texas Permian Basin, Odessa, Texas, USA
(zobaa_m@utpb.edu)
Institute of Mineralogy and Geology, University of Miskolc, Hungary
(askmf@uni-miskolc.hu)
Department of Geology and Meteorology, University of Pécs, Pécs, Hungary
(hamorvido@gmail.com)

Abstract: We conducted a detailed organic facies analysis on 27 core samples from the Upper Mancos Formation in the San Juan Basin, USA. The aim was to evaluate thermal maturity of the dispersed organic matter, interpret paleoenvironmental conditions, and define the oil- or gas-prone nature of the existing organic facies in the interval between 315.5–188.7 m at the Melrich-Shaft-Site drilled in Smith Lake Field, McKinley County, New Mexico. The studied section displayedthree organic facies associations (PF-1, PF-2, and PF-3) based on the relative abundances of three groups of dispersed organic matter (phytoclasts, palynomorphs, and amorphous organic matter). PF-1 (315.5–267.0 m in depth) is characterized by abundant amorphous organic matter (AMOM) up to 80.2% with lesser quantities of opaque wood tissue origin phytoclasts, degraded phytoclasts, and small quantities palynomorphs of marine plankton origin of dinoflagellate cysts and solitary alga (avg 0.5%). PF-2 sequence (267.0–224.0 m in depth) represents a transitional facies between the amorphous matter and marine plankton origin PF-1 zone and the mostly terrigenous type PF-3 sequence which occurs at depth between 224.0 and 188.7 m and dominated by degraded, structured phytoclasts (avg. 63.3%), opaque wood tissue origin phytoclasts (avg. 31.9%) and in minor amounts palynomorphs (avg. 4.5%). Recognized kerogen types include type-II, mixed type-II/III, and type-III materials. Observed spore/pollen colors (yellowish-orange to light orange) and vitrinite random reflectance (0.245–0.414%) indicate immature source rock with significant hydrocarbon generation potential.

*Keywords: palynofacies, vitrinite reflectance, thermal maturity, kerogen type, Mancos Formation, San Juan Basin*

1. INTRODUCTION

The study of sedimentary organic matter is essential for the evaluation of an identified source rock unit in a prospective basin. It provides a plethora of information which is necessary for accurate prediction of the source rock petroleum generation

potential. The San Juan Basin is primarily a mature natural gas producer for both conventional extraction and as occurrences of unconventional tight gas sand. Numerous authors studied this area, particularly the rocks of Cretaceous age of coal and hydrocarbon resources which are abound and well exposed in the basin [1, 2, 3]. The Upper Cretaceous Mancos Shale preserves sufficient amounts of organic matter, which have sourced significant hydrocarbon reserves. It is considered an important regional source rock in the San Juan Basin for oil and natural gas from conventional reservoirs, as well as a promising unconventional gas resource [4]. Previous studies on the Mancos Formation did not include organic facies data and were mostly from the northern part of the San Juan Basin [4, 5, 6]. In this study, the hydrocarbon potential of the Upper Mancos Formation is evaluated based on organic facies and organic thermal maturity parameters.

2. LOCATION OF THE STUDIED SECTION

The studied section is located in McKinley County in the southwestern part of San Juan Basin, New Mexico. The location is defined by latitude 35°23'56.4" N and longitude 107°42'25.2" W as shown in *Figure 1*.
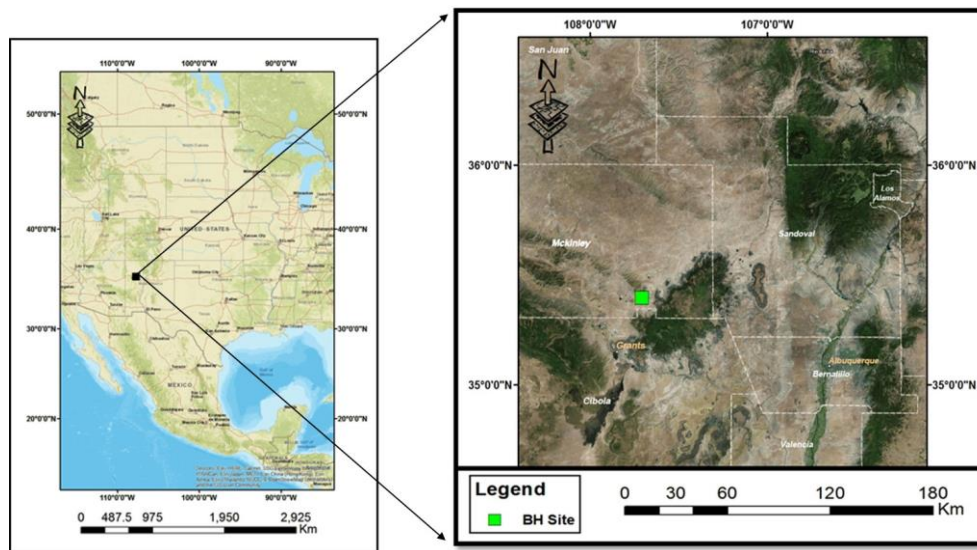
Figure 1
Location map of the studied section in McKinley County in the vicinity of Lee Ranch Mine, New Mexico, USA

3. METHODS

A total of 27 core samples representing the Upper Mancos Formation were prepared for organic facies studies in the Mining and Geological Survey of Hungary following the standard preparation techniques described by Traverse [7]. All slides

were examined using a Zeiss Axio Imager microscope equipped with AxioCam MRc5 camera. Palynofacies point counts were made by traversing across each slide and recording the first 200 organic particles encountered. Identified organic matter particles were grouped following the classification scheme of Zobaa et al. [8]. Six polished blocks were prepared at the laboratories of MOL Public Company, Hungary for vitrinite reflectance (Ro%) measurements. Fifteen reflectance readings were possible on each sample with Zeiss Axioplan microscope, NEOFLUAR 50× oil immersion objective, according to the guidelines of the ISO 7404-5 [9] and described in [10]. The lithostratigraphy and samples depths of the studied Upper Mancos interval are shown in *Figure 2*.
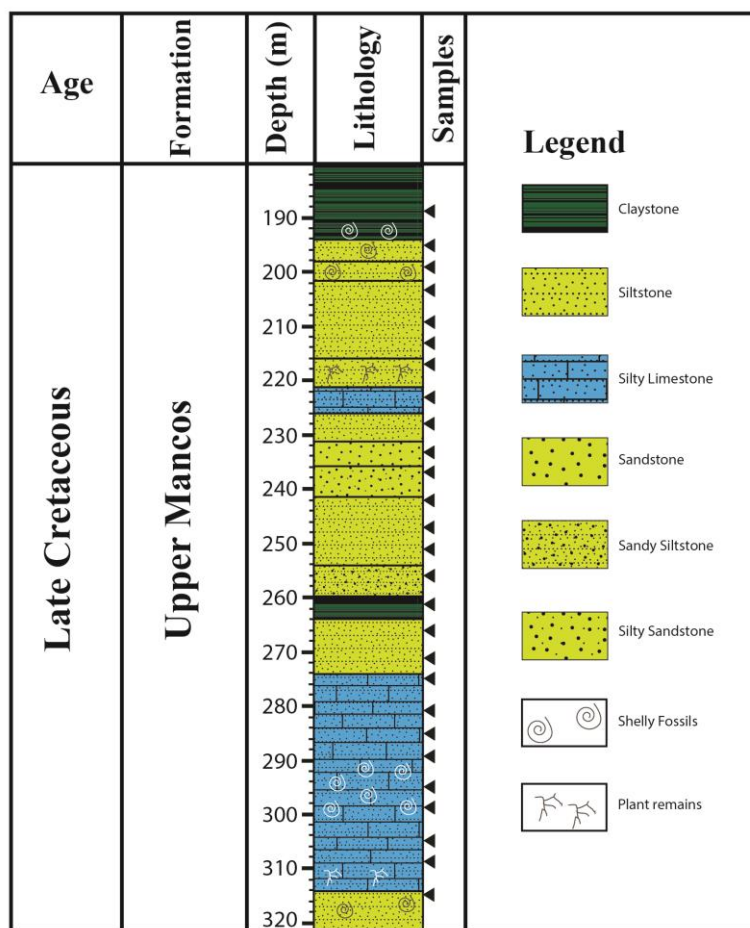
Figure 2
Stratigraphic column showing the lithostratigraphy and samples depths of the studied   Upper Mancos interval. The black triangles on right side of the stratigraphic column are representing the depth interval of the studied samples.

4. RESULTS

4.1. Palynofacies data

Based on the vertical distribution of organic facies components throughout the studied section, three organic facies associations were recognized from Nannofossil biostratigraphically older to younger sections [11]:

4.1.1. Palynofacies-1 (PF-1)

PF-1 represents the organic facies of the interval between 315.5 and 267.0 m. It contains abundant amounts of amorphous organic matter (AMOM) reaching up to 80.2% *(Figure 3, Plate 1)*. Opaque, wood tissue origin phytoclasts (avg. 19.1%) and structured phytoclasts (avg. 12.2%) come next in abundance in this palynofacies, while palynomorphs represent negligible proportions (0–1.9%). No cuticles were recorded as part of the counted phytoclast particles.
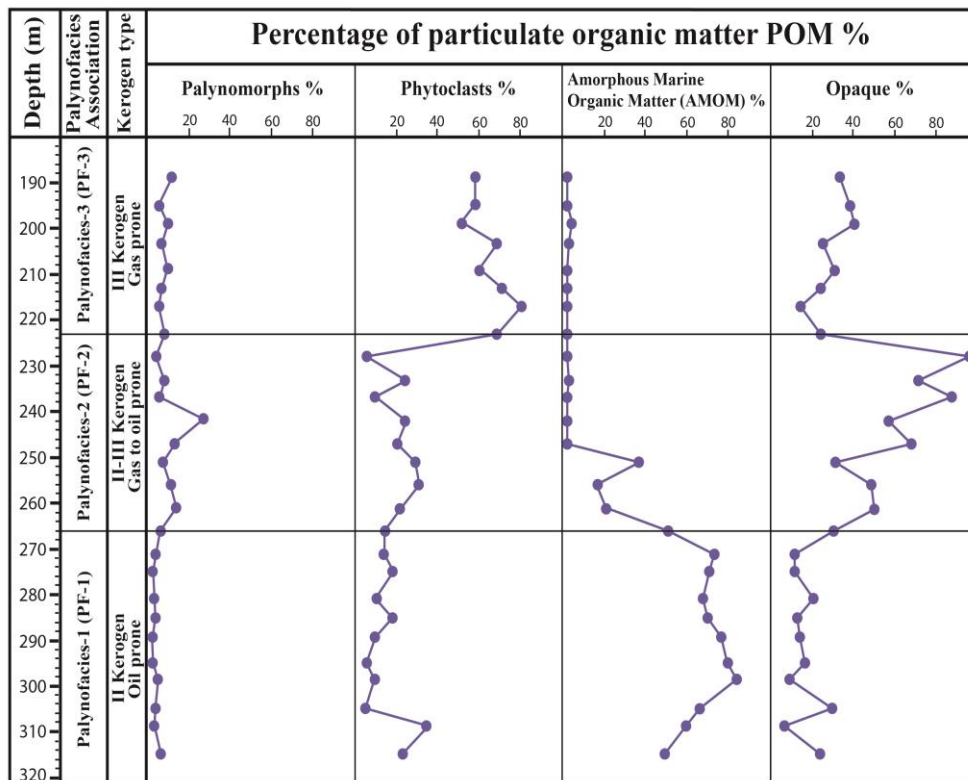
Figure 3

Percentage distribution of organic facies categories counted in the present study along with interpreted kerogen types and hydrocarbon source rock potential
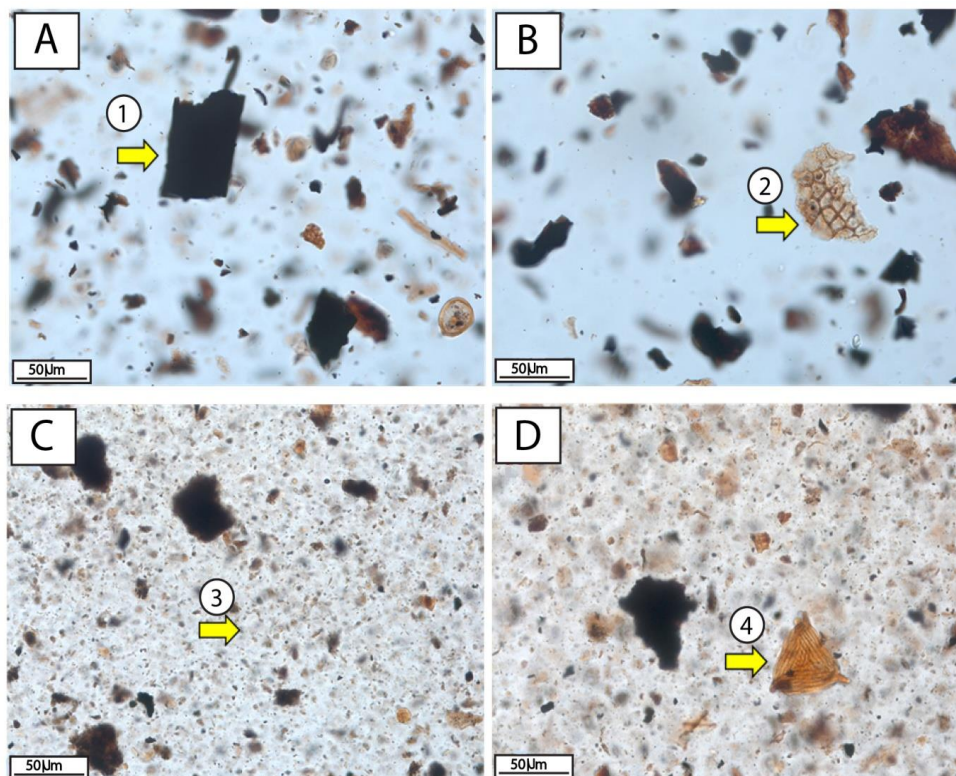
Plate 1
*Photomicrographs of the example organic facies constituents encountered
in the present study. All images were taken in transmitted white light
at 40× magnification. 1) Opaque wood tissue phytoclast, depth 255.0 m. 2)
Cuticle phytoclast, depth 246.0 m. 3) Amorphous marine organic matter AMOM,
sample no. 121 depth 300.0 m. 4) Terrigenous palynomorph (trilete spore),
depth 270.0 m.*

4.1.2. Palynofacies-2 (PF-2)

This facies occurs in the interval between 267.0 and 224.0 m. It is composed of
large amounts of opaque wood tissue origin phytoclasts (avg. 62%) along with
close to equal amounts of structured and degraded phytoclasts (avg. 17.8%) and
AMOM (avg. 13.6%). Palynomorphs (mostly terrestrial) represent only an average
of 6.6% in this organic facies (*Figure 3*; Plate 1). Among the counted structured
phytoclast particles, cuticles represented only 0–2.4%.
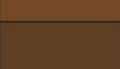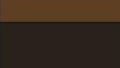
4.1.3. Palynofacies-3 (PF-3)
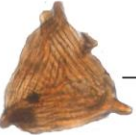
PF-3 takes place within the interval between 224.0 and 188.7 m. It is comprised
primarily of degraded and structured phytoclasts (avg. 63.3%), opaque wood tissue

origin phytoclasts (avg. 31.9%), in addition to minor amounts of palynomorphs (avg. 4.5%). AMOM was very rare in this palynofacies (*Figure 3*, Plate 1). Cuticles and tracheids occurred only in small portions (avg. 1.1%).

4.2. Thermal Alteration Index (TAI) and vitrinite reflectance (Ro%)

Observed spore/pollen exine colors in the investigated samples ranged from yellowish-orange to light orange, which correspond to TAI values of 2–2+ *(Figure 4)*. Measured Ro% values ranged from 0.31 and 0.42% throughout the entire studied interval *(Figure 5)*.

Figure 4
Pearson's spore/pollen color chart [12] compared to example palynomorphs from the present study (modified from Traverse [13]). The random vitrinite reflectance of the studied samples are ranging from 0.245 to 0.414 %"
in a boarder scale correspond to the TAI colors of the palynomorphs
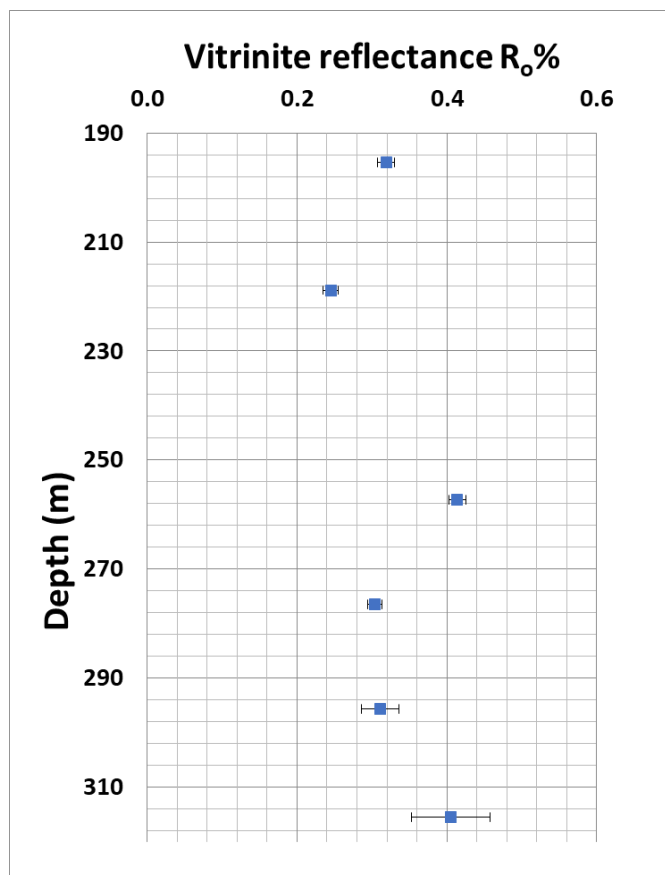
Figure 5
Vitrinite random reflectance (Ro%) data versus depth representing the thermal
maturity of the immature studied samples and the standard deviation

5. DISCUSSION

5.1. Source rock potential and organic matter type

The observed vertical variation in organic matter composition throughout the studied section was the main parameter considered in defining kerogen types and thus hydrocarbon source rock potential *(Figure 3)*. For the established three organic facies assemblages, PF-1 was mostly dominated by oil-prone materials, primarily amorphous organic matter that is derived largely from the degradation of phytoplankton or bacteria under suboxic to anoxic conditions [14, 15]. This is similar to results by Pasley et al. [5] who concluded that the transgressive Upper Mancos Formation in the San Juan Basin contains mostly amorphous marine organic matter; possessing excellent source potential. After the deposition of PF-1 and as the sea-level was apparently falling, higher amounts of transported terrigenous organic

matter increases to PF-2 which is essentially a mix of terrigenous type-III (gas-prone) and marine type-II (oil-prone) kerogen. PF-2 sequence represents the transition between the marine dominant PF-1 conditions and the terrestrially influenced PF-3 organic matter accumulation. PF-3 is interpreted to contain type-III kerogen based on the presence of high percentages of gas-producing materials, which are mainly derived from terrigenous macrophyte fragments such as xylem, phloem, and cortex tissues along with oxidized plant particles [16].

5.2. Thermal maturity of the organic matter

Observed spore/pollen coloration in the investigated samples varied from yellowish-orange to light orange under transmitted white light. These colors correlate with 2–2+ values on the TAI scale *(Figure 4)* and indicate negligible chemical change in the thermal maturity path [17]. Vitrinite reflectance (Ro%) measurements ranged from 0.245 % to 0.414 %, further confirming that the preserved organic matter in the studied section has not reached the oil window. Thus, the Upper Mancos Formation is considered as a promising oil and gas prone unit pending sufficient thermal stress to promote it to enter the oil window. These findings are consistent with the interpretation of Gentzis [6] and Broadhead [4] for the Upper Mancos along the southwestern flank of the San Juan Basin. At the present stage of maturation, the Upper Mancos sediments can only produce biogenic gas of carbon dioxide and some methane.

6. SUMMARY

Detailed palynofacies analysis was carried out on 27 core samples from the Upper Mancos Formation in McKinley County in the southwestern part of San Juan Basin, New Mexico, USA. Three palyno facies associations were recognized based on the vertical distribution of the various types of organic matter throughout the studied section. The PF-1 older sequence is dominated marine plankton and solitary alga origin fossils containing primarily type-II kerogen materials (oil-prone). PF-2 (transitional) contains a mix of marine and terrestrial organic constituents, characteristic of type-II/III kerogen (oil and gas prone). PF-3 is terrestrially dominated containing type-III kerogen materials (gas-prone). All samples were found to be thermally immature based on observed spore/pollen colors and vitrinite reflectance measurements.

REFERENCES

[1]   Faulkner, A. B., Zobaa, M. K. (2018). Paleoenvironment and hydrocarbon potential of the Cretaceous Mancos Shale in Rio Arriba County, New Mexico. 2018 *WTGS Annual Fall Symposium* "A DECADE OF SHALE", Midland, TX, USA. September 26–27. Schedule and Abstracts, p. 71.

[2]   McCrary, C., Zobaa, M. K. (2018). Palynofacies and organic geochemical analyses of the Mancos Shale Formation in the Burham-1 well, San Juan Basin, New Mexico. 2018 *SWS AAPG Annual Convention*, El Paso, Texas, USA. April 7–10, 2018. Schedule and Abstracts, p. 84

[3]   Moghazi, A. H., Hamor-Vido, M., Zobaa, M. K. (2019). Organic petrography of the Upper Cretaceous Mancos Shale in the San Juan Basin, New Mexico, USA. 2019 EGU General Assembly, Vienna, Austria. *Geophysical Research Abstracts*, V. 21. April 7–12, 2019.

[4]   Broadhead. R. F. (2018). *The Upper Mancos Shale in the San Juan Basin: Three Oil and Gas Plays*. Conventional and Unconventional: Update, p. 11096.

[5]   Pasley, M. A., Gregory, W. A., Hart, G. F. (1991). Organic matter variations in transgressive and regressive shales. *Organic geochemistry*, 17 (4). pp. 483–509.

[6]   Gentzis, T. (2013). A review of the thermal maturity and hydrocarbon potential of the Mancos and Lewis shales in parts of New Mexico, USA. *International Journal of Coal Geology*, 113, pp. 64–75.

[7]   Traverse, A. (2007). *Paleopalynology*. Topics in Geobiology, second ed. Springer, Dordrecht, Netherlands. 2007.

[8]   ISO 7404-5 (2009). *Methods for the Petrographic Analysis of Coal—Part 5: Methods of Determining Microscopically the Reflectance of Vitrinite*. International Organization for Standardization, Geneva, Switzerland. 14 p.

[9]   Zobaa, M. K., El Beialy, S. Y., Taha, A. A., Oboh-Ikuenobe, F. E. (2015). Improved GraphicalRepresentation of Sedimentary Organic Matter as Paleoenvironmental Parameters. 2015 GSA Annual Meeting, Baltimore, Maryland, USA. *Abstract*, V, 47 (7), p. 365.

[10] Taylor, G. H., Teichmüller, M., Davis, A., Diessel, C. F. K., Littke, R., Robert, P. (1998). Organic Petrology. Gebrüder Bontraeger, Berlin.

[11] Schueth, J. D., Lees, J. A. (2019). Pioneer nannofossil assemblages from the initial transgression of the Niobrara seaway in the Turonian. San Juan Basin, New Mexico, USA. *MarMP*, 151, p. 101771.

[12] Pearson, D. L.: Pollen/Spore Colour ''Standard'', Version 2. Phillips Petroleum Company, Privately Distributed.

[13] Traverse, A. (1988). *Paleopalynology*. Unwin Hyman, Boston, p. 600.

[14] Kus, J., Araujo, C. V., Borrego, A. G., Flores, D., Hackley, P. C., Hámor-Vidó, M., Kalaitzidis, S., Kommeren, C. J., Kwiecińska, B., Mastalerz M., Mendonça Filho J.,G. (2017). Identification of alginite and bituminite in rocks other than coal. 2006, 2009, and 2011 round robin exercises of the ICCP Identification of Dispersed Organic Matter Working Group. *International Journal of Coal Geology*, 178. pp. 26–38.

[15] Pickel, W., Kus, J., Flores, D., Kalaitzidis, S., Christanis, K., Cardott B. J., Misz-Kennan, M., Rodrigues, S., Hentschel, A., Hamor-Vido, M., et al. (2017). Classification of liptinite — ICCP System 1994. 169, 40–61.

[16] Tyson, R.V. (1995). *Sedimentary Organic Matter: Organic Facies and Palynofacies*. Chapman and Hall, London.

[17] Batten D. J. (1980). Use of transmitted light microscopy of sedimentary organic matter for evaluation of hydrocarbon source potential, in *Fourth International Palynological Conference*: Proceedings, Volume 2, Lucknow, India, Birbal Sahni Institute of Palaeobotany, pp. 589–594.

INTENSIFICATION OF THE BIODEGRADATION
OF WASTEWATER SLUDGE BY MICROWAVE IRRADIATION

L. HARANGHY[1] – SZ. KERTÉSZ[1] – G. VERÉB[1] –
ZS. LÁSZLÓ[1] – A. VÁGVÖLGYI[2] – Z. JÁKÓI[1] – I. CZUPY[2] –
C. HODÚR[1, 3] – G. RÁKHELY[3] – S. BESZÉDES[1*]

[1]*Department of Process Engineering, Faculty of Engineering, University of Szeged*
[2]*Institute of Forest and Environmental Techniques, Faculty of Forestry,*
University of Sopron
[3]*Institute of Environmental Science and Technology,*
Faculty of Science and Informatics, University of Szeged
*beszedes@mk.u-szeged.hu

Abstract: The applicability of microwave (MW) irradiation for sludge treatment has been intensively investigated in the last 20 years. Studies have focused on the detailed analysis of MW irradiation on waste activated sludge. Results have been derived from batch experiments.

In this study, continuous flow microwave (MW) treatment with different irradiated energy and power intensity was applied in order to improve the chemical oxygen demand (COD) solubilization and biodegradability of thickened primary dairy sludge. The efficiency of MW treatment was examined by batch mesophilic anaerobic digestion (AD) tests, as well. Our results show that the solubilization ratio (soluble to total COD, SCOD/TCOD) and aerobic biodegradability (expressed as the ratio of biochemical oxygen demand to soluble COD: BOD/SCOD) was influenced by energy input, as well as by the MW power. Increased power and/or enhanced energy input resulted in higher solubilization and biodegradability. Nevertheless, the ratios SCOD/TCOD and BOD/SCOD worsened if irradiated energy exceeded the critical value of 90 kJ/L and of 200 kJ/L with power intensity of 600 W, respectively. Biogas production is influenced mainly by the input energy.

Compared to the untreated sludge, the MW energy input of 120 kJ/L and 220 kJ/L resulted in biogas yield increments of 174% and 210%, respectively. Power intensity did not affect the cumulative biogas product, but it can be an influential parameter for the rate of anaerobic digestion. Applying 220 kJ/L energy input with different power intensities (300-600 W), it was found that 300 W power intensity resulted in accelerated anaerobic digestion; approximately 80% of total biogas volume was produced in the first 15 days of the fermentation process.

Keywords: MW treatment, wastewater sludge, sludge utilization technologies

1. INTRODUCTION

In the EU approximately 60% of renewable energy generation is based on biomass, but 80% of biomass energy originates from wood utilization [1]. The diversification of bioenergy raw materials should be encouraged and the role and ratio of waste and

byproduct in the bioenergy production should be increased, according to the waste-to-energy (W2E) concept. Because of its high organic matter content, the sludge originating from municipal wastewater treatment plants and agrifood industry has high potential for biofuel – mainly for biogas – production.

Sludge generation is continuously rising, because of the growing urbanization and the concentration of industrial activities into industrial parks, respectively. In cities and industrial parks the wastewater purification technology has high removal efficiency; mainly in the mechanical (primary) stage of technology but also in biological wastewater treatment (secondary) stage a huge amount of sludge is produced containing the wastewater pollutants in a concentrated form. During the conventionally used wastewater treatment technologies approximately 8–10 kg/m^3 of waste activated sludge is produced [2]. Furthermore, the specific sludge generation of several types of industry effluents is higher than that for municipal wastewater; therefore, sludge handling has become more and more costly for companies in recent decades. Among the numerous methods availalbe, anaerobic digestion (AD) is often applied for both sludge stabilization and biogas production. Involving sludge in biomass based energy generation has several benefits: it provides facilities to stabilize the sludge with reduced environmental hazard, it makes the utilization of nutrients for agriculture possible, (the main concept of the circular economy), and it reduces the net CO_2 emissions.

In most cases, bioenergy generation based on biotransformation (fermentation) processes needs pre-treatments to make biological degradation and enzymatic hydrolysis possible, or to increase their efficiencies [3]. The direct energetic utilization of biomass needs pretreatment, as well, to increase the energy density of raw materials [4]. Conventional thermal pre-treatments, often in combination with chemical methods, are widely used in practice, but more and more attention is being devoted to finding alternative, non-conventional heating sources that can be applied for enhanced sludge processing [5].

Due to its volumetric and selective heating effect, microwave irradiation provides an energetically effective method for biomass treatment, especially for materials with high water content, such as sludge. Microwave effects on sludge can be explained by three different mechanisms, thermal (heat generation); specific non-thermal effects of the electromagnetic field; and catalytic oxidation [6]. Because of the polar characteristic, water molecules and other polar components have high energy dissipation capability. Therefore, in the processing of high water content sludge by high MW energy intensity the thermal effect dominates over the non-thermal effect [7]. The dielectric behavior of sludge leads to high temperature increase during microwave heating, and the high heat stress and temperature gradient generated inside the processed materials manifests in rapid hydrolysis of macromolecular components, and disruption of cell walls, respectively [8]. It can be noted that the ability of molecules to oscillate is different for the free and bounded water content.

Summarizing the results available in the scientific literature, it can be concluded that microwave (MW) treatment is suitable to increase the soluble chemical oxygen demand (SCOD) of sludge. The increment in the solubility of organic matters,

disruption of cell walls and extracellular polymeric network, furthermore the destruction of original aerobic microbial community leads to intensified anaerobic digestion process of sludge. Increment of solubility degree is influenced by the type (origin) of sludge, time of MW irradiation, microwave power, physicochemical and dielectric properties of components, and total and volatile solid content of materials. In MW treatment, higher initial volatile solid concentration resulted in a higher degree of solubilization [9].

The majority of research papers deal with relatively low total solid (TS) content sludge. Very little research has focused on the efficiency analysis of the MW treatment of thickened sludge, or sludge cake from dewatering processes (sludge belt and screw press, sludge filtering press, etc.). Sludge with a high content of solid and organic matter is sensitive to the use of an appropriate temperature range. In research practice, the temperature range over the boiling point (120–200 °C) is used for sludge treatment, mainly on the lab scale, with batch pressurized reactors. But in sludge with a high protein and carbohydrate content (from the primary dairy industry or canning industry, for instance) the macromolecular components are rapidly decomposed to free amino acids and reducing sugars, which contribute to the occurrence of Maillard-type reactions [10] , whose products are resistant to biodegradation.

Unfortunately, studies available in the field of microwave irradiation of sludge have focused mainly on batch treatment with small sludge samples (10–200 mL). Therefore the irradiated MW energy range was varied widely in the range of 50–80,000 kJ/g VS, depending on the quantity of the sample, irradiation time and the power of microwave equipment. Considering the type of processed sludge, it can be concluded that mainly the effects of MW irradiation on waste activated sludge have been investigated; very few papers have been concerned with primary sludge treatments. Therefore, our research focused on the investigation of the applicability and efficiency of microwave pre-treatment on the biodegradability of primary, thickened sludge from the food industry.

2. MATERIALS AND METHODS

The thickened wastewater sludge samples originated from a dairy in Szeged, Hungary. The main characteristics of the sludge are summarized in *Table 1*. Sludge samples were stored refrigerated (+4 °C) in closed plastic containers before processing to avoid dehydration and the solubility change from freezing-thawing.

Table 1

Main characteristics of sludge

TS [%]	pH [-]	COD [mg/L]	SCOD/TCOD [%]	BOD$_5$ [mg/L]
4.9±0.22	6.2±0.32	23910±421	23±1.8	1424±63

TS-total solids; SCOD and TCOD-soluble and total chemical oxygen demand;
BOD$_5$-5 day biochemical oxygen demand

Microwave pre-treatments were carried out in a semi-pilot, specially-made microwave unit equipped with a magnetron with variable nominal power in the range of 200–650 W at an operating frequency of 2,450 MHz. In continuous flow operation mode the sludge flows through a toroidal pipe (inside diameter 10 mm) placed inside the microwave cavity. The flow rate was varied in the range of 5–60 L/h by the revolution of a peristaltic pump. Energy input (kJ/L) was calculated from the magnetron power, volumetric flow rate and residence time of sludge in microwave reactor.

The total solid content (TS) of sludge was measured by drying cabinet method at 105 °C. Chemical oxygen demand (COD) was determined by photometric method according to ISO 6060-1989 with HACH cuvette tests. To separate the soluble organic matters (expressed as SCOD) sludge samples were centrifuged (RCF of 10,000 G for 20 minutes) and filtered (0.45 mm syringe filter), after dilution (dilution factor was 10). Biochemical oxygen demand (BOD_5) was measured in a respirometric BOD meter (Oxidirect) at 20 °C for 5 days (according to the DIN 38409H51 method). Each analytical test was carried out three times.

Batch mesophilic anaerobic digestion (AD) test was applied to determine the biogas production of sludge at 37 °C for 30 days. AD tests were carried out in lab-scale, continuously stirred glass reactors (volume of 250 mL with sample volume of 100 mL, head space of 150 mL), applying adapted mesophilic municipal sludge as inoculum at a dosage of 10 vol%. The pH of sludge samples was adjusted to 7.2 and nitrogen purging was used before the tests to ensure the anaerobic condition. The volumetric biogas production was determined by manometric method, pressure increment was detected by Oxitop-C measuring heads, gas volume was calculated by ideal gas law. AD tests were triplicated; biogas product was given as the mean of the calculated volumes.

3. RESULTS AND DISCUSSION

Studies have reported that the divalent cations can bind to extracellular polymeric substances (EPS), which produce larger and more compact flocs. MW treatment is suitable to disrupt the polymeric matrix formed by polysaccharides, proteins, and products of microbial metabolism. Microwave induced disintegration of sludge flocks assists in releasing organic matter from i) the polymeric network, and ii) intracellular space due to the cell wall disruption effect, therefore the solubility of COD (given by the SCOD parameter) increases. In the MW sludge treatment process the COD solubilization is influenced by the pH, TS content, and energy input. Our preliminary results show that in batch processing, beside the irradiation time and energy, the specific MW power intensity also has an effect on the disintegration degree [11].

The results of our continuous flow treatment show that the solubilization ratio (SCOD/TCOD) of thickened primary dairy sludge was influenced by both energy input and the MW power. At lower power intensity (in the range of 300–500 W), increasing energy input resulted in the enhancement of SCOD/TCOD. Solubility of organic matters of raw sludge (23%, data not shown in figures) improved by over

40% after MW treatments. But a worsening effect of energy input increment was found for MW treatment at 600 W, if energy input exceeded 90 kJ/L (*Figure 1*).
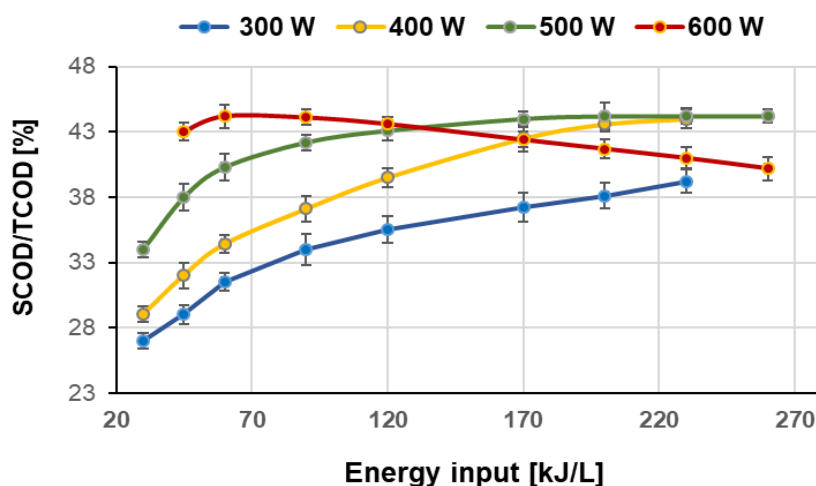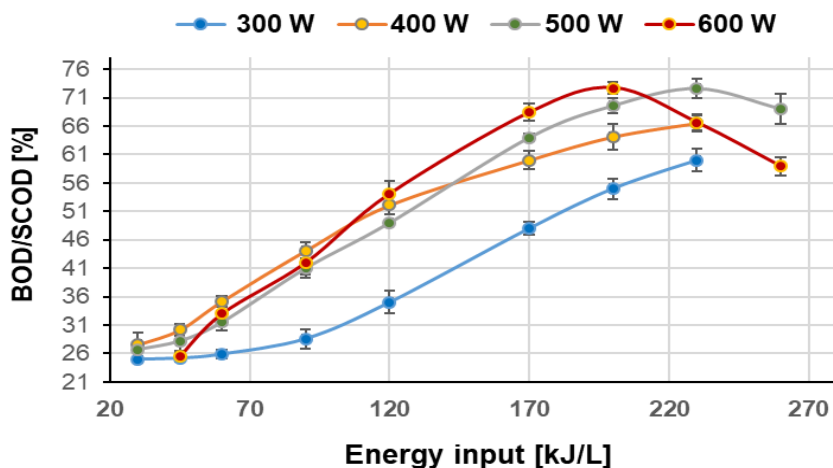

Figure 1
Organic matter solubility (SCOD/TCOD) as a function
of MW energy input (kJ/L) and power intensity (W)
(SCOD-soluble chemical oxygen demand, TCOD-total chemical oxygen demand)

Ahn et al. [12], Uma et al. [9], and Ebenezer et al. [13] reported the specific irradiated MW energy (energy input) to be the main factor in organic matter solubilization. Their batch MW waste activated sludge disintegration tests verified that over a certain value energy input (14,000–82,000 kJ/kg TS, depending on the type of sludge) the SCOD/TCOD worsens. In our experiments a lower amount of energy was irradiated, but it has been clearly verified that the MW irradiation applied to continuously flowing sludge was suitable to increase the COD solubilisation. However, because the increment of organic matter solubility is limited, no further enhancement in SCOD/TCOD was observed when the sample was MW irradiated at 200 kJ/L or higher *(Figure 1)*.

Increased organic matter solubility is reported to be advantageous because it stimulates improvement in biodegradability [14], [15]. MW pre-treatment for sludge, applied prior to biological transformation processes (such as anaerobic digestion or composting), has great potential because enhanced solubility makes the biodegradation and enzymatic hydrolysis processes faster. In order to quantify the efficiency of MW treatment of sludge on the change of biodegradability, the ratio of biochemical oxygen demand (BOD) to soluble chemical oxygen demand (SCOD) was calculated. This parameter indicates the bioavailability (in this study, the ability to undergo aerobic microbial degradation in a 5-day period) of organic matter in the soluble phase of sludge.

Results show the same tendency which has been revealed for SCOD/TCOD, i.e. the increment of irradiated energy and MW power had a positive effect on biodegradability, but over a certain energy input (200 kJ/L), application of the higher power intensity range (500–600 W) led to a decrease in the ratio of biodegradable organic matter *(Figure 2)*.

Figure 2
BOD/SCOD of sludge pre-treated by MW
with different power intensity (W) and energy input (kJ/L)
(BOD-biochemical oxygen demand, SCOD-soluble chemical oxygen demand)

Similarly to the change of organic matter solubility, aerobic biodegradation is supposed to be inhibited by compounds formed in high energy and/or high temperature MW treatment [16]. It should be noted that there was no significant difference in BOD/SCOD if the power intensity was varied in the range of 400–600 W when energy input of 50–120 kJ/L was applied.

For the evaluation of the efficiency of MW treatment for enhanced biodegradability, mesophilic AD tests are the most frequently used method. In general, MW irradiation is suitable to intensify the anaerobic digestion process. The main effect of MW irradiation, applied as a pre-treatment step in biogas technology, is attributed to the hydrolysis stage of anaerobic digestion [17]. Hydrolysis is considered the main rate-limiting step of AD; therefore, MW pre-treatments are suitable to increase the specific biogas yield (on TS, i.e. total solid or VS, i.e. volatile solid basis), and also accelerate the digestion process.

Sludge contains different microbial cells and organic and inorganic components that work together with extracellular polymeric substances to build up a special physicochemical structure that is resistant to anaerobic digestion. Kavitha et al. [18] concluded that the energy efficiency of MW treatments aiming at biomass lysis and enhanced hydrolysis (and therefore increasing the methane production) was higher if

EPS and sludge flocs are disrupted in a preliminary stage using mechanical (ultra-sonication) and/or chemical (alkali dosage) methods. These methods are suitable for decreasing the average size of solid particles and increasing the specific surface area of particles and flocs. These effects result in easier penetration for electromagnetic waves (higher penetration depth) and higher dissipation of irradiated MW energy.

The release of divalent cations from sludge flocs, which is due to i) the defloccu-lating effect of MW and ii) release of ionic components from intracellular space from cell wall disruption, has a synergetic effect that leads to an increase in ionic strength. Therefore, further research is needed to investigate the effect of the change of ionic strength on the microbial activity in the different stages of the anaerobic digestion (AD) process [2]. Effects of high-intensity microwave irradiation on contaminants of emerging concern (CECs) have not yet been examined in detail. Further research is needed to explore the pathways of transformation of CECs exposed to a high-intensity electromagnetic field, mainly in real, multicomponent, and biological active systems such as sludge.

Beyond the promising results related to MW irradiation when using it as a pre-treatment method for AD, it should be highlighted that the production of wastewater sludge in sewage treatment plants is continuous, therefore the detailed investigation of continuous flow microwave sludge processing is needed. In our research the mesophilic biogas production of sludge samples treated at different MW power and specific MW energy input (determined from volumetric flow rate, residence time in microwave reactor, sample volume and magnetron power) was measured in a 30-day fermentation period. The specific volumetric biogas product was given on a TS basis *(Figure 3).* It can be concluded that continuous flow MW irradiation of sludge increased the biogas product. Application of MW treatment with an energy input of 120 kJ/L and 220 kJ/L resulted in biogas yield increments of 174% and 210%, respectively, compared to the biogas product of raw sludge (118 mL/g TS, data not shown in figures).

Results of the AD tests show that at higher levels of irradiated energy (120–220 kJ/L) the power intensity of MW treatment has no significant effect on the biogas production *(Figure 3)*. If irradiated energy was in the range of 45–60 kJ/L the power intensity has a slight effect on the biogas yield. The difference between the biogas yield of sludge exposed to 300 W and 600 W MW power with energy input of 45 and 60 kJ/L was 15% and 21%, respectively. Microwave treatments applied prior to AD are reported as a suitable method to increase the biogas production. Several studies highlighted that microwave irradiation alone – or in combination with chemical methods – under optimized conditions resulted in a higher methane ratio in the produced biogas [19], [20]. There are no known sludge pre-treatment methods especially designed and optimized to produce substrate exclusively to methanogenic archaea. Microwave irradiation is widely used in the industry, but there is not enough experience derived from semi-pilot and pilot systems to implement directly to industry scale sludge processing. Among many factors of scale-up, one difficult question that arises is how to define control parameters. In lab-scale studies the biogas yield is given as the maximum achievable cumulative values in 30–60 days anaerobic digestion

process. The AD process operating on the industrial scale through continuous flow and one-stage digester in the mesophilic temperature range is decidedly not controlled to achieve the maximum biogas yield. On the other hand, the economic motivations are to minimize the capital costs for installing digesters and other service units and to minimize the operation expenditures of AD plants, while at the same time the technology should remain 'flexible' to variable feed quantity and quality. From this aspect the biogas production rate is considered as an important parameter [21].
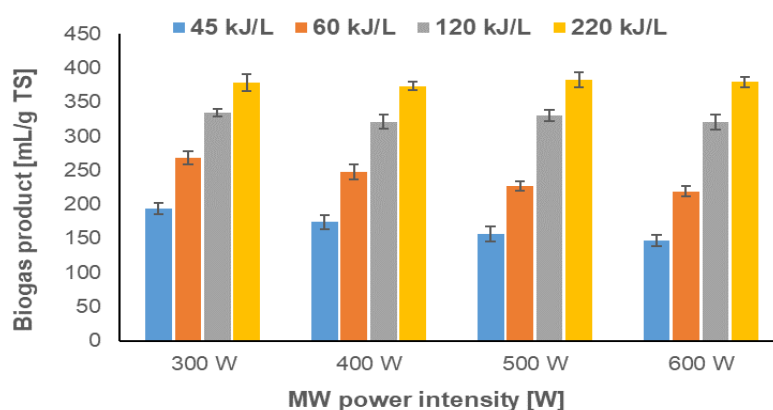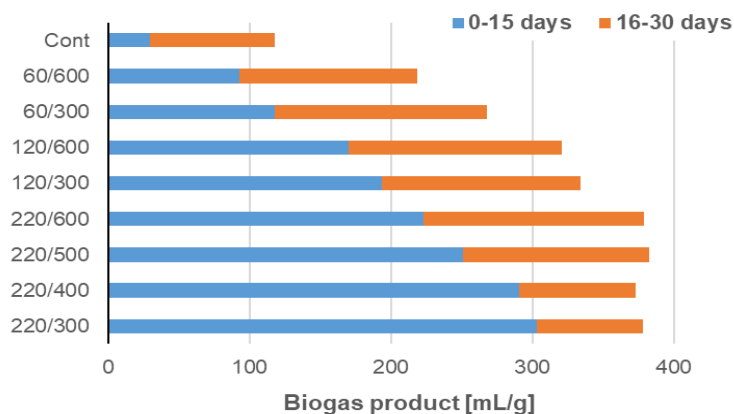

Figure 3
Biogas product of MW pre-treated sludge
(biogas product is given on total solid basis)

In order to quantify the effect of MW treatment on the rate of anaerobic digestion the cumulative biogas production of the first period (0–15 days) and second period (16–30 days) of the AD process was calculated from the daily volumetric biogas production. Results related to the contribution of the two periods to total biogas yield show that MW pre-treatment can accelerate the anaerobic digestion process. Compared to the raw sludge (Cont), the MW pre-treated sludge produced a greater amount of biogas in the first 15 days of fermentation *(Figure 4)*.

A study by Gil et al. [16] verified the positive effect of MW irradiation on methane production rate for mixed sludge (primary and secondary sludge, originating from 80% municipal and 20% agrifood-industry wastewater). The results of our AD tests show that the total cumulative biogas product is mainly influenced by the irradiated energy; in the range of energy input of 120–220 kJ/L the power intensity has no significant effect on biogas production. But considering the daily volumetric biogas production, our results reveal that the power intensity applied has an effect on the rate of anaerobic digestion process. As *Figure 4* shows, applying the same energy input of 220 kJ/L with different power intensity (300–600W), the lower power intensity resulted in accelerated anaerobic digestion, with approximately 80% of the total biogas volume being produced in the first 15 days of the fermentation process.

Therefore, in continuous flow MW treatment of sludge, the MW power intensity does not affect the cumulative biogas yield, but can be an influential parameter for the rate of anaerobic digestion.

Figure 4
Cumulative biogas product in the 1st (0–15 days) and
2nd (16–30 days) period of AD process
(Cont- non treated sample; MW pre-treatments are encoded
as energy input [kJ/L] / power intensity [W])

4. CONCLUSIONS

Many studies have verified the rapid and strong sludge disintegration effect of microwave (MW) irradiation, applying it as stand-alone method or coupled with conventional chemical method, advanced oxidation processes, enzymatic treatment, or ultrasonication. Increased organic matter solubility is induced by disintegration, which is also manifested in higher biogas production. Most studies available present results obtained from batch MW treatment of municipal waste activated sludge; however, detailed information about the efficiency and applicability of continuously flow MW treatment for enhanced biodegradability is missing. In our earlier research the advantages of batch MW pre-treatment for enhanced disintegration of sludge and accelerated anaerobic digestion were verified. In the present research, the efficiency of continuous flow MW treatment of thickened primary dairy industry sludge was investigated. Our experimental results verified that MW pre-treatment was suitable to increase the SCOD/TCOD, which indicated an enhanced degree of solubilization. Furthermore, the aerobic biodegradability (expressed in BOD/SCOD) and the biogas production improved by 170–210% (depending on the MW power and irradiated energy). Results revealed that the power intensity of MW irradiation has an effect on COD solubilization and irradiated energy affects biogas yield. Increasing the irradiated energy (energy input) and microwave power intensity resulted in higher organic matter solubility. However, irradiated energy at levels over 90 kJ/L had a negative

effect on COD solubility, and 200 kJ/L at 600 W power intensity, worsened aerobic biodegradability. Results of mesophilic AD tests revealed that the biogas yield increased due to the use of MW irradiation as a pre-treatment; furthermore, the rate of anaerobic digestion process accelerated. Analysis of the effects of MW-related process parameters on the efficiency of AD shows that the cumulative biogas production is influenced mainly by the energy input. The power intensity of MW irradiation has only a slight effect on biogas yield, if energy input exceeds 120 kJ/L, but it can be an influential parameter for the rate of anaerobic digestion/biogas production. Our experiments verified that continuous flow microwave treatment can assist in achieving higher utilization of organic matter in primary food industry sludge in the form of biogas. We conclude that MW processing technology – under optimized conditions – can be an answer to the challenge of achieving higher utilization of waste and byproduct towards the valorization of secondary resources. With well-designed MW pre-treatments the availability of organic matter fraction of sludge can be increased, which will lead to accelerated anaerobic digestion and higher biogas yield. These results contribute to achieving higher valorization of sludge with reduced environmental impact of digestate and higher energy efficiency of sludge utilization technologies.

REFERENCES

[1] Proskurina, S., Sikkema, R., Heinimö, J., Vakkilainen, E. (2016). Five years left–How are the EU member states contributing to the 20% target for EU's renewable energy consumption; the role of woody biomass. *Biomass Bioenerg.*, 95, pp. 64–77.

[2] Yigit, B. C., Apul, O. G. (2020). Critical review for microwave pretreatment of waste-activated sludge prior to anaerobic digestion. *Curr. Opin. Env. Sci. Health*, 14, pp. 1–9.

[3] Chen, Y., Cheng, J. J., Creamer, K. S. (2008). Inhibition of anaerobic digestion process: a review. *Bioresour Technol.*, 99 (10), pp. 4044–4064.

[4] Van Quyen, T., Nagy, S. (2015). Effect of various production parameters on biomass agglomeration. *Geosci. Eng.*, 4 (7), pp. 86–96.

[5]   Remya, N., Lin, J. G. (2011). Current status of microwave application in wastewater treatment—a review. *Chem. Eng. J.*, 166 (3), pp. 797–813.

[6]   Kostas, E. T., Beneroso, D., Robinson, J. P. (2017). The application of microwave heating in bioenergy: A review on the microwave pre-treatment and upgrading technologies for biomass. *Renew. Sustain. Energ. Rev*., 77, pp.12–27.

[7]   Géczi, G., Horváth, M., Kaszab, T., Alemany, G. G. (2013). No major differences found between the effects of microwave-based and conventional heat treatment methods on two different liquid foods. *PLOS ONE*, 8 (1), e53720, 12 p.

[8]   Coelho, N., Droste, R. L., Kennedy, K. J. (2014). Microwave effects on soluble substrate and thermophilic digestibility of activated sludge. *Water Environ*., 86, pp. 210–222.

[9]   Uma, R. R., Kumar, A., Kaliappan, S., Yeom, I. T., Banu, R. J. (2013). Impacts of microwave pre-treatments on the semi-continuous anaerobic digestion of dairy waste activated sludge. *Waste Manage*., 33, pp. 1119–1127.

[10] Richel, A., Jacquet, N. (2015). Microwave-assisted thermochemical and primary hydrolytic conversions of lignocellulosic resources: a review. *Biomass Conv. Biorefin.*, 5 (1), pp. 115–24.

[11] Beszédes, S., László, Z., Szabó, G., Hodúr, C. (2009). Examination of the effect of microwave heating on the biodegradable and soluble fraction of organic matter of sludge. *Ann. Fac. Eng. Hun.*, 7, pp. 87–90.

[12] Ahn, J. H., Shin, S. G., Hwang, S. (2009). Effect of microwave irradiation on the disintegration and acidogenesis of municipal secondary sludge. *Chem. Eng. J.*, 153, pp. 145–150.

[13] Ebenezer, A. V., Kaliappan, S., Adish Kumar, S., Yeom, I. T., Banu, J. R. (2015). Influence of deflocculation on microwave disintegration and anaerobic biodegradability of waste activated sludge. *Bioresour Technol*., 185, pp. 194–201.

[14] Beszédes, S., László, Z.; Szabó, G.; Hodúr, C. (2008). Enhancing of biodegradability of sewage sludge by microwave irradiation. *Hung. J. Ind. Chem.*, 36, pp. 11–16.

[15] Houtmeyers, S., Degrève, J., Willems, K., Dewil, R., Appels, L. (2014). Comparing the influence of low power ultrasonic and microwave pre-treatments on the solubilisation and semi-continuous anaerobic digestion of waste activated sludge. *Bioresour. Technol*., 171, pp. 44–49.

[16] Gil, A., Siles, J. A., Toledo, M., Martín, M. A. (2019). Effect of microwave pretreatment on centrifuged and floated sewage sludge derived from wastewater treatment plants. *Process Saf. Environ. Prot*., 128, pp. 251–258.

[17]   Beszédes, S., Szabó, G., Géczi, G. (2012). Application of thermal and micro-wave pre-treatments for dairy wastewater sludge. *Ann. Fac. Eng. Hun.*, 10, pp. 231–235.

[18]   Kavitha, S., Banu, J. R., Kumar, G., Kaliappan, S., Yeom, I. T. (2018). Prof-itable ultrasonic assisted microwave disintegration of sludge biomass: Model-ling of biomethanation and energy parameter analysis. *Bioresour. Technol.*, 254, pp. 203–213.

[19]   Liu, J., Tong, J.; wie, Y.; Wang, Y. (2015). Microwave and its combined pro-cesses: an effective way for enhancing anaerobic digestion and dewaterability of sewage sludge? *J Water Reuse. Desalin.*, 5 (3), pp. 264–70.

[20]   Kuglarz, M., Karakashev, D., Angelidaki, I. (2013). Microwave and thermal pretreatment as methods for increasing the biogas potential of secondary sludge from municipal wastewater treatment plants. *Bioresour. Technol.*, 134, pp. 290–297.

COST ESTIMATION OF COMBINED MEMBRANE SEPARATION AND DIFFERENT ADVANCED OXIDATION PROCESSES PRE-TREATMENT OF OILY WASTEWATER

ZS. LÁSZLÓ[1, 2 *] – Á. FAZEKAS[1] – C. HODÚR[1, 2] – G. ARTHANAREESWARAN[3] – G. VERÉB[1]

[1]*Institute of Process Engineering, Faculty of Engineering, University of Szeged, HU-6725, Moszkvai Blvd. 9., Szeged, Hungary*
[2]*Institute of Environmental Science and Technology, University of Szeged, H-6720, Tisza Lajos Blvd. 103, Szeged, Hungary*
[3]*Membrane Research Laboratory, Department of Chemical Engineering, National Institute of Technology, Tiruchirappalli-620015, Tamilnadu, India*
* e-mail address: zsizsu@mk.u-szeged.hu

Abstract: The current study deals with comparison of the cost of oily wastewater treatment by membrane filtration associated with different pretreatment methods. The cost evaluation was completed for model oily wastewaters containing 100 ppm crude oil in saline or distilled water, and in some cases for real produced water, aiming at elimination of oil content. Three different pre-treatment methods – ozonation, Fenton and photo-Fenton pretreatments – and the modification of the used membrane surfaces with photocatalytic nanoparticles were used for the mitigation of fouling and enhancing oil elimination efficiency during the process. The cost estimation was evaluated on the basis of flux decline and the cost of pre-treatments. Results showed that pre-oxidation enhances the flux, thus potentially decreasing the cost of combined treatment. The lower cost was achieved by the application of modified membrane surfaces, which shows that the development of antifouling surfaces may further decrease costs of membrane filtration.

Keywords: Oily wastewaters, membrane filtration, waste reduction, titanium dioxide, carbon nanotubes, cost evaluation

1. INTRODUCTION

Oily wastewaters originate from several industries, especially the oil industry, oil mining, oil refining, oil storage transportation, and petrochemical industries. Besides them, other industries like machinery or food industry also produce a considerable amount of oily wastewaters. The composition and characteristics of these waters strongly depend on the releasing industry; however many of them contaminated by crude oil, with nondescript composition. As crude oil is a mixture of different organic and inorganic compounds, which are often toxic, discharged oily wastewaters pollute surface and underground water, endangering aquatic resources and human health [1], [2].With the continuous improvement in environmental standards, the existing

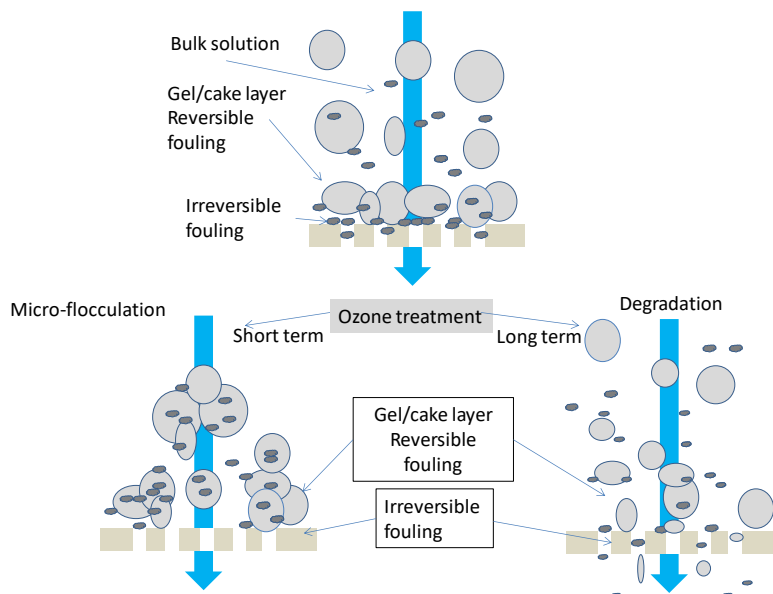methods have been unable to meet the requirements, thus more efficient technologies should be developed [1].

In order to meet environmental standards and to achieve reusable and recyclable water from oily wastewaters, several investigations have been focused on developing water treatment technologies for oily wastewaters [3]. Conventional water treatment technologies involve physical, chemical and biological methods. Although the biological treatments are cost-effective, these industries produce large volumes of wastewater contain recalcitrant compounds, possibly toxic organic pollutants which are difficult to treat by biological methods [4].

In oily wastewater emulsions, the typical oil concentrations vary from 50 up to 1,000 ppm of oil [5]. Several techniques have been used for oil-in-water emulsion purification, such as air flotation, heating, ozonation, coagulation-flocculation, and membrane filtration [6]. The physical and chemical methods that can be applied have high capital costs, and the cost of chemicals for chemical treatment is high [3]. Moreover, the current methods cannot remove the dispersed, suspended oil content.

Among the physical processes, membrane-based separation is a promising technology for 21st century since there is no necessity for chemical additives and the energy costs are relatively low [6]. Ultrafiltration (UF) is the most effective treatment for oily wastewater, possessing high oil-removal efficiency however, membrane fouling is a considerable limiting factor.

Membrane separation processes combined with pretreatments may enhance the elimination efficiency and reduce the filtration resistance. Earlier studies showed that pre-oxidation of oily wastewaters may be an advantageous solution, as it degrades the organic pollutants in oily wastewaters, and in parallel, it may improve the flocculation efficiency and particle removal during the filtration step [7], [8]. These advanced oxidation processes may include ozone, UV/hydrogen peroxide, Fenton or photo-Fenton reaction, and heterogeneous photocatalysis. Advanced oxidation processes and ozone treatment generate free radicals, which are able to react with the contaminants directly and indirectly, and finally decompose to oxygen. In these reactions two typical pathways have been observed, influencing membrane filtration parameters: (1) the micro-flocculating effect producing associated colloidal particles, and (2) degradation of organic materials *(Figure 1)*. The latter decreases the retention of pollutants and may increase the pore fouling, thus short-term oxidation pretreatment may lead to micro-flocculation and result in large floccules, thereby reducing membrane fouling [9], [10]. This means that for combined techniques the pre-oxidation processes should be optimized in terms of filtration parameters.

Another approach to membrane fouling mitigation is to modify membranes with photocatalytic nanoparticles, therefore combining the advantages of membrane filtration (physical separation) and the advantage of photocatalysis (non-selective organic matter degradation) [12]. TiO_2 is one of the most commonly used photocatalysts due to its good physical and chemical properties, availability, high photocatalytic activity, and desirable hydrophilic properties [13–17], but recently the application of new nanoparticles is being widely investigated [18].

Bulk solution

**Gel/cake layer
Reversible
fouling**

**Irreversible
fouling**

Micro-flocculation

Ozone treatment

Short term　　　　**Long term**

Degradation

**Gel/cake layer
Reversible
fouling**

**Irreversible
fouling**

Figure 1
Possible effects of ozone pretreatment on membrane filtration [11]

Several investigations have focused on the optimal operational conditions, and only a few works contain cost evaluation, which is essential to choose an appropriate method for water treatment technology. The cost of water treatment depends on both the technological aspects and the regulation requirements.

The economics of membrane filtration are determined by the initial investment cost of the membrane modules, equipment, and facilities. The key parameter is the permeate flux, which is determined by the driving force (typically the transmembrane pressure) and the hydrodynamic resistance of the membrane and the particle layer accumulates on the membrane surface, namely the fouling. Membrane fouling affects both capital and operating costs by affecting the membrane area and energy requirements [19].

For estimating the cost of technology to be chosen, preliminary design and economic potential estimation should be attained [20]. Preliminary experimental data provide a basis for the operational parameters and technical requirements, while economic evaluations give an estimate of capital and operational costs. The costs of advanced oxidation processes are highly dependent on the quality of the source water to be treated and effluent treatment goals [21]. Although very few studies aim at investigation of advanced oxidation processes (AOPs) involving cost estimation analysis, summarizing them, they conclude that the main factors influencing the prices are the removal efficiency and flow rate; capital, operational and management costs increased with higher removal efficiency [22].

Although AOPs are known to be relatively expensive processes, by applying them as pre-treatment, without aiming for total pollutant elimination during oxide-

tion, their cost may become competitive to membrane filtration. In this work a comparison of the cost of oily wastewater treatment by membrane filtration associated with different pre-treatment methods was performed. The cost evaluation was completed for model oily wastewaters containing 100 ppm crude oil in saline or distilled water, and in some cases for real produced water, aiming elimination of oil content. In the present study the four different promising methods of pre-ozonation [23], Fenton or photo-Fenton reaction, and photocatalytic nanoparticle modified membranes [18], [12] were used for the mitigation of fouling during membrane filtration. The cost estimation was evaluated on the basis of flux decline and the cost of pre-treatments.

2. EXPERIMENTAL

2.1. Materials and methods

Model wastewater composition: oil in water (o/w) emulsions ($c_{oil} = 100$ mg L^{-1}; $d_{droplets}$ < 1.5 μm) were prepared in 2 steps, using crude oil (provided by MOL Zrt.; Hungary), and ultrapure water (PureLab Pulse, ELGA Labwater, UK). Intensive stirring (35,000 rpm, 1 min) of crude oil and water was followed by 10 min ultrasonic homogenization (Hielscher UP200S, Germany) at 25 °C (using maximal amplitude and cycle). For the photocatalytic experiments 20 ppm oil concentration was set by the dilution of the emulsion. In case of saline water, a model of real groundwater located in south Hungary was prepared, which contained the following salts: 2.26 g L^{-1} $NaHCO_3$; 53.4 mg L^{-1} NH_4Cl; 19.1 mg L^{-1} $CaCl_2$; 20.9 mg L^{-1} KCl; 93.5 mg L^{-1} NaCl; 4.5 mg L^{-1} $FeCl_3$ and 35.1 mg L^{-1} $MgSO_4$ (Sigma Aldrich; analytical grade).

The investigated real wastewater was produced from the southern part of Hungary, containing crude oil. (Extractable oil content 28±2 ppm, turbidity 44.2±0.5 NTU, pH 7.95±0.05, COD 927±10 mg L^{-1}.)

Pre-ozonation was carried out in a glass batch reactor, the ozone was generated from clean oxygen (Messer; 3.5) by a flow-type ozone generator (BMT 802N, Germany) and it was bubbled through a diffuser into a batch reactor containing 400 mL of the given oil-in-water emulsion, equipped with a magnetic stirrer (Fig. 2a). The applied flow rate was 1 L min^{-1} and ozone concentration of inlet and outlet was measured using a WPA Biowave II type UV spectrophotometer, with the wavelength set at $\lambda = 254$ nm) to determine the absorbed volume of ozone. If pre-ozonation was applied, its duration was only 5 minutes in all cases, since our previous studies [23], [24] proved that longer pre-ozonation can result in pore blocking (due to the fragmentation of the oil droplets) and also results in lower purification efficiency because of the generated water-soluble organic oxidation by-products. The applied 5 min long pre-ozonation resulted in 30 ± 5 mg L^{-1} of absorbed ozone dose. The remaining dissolved ozone was purged by oxygen after the treatment to avoid damage of the used membrane. In the case of real wastewater, the duration of ozone treatment was 2 min, with 28±2 mg L^{-1} absorbed ozone.

Fenton-type reactions were carried out at pH = 4, the concentration of H_2O_2 (VWR Hungary) was 300 ppm, ratio of n_{Fe}:$n_{H2O2} = 1 : 25$ *(Figure 2b)*, and before membrane filtration the pH was set to be 7, and (possibly) remaining H_2O_2 was

decomposed enzymatically with catalase enzyme. Photo-Fenton reactions were carried out by the irradiation of the emulsion with an immersed compact fluorescent UV-tube ($\lambda_{max} \approx 254$ nm, 10 W, Lighttech Ltd, Hungary). For determination of the residual amount of hydrogen peroxide, COD measurements were performed before and after the addition of catalase enzyme.

For the membrane surface modification, commercial titanium dioxide (TiO$_2$; Aeroxide P25, Germany, d = 25–39 nm, a^S_{BET} = 50.6 m^2 g^{-1}) and carbon nanotubes (CNT; Nanothinx NTX1 multi-walled carbon nanotube, Greece, l $\geq$ 10 μm; d = 15-35 nm) were applied. Nanomaterials (TiO$_2$ and CNT) by themselves or in composites (TiO$_2$ with 1 wt% CNT) were suspended in 2-propanol (c = 400 mg L^{-1}) by 1 min ultrasonic homogenization (Hielscher UP200S, Germany) at 25 °C (maximal amplitude and cycle were applied). 40 mg of the given nanomaterial (suspended in 100 mL of 2-propanol) was immobilized on a polyvinylidene fluoride (PVDF) membrane (New Logic Research INC, USA, 100 kDa; ~1.0 mg cm^{-2} catalyst coverage) by physical deposition method: the suspension was filtered through the membrane, applying 0.3 MPa transmembrane pressure in a batch-stirred membrane reactor (Millipore, XFUF07601, USA), followed by drying in air at room temperature *(Figure 2c)*.

Membrane filtration experiments were carried out in a Millipore XFUF07601 batch-stirred membrane reactor, which was equipped with commercial polyethersulfone (PES) or polyvinylidene fluoride ultrafilter membranes (PVDF, 100 kDa), or in the case of Fenton-type reactions microfiltration PES membranes (pore size 0.2μm) (New Logic Research INC, USA) or with photocatalytic nanomaterial covered membranes. Filtration was carried out using 0.1 MPa transmembrane pressure and 5.83 s^{-1} stirring speed (350 rpm). In all filtration experiments, 250 mL emulsion was filled into the reactor and filtered until the production of 200 mL permeate (volume reduction ratio: VRR = 5).

The purification efficiencies were determined by measuring the chemical oxygen demand (COD) and the extractable oil content (TOG/TPH) of the feed and the permeate. COD was measured by a standard potassium-dichromate oxidation based method, using standard test tubes (Lovibond). The digestions were carried out in a COD digester (Lovibond, ET 108) for 2 h at 150 °C and the COD values were measured with a COD photometer (Lovibond PC-CheckIt). Extractable oil content was measured by a Wilks InfraCal TOG/TPH type analyzer, using hexane as extracting solvent. The purification efficiency (R) was calculated as:

$$R = \left(1 - \frac{c}{c_0}\right) \cdot 100\% \, , \tag{1}$$

where c_0 is the COD or the TOG/TPH value of the feed and c indicates the values of the permeate.

To compare the performance of different AOPs, Oxygen-equivalent Chemical-oxidation Capacity (OCC, kg O$_2$/m^{-3}) was used to quantify the oxidants used in the

ozone treatment and Fenton process, and was determined on the basis of stoichiometric calculations as [22]:

$$OCC=1.000[O_3] =0.471[H_2O_2], \tag{2}$$

where $[O_3]$ is the demanded ozone concentration (kg O_3/m^3) and $[H_2O_2]$ is the demanded hydrogen peroxide concentration (kg H_2O_2 / m^3).
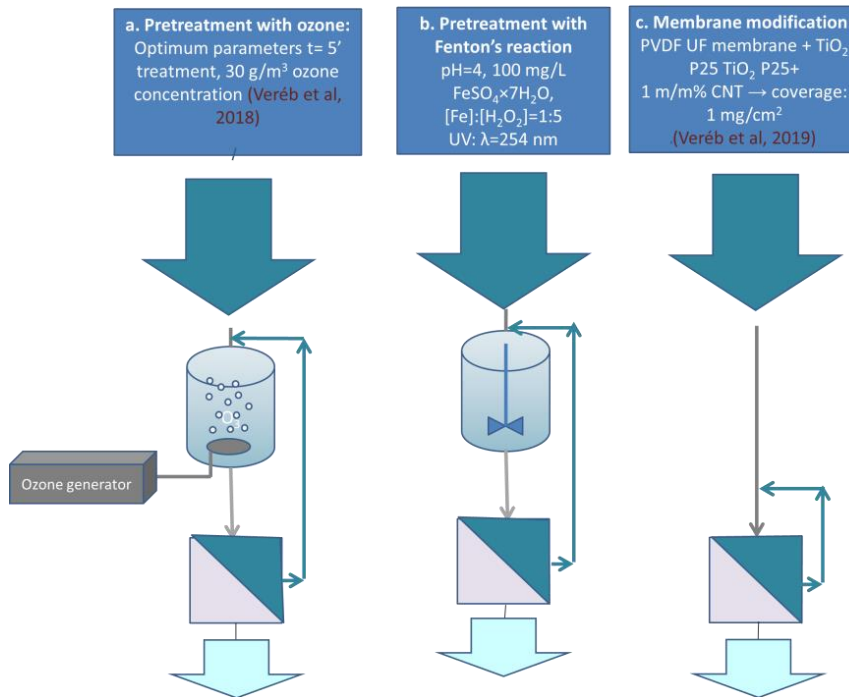
Figure 2

Experimental design of pre-treatments and membrane filtration experiments
[24], [18]

2.2. Cost estimation methodology

The cost estimation of combined processes was based on the costs of membrane filtration and pretreatments. During calculations 1,000 m^3/day feed volume was assumed *(Figure 2)*. Amortization was assumed to be 30 years. Taking into consideration the capital investments and operational costs, the total cost of 1 m^3 of wastewater purification was calculated. The calculation of costs of membrane filtration was carried out by the work published by [20]. The calculation of total capital investment for the membrane unit and plant includes fixed capital and working capital (operational cost) investments, while fixed capital investment comprises both direct and indirect costs. A similar method was applied for the cost calculation of the pretreatments [21].

3. RESULTS AND DISCUSSION

3.1. Effect of different pre-treatments on pollutant elimination efficiencies

In order to make the oxidation pre-treatments comparable, the Oxygen-equivalent Chemical-oxidation Capacity (OCC) was calculated during the pretreatments. Due to the negative long-term effects of pre-oxidation on filtration efficiency, short time (5 min, and in case of real wastewater 2 min) pretreatments were performed. In case of ozone treatments, the OCC was 30 ± 5 g m^{-3}, in case of real wastewaters 28 ± 2 g m^{-3}. In case of Fenton reaction, the OCC was 11.28, and in case of photo-Fenton 33 g m^{-3}. In case of catalyst-modified membrane surfaces, in one set of experiments the wastewaters were not pretreated before filtration; in these cases the photocatalytic effect was used for cleaning the membranes [24], while in another set of experiments ozone-pretreatments were performed (OCC=28 ± 2 g m^{-3}).

The pretreatments alone caused only a slight, if any, decrease in COD and extractable oil content. After the filtration, the overall extractable oil elimination was very high, while COD elimination efficiency was a little bit lower, but generally above 97% *(Table 1)*. The salinity of the water generally decreased the elimination efficiency.

Table 1

Chemical oxygen demand (COD) and extractable oil elimination efficiency after different pre-treatments and membrane filtration in case of model wastewaters (DW in distilled water, SW in saline water).

	MF (DW)	MF (SW)	UF	UF+TiO$_2$	UF+ TiO$_2$/CNT	Ozone +MF DW	Ozone +MF SW	Fenton + MF	Photo-Fenton +MF
Extractable oil elimination (%)	>99	>99	>99	97	97	99	99	98	98
COD elimination (%)	98	98.3	99	97	97	97.5	93	98	98

In case of real wastewater, the short term ozone treatment alone resulted in 10.6% COD elimination, and 30% elimination of extractable oil content. After filtration (Table 2), the extractable oil elimination efficiencies were lower than in the case of model wastewaters, presumably due to the saline water matrix. The pre-ozonation worsened the oil retention, presumably due to decomposition of oil to smaller molecules. The COD elimination efficiency was very low (around only 20%), which means that in this case the chemical oxygen demand mainly related to small organic and inorganic pollutants, not to oil.

COD and extractable oil elimination efficiency after different pre-treatments and membrane filtration in case of real produced water

	UF	UF+TiO$_2$	UF+TiO$_2$+CNT	Ozone+ UF	Ozone+ UF+TiO$_2$	Ozone+ UF+TiO$_2$+CNT
Extracable oil elimination (%)	83	98	99	87	95	98
COD elimination (%)	22	25.5	24	24	24.1	23

3.2. Effect of different pre-treatments on permeate flux

Separation performance of the selected membranes was studied in this and earlier studies [23], [24], [18]. A preliminary design can be developed on the basis of flux data by calculating the membrane area. During preliminary experiments the membrane filtration was done until VRR = 5. The measured flux at VRR = 5 (*Tables 3* and *4*) was considered as steady-state flux and used for calculations. Assuming 1,000 m^3 d^{-1} feed volume, the membrane area was calculated by the following equation:

$$A = \frac{Y \cdot V_F}{J} \tag{3}$$

where A is the filtration area (m^2), Y is the yield of the process, V$_F$ is feed volume (L h^{-1}), and J is the flux (L m^{-2} h^{-1}) at VRR = 5.

It was found that pretreatments significantly increased the flux. Although the ozone pretreatment significantly increased the flux, both Fenton pretreatment, and membrane surface modification were found to be more effective *(Table 3)*.

Steady-state flux and calculated membrane area for filtration of pre-treated model wastewaters

	MF (DW)	MF (SW)	UF	UF+TiO$_2$	UF+ TiO$_2$/CNT	Ozone +MF DW	Ozone +MF SW	Fenton +MF	Photo-Fenton +MF
Flux (L m^{-2} h^{-1})	54	46.0	45	150	294	173	85	278	244
Membrane area (m^2)	616	723.0	740	222	113	192	392	119	136

Similar results were obtained in case of real produced water; while ozone treatment slightly decreased the flux, the effect of membrane modification was more expressed. However, in this case – unlike in model wastewaters – the presence of

carbon nanotubes did not enhance the flux, and this effect was observed after pre-ozonation, too. The explanation of this finding requires more experiments, but the salinity of the water may play an important role in the fouling behavior of modified membrane surfaces.

Table 4

Steady-state flux and calculated membrane area for filtration of pre-treated real produced waters

	UF	UF+TiO$_2$	UF+TiO$_2$+CNT	Ozone+ UF	Ozone+ UF+TiO$_2$	Ozone+ UF+TiO$_2$+CNT
Flux (L/m^{2}h)	121.00	326.0	301.00	155.00	362.00	339.00
Membrane area (m^2)	275.04	102.1	110.56	214.71	91.93	98.17.

3.3. Cost evaluation

For the estimation of AOPs cost, Kommineni's method was followed [21]. The costs were divided into categories direct investment costs, indirect costs and operating costs *(Table 5)*. Amortization was assumed to be 30 years, 7% discount rate. The volume of ozonation reaction vessel was estimated by the ozone demand (30 g m^{-3}), and the contact time (5 min). On the basis of the feed volume, the volume of the tank is:

$$V=V_F/t = 1000 \text{ m}^3 \text{ d}^{-1}/5 \text{ min} = 3.47 \sim 4 \text{ m}^3, \qquad (4)$$

The amount of absorbed ozone is 1,440 g/4 m^3/h, which can be provided by 18 × 80 g/h ozone generator. The price of a 80 g/h ozone generator starts from 700 EUR, but it strongly depends on the manufacturer and other specifications; thus the costs calculated are minimum costs. Energy cost calculations were based on the power of ozone generators (680 W/item), 350 working days/year was assumed.

For calculation of Fenton and photo-Fenton treatment costs 120 min contact time was assumed, thus a 3 × 30 m^3 flocculator tank was considered (approx. 10,000 EUR each). The chemical demand was calculated as 100 g m^{-3} FeSO$_4$ and 0,2 Lm^{-3} H$_2$O$_2$. For the photo-Fenton process, lamps with 1,300 W power were considered in each reactor, and the UV energy demand was 0.096 kWh m^{-3}.

According to the method previously described by Salehi et al. [20] the total capital investment for the membrane unit includes can be divided into fixed capital and working capital investments. Fixed capital investment contains both direct and indirect costs, according to *Table 5*. The results of calculations are summarized in *Tables 6* and *7*.

Table 5

Cost estimation methodology

	Costs of Advanced Oxidation Processes [21]	Membrane separation costs [20]
Direct investment costs	a) Advanced oxidation unit b) Piping, valves, electrical (30% of (a)) c) Site work (10% of (a))	a) Main operating system (membrane systems). b) Installation of main systems (15% of (a)) c) Instrumentation and controls (6% of (a)) d) Electrical (10% of (a)) e) Installation (30% of (a)) f) Buildings, yard and auxiliary (15% of (a)) g) Land (6% of (a))
Indirect costs	Contractor's fees (15% of direct costs Engineering (15% of Direct costs +contractor) Contingency (20% of subtotal)	Engineering and supervision (30% of (a)) Contractor's fees (5% of direct cost) Construction expenses (10% of direct costs) Contingency (8% of fixed capitals)
Operating costs (annual)	Replacement Parts (1.5% of capital cost) Labor (3% of fixed capital) Analytical costs (2% of fixed capital) Chemical costs (based on experiments) Power (0.08 EUR/kWh)	Energy consumption (4% of fixed capital) Maintenance (4% of fixed capital) Operation and performance (2% of fixed capital) Labor (3% of fixed capital) Cleaning (3% of fixed capital)
Total annual cost	Amortization + annual operating costs Amortization: (based on 30-year period, 7% discount rate)	Amortization: lifetime of the polymeric membranes is 2 years. Amortization: (1/30) maintenance cost + (1/15) engineering and supervision + (1/2) membrane system

Table 6

Cost estimation results of combined pretreatment + membrane filtration processes in model wastewaters

	MF (DW)	MF (SW)	UF	UF+ TiO$_2$	UF+ TiO$_2$/ CNT	Ozone +MF DW	Ozone +MF SW	Fenton + MF	Photo -Fenton+ MF
Direct costs (investm.) (EUR)	140207	216410	168249	50475	25752	83314	128623	49285	60080
Indirect costs (EUR/year)	21031	24689	25237	7571	3863	29780	36577	17029	21707
Operating costs (EUR/year)	29496	34626	35395	10619	5418	22426	31958	71332	75541
Total annual cost (EUR)	69801	81940	83761	25128	12821	40028	62584	81961	88149
Water treatment cost (EUR/m^3)	**0.199**	**0.223**	**0.239**	**0.072**	**0.037**	**0.114**	**0.179**	**0.234**	**0.252**

The results show that the salinity of the water slightly increases the costs, in spite of this technology aiming only at oil removal (salinity removal requires more complex and expensive technology). The low costs of ozone pretreatment (assuming the cheapest ozone generators in the market) may be surprising, but it can be noted that the price is mainly determined by the cost of filtration, not by the ozone pretreatment, due to the short contact time. As the Fenton processes were considered with longer contact time (120 min), its investment costs were considerably higher than those of the ozone treatment unit. Together with its relatively high operating costs this resulted in higher total costs. The membrane surface modification presents the lowest investment cost with low operational costs, resulting in the most beneficial cost/m^3 wastewater. Although this technology would be very beneficial, it should be noted that these types of modified membranes are not available on the market at this time. Nevertheless, our results show that due to their good antifouling properties, the development of modified membrane surfaces may lead to a decrease in membrane filtration costs. Accordingly, the development of these kinds of commercial membranes is of great interest, and their widespread application is expected in several industrial activities.

In case of real wastewater *(Table 7)*, due to the lower oil content of the produced water, the cost of oil elimination decreased further. Although in terms of flux, the ozone treatment before filtration through modified membranes was beneficial – pre-ozonation enhanced the flux – in terms of costs this cannot be stated. The investment and operational costs of ozone treatment unit cannot be compensated by gains in smaller membrane area.

Table 7

Cost estimation results of combined pre-treatment +
membrane filtration processes in real wastewaters

	UF	UF+TiO$_2$	UF+TiO$_2$+CNT	Ozone+ UF	Ozone+ UF+TiO$_2$	Ozone+ UF+TiO$_2$+CNT
Direct costs (investments) (EUR)	62572	23225	25153	88396	60465	62575
Indirect costs (EUR/year)	9386	3484	3773	7327	26353	23622
Operating costs (without amortization) (EUR/year)	13163	4886	5292	23495	17619	17989
Total annual cost (EUR)	31151	11562	12522	42558	28653	29518
Water treatment cost (EUR/m^3)	0.089	0.033	0.036	0.122	0.082	0.084

4. CONCLUSIONS

The current study deals with a comparison of the cost of oily wastewater treatment by membrane filtration associated with different pretreatment methods. The cost

evaluation was completed for model oily wastewaters containing 100 ppm crude oil in saline or distilled water, and in some cases for real produced water, aiming at elimination of oil content. Three different pre-treatment methods (ozonation, Fenton and photo-Fenton pretreatments) and the modification of the used membrane surfaces with photocatalytic nanoparticles were used for the mitigation of fouling and enhancing the oil elimination efficiency during the process. The cost estimation was evaluated on the basis of flux decline and the cost of pretreatments. Results showed that pre-oxidation enhances the flux, and thus may decrease the cost of combined treatment.

Comparison of model and real wastewater's costs allows us to conclude that the cost depends on pollutant concentration – a lower oil concentration decreases the cost.

Analyzing the costs of AOPs and membrane separation, it appears that the capital cost of the ozone treatment unit may be reasonable, as the price is mainly determined by the cost of filtration rather than by the ozone pretreatment, due to the short contact time.

The membrane surface modification showed the lowest investment cost with low operational costs, resulting in the most beneficial cost/m^3 treated wastewater; due to their good antifouling properties, the development of modified membrane surfaces may lead to decreasing of membrane filtration costs, so there will be great interest in the development and the widespread application of these kind of commercial membranes in the near future, due to the continuously tightening emission limits.

REFERENCES

[1]   Yu, L., Han, M., He, F. (2017). A review of treating oily wastewater. *Arabian Journal of Chemistry*, 10, S1913–1922.

[2]   Erten-Unal, M., Gelderloos, A. B., Hughes, J. S. (1998). A toxicity reduction evaluation for an oily waste treatment plant exhibiting episodic effluent toxicity. *Sci Total Environ*, 218, pp. 141–152.

[3]   Fakhru'l-Razi, A., Pendashteh, A., Abdullah, L. C., Biak, D. R., Madaeni, S. S., Abidin, Z. Z. (2009). Review of technologies for oil and gas produced water treatment. *J. Hazardous Materials*, 170, pp. 530–551.

[4]   Aljuboury, D. A. D. A., Palaniandy, P., Abdul Aziz, H. B., Feroz, S. (2017). Treatment of petroleum wastewater by conventional and new technologies – A review. *Global NEST Journal*, 19 (3), pp. 439–452.

[5]   Hua, F. L., Tsang, Y. F., Wang, Y. J., Chan, S. Y., Chu, H., Sin, S.N. (2007). Performance study of ceramic microfiltration membrane for oily wastewater treatment. *Chem Eng J*., 128, pp. 169–175.

[6]   Padaki, M., Surya Murali, R., Abdullah, M. S., Misdan, N., Moslehyani, A., Kassim, M. A., Hilal, N., Ismail, A. F. (2015). Membrane technology enhancement in oil-water separation. A review. *Desalination*, 357, p. 197

[7]   Paode, R. D., Chandrakanth, M., Amy, G. L., Gramith, J. T., Ferguson, D. W. (2005). Ozone Versus Ozone/Peroxide Induced Particle Destabilization And Aggregation: A Pilot Study. *Ozone-Sci Eng*., 17, pp. 25–51.

[8]   Chang, I-S., Chung, C-M., Han, S-H. (2001). Treatment of oily wastewater by ultrafiltration and ozone. *Desalination*, 133, pp. 225–232.

[9]   Zhu, H.T., Wen, X. H., Huang, X. (2008). Pre-ozonation for dead-end microfiltration of the secondary effluent: suspended particles and membrane fouling. *Desalination*, 231, pp. 166–174.

[10]   László, Zs., Kertesz, Sz., Beszedes, S., Hovorka-Horvath, Zs., Szabo, G., Hodúr, C. (2009). Effect of pre ozonation on the filterability of model dairy waste water in nanofiltration. *Desalination*, 240, pp. 170–177.

[11]   Zakar, M., Lakatos, E., Keszthelyi-Szabó, G., László, Zs. (2017). Purification of dairy wastewaters by advanced oxidation processes and membrane filtration. *Review of Faculty of Engineering Analecta Technica Szegediensia* (ISSN: 1788-6392, eISSN: 2064-7964), 11/1., pp. 32–38.

[12]   Kovács, I., Veréb, G., Kertész, S., Hodúr, C.,László, Z. (2018). Fouling mitigation and cleanability of TiO2 photocatalyst-modified PVDF membranes during ultrafiltration of model oily wastewater with different salt contents. *Environmental Science and Pollution Research*, 25, p. 34912.

[13]   Bet-moushoul, E., Mansourpanah, Y., Farhadi, Kh., Tabatabaei M. (2016). TiO$_2$ nanocomposite based polymeric membranes: A review on performance improvement for various applications in chemical engineering processes. *Chemical Engineering Journal*, 283, pp. 29–46.

[14]   Molinari, R., Lavorato, C., Argurio, P. (2016). Recent progress of photocatalytic membrane reactors in water treatment and in synthesis of organic compounds. A review. *Catalysis Today*, 281, pp. 144–164.

[15]   Yi, X. S., Yu, S. L., Shi, W. X., Sun, N., Jin,, L. M., Wang, S., Zhang, B., Ma, C., Sun L. P. (2011). The influence of important factors on ultrafiltration of oil/water emulsion using PVDF membrane modified by nano-sized TiO2/Al2O3. *Desalination*, 281, pp. 179–184.

[16]   Hu, B., Scott, K. (2008). Microfiltration of water in oil emulsions and evaluation of fouling mechanism. *Chemical Engineering Journal*, 136, pp. 210–220.

[17] Leong, S., Razmjou, A., Wang, K., Hapgood, K., Zhang, X., Wang, H. (2014). TiO2 based photocatalytic membranes: A review. *Journal of Membrane Science*, 472, pp. 167–184.

[18] Veréb, G., Kálmán, V ; Gyulavári, T ; Kertész, Sz ; Beszédes, S ; Kovács, G ; Hernádi, K ; Pap, Zsolt ; Hodúr, C ; László, Zs. (2019). Advantages of TiO2/carbon nanotube modified photocatalytic membranes in the purification of oil-in-water emulsions. *Water Science and Technology-Water Supply*, 19, pp. 1167–1174.

[19] Sethi, S., Wiesner, M. R. (2000). Cost modeling and Estimation of Crossflow Membrane Filtration Processes. *Environmental Engineering Science*, 17 (2), pp. 61–79.

[20] Salehi, E., Madaeni, S. S., Shamsabadi, A. A., Laki, S. (2014). Applicability of ceramic membrane filters in pretreatment of coke- contaminated petrochemical wastewater: Economic feasibility study. *Ceramics International*, 40, pp. 4805–4810.

[21] Kommineni, S., Zoeckler, J., Stocking, A., Liang, P. S., Flores, A., Rodriguez, R., Browne, T., Roberts, P. E., Brown, A. (2000).: 3.*0 Advanced Oxidation Processes*. Center for Groundwater Restoration and Protection, National Water Research Institute.

[22] Cañizares, P., Paz, R., Sáez, C., Rodrigo, M. (2009). Costs of the electrochemical oxidation od wastewaters: a comparison with ozonation and Fenton oxidation Processes. *J Env. Management*, 90 (1), pp. 410–420.

[23] Veréb, G., Mihály, Z., Kovács, I., Pappné Sziládi, K., Kertész, Sz., Hodúr, C., László, Zs. (2017). Effects of pre-ozonation in case of microfiltration of oil contaminated waters using polyethersulfone membrane at various filtration conditions. *Desalination and Water Treatment*, 73, pp. 409–414.

[24] Veréb, G., Kovacs, I., Zakar, M., Kertész, S., Hodúr, C., László, Zs.(2018). Matrix effect in case of purification of oily waters by membrane separation combined with pre-ozonation. *Environmental Science and Pollution Research*, 25 (35), pp. 34976–34984. DOI: 10.1007/s11356-018-1287-9.